UNIVERSITÀ DI TRENTO

DEPARTMENT OF CIVIL, ENVIRONMENTAL AND MECHANICAL ENGINEERING

Master's Degree Course in

Civil Engineering

ANALYSIS OF THE PLASTIC SLIP CAPACITY OF STEEL-CONCRETE COMPOSITE DOWELS SHEAR CONNECTORS: DEVELOPMENT OF AN ANALYTICAL SIMPLIFIED MODEL

Supervisors

Prof. Nicola Tondini

Eng. Riccardo Zanon

Eng. Rui Matos

Candidate

Francesco Profico

Academic Year 2021/2022

Abstract

The shear connection is that part of a steel-concrete composite member that provides transfer of shear between the steel and concrete part of the element. The design rules EN1994-1-1 introduce a classification of the shear connectors based on the plastic slip capacity. In the present version of EC4 a minimum threshold value of 6mm is adopted in order to classify shear connectors as ductile. The classification will be adopted also in the forthcoming new version of EC4, with a more complex differentiation. The concept of classification is important in order to guarantee sufficient deformation capacity of the shear connection, especially to provide the correct shear flow redistribution in case of a plastic design of the shear connection in buildings. Moreover the concept is crucial to set the minimum degree of shear connection in members in Partial Shear Connection.

In recent decades new types of shear connectors have been developed. Composite dowels shear connectors are a relatively recent solution on the market and will be the subject of design rules in the forthcoming version of EC4. So far numerous application cases of this technology exist in bridge construction. The behaviour of composite dowels for composite members in buildings is still under study. The plastic slip capacity of this type of shear connectors must be assessed in order to provide the correct classification according to EC4. In this work an analytical simplified method and a numerical Finite Elements Analysis parametric study are proposed to assess the plastic slip capacity of composite dowels. The plastic slip capacity is studied under different failure modes of the composite dowels. Analytical models of the plastic slip capacity of composite dowels are proposed and compared.

Aside of the main research scope of the work, the behaviour of composite simply supported beams is studied by mean of a numerical one-dimensional finite differences numerical method. This method allows for the computation of the slip demand and the shear flow along the shear connection of the member.

Innovative design case studies are proposed as annex of the work. On these technologies using composite dowels shear connections a parametric study to identify the optimal solutions is also proposed.

Keywords

Composite beams, Composite dowels, Shear connection, Plastic slip capacity, Analytical model

Preface

The present Master's Degree thesis has been developed in conjunction with a period of internship in the Global Research and Development department in Esch-Sur-Alzette, Luxembourg of the company ArcelorMittal. The work is the result of a period of deep diving into the topic, not only limiting the area of interest at the mere academic scope of it, but also broadening the studied field at the surrounding related topics. Aside of the technical content that will be introduced and discussed in the body of the thesis, in this work I try to summarize the deep passion, interest and curiosity I have into science in general. More in detail engineering, physics, math and informatics have been always attractive subjects to me. In presenting the technical work of the thesis, I also try to bring out these personal interests which are not strictly linked to the engineering area. In growing up as an engineer I always considered physics as the set of rules to face, math as the language to describe them and programming as a powerful instrument to solve engineering problems. Engineering has the natural position to link these branches of science. This work has the aim to represent this line, transmitting my passion and curiosity in all these fields, hoping to be inspirational and trying to give a contribute to the development of the specific technical subject.

Contents of the work are for the largest part self-prepared. Drafting, reporting, technical drawings of images, programming, workflow automation, numerical analysis, renderings, the ability to perform calculations according to design rules, data management and report, and much more are all competences that I tried to put into play to finalize this work. This work is a frame showing my engineering skills. It gives me confirmation of the person who I am and and of the interests I want to grow. It represents a milestone for my personal formation as engineer, and can potentially be a starting point for my future professional career.

I hope the reader will in general perceive and appreciate the effort and passion I putted in this work.

Acknowledgements

I would like to thank my supervisor Prof. Nicola Tondini, who followed me in my work and allowed me to get in touch with ArcelorMittal's R&D department, giving me an exceptional opportunity for personal and professional growth. Special thanks go to my company supervisors, Eng. Riccardo Zanon and Eng. Rui Matos, who stimulated me to give my best for the success of the work, and made me live the internship experience (Fig.1, Fig.3, Fig.4) in the company to the full. These three people deserve the main credit for directing my research efforts. I would like to thank the company ArcelorMittal for the opportunity offered to

Figure 1: Visit at the beam finishing center

me to know this reality from close. In these three months of experience, I came into contact with a centre of excellence and a hub of research in the field of steel structures. I would like to thank the entire R&D team (Fig.2) of ArcelorMittal in Esch-Sur-Alzette for having welcomed me among you with enthusiasm and passing on your passion for research. A big thanks goes to Teodora but also Fırat and Majeck who gave me feedbacks for setting up the numerical analysis.

Figure 2: The R&D team

An important thanks goes to my family, to my parents who have always encouraged me in my choices and supported me, to my brother who is a great person, to my grandparents who raised me and gave me the best. A deep thank you goes to my girlfriend, Daila. We encouraged and motivated each other often in

our goals. I am happy to have shared these years and so many adventures with you.

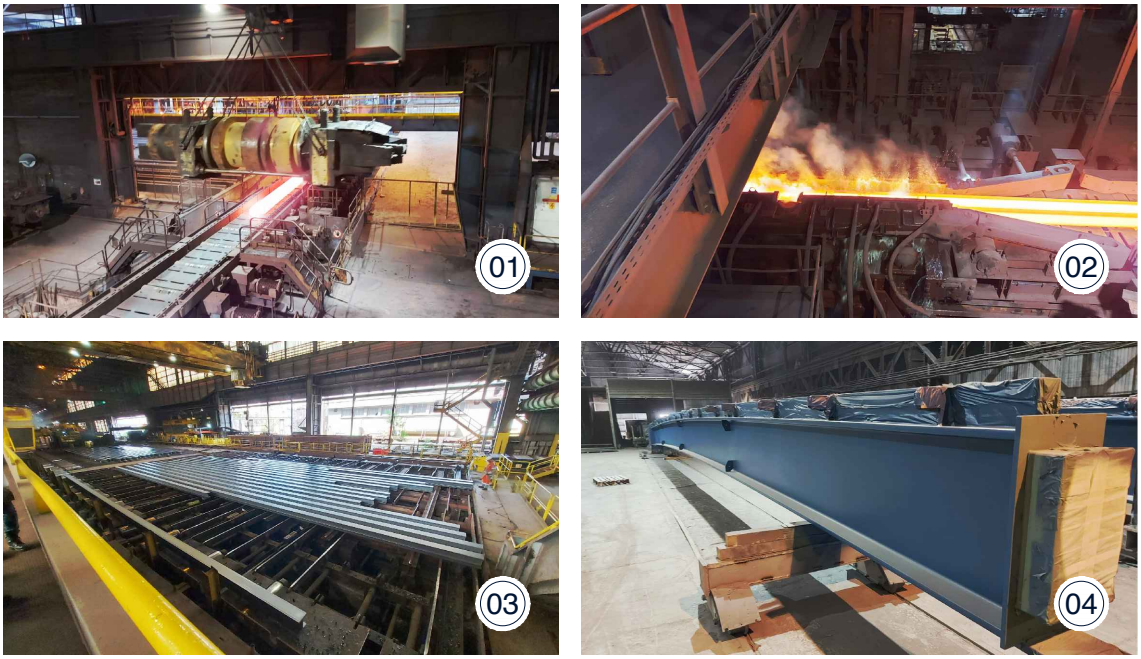

Figure 3: some pictures of the visits I took at the hot-rolling plant and beam finishing center plant: 01) a long product under hot rolling process; 02) a long product under Quenching and Self Tempering (QST) process; 03) a stock of hot-rolled long products; 04) a bridge beam

I thank my friends Daniel, Lorenzo, Dalle, Marti, Thomas, Milena, Nicole, Valeria, Giulia, Sara. I thank Andrea, Mello, Gabriel, Kevin, Dymitri, Chiara for all being such good friends and fellow adventurers. A significant thank you is directed to Professor Francesco Catania, who was my high school teacher. I will never forget the passion he passed on to me for technical subjects. It is mainly thanks to him and the enthusiasm he put into his job that I was directed to study engineering. The thanks that go to him are those directed to all those who participated in my education.

I thank the colleagues with whom I have lived the university experience over the last few years, with whom I have pursued my studies and group projects. In particular, a thought goes to Stefano Zorzi, one of the toughest engineers I have ever met, with whom I have teamed on university projects, but I am not forgetting Alessandro, Enrico, Andrea, Alice, Elena, Miriana, Monica.

Figure 4: some pictures of the visits I took at the hot-rolling plant and beam finishing center plant: 01) a partial encased beam for a building project in preparation; 02) a set of car park beams with welded headed studs and bars; 03) headed studs shear connectors; 04), 05) and 06) a set of composite dowels beams with Modified Clothoidal Shape (MCL) type thermal cutting

Contents

Notations

$(1/r)$	curvature of section
$(1/r)_u$	ultimate curvature of section
χ	curvature
χ_u	ultimate curvature
χ_x	reduction coefficient for interaction of dowels arranged in the same row
χ_y	reduction coefficient for interaction of dowels arranged in the parallel rows
$\Delta h_{pl,\chi}$	height of plastic hinge
$\Delta h_{pl,\delta}$	height of plastic plane
Δt	numerical resolution time increment or time step increment
δ	slip
δ_u	plastic slip capacity the shear connector
δ_{max}	maximum imposed slip
Δ_x	discretization step
δ_y	first yielding slip
ϵ	concrete damage plasticity eccentricity or generic strain component
$\epsilon_{a,interface}$	strain of structural steel fibre in correspondence of the steel-concrete interface
ϵ_{au}	ultimate strain of structural steel
ϵ_{ay}	yielding strain of structural steel
$\epsilon_{c,interface}$	strain of concrete fibre in correspondence of the steel-concrete interface
ϵ_{cf}	concrete upper fibre strain in full shear interaction condition
ϵ_{cu}	ultimate compression strain of concrete
ϵ_c	concrete upper fibre strain or concrete fibre strain
ϵ_{el}	elastic strain
ϵ_{eq}	equivalent strain
ϵ_{in}	inelastic strain
ϵ_{pl}	plastic strain
ϵ_{slip}	strain slip
ϵ_{su}	ultimate strain of reinforcement steel
ϵ_{sy}	yielding strain of reinforcement steel

ϵ_{tot}	total strain
ϵ_y	yielding strain of steel
η	degree of shear connection
η_D	coefficient for the concrete dowel shearing resistance calculation
η_{min}	minimum degree of shear connection
γ	shear angular slip
γ_u	ultimate shear angular slip
γ_v	partial safety factor for shear connection's resistance
λ_{geo}	shape factor for steel dowel yielding resistance
μ	concrete damage plasticity viscosity parameter
$\mu_{Friction}$	tangential friction coefficient
ν	material's Poisson's modulus
ϕ	section rotation
ψ	concrete damage plasticity dilation angle
ψ_{crack}	reduction factor for pryout failure resistance due to transverse cracking of slab
ρ	material's density
σ	stress
σ_{ct}	concrete tensile stress
θ	steel dowel rotation
θ_u	steel dowel ultimate rotation
A_b	bottom reinforcement area
$A_{D,j}$	effective concrete dowel area
A_D	concrete dowel area
A_t	top reinforcement area
b	flange width or section fibre width or steel dowel base dimension
$c_{D,o}$	upper concrete cover
$c_{D,s}$	side concrete cover
$c_{D,u}$	lower concrete cover
d_c	concrete compression damage
d_t	concrete tensile damage
E	material's elastic modulus
E_s	elastic modulus of steel
e_x	composite dowel size or shear connector spacing
E_a	elastic modulus of structural steel
E_{cm}	mean elastic modulus of concrete
E_{CW}	constraint penalties work
E_{FD}	friction dissipated energy
E_{IHE}	internal heat energy

E_I	internal energy
E_{KE}	kinetic energy
E_{MW}	propelling added masses work
E_{PW}	contact penalties work
E_{TOT}	total energy
E_{VD}	viscous dissipated energy
E_W	work energy
f_y	steel yielding resistance
f_{au}	ultimate resistance of structural steel
f_{ay}	yielding resistance of structural steel
f_{ck}	cylindrical compression characteristic resistance of concrete
f_{cm}	mean value of compression resistance of concrete
f_{ctm}	concrete mean tensile resistance
f_{ct}	concrete tensile resistance
f_c	concrete compression resistance
f_{su}	ultimate resistance of reinforcement steel
f_{sy}	yielding resistance of reinforcement steel
$f_{y,red}$	reduced yielding resistance of steel due to shear-moment interaction
G_f	fracture energy
h	section height
h_{crit}	height of critical section
h_D	steel dowel height
h_{po}	concrete pryout cone height
h_P	height of force application
h_{slab}	concrete slab height
h_{TOT}	composite section total height
k_1	coefficient for the pryout resistance calculation
L	span length
L_{min}	minimum finite element dimension
M	bending moment
M_{Ed}	design acting bending moment
M_{max}	maximum bending moment
$M_{pl,a,Rd}$	plastic resistant design bending moment in of the steel part
$M_{pl,f,Rd}$	plastic resistant design bending moment in FSC conditions of the composite section
$M_{pl,Rd}$	plastic resistant design bending moment of the composite section
M_{pl}	plastic resistant moment
MSF	mass scaling factor
n	number of shear connectors between two critical sections

N_{cf}	compression force on the concrete part in FSC and ULS conditions
N_c	compression force on the concrete part
P	shear load
$P_{max,b}$	maximum resistant force on the composite dowel due to bending failure
$P_{max,v}$	maximum resistant force on the composite dowel due to shear
P_{max}	maximum force on the composite dowel
$P_{pl,k}$	steel dowel yielding characteristic resistance
$P_{po,k}$	concrete pryout characteristic resistance
$P_{poe,k}$	concrete edge-pryout characteristic resistance
P_{Rd}	shear connection design shear resistance
P_{Rd}	shear design resistance of the single shear connector or composite dowel
P_{Rk}	shear connection characteristivc shear resistance
$P_{sh,k}$	concrete dowel shearing characteristic resistance
q	distributed load
r	fillet radius
T	numerical resolution step time period
t_w	web thickness of the steel section
t_f	flange thickness
u	displacement
u_a	displacement of structural steel fibre
u_c	displacement of concrete fibre
V	shear
v_L	longitudinal shear flow
V_{Ed}	design value of acting shear
V_{el}	elastic shear
$v_{L,Rd}$	shear flow design resistance of the shear connection
V_{pl}	plastic shear
w	concrete crack opening
x	element coordinate
$x_{pl,1}$	position of first neutral axis of the composite section
$x_{pl,2}$	position of second neutral axis of the composite section
y	sectional coordinate of fibre or vertical displacement

Definitions

composite action configuration such that two former individual elements act together as one cohesive component, with a consequent higher resistance and stiffness.

composite beam a composite member subjected mainly to bending.

composite dowel Composite shear connector of steel cut out of hot-rolled steel plates, sections or bars and encased in reinforced concrete to achieve composite action between steel part and concrete part of the composite member.

composite section section made up of different parts of different materials.

dowel shape particular cutting separation geometry that defines the composite dowels shear connection conformation.

plastic slip capacity slip correspondent to the 90% of the peak shear resistance of the shear connection on the post-critical branch of the load-slip curve. Definition in accordance with EC4[11].

PreCoBeam solution prefabricated composite beams based on composite dowels shear connection.

shear connection an interconnection between the concrete and steel components of a composite member that has sufficient strength and stiffness to enable the two components to be designed as parts of a single structural member.

slip demand required slip on the shear connection. The value is related to the composite member behaviour, properties and loading conditions.

steel dowel steel mechanical device loaded under shear action composing the shear connection.

steel-concrete composite member a structural member with components of concrete and of structural or cold-formed steel, interconnected by shear connection so as to limit the longitudinal slip between concrete and steel and the separation of one component from the other.

Acronyms

CDP Concrete Damage Plasticity.

FEA Finite Element Analysis.

FEM Finite Element Method.

FSC Full Shear Connection.

FSI Full Shear Interaction.

HPC High Performance Concrete.

MCL Modified Clothoidal Shape.

MPZT Modified PZT Shape.

MSF Mass Scaling Factor.

POST Push Out Standard Test.

PSC Partial Shear Connection.

PSD Partial Shear Diagram.

PSI Partial Shear Interaction.

PZ Puzzle Shape.

PZT Modified Puzzle Shape.

RP Rigid Plastic analysis.

SA Fin Shape.

SL Strain Limited analysis.

SLS Serviceability Limit State.

UHPC Ultra High Performance Concrete.

ULS Ultimate Limit State.

Chapter 1

Introduction

1.1 Composite steel-concrete beams

The use of structural solutions in the field of civil engineering with the combined use of steel and concrete optimises the element's performance by exploiting the complementary characteristics of the two materials. The concept, also used in the case of reinforced concrete, is applied in steel-concrete steel-concrete composite members. Composite structural elements can bring advantages both on a mechanical level and on an economic level, in terms of speed and ease of erection. There is a potential gain in the reduction of deformations, thicknesses and weights of structural elements. In civil engineering, the use of steel-concrete composite members is extended to both buildings and bridges. In composite elements the adequate transmission of forces between steel and concrete parts must be guaranteed. The use of a shear connection guarantees a transfer of shear actions. The problem is known in particular in the case of elements in predominantly bending such as composite beams and slabs. In these cases, there is usually an upper concrete slab connected by means of steel elements to a welded or hot-rolled profile at the lower end. The shear connection allows to gain resistance and stiffness achieving the composite action. In the absence of a shear connection, the composite action would not be achieved with a non-optimal utilisation of the two materials. The concept is illustrated in Fig.1.1.

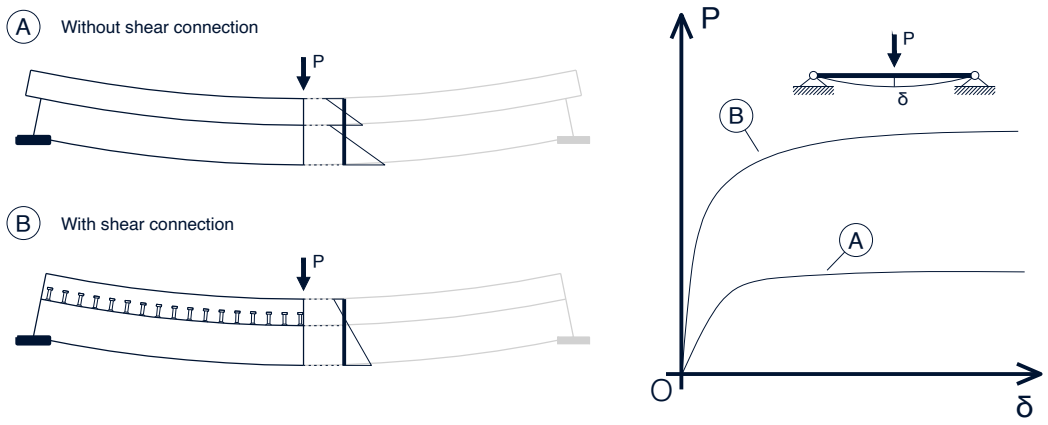

Figure 1.1: composite behaviour of beams

1.2 Development of composite dowels solutions

The composite action is achieved by means of mechanical devices known as shear connectors. The development of interest in steel-concrete steel-concrete composite members has led to an evolution throughout the history of shear connectors. From the first patents dating back to the beginning of the 20th century, such as the solution proposed by Julius Kahn in 1903 (Fig. 1.2), the connectors have evolved in different forms arriving successively at the welded head-stud connectors, which appeared for the first time in 1956 but only became established in the 1980s. These are now widely used in various construction solutions in civil engineering.

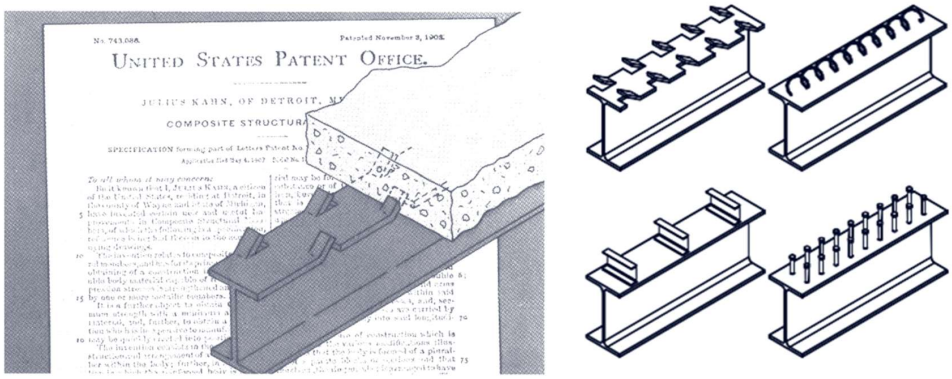

Figure 1.2: examples of shear connectors

In recent decades, research has moved towards new technologies with a higher degree of material utilisation, partly as a result of the interest in obtaining more competitive solutions on the market. The first studies carried out by Leonhardt in 1987 on the "Perfobond-Leiste" (PBL) technology based on continuous connection elements realised by means of a steel strip perforated at discrete intervals and joined to the

concrete date back to the end of the 1980s. In this case, the connectors are materialised by the concrete parts inside the holes which are loaded in shear and can develop various failure mechanisms. However, the study focused and modelled the failure for the concrete dowel side. Studies then developed the 'Kombi-Dowel' technology in the late 1990s. The subsequent evolution led to the development of steel-concrete 'continuous composite dowels' (Fig.1.5, Fig.1.3). The term composite dowels, 'Verbunddübel' in German, has been adopted because both the steel and concrete dowels can fail. One of the relevant research work on the topic was done in the frame of the PrecoBeam project. The objective was to carry out research on the technology of composite dowels applied in the field of bridge beams of medium-short span and tall buildings, examining mainly the mechanical aspects of their behaviour under static, cyclic and fire loads, considering their fatigue behaviour and durability and acquiring knowledge on the influence of the geometrical characteristics and the materials used.

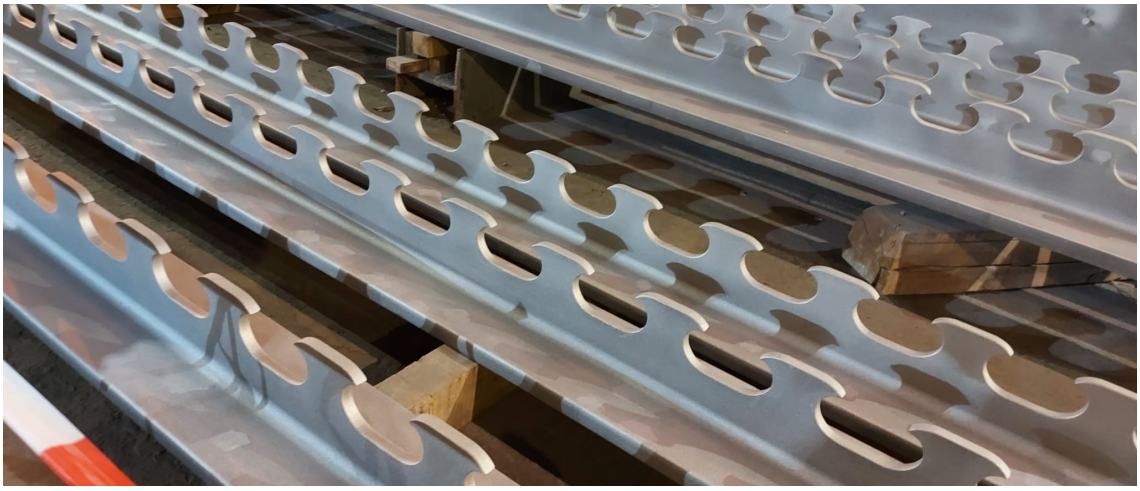

Figure 1.3: an example of MCL shaped steel profile

In the study, the potential of exploiting advantageous aspects of the following two technologies is highlighted:

- The "Filler-Beam Deck" is a construction technology that has been widely used in the past and guarantees the strength and slenderness of the element.
- "VFT" (Verbundfertigteil - Träger) is a construction technology widely used since 1998 for bridges. It guarantees a high degree of prefabrication and short erection times. The upper concrete flange is connected to the steel profile by head studs connectors. The concrete slab, as well as acting as a formwork for the subsequent casting of the completion slab in situ, guarantees the stability of the steel profile and makes it possible not to use propping during the erection phase.

The use of composite dowels beams opened up the possibility of having the robustness and slenderness of Filler-Beam elements and the degree of prefabrication of VFT technology.
A T-profile, obtained by separation by longitudinal cut at the web height of double-T laminated elements, is connected to the concrete upper part. The slenderness of the element is greater when compared to

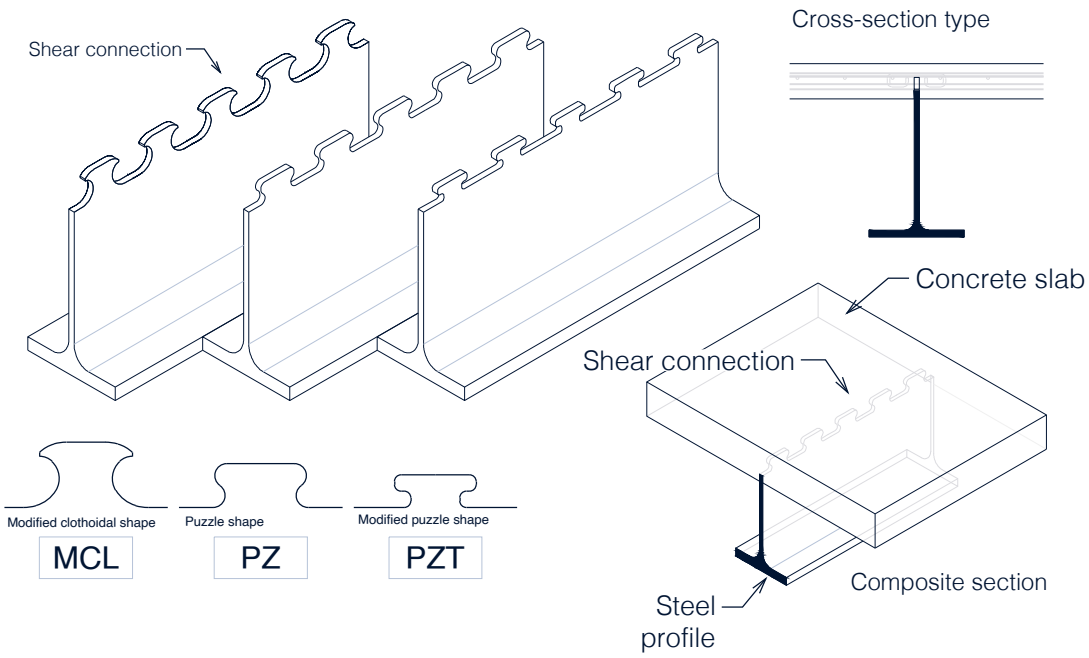

Figure 1.4: composite dowels: concept

conventional solutions using double-T beams. This leads to design advantages such as less soil moving and fewer access works or a higher river or road clearance in case of bridges. The cutting shape is such that two T-sections of equal cutting shape are obtained. In addition to the high load-bearing capacity, the most relevant implications of composite dowels are the use in composite sections without upper flange of the steel profile and a deformation capacity that can respect the ductility criterion of EC4 [11]. They can guarantee a complete and consistent design.

Following the Precobeam project, the ECOBRIDGE project (Demonstration of economical bridge solutions based on innovative composite dowels and integrated abutment) was carried out, with which the first works using the continuous composite connector technology were designed and built in three different European countries. Further research work led with Project FOSTA P804 [45] to the formulation and approval of the first technical regulations in Germany [4].

At present, research on composite dowels is still under development, in particular with the long-term goal of being able to include guidelines for the calculation of structures using the technology in subsequent versions of Eurocode 4. This would make it possible to expand the use of the technology.

1.3 Research topic introduction

In composite beams a relative slip at the concrete-steel interface occurs (Fig.1.6). This is due to the non infinite stiffness of the shear connection. A shear flow is transmitted through the shear connection. The slip and the shear flow are related by the mechanical behaviour of the shear connection (Fig.1.7). If the shear

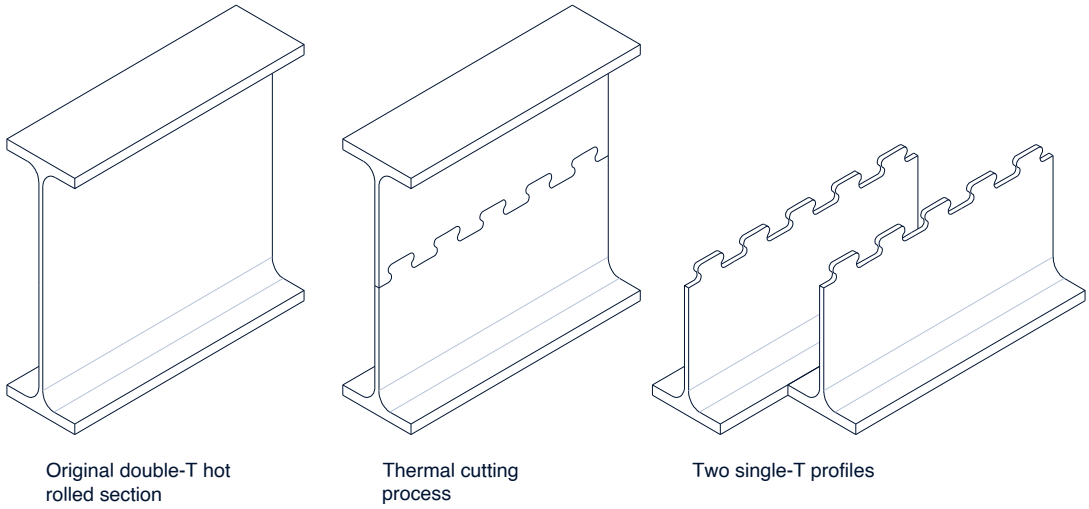

Figure 1.5: thermal cutting of steel profile

connection yields, redistribution of shear flow occurs. A Full Shear Connection (FSC) regime occurs when the sectional resistance of the beam is not limited by the shear connection's resistance. In the opposite case a Partial Shear Connection (PSC) occurs (Fig.1.8).

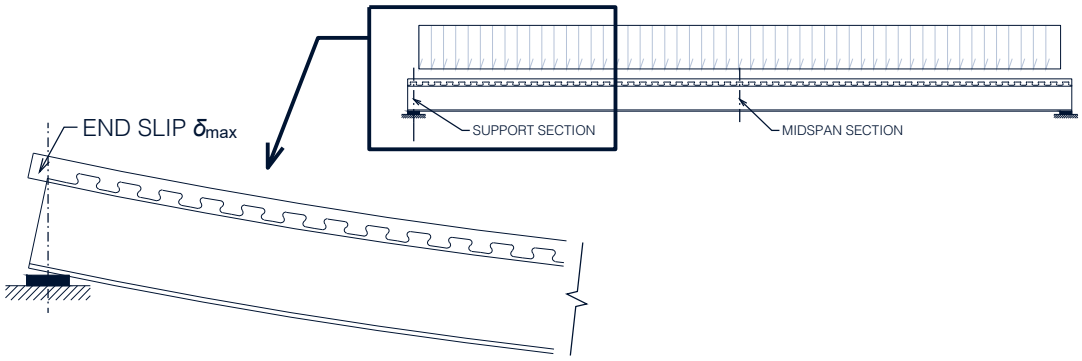

Figure 1.6: slip at steel-concrete interface

So far the composite dowels technology has been widely applied in the bridge construction. Here an elastic design approach is commonly used for the shear connection (Fig.1.8). At limit a yielding, with reaching of the plastic resistance of the most loaded shear connector is allowed. This occurs at support for simply supported composite beams. No reaching of the plastic resistant shear flow is admitted along the shear connection. Research has then enlarged toward buildings applications. Here a plastic approach can be used in the design process. A redistribution of the plastic flow along the shear connection is allowed. Under these circumstances the ductile failure mode of the shear connection has to be guaranteed. If not, the proper redistribution can not be successfully achieved, leading to brittle and undesired failures of the steel-concrete composite member. The plastic slip capacity of the shear connection has therefore to be

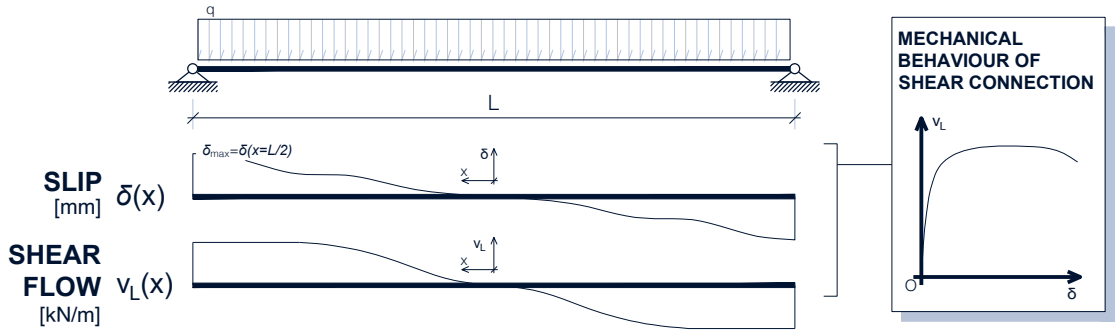

Figure 1.7: shear flow and slip relation

correctly assessed. Furthermore, Partial Shear Connection (PSC) regimes are also allowed in buildings. It's known from research that in PSC the end-slip (fig.1.6) of simply supported beams tends to increase sharply at Ultimate Limit State (ULS) conditions. This represents a significant slip demand on the shear connection. Comparing the plastic slip capacity with the slip demand is important in order to prevent brittle failure modes of the steel-concrete composite member. The required deformation on the shear connection must not be greater than the plastic slip capacity. From this concept, design checks on the minimum degree of shear connection are already present in the version of EC4 [11]. In the present version shear connection devices meeting the criteria of ductility of 6mm are classified as ductile. Research has to be done in order to improve the knowledge on the plastic slip capacity of composite dowels. Moreover, this has to be done looking forward to the forthcoming version of EC4, which is currently under development. This new version of the deign rules is evolving toward a more differentiated classification of the ductility of shear connection devices.

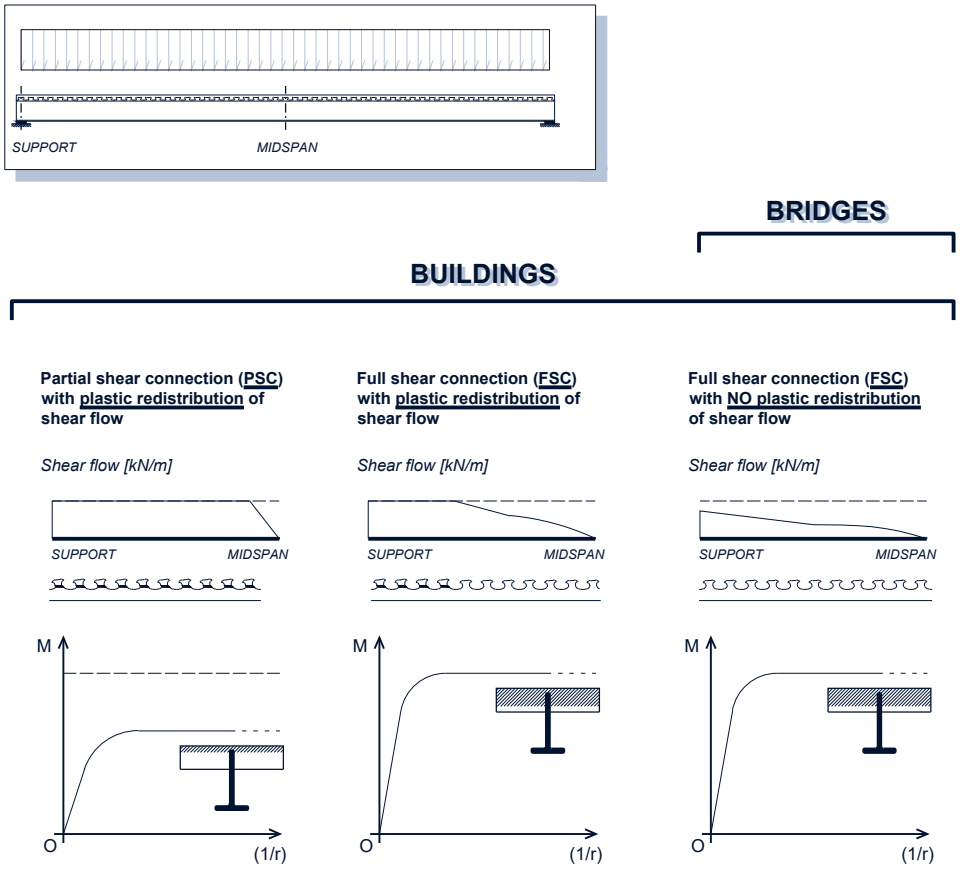

Figure 1.8: concepts of partial and full shear connection and concept of redistribution of shear flow

1.4 Research objectives

The main focus of the present work is to assess with analytical simplified models and numerical analysis the plastic slip capacity of the composite dowels technology. The plastic slip capacity should be assessed under both concrete pryout and steel yielding failure modes. The plastic slip capacity is derived by means of two different methods. Both an analytical simplified approach and numerical simulations are used. A numerical one-dimensional model to assess the slip demand along the beam is also presented. This has been developed in order to gain confidence with the topic and understand the phenomena. In addition this numerical method allows to compare between the slip demand and the plastic slip capacity of the composite dowels shear connection.

1.5 Related topics

Alongside the main topic of the present research work, worked calculation examples are presented for the composite dowels technology. These can be found in the annexes for two different innovative cases. In

annex B the calculation of a Carpark composite dowels beam is presented. In annex A the calculation of an office composite dowels slim floor decking technology is shown. Worked cases are developed and discussed. These have also been important parts of the work in order to gain confidence with the main argument and to taste a more application side of the solutions. An excel design sheet was developed in the frame of the present research work. The two computational examples in the annexes have been calculated with this tool. Thanks to this tool, a set of parametric studies has been carried out in order to identify the optimized solutions for both the worked examples in the annexes. This parametric analysis is presented in annex C and extended results are shown in annex F. Due to the composite wood-steel-concrete nature of the technology presented in annex A and annex C, analysis on the optimization of the wood-concrete decking solution are presented in annex D.

A significant number of Python language coding is being used in the whole work in order to automate the analysis, to post-process the results and print significant charts. These codes are not presented as annex, but can be requested to the author.

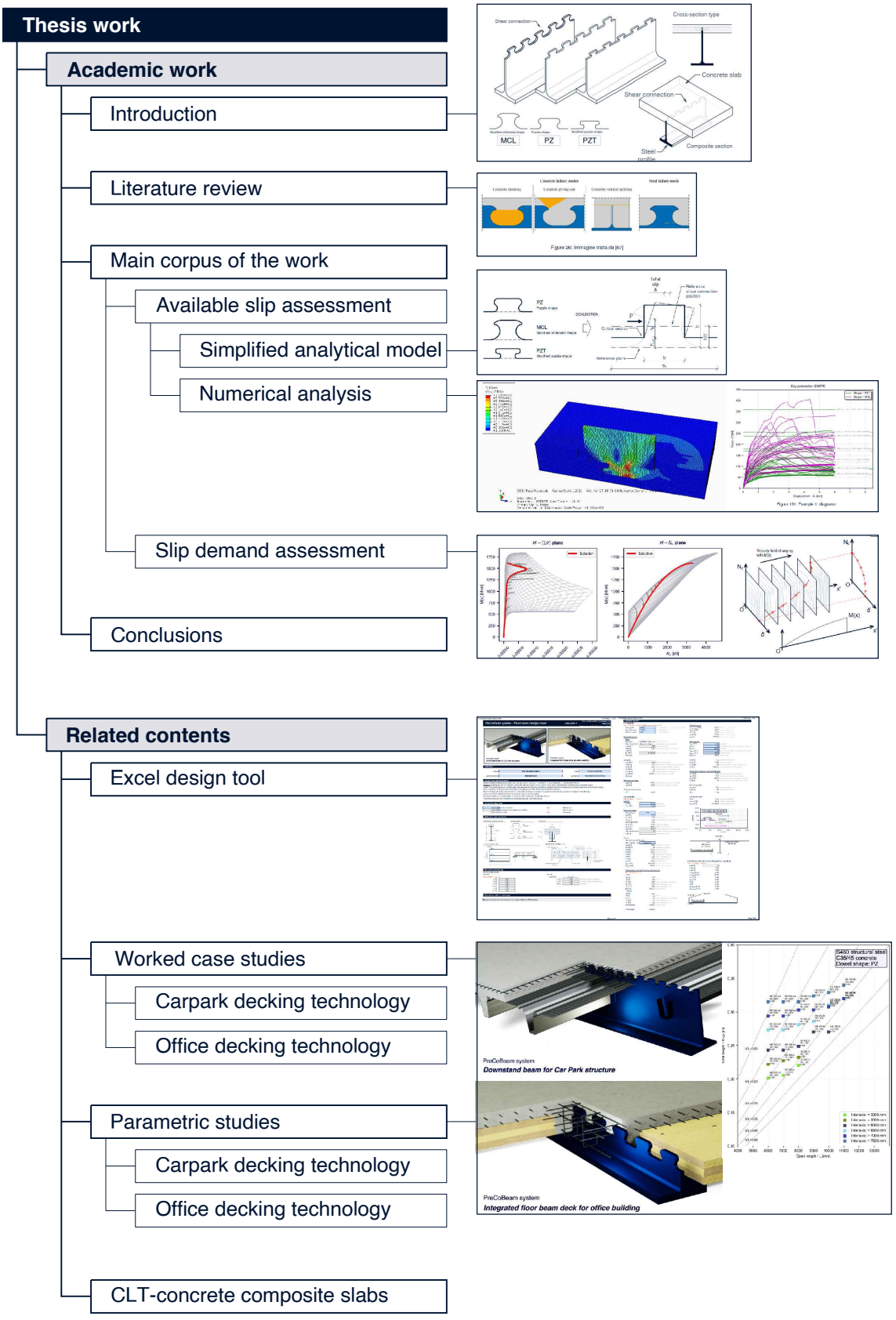

Figure 1.9: thesis work organization

Chapter 2

Literature review

In this section, the literature review on composite dowels is presented. After the description of the search criteria, a classification of the publications is carried out. The contents are analysed and the literature review is done for those aspects which are useful for the present research work.

2.1 Search criteria and literature found

On 22 September 2021, the analysis with the online engine "Scopus" was carried out [14]. The following key was used to search through article titles, keywords and abstracts of the publications:

« ("Composite dowels" OR "Precobeam" OR "Rib shear connection") AND ("steel" OR "concrete" OR "composite section" OR "composite elements") AND NOT (timber OR wood) »

The search produced 124 results. Restricting the subject area to engineering and materials science the number of publications found reduced to 113. Both English- and German-language publications are examined. Further selection is made by examining the summaries and bibliographies of the publications found.
The growth of research interest in composite dowels over the last two decades is evidenced by the increasing trend in the number of publications per year on the subject (Fig. 2.1).
The research is mainly concentrated in Germany and Poland (Fig. 2.5), between the "Lehrstuhl und Institut für Massivbau" in Aachen (DE) and the "Wroclaw University of Science and Technology" (PL) (Fig. 2.3). From Fig. 2.2 it is possible to get an overview of the main authors of the publications found.
In the list of 113 publications found, special attention is given to the analysis of articles with:

- the highest number of citations, probably those which are most interesting for having characterised the development of the subject in the course of the past research and breakthrough discoveries;
- the most recent date, in order to get a clear picture of the latest research developments on the topics

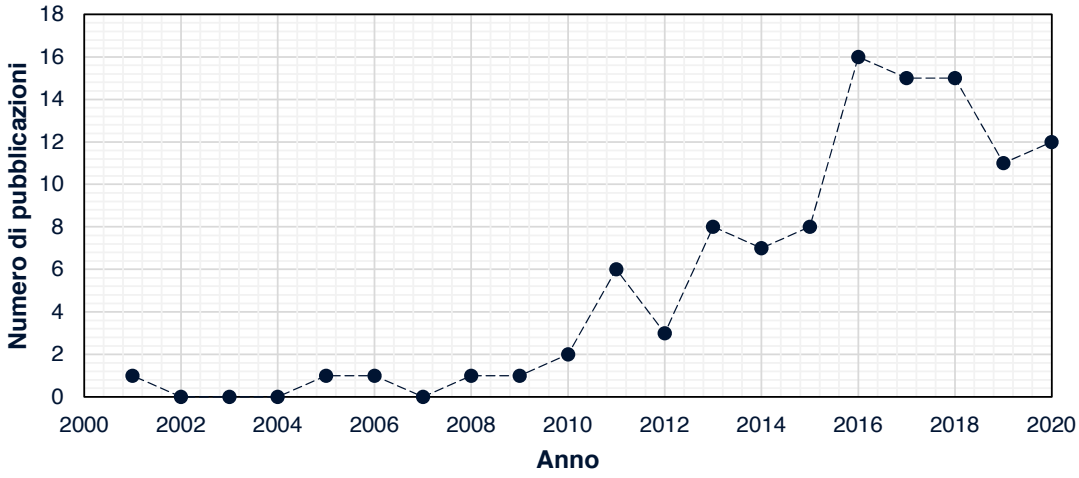

Figure 2.1: publications per year of the composite dowels topic

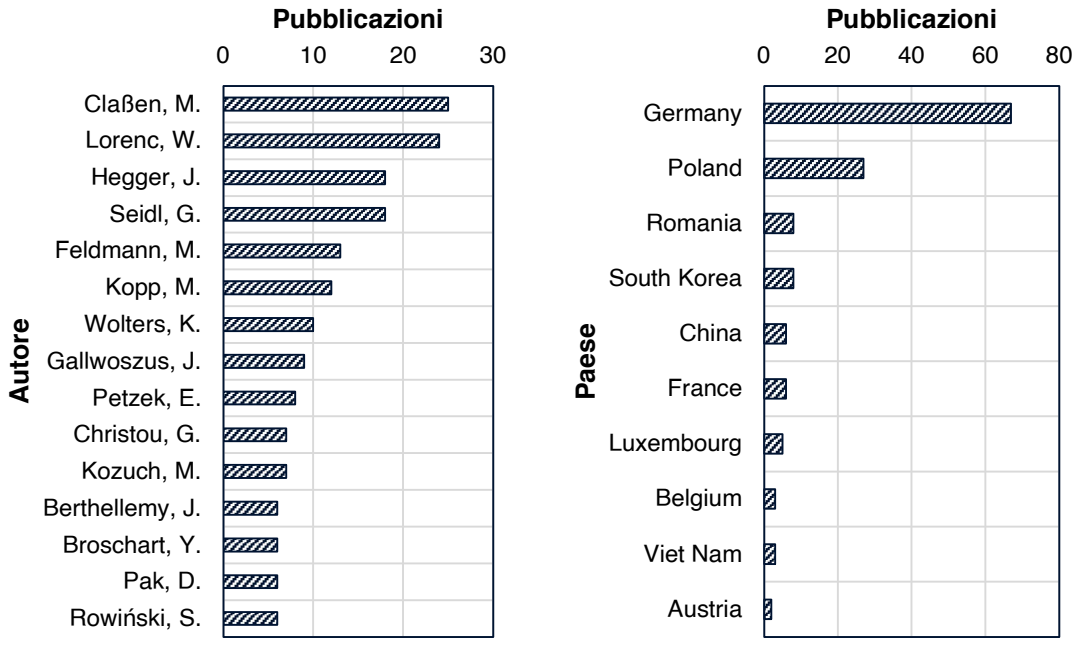

Figure 2.2: publications per author and per country on the composite dowels topic

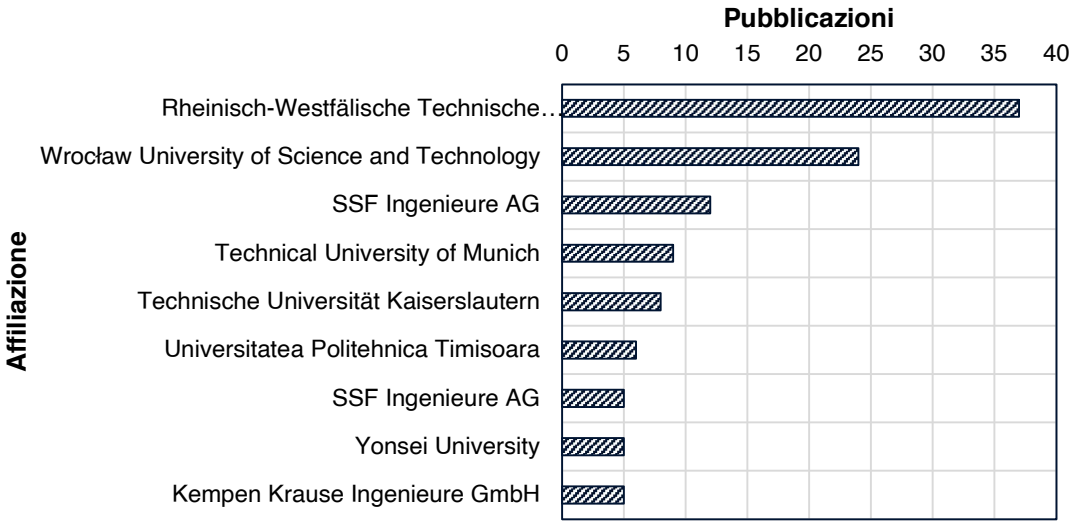

Figure 2.3: publications per affiliation on the composite dowels topic

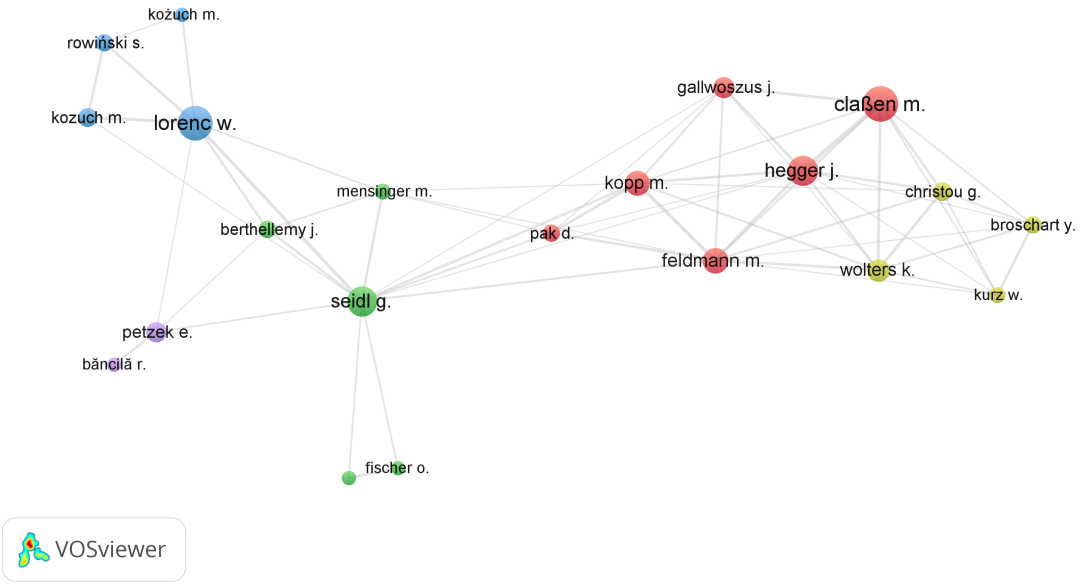

Figure 2.4: relevant authors map from VOSviewer

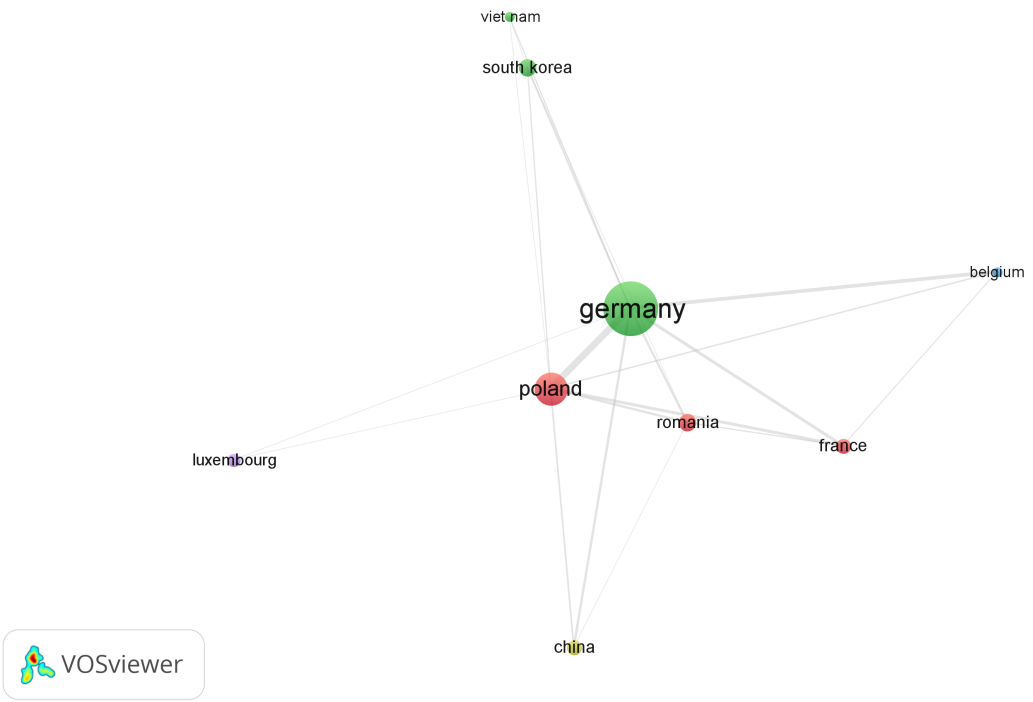

Figure 2.5: countries where the research on composite dowels has major activity: conceptual map from VOSviewer

covered.

Where relevant, publications included as references within the main articles are also considered. Given the nature and scope of this research work, particular attention is given to the techniques described and employed in the literature for the numerical Finite Element Method (FEM) simulation of the mechanical behaviour of composite dowels.

2.2 Classification of literature

It is possible to introduce a classification of the reviewed literature on the basis of the following criteria:

- work tipology:
  - article;
  - book part;
  - technical specification or standard;
  - MSc or Phd dissertation.
- macro-topic:
  - mechanical behaviour of composite dowel;
  - numerical simulation techniques and methods;
  - realized constructions;
  - fabrication aspects;
  - constructive, executive and economical aspects;
  - technical specifications and standards.

2.3 Economical and executive aspects about composite dowels

Exploiting the technology of composite dowels can lead to savings in the amount of steel used. In composite beams with a double-T steel profile, the upper flange is occupied in bending and used to weld head-studs mechanical devices on top, which act as shear connection. In a solution with composite dowels, an optimised configuration is obtained in which the lower steel flange and the upper concrete slab are occupied in bending and the steel web is occupied in shear. The shear connection transmits a shear flow. A significant amount of steel can be saved. The costs of the final element are governed mainly by the amount of steel, therefore leading to cost savings. A further saving in the preparation of the steel-concrete composite member can result from the absence of welding of the head studs. The only process required is cutting the steel web to the desired shape. The cutting is done in the workshop. It should be noted that from a standard double-T beam, two complementary T-beams are obtained, both of which can be used to make a steel-concrete composite member with a composite dowels shear connection. There is therefore minimal waste of steel. Steel-concrete composite members can be prefabricated or cast on site. The result

in both cases is speed and ease in erecting and assembling the structure. In both cases, the installation involves the lifting of lightweight and more manageable solutions when compared to prestressed reinforced concrete ones.

The cutting of the double-T girder in order to obtain two T-profiles with the shape in the longitudinal direction of the steel dowels creates a redistribution of the residual stresses already present in the profile in the form of an internal state of stress. This results in non-rectilinear profiles with a curvature similar to the product of cambering [55]. A better technology than gas cutting is plasma cutting, which provides smoother surfaces although the costs are higher [55].

2.4 Examples of composite dowels applications

Some application examples are listed here and briefly described. References are given. The majority of the realised cases consist in bridge composite beams crossing streets, rails or rivers. Just one case [94] was found to be exploited for buildings applications. This is testifying that the potential for building applications has still to be tested and studied. As described in the following cases, multiple typologies of sections have been developed and successfully exploited in the past years. Most of these have been designed in the Precobeam [89] project frame. These consists in prefabricated solutions with a cast in situ concrete slab. Some of these technologies such as the VFT, VFT-WIB and the VFT-Rail are patented by the SSF Ingenieure AG engineering company.

The **Pocking bridge** [84, 88] (Fig.2.6), located in Germany in the great Munich area, is one of the first applications of the composite dowels technology. The prefabricated elements are more appropriately identified as PreCoBeam technology, which stands for Prefabricated Composite Beams enduring elements. It consists of a road bridge crossing over the railway. This technology was chosen because of its ease of erection and short interruption of the railway line. The total bridge length consists in two spans of 8.35 meters. It was built in 2003. Profiles were obtained from HEM 1000 standard profiles with structural S460 strength class steel.

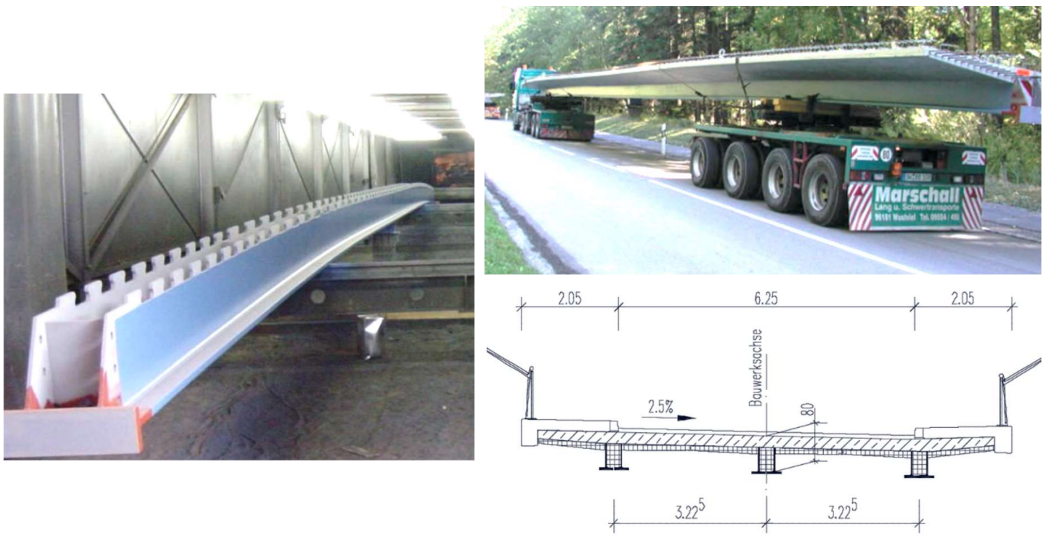

Figure 2.6: Pöcking (DE) bridge example. Images from [84, 88]

Between 2009 and 2012 in Poland an example of duo type bridge has been built [88]. The bridge is located between **Olsztynek and Nidzica** and crosses the S7 speedway. The slenderness (length over height ratio) of the final solution is 22. Here S355M steel with HEA, HEB, HEM 1000 standard hot rolled sections have been exploited.

The **Simmerbach** railway bridge [49, 87] consists in two simply supported spans each of length 12.75 m. The solution consists of a composite solution with integrated rails. The shape of connector used is the MCL. The solution was chosen in order to minimise the interruption time of the railway line and to optimise the slenderness of the structure at the same time.

The **Wiesbaden (DE) Coulinstrasse "Parkhaus"** [94] (Fig.2.7) is an interesting example of composite dowels solution for application in building construction. The building is an off-ground parking of eight stories. Here traditional and innovative composite dowels solutions were both exploited. The solution is coupled with a Cofraplus®220 decking sheeting technology. Wings are welded aside the steel profiles web and act as supports for the Cofraplus® sheeting. Here 18.55 meters spanlength were used. The main beams interaxis is 5 meters. The total sectional height is 0.55 m. Profiles ranging from HEAA700 to HEB900 profiles are exploited. The shear connection consists in PZ shaped dowels. This example will be the reference and inspiration for the downstand beam for carpark structure case study that will be considered in the present work in annex B.

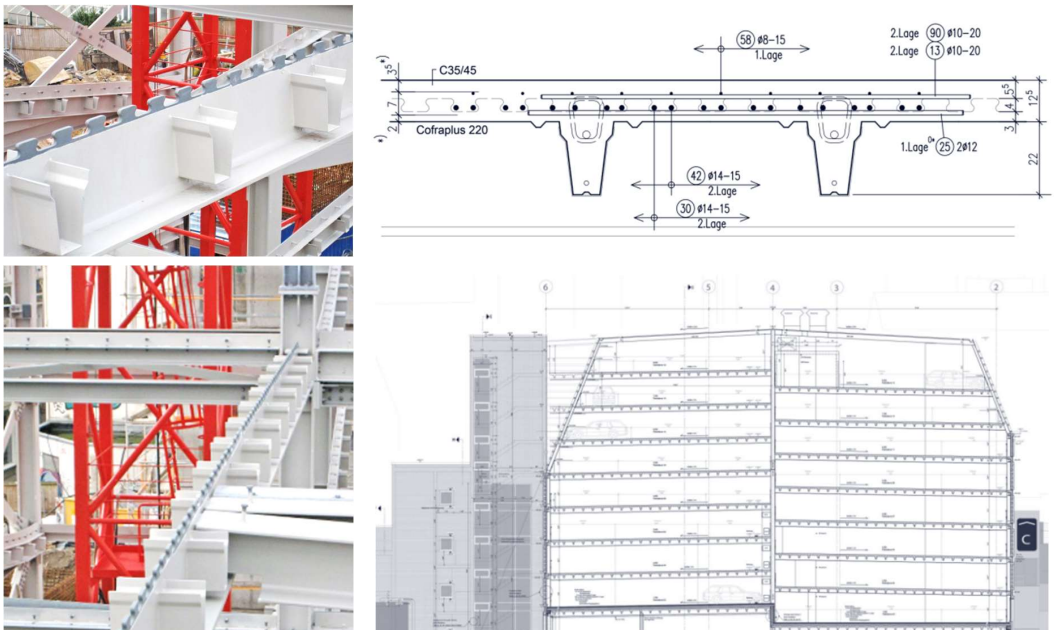

Figure 2.7: the Wiesbaden Parkhaus example of composite dowels use. Images from [94]

The **Kaprun** (Austria) example [43, 86, 85] crosses the Salzach river.

The **Martwa Wisla River** [85] (Fig.2.8) near Danzig is an example of drawbridge project crossing a river. Here variable section composite elements are used exploiting MCL shaped dowels. Elements are 25.00 meters long. In this example composite dowels elements are used not only for beams but also for the embedded ancorage steel elements contained in the drawbridge piles. This is an interesting example of how the composite dowels technology can be exploited also in other situations different than for beams.

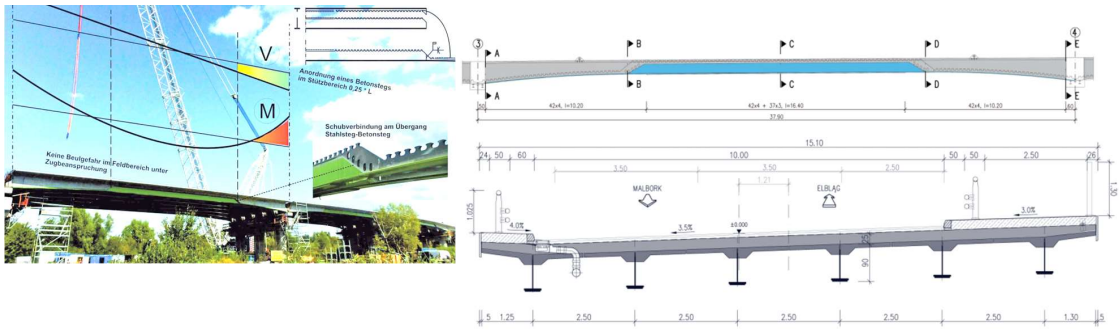

Figure 2.8: Martwa river bridge. Images from [85]

The **Elblag** (Poland) bridge [73] was designed in order to replace the old bridge structure crossing the railway and the river. The solution was chosen because of the short erection terms. Here an alternative

solution to the final technology chosen by the administration was proposed. Various design options were considered in order to create the composite girder element. The spanlength of the element is about 38.00 meters. HL1000x539 and HL1000x748 with steel strength S460ML are exploited.

The **Romanian bridge crossing the A1 motorway** [81] is an example of PreCoBeam solution application. The project was developed in the frame of the Ecobridge [48] project. The prefabricated elements are used for an overpass construction. The beam is joined with the bridge piles forming a frame static scheme. Here MCL shaped dowels are used. The span is 39.00 meters long. The slenderness, in terms of element's height over spanlength ratio, of the horizontal element is of about 1/29.

Further structures can be found in [88] and include the crossing bridge over the S5 street between **Chorzow Batory-Tczew** is an example of innovative prefabricated section. The project was realized in 2009. Another example is the **Lososina river bridge**. The **Kuhl** example (Austria) is another case exploited for railway crossing bridges. The **"Wilde Saale" in Halle** is also exploiting the technology. The **Ursulau in Saalfelden bridge** is crossing a river and is 18.15 m long.

Other cases can be found in [91] (**Greiselbach bridge**), [93] in Czech Republic, [72] for the **Wierna Rzeka bridge**. More information about completed works and future applications can be discovered in [23, 61, 29, 62, 21].

2.5 Composite beams

Composite beams have a composite section made up of a steel part and a concrete part. The bending resistance of the composite section can be assessed by means of Rigid Plastic analysis (RP) or Strain Limited analysis (SL) approaches. The bending resistance of the composite beam is $M_{pl,Rd}$ and is dependent on the resistance of the shear connection.

EC4 [11] allows the bending resistance to be assessed by RP method with equilibrium at cross-sectional level.

2.5.1 Degree of shear connection

The degree of shear connection is computed as:

$$\eta = \frac{n \cdot P_{Rd}}{N_{cf}} \qquad \text{Degree of shear connection} \tag{2.1}$$

If $\eta \geq 1$ the element is in Full Shear Connection (FSC). An addition of shear connectors does not improve the bending capacity of the element. If $\eta < 1$ the element is in Partial Shear Connection (PSC). The resistance of the shear connection affects in this case the bending resistance of the element.

In case of $\eta = 1.0$ the plastic resistant design bending moment $M_{pl,Rd}$ of the element is equal to the one of Full Shear Connection (FSC) $M_{pl,f,Rd}$. Namely:

$$M_{pl,Rd}(\eta \geq 1) = M_{pl,f,Rd} \tag{2.2}$$

In case of $\eta = 0.0$ the plastic resistant design bending moment $M_{pl,Rd}$ of the element is equal to the one of the steel part of the composite section $M_{pl,a,Rd}$. Namely:

$$M_{pl,Rd}(\eta = 0) = M_{pl,a,Rd} \tag{2.3}$$

In the intermediate cases the function $M_{pl,Rd}(\eta)$ can be defined and if plotted in the $M - \eta$ plane this defines the Partial Shear Diagram (PSD) (Fig.2.9).
For small degrees of shear connection η the bending resistance obtained with a Rigid Plastic analysis (RP) approach can lead to unsafe results due to the fact that the slip at the interface exceeds the plastic slip capacity of the shear connection devices. Assuming unlimited plastic slip capacity of the shear connection is in this case unsafe.

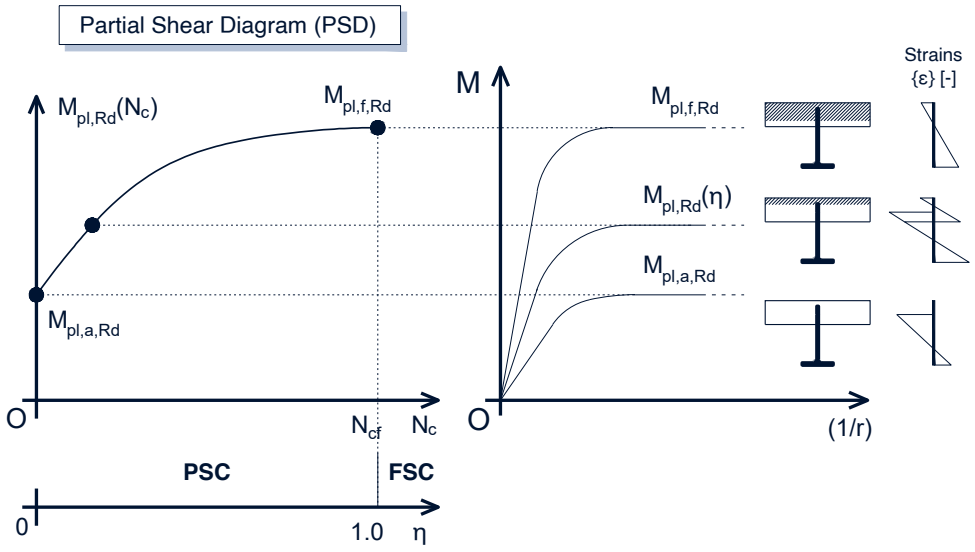

Figure 2.9: Partial Shear Diagram (PSD) construction

2.5.2 Minimum degree of shear connection

If the maximum slip demand on the composite beam matches the plastic slip capacity of the connector, a concept of minimum degree of shear connection (η_{min}) can be defined. In order to assess the value of η_{min} step-by-step variation of the degree of connection η in numerical simulations is generally used as approach [36]. An important result that has to be pointed out is that η_{min} is dependent on the span of the element. It is well known from literature, as stated in [36], that an increase of span length for a simply supported element, leads to an increment in slip demand. Consequently the parameter η_{min} gets affected and increases. The present relations contained in EC4 [11] are derived from experimental results.
Further elements on the studies from which the EC4 [11] relations were derived can be found in [36].

$$\eta_{min} = \begin{cases} 1 - (355/f_y) \cdot (0.75 - 0.03 \cdot L_e) \geq 0.4, & \text{if } L_e \leq 25m \\ 1, \text{ if } L_e > 25m \end{cases} \tag{2.4}$$

$$\eta_{min} = \begin{cases} 1 - (355/f_y) \cdot (0.3 - 0.015 \cdot L_e) \geq 0.4, & \text{if } L_e \leq 20m \\ 1 \text{ if } L_e > 20m \end{cases} \tag{2.5}$$

Those relations are only valid for headed studs with sufficient deformation capacity ($\delta_u > 6mm$) ("ductile connectors"), equally spaced used for sagging moment regions under uniformly distributed loads in building construction. Elements should have sufficient rotational capacity. Therefore Class 3 and Class 4 sections according to [9] and prestressed elements are excluded from the application range. Furthermore EC4 [11] refers to composite sections with double-T steel elements having a bottom flange area of at least three times the top one. Another limitation is the one governing the plastic resistance moment of the composite section over the one of the steel profile section ratio that has to respect $M_{pl,a,R}/M_{pl,f,Rd} > 0.4$.

As specified in [36], the definition of η_{min} has to be associated with $\delta_u = 6mm$. The 6mm threshold value has been selected as an arbitrary quantity for the standards, but it has to be remembered that further relations in order to compute η_{min} are also calibrated with this arbitrary definition of ductile connector. Shear connector devices allow for perfectly plastic redistribution when the ductility criteria is met associated with a degree of shear connection greater with respect to η_{min}. The value 6 mm comes from [60].

Despite of the fact that beams single-T sections have already been designed following EC4 rules in engineering practice, researches such [32] pointed out that rib shear connections have higher stiffness compared with headed studs and in case of pry-out failure the deformation capacity can be smaller than 6mm. A direct application of EC4 rules to continuous shear connectors is therefore not recommended as demonstrated in [36].

Limitations to the use of partial shear connections in composite beams with continuous shear connections were studied in [36]. In this research work different deformation capacities on three different cross sections have been analyzed. Furthermore the variation of the $M_{pl,a,R}/M_{pl,f,R}$ ratio is considered. The loading configuration affects the plastic demand along the element. Developing a design approach considering a uniformly distributed load is on the safe side.

The plastic slip capacity of connectors has a significant influence on the value η_{min}. The minimum degree of shear connection in order to have a fully plastic behaviour η_{min} of the connector increases significantly with decreasing plastic slip capacity.

Given the above stated observations, an analytical approach is proposed in [36]. The final model can be summarized in the following design equation:

$$0.7 \leq \eta_{min} = (0.3/\delta_u)^{1.25} \cdot L_e + 0.62 \leq 1.0 \tag{2.6}$$

Moreover the following ratio has to be guaranteed:

$$M_{pl,a,R}/M_{pl,f,Rd} \geq 0.15 \tag{2.7}$$

2.6 Mechanical behaviour of composite dowels

In this section, the content of the publications found regarding the mechanical behaviour of composite dowels is examined. It can be seen that the research is directed towards deriving calculation methods that allow a complete and consistent design approach.
A direct comparison between the performance of a standard section with a composite dowels section can be found in [36].

2.6.1 Classification of the literature on mechanical behaviour

It is possible to classify the topics dealing with in the literature on mechanical behaviour according to the following criteria:

- imposed solicitation:
  - longitudinal shear;
  - pure tensile load;
  - shear-tension interaction.
- loading stage considered:
  - Serviceability Limit State (SLS);
  - Ultimate Limit State (ULS).
- load variability with time:
  - static loading;
  - dynamic and cyclic loading.
- dowel shape;
- cracked stage of the element;
- boundary solicitation on the concrete part.
- investigation mode:
  - loading tests on specimens;
  - numerical simulation;
  - development of analytical and empirical models.

No studies were found on the robustness of the elements. In some cases, the research addresses more specific topics such as the behaviour of connectors in the presence of High Performance Concrete (HPC) and Ultra High Performance Concrete (UHPC).
The publications found are mostly journal articles and parts of scientific journals. There are also five relevant PhD theses by the authors Classen [40], Broschart [27], Lechner [68], Seidl [90], Heinemeyer [58]. In the past research important effort and contribute was given by the "FOSTA P804" project [45]. This research was conducted in order to develop consistent design approaches and led to the approval of the first technical regulations in Germany [4]. Another important work is and P1208 project [46]. Some

engineering companies were found to be active in research on composite dowels, such as SSF Ingenieure AG [16].

2.6.2 Definitions

The geometric quantities of Fig.2.10 are here defined.

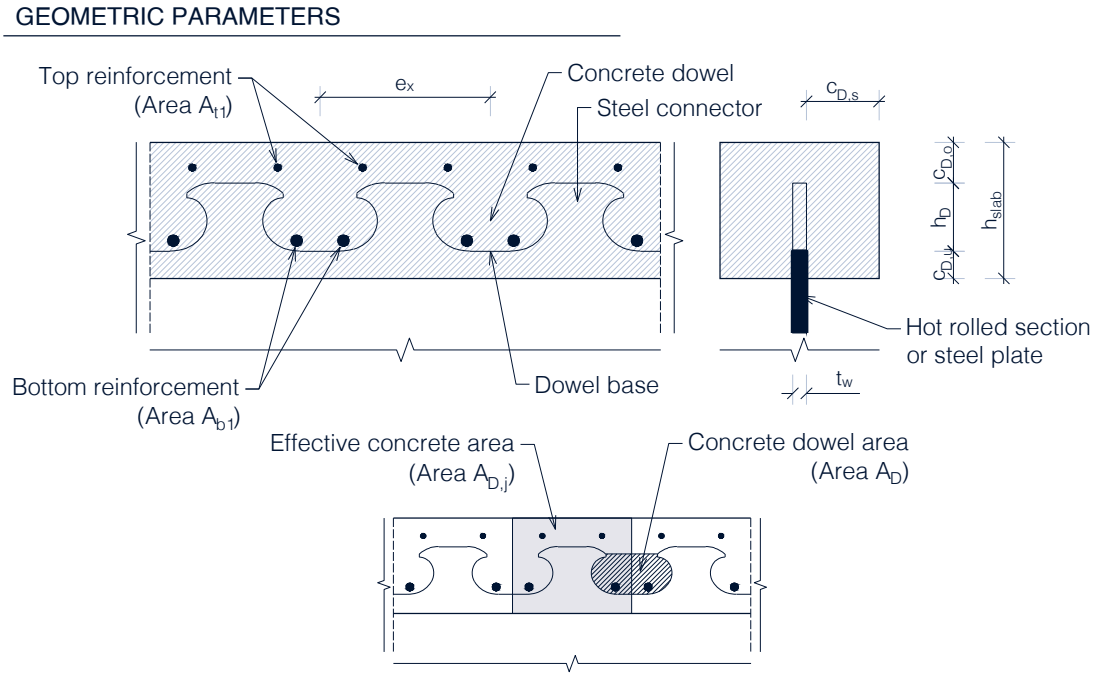

Figure 2.10: relevant geometric quantities definition

Moreover further definitions are here introduced:

- P: bearing force on the connector;
- δ: relative slip of the shear connection;
- δ_u: plastic slip capacity of the shear connection (define din accordance with EC4 [11]);
- P_{Rk}: characteristic value of the shear resistance of the shear connector;
- P_y: yealding shear force of the connector;
- δ_u: ultimate slip;
- e_x: dowel size;
- $c_{D,s}$: side concrete cover;
- $c_{D,o}$: upper concrete cover (index ’o’ derives from german "oben");
- $c_{D,u}$: lower concrete cover (index ’u’ derives from german "unten");
- $A_{b,1}$: bottom reinforcement area in the single concrete dowel;
- $A_{t,1}$: top reinforcement area in the dowel;
- A_D: concrete dowel area;

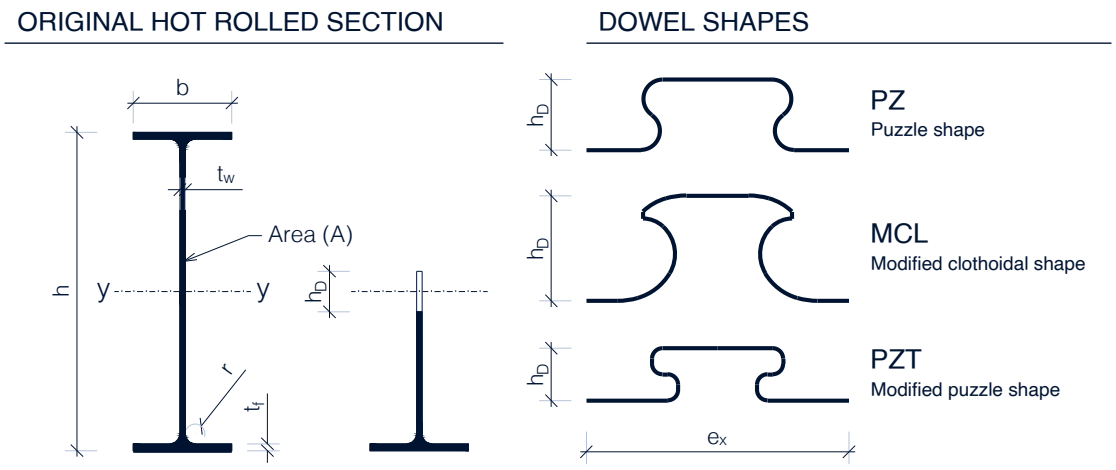

Figure 2.11: standard hot rolled section, single T cutted profile and steel dowel relevant dimensions and shapes

- $A_{D,j}$: effective concrete area;
- h_{slab}: concrete slab height;

The coordinate s is here introduced, arclength coordinate running along the edge of the connector with origin at the connector root (Fig. 2.12)

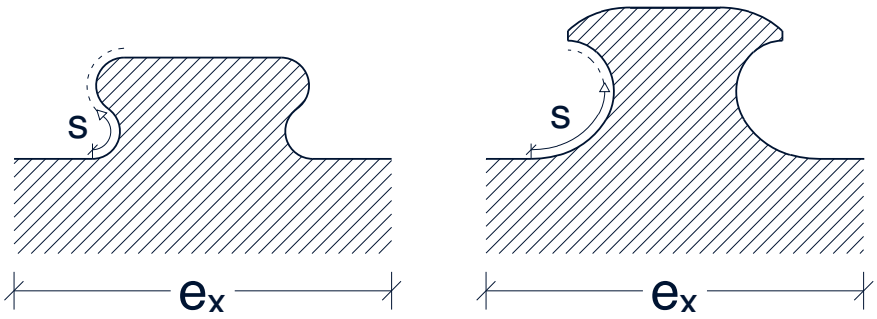

Figure 2.12: reference arc-length coordinate for the steel dowel

2.6.3 Influence of the composite dowel shape

The dowel shapes found in the literature are summarised in the Fig.2.13.

The first shape used for bridge construction was the Puzzle Shape (PZ) [84]. The Modified Clothoidal Shape (MCL) shape, was originally studied with the 2008 development of the railway bridge over the Łososina in Poland. [88]. Due to the important role of the dowel shape in both mechanical and manufacturing aspects, studies on the problem can be found in the literature. Researches on the behaviour of the 'PZ' shape of the connector have been done in [74] and later described by the author in more detail in [75]. In [95] several shapes of type 'PZ' are studied.

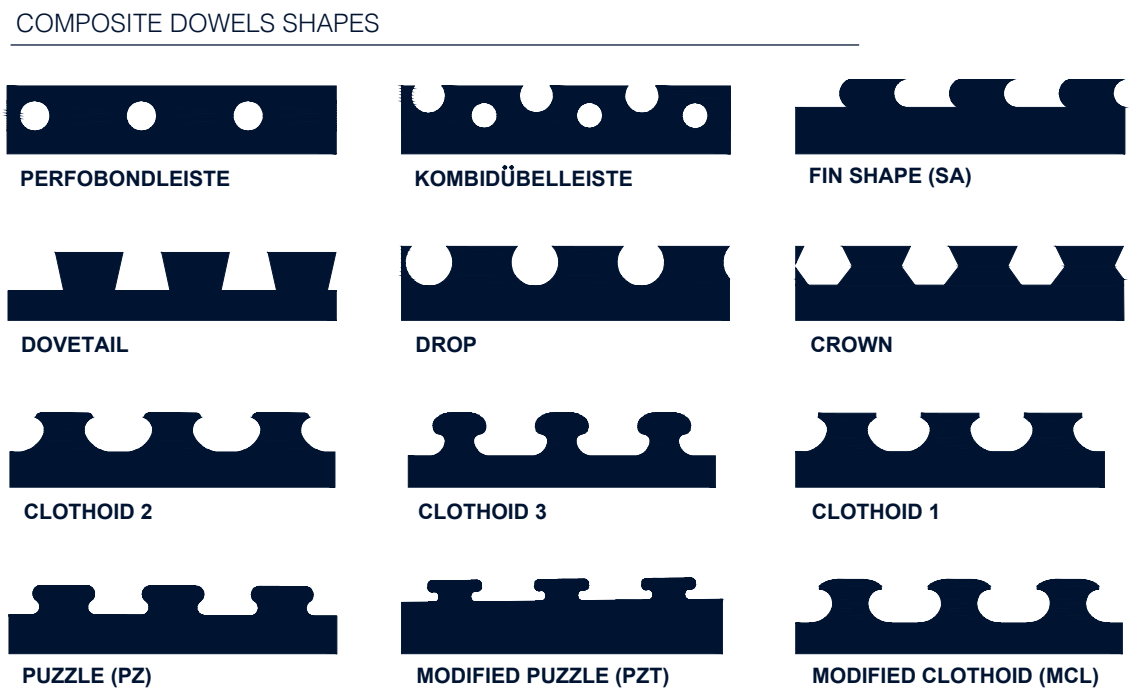

Figure 2.13: composite dowels possible shapes

Already within the framework of the PreCoBeam research project, numerous experiments and numerical tests were carried out on the load-bearing capacity of connectors in relation to various dowel shapes. Although the SA, shows a higher strength under static load, the Puzzle Shape (PZ) and Modified Clothoidal Shape (MCL) shapes show better fatigue behaviour. The better fatigue behaviour of the 'MCL' shape compared to the 'PZ' shape is shown in [55]. Precisely because of the stress concentration created by the SA shape at the base of the connector due to the strong discontinuity present and the consequent problems induced above all as regards fatigue, a substantial abandonment of the adoption of this shape is observed. Recently a Modified Puzzle Shape (PZT) has been developed.

In order to simplify the cutting process recently a Modified PZT shape has been introduced. This is referred in this work as Modified PZT Shape (MPZT) shape.

For the present study purposes three shapes are relevant. These are PZ, PZT and MCL. However, this sha;pe is not studied in deep in the present work.

The geometric description of the steel dowels shapes for 'PZ', 'PZT' and 'MCL' is illustrated in figure 2.14. Note that here a one-to-one relationship between the nomenclature and the geometry is introduced.

From the point of view of the mechanical behaviour of the steel dowel, the shape is crucial. At the base of the steel dowel, the discontinuity created by thermal cutting interruption produces a more sensitive region to the problem of high-cycle fatigue and stress concentration in the elastic field on the steel dowel, called the "hotspot" zone. The introduction of a clothoid arc makes it possible to pass gradually from an infinite to a finite radius of curvature. In reality these are formed as illustrated above (Fig. 2.14) by a succession of circumferential arcs, thus having a constant radius of curvature at intervals. The use of the chlotoid shape,

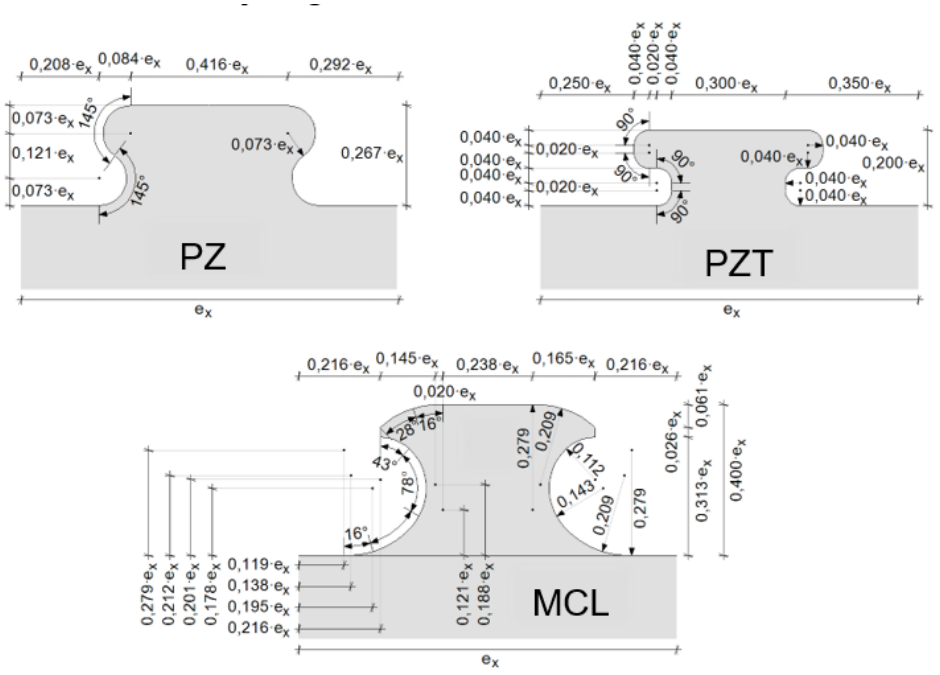

Figure 2.14: PZ and MCL shapes descriptions

however, allows for more than doubling the radius of curvature by decreasing the concentration of stress in the hotspot [21].

Prior to the PreCoBeam project, studies on the mechanical behaviour of the steel dowel had already been carried out in [69] with the proposal of a method for the optimisation of the shape.

The distribution of pressures along the side of the steel dowel has been studied in research works. In order to describe the relations between the pressures distribution and the size a size factor is introduced by Lorenc [69].

2.6.4 Elastic state and Serviceability Limit State (SLS)

The elastic behaviour of the steel dowel occurs for loads lower than the first yield stress P_y which is lower than the connector capacity P_{Rk}. In contrast to the initial development phases of the composite dowels technology where the classical approach based on standard push-out tests was used for the design of the steel dowel, as stated by [69], the research showed that the geometry of the steel dowel should be designed according to elastic stress-based criteria. Given the complexity of the geometry and the coexistence of multiple materials, there is a heavy reliance on Finite Element Method (FEM) supported and calibrated on the basis of strain gauges and trying to synthesise analytical engineering models.

The steel dowel has a stress state composed by a local contribution (L) given by the shear acting on the steel dowel and a global one (G) given by the global bending action of the element working as a beam. An additional uplift force is mentioned in some works [57]. When partitioning a composite section, the dowel shape must be such as to avoid potential propagation of the crack to the stressed steel dowel. [69].

The model proposed in [69] is derived from considerations made within the framework of numerical analy-

ses carried out on beam models by varying the position of the composite dowel with respect to the neutral axis. A further model can be traced in [56]. The model proposed in [59] for the PZ shape was taken as a starting point. Further reference is the work [65].
The model derived in [69] presents the following formulation in order to compute the stress in correspondence of the hotspot area.

$$\sigma = \sigma_L + \sigma_G = k_{f,L} \cdot v_L / t_w + k_{f,G} \cdot (\sigma_M + \sigma_N) = k_{f,L} \cdot \frac{V \cdot S_y}{I_y \cdot t_w} + k_{f,G} \cdot \left(\frac{M}{I_y} \cdot z_D + \frac{N}{A} \right) \tag{2.8}$$

Here $k_{f,G}$ is the concentration factor due to global effects, $k_{f,L}$ is the concentration factor due to local effects, V, M, N are respectively the shear, moment and axial actions. I_y, S_y, A, z_D are respectively the second moment of section, the static moment of the part of the section above the shear connection, the area and the internal lever arm. This formulation is based on:

- the summation of local (σ_L) and global (σ_G) stress states effects;
- the approximation of the actual stress distributions with second order polynomia;
- the derivation of the arclength coordinate of the hotspot area, i.e. the point where the maximum stress finds;
- the derivation of an elliptical elastic domain in the shear flow-normal stress plane by imposing the equality with f_y of the maximum stress;

The values of the stress concentration factors $k_{f,G}$ and $k_{f,L}$ are calculated through FEA modelling. The obtaining of the values is proposed in [89] for the dowel shape PZ and in [69, 45].

2.6.5 Ultimate Limit State (ULS)

The experimental tests campaigns have shown different failure modes [62, 89]. In accordance with the studies carried out, calculation formulas for the failure modes were developed. This was done from existing, modified or newly developed models through a statistical analysis of the test results. By means of result databases, test results were compared with expected test outcomes according to theoretical concepts. The derivation of the formulae was done in accordance with Annex D of EC0 [6]. These are taken also by the German technical specifications Z-26.4-56 [4]. The identified failure modes are:

- steel dowel yielding;
- concrete shearing;
- concrete pryout;
- concrete web splitting.

An illustration of the different failure modes is given in Fig.2.15. For the case of horizontal arrangement close to the edge of the composite dowels in the concrete slab, a further failure mode called 'edge pry-out failure' can be observed. This failure mode was widely studied in [25, 26].

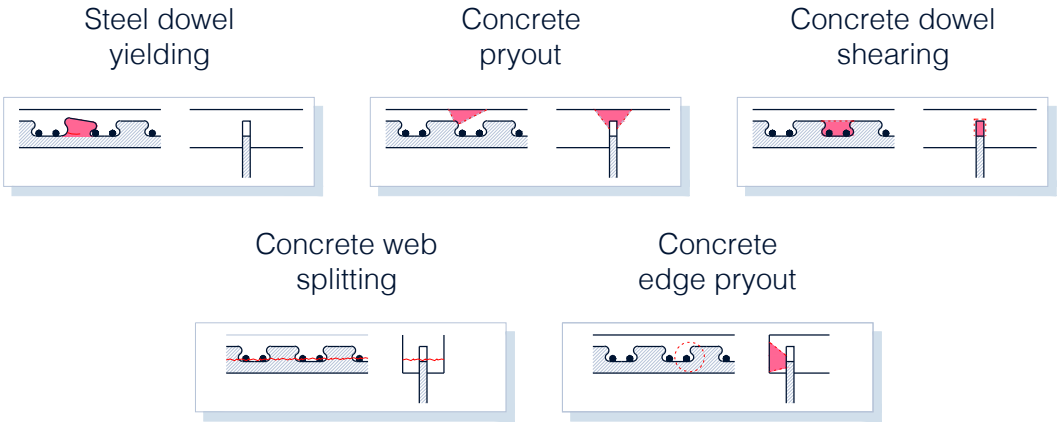

Figure 2.15: schematic representations of the possible failure modes

The steel dowel failure depends mainly on the geometry of the connector. The failure on the concrete side, on the other hand, is similar when comparing those observed for the MCL form and those for the PZ form [64].

Steel dowel yielding failure

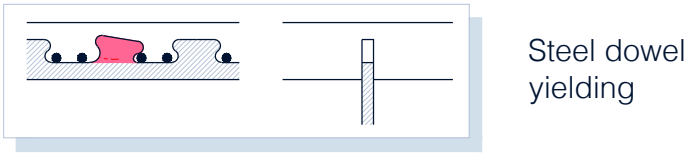

Figure 2.16: schematic representation of steel yielding failure mode

The failure of the steel dowel can occur in the case of low steel web thickness or low strength values of the T-profile steel. A bending stress state combined with shear induces horizontal fractures on the steel plate. This failure mode is ductile and accompanied by high plastic deformations [47, 63]. Mechanical tests on samples using Push Out Standard Test (POST) show that the fracture is initiated at various heights of the steel dowel between dowels of the same specimen [74] (Fig. 2.17). This is due to the variable entity of the global stress contribute in the longitudinal direction of the specimen. Tests show that the smaller the overall compression effects are compared to the local effects on the steel connector, the closer the fracture is located to the base of the connector [64]. Here the following definitions apply:

- e_x is the dowel size according to Fig.2.10;
- f_y is the yealding resistance of the steel single T profile;
- t_w is the web thickness of the single T steel profile.

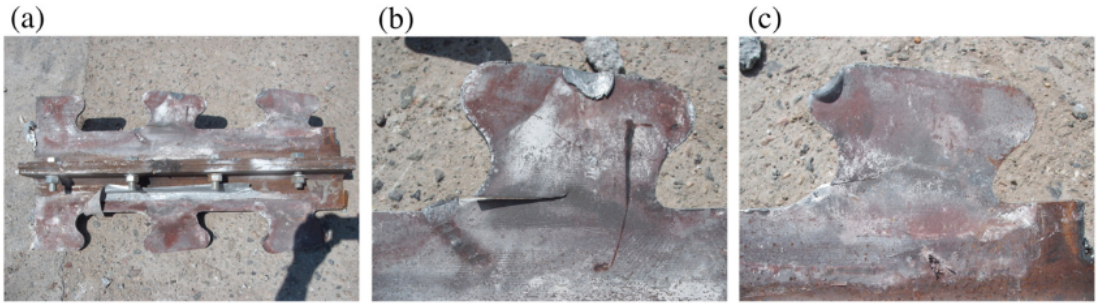

Figure 2.17: steel dowel yielding failure observed in test specimen. Image from [74]

The strength of the steel connector can be calculated according to the following formula:

$$P_{pl,k} = \lambda_{geo} \cdot f_y \cdot t_w \cdot e_x \tag{2.9}$$

The accepted values for the three relevant shapes are:

Shape	λ_{geo}
MCL	0.259
PZ	0.286
PZT	0.186

The formulation was initially introduced in the PreCoBeam project frame [89]. This was derived starting from the subsequent observations:

- the nature of the steel dowel failure mode is ductile [75]. This supports the approach based on yield stress f_y for calculating the strength of the steel connector rather than on the ultimate failure resistance f_u, in contrast to the formulations present for head studs where the ultimate resistance is used f_u. The model of large plastic shear deformations ensured by the redistribution of stresses was therefore implicitly assumed. Plastic deformations are still small enough to be outside the plastic hardening region of the material's constitutive law [71]. Furthermore, the author of [75] proposes, in line with what has been observed, the use of a partial safety coefficient of γ_{M0} rather than $\gamma_v = 1.25$.
- The resistance per unit length of a shear connection does not depend on the size e_x of the connector and ductility is a linear function of the connector size e_x. The assumption is discussed in [71, 74, 75] and finds experimental confirmation.
- The unit-length capacity of the steel connector is a linear function of the web thickness t_w [74].
- The amount of reinforcement has practically no influence on the strength of the steel connector [74]. The post-critical behaviour does not depend in the final stage on the thickness t_w and depends on the transverse reinforcement.

The formulation was initially proposed by Wurzer [96]. The coefficient λ_{geo} can be equivalently identified in some literature cases [64] as A_{ULT} or as β_{ULS}, and is known as "shape factor" of the steel dowel.
In this approach the shape factor λ_{geo} plays a key role and is related to the geometry of the dowel. The derivation in the literature according to different approaches:

1. simplified engineering analytical model derivation;
2. numerical method derivation;
3. derivation from mechanical tests.

These three different derivation methods will be briefly reviewed below.

Engineering simplified analytical model

The analytical and semi-empirical relationships in the literature are derived from the same model in which a linear dependence is presented with t_w, the critical section width b_{crit} and the steel strength f_y. Various derivations in the literature may however differ in the identification of the critical section and the resulting critical width b_{crit} [63]. The derivation of the resistance formula is retraced in [63]. According to [64] however [63] does not make explicit the mechanical model from which it derives these values. The starting hypothesis is that of constant transferred stress along the effective height h_{eff} of the steel dowel. A stress state induced by an horizontal shear force P_2 in conjuction with a moment $P_2 \cdot z_{p2}$ is considered. The critical section is identified by solving the minimum problem, considering the trade-off between the decrease in P_2 and the larger lever arm z_{p2} varying the considered horizontal section. Note that the variability of the cross-section of the steel connector on which the stress state is calculated must also be taken into account [47]. Following, the Von Mieses failure criteria is imposed.
The following is derived:

$$P_{pl} = \frac{h_{eff}}{h_{eff} - h_{krit}} \cdot \frac{b_{krit}^2}{\sqrt{16 \cdot b_{s,krit}^2 + 3 \cdot b_{krit}^2}} \cdot t_w \cdot f_y \tag{2.10}$$

In this relation the following holds:
$h_{krit}(\alpha), h_{s,krit}(\alpha), b_{krit}(\alpha)$ and $\alpha = f(\partial P / \partial \alpha \rightarrow min)$.
When using the specific geometric parameters relating to the clothoid or puzzle shape [54] the derived formulation gets [63]:

$$P_{pl,MCL} = 0.243 \cdot e_x \cdot t_w \cdot f_{yk} \tag{2.11}$$

$$P_{pl,PZ} = 0.269 \cdot e_x \cdot t_w \cdot f_{yk} \tag{2.12}$$

The author of [64] strongly criticises the oversimplification of the previously described model for the plastic failure of the steel-side connector and recommends its abandonment. In particular:

- shows that neglecting the forces applied to the top of the steel connector is a mistake, also demonstrated in [75] for 'PZ' type connectors;
- it is claimed that taking into account a constant distribution of the pressures applied to the connector is over-simplifying. The claim is supported by showing the distribution of pressures and shear applied on the connector along the arc-length coordinate;

- argues that although the value $\lambda_{geo} = 0.250$ for MCL and PZ is in some research cases derived from the criticised model, statistical analysis on experimental tests and rigorous FEA analyses confirm its reliability.

Other different models are observed in the literature, the first proposed for the 'PZ' shape in [1, 59], the second proposed for the 'MCL' shape in [76].

Numerical derivation

From [64] by exploiting numerical analysis values of 0.254 and 0.349 for MCL shapes can be derived. In [76] the value of λ_{geo} is 0.254 if an elastic-perfectly plastic material model is exploited and is 0.344 if an elastic with plastic hardening branch material law is used. These values well represent the tests results from research [76].

The vectors of the resultant forces (including direction and line of application) on the two faces of the 'MCL' connector are derived in [76] from the contact pressure distributions for both SLS and ULS.

Tests derivation

In [64] the value is calculated from experimental tests results and is 0.358. In the research [64] the model with constant horizontal load along the connector height is used as an analytical comparison.

Observation

Following [76], the shear flow in a steel plate without openings is:

$$v_L = \frac{1}{\sqrt{3}} t_w \cdot f_y = 0.577 \cdot t_w \cdot f_y \tag{2.13}$$

With openings of ratio 0.5:

$$v_L = \frac{1}{2} \cdot \frac{1}{\sqrt{3}} t_w \cdot f_y = 0.289 \cdot t_w \cdot f_y \tag{2.14}$$

This is a close value to the ones derived with tests, numerical analysis and analytical approaches.

A comparison of contact pressures at SLS and ULS between steel and concrete for an 'MCL' shaped connector can be found in [76]. However, the distributions do not take into account the concrete material nonlinearity.

Concrete shearing failure

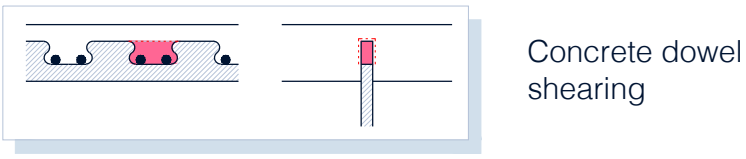

Figure 2.18: schematic representation of concrete dowel shearing failure mode

In case of a thick steel profile web t_w or small spacing between steel connectors e_x, failure exhibits by concrete shearing of dowel with a double shear plane. The shear failure resistance of the concrete dowel

is evaluated according to the formula:

$$P_{sh,k} = \eta_D \cdot e_x^2 \cdot \sqrt{f_{ck}} \cdot (1 + \rho_D) \tag{2.15}$$

here the following definitions apply:

- e_x is the size of the dowel;
- f_{ck} is the cylindrical concrete characteristic strength in compression;
- $\rho_D = E_s \cdot A_b/(E_{cm} \cdot A_D)$;
- E_s is the steel elastic modulus;
- E_{cm} is the concrete average elastic modulus;
- A_b is the area of the transverse reinforcement passing through the concrete dowel;
- A_D is the shear stress area of the concrete connector and can be computed as:
  $A_{D,MCL} = 0.2 \cdot e_x$
  $A_{D,PZ} = 0.13 \cdot e_x$;
- $\eta_{D,MCL} = 2 - e_x/400$
  $\eta_{D,PZ} = 3 - e_x/180$

The derivation of a calculation formula is based on considerations and research carried out for failures in Perfobond systems (PBL). The following phenomena are observed:

- In the case of large openings, it is possible that consecutive shear planes are joined. The effect is taken into account by the size-dependent parameter η_D;
- The transverse reinforcement in the connector has a significant effect on the load-bearing resistance and provides an additional reserve of load-bearing capacity [47, 63]. This effect is accounted by the parameter ρ_D;
- it emerges that the concrete shearing failure model is transferable and adaptable to any shape of steel connector [63];
- the capacity against shear failure of the concrete connector is proportional to the tensile strength of the concrete f_{ct}. This is known in the literature to be linked with the related compression resistance with the relation $f_{ct} \propto \sqrt{f_c}$.

The application range and the geometrical limitations provided by [4], allow to consider the shear failure of the concrete connector as a ductile failure [47]. Further considerations on the derivation of the calculation formulation can be found in [63]. The author justifies the choice of formulation by further proposals in the literature and by analysing their adherence to the results of experimental tests collected in a database. Further references include [18, 90].

Concrete pryout failure

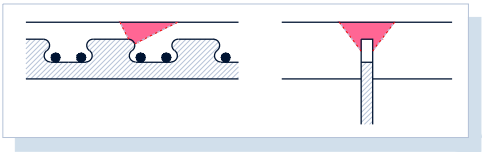

Figure 2.19: schematic representation of the concrete pryout failure mode

For limited distances between the concrete external surfaces and the steel connector, pryout failure occurs. This can occur either at the lower or upper concrete interface. The hydrostatic pressures in the area of load introduction create transverse tensile stresses which lead to a cone shaped failure. The formation of a pryout cone shows. Pryout failure generates a loss of hydrostatic pressure which triggers a secondary failure [47, 63]. The failure mode is considered to be ductile. The resistance for this failure mode can be evaluated as follows:

$$P_{po,k} = k_1 \cdot \chi_x \cdot \chi_y \cdot h_{po}^{1.5} \sqrt{f_{ck}} \cdot \psi_{crack} \tag{2.16}$$

Here h_{po} is the concrete pryout cone height and can be computed accrding to:

$$h_{po}(PZ) = \min\left(c_{D,o+0.07\cdot e_x}, c_{D,u+0.08\cdot e_x}\right) \tag{2.17}$$

$$h_{po}(PZT) = \min\left(c_{D,o+0.05\cdot e_x}, c_{D,u+0.06\cdot e_x}\right) \tag{2.18}$$

$$h_{po}(MCL) = \min\left(c_{D,o+0.07\cdot e_x}, c_{D,u+0.13\cdot e_x}\right) \tag{2.19}$$

The coefficient k_1 is dependent on the shape, and is:

$$k_1(PZ) = 71 \qquad k_1(PZT) = 71 \qquad k_1(MCL) = 95 \tag{2.20}$$

The coefficient ψ_{crack} accounts for transverse cracking of the concrete. The formulation is at present under discussion. However this coefficient is not relevant for the present study.
In the case of close dowels along the longitudinal axis, overlapping of the failure cones is observed. In this case, the Pry-Out failure capacity of the concrete is reduced by multiplying it by a reduction coefficient χ_x defined as:

$$\chi_x = \frac{e_x}{4.5 h_{po}} \tag{2.21}$$

This effect is also observed when several rows of connectors are placed side by side in the transverse direction. In the same way, the reduction coefficient χ_y defined as:

$$\chi_y = 1 \text{ for } e_y \geq 9 \cdot h_{po} \tag{2.22}$$

$$\chi_y = 1/2 \cdot \left(\frac{e_x}{9 h_o} + 1\right) \leq 1 \text{ for } 120mm < e_y < 9 \cdot h_{po} \tag{2.23}$$

The coefficients χ_x and χ_y have been derived in [90]. The structure of the formula is taken from [58] which proposes a simple formula taking into account the transverse reinforcement ratio.
Pryout failure of the concrete is negligible if the concrete is supported by the flanges of the steel profile and the section is provided with confinement stirrups [47]. Further information on the derivation of the calculation formulas can be found in [63]. In the paper, several model proposals for the calculation of Pryout strength on the basis of the height of the failure cone h_{po} are mentioned and the results of the statistical and sensitivity analysis of the chosen model including the correction factors χ_x and χ_y for overlapping failure cones are presented.
The influence of transverse cracking is taken into account by the reduction factor ψ_{crack}. The German regulations [4] do not contain any specific indications for the case of a cracked section. Studies conducted on the influence of cracking are [34, 41] in order to determine the parameter ψ_{crack}. In [33], the main observations are:

- the presence of cracking affects the bearing capacity and stiffness. The size of the failure cone is reduced by the presence of cracks. The formation of smaller ejected concrete bodies is noticeable.
- the strength decreases approximately proportionally as the crack spacing decreases.
- as the crack width increases the bearing capacity decreases. For small crack widths there is shear stress transfer between adjacent segments of the crack resulting in the formation of a consistent failure cone between the sides of the crack. For large crack amplitudes there is no shear transfer between the crack interfaces and the resulting failure cone is cut.
- the cracking has led to an increase in deformation capacity and ductility. The composite dowel can transfer stresses from cracked areas to less stressed areas of the beam.

Starting from the results obtained in the experimental programme described in [33], in the subsequent research work [39], the authors propose an engineering model to predict the behaviour of a connector inserted in a transversely cracked concrete section. In the present research work, transverse cracking does not play a key role in the configurations studied. The effect is neglected in the calculation formulae by setting $\psi_{crack} = 1.0$.

Splitting failure of concrete web

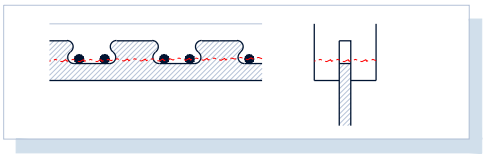

Figure 2.20: schematic representation of the concrete web splitting failure mode

Splitting fracture is prevented by design prescriptions on transverse reinforcement and minimum concrete thickness. This failure mode can in this case be neglected. A calculation formulation can however be found in [58] for the case of high performance concretes.

Edge pry-out concrete failure

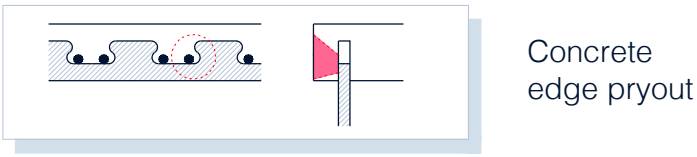

Figure 2.21: schematic representation of the concrete edge pryout failure mode

The continuous composite dowels connection can be placed horizontally in the concrete flange. In this case, the edge pry-out failure mode can be observed, which develops for low distances between the steel dowel and the concrete surfaces. This is studied in [27] and also examined in [25, 26, 24] on beam specimens and push-out tests by examining its influence for different parameters (concrete strength, thickness of the concrete section, presence of stirrups, depth of immersion of the connector in the concrete slab, strength of the steel). The addition of an helicoidal reinforcement is also studied. The development of three cracking phases leading to a pry-out failure of the concrete side is shown in [25, 26, 24]. Further research is contained in [52]. Through an extensive study carried out with load tests and numerical analysis, the work of Broschart arrives at the development of a calculation model. In [24] an analytical model is developed and described. The proposed formulation is summarised below.

$$P_{poe,k} = 2.16 \cdot \sqrt{f_{ck}} \cdot k \cdot c_{D,s} \cdot \sqrt[3]{t_w \cdot h_{d,eff}} \cdot \sqrt[3]{e_x} \tag{2.24}$$

In the present work this failure mode plays a minor role. The shear connection is considered vertically positioned in the concrete slab. This failure mode has also to be considered for vertical shear connections near slab ends.

Characteristic and design values of resistance

The characteristic shear resistance of the connector is defined as the minimum value obtained among the failure modes:

$$P_{Rk} = \min\left(P_{sh,k}; P_{po,k}, P_{pl,k}, P_{poe,k}\right) \text{ in } [kN/dowel] \tag{2.25}$$

The transition from the characteristic value to the design value of the load-bearing capacity of the connector takes place through the reduction by mean of the partial safety factor $\gamma_v = 1.25$ [47]:

$$P_{Rd} = P_{Rk}/\gamma_v \tag{2.26}$$

For design purposes a more significant value is the resistance offered by the shear connection per unit length. This is the resistant shear flow, and is computed as:

$$v_{L,Rd} = P_{Rd}/e_x \tag{2.27}$$

Comparison of the shear connection resistance with changing size and shapes of the dowels are more significant if expressed in terms of resistant shear flow.

2.6.6 Plastic slip capacity

The definition of plastic slip capacity (δ_u) according to EC4 [11] is shown in Fig.2.22.

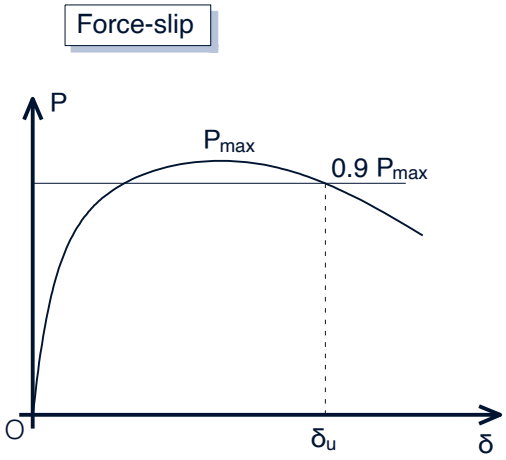

Figure 2.22: concept of plastic slip capacity according to EC4 [11]

According to [71] in the steel dowel yielding failure mode the ductility of the shear connection can be considered as a linear function of the dowel size (Fig. 2.23). The concrete shearing and pryout failure modes appear as more brittle compared with the steel dowel plastic failure.

According to results presented in [75] for 'PZ' type shape of the steel connector, 90% of the deformations at failure are due to shear. The relationship between the first yield strength and the bearing capacity P_y/P_{Rk} depends mainly on the connector shape and the height/length ratio [70].

As demonstrated in [36] models can be derived in order to design elements using plastic procedures also having $\delta_u < 6mm$, leading to a more economical and still safe design approach of single-T sections. Thus an innovative approach is proposed considering the influence of the deformation capacity of the connection rather than defining a ductility criterion such as the state of the art limit of 6mm in order to consider a fully plastic behaviour of the connection. As stated by the author in [36], further research effort has to be made in order to understand the influence of other parameters such as the steel strength.

FEA simulations show that δ_u is strongly dependent on the constitutive bond chosen for the steel.

The ductility requirement according to EC4 is $\delta_u > 6mm$.

The difference in ductility between the failure modes of steel and concrete is appreciable in the [67] study for the use of high performance concretes (HPC).

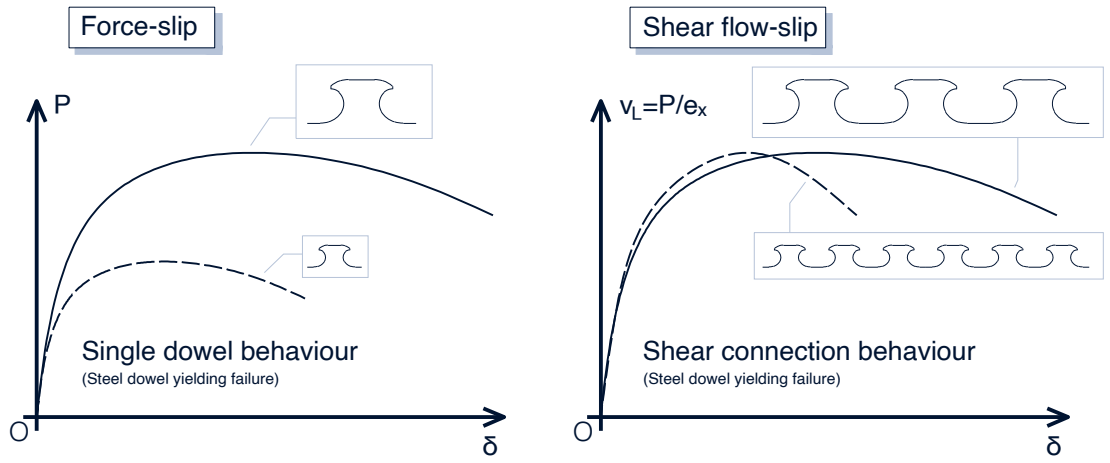

Figure 2.23: concept of load-slip curve for the single steel dowel and for the shear connection for the steel dowel yielding failure mode

2.6.7 Shear-slip behaviour modeling

The shear-slip curve for the individual connector is referred to as the 'dowel characteristic curve' and provides information on the ultimate load (P_u) and consequently on the characteristic resistance defined as $P_{Rk} = 0.9 \cdot P_u$, the deformation capacity (δ_u), which is equal to the displacement δ) of the point at which P_{Rk} is reached in the post-critical branch, and the initial stiffness, relative to the linear elastic branch of the curve (C_{el}).

The typical decomposition of the bearing capacity contributes is described in [22, 89].

The load capacity contributes for the different loading stages are:

- at beginning of the load, the load-bearing contribution is provided by static friction (A) up to the load P_{adh} after which it decreases to the constant slip friction level;
- contact forces develop between the steel and metal parts (B), the loading behaviour is comparable to that of a steel element immersed in a concrete medium. The contribution increases until failure through pulverisation of the confined concrete wedge is generated at the interface at which the stress exchange occurs;
- in this state the concrete bears a multiple of the one-axial compression strength (C);
- the load can be further increased by the multi-axial stress. In this state, cracking takes place.
- when the maximum load is reached, the transverse reinforcement (D) is activated;
- further contribution is made in the post-critical phase by the confinement given by the reinforcements arranged in the concrete dowels (E).

An example of a study of shear-slip behaviour with metal connector failure can be found in [74, 75].

Different models for describing the shear-slip action behaviour must be adopted depending on whether the failure situation is described on the steel or concrete dowel side [32].

Shear-slip behaviour in the case of steel dowel yielding failure

The steel dowel yielding failure mode is descrived in the work [38]. A multilinear approach is used here.

Shear-slip behaviour in the case of concrete pryout failure

In the case of concrete pryout failure the research [32] proposes a mathematical description of the behaviour using a multilinear model. It is limited to PZ and MCL connector shapes and is derived on the basis of curves obtained from experimental tests in the literature. The author observes the similarity between the test curves represented in the plane with normalised axes ($P/P_{po}; \delta/\delta_{el}$). All test curves up to 70% of the shear strength behave substantially elastically. The value of δ_{el} is therefore defined as the slip corresponding to a load of 70% of the shear strength. The value P_{po}, on the other hand, is derived as per the formulation (2.16). Observing the normalised curves, a variability of the inelastic branch is observed. The author concludes that the influence can be attributed to:

- the volume of the pryout cone, which is dimensionally related to the cube of the cone height $V_{po} \approx h_{po}^3$;
- to the measure of brittleness referred to as 'characteristic length' and derived as $l_{ch} = G_f \cdot E_c / f_{ct}^2$ where G_f is the fracture energy, f_{ct} is the tensile strength of the concrete, E_c is the modulus of elasticity of the concrete.

On the other hand, the shape of the steel connector has no particular influence. The parameter χ_{po} is defined and appropriately calibrated on the basis of the available evidence:

$$\chi_{po} = l_{ch}/350 \cdot (h_{po,s}/60)^3 \tag{2.28}$$

Using a model of three springs arranged in series, the stiffness of the elastic branch of the curve ($C_{el,CD}$) is derived:

$$C_{el,CD} = (1/C_{S,flex} + 1/C_{S,s} + 1/C_C)^{-1} \tag{2.29}$$

In which $C_{S,flex}$, $C_{S,s}$, C_C are the stiffnesses with respect of the bending slip of the steel dowel, the shear slip of the steel dowel and the compression slip of the concrete dowel, respectively. For the explicit calculation refer to the formulations contained in [32]. From the definition of the elastic end shear and initial stiffness, it is possible to derive, according to the observations made earlier:

$$\delta_{el} = 0.7 \cdot P_{po}/C_{el,CD} \tag{2.30}$$

The shear-slip curve can be described by a multilinear by defining its points as a function of only the parameters $\delta_{el}, P_{po}, \chi_{po}$ One use of this model can be found in [30]. The derived formulation makes it possible to obtain the deformation capacity δ_u and to perform parametric analyses. Further analysis done in [32] shows that:

- in the range $100mm < e_x < 350mm$ the CL-type shape can guarantee more ductility in a comparison made with the PZ shape with all other parameters being equal;

- an increase in the thickness of the steel web leads to a reduction in deformation capacity;
- an increase in concrete strength leads to a decrease in deformation capacity;
- the most influential parameter on the deformation capacity is the concrete cover. Below 30 mm of concrete cover, only MCL connector shapes with $e_x > 175mm$ can achieve the deformation capacity of 6 mm required by [11] as ductility requirement. The author of [32] concludes by asserting that there is therefore a need to raise the minimum concrete cover proposed by the German regulations [4] to 20 mm.

2.6.8 Pure tensile load

Shear connectors may be subject to accidental tensile loading, however they may also be intentionally designed to resist pull-out action. In accordance with the standards, shear connectors must be designed to resist 10% of the longitudinal shear resistance while providing sufficient anchorage strength.
In [31] results of an experimental and numerical simulation campaign to determine the pure tensile behaviour of the connector are documented. A 'break-out cone' collapse is observed. In cases where there is no longitudinal stress, the break-out cone occurs at angles between 30° and 35°. The influence of various parameters is observed. In particular:

- the presence of transverse reinforcement decreases the initial stiffness of the connector due to the introduction of a local discontinuity, but increases its strength and deformation capacity due to the growth of activated area in concrete.
- consecutive connectors have a mutual interaction which leads to a decrease in load-bearing capacity due to the fact that the fracture cones come together to form a single wedge.
- the effect of a longitudinal pre-stressing state in the slab is stiffening in both tensile and compressive cases. While in tension the bearing capacity decreases by about 10% and leads to a less ductile fracture, in compression an increase in pull-out strength is observed.
- the point at which most of the stress transference between the concrete part and the steel connector occurs is at the notches in the front faces of the connector. The two cones of stress transmission overlap. A parametric analysis shows the dependence between the maximum pull-out resistance relative to the single point of load insertion and the depth of immersion in the concrete $P \approx h^{1.8}$.

In particular, the presence of longitudinal stresses in the concrete is taken into account by the factor ψ which reduces the capacity of the connector by 10% in the case of longitudinal traction in the concrete which is greater than the tensile strength of the concrete. The dependence of the strength with respect to the immersion height has an exponent of 1.5. This is to include the applicability of the model for large immersion heights of the connector. Results of static loading tests for tensile composite connectors in high performance concrete are available in [53] where the fatigue behaviour is also presented. The model developed in [31] is employed in this last cited study.

2.6.9 Shear-tension interaction

The shear-tension interaction behaviour of composite dowels is studied in [35]. Here an interaction domain is proposed in the tension-shear plane.

2.6.10 Composite dowels with High Performance Concrete (HPC)

The high density of the UHPC microstructure allows for an improvement in the strength and durability of the concrete. This leads to a saving in the weight of the structural element [67]. Ultra high-performance concretes (UHPC) behave elastically up to 80-90% of their failure load under uniaxial stress [53]. The elastic moduli are around 43000 MPa and 55000 MPa. With the addition of fibres, a more ductile fracture can be achieved.

Shear behaviour in high-performance concretes is studied by means of POST push-out tests in [67]. The tests show that in the case of steel connector failure the calculation formula is not economical. The influence of the degree of connection, the thickness of the metal profile and the grade of steel, and the amount of reinforcement is examined. The study shows the importance of reinforcement in preventing brittle shear failure of the concrete core. The composition of the high-performance concrete and the thickness of the concrete element are also examined. A strong influence of steel core thickness, steel strength and concrete thickness is shown.

The behaviour under tensile stress in high-performance concrete is studied in [37].

The behaviour of continuous connectors under tensile stress in high-performance concretes is studied in [53] for both the static and fatigue case.

The fatigue behaviour in the case of tensile stress in UHPC is investigated in [53]. In the study, the influence of the maximum load and the stress range for cyclic load tests is examined by deriving the number of cycles-slip relative curves. The higher load has an influence on the relative slip in the elastic phase while it has no significant influence on the progression of the inelastic creep in the fatigue phases. The load amplitude has a strong influence on the development of inelastic slip during loading cycles. As a result, the research [53] proposes a first model to quantify the lifetime of tensile composite connectors in the absence of transverse reinforcement. The model is elaborated from the model developed in [31]. Further reference is [37].

Further reference is[51].

2.7 Regulatory framework

The current limitations for the application of Eurocode 4 [11] exclude the possibility of applying T-sections. The scope of application of Eurocode 4 is in fact reduced to that of double-T profiles with a minimum number of shear connectors. The minimum ductility value i order for a connector to be classified as ductile is 6 mm. The first regulations on calculation and construction requirements for composite dowels are the [4], first introduced in 2013, renewed in 2018 and with a validity expiry date set for the year 2023. The analogous

regulations for Perfobond and Kombi-Dübel systems are respectively [3] and [2]. The development of the German technical regulations [4] was in accordance with the Eurocodes [8, 9, 11].

The scope of application is beams made by shear connection of a clothoid (CL) or puzzel-shape (PZ) connector profile together with a concrete flange. The size of the connector is limited to between 150 mm and 500 mm. The lower limit ensures ductile behaviour in shear failure of the concrete connector. The indications are particularly aimed at the area of bridge constructions and tall buildings [47, 63]. Excluded from the scope of application of the regulations are [4] elements subject to centred tension under non-primarily static loads perpendicular to the connectors. This is to prevent a degradation of the shear connection [47, 63]. Geometric tolerances for the nominal connector gauge are given. In particular, a deviation of +2/-4 mm is accepted where the '+' refers to an increase in material. The shape of the cut must comply with the indications of Table 8.1 of the standards [10]. If you fall in the case of construction detail 4, category 140 will be used. If, on the other hand, construction part 5, category 125 is used.

The regulations also contain information on production controls and conformity tests, materials and geometries to be used, design and dimensioning guidelines with explicit reference to the safety requirements introduced by EN1994-1-1, EN1994-2 [11, 12].

Contrary to the statement of [11], which in the case of the minimum requirement of degree of connection is satisfied provides for the possibility of inserting equidistant connectors with both positive and negative moments, in the case of composite beams without an upper flange of the steel profile the equidistance of the connectors is permitted if the following requirements are met: (1) the degree of connection in shear is at least 0. 5 ($\eta \geq 0.5$), (2) the span does not exceed 18m, (3) the plastic moment of the composite section is less than 10 times that of the steel profile alone, (4) the reduction of the shear capacity of the connector must not fall below the longitudinal shear force by more than 25%.

The minimum permissible distance $c_{D,o}$ between the upper edge of the steel connector and the outer surface of the concrete is set at 20 mm. The same limitation applies to the distance ($c_{D,u}$) at the base of the compound connector. This is to ensure the complete development of the Pry-Out cone [47]. The concrete classes that can be used are C20/25 to C60/75. The minimum section width is 250mm.

From a Strut And Tie model with 45° inclined struts [47, 63] the minimum prescribed amount of reinforcement to be inserted is derived:

$A_b = 0.5 \cdot P / f_{sd}$

where $P = P_{Rd}$ or alternatively $P = P_{Ed}$.

At present new design regulations are under development. These will be included as annex for the forthcoming version of the Eurocode 4.

The stirrups must extend for a distance of at least $\Delta = 0.15 \cdot e_x$ beyond the lower level of the connector. In order to achieve ductile behaviour [47], at least two stirrups must be placed $\phi 10$ per opening. The limitation on the spacing of the confining reinforcement to $\min e_x; 300mm$ is justified by the fact that the reinforcement must be included in the concrete strut [47].

Chapter 3

Shear flow-slip: numerical one-dimensional method

3.1 Introduction

For low degrees of partial shear connection in composite steel concrete elements a sharp increase of the deformation demand on the shear connector is observed. This can create an impediment for the composite member behaviour in reaching the expected bending resistance of PSC situation, generating undesired and unsafe premature failures. Moreover it creates limitations [28] in the assessment via the widely used Rigid Plastic analysis (RP) method allowed by EC4 [11].

Practically this phenomena is prevented by the design codes such as EC4 [11] by introducing a lower bound as limitation on the degree of shear connection η. This minimum degree of shear connection η_{min} is proposed in the present version of Eurocode 4 [11] as a function of the element's span length L and of the steel strength f_y. The present design rules are strictly related and calibrated on the basis of the minimum available deformation requirement which the connector must satisfy. This value is set to $6\,mm$ in EC4 [11], therefore a shear connector matching this requirement is labeled as "ductile". These formulas, as stated in [28], are robust but consist in a coarse approximation of the actual behaviour of the element and end up being non advantageous for exploiting more ductile connectors. The use of low deformation capacity shear devices would also be possible by increasing the values of η_{min}.

For the forthcoming version of the Eurocode 4 initiatives are promoting the implementation of new kinds of shear connections. These imply the exploiting of different situations not covered by the present EC4 version. In particular mechanical connector devices such as continuous composite shear connections [63] often imply a presence of single T sections, thus exiling from the present EC4 limits of double symmetrical or nearly double symmetrical steel profiles. In these cases the research is spending effort in determining the structural behaviour of the member for low degree of shear connection, studying if the present rules are also suitable to be extended for the single-T profile applications. Moreover, researches such as [36], are

promoting a shift of approach toward more "performance based" design rules. This is done by implementing limitations on the degree of shear connection which take into account also the plastic slip capacity δ_u offered by the shear connection device and proposing formulations depending both on the span length and the steel strength but also on the available ductility δ_u. Shear connection technologies such as composite dowels can be applied in different sizes, and the plastic slip capacity δ_u has been proved to be a linear function of the connector size in case of steel yielding failure mode. [71], thus covering a wide spectrum of deformation capacities.

In the present work a numerical one-dimensional method is presented in order to assess the overall element mechanical behaviour in bending. This is based on the work from Zhang [97]. The method takes into account both the shear connection behaviour and the sectional response on the overall span length and is developed in order to quantify the slip demand of the shear connection, especially in the partial shear connection regime.

After presenting the case study's cross-section and main features, a theoretical background is done which contains also the numerical method formulation description. Following, five numerically solved examples are presented and discussed. Thus a restricted parametric study is presented varying the span length and the load level. The method is developed in order to carry out a more intense parametric study to assess the dependence of the ductility demand of the shear connection as function of the span length and the degree of shear connection η.

The broadening of the numerical study aims for future purposes to assess new design rules proposals for the formulation of a minimum degree of shear connection η_{min} design formulation, taking into account also the available deformation capacity of the shear connection.

3.2 Case study

The case study is a simply supported beam of span length L under a uniformly distributed load q. The reference case is shown in Fig.3.1. The reference frame has origin at the midspan section and the generic section S is identified by its coordinate $x(S)$. In particular the x coordinate of the support section is $x = L/2$. Under these assumptions the moment distribution $M(x)$ along the beam is known from the structural analysis. The structure is statically determinate and is solicited by sagging moment.

$$M(x) = q \cdot L^2/8 \cdot \left(1 - (\frac{x}{L/2})^2\right) \tag{3.1}$$

More in detail the maximum bending moment is:

$$M_{max} = M(x = 0) = q \cdot L^2/8 \tag{3.2}$$

3.2.1 Composite cross-section

Geometry

The composite cross-section is obtained from an original standard hot-rolled HE1000AA profile. The

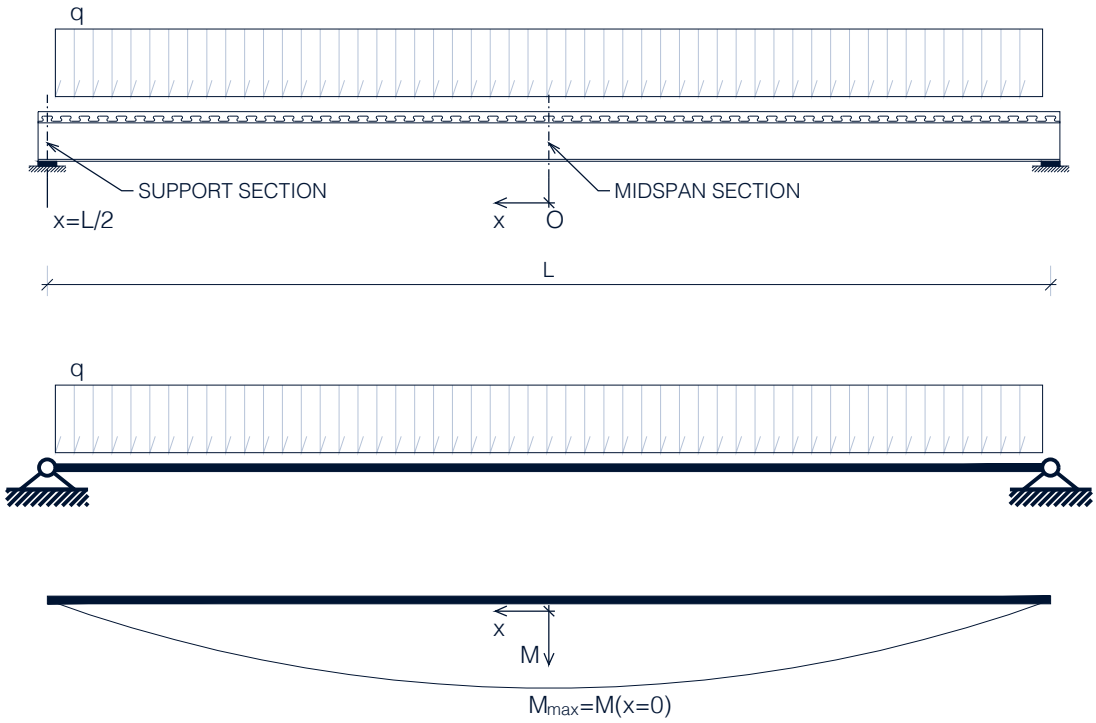

Figure 3.1: case study: element, static scheme and acting moment diagram

considered shear connection is a PZ shape spaced $e_x = 150.0\ mm$ but the method is in general valid for any shear connection. The concrete slab is $120\ mm$ thick. Considering a $5000\ mm$ of beams interaxis leads to an effective width of $4000\ mm$. The geometry is illustrated in detail in Fig.3.2.

Materials

The considered materials are an S355 structural steel, a B500 reinforcement steel and a strength class C55/67 concrete.

sectional bending resistance

The relevant cross sectional bending resistance properties are the plastic resistant design bending moment in full shear connection condition $M_{pl,f,Rd}$, the plastic resistant design bending moment of the isolated steel single T profile $M_{pl,a,Rd}$, the concrete compression force in a ULS condition with full shear connection N_{cf}. These are:

$$M_{pl,f,Rd} = 1846\ kNm \tag{3.3}$$

$$M_{pl,a,Rd} = 550\ kNm \tag{3.4}$$

$$N_{cf} = 4500\ kN \tag{3.5}$$

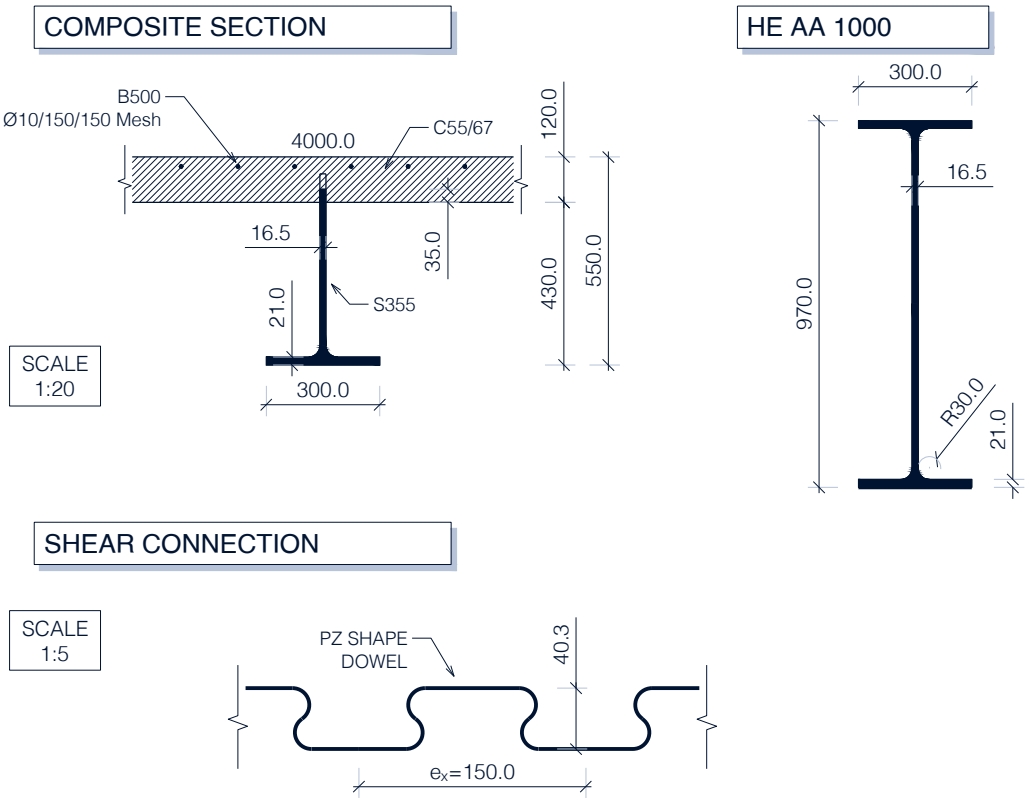

Figure 3.2: case study: section and shear connection

3.3 Theoretical background

3.3.1 Composite beam general considerations

While for a homogeneous section the element's flexural behaviour strictly depends on the sectional properties, in a steel-concrete composite member the response depends on the interaction between the shear connection and the sectional behaviours. Generally particular sections labeled as "critical sections" are identified. For the simply supported beam under a uniform load, the two critical sections of interest are the one at support and the midspan. While at midspan the maximum bending moment accompanied by the maximum compression force in the concrete part $\max(N_c)$ occurs, in the support region the pinned end implies an absence of bending moment and a consequent null concrete compression resultant $N_c = 0$. Thus, the shear connection provides between the two critical sections the force transfer, allowing the boundary conditions to be satisfied. The concrete compression N_c can be interpreted as a continuous function $N_c(x)$ varying between N_c at midspan and zero at support. Because of force equilibrium reasons taken the generic two sections A and B the following should be satisfied:

$$N_c(B) - N_c(A) = -\sum_i P_i \tag{3.6}$$

where A and B are the two sections considered and P_i are the forces applied at the $i-th$ connector with i ranging from 1 to the number of connectors between the two sections. Alternatively, rather than a discrete approach, a continuous interpretation can be used:

$$N_c(B) - N_c(A) = \int_{x_A}^{x_B} dN_c = -\int_{x_A}^{x_B} dP = -\int_{x_A}^{x_B} \frac{d\,P}{dx}\,dx = -\int_{x_A}^{x_B} v_L(x)\,dx \tag{3.7}$$

where v_L consists in the shear flow and is defined as:

$$v_L(x) = \frac{d\,P(x)}{dx} = -\frac{d\,N_c(x)}{dx} \approx \Delta P/\Delta x = P(x)/e_x \tag{3.8}$$

An average value of the shear flow between the two critical sections may be defined as:

$$\overline{v}_L = \frac{N_c}{L/2} \tag{3.9}$$

Important definitions for assessing the composite member behaviour are [17]:

- slip (δ): in a deformed state for a particular section the longitudinal displacements for the concrete fibre at the steel-concrete interface $u_c(x)$ and the one of the steel fibre at the steel-concrete interface $u_a(x)$ are recognisable. The slip is defined as: $\delta(x) = u_c - u_a$ and it has length dimensions.
- slip strain (ϵ_{strain}): is the difference between the concrete strain and the steel strain in correspondence of the steel-concrete interface ($\epsilon_{c,interface}(x) - \epsilon_{a,interface}(x)$). It can be recognised as: $\epsilon_{slip}(x) = d\,\delta(x)/dx = d\,u_c/dx - d\,u_a/dx = \epsilon_{c,interface}(x) - \epsilon_{a,interface}(x)$. The slip strain is dimensionless.
- full shear interaction (FSI): it consists in null slip strain situation. It's the particular case at which the longitudinal stiffness of the shear connection is infinite and no slip occurs between concrete and steel interface.

- Partial Shear Interaction (PSI): it consists in a positive slip strain situation. In this case the longitudinal stiffness of the shear connection is finite.
- no interaction: it's a limit case of Partial Shear Interaction (PSI) where the slip strain reaches it's maximum. In this case the shear connection has zero longitudinal stiffness.

In the following part a simplified approximated but practically exploited straightforward method is presented in order to assess the global behaviour of a simple supported beam under uniform load with uniformly spaced connectors with spacing e_x. The method is conceptually useful in order to understand the whole model and will be taken as a reference for the subsequent sections. The model assumes the linearity of the slip demand along the beam and the elastic-perfectly plastic behaviour of the connection. The linearity of the slip demand is verified at low load levels coming directly from the well known Jourawski formulation of the shear flow:

$$v_L(x) = \tau(x) \cdot b(y) = \frac{V(x) \cdot S^*(y)}{I_y} \tag{3.10}$$

Because the shear distribution $V(x)$ varies linearly and the section is constant, a linear distribution of the shear flow must exist. If the shear connection behaves linearly the slip demand $\delta(x) \propto v_L(x)$ will also be linear. Of course this is valid only under linear elastic assumptions but is approximately verified also at ultimate limit states for an elastic behaviour of the shear connection. A perturbation of the elastic distribution appears in the midspan region because of the plastic hinge generation. This phenomenon is in detail described by Zhang [97] and testifies the need to discard the simplified model, which could despite of that be taken as a "starting reference" for subsequent observations.
Taking into account the fact that the connector has a limited bearing capacity P_{Rd}, the maximum transferable force between the two critical sections can be computed as:

$$\sum_{i=1}^{n} P_{Rd,i} = n \cdot P_{Rd} \tag{3.11}$$

Where n is the number of shear connectors between the two critical sections, namely:

$$n = \frac{L/2}{e_x} \tag{3.12}$$

If the shear connection is capable of transferring the whole N_{cf} force the shear connection is named Full Shear Connection (FSC). On the contrary if the shear connection is not capable of transferring all N_{cf} the connection is named "partial shear connection" (PSC). In both cases the failure occurs at sectional level, but while in the FSC case the whole sectional capacity is exploited, in PSC case the sectional bending capacity "adapts" to the fact that the shear connection has reached the maximum transferable force. In the PSC case the actual transferred concrete compression force is $N_c = \sum P_{Rd,i} < N_{cf}$. In the FSC case the concrete compression force will be exactly $N_c = N_{cf} \leq \sum P_{Rd,i}$. The FSC condition, as defined by EC4 [11], is the condition where a further increase of the number of shear connectors does not lead to an increase of the plastic bending resistance.

Formally the shear connection degree η can be defined as:

$$\eta = \frac{n \cdot P_{Rd}}{N_{cf}} \tag{3.13}$$

In accordance with the above done statements, the two cases can be distinguished as:

$$\begin{cases} \eta = \frac{n \cdot P_{Rd}}{N_{cf}} \geq 1 & \text{FSC} \\ \eta = \frac{n \cdot P_{Rd}}{N_{cf}} < 1 & \text{PSC} \end{cases} \tag{3.14}$$

The $\eta \approx 1$ region can be interpreted as an optimum exploiting of both the shear connection capacity and the sectional bending capacity. Of course, the designer, is more interested in exploiting the maximum bending capacity of the element, rather than the maximum bearing capacity of the shear connection, making it preferable to have a FSC condition $(\eta \geq 1)$.

In a continuous approach a maximum transferable shear flow $v_{L,Rd}$ can be defined:

$$v_{L,Rd} = P_{Rd}/e_x \tag{3.15}$$

Notice that, following from the definition of the number of connectors, the degree of shear connection η can also be defined as:

$$\eta = \frac{n \cdot P_{Rd}}{N_{cf}} = \frac{L/2/e_x \cdot v_{L,Rd} \cdot e_x}{(N_{cf})} = \frac{v_{L,Rd}}{(2N_{cf}/L)} \tag{3.16}$$

This is the ratio between the maximum admissible shear flow by the shear connection and the average shear flow in case of full shear connection.

Another important phenomenon that has to be considered is the one of redistribution at shear connection level. In case all the shear connectors are behaving in a linear elastic way, no redistribution occurs. As a connector starts yielding, redistribution along the shear connection exhibits. As the degree of shear connection η becomes lower than the unit value entering in the PSC region, the shear connection will be fully yielded as each connector is participating balancing the N_c force with its resistance P_{Rd}. For a given value P_{Rd}, wheter redistribution occurs depends on the N_{cf} value which depends on the choice of the section. In an elastic situation the distribution of forces along the shear connection is given by:

$$P_i = x_i/(L/2) \cdot P_{max} = i/n \cdot P_{max} \tag{3.17}$$

The previous written equation implicitly assumes also a linear distribution of the slip δ and a uniform connectors spacing. Where P_{max} is the bearing force on the most loaded connector, that is the one at support. In detail, if the most loaded connector in an elastic assumption reaches P_{Rd}, then redistribution occurs. For equilibrium reasons the next relation must be fulfilled:

$$\sum_{i=1}^{n} P_i = P_{max}/n \sum_{i=1}^{n} i \approx n/2 \cdot P_{max} = N_{cf} \tag{3.18}$$

Therefore the value of P_{max} is $2N_{cf}/n$. Thus, the bound condition is represented by:

$$P_{max} = 2N_{cf}/n = P_{Rd} \quad \rightarrow \quad N_{cf} = n \cdot P_{Rd}/2 \tag{3.19}$$

In terms of shear flow it becomes $N_{cf} = L/ \cdot v_{L,Rd}/4$. This condition can also expressed in terms of η:

$$\begin{cases} \eta = n \cdot P_{Rd}/N_{cf} < 2 & \text{REDISTRIBUTION} \\ \eta = n \cdot P_{Rd}/N_{cf} \geq 2 & \text{NO REDISTRIBUTION} \end{cases} \tag{3.20}$$

The cross sectional behaviour assessment will be discussed in the next section (Sec.3.3.2). With these methods it's possible to derive how the plastic resistant bending moment is affected by the degree of shear connection. In detail it's possible to reconstruct the function $M_{pl,Rd}(\eta)$ or equivalently $M_{pl,Rd}(N_c)$. Notice that for a given section there is a related value of N_{cf}. Therefore in the PSC situation referring to η or to N_c is the same as there is a direct proportionality $N_c = \eta \cdot N_{cf}$. The function $M_{pl,Rd}(N_c)$ in a PSC condition is referred as Partial Shear Diagram (PSD).

Remembering the simplification of this approach the frame in Fig.3.3 can be used as a quick summary.

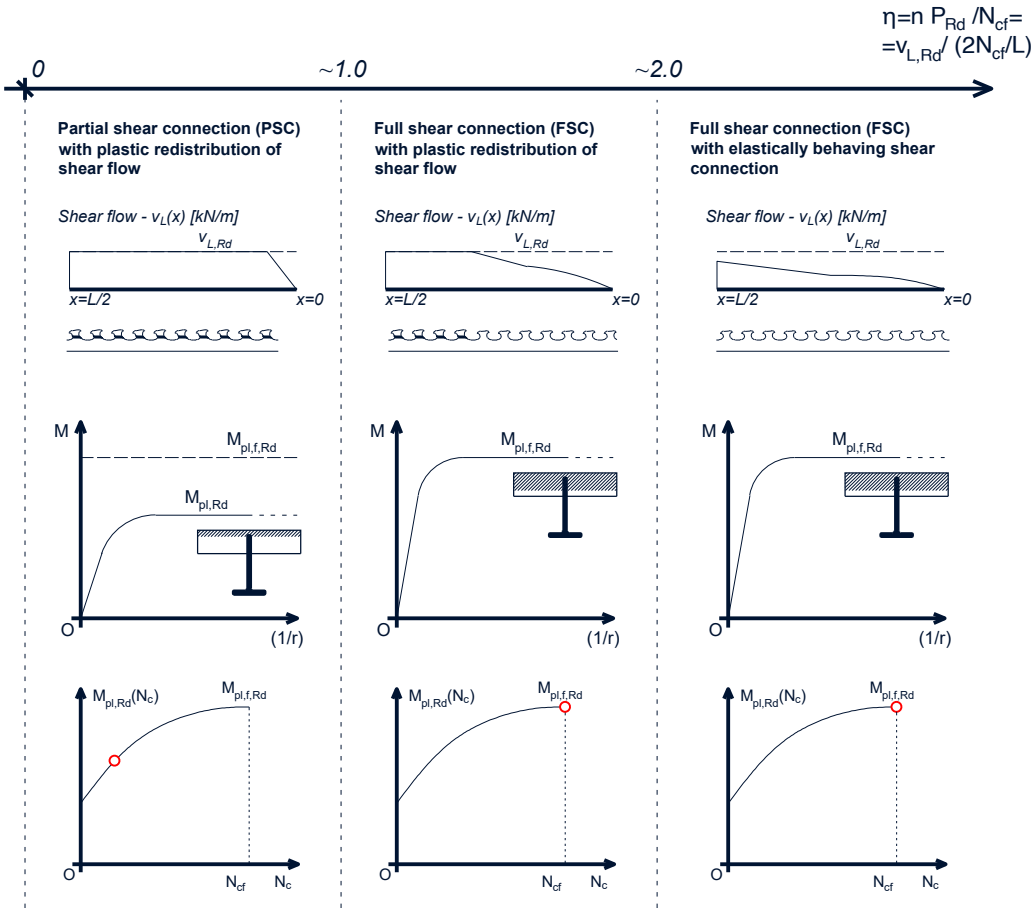

Figure 3.3: composite beam mechanical behaviour. Concept of Partial Shear Connection (PSC) and Full Shear Connection (FSC) and concept of redistribution of shear flow

Deformation behaviour of a composite beam

The generic deformation stage of a composite member can be described as a sum of an elastic component and a rigid-plastic contribution [28]. This can be used also in order to derive the end-slips δ_{max}.

The elastic quote is often described analytically by the differential equations of the composite action, or by approximated methods such as the "γ-method" [80] also exploited for wood structures and implemented in the Eurocode 5 [13]. The plastic contribution consists in a concentrated (null length) plastic hinge formation. This methods are in the present study still not used, but might consist a useful reference point in order to check and compare future results.

3.3.2 Sectional model

One simplified method in order to assess the flexural behaviour, also allowed by EC4 [11], is the rigid plastic (RP) analysis also known as "equilibrium method" [17]. This is because in performing the computation the only kinematic consideration consists in the determination of the plastic neutral axis. Following this an infinite curvature is assumed which leads to the consideration of uniform stress distributions along the section. The only unknown quantity under this assumptions is the position of the plastic neutral axis (PNA) which guarantees the equilibrium assuming a particular degree of shear connection. Traditionally this approach found a wide exploiting for practical purposes. Nowadays thanks to accessible and available computational software the trend is away from Rigid Plastic analysis (RP) methods towards Strain Limited analysis (SL) methods which will be described in the following section.
In order to model the sectional behaviour a Strain Limited analysis (SL) method is used. The following assumptions are made:

- on the steel part strains are linear;
- on the concrete part strains are linear;
- perfect bond exists between the reinforcement steel and the concrete part. This implies kinematic congruence for adjacent concrete-reinforcement steel fibres;
- concrete part and steel part have the same curvature;
- material laws depicted in Fig.3.4 are considered:
  - for the concrete part a parabola-rectangle relation is used;
  - for the structural steel part an elastic with plastic hardening branch is used;
  - for the reinforcement steel part an elastic with plastic hardening branch is used.

For the material laws other possible choices are to implement a Sargin parabola model [83], also given in [8]. For the structural steel another feasible choice is to use a quartlinear approximation of the stress-strain curve exploited for example in [97].
For the subsequent application the reinforcement bars in compression will not be accounted as considered negligible. The concrete slab basis length is assessed by mean of the concept of "effective width" from Eurocode 4 [11]. Notice that a limitation of the method is the impossibility to take into account for

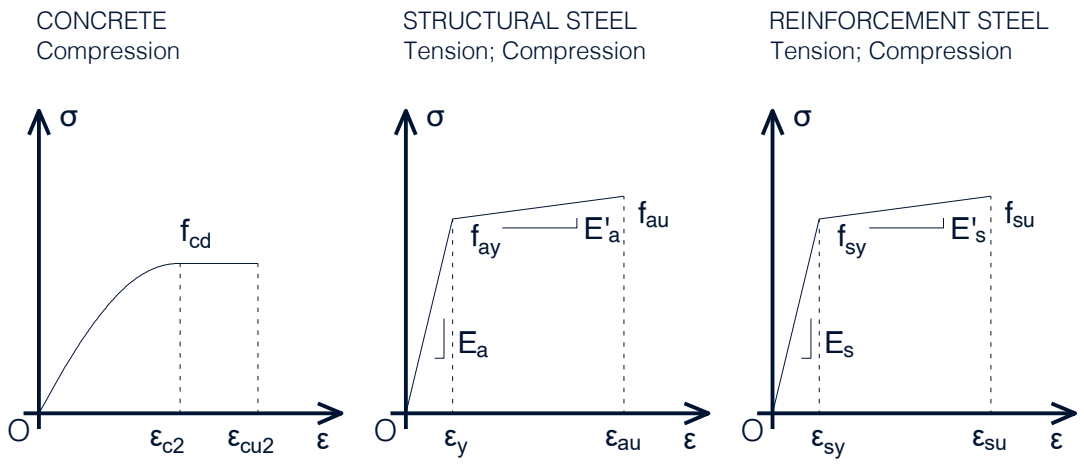

Figure 3.4: considered material laws

local buckling phenomena. Despite of that, local instabilities can be taken into account with the section classification.

Notice that due to the fact that the concrete part and the steel part belong to the same element the deflections should be the same for compatibility reasons ($y_c(x) = y_a(x) = y(x)$), where $y_c(x), y_a(x), y(x)$ are respectively the deflection of concrete, the deflection of steel and the deflection of the composite element. So also the first derivative (rotation) and the second derivative (curvature) have to be equal leading to the aforementioned hypothesis $y_c'' = y_s'' = y''(x) = (1/r)(x)$.

Specifying a sectional state

Under these assumptions, a certain state of the cross section is specified by a set of three kinematic parameters. These can be chosen between:

- curvature $(1/r)$;
- the position of the concrete plastic neutral axis $x_{pl,1}$;
- the position of the steel plastic neutral axis $x_{pl,2}$;
- the strain of a fibre belonging (or ideally belonging) to the concrete part, for example the strain of the upper fibre of the concrete part ϵ_c;
- the strain of a fibre belonging (or ideally belonging) to the steel part, for example the strain of the upper fibre of the concrete part as if would belong to the steel part ϵ_{cf}.

In order to identify the generic fibre of the section a y coordinate is introduced. The sectional reference frame is set with origin on the upper concrete fibre. The calculation scheme for a generic deformed state of the section is shown in figure 3.10. For performing the analysis choosing the sign conventions is fundamental. The sign conventions as taken in the analyses are described, despite of that this is not a key

point for the subsequent part of the reading. Following sign conventions are assumed: - Tensile stresses $\sigma(y)$ are positive; - Elongation strains $\epsilon(y)$ are positive; - Parameters $\epsilon_c, \epsilon_{cf}$ are considered positive when a compression is associated with them; - Compression forces are positive; - Positive ϵ_{slip} is associated with positive difference $\epsilon_{cf} - \epsilon_c$. - Positive curvature generates positive strains on the lower fibre and negative strains on the upper fibre; - A positive bending moment is associated with a positive curvature.
The state of the section can thus be specified in a three-dimensional space by a set of three independent kinematic parameters, for example by $(1/r) - \epsilon_c - \epsilon_{slip}$ or $(1/r) - x_{pl,1} - x_{pl,2}$.
In the following procedure the basic chosen kinematic parameters are $(1/r, \epsilon_{cf}, \epsilon_{slip})$. The kinematic relations between the quantities are derived simply by exploiting the linearity of the strain distribution on the two parts of the section.:

$$\epsilon_c = \epsilon_{cf} - \epsilon_{slip} \tag{3.21}$$

$$\epsilon_a(y) = (1/r) \cdot y - \epsilon_{cf} \tag{3.22}$$

$$\epsilon_c(y) = (1/r) \cdot y - \epsilon_{cf} + \epsilon_{slip} \tag{3.23}$$

$$x_{pl,1} = (\epsilon_{cf} - \epsilon_{slip})/(1/r) \tag{3.24}$$

$$x_{pl,2} = \epsilon_{cf}/(1/r) \tag{3.25}$$

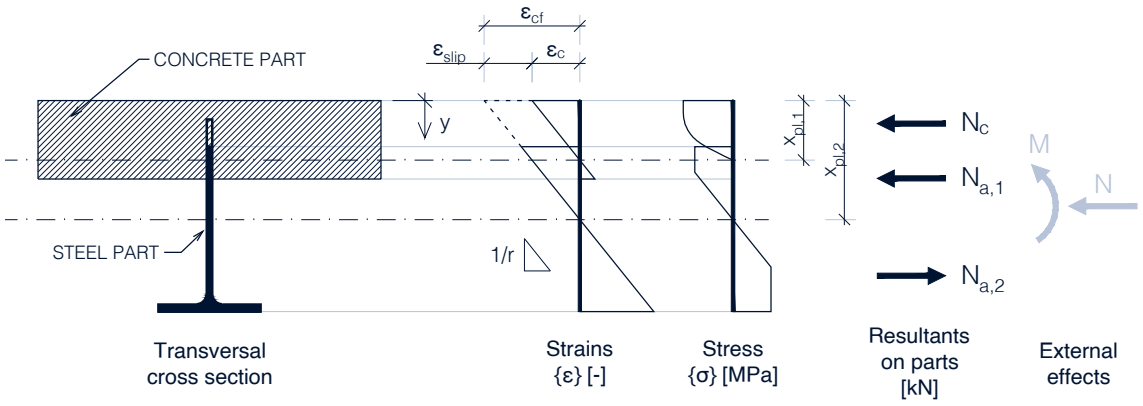

Figure 3.5: generic deformed state on the composite section: calculation scheme

Given the three kinematic parameters, the strain field is known along the section and following from the material laws the stress distribution is also determined:

$$\sigma_a(y) = \sigma_a(\epsilon_a(y)) \tag{3.26}$$

$$\sigma_c(y) = \sigma_c(\epsilon_c(y)) \tag{3.27}$$

The resultants are uniquely specified by integration of the stress distribution and static parameters can be determined deriving the following quantities:

- the acting external moment M;

$$M = \int_{Section} \sigma(y) \cdot b(y) \cdot y \, dy \tag{3.28}$$

- the acting external axial force N

$$N = \int_{Section} \sigma(y) \cdot b(y) \, dy \tag{3.29}$$

- the resultant on the concrete part N_c.

$$N_c = \int_{Concrete\,part} \sigma(y) \cdot b(y) \, dy \tag{3.30}$$

More formally a function relating the kinematic quantities and the static derivations can be written:

$$(M, N, N_c) = f(1/r, \epsilon_c, \epsilon_{slip}) \tag{3.31}$$

Notice that if f is continuous and monotonically increasing an inverse function f^{-1} between the (M, N, N_c) space and the $(1/r, \epsilon_c, \epsilon_{slip})$ space exists. Further observations on this concept can be found in [97]. In this case f is a is a one-to-one function and the following inverse relation can be written:

$$(1/r, \epsilon_c, \epsilon_{slip}) = f^{-1}(M, N, N_c) \tag{3.32}$$

While specifying the kinematic parameters $(1/r, \epsilon_c, \epsilon_{slip})$ of the strain field along the section allows a direct computation of the resultants (M, N, N_c), the inverse procedure requires the implementation of an iterative procedure first guessing the $(1/r, \epsilon_c, \epsilon_{slip})$ point and verifying if the correctness of the resultants is met. If not a new point $(1/r, \epsilon_c, \epsilon_{slip})$ has to be chosen. Observe that choosing an elastic plastic hardening material law rather than an elastic perfectly plastic one, can be favourable in allowing a one-to-one function property. Notice that every time three parameters are specified the others turn out to be a consequence. Thus if $1/r, \epsilon_c, \epsilon_{slip}$ are set as independent variables, the other dependent variables $(M, N, N_c, x_{pl,1}, x_{pl,2}, ...)$ are mere results coming from a choice of $1/r, \epsilon_c, \epsilon_{slip}$.

For the purpose of the present numerical experience only elements under pure bending actions are considered. Thus another constraint for the considered state of the section is that the external axial force on the section should be zero:

$$N = \int_{Section} \sigma(y) \cdot b(y) \, dy = 0 \tag{3.33}$$

Under the newly added assumption $N = 0$ the state of the cross-section that fulfills the conditions belongs to a two-dimensional space. Points in the $(1/r, \epsilon_c, \epsilon_{slip})$ space which satisfy the pure bending $(N = 0)$ condition belong to a surface and can be found by sampling a mesh of two of the three parameters, say $1/r, \epsilon_c$ points, and changing by successive iterations the third parameter ϵ_{slip} until the value that satisfies the equilibrium condition $N = 0$ is found.

The chosen way of mapping the two dimensional domain is by sampling points on a uniform grid in the $(1/r) - \epsilon_c/\epsilon_{cf}$ plane and finding the ϵ_{cf} value that satisfies $N = 0$.

For each point $(1/r, \epsilon_c, \epsilon_{slip})$ of the surface there are also the static counterparts N_c and M associated. So it's possible to remap the surface in the $M - N_c - (1/r)$ space obtaining the $M - N_c - (1/r)$ surface (Fig.3.6). The $M - N_c - (1/r)$ surface was firstly introduced by Zhang in [97] and will be exploited in the subsequent sections as the mechanical model of the cross-section just in the same way as a moment-curvature diagram would be used for a canonical non-composite section of an element. The only difference, as depicted above, is the presence of a new degree of freedom along the element which is the compression on the concrete part N_c or equivalently,if f is a one-to-one function, the kinematic counterpart slip strain ϵ_{slip}.

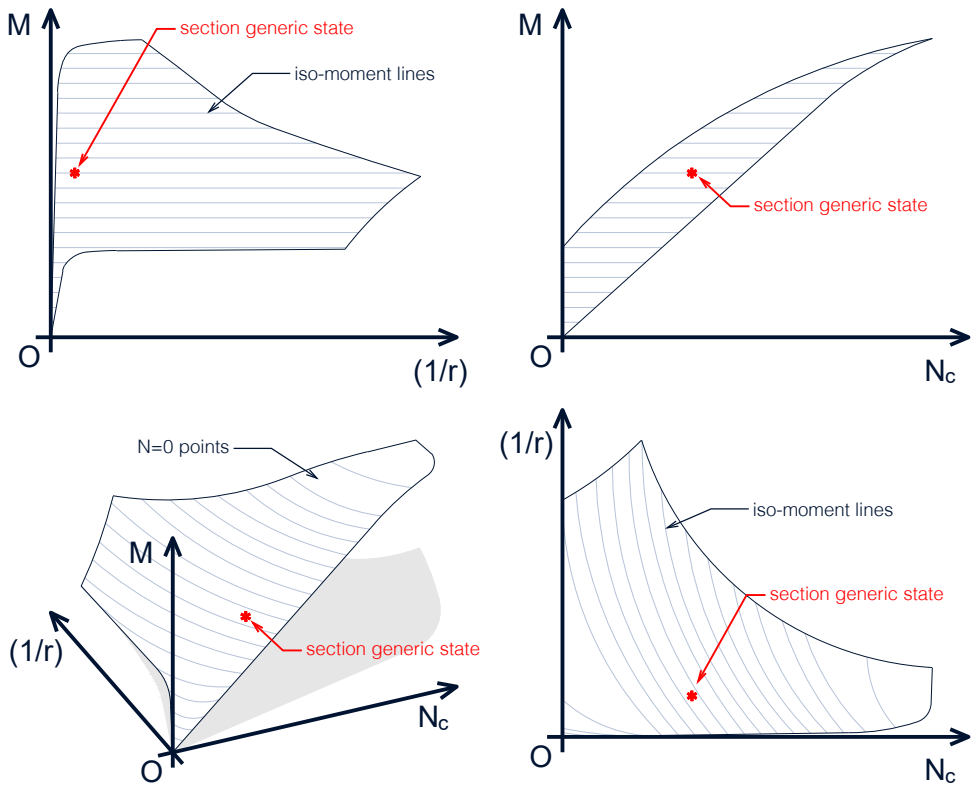

Figure 3.6: moment-concrete compression-curvature surface: generic sectional state

One point on the $M - N_c - (1/r)$ surface represents the state of a section. As an example considering a particular section S of the element associated with the respective coordinate $x(S)$, the values of two parameters such as $N_c(x)$ and $M(x)$ knowing that $N = 0$ can uniquely define the state of the section, and the derivation of all the dependent variables is possible if the function f is monotonically increasing.
If the functions $N_c(x)$ and $M(x)$ are known for each x along the element, the state of every section of the element can be derived and represented on the $M - N_c - (1/r)$ surface. Alternatively a single section evolution can be represented on the surface under increasing load (Fig.3.7).

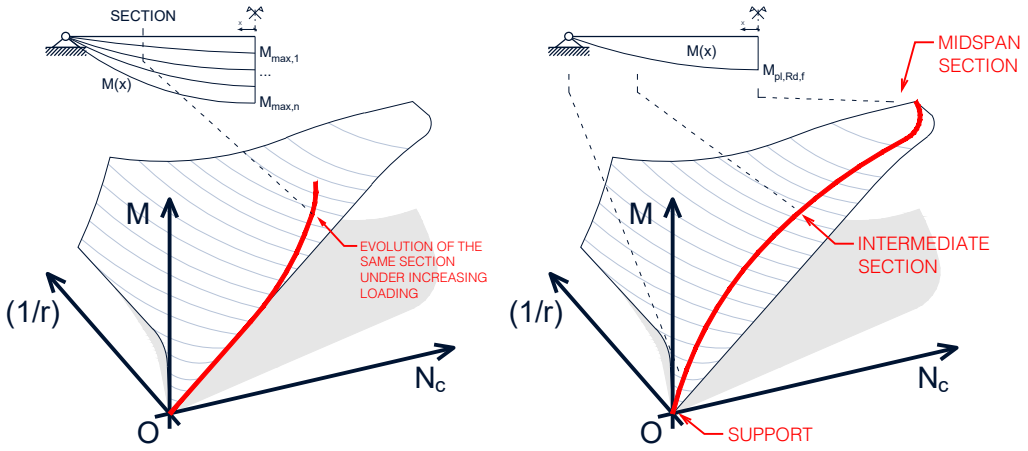

Figure 3.7: moment-concrete compression-curvature surface: representation of element state and sectional evolustion state under increasing load

Ultimate Limit State (ULS) The Ultimate Limit State (ULS) is the particular deformation state at which the first fibre reaches the limit strain along the section (Fig. 3.12). With the ULS deformation condition is associated the relative stress field. By integration of the stress field the design resistant bending moment under a particular axial force N and at a degree of shear connection η can be found.

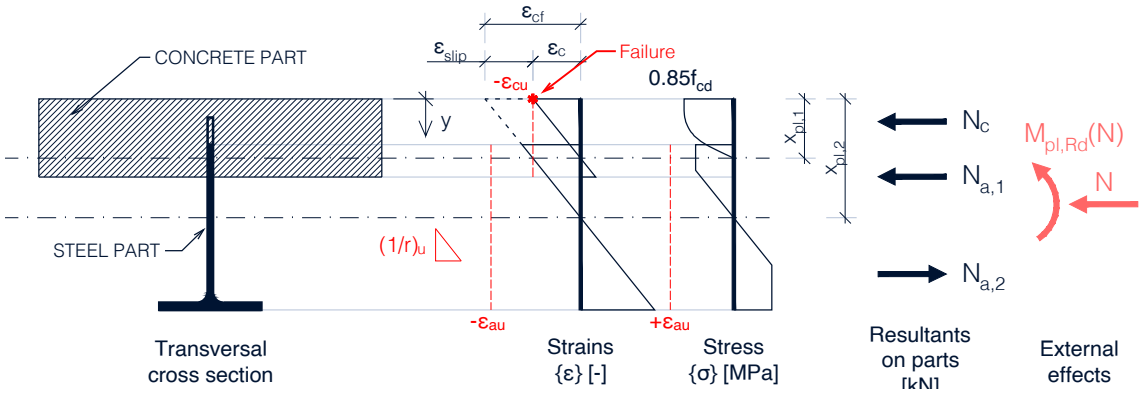

Figure 3.8: ULS deformed state of the composite section: calculation scheme

Notice that in case the pure bending case $N = 0$ is considered the ULS is dependent only on the degree of shear connection η and in the $M - N_c - (1/r)$ space the set of failure points is represented by a curve (Fig.3.9). The projection of this curve on the $M - N_c$ plane consists in the partial shear diagram.
Failure by reaching of the limit strain deformation can occur both by reaching of the ultimate limit concrete compression strain ϵ_{cu}, in this case failure by crushing of concrete shows, or by reaching of the structural steel limitation strain ϵ_{au} both for compressive and tensile stress. For realistic values of limit strains of steel and concrete, geometries and materials failure due to concrete crushing is expected for high values of degree of shear connection. Failure on the structural steel side is instead expected in case of low degree

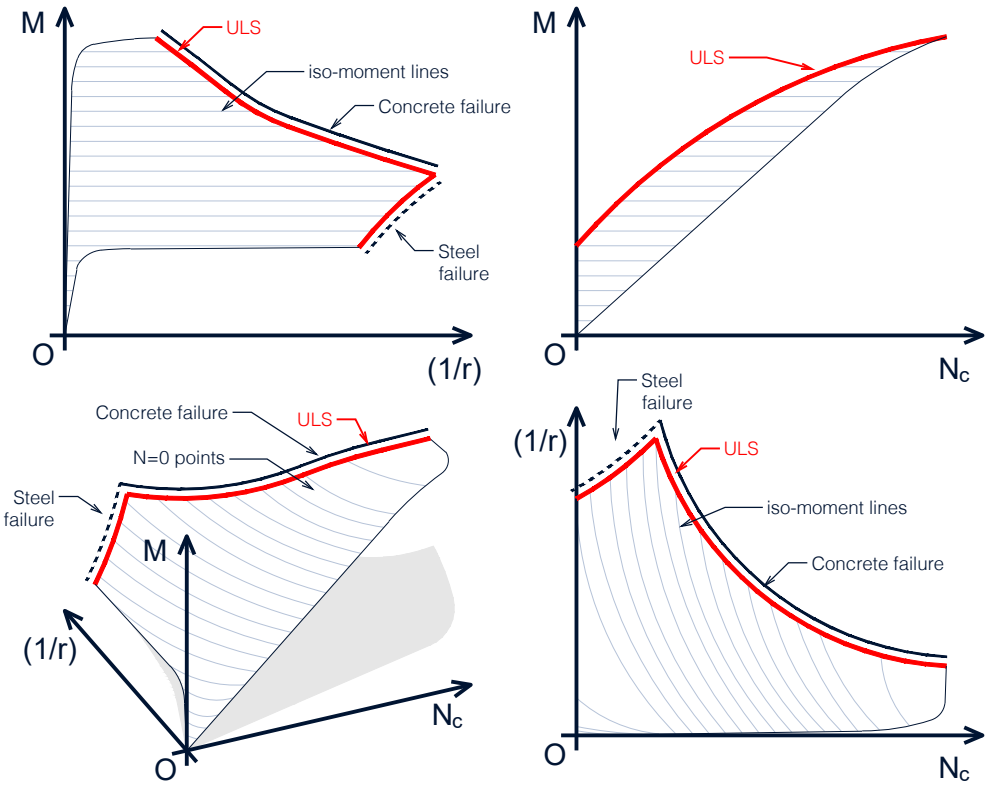

Figure 3.9: moment-concrete compression-curvature surface: ULS sectional state

of shear connection.

Using the degree of shear connection η as a control parameter to derive the ULS points would require an inverse iterative procedure, in fact choosing a particular η^* there would be the necessity of deriving a particular deformed state $(1/r)_u, \epsilon_c, \epsilon_{slip}$ that satisfies $N = 0$ and $\eta = \eta^*$. Thus it's more convenient to use kinematic-related parameters such as the ratio ϵ_c/ϵ_{cf}. The applied way of deriving the failure points is:

1. imposing ϵ_c/ϵ_{cf};
2. guessing the value of ϵ_{cf};
3. searching for the ultimate curvature i.e. the curvature at which the first fibre fails due to the strain limitation;
4. checking the axial force equilibrium condition $N = 0$. If the condition is not met return to point 2. If it is then exit the procedure.

Full Shear Interaction (FSI) The zero slip strain condition is the particular state of the section at which $\epsilon_{slip} = 0$ occurs.

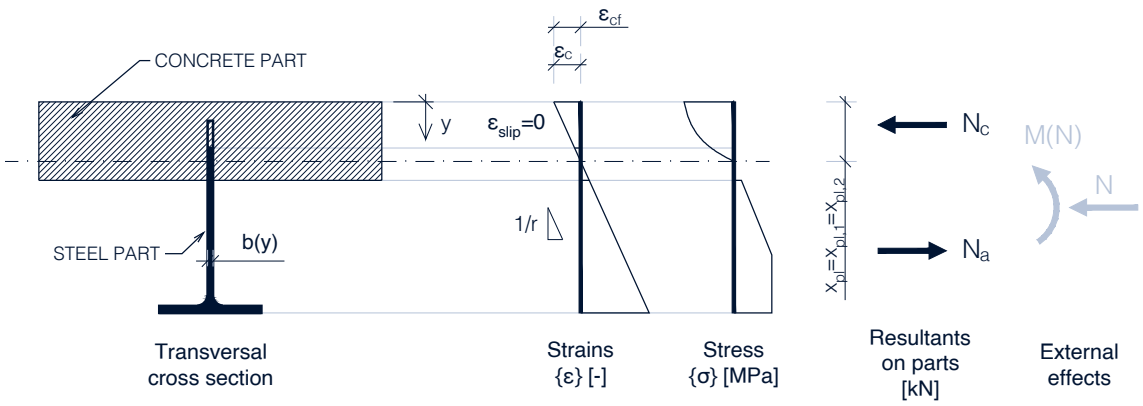

Figure 3.10: generic full shear interaction deformed state on the composite section: calculation scheme

By adding this constraint to the pure bending $N = 0$ condition the state of the section is specified just by one free parameter which could be taken for example as the curvature (Fig.3.11).

Moreover if the ULS condition is considered, the failure point has full degree of shear connection, the compression force on concrete part reaches the one of FSC $N_c = N_{cf}$ and the plastic resistant design moment reaches the value of FSC $M_{pl,f,Rd}$.

By projecting the curve to the $M - (1/r)$ plane the moment-curvature curve of the fsi section can be obtained.

Practical way of deriving the zero slip curve is described:

1. Set the curvature $1/r$ to a specified value;
2. Set $\epsilon_c/\epsilon_{cf} = 1$;

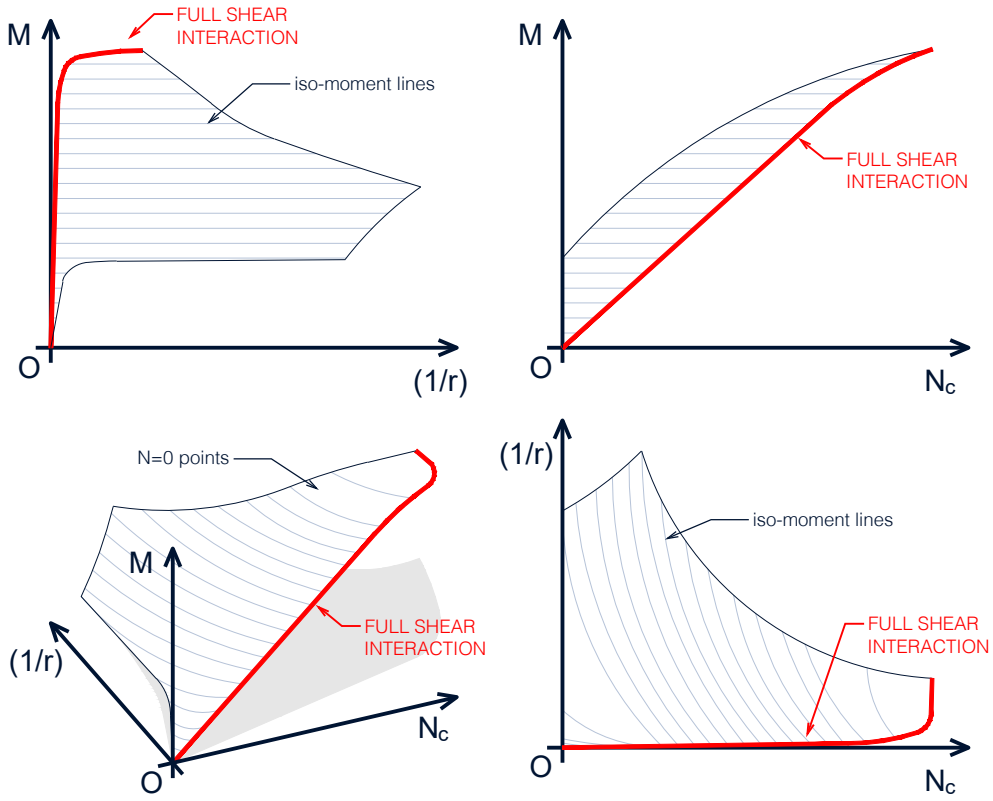

Figure 3.11: moment-concrete compression-curvature surface: FSI region

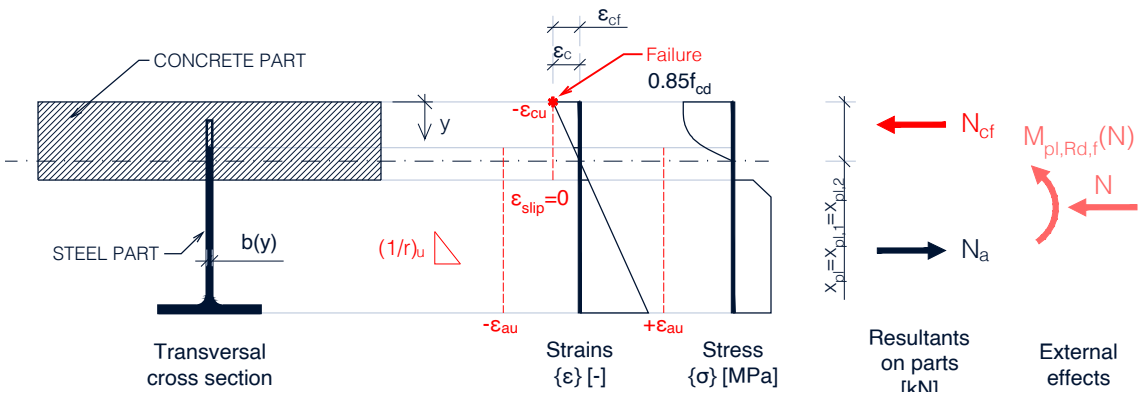

Figure 3.12: ULS-full shear interaction deformed state on the composite section: calculation scheme

3. Search by iterations for the value of ϵ_c (or equivalently ϵ_{cf}) that satisfies $N = 0$.

4. Once the solution is obtained the related quantities such as N_c and M can be derived.

5. Change the curvature at point 1 and repeat.

No shear interaction In Fig.3.13 the points of the surface having no shear connection are identified.

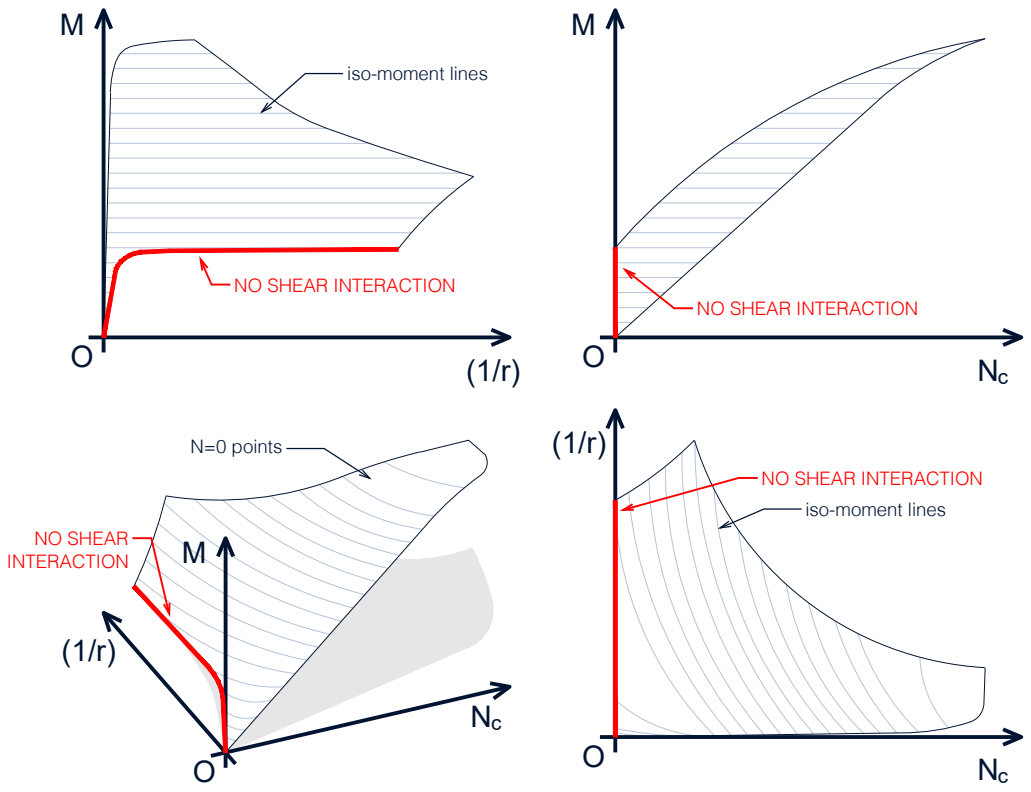

Figure 3.13: moment-concrete compression-curvature surface: zero shear interaction region

Numerical computation method for strain limited design In [97] a few techniques in order to implement a strain limited approach are given. In this work a fiber method has been exploited in order to derive the sectional model. The accuracy of this method depends on the discretization step. In this work a constant discretization step of $1\ mm$ has been exploited. The work [97] provides also interesting observations in order to improve the computational efficiency implementing a non constant fibre step.
More efficient ways of computation can be implemented such as "finite cells method", "integral strain methods", "direct analytical methods" according to [97].

3.3.3 Shear connection model

The mechanical behaviour of the shear connection is described by the characteristic curve of the shear connection. Due to the fact that in the following procedure the shear flow v_L is used as the reference quantity for the continuous approach, the reference shear connection model will be a shear flow-slip $v_L - \delta$ curve (Fig.3.14) rather than a bearing force-slip $P - \delta$ one. The shear flow as a function of slip is derived by simply dividing the bearing force P by the dowel spacing e_x:

$$v_L(\delta) = P(\delta)/e_x \tag{3.34}$$

Notice that the dowel spacing e_x is constant along the x coordinate.

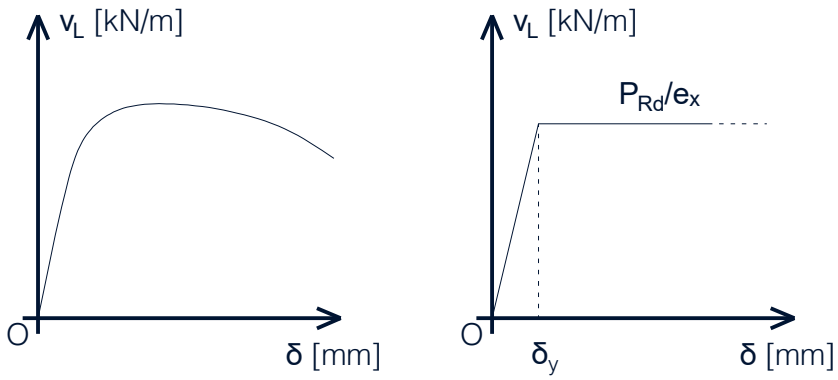

Figure 3.14: shear flow-slip shear connection's law. Right: model behaviour; Left: real behaviour

For the following numerical procedure the simplified bi-linear model elastic-perfectly plastic is used as reference (Fig.3.14 right). This behaviour is described by only two parameters:

- the maximum admissible shear flow P_{Rd}/e_x;
- the yielding slip δ_y

Notice that for two chosen values of these parameters the stiffness k of the shear connection is given by:

$$k = \frac{P_{Rd}/e_x}{\delta_y} \tag{3.35}$$

More realistic models can be implemented in the following procedure such as the curves introduced by Claßen in [32] and [38] modelling respectively the pry-out failure and the steel failure of the dowel. In order to keep the things simple and to gain sensitivity with the basic parameters a simple bi-linear model is exploited in the following sections.

Another important parameter of the shear connection model is the slip ultimate capacity δ_u. This parameter plays a key role in the present study but will be introduced just after the derivations of the required slip resulting from the present model.

3.3.4 Equilibrium on the concrete part

The differential way of writing the equilibrium equation consists in considering an infinitesimally small part of the concrete part of length dx and listing the acting forces on the boundaries of the considered piece write the equilibrium relation. With reference at the figure Fig. 3.15, the following equation is written:

$$N_c(x) + dN_c(x) + v_L(x)dx = N_c(x) \tag{3.36}$$

Therefore, the following differential expression can be derived:

$$\frac{d\,N_c(x)}{dx} = -v_L(x) \tag{3.37}$$

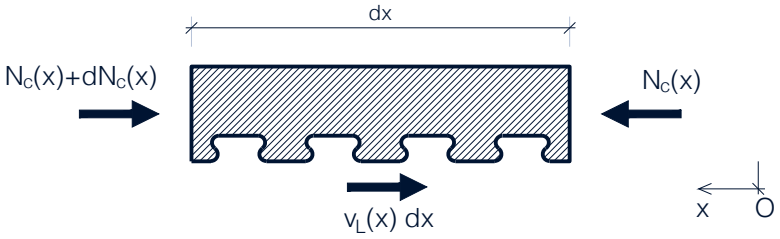

Figure 3.15: free body diagram: acting forces on an infinitesimally small concrete slab piece

This relation states that the changing ratio of the concrete part compression along the beam is the shear flow $v_L(x)$ changed with sign. Therefore, following the assumptions, if a positive shear flow acts on the beam the compression force on the concrete N_c part will decrease with x.
Notice that, following from the previous written relations at shear connection level the way v_L changes with the x coordinate is directly affected by the slip function:

$$v_L(x) = v_L(\delta(x)) \tag{3.38}$$

3.3.5 Kinematic compatibility of the shear connection

The slip δ is related with the slip strain with the following relation (Fig.3.16):

$$\frac{d\,\delta(x)}{dx} = \epsilon_{slip}(x) \tag{3.39}$$

At a positive slip strain at sectional level directly follows an increase of the slip of the shear connection.
Notice that, following from the previous written relations at sectional level the way ϵ_{slip} changes with the x coordinate is directly affected by the compression force on the concrete part and the bending moment $M(x)$:

$$\epsilon_{slip}(x) = \epsilon_{slip}(N_c(x), M(x)) \tag{3.40}$$

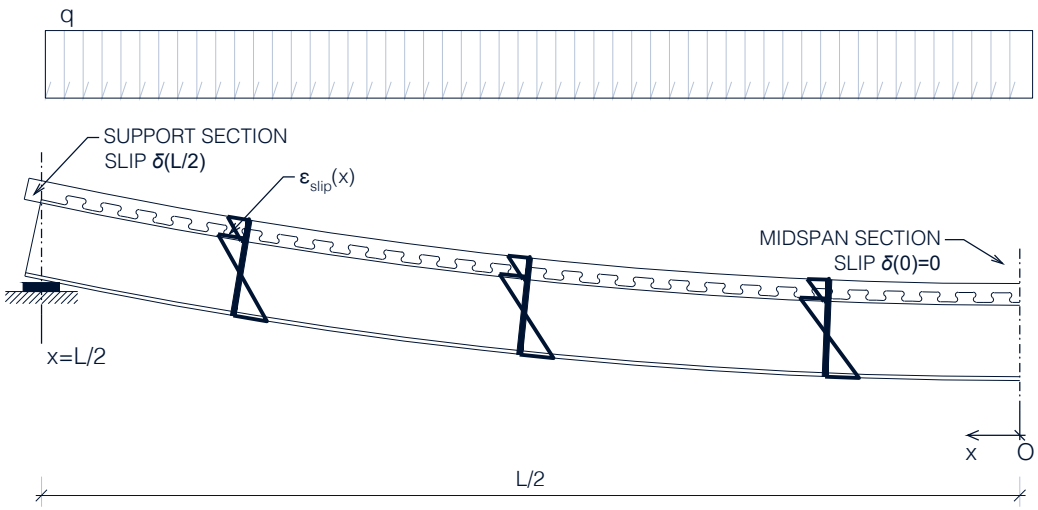

Figure 3.16: kinematic overview

3.3.6 Element model

While the sectional behaviour is described by the $M - N_c - (1/r)$ surface and the shear connection by the assumed $v_L - \delta$ model derived from the dowel characteristic curve, the quantities are related by the following ODEs system:

$$\begin{cases} \frac{d\,N_c(x)}{dx} = -v_L(\delta(x)) \\ \frac{d\,\delta(x)}{dx} = \epsilon_{slip}(N_c(x), M(x)) \end{cases} \tag{3.41}$$

This is a system composed by a pair of nonlinear first-order non-homogeneus differential equations. The equations are coupled and a mutual dependency of the quantities $\delta(x)$ and $N_c(x)$ can be observed. The signs in the equations directly follow from the assumption of the reference frame. In case of a flipped reference frame, starting from the support, pointing midspan, the signs have to be swapped.
Notice that because of the statically determinate situation, there is no dependency of the moment distribution on the internal stiffness variation of the element.

Boundary conditions

In addition of the previous described differential equations which govern the relations between slip and slip strain, compression on concrete part and shear flow in the studied domain ($x \in (0, L/2)$), the following boundary conditions have to be satisfied:

- Zero slip at midspan section:

$$\delta(x = 0) = 0.00\,mm \tag{3.42}$$

  This condition applies because of symmetry reasons.

- Zero compression on the concrete part at the support section

$$N_c(x = L/2) = 0.00\,kN \tag{3.43}$$

This condition applies because at support there is no external axial force applied at the concrete slab.

Rotation and deflection

Following from the assumed small deflection Euler-Bernoulli theory, the kinematic compatibility relations between the curvature, the rotation and deflection are valid:

$$(1/r)(x) = \frac{d\,\phi(x)}{dx} \tag{3.44}$$

$$\phi(x) = \frac{d\,y(x)}{dx} \tag{3.45}$$

Knowing the curvature function $(1/r)(x)$, rotation and deflections can be derived by integration:

$$\phi(x) = \phi(0) + \int_{x'=0}^{x'=x} (1/r)(x')\,dx' \tag{3.46}$$

$$y(x) = y(L/2) - \int_{x'=L/2}^{x'=x} \phi(x')\,dx' \tag{3.47}$$

Where the values of $\phi(0)$ and $y(L/2)$ are the one which permit the satisfaction of the constraint boundary conditions. For the simply supported beam:

$$y(L/2) = 0 \tag{3.48}$$

$$\phi(0) = 0 \tag{3.49}$$

3.3.7 Additional observations

Second derivative of N_c and δ

Applying the chain derivative rule to the shear flow function and the slip strain function is possible to derive:

$$\frac{d\,v_L(x)}{dx} = \frac{d\,v_L(\delta(x))}{dx} = \frac{d\,v_L(\delta)}{d\delta} \cdot \frac{d\,\delta(x)}{dx} = \frac{d\,v_L(\delta)}{d\delta} \cdot \epsilon_{slip}(x) \tag{3.50}$$

$$\begin{aligned} \frac{d\,\epsilon_{slip}(x)}{dx} &= \frac{d\,\epsilon_{slip}(M(x), N_c(x))}{dx} = \\ &= \frac{d\,\epsilon_{slip}(M)}{dM} \cdot \frac{d\,M(x)}{dx} + \frac{d\,\epsilon_{slip}(N_c)}{dN_c} \cdot \frac{d\,N_c(x)}{dx} = \\ &= \frac{d\,\epsilon_{slip}(M)}{dM} \cdot V(x) - \frac{d\,\epsilon_{slip}(N_c)}{dN_c} \cdot v_L(x) \end{aligned} \tag{3.51}$$

Thus the second derivatives of N_c and δ are:

$$\frac{d^2\,N_c}{dx^2} = -\frac{d\,v_L(x)}{dx} = -\frac{d\,v_L(\delta)}{d\delta} \cdot \epsilon_{slip}(x) \tag{3.52}$$

$$\frac{d^2\,\delta}{dx^2} = \frac{d\,\epsilon_{slip}(x)}{dx} = \frac{d\,\epsilon_{slip}(M)}{dM} \cdot V(x) - \frac{d\,\epsilon_{slip}(N_c)}{dN_c} \cdot v_L(x) \tag{3.53}$$

Local linearization

Assuming a local linearization of $M - N_c - \epsilon_{slip}$ and $v_L - \delta$, namely:

$$\epsilon_{slip} = \epsilon_{slip,0} + k_1 \cdot M + k_2 \cdot N_c \tag{3.54}$$

$$v_L = k_3 \cdot \delta \tag{3.55}$$

The previously written relations become:

$$\frac{d\, v_L}{dx} = k_3 \cdot \epsilon_{slip} \tag{3.56}$$

$$\frac{d\, \epsilon_{slip}}{dx} = k_1 \cdot V(x) - k_2 \cdot v_L \tag{3.57}$$

3.4 Numerical method description

The applied numerical method consists in a forward finite differences method. The studied domain is discretized in n slices as shown in figure Fig.3.17. The length of the discretization step Δx is therefore:

$$\Delta x = \frac{L/2}{n-1} \tag{3.58}$$

The continuous domain $x \in [0, L/2]$ becomes a set of coordinates x_i for $i = 1, 2, ..., n$. The continuous functions in the continuous domain are defined on the discrete domain with the correspondent values:

$$\{x,\ M(x),\ v_L(x),\ N_c(x),\ \delta(x),\ \epsilon_{slip}(x),\ (1/r)(x),\ \phi(x),\ y(x)\} \quad \text{with} \quad x \in [0, L/2] \tag{3.59}$$

$$\{x_i,\ M_i,\ v_{L,i},\ N_{c,i},\ \delta_i,\ \epsilon_{slip,i},\ (1/r)_i,\ \phi_i,\ y_i\} \quad \text{for} \quad i = 1, 2, ..., n \tag{3.60}$$

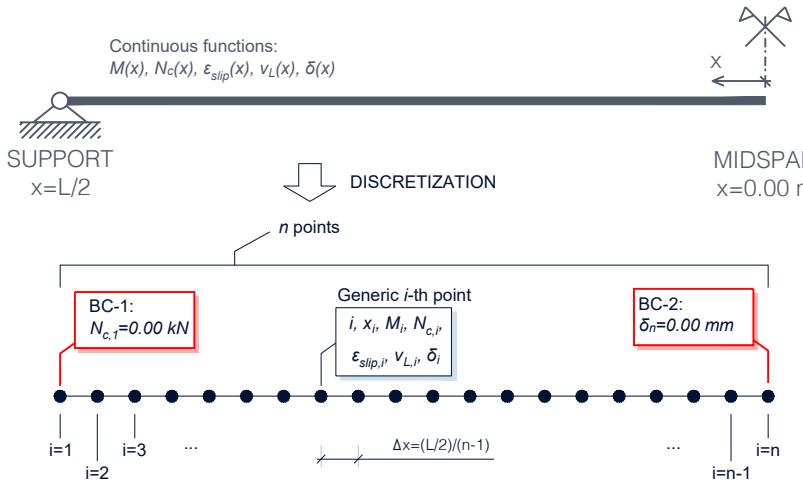

Figure 3.17: element discretisation

In the discretized domain the first derivatives are approximated by a forward difference method. Following relations can be derived:

$$\epsilon_{slip,i} = \frac{\delta_{i+1} - \delta_i}{\Delta x} \tag{3.61}$$

$$v_{L,i} = -\frac{N_{c,i+1} - N_{c,i}}{\Delta x} \tag{3.62}$$

Knowing the quantities related to the i-th element, the quantities of the following $(i+1)$-th element can be derived by inverting the previously written relations:

$$\delta_{i+1} = \epsilon_{slip,i} \cdot \Delta x + \delta_i \tag{3.63}$$

$$N_{c,i+1} = N_{c,i} - v_{L,i} \cdot \Delta x \tag{3.64}$$

The terms $\epsilon_{slip,i}$ and $v_{L,i}$ are locally determined respectively from the $M - N_c - (1/r)$ surface of the section and the $v_L - \delta$ curve of the shear connection from the following relations:

$$\epsilon_{slip,i} = \epsilon_{slip}(M_i, N_{c,i}) \tag{3.65}$$

$$v_{L,i} = v_L(\delta_i) \tag{3.66}$$

Boundary conditions consists in the following relations:

$$N^*_{c,i=1} = N_c(x = L/2) = 0 \tag{3.67}$$

$$\delta^*_{i=n} = \delta(x = 0) = 0 \tag{3.68}$$

The numerical method consists in applying the first boundary condition $N_{c,1} = N^*_{c,i=1} = 0$ and guessing the value of $\delta_1 = \delta_1^{(guess)}$. By numerical integration exploiting equations 3.63 and 3.64 the values $\delta_i, N_{c,i}$ are derived at every point of the discretized domain (for i in 1,2,...,n). The second known boundary condition is then checked:

$$\delta_n \stackrel{?}{=} \delta^*_n \tag{3.69}$$

If the condition is verified, then the guess value $\delta_1^{(guess)}$ was the one respecting both boundary conditions for the given governing equations in the domain. If not a new $\delta_1^{(guess)}$ value has to be tried.

Because of the structure of the numerical method, first guessing the boundary conditions on one side of the domain and then verifying if the second boundary condition is met on the other side of the domain, the applied method is often referred in literature as "shooting method".

Notice that the moment distribution $M(x)$ for a static determined structure such as the one of the case study is known a priori from the structural analysis. The discrete values $M_i = M(x_i)$ are therefore a given data of the problem and are not changing performing the iterative process of searching the correct value of $\delta_1^{(guess)}$.

Because of the boundary conditions and the imposed external bending moment the values $v_{L,n}$ and $\epsilon_{slip,1}$ are also known. In detail:

$$v_{L,n} = v_L(\delta_n) = 0.00\ kN/m \tag{3.70}$$

$$\epsilon_{slip,1} = \epsilon_{slip}(M_1, N_{c,1}) = 0.0 \tag{3.71}$$

The numerical method can be visualized as structured in matrix form:

$$1/\Delta x \cdot \begin{pmatrix} 1 & -1 & 0 & & & \\ 0 & 1 & -1 & 0 & & \\ & 0 & 1 & -1 & 0 & \\ & & \ddots & \ddots & \ddots & \\ & & 0 & 1 & -1 & 0 \\ & & & 0 & 1 & -1 \end{pmatrix} \begin{pmatrix} N_{c,1} \\ N_{c,2} \\ N_{c,3} \\ \vdots \\ N_{c,n-1} \\ N_{c,n} \end{pmatrix} = \begin{pmatrix} v_{L,1} \\ v_{L,2} \\ v_{L,3} \\ \vdots \\ v_{L,n-1} \\ v_{L,n} \end{pmatrix} \tag{3.72}$$

$$1/\Delta x \cdot \begin{pmatrix} -1 & 1 & 0 & & & \\ 0 & -1 & 1 & 0 & & \\ & 0 & -1 & 1 & 0 & \\ & & \ddots & \ddots & \ddots & \\ & & 0 & -1 & 1 & 0 \\ & & & 0 & -1 & 1 \end{pmatrix} \begin{pmatrix} \delta_1 \\ \delta_2 \\ \delta_3 \\ \vdots \\ \delta_{n-1} \\ \delta_n \end{pmatrix} = \begin{pmatrix} \epsilon_{slip,1} \\ \epsilon_{slip,2} \\ \epsilon_{slip,3} \\ \vdots \\ \epsilon_{slip,n-1} \\ \epsilon_{slip,n} \end{pmatrix} \tag{3.73}$$

Rotation and deflection

After the computation of the solution the value of the function $N_c(x)$ is known on the discrete domain. The moment $M(x)$ is known from the structural analysis. So the curvature can be determined uniquely if the $M - N_c - (1/r)$ curvature is monotonically increasing:

$$(1/r, \epsilon_{slip}, \epsilon_{cf}) = f^{-1}(M, N_c, N = 0) \tag{3.74}$$

Thus, with the derivation of the values $N_{c,i}$ and knowing the values M_i for $i = 1, 2, ..., n$, the rotations $(1/r)_i$ can be derived as well:

$$(1/r)_i = (1/r)(M_i, N_{c,i}, N = 0) \tag{3.75}$$

By numerical integration it's possible to derive the values of the rotation ϕ_i and the deflection y_i for each point $i = 1, 2, ..., n$. This is done with a trapezoidal rule numerical integration:

$$\phi_i = \sum_{j=1}^{j=i} 1/2 \cdot ((1/r)_i + (1/r)_{i-1}) \cdot \Delta_x + \phi_1 \quad \text{for} \quad i = 2, 3, ..., n \tag{3.76}$$

Where ϕ_1 is fixed to zero in order to respect the boundary conditions. Similarly:

$$y_i = \sum_{j=n-1}^{j=i} 1/2 \cdot (\phi_i + \phi_{i+1}) - y_n \cdot \Delta x \quad \text{for} \quad i = n-1, n-2, ..., 1 \tag{3.77}$$

Where y_n is fixed to zero in order to respect the boundary conditions.

3.4.1 Visualization of the numerical method

The solution can be visualized as a parametric curve in the $N_c - \delta$ plane varying with x:

$$\gamma(x) = [\delta(x), N_c(x)] \tag{3.78}$$

For this curve, because of the structure of the problem, the velocity is given by the vector:

$$\gamma'(x) = \frac{d\,\gamma(x)}{dx} = \left[\frac{d\,\delta(x)}{dx}, \frac{d\,N_c(x)}{dx}\right] = [\epsilon_{slip}(M(x), N_c(x)),\ v_L(\delta(x))] \tag{3.79}$$

If a constant value of M is considered a velocity field can be constructed in the $N_c - \delta$ plane (Fig.3.18). Notice that in correspondence of the $N_c = 0$ axis if the moment is such that $M = 0$, the velocities are vertical because the first component of the velocity is zero for $N_c = 0$ following from the $M - N_c - (1/r)$ surface:

$$\epsilon_{slip}(M = 0, N_c = 0) = 0 \tag{3.80}$$

Equally the velocities are horizontal in correspondence of the $\delta = 0$ axis. This is because the second component of the velocity is zero for $\delta = 0$:

$$v_L(\delta = 0) = 0 \tag{3.81}$$

Because of the variable moment $M(x)$ as function of x, the velocity field is also changing with the coordinate x because of the dependency of ϵ_{slip} with the bending moment M.

The integration process can be visualized as a curve following the velocity field for a given starting point. As more starting conditions are given more streamlines can be obtained. The searched solution can be imagined as a curve remaining tangent at the velocity field in every point as the coordinate x varies and respecting the boundary conditions $\delta(x = 0) = 0$ and $N_c(x = L/2) = 0$. These last conditions are met if the curve starts on the horizontal axis $N_c = 0$ for $x = L/2$ and ends up on the vertical axis $\delta = 0$ for $x = 0$. The iterative numerical "shooting" method is based on the progressive changing of the first point coordinate $\delta(L/2)^{guess}$ and integration in order to find the curve which ends for $x = 0$ with a zero slip condition $\delta = 0$, respecting the second boundary condition. Notice that as the solution is found, the compressive force on the concrete part at midspan $N_c(0)$ value comes out as a result.

The solution can be represented in the $\delta - N_c$ plane, noting that on the found streamline the moment can be variable. Thus in a generic solution with $M(x)$ changing with x would not be correct to unwrap the velocity field for a constant moment with the resulting curve.

Notice that, as the value of ϵ_{slip} is given by the $M - N_c - (1/r)$ surface which is defined on a restricted domain, some curves may loose the $M - N_c - (1/r)$ surface requesting "out of domain" points. In this case the integration is stopped, and the curve interrupts for coordinates which are less than correspondent to an intermediate point between the support section and the midspan section. If this happens the found curve is treated as wrong.

As the solution is found the values of the function $N_c(x)$ are known on the discrete numerical method domain. Thus, knowing for every point also the value of the bending moment, the state of the element can be visualized on the $M - N_c - (1/r)$ surface.

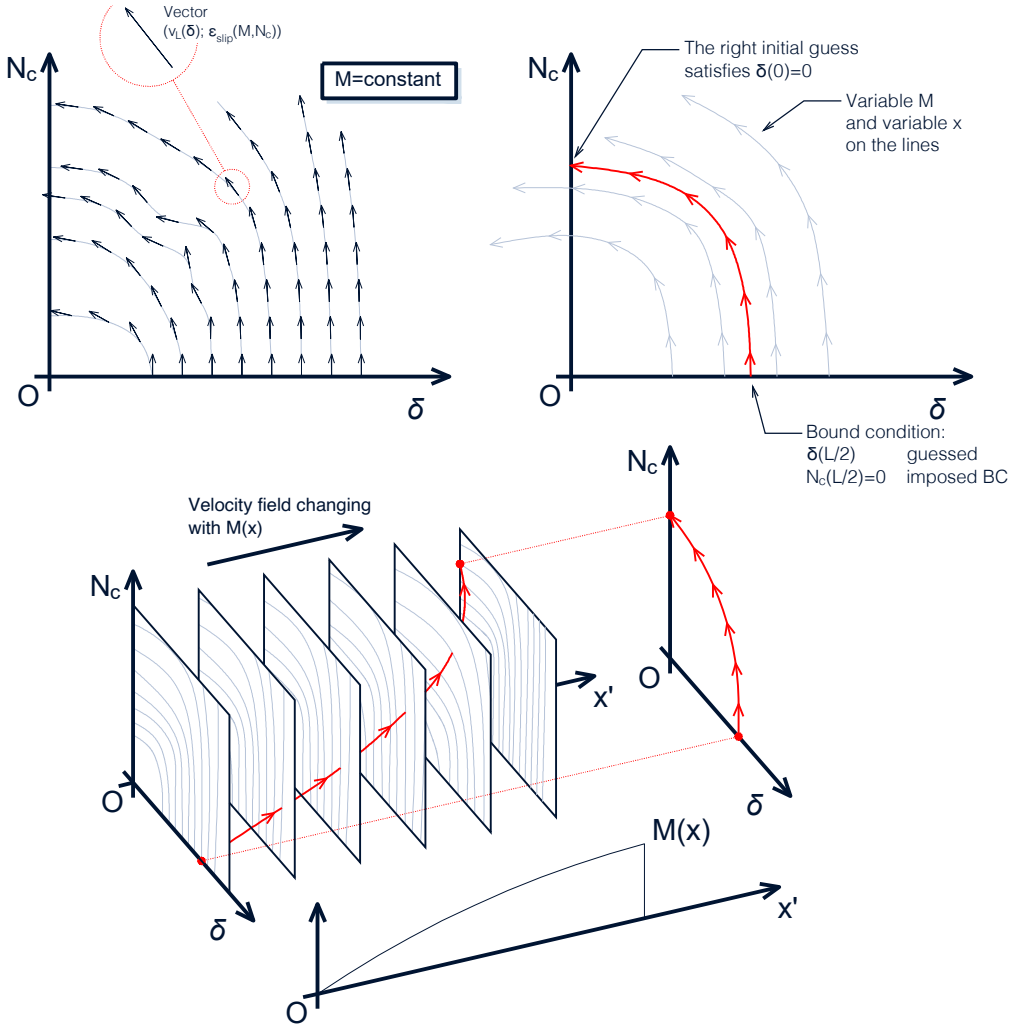

Figure 3.18: numerical shooting method visualisation

3.5 Numerically solved examples

In the present section five examples are introduced, numerically resolved and discussed. Every studied case has the same cross-section and the same span length:

$$L = 16.000\, m \tag{3.82}$$

3.5.1 Example 1: fully elastic case

The first example is a low level load case with both the shear connection and the sections behaving in a linear elastic way. The input data are as follows:

- $M_{Ed} = 1350\, kNm$
- $P_{Rd}/e_x = 1237.5\, kN/m$
- $\delta_y = 2\, mm$

Notice that the acting bending moment is much lower compared with the plastic bending moment of the composite section in the full shear connection case:

$$M_{Ed} << M_{pl,f,Rd} \tag{3.83}$$

Furthermore, considering the shear connection, the average shear flow for the full shear connection case is less than half the maximum admissible shear flow:

$$\frac{N_{cf}}{L/2} < 1/2 \cdot P_{Rd}/e_x \tag{3.84}$$

Thus, both the cross sectional behaviour and the shear connection's one, are expected to be fully elastic. The resulting diagrams are shown below.
As expected, the moment is proportional to curvature and the shear flow is proportional to the slip, confirming the elastic behaviour (Fig.3.19). The maximum slip occurs in the support region and it's around $1\, mm$. The solution occupies the elastic region on the $M - N_c - (1/r)$ surface (Fig.3.20):
The solution streamline can be represented in the $N_c - \delta$ plane (Fig.3.21). The satisfaction of the bound conditions can be observed. A high dependency of the streamline path with the starting conditions can be observed.

3.5.2 Example 2: close to ULS, full shear connection case with elastic shear connection

The second example is a higher level load case, with the midspan section approaching the ultimate limit state and the shear connection behaving in a linear elastic way. The input data are as follows:

- $M_{Ed} = 1842\, kNm$

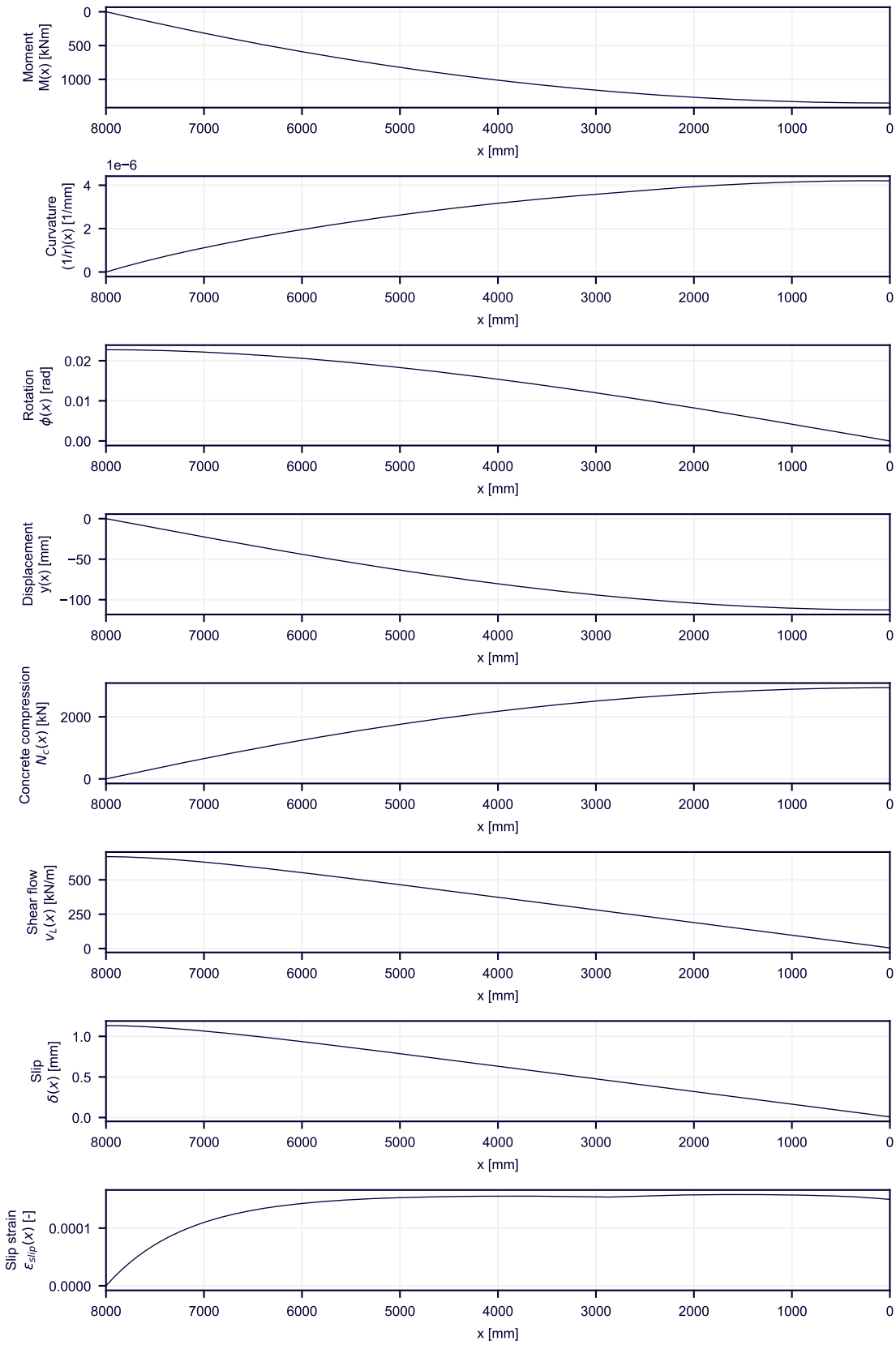

Figure 3.19: Example 1: diagrams

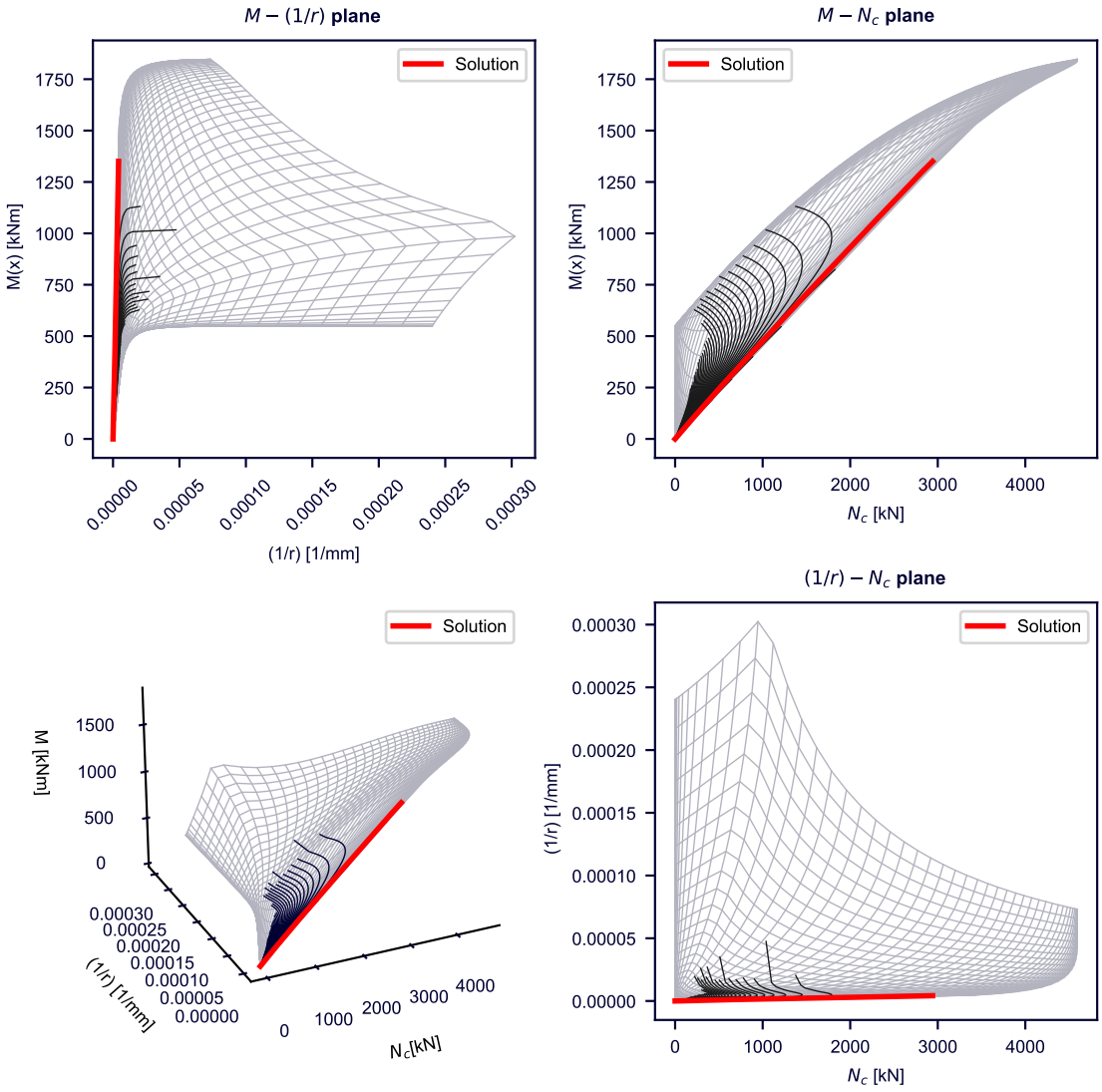

Figure 3.20: Example 1: moment-concrete compression-curvature surface

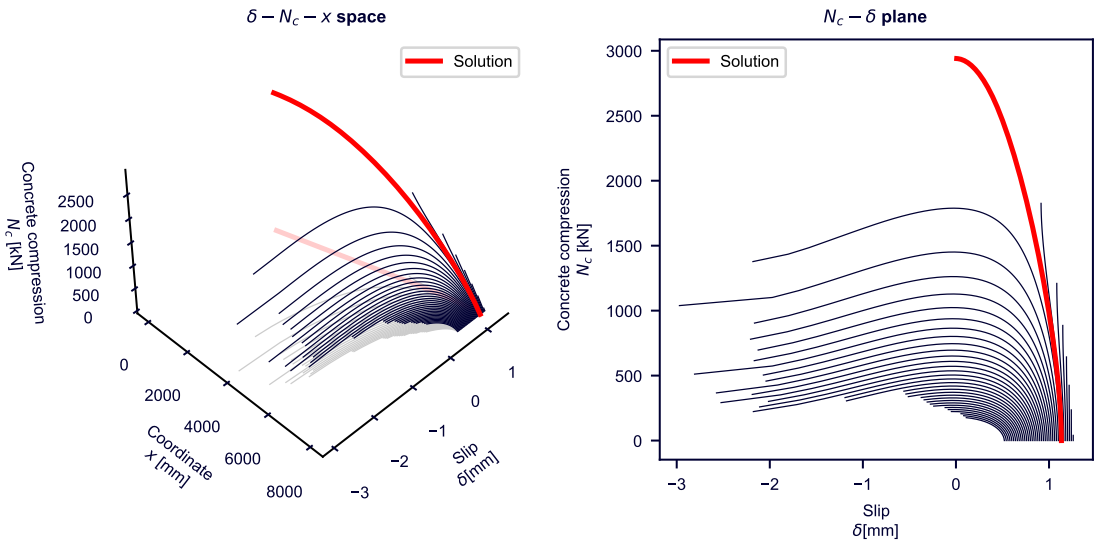

Figure 3.21: Example 1: numerical method streamlines

- $P_{Rd}/e_x = 1237.5\,kN/m$
- $\delta_y = 2\,mm$

In this case the bending acting moment is really close to the bending design resistance of the section in the full shear connection case:

$$M_{Ed} \approx M_{pl,f,Rd} \tag{3.85}$$

Like in the previous example, considering the shear connection, the average shear flow for the full shear connection case is less than half the maximum admissible shear flow:

$$\frac{N_{cf}}{L/2} < 1/2 \cdot P_{Rd}/e_x \tag{3.86}$$

The studied case is expected to reach a failure state in a full shear connection condition. Because of the strong elastic behaving shear connection, a full shear connection with no redistribution is expected. The resulting diagrams are shown below (Fig.3.22).

While the shear flow is still proportional with slip like in the previous example, the moment looses its proportionality with the curvature. A sharp increasing of the curvatures appears in the midspan region testifying the yielding of the central part of the element. In the shear flow and in the slip diagram a hump appears in the central part of the element. This is reconcilable with the higher curvature and consequent higher slip strain in the region. Because of the fact that the slip strain ϵ_{slip} is the first derivative of the slip δ, where the slip strain increases the hump appears as a result of the integration process. This phenomenon is also observed in [97]. The slip maximum demand along the beam occurs at the support region and is about $\delta_{max} = \delta(L/2) = 1.5\,mm$.

The solution occupies the FSC region on the $M - N_c - (1/r)$ surface (Fig.3.23). The midspan section is approaching the ULS.

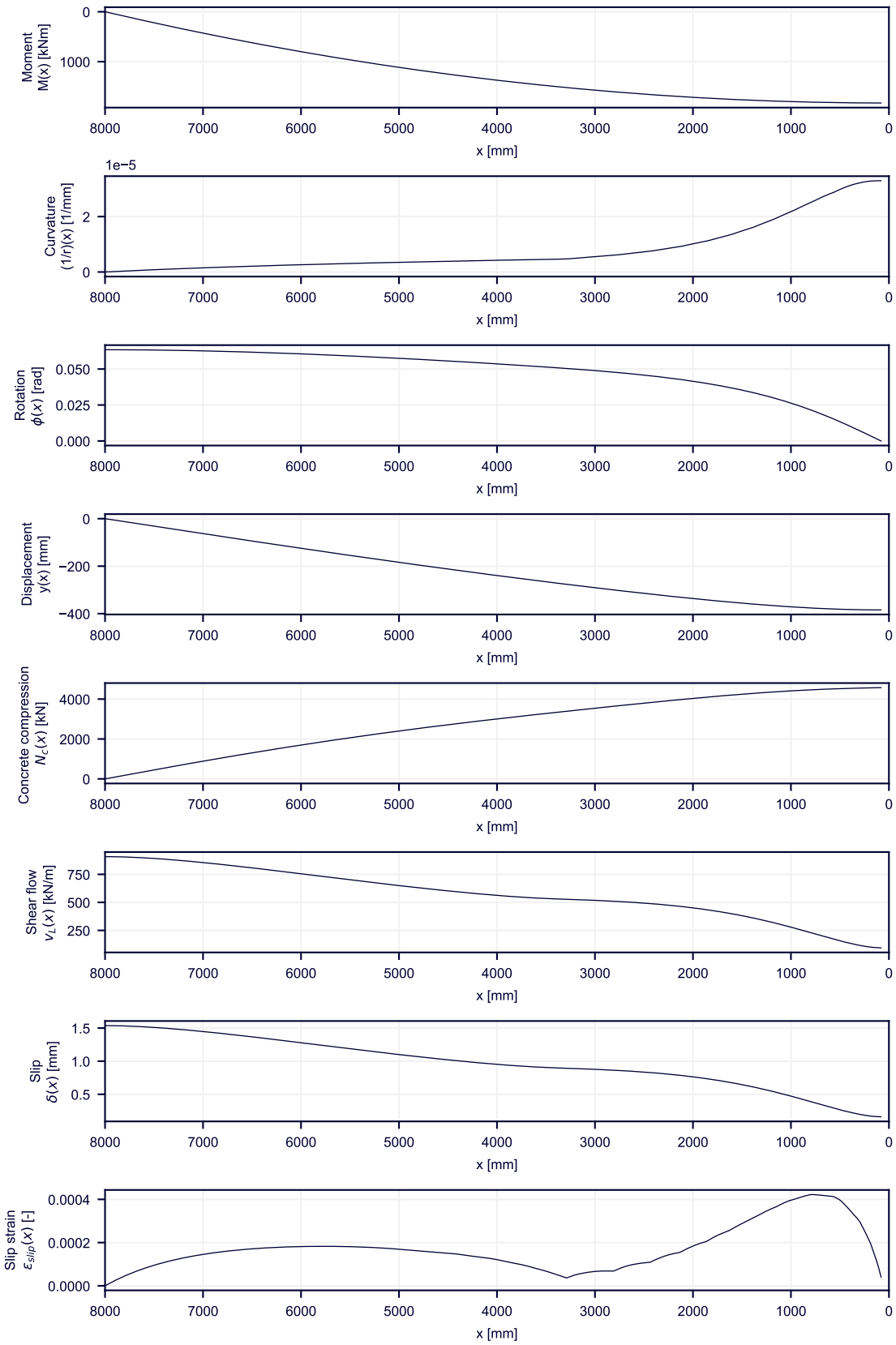

Figure 3.22: Example 2: diagrams

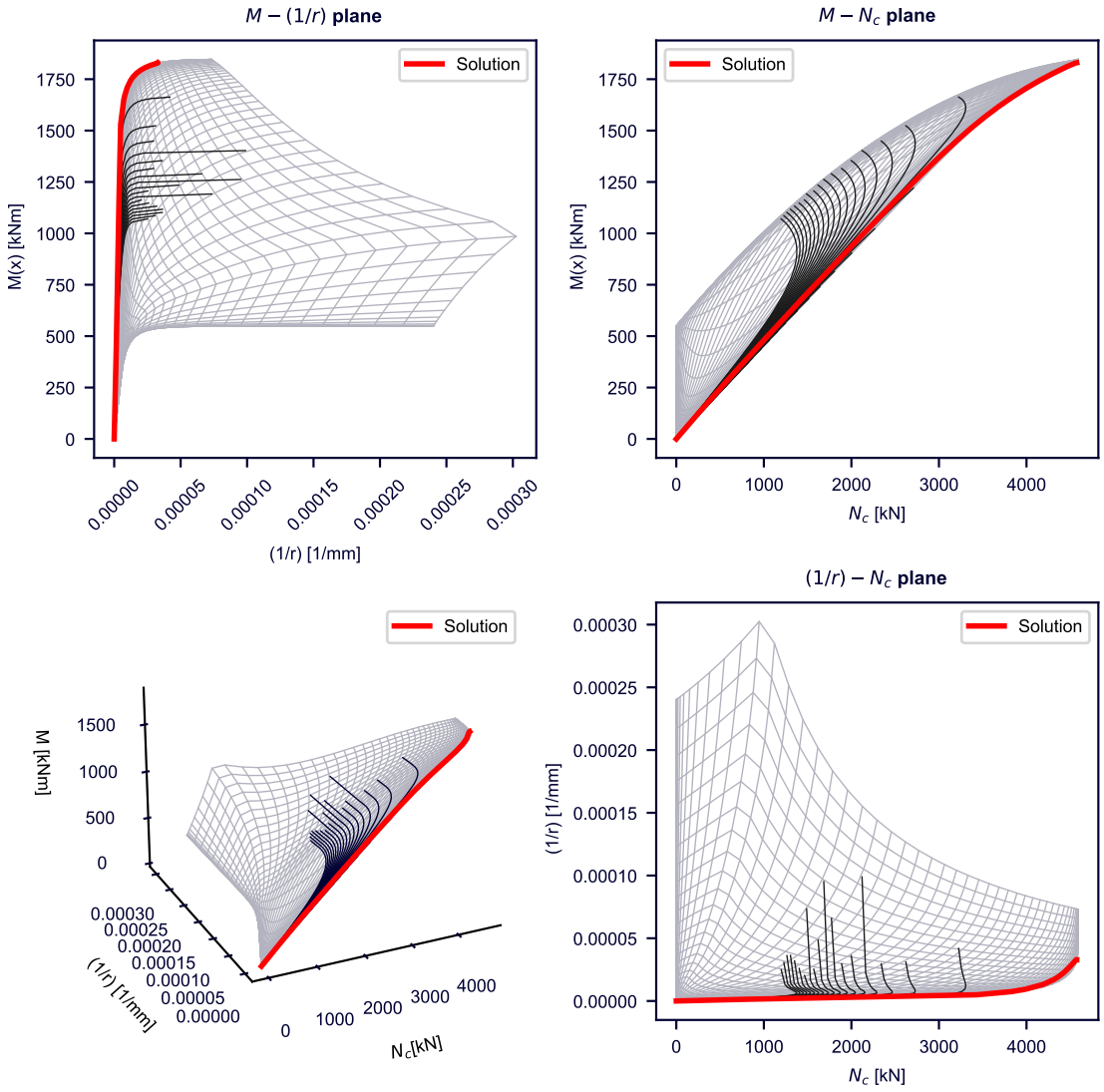

Figure 3.23: Example 2:Moment-concrete compression-curvature surface

The solution streamline can be represented in the $N_c - \delta$ plane (Fig.3.24). The satisfaction of the bound conditions can be observed. A high dependency of the streamline path with the starting conditions can be observed. Notice that in proximity of the $\delta = 0$ axis the derivative of the solution is not completely horizontal, this can be brought back to a numerical error of closing because of the tolerance condition in the iterative loop.

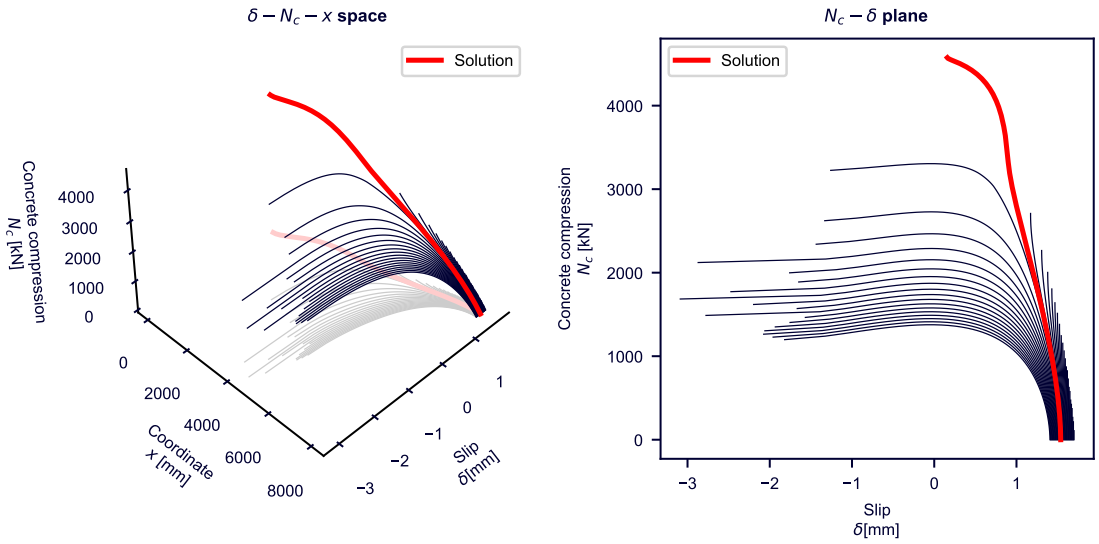

Figure 3.24: Example 2: numerical method streamlines

3.5.3 Example 3: close to ULS, full shear connection case with redistribution along the shear connection

The third example has the same load level as the second example. Differently, the resistance of the shear connection is set to a lower level.

The input data are as follows:

- $M_{Ed} = 1842\, kNm$
- $P_{Rd}/e_x = 731.3\, kN/m$
- $\delta_y = 1\, mm$

In this case the bending acting moment is really close to the bending design resistance of the section in the full shear connection case:

$$M_{Ed} \approx M_{pl,f,Rd} \tag{3.87}$$

Considering the shear connection, the average shear flow for the full shear connection case is greater than half but less than the maximum admissible shear flow:

$$\cdot 1/2 \cdot P_{Rd}/e_x < \frac{N_{cf}}{L/2} < \cdot P_{Rd}/e_x \tag{3.88}$$

The studied case is expected to reach a failure state in a full shear connection condition and a plastic redistribution is expected along the shear connection. The resulting diagrams are shown below (Fig.3.25). Like in the previous case, a sharp increase of the curvature in the midspan region shows, testifying the plastic hinge formation reaching the failure state. Differently, the shear flow is no more proportional to the slip. The maximum admissible shear flow is reached and redistribution occurs. The slip maximum demand along the beam occurs at the support region and is about $\delta_{max} = \delta(L/2) = 3\,mm$. The solution does no more occupy the zero slip condition region in the $M - N_c - (1/r)$ surface (Fig.3.26).
The solution streamline can be represented in the $N_c - \delta$ plane (Fig.3.27).

3.5.4 Example 4: close to ULS, partial shear connection

The fourth example presents a lower load level compared with the second and third examples. The resistance of the shear connection is set to an even lower value respect with the third example.
The input data are as follows:

- $M_{Ed} = 1611\,kNm$
- $P_{Rd}/e_x = 421.9\,kN/m$
- $\delta_y = 1\,mm$

Notice that the acting bending moment is lower compared with the plastic resistant design moment for the full shear connection case:

$$M_{Ed} < M_{pl,f,Rd} \tag{3.89}$$

The average shear flow in the full shear connection case surpasses the maximum admissible shear flow:

$$\frac{N_{cf}}{L/2} > P_{Rd}/e_x \tag{3.90}$$

Therefore the beam is expected to fail for a lower bending moment compared with the plastic resistant design bending moment in the FSC case. The shear connection is not capable of transferring the whole maximum concrete compression N_{cf} between the two critical sections. Thus, is the resistant bending moment which has to adapt to the limited bearing capacity of the shear connection. The resulting diagrams are shown below (Fig.3.28).
The shear connection is nearly fully yielded. The midspan region of the shear connection is still behaving elastically. This is because of the fact that boundary condition $\delta(0) = 0$ has to be fulfilled and imposes also a sorrounding part to behave elastically. Notice that in this case the yielding region of the beam at sectional level is no more the midspan zone. A sharp increase of the curvatures occurs not at midspan. This phenomenon is well represented in the $M - N_c - (1/r)$ surface. The first section that approaches the ULS condition is not the midspan one. The phenomena is also recognized in [28].
The slip maximum demand along the beam occurs at the support region and is $\delta_{max} = \delta(L/2) = 40\,mm$ showing a relevant increase respect with the previous studied example (Example 3).

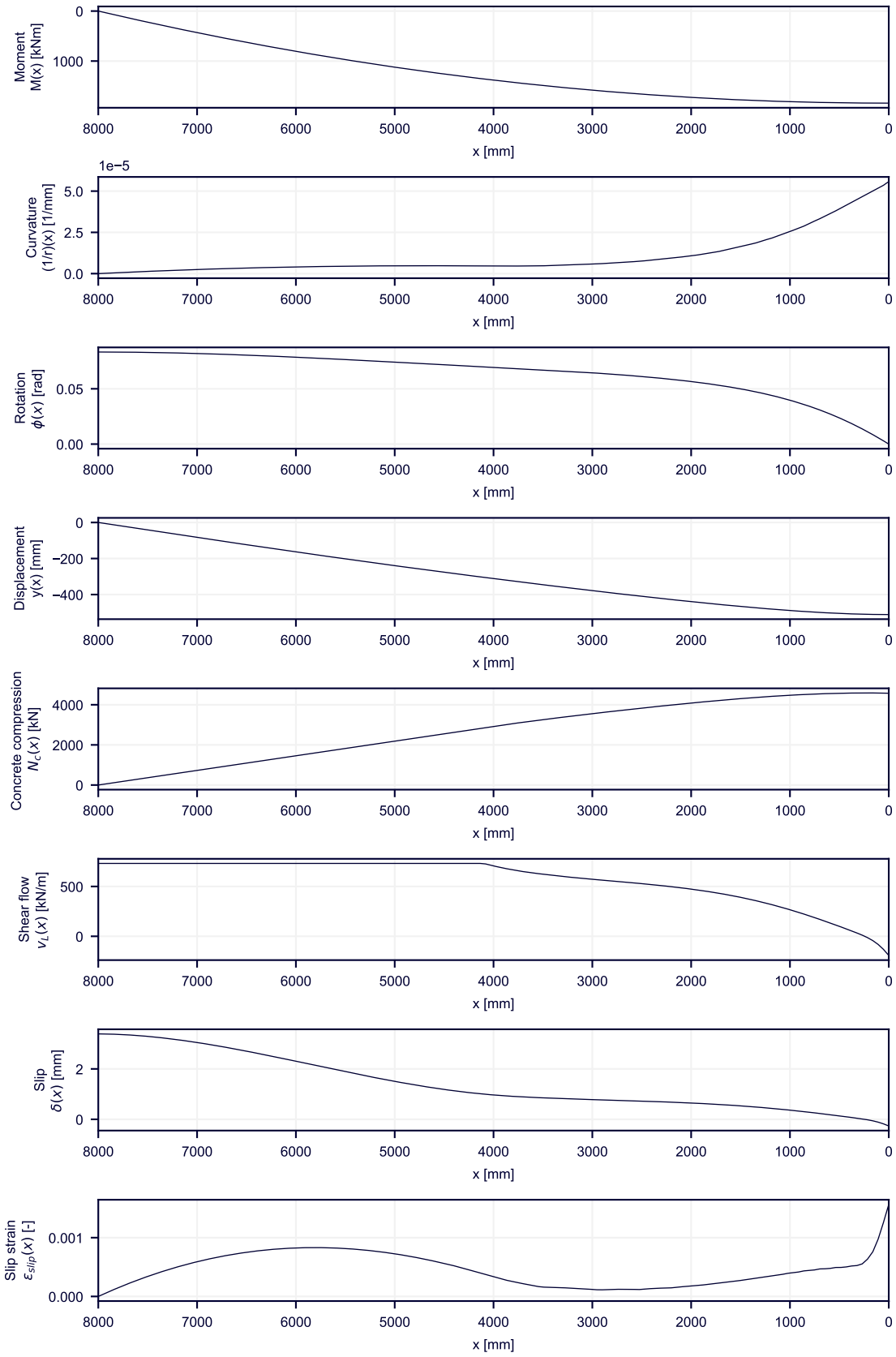

Figure 3.25: Example 3: diagrams

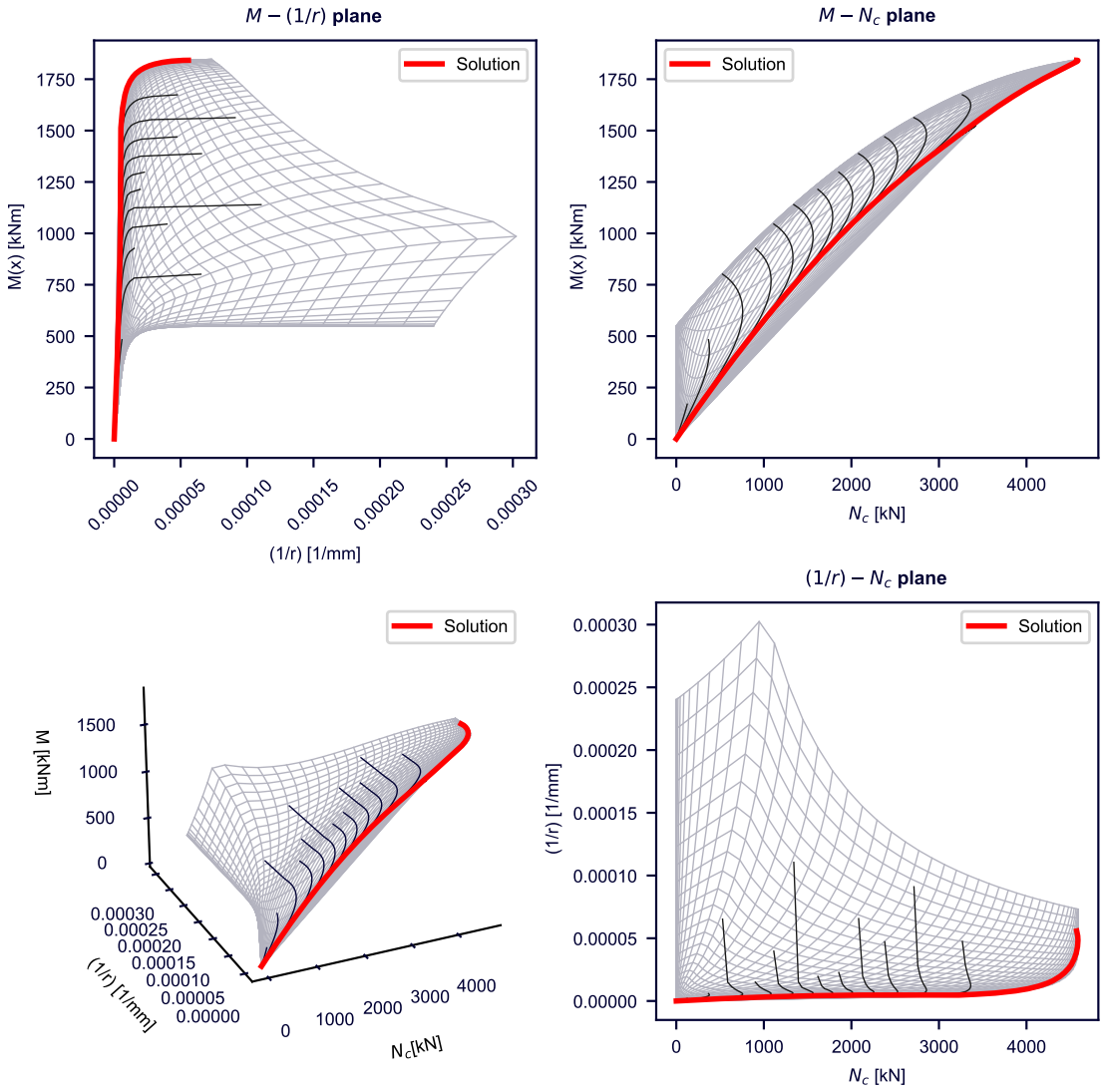

Figure 3.26: Example 3: moment-concrete compression-curvature surface

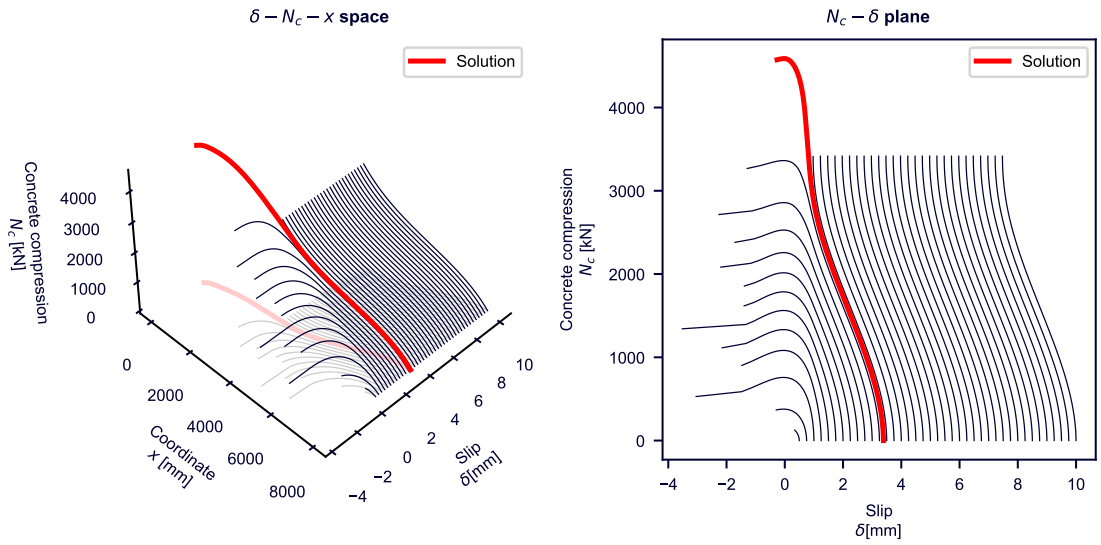

Figure 3.27: Example 3: numerical method stramlines

The solution is represented on the $M - N_c - (1/r)$ surface (Fig.3.29). The approaching ULS of one of the section is well shown in the $M - N_c$ plane with a section almost coincident with one point of the partial shear diagram.

The solution streamline can be represented in the $N_c - \delta$ plane (Fig.3.30). Notice that the the streamline path evolution is less sensitive with the chosen starting conditions compared with the previous studied cases.

3.5.5 Example 5: close to ULS, partial shear connection

Another example similar to the one of example 4 is presented. The load level is set lower and the resistance of the shear connection is set to an even lower value respect with the fourth example.

The input data are as follows:

- $M_{Ed} = 1280\ kNm$
- $P_{Rd}/e_x = 225\ kN/m$
- $\delta_y = 1\ mm$

The acting bending moment is lower compared with the plastic resistant design moment for the full shear connection case:

$$M_{Ed} < M_{pl,f,Rd} \tag{3.91}$$

The average shear flow in the full shear connection case surpasses the maximum admissible shear flow:

$$\frac{N_{cf}}{L/2} > P_{Rd}/e_x \tag{3.92}$$

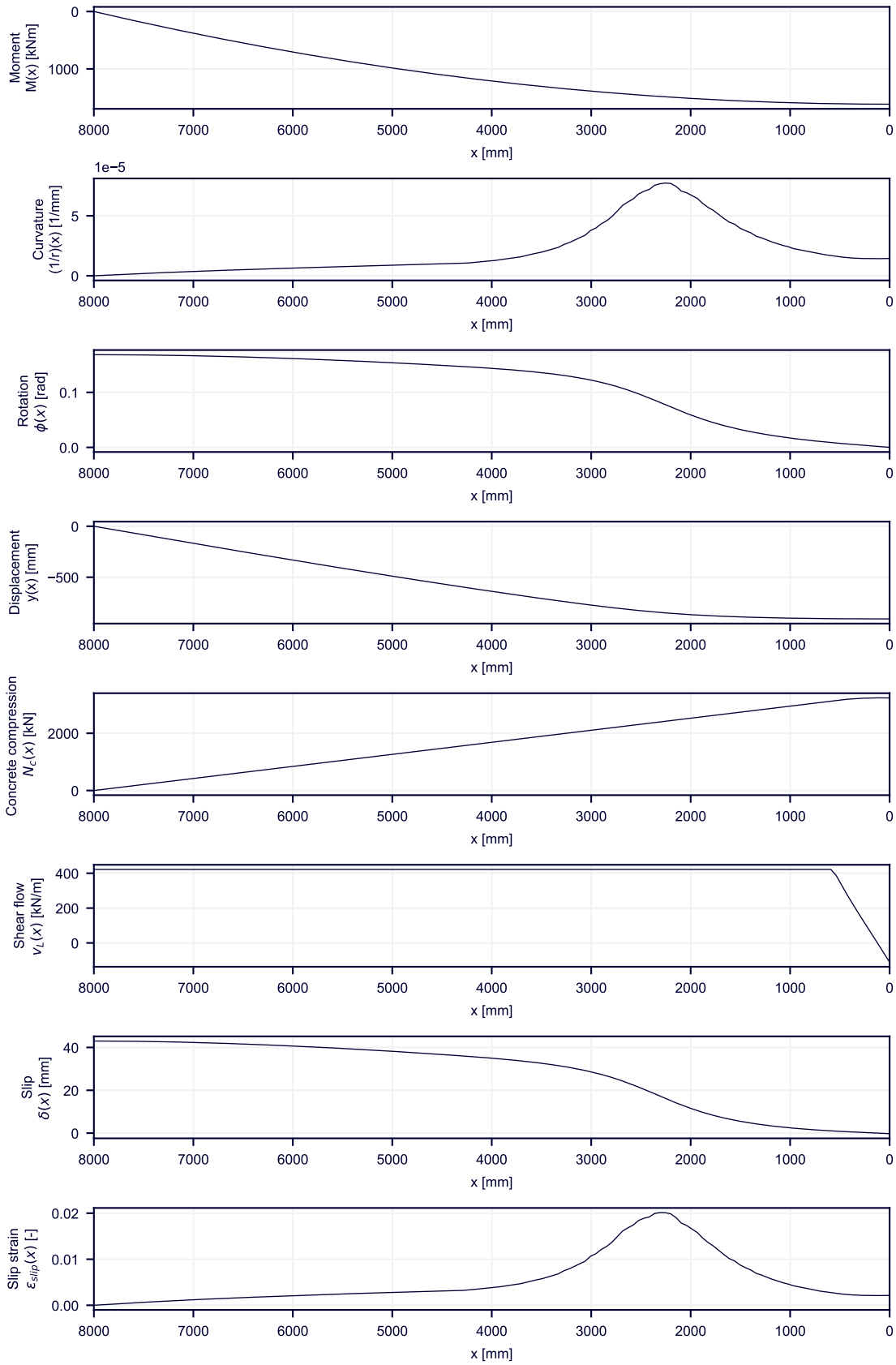

Figure 3.28: Example 4: diagrams

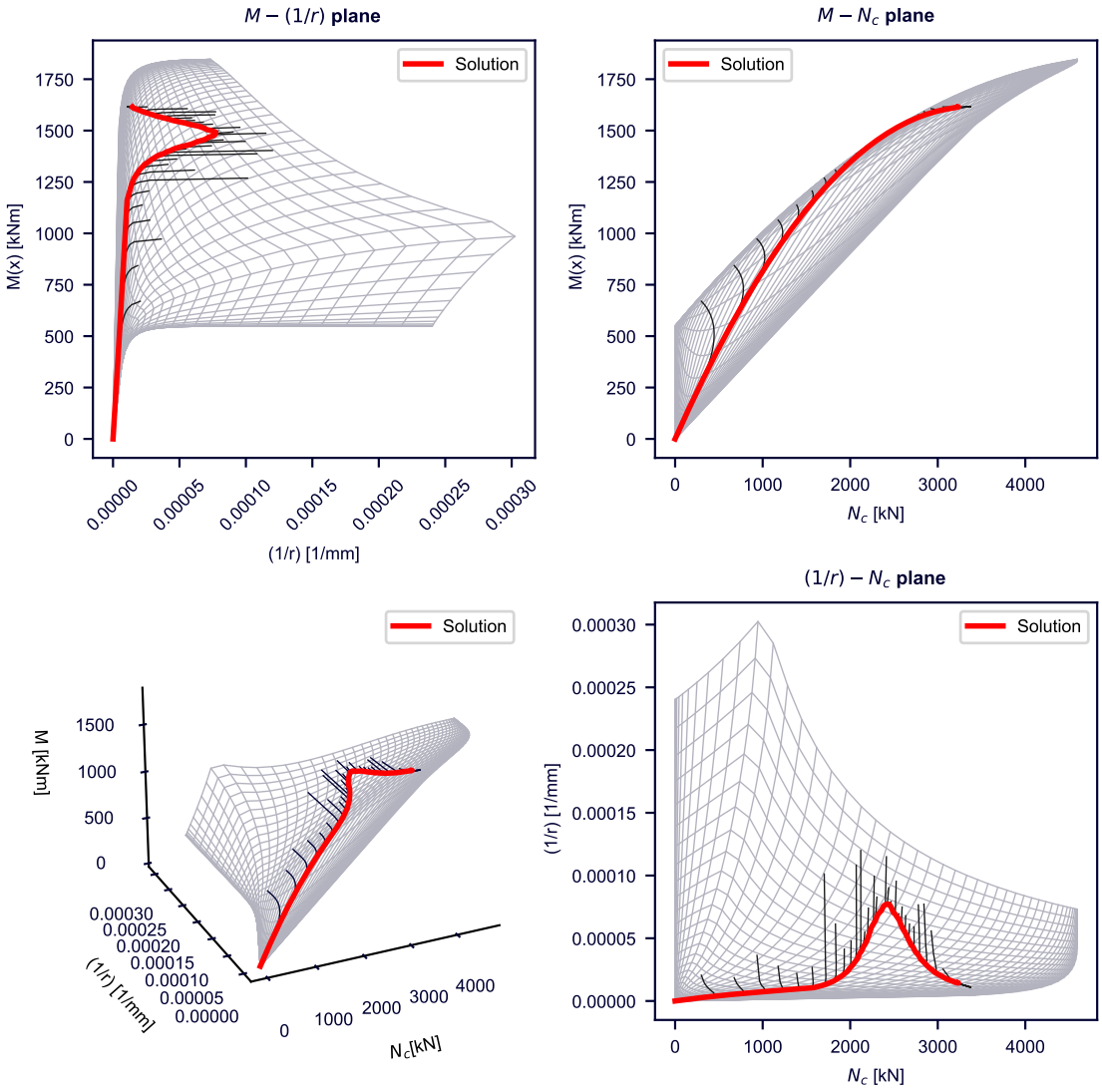

Figure 3.29: Example 4: moment-concrete compression-curvature surface

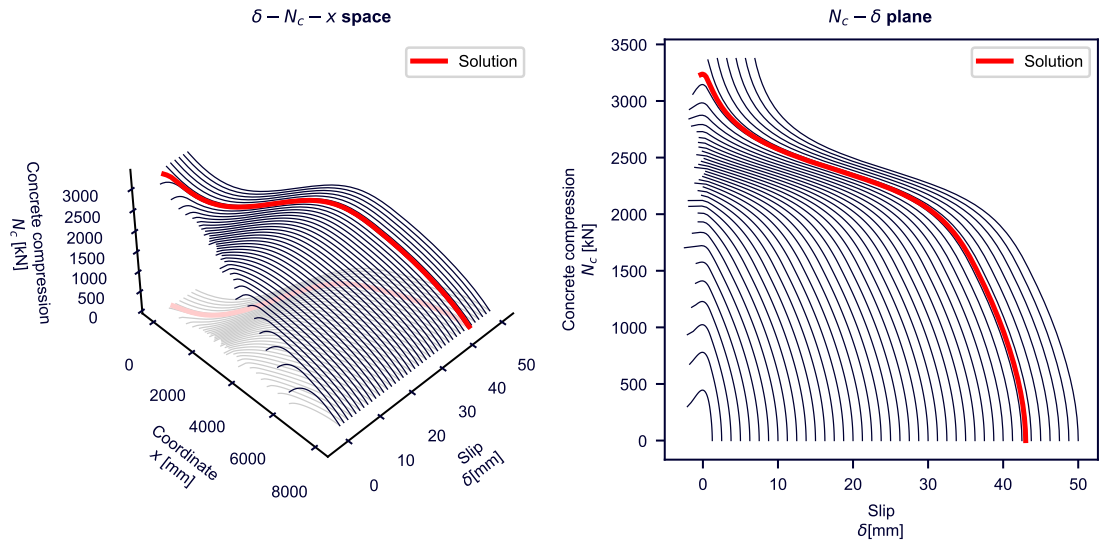

Figure 3.30: Example 4: numerical method streamlines

Therefore the beam is expected to fail for a lower bending moment compared with the plastic resistant design bending moment in the FSC case. The results are expected to be similar with the one relative to the example 4 (Fig.3.31).

Again, there is an extended area of yielded shear connection and sectional failure shows in a different coordinate than the one of midspan.

The slip maximum demand along the beam occurs at the support region and is $\delta_{max} = \delta(L/2) = 40\,mm$ and the value is similar with the one of example 4 but still much larger than the one of examples 1,2,3. The solution is represented on the $M - N_c - (1/r)$ surface (Fig.3.32):

The solution is represented in the $N_c - \delta$ plane (Fig.3.33). Notice that similarly with the example 4 the streamline path evolution is less sensitive respect with the starting conditions.

3.5.6 Plastic bending moment assessment in a partial shear connection case

In a partial shear connection case for a uniformly loaded simply supported beam, for a bi-linear shear connection shear flow-slip $v_L - \delta$ law, the shear flow will be constant to the maximum admissible value along the beam until the midspan proximity gets reached. In the closeness of the midspan section the shear flow recovers its proportionality with the slip, which must be zero at midspan section. Referring to the support reference frame with the relative x' coordinate, for the constant flow area of the element the following relation can be written:

$$N_c(x') = P_{Rd}/e_x \cdot x' \tag{3.93}$$

Notice that implicitly the $N_c(x' = 0) = 0$ boundary condition has been used. Moreover the distribution of the plastic resistant bending moment as a function of N_c is known from the partial shear diagram. This function can be more or less complicate depending on how ULS condition is defined. In this application

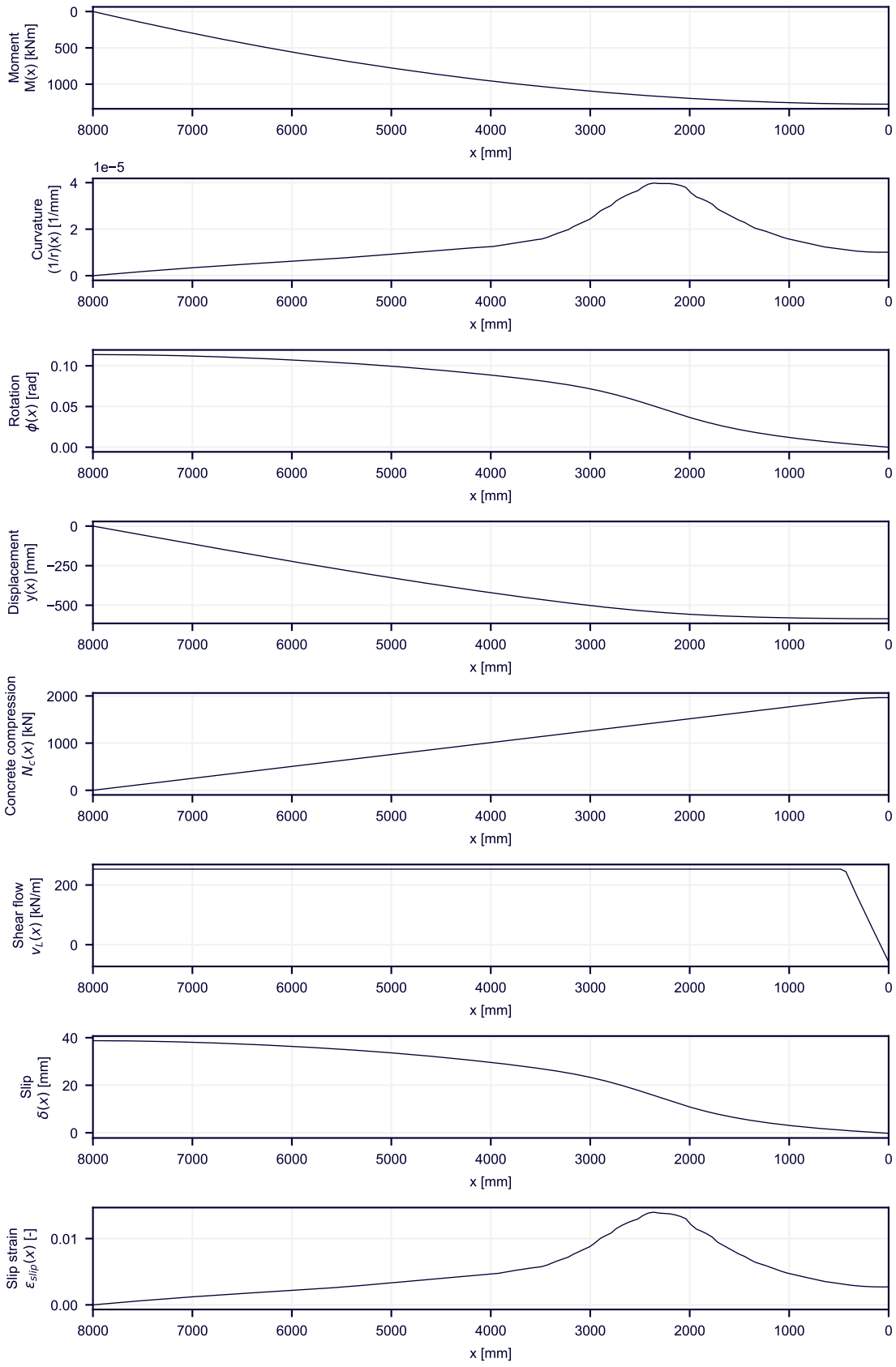

Figure 3.31: Example 5: diagrams

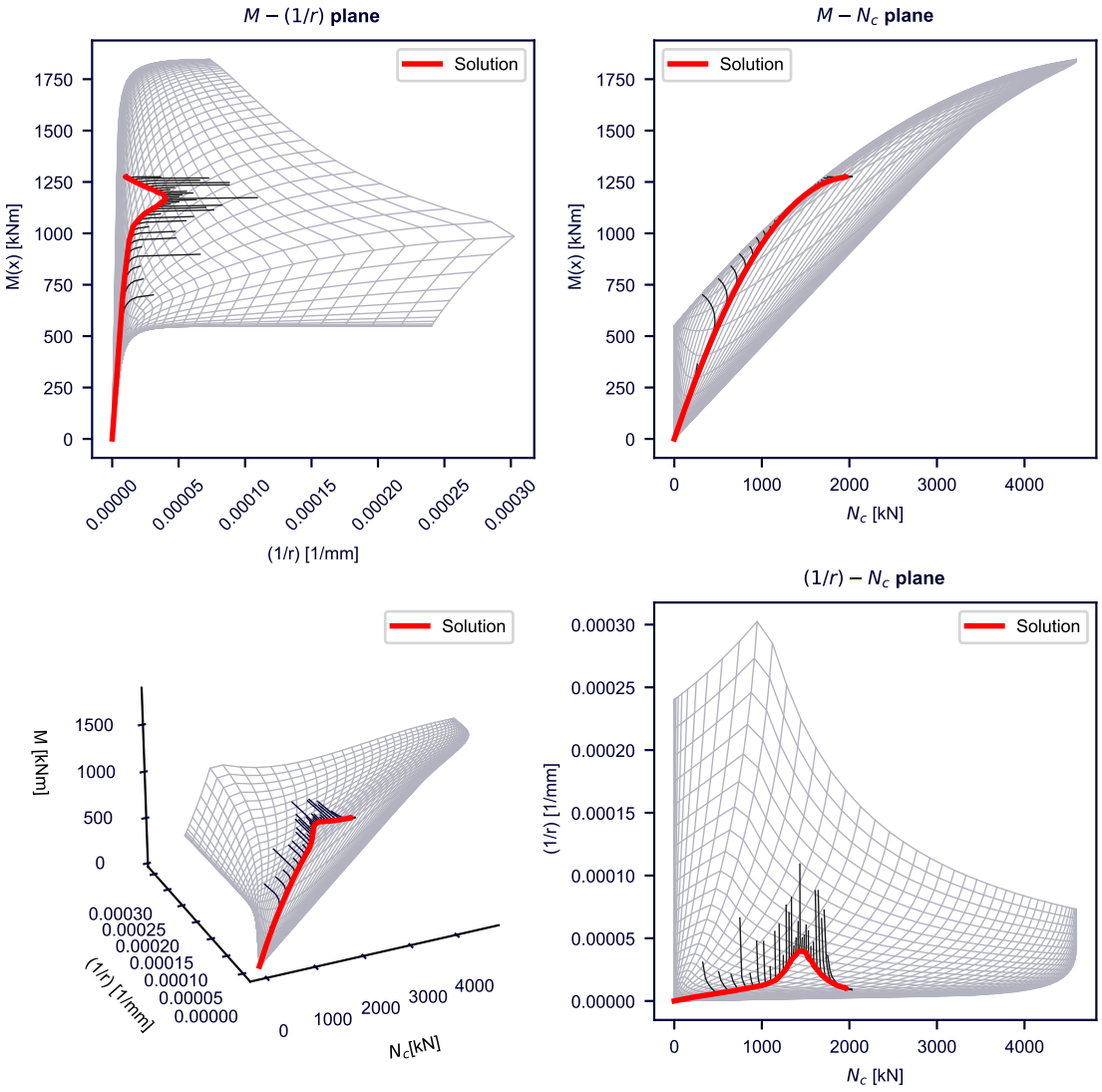

Figure 3.32: Example 5: moment-concrete compression-curvature surface

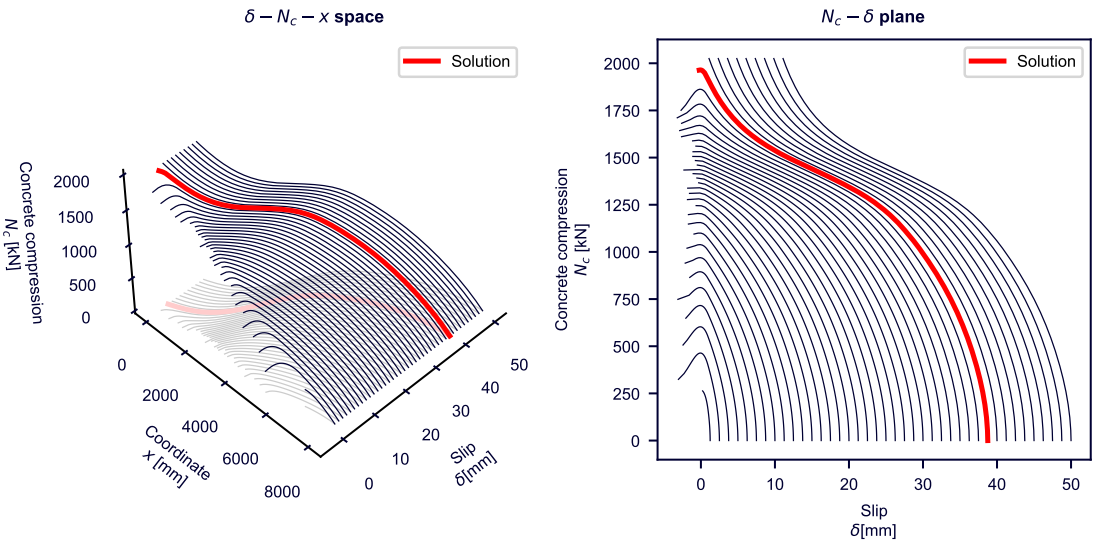

Figure 3.33: Example 5: numerical method streamlines

the partial shear diagram was derived by mean of a strain limitation approach (SL), but it can be also be derived by a traditional simpler Rigid Plastic analysis (RP) approach. The key point is that it can be derived, so let's assume the function $M_{pl,Rd}(N_c)$ is known.

Therefore, the following variation of the plastic resistant bending moment can be found as a function of the coordinate:

$$M_{pl,Rd}(x') = M_{pl,Rd}(N_c(x')) = M_{pl,Rd}(P_{Rd}/e_x \cdot x') \tag{3.94}$$

The moment distribution along the beam is also known from the structural analysis. For the considered case the acting bending moment varies in a quadratic way:

$$M(x', M_{max}) = q \cdot L/2 \cdot x' - q \cdot x'^2/2 = 4 \cdot M_{max}/L^2 \cdot (L - x') \cdot x' \tag{3.95}$$

Notice that the function $M_{pl,Rd}$ refers to the resistance of the section considered. While M_{max} consists in the maximum acting bending moment on the beam. The purpose is to assess the particular $M_{max} = M_{max,Rd}$ which creates failure at one particular section of the beam, generally it might not be coincident with that one of midspan. While $M_{pl,Rd}$ is the sectional resistant bending moment, the value of $M_{max,Rd}$ is the one of the whole element.

In order to assess the plastic resistant bending moment three conditions are imposed:

- in a particular section of coordinate $\overline{x'}$ failure exhibits. Therefore for this particular section the acting moment is equal to the resistant moment and the following equation is imposed:

$$M_{pl,Rd}(\overline{x'}) = M(\overline{x'}, M_{max}) \tag{3.96}$$

- in the same coordinate the two functions are tangent. If it were not, considering two continuous function with continuous derivative, it would exist in the proximity of the considered coordinate a

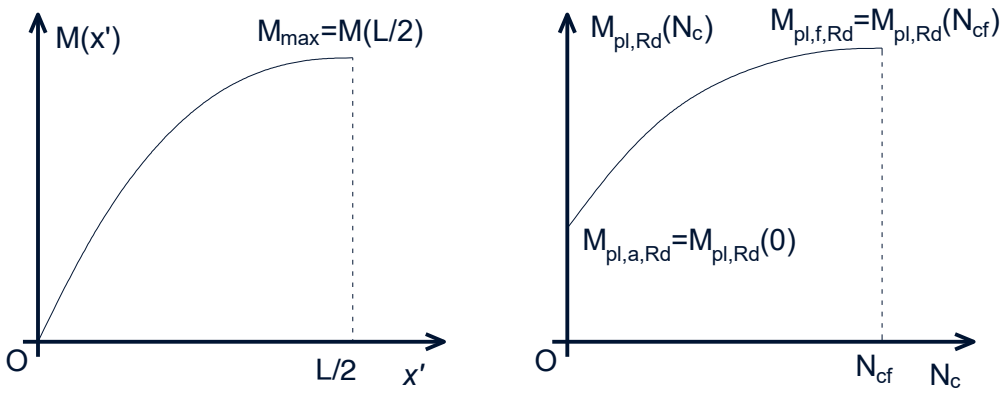

Figure 3.34: acting moment diagram and partial shear diagram

section with acting moment greater than the resistant moment. Thus:

$$\frac{d\,M_{pl,Rd}(\overline{x'})}{dx'} = \frac{d\,M(\overline{x'}, M_{max})}{dx'} \tag{3.97}$$

- Because the final purpose is to assess the particular M_{max} which creates global failure M_{max} should be equal to $M_{max,Rd}$:

$$M_{max} = M_{max,Rd} \tag{3.98}$$

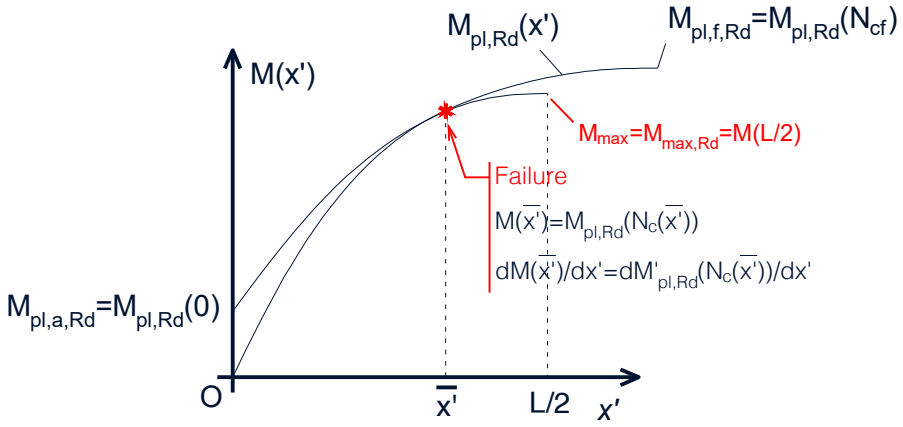

Figure 3.35: failure condition identification

As an example let's assume the plastic resistant bending moment for the cross section varies in a parabolic way:

$$M_{pl,Rd}(N_c) = M_{pl,a,Rd} + N_c/N_{cf} \cdot (2 - N_c/N_{cf}) \cdot (M_{pl,f,Rd} - M_{pl,a,Rd}) \tag{3.99}$$

$$M(x'/L) = 4 \cdot M_{max} \cdot (1 - x'/L) \cdot x'/L \tag{3.100}$$

Substituting the linear variation law $N_c(x) = v_{L,Rd} \cdot x'$ in the partial shear connection case would lead to:

$$M_{pl,Rd}(x') = M_{pl,a,Rd} + (v_{L,Rd} \cdot x')/N_{cf} \cdot (2 - (v_{L,Rd} \cdot x')/N_{cf}) \cdot (M_{pl,f,Rd} - M_{pl,a,Rd}) \tag{3.101}$$

Applying the three equations leads to the following system:

$$\begin{cases} M_{pl,Rd}(\overline{x'}) = M(\overline{x'}, M_{max}) \\ \frac{d\, M_{pl,Rd}(\overline{x'})}{dx'} = \frac{d\, M(\overline{x'}, M_{max})}{dx'} \\ M_{max} = M_{max,Rd} \end{cases} \tag{3.102}$$

More in detail the system becomes:

$$\begin{cases} \frac{4M_{max} \cdot (L - \overline{x'}) \cdot \overline{x'}}{L^2} = M_{pl,a,Rd} + \frac{(M_{pl,a,Rd} - M_{pl,f,Rd} \cdot v_{L,Rd} \cdot \overline{x'} \cdot (-2 \cdot N_{cf} + v_{L,Rd} \cdot \overline{x'}))}{N_{cf}^2} \\ \frac{4M_{max} \cdot (L - 2 \cdot \overline{x'})}{L^2} = -\frac{2(M_{pl,a,Rd} - M_{pl,f,Rd} \cdot v_{L,Rd} \cdot (N_{cf} - v_{L,Rd} \cdot \overline{x'}))}{N_{cf}^2} \\ M_{max} = M_{max,Rd} \end{cases} \tag{3.103}$$

The system can be solved for the unknown variables $M_{max,Rd}$ and $\overline{x'}$ by expressing them as function of the adimensionalized parameters $M_{pl,a,Rd}/M_{pl,f,Rd}$ and $v_{L,Rd}/(N_{cf}/(L/2))$ deriving the expressions for the adimensionalized position of the failure section $\overline{x'}/(L/2)$ and the adimensionalized resistant bending moment of the element $M_{max,Rd}/M_{pl,f,Rd}$. With the derived relations the diagram of Fig.3.36 can be plotted.

On the left side of Fig.3.36 the position relative to half length of the element is plotted as function of the normalized shear connection resistance $v_{L,Rd}/(2N_{cf}/L)$ and the full shear connection plastic moment design resistance over the zero shear connection plastic moment design resistance $M_{pl,a,Rd}/M_{pl,f,Rd}$. The shifting of the failure section appears to have a maximum in proximity of the value $v_{L,Rd}/(2N_{cf}/L) = 0.5$ and it vanishes for increasing $M_{pl,a,Rd}/M_{pl,f,Rd}$ ratios. If the $v_{L,Rd}/(2N_{cf}/L)$ ratio is zero or unitary the failure appears at midspan. On the right side of Fig.3.36 the maximum applicable moment on the element normalized with the plastic resistant bending moment of the full shear connection case $M_{max,Rd}/M_{pl,f,Rd}$ is plotted. The condition $M_{max,Rd} = M_{pl,f,Rd}$ for $v_{L,Rd}/(2N_{cf}/L) = 1$ and $M_{max,Rd} = M_{pl,a,Rd}$ for $v_{L,Rd}/(2N_{cf}/L)$=0 is respected. Increasing the $M_{pl,a,Rd}/M_{pl,f,Rd}$ ratio generate an increasing also in the value of $M_{max,Rd}$. The transition to the value of $M_{pl,a,Rd}$ to $M_{pl,f,Rd}$ is non-linear. In the limit of $M_{pl,a,Rd}/M_{pl,f,Rd}$ ratio going to zero an almost linear relation shows.

The derived relations, or equivalently the plotted diagrams, can be exploited in order to assess the maximum applicable moment $M_{max,Rd}$ of the element for the previously analyzed Example 4 and 5 which exhibit a partial shear connection failure.

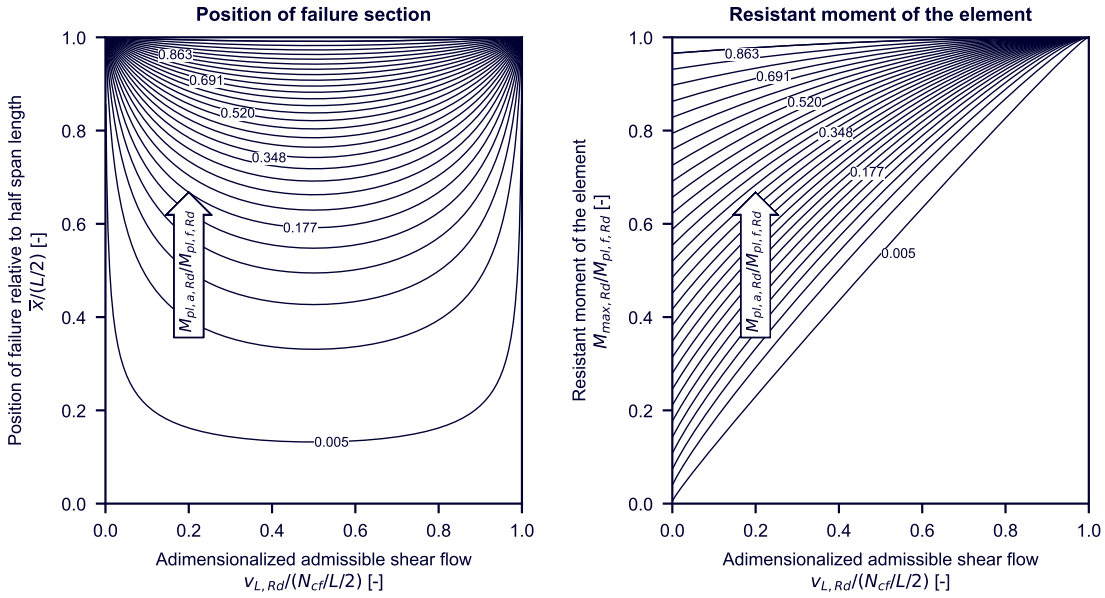

Figure 3.36: plastic resistant bending moment and position of failure section in PSC assessment: resulting diagrams. The adimensional admissible shear flow is the degree of shear connection η

General data:

$$M_{pl,f,Rd} = 1846\ kNm \quad M_{pl,a,Rd} = 550\ kNm \quad L = 16.0\ m \quad N_{cf} = 4500\ kN \tag{3.104}$$

Applying the formulations for example 4 returns:

$$v_{L,Rd} = 421.9 kN/m \tag{3.105}$$

$$M_{max,Rd}(\frac{v_{L,Rd}}{2N_{cf}/L}, \frac{M_{pl,a,Rd}}{M_{pl,f,Rd}}) = 1704.5 kNm \tag{3.106}$$

$$\overline{x'}(\frac{v_{L,Rd}}{2N_{cf}/L}, \frac{M_{pl,a,Rd}}{M_{pl,f,Rd}}) = 6.00 m \tag{3.107}$$

Applying the formulations for example 5 returns:

$$v_{L,Rd} = 225 kN/m \tag{3.108}$$

$$M_{max,Rd}(\frac{v_{L,Rd}}{2N_{cf}/L}, \frac{M_{pl,a,Rd}}{M_{pl,f,Rd}}) = 1290 kNm \tag{3.109}$$

$$\overline{x'}(\frac{v_{L,Rd}}{2N_{cf}/L}, \frac{M_{pl,a,Rd}}{M_{pl,f,Rd}}) = 5.70 m \tag{3.110}$$

In the first case $M_{max,Rd}$ overestimates the actual value of maximum bending moment that was applied at which failure was showing:

$$M_{max,Rd,Ex.4} = 1704.5\ kNm > M_{max,Ex.4} = 1611\ kNm \tag{3.111}$$

In the second case $M_{max,Rd}$ provides a better estimation of the actual value of maximum bending moment that was applied at which failure was showing:

$$M_{max,Rd,Ex.5} = 1290\ kNm \approx M_{max,Ex.5} = 1280\ kNm \tag{3.112}$$

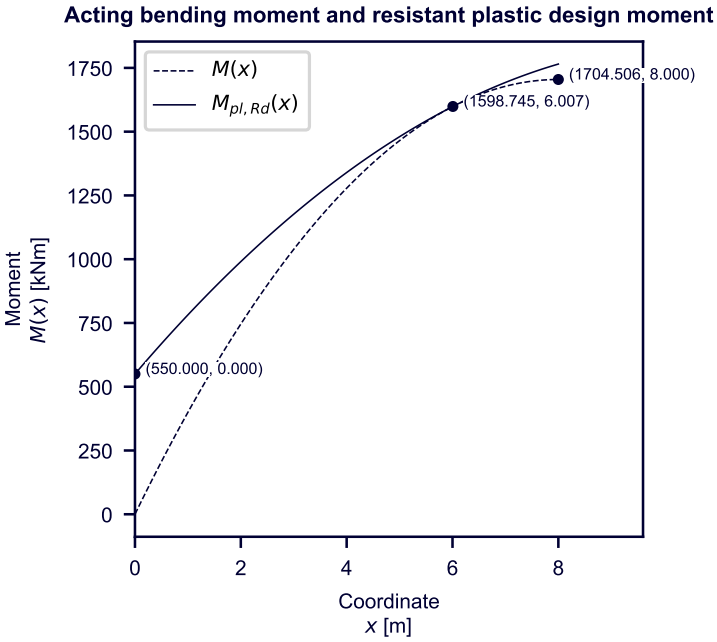

Figure 3.37: Example 4: failure state assessment

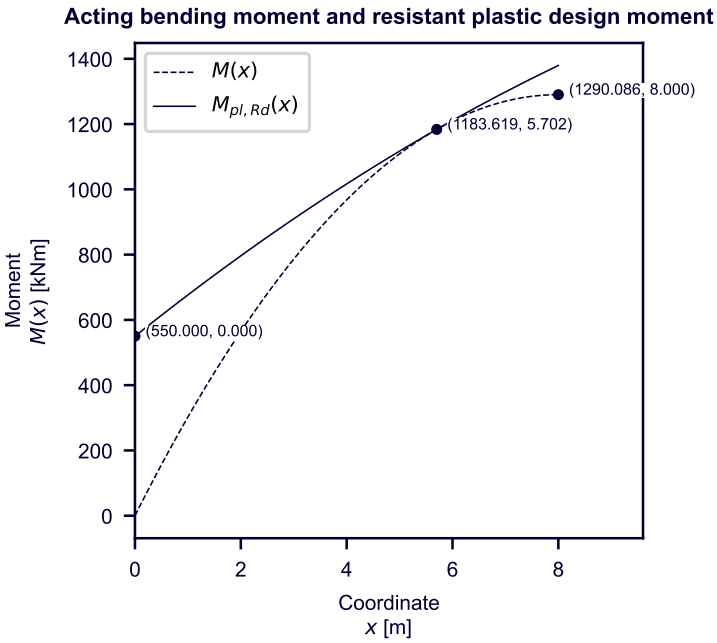

Figure 3.38: Example 5: failure state assessment

3.6 Slip demand parametric study

In order to assess the slip demand along the beam a parametric study has been conducted exploiting the previously described numerical method.
The properties of the shear connection has been set as follows:

$$P_{Rd}/e_x = 450\,kNm \quad \delta_y = 1\,mm \tag{3.113}$$

Notice that because of the imposed shear connection properties the full shear connection condition is expected at about:

$$L_{FSC} = 2 \cdot \frac{N_{cf}}{P_{Rd}/e_x} = 20.0\,m \tag{3.114}$$

Thus, for $L < L_{FSC}$ a partial shear connection is expected while for $L \geq L_{FSC}$ a full shear connection is forecast with the value of the applied midspan moment M_{max} reaching the the one of $M_{pl,f,Rd}$. This limit has to be considered just as a reference.
The slip demand has been studied as a function of the following variables Fig.3.39:

- the span length L of the element. In particular the region of lengths $L \in [9.500\ m; 25.500\ m]$ is examined ;
- the bending moment at midspan M_{max} under a uniformly distributed simply supported beam condition. More in detail the values of $M_{max} \in (800\ kNm; M_{pl,f,Rd} = 1846\ kNm)$ are considered. Notice that for a partial shear connection condition no plastic bending resistant moment for full shear connection $M_{pl,f,Rd}$ will be reached by the structure, resulting in non-convergent analyses, thus the examined range will be narrower.

3.6.1 Results

For each couple of sampled (M_{max}, L) point the value of the maximum slip along the beam is collected. Notice that due to the fact that no negative ϵ_{slip} are examined in the whole procedure, as a consequence of the fact that along x the slope increasing ratio of the slip δ can only be positive follows that the maximum slip occurs in the support region.
The sampled points $(M_{max}, L, \delta_{max})$ can be plotted in a three dimensional plot (Fig.3.40). A surface well approximates the points position region.
The ductility demand δ_{max} is higher with decreasing span length L. Notice that the results can be counter-intuitive: one can expect that with increasing span length, because the slip is obtained with an integration of the slip strains, for an increasing span length the resulting slip increases. Despite of that also the ϵ_{slip} distribution dependency with L has to be taken into account. By decreasing the span length, with the same given shear connection, also the shear flow distribution changes.
The relations derived in section 3.5.6 for the assessment of the plastic bending resistant moment can be exploited in order to predict how the maximum applicable moment at midspan $M_{max,Rd}$ varies with the

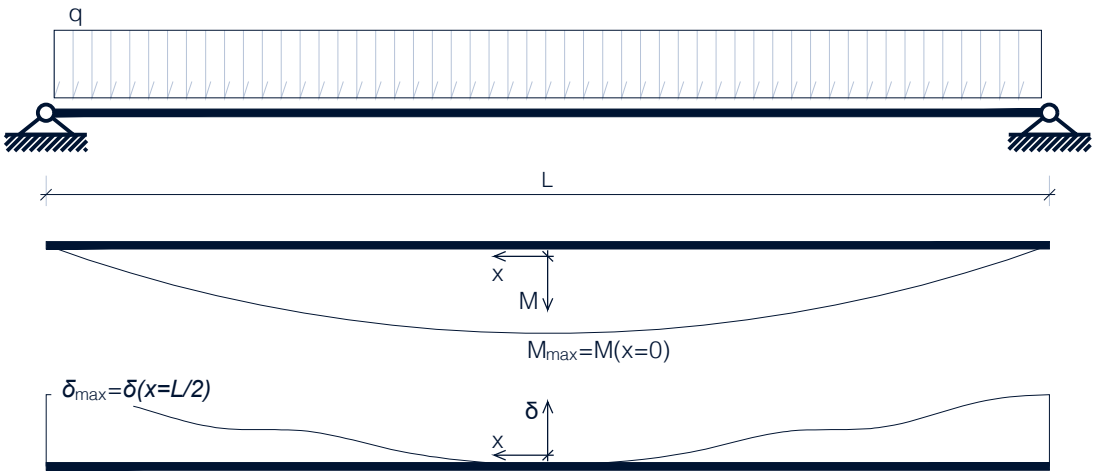

Figure 3.39: Slip demand study: parameters

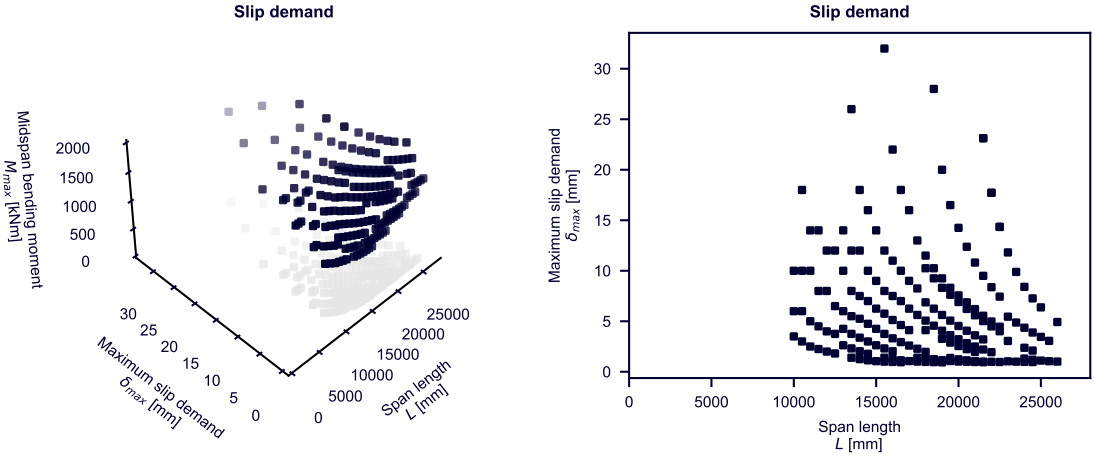

Figure 3.40: Slip demand distribution for fixed admissible shear flow and section and variable acting moment and span length

span length for the given section and shear connection. Remember that the relations were derived under the simplified approximated assumption of parabolic trend of the function $M_{pl,Rd}(N_c)$.
Using the following equation:

The value of $M_{max,Rd}$ can be plotted as a function of L:

$$M_{max,Rd}(L) \tag{3.116}$$

The function can be plotted and overlapped with the sampled points in the $M - L$ plane, deriving the diagram of Fig.3.41. The curve consists in an upper limit of the sampled points.

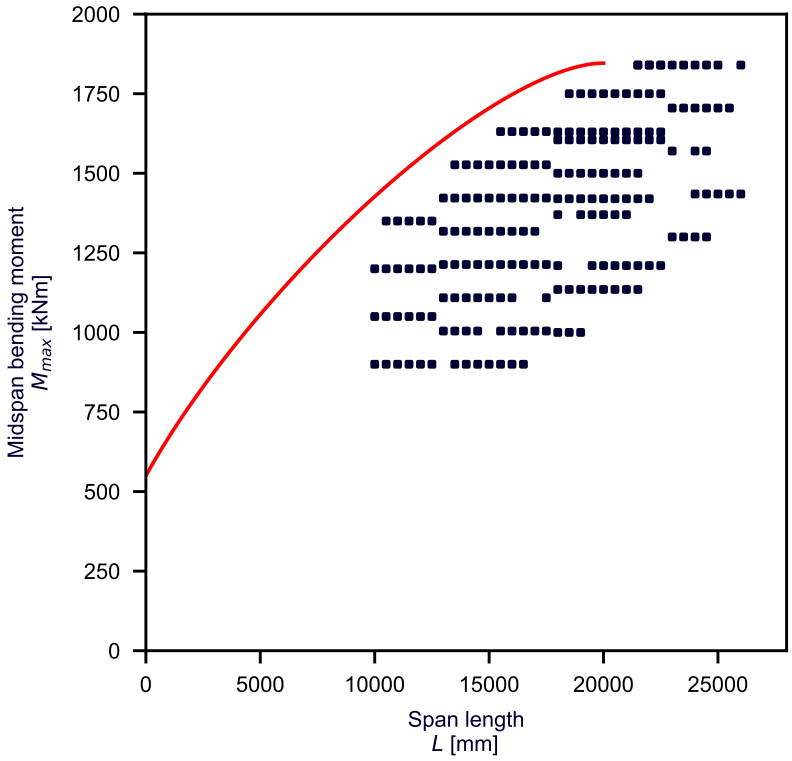

Figure 3.41: scatter plot of the sampled points in the moment-span length plane with maximum resistant bending moment of the element assessed with the simplified method presented in section 3.5.6

3.6.2 Results consistency

For design purposes the limitation in order to prevent an excessive ductility demand δ_{max}, which would exceed the available ductility δ_u, is set on the degree of shear connection η. The suddenly slip increase for in the partial shear connection situation is also observed in [97] which Notices how with a global yielding of the shear connection the slip increases sharply under the same amount of load increasing. This is because the shear connection looses the stiffness turning the system in a mechanism. Other tests are conducted

in [42]. In particular limitations in the following form are present in the present version of Eurocode 4 [11]:

$$\eta \geq \eta_{min} = \eta_{min}(L, f_y) \tag{3.117}$$

This relation has been calibrated on the basis of the minimum deformation capacity requested by the EC4 for a connector, which is actually $6\ mm$. The relation is therefore strictly related with this value. For the forthcoming version of the Eurocode 4, research is investing effort in pushing the design rules toward a "performance based" approach. In detail in researches like [36] new proposals of the limitations take into account also the available ductility δ_u, which represents the deformation capacity of the shear connection, in the formulation, trying to put the limitation in the more advanced form:

$$\eta \geq \eta_{min} = \eta_{min}(L, f_y, \delta_u) \tag{3.118}$$

In the $\eta - L$ plane constant $v_{L,Rd}$ lines are represented by straight lines coming out from the origin of the plane (Fig.3.42). This comes from:

$$\eta = \frac{n \cdot P_{Rd}}{N_{cf}} = \frac{L \cdot v_{L,Rd}}{2N_{cf}} \tag{3.119}$$

In this relation the proportionality between the degree of shear connection η and the span length L can be observed for fixed values of the shear connection resistance. Due to the fact that in the sampled cases the maximum admissible shear flow $v_{L,Rd}$ is set to a constant value, in the $\eta - L$ plane the sampled analysed region is represented by a straight line (Fig.3.42). On this line the maximum ductility demand has been found to be decreasing with the span length. When overlaying the result of the present study with the Claßen's proposed limitations on η, the results are found to be qualitative consistent. Also the results from Claßen's express a decreasing of the ductility demand following the straight line $v_{L,Rd} = 450\ kN/m$.

3.6.3 Assessing the limitation on the degree of shear connection

One way in order to assess the function $\eta_{min} = \eta_{min}(L, f_y, \delta_u)$ is (Fig. 3.43):

- sampling the function of the maximum slip along the beam in the variables M_{max}, L deriving for constant values of $v_{L,Rd}$:

$$\delta_{max}(M_{max}, L, v_{L,Rd}) \tag{3.120}$$

- deriving the $\delta_{max}(M_{max}, L, v_{L,Rd})$ values at the bending resistant moment of the element, thus considering the bending ULS condition and deriving:

$$\delta_{max,ULS} = \delta_{max}(M_{max,Rd}, L) = \delta_{max,ULS}(L, v_{L,Rd}) \tag{3.121}$$

- the function $\delta_{max,ULS}(L, v_{L,Rd})$ can be viewed equivalently as $\delta_{max,ULS}(L, \eta)$. Thus, "iso-deformation request" lines can be plotted in the $\eta - L$ plane or derived as functions $\eta = f(\delta_{max,ULS}, L)$.

- imposing the condition $\delta_{max,ULS} \leq \delta_u$ means limiting the required deformation capacity to the available deformation capacity, thus in terms of the degree of shear connection means imposing the following limitation: $\eta \geq \eta_{min} = f(\delta_u, L)$. These lines are the searched functions.

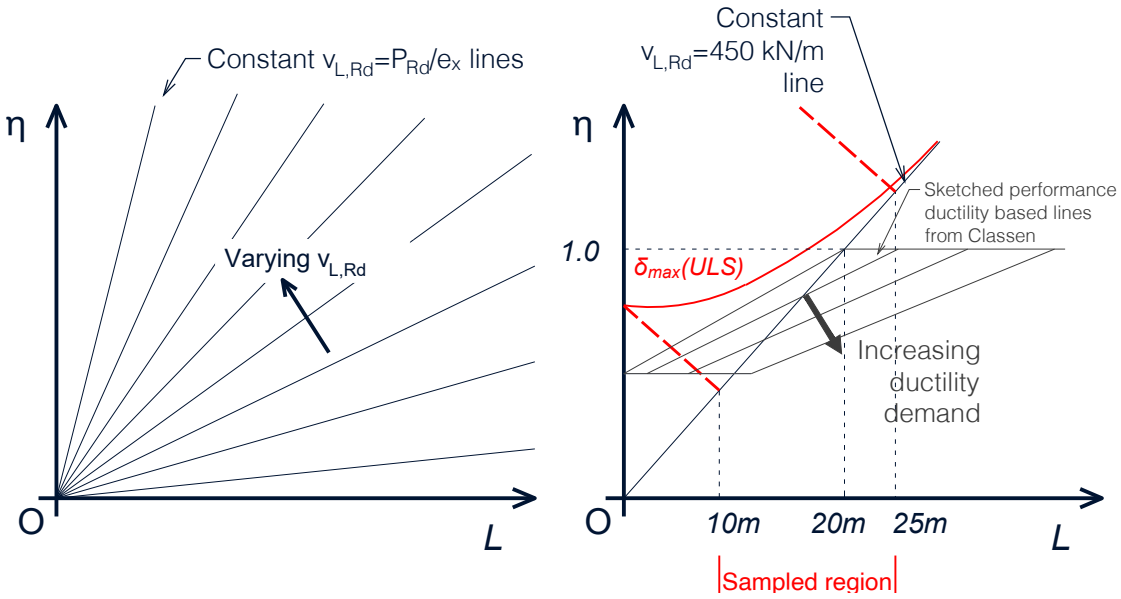

Figure 3.42: constant shear connection resistance lines in the degree of shear connection-span length plane (left) and qualitative consistency with Classen's results (left)

Another feasible way could be by sampling the $\delta_{max}(M_{max}, L, v_{L,Rd})$ points directly from varying the degree of shear connection $\delta_{max}(M_{max}, L, \eta)$ instead of varying the shear connection resistance $v_{L,Rd}$. The two methods are equivalent.

Possible criticality in the assessment of the minimum degree of shear connection

As the function $\eta_{min}(\delta_u, L)$ is derived examining the deformation demand of bending ULS $\delta_{max,ULS}$, a possible critical point can arise. Reaching the bending resistance of the element in a partial shear connection condition $M_{max} \rightarrow M_{max,Rd} \leq M_{pl,f,Rd}$, at shear connection level the structure is progressively reaching a kinematism condition, i.e. a mechanism is forming both at sectional level and at shear connection level. Thus, the determination of the value of $\delta_{max,ULS}$ as the particular value δ_{max} where the bending resistance $M = M_{max,Rd}$ is reached, may be over-sensitive on the choice of the shear connection model (3.44).

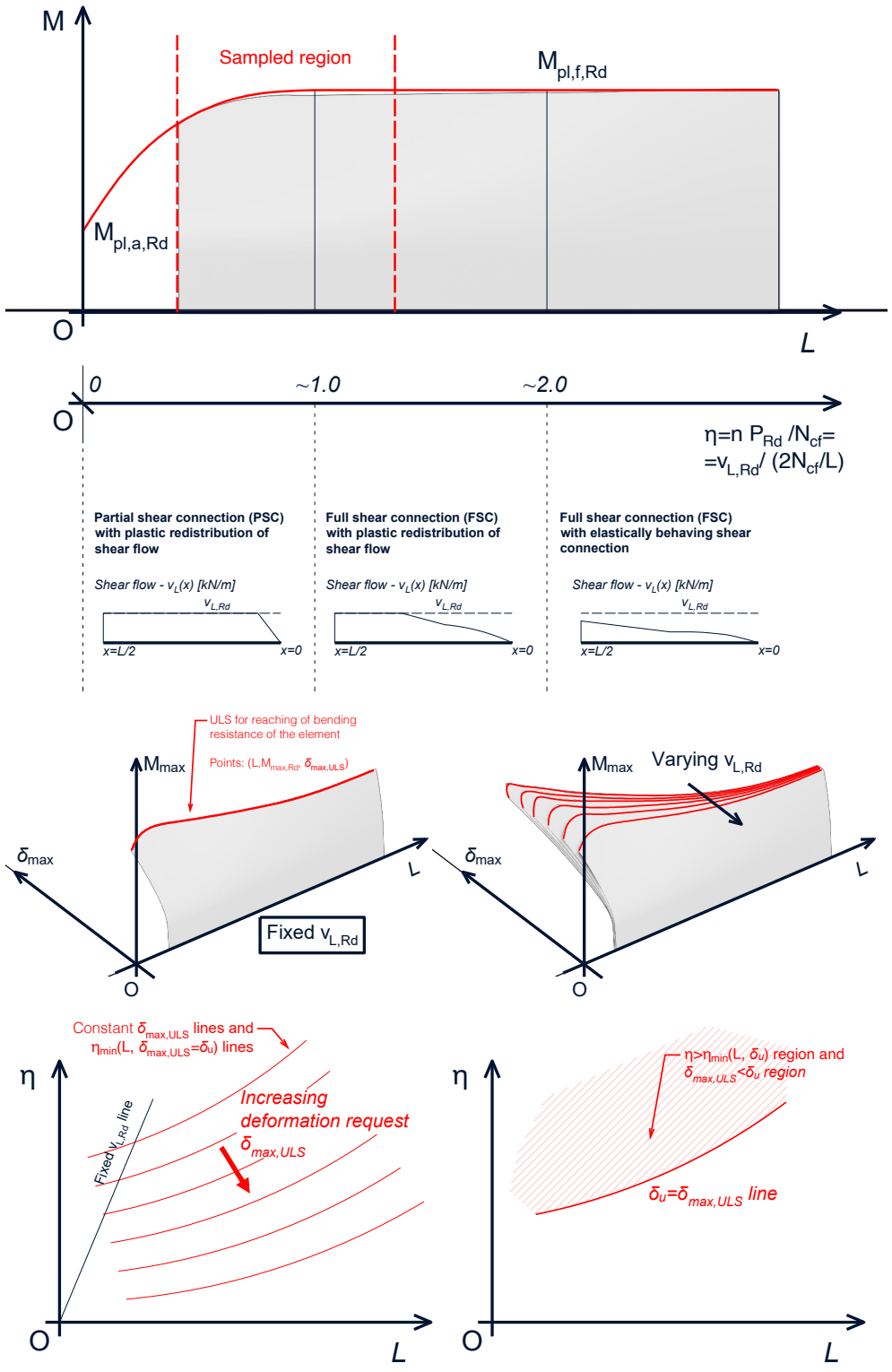

Figure 3.43: identification of the minimum degree of shear connection requirements on the basis of the slip demand: conceptual drawings. Surfaces are not derived from numerical derived results

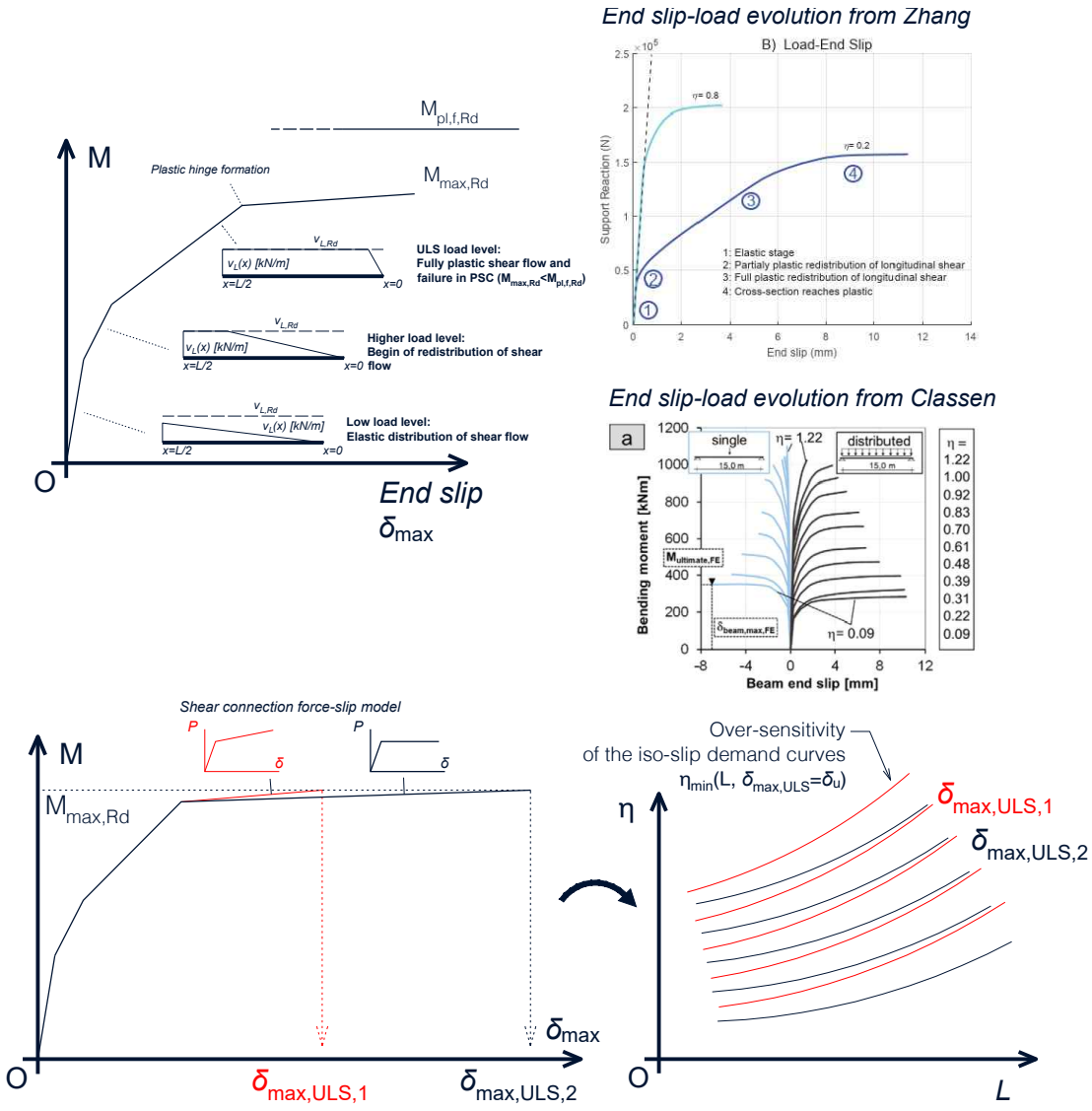

Figure 3.44: sensitivity of the slip demand result on the chosen mechanical behaviour model of the shear connection

Chapter 4

Analytical model for the plastic slip capacity assessment

In this section considerations are made in order to develop an analytical simplified mechanical model of the composite dowels shear connection. The scope is to compute the plastic slip capacity. The model development is guided by literature data analysis, failure mode observations and engineering intuition.

4.1 Scopes of the model derivation

The scope is to quantify the plastic slip capacity. On the other hand the slip demand can be assessed through the shear flow-slip one dimensional model that was described in section 3.
An important point is to estimate the maximum composite dowels resistance. According to the literature review that has been carried out this has already been done and is also contained in the existing technical specifications and standards. However the final purpose of a consistent design approach is to guarantee a ductile failure mode. A high ductility guarantees the correct plastic redistribution of the shear connection. Here it's important to guarantee the ductile failure mode. This is done by preventing more brittle failure modes. These are the shearing of concrete dowel and the concrete pryout. The succession of resistant mechanisms forming the composite dowels shear connection are connected in series. The bearing force has in fact first to be transmitted to the concrete chord to the concrete part that forms the immediate nearby region of the steel dowel. Then the force has to be transferred to the steel dowel and transmitted through the steel web. This is how the equilibrium at sectional level works and how the shear flows through the shear connection. In order to prevent the more brittle failure modes and to promote the steel dowel failure, a hierarchy of resistances principle is generally exploited in the modern design rules and approaches. This is done by ensuring that the ductile resistance of the steel mechanism of the resistances chain is less than the ones of the more brittle failure modes. In the composite dowels case the resistance of the steel dowel must be lower compared with the one of the concrete shearing and pry-out failure modes. In the ULS checks an underestimation of the steel dowel resistance would lead the designer to be on the safe side. In

the hierarchy of resistances approach an excessive underestimation of this value would lead for this ductile mechanism not to occur. Thus, leading to brittle failures. Here the importance of correctly estimating the steel dowel resistance is underlined. Accounting for effects such as the plastic hardening of the steel is also important. The resistance of the steel dowel must be correctly assessed. The more brittle mode resistances must then satisfy the relation:

$$P_{S,brittle} \geq \gamma \cdot P_{S,ductile} \tag{4.1}$$

Here the γ factor is introduced in order to distance sufficiently the desired ductile mode to the unwanted brittle ones.

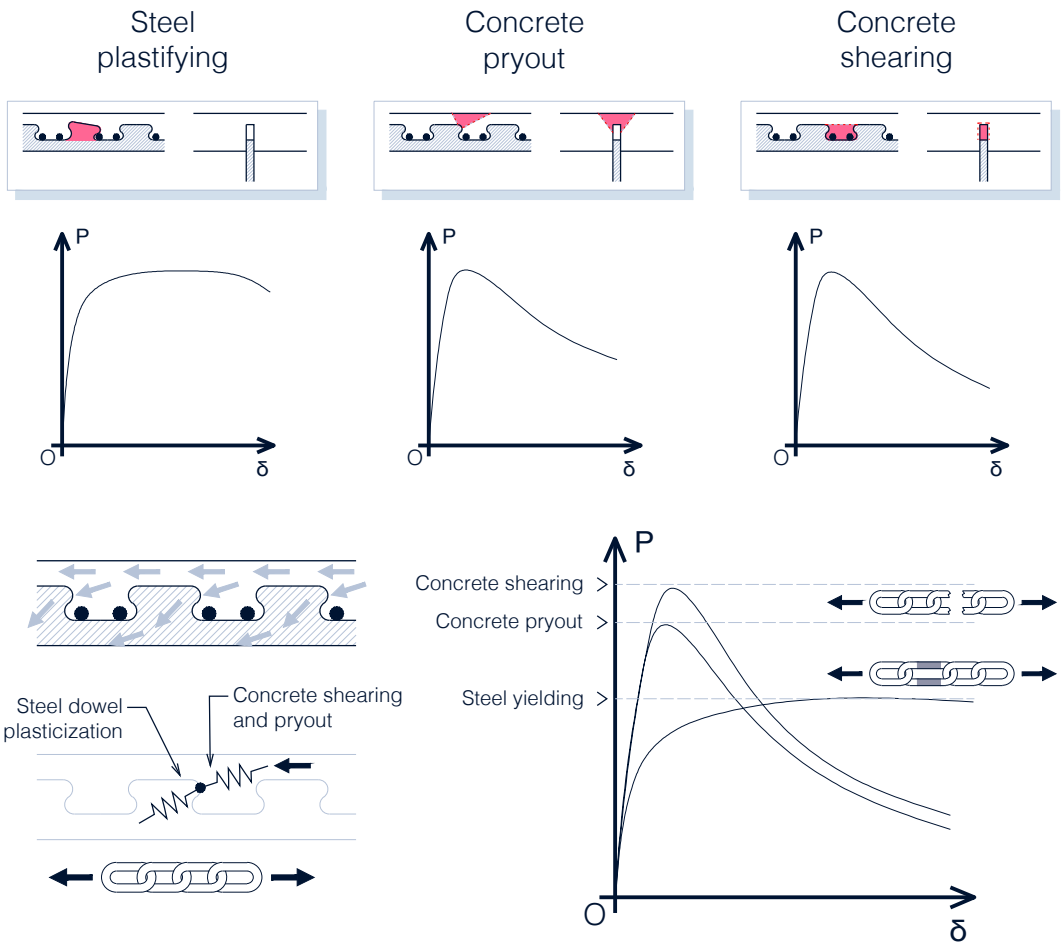

Figure 4.1: conceptual load-slip curves according to the different failure modes and concept of hierarchy of resistances

4.2 Failure modes resistances comparison

According to the recent literature results, three failure modes are relevant for a composite dowels beam with the shear connection embedded in a concrete slab. These are the steel dowel yielding, the concrete

dowel shearing and the concrete pryout failure modes. The three related resistances can be computed according to the following formulas. These are under development for the forthcoming design rules and have been reviewed in section 2.6.5.

Calculation formula	Failure mode
$P_{pl,k} = \lambda_{geo}\, f_y\, t_w\, e_x$	Steel dowel yielding
$P_{po,k} = k_1\, \chi_x(e_x)\chi_y h_{po}^{1.5}(e_x)\sqrt{f_{ck}}$	Concrete pryout
$P_{sh,k} = \eta_D(e_x)\, e_x^2\sqrt{f_{ck}}(1+\rho_D(e_x))$	Concrete dowel shearing

The terms involved in the three equations have been previously discussed in the section 2.6.5. In the steel dowel yielding the parameter λ_{geo} depends on the dowel shape. In the pryout failure modes the parameter k_1 depends on the dowel shape. While χ_y is equal to 1 for a single dowel row. Account for transverse cracking is here not done, thus $\psi_{crack} = 1$ is assumed. In these formulas the size (e_x) dependency has been highlighted. In the design process of composite beams, the value of the shear flow $v_{L,k}$ is more relevant compared with the value of the bearing resistance of the composite dowel P_k. Thus, for the following observations the shear flow will be used. This is derived with:

$$v_{L,k} = \frac{P_k}{e_x} \tag{4.2}$$

The three shear flow resistance formulas can be plotted as function of the dowel size e_x. This is done for specific values of the parameters $c_{D,u}$, $c_{D,o}$, A_b, t_w and for specific steel (E_s, f_y) and concrete (E_{cm}, f_{ck}) values. The dowel shape is also varied. The result is shown in Fig.4.2.

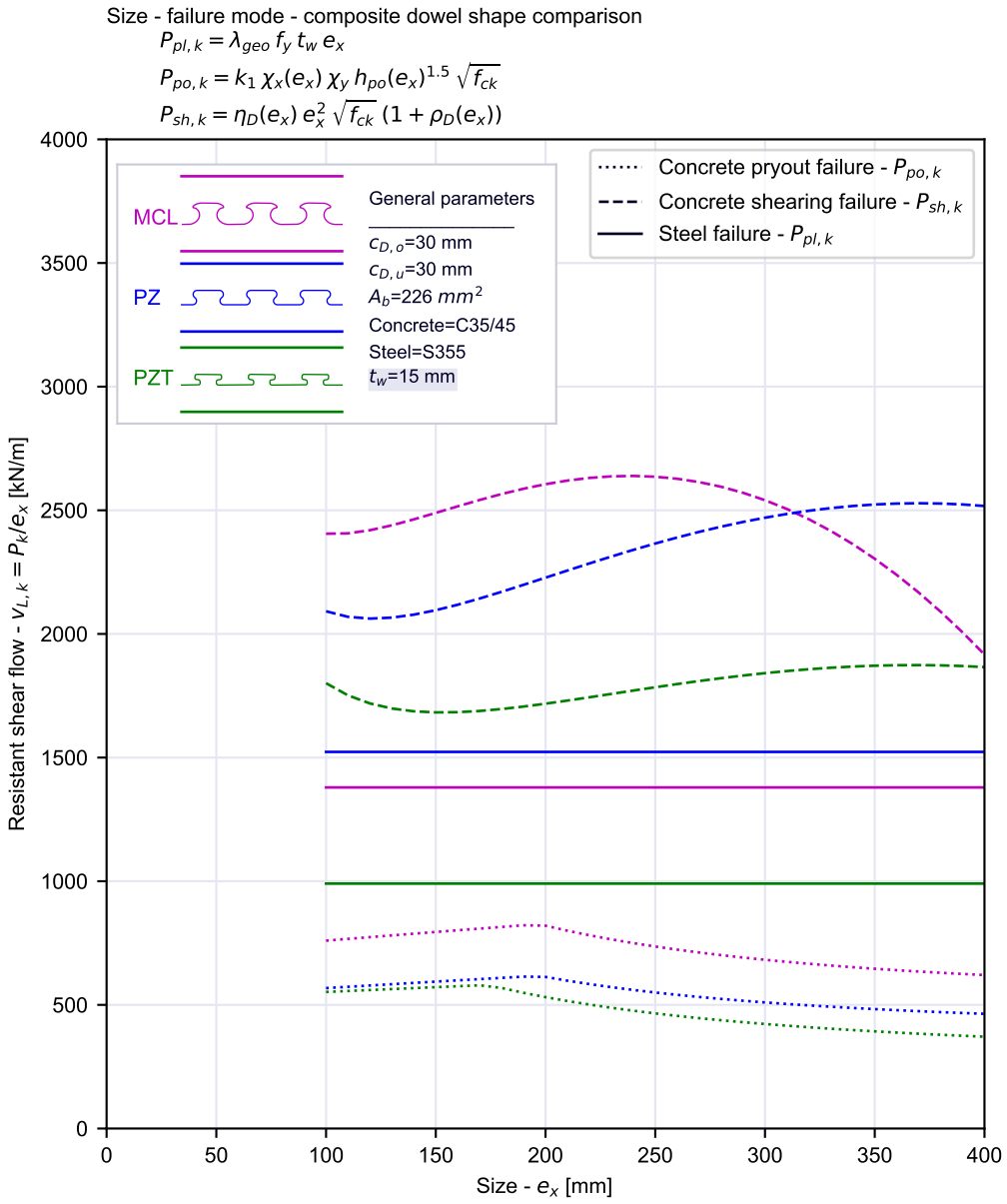

Figure 4.2: comparison of resistance values of the different failure modes for the given listed input data. For the specific case the pryout failure mode is the dominant fo all three shapes

It can be observed that the concrete pryout is the critical failure mode for the specified values of the parameters in all the three different dowel shapes. Note that $P_{po,k}$ and $P_{sh,k}$ are not dependent on the web thickness t_w. Note that the resistant shear flow related with the steel dowel failure is not dependent on the dowel size e_x. If the purpose is to encourage the steel yielding failure mode for fixed distances to the concrete surfaces $c_{D,u}$ and $c_{D,o}$ and for fixed materials, the only choice a designer has is to reduce the web thickness t_w. The amount of reinforcement steel A_b just plays a role in the concrete shearing mode. However this failure mode is not the dominant. The discriminant in the critical failure mode can be identified

in the values t_w and $c_{D,o}$, $c_{D,u}$. For each dowel shapes the failure modes domain can be plotted in the size-web thickness plane $e_x - t_w$ for different values of $c_{D,o} = c_{D,u}$. Results are shown in Fig.4.3, Fig.4.4 and Fig.4.5.

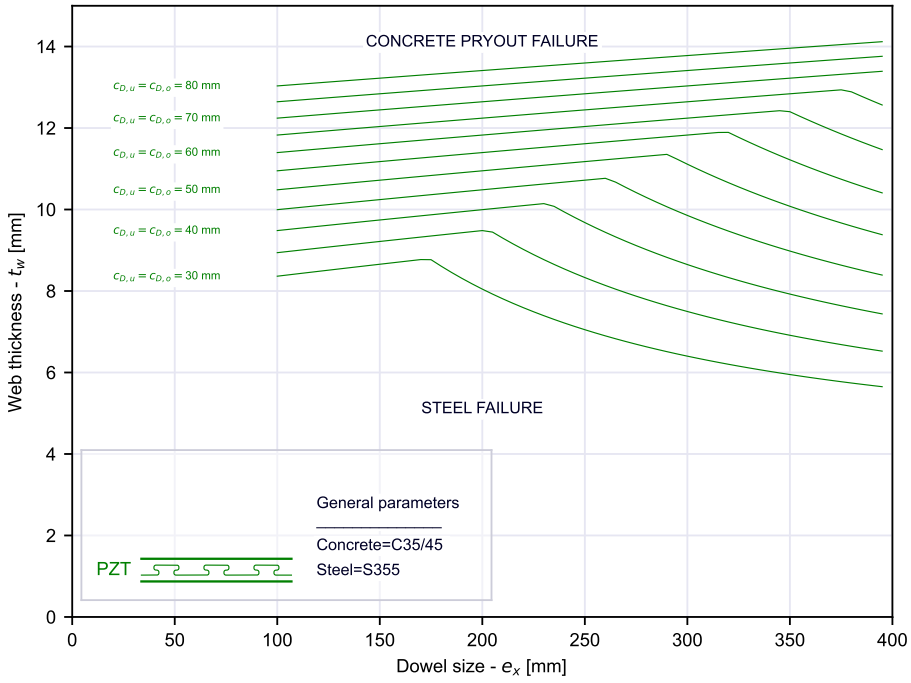

Figure 4.3: failure mode domains for the PZT dowel shape

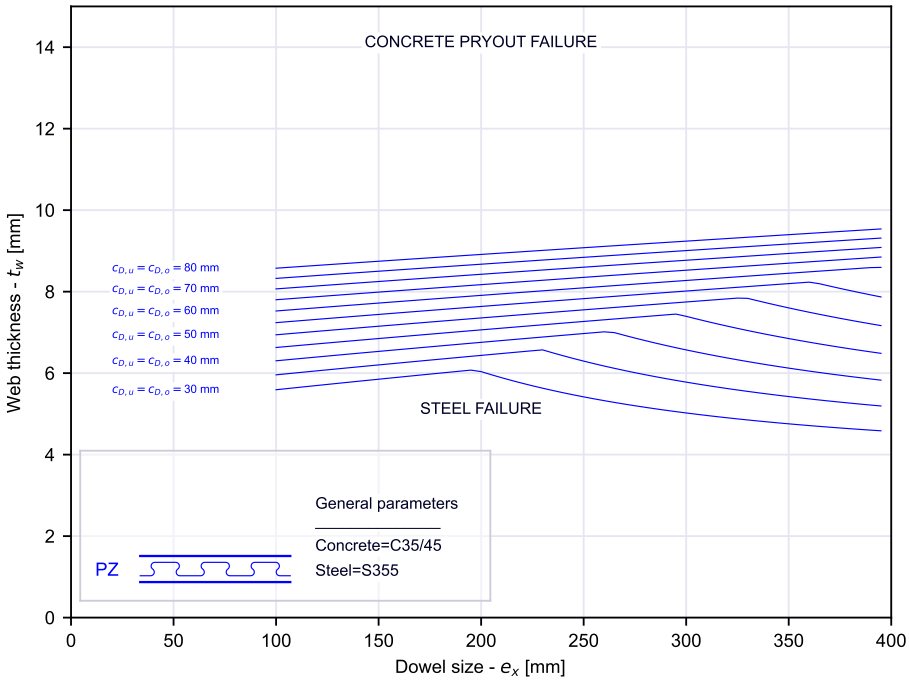

Figure 4.4: failure mode domains for the PZ dowel shape

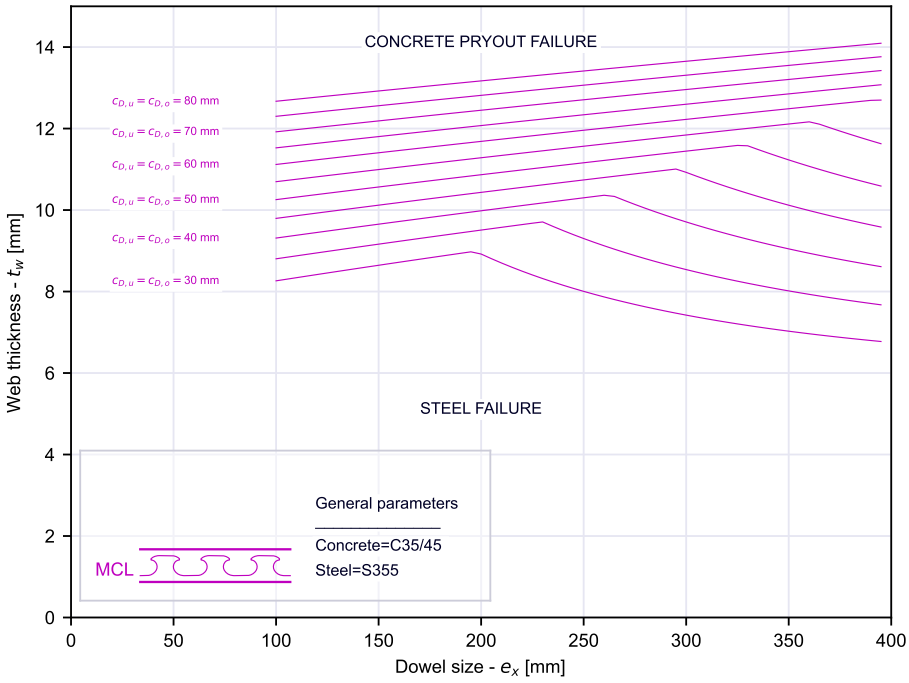

Figure 4.5: failure mode domains for the MCL dowel shape

MCL and PZT types are more likely to show a steel dowel yielding failure mode. Note that for reasonable values of $t_w \in [8, 15mm]$ is hard to obtain a steel dowel failure. Commercial sections used in the composite dowels technology normally have $t_w \geq 10mm$. Hence, a concrete pryout failure is expected in the common design situations.

4.3 General setup of the model

A first important conclusion is that in the composite dowels solutions with the shear connection embedded in a concrete slab the yielding failure is not likely to happen and more brittle failure modes show (Fig.4.6). In this frame is important to correctly assess the ductility in both failure mode cases. The slip deformation is a result of a sum of the concrete deformation contribute and the steel deformation contribute (Fig.4.7).

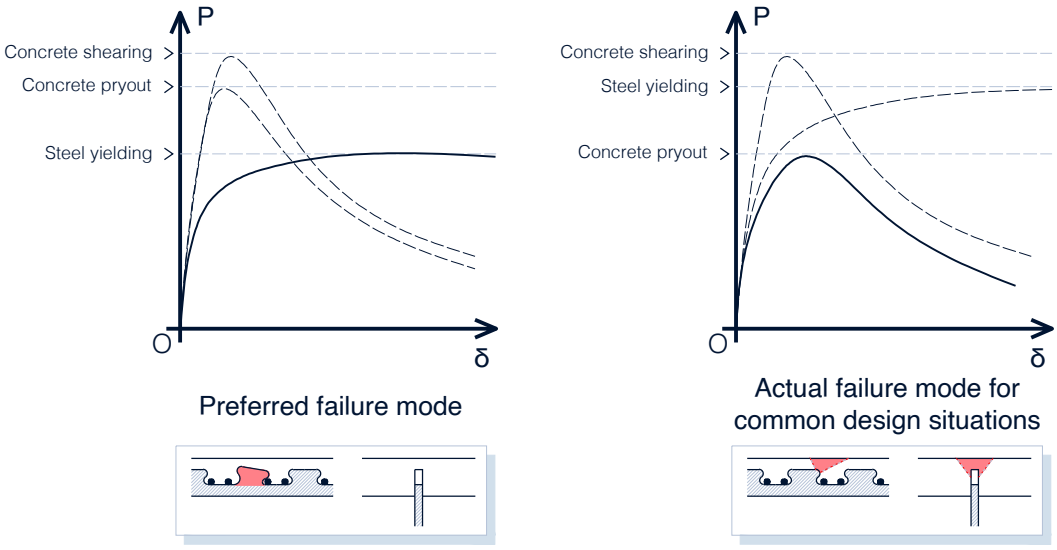

Figure 4.6: conceptual load-slip curves of the shear connection for the desired situation and the common design situation

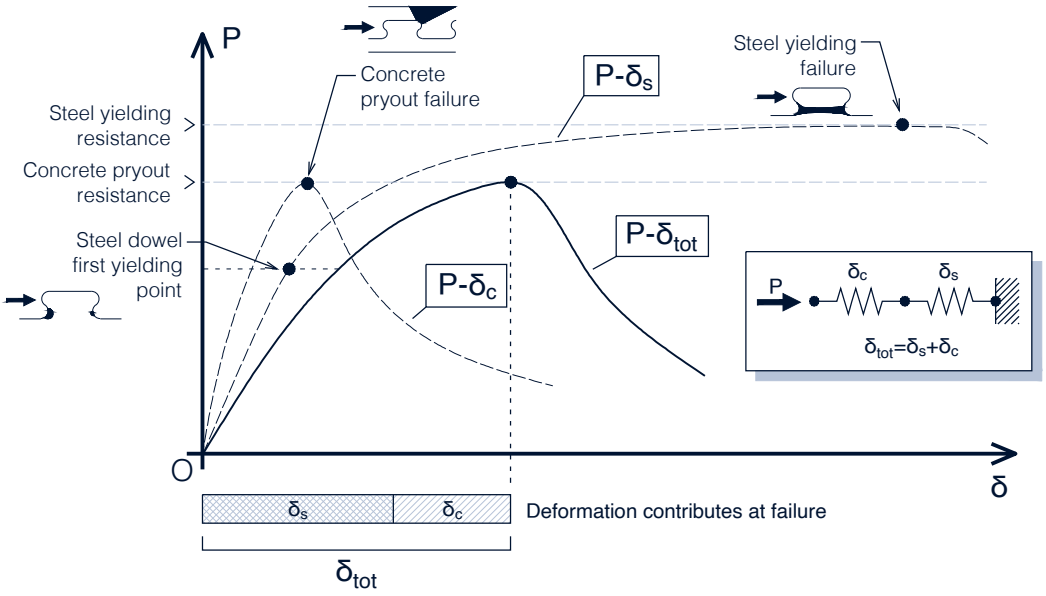

Figure 4.7: conceptual slip contributes in case of concrete pryout failure

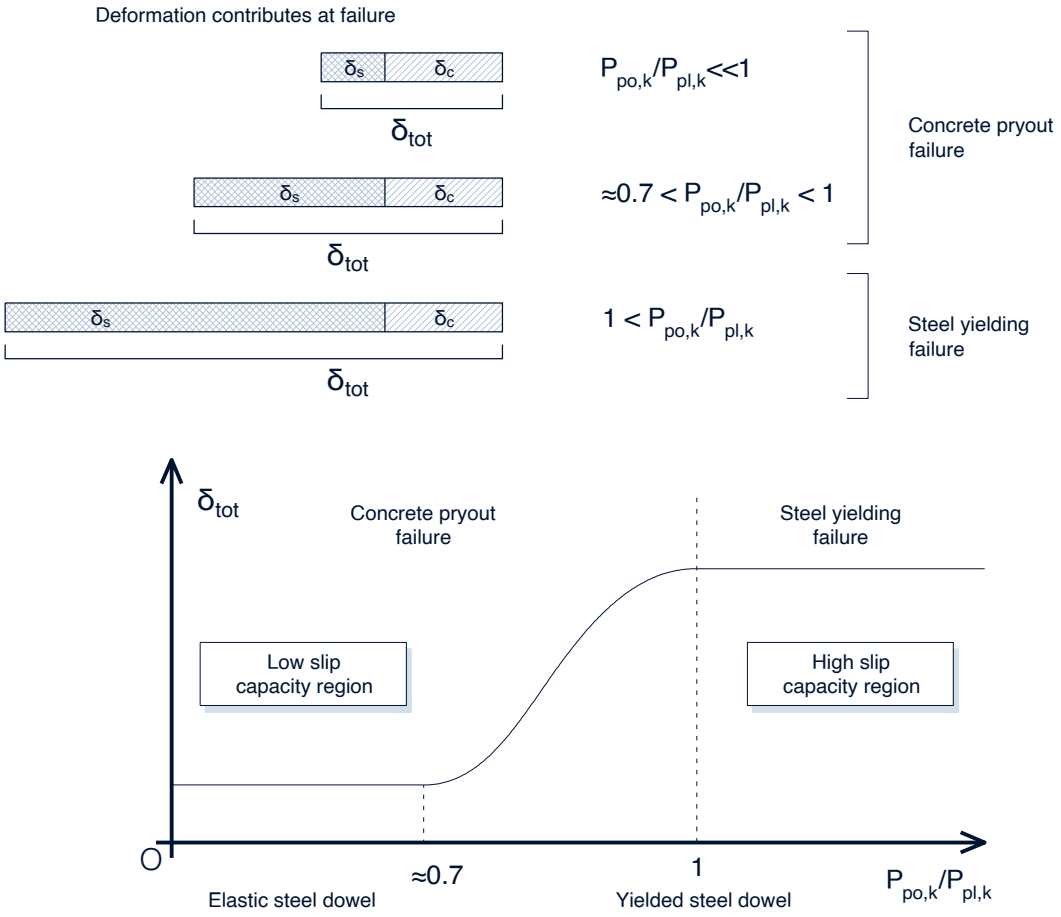

Figure 4.8: conceptual graph of transition from high slip capacity failure to low slip capacity failure mode

4.4 Steel dowel yielding failure model

Due to the multiple complications in deriving analytically a model for the steel dowel mechanical behaviour, as first point critical aspects are listed. Multiple simplifications are done in the assumptions. These are underlined in the development of the model. The consistency of the results with the expectations is tested and a sensitivity analysis of the most important parameters characterizing the model is carried out.

4.4.1 Preliminary observations

Observations done in literature are here briefly summarized. These are useful for the following considerations.

- according to Lorenc [71] the ductility in case of steel dowel yielding failure is proportional to the size of the dowel. Considerations are done in [22]. The concept has been reviewed in section 2.6.6.
- according to [75] for PZ shaped dowels 90% of the plastic strains at failure were due to shear in numerical analysis. Some equivalent analysis for the MCL shaped dowel were made in [64]. Here

the plastic shear deformation is clearly visible in the failure configuration. A rotational component is also visible. On Push Out test specimens at failure similar considerations can be done. These concepts have been analysed in the literature review section 2.6.6.

- simple considerations in order to derive with analytical models the failure load are done in [76]. Here the resistance was estimated considering a pure shear failure mode. These has been analysed in the literature review section 2.6.5.
- simplified analytical approaches have been already developed in order to model the behaviour of the steel dowel. The "critical section approach" was developed in [63, 44]. In [64] drawbacks of these models are expressed. These have been analysed in the literature review section 2.6.5.
- multi-linear models have already been developed [38] in order to predict the steel dowel yielding failure mechanical behaviour of the composite dowels shear connection. These have been analysed in the literature review section 2.6.7.

Before developing the model a set of comments is done. The critical aspects in the development of the model are here highlighted.

- The actual nature of the studied problem is three dimensional. A steel dowel is embedded in a concrete chord. Both materials are nonlinear. Rebars can provide a confinement effect and an additional bearing capacity. The model can be reduced to a two-dimensional one, still preserving the reliability. In the next procedure the problem will be reduced to a one-dimensional cantilever model. This creates of course significant limitations on the reliability of the developed model because of the oversimplification.
- The actual static model of the steel dowel is that of a deep beam. The "Saint Venant" beam model, the "Euler-Bernoulli" or the "Timoshenko" beams model would result in an over simplification. The load application point has a significant influence on the behaviour. In case of deep beams the distribution of strains along the section is nonlinear already in the elastic phase. Analytical solutions for these elastic problems are provided in literature like the Airy potential functions. The case study however is nonlinear.
- in assessing the load capacity of the steel dowel, limit analysis theorems such as the static theorem or the kinematic theorem can be helpful. Especially in trying to circumscribe the actual failure load with an upper and a lower load limit.
- assessing the ductility of a system is more difficult. Both using analytical derived model and numerical analysis, the ultimate ductility is significantly affected by the input material law curve. This aspect is clearly visible in the study [76]. This is especially true regarding the ultimate strain value of the steel and the plastic branch choice of the model. Significant scattering in the steel dowel ductility have been observed in [38] under experimental test conditions.

4.4.2 Model development

A one dimensional model is here used. Limitations and drawbacks of this choice have been highlighted before in section 4.4.1.

Two limit cases

Two limit cases can be identified. These are depicted in Fig.4.9. In both cases a rectangular section is considered with base b and height t_w. The steel model consists in an elastic-perfectly plastic behaviour. The first limit case considers a slender dowel, where the eccentricity h_P of the force is significantly larger compared with the base b of the section. In this case a bending failure is expected. The ultimate bending moment of the section is:

$$M_{pl} = 1/4 \cdot f_y t_w b^2 \tag{4.3}$$

By dividing this value with the eccentricity h_P of the force P, the maximum applicable force before a bending failure occurs can be derived as:

$$P_{max} = P_{max,b} = M_{pl}/h_P = 1/4 \cdot f_y t_w b^2/h_P \tag{4.4}$$

In the second limit case, the steel dowel is considered as non slender. In this case the force eccentricity h_P is considerably lower compared with the section dimension b of the steel dowel. In this case the ultimate load P_{max} is the one related with a plastic shear failure:

$$P_{max} = P_{max,v} = \frac{1}{\sqrt{3}} f_y t_w b \tag{4.5}$$

In the bending failure case $P_{max,b}$ is dependent on the dowel slenderness h_P/b. If the value of the resistance is plotted as function of the slenderness h_P/b (Fig.4.10) the resistance domain is represented by the region under the hyperbolic curve. This hyperbole represents this failure criteria. In the shear failure case $P_{max,v}$ is not dependent on the dowel slenderness h_P/b. If the value of the resistance is plotted as function of the slenderness h_P/b (Fig.4.10) the resistance domain is represented by the region under a constant value. So an horizontal line represents this failure mode. These failure criteria are valid in case the slenderness will be very high ($h_P/b >> 1$) for the bending failure mode, or very low ($h_P/b << 1$) for the shear failure mode. In these limit regions, the lower value of the resistance will govern the failure mode. In the middle region the failure will occur with a combination of the two modes. Here the actual resistance of the steel dowel can be smaller than the minimum of the two values representing the limit cases. In particular if the two failure modes are imposed to be equal, an idea of where the interaction of the two failure modes occurs can be derived. This is done as follows:

$$P_{max,b} = P_{max,v} \qquad \rightarrow \qquad \frac{1}{\sqrt{3}} = 1/4 \cdot b/h_P \tag{4.6}$$

So, the slenderness value where the two resistances are equal is:

$$(h_P/b)^* = \frac{\sqrt{3}}{4} \approx 0.433 \tag{4.7}$$

It is supposed that the dowels with a slenderness close to this value will have a mixed type of failure, which will involve an interaction of the bending failure mode and the shear failure mode. Because of this interaction the resistance value will be also affected. Furthermore also the ductility value will be conditioned. To determine how wide this interaction zone is, is not immediate. It can just be concluded that at a sufficient distance of this region the dowel capacity will be governed by just one of the two failure modes under the hypotheses. A further observation can be made concerning the particular dowel shapes introduced by the technical approval for the compoite dowels. In this case the PZ, PZT and MCL shapes are adopted. Without formally defining the eccentricity of the force h_P and the section dimension b, a raw estimation of the dowel slenderness can be made. This was done in one case doing reasonable assumptions and trying to maximize the dowel slenderness (high case scenario), and in another case to minimize the same quantity (low case scenario). This procedure is not objective. Another author can identify different values for the low case and high case scenarios, but the resulting range would be similar. The scope of this procedure is just to identify a range of interest for the composite dowels applications. The following table summarises the results.

CEN-TS dowel shapes

Shape	High case scenario	Low case scenario
MCL ($e_x = 150\,mm$)	$b = 60mm$	$b = 70mm$
	$h_P = 60mm$	$h_P = 30mm$
	$h_P/b = 1.00$	$h_P/b = 0.43$
PZ ($e_x = 150\,mm$)	$b = 65mm$	$b = 85mm$
	$h_P = 40mm$	$h_P = 20mm$
	$h_P/b = 0.62$	$h_P/b = 0.24$
PZT ($e_x = 150\,mm$)	$b = 60mm$	$b = 90mm$
	$h_P = 30mm$	$h_P = 20mm$
	$h_P/b = 0.5$	$h_P/b = 0.22$

The largest value is obtained for the MCL case. The smallest value is obtained for the PZT case. A reasonable application range for the composite dowels slenderness can be identified in:

$$\text{Composite dowels application range} = R \tag{4.8}$$

So the slenderness will belong to this interval:

$$h_P/b \in R = [0.22, 1.00] \tag{4.9}$$

From this simple concept, the clear fact that the application range of the composites dowels falls exactly in the bending-shear failure interaction region can be appreciated. The value $(h_P/b)^* \approx 0.433$ is in the

middle of this region. For both the resistance and the ductility the bending and the shear contributes play a significant role. This conclusion is in accordance with the preliminary observations that were carried out.

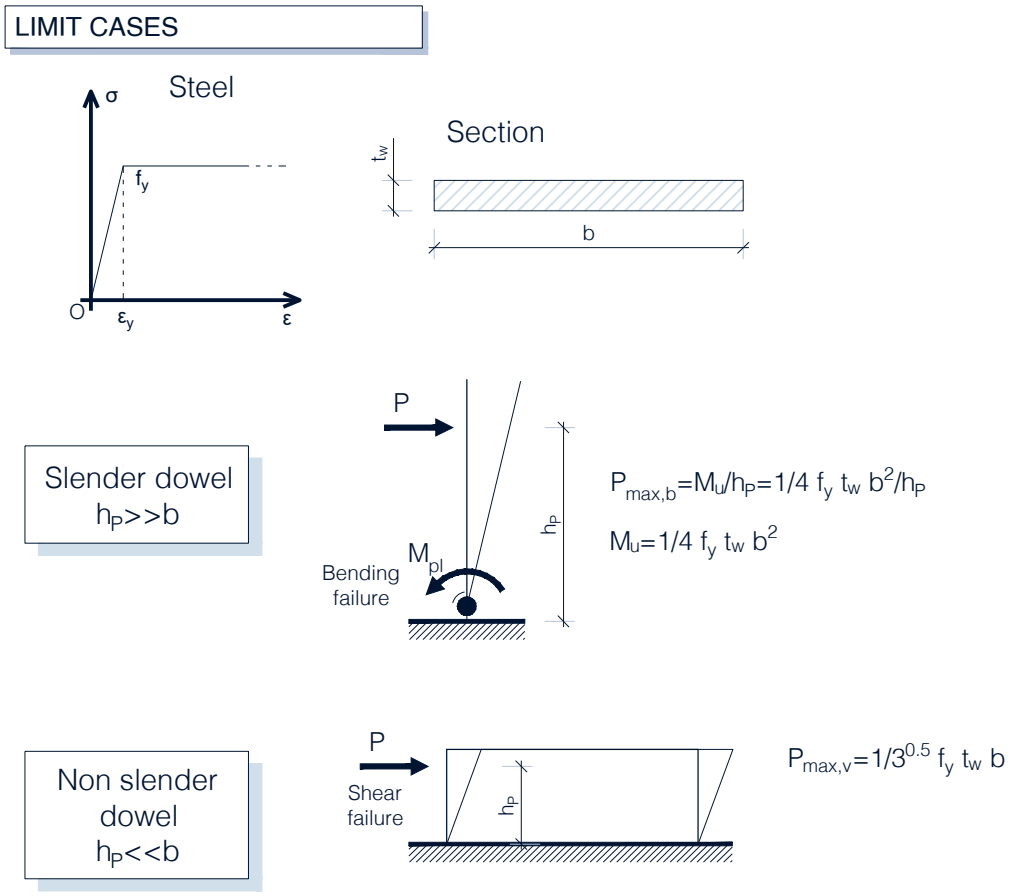

Figure 4.9: limit cases identification

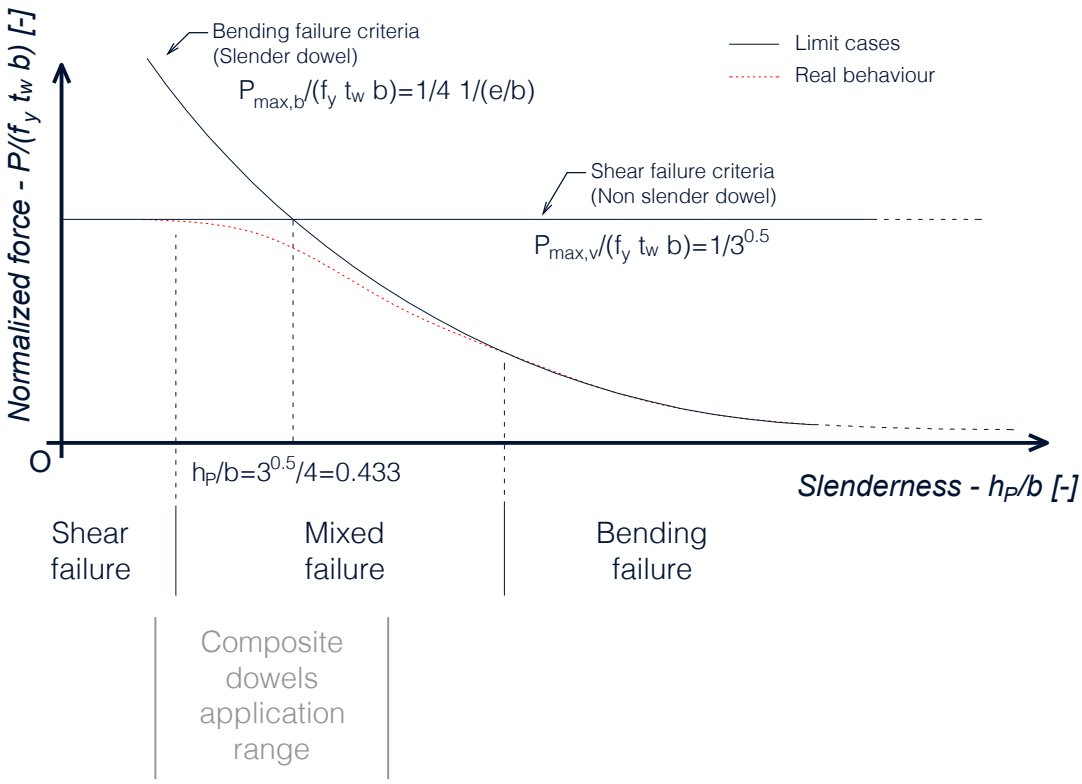

Figure 4.10: conceptual slenderness-resistance and failure modes diagram for the steel dowel yielding failure

Model description

The simplified model consists in a cantilever beam. In the fixed end proximity a localized rotational spring and a localized shear spring are placed. The two springs are nonlinear and are connected in series. The shear spring has the scope to reproduce the shear-angular slip behaviour of the dowel. The rotational spring has the objective to model the moment-rotation mechanical behaviour of the dowel. These two springs are ideally placed in the same point. The simplified model is based on these two fundamental assumptions:

- the plastic deformation are much more significant compared with the elastic contributes;
- the plastic deformations are concentrated in a specific region of the dowel;

The dowel has size e_x and thickness t_w. For each of the three dowel shapes the reference plane is identified as that one located at the bottom boundary of the connector. From this plane the dowel's height h, the reference shear connection height $h/2$ and the critical section position h_{crit} are measured. The shear force P is impressed on the dowel with a lever arm of h_P respect with the critical section position. The critical section has base b. The model setup is shown in Fig.4.11.

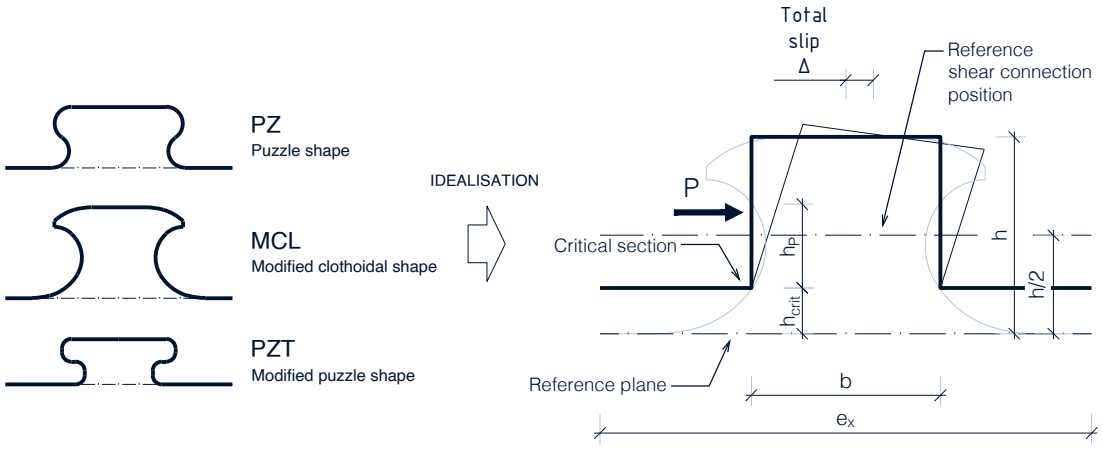

Figure 4.11: simplified analytical model for the steel dowel yielding failure setup: identification of the geometric quantities

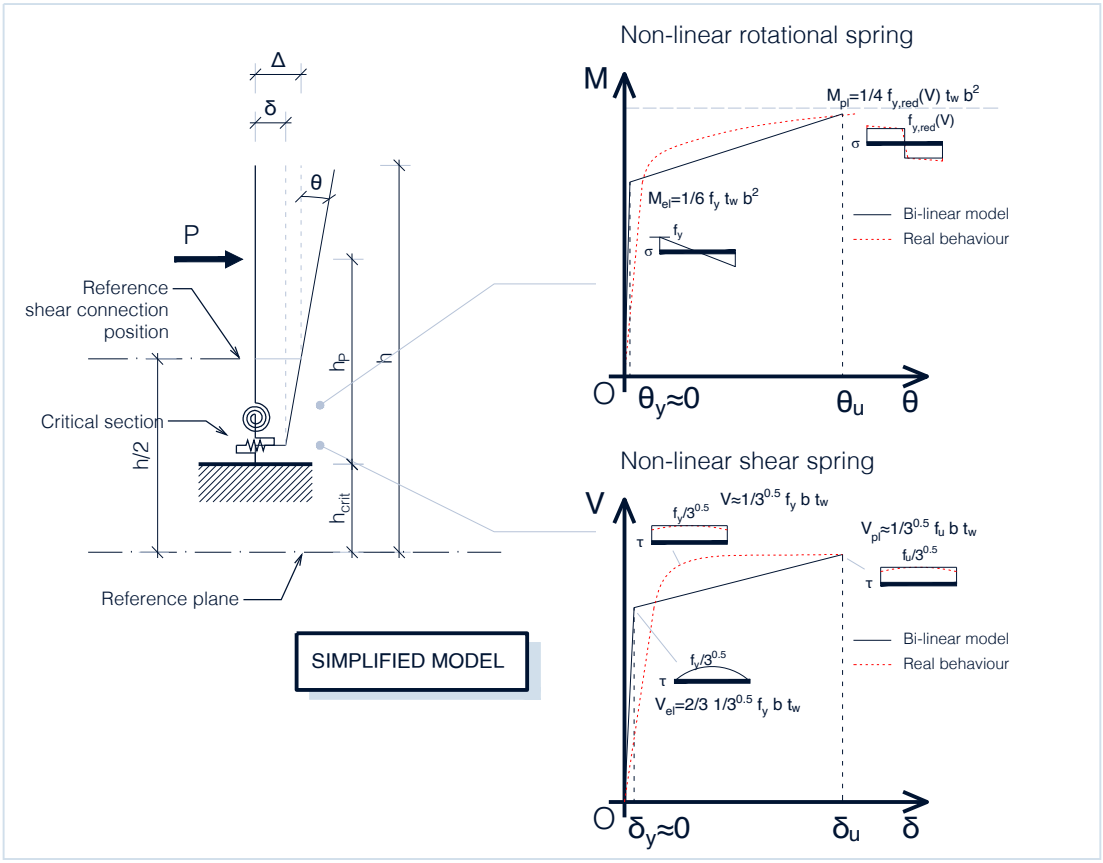

Figure 4.12: simplified analytical model for the steel dowel yielding failure setup: model setup and mechanical curves for the two nonlinear springs

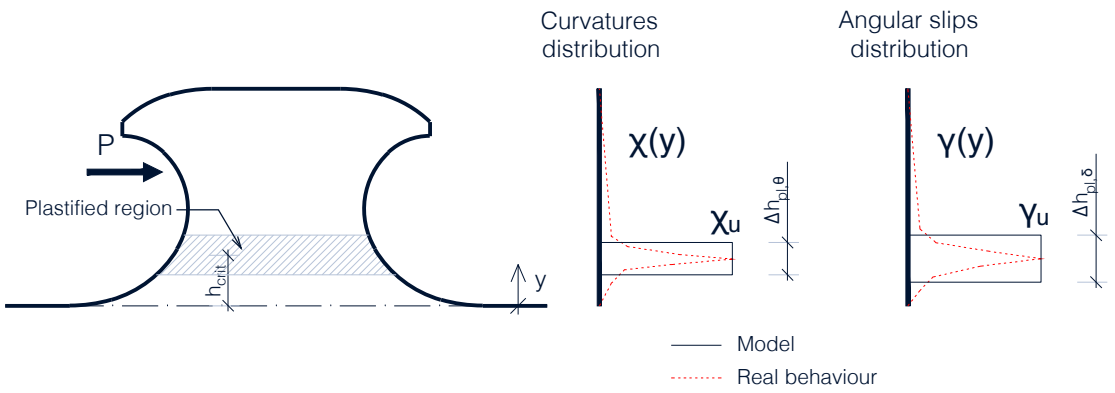

Figure 4.13: simplified analytical model for the steel dowel yielding failure setup: concept of plastic hinge length and plastic plane length

Kinematic description

The total slip Δ is measured in correspondence of the shear connection reference position. A pure shear slip contribute is given by a rigid translation of the beam. This degree of freedom is labelled as δ. A rotational contribute is given by the rigid rotation of the dowel with an angle θ. So, following from the kinematical description given in Fig.4.12, the following equation holds:

$$\Delta = \delta + (h/2 - h_{crit}) \cdot \sin\theta \tag{4.10}$$

If the geometrical nonlinearity is neglected, thus considering a small displacements regime, the previous relation reduces to:

$$\Delta = \delta + (h/2 - h_{crit}) \cdot \theta \tag{4.11}$$

Equilibrium conditions

The simple equilibrium equations of a cantilever beam are considered. The reaction bending moment offered by the rotational spring is:

$$M = P \cdot h_P \cdot \cos\theta \tag{4.12}$$

Again, if the geometric nonlinearity is neglected, the previous relation reduces to:

$$M = P \cdot h_P \tag{4.13}$$

The shear force in correspondence of the critical section is equal to the applied bearing force P.

$$V = P \tag{4.14}$$

Material laws of the shear spring

The shear resistance V_{el} is computed according to:

$$V_{el} = 2/3 \cdot \frac{1}{\sqrt{3}} f_y \cdot t_w \cdot b \tag{4.15}$$

Before this shear value the dowel is assumed to behave elastically. The ultimate shear load V_{pl} is assumed to be equal to:

$$V_{pl} = \frac{1}{\sqrt{3}} f_y \cdot t_w \cdot b \tag{4.16}$$

Between the first yielding value of shear V_{el} and the ultimate value of the plastic shear V_{pl}, the dowel will gradually plastify. A linear plastic hardening branch is assumed between the first yielding shear and the ultimate shear. The elastic yielding slip δ_y of the nonlinear shear spring is assumed to be much lower ($\delta_y \approx 0$) compared with the ultimate slip value δ_u. So the elastic deformation contribution of the shear spring has been neglected by assuming an infinite stiffness elastic branch.

The angular slips due to shear are in the real steel dowel behaviour non uniform along the height. The distribution of the angular slips can be expressed by a function $\gamma(y)$. Similarly to the nonlinear rotational spring case, the plastic shear angular slips are assumed to be uniformly distributed in a region of height $\Delta h_{pl,\delta}$. This region will be referred as plastic plane, and the concept is similar to that one of the plastic hinge for the bending mechanical behaviour. The following equation must hold:

$$\delta = \int_0^h \gamma(y) dy = \int_{h_{crit}-\Delta h_{pl,\delta}/2}^{h_{crit}+\Delta h_{pl,\delta}/2} \gamma_{max} dy = \gamma_{max} \cdot \Delta h_{pl,\delta} \tag{4.17}$$

Similarly to the nonlinear rotational spring case, the total slip due to the shear angular slips should be equal in the real case and in the simplified model. The ultimate slip δ_u is computed by considering the ultimate angular slip δ_u of a steel component subjected to pure shear. The equivalent Von Mieses strains are computed according to:

$$\epsilon_{eq} = \frac{2}{3} \cdot \sqrt{\frac{3\gamma^2}{4}} = \frac{\sqrt{3}}{3}\gamma \tag{4.18}$$

Here the limit equivalent Von Mieses strain ϵ_{eq} is set to ϵ_{su}. So the ultimate angular slip is:

$$\gamma_u = \frac{3}{\sqrt{3}}\epsilon_u \tag{4.19}$$

This leads to an ultimate slip of δ_u equal to:

$$\delta_u = \gamma_u \cdot \Delta h_{pl,\delta} \tag{4.20}$$

The model results in a bilinear $V - \delta$ mechanical behaviour of the nonlinear shear spring. The difference between the real expected behaviour and the simplified model bilinear function is conceptually highlighted in Fig.4.12.

Material laws of the rotational spring

The rotational spring has a nonlinear moment-rotation behaviour. The yielding moment M_{el} consists in the particular M value at which the first fibre of the section yields. The moment-shear (M-V) interaction is taken into account here reducing the yielding stress to:

$$f_{y,red} = f_y \cdot \sqrt{1 - \left(\frac{V}{V_{pl}}\right)} \tag{4.21}$$

Note that the reduced yielding resistance due to M-V interaction is therefore a function of the shear:

$$f_{y,red} = f_{y,red}(V) \tag{4.22}$$

This is computed by considering a rectangular section:

$$M_{el} = \frac{1}{6} f_{y,red} \cdot t_w \cdot b^2 \tag{4.23}$$

Note that here the linear stress distribution and implicitly the linear strain distribution, consist in an approximation. In fact due to the deep height nature of the beam the stress and the strains are nonlinear on a straight section.

The ultimate bending moment M_{pl} is considered equal to the following:

$$M_{pl} = \frac{1}{4} f_{y,red} \cdot t_w \cdot b^2 \tag{4.24}$$

This is ideally reached for an infinite curvature ($\chi \to \infty$) value of the section. The infinite curvature situation is clearly ideal. Despite of that, the bending moment for a rectangular steel section can be demonstrated to approach the ultimate bending moment value M_{pl} even for high but reasonable values of curvatures χ. This can be appreciated in literature in [78] for slender beam cases. Again the linear strain and consequently the curvature representation assuming plane sections consists in an approximation in the present model.

The elastic contribute in the deformation is neglected ($\theta_y \approx 0$). Thus, an infinite stiffness is ideally characterizing the elastic branch of the spring.

In the real behaviour of the steel dowel, the distribution of the curvatures is assumed to be non uniform along the dowel height. A sharp increase of the curvatures will appear in the yielding region of the dowel. The model assumes the curvature to be approximated by a rectangular function, with value equal to the maximum curvature χ_{max} in a region of height $\Delta h_{pl,\theta}$. Here $\Delta h_{pl,\theta}$ has to be chosen in such a way that the following equation holds:

$$\theta = \int_0^h \chi(y) dy = \int_{h_{crit}-\Delta h_{pl,\theta}/2}^{h_{crit}+\Delta h_{pl,\theta}/2} \chi_{max} dy = \Delta h_{pl,\theta} \cdot \chi_{max} \tag{4.25}$$

This means that the rotation of the dowel should be the same in the real behaviour and in the simplified model behaviour. Here a similar concept to that of the effective width of the concrete slab in the composite sections computation is used.

The ultimate curvature χ_u is defined starting from the ultimate strain ϵ_u and considering a linear strain distribution along the critical section.

$$\chi_u = \frac{\epsilon_u}{b/2} = 2 \cdot \frac{\epsilon_u}{b} \tag{4.26}$$

The failure angle θ_u is defined by integrating the failure curvature χ_u over the plastic hinge formation length $\Delta h_{pl,\theta}$. So the failure angle results in:

$$\theta_u = \int_{-\Delta h_{pl,\theta}/2}^{\Delta h_{pl,\theta}/2} \chi_u \, dy = \chi_u \cdot \int_{-\Delta h_{pl,\theta}/2}^{\Delta h_{pl,\theta}/2} dy = \Delta h_{pl,\theta} \cdot \chi_u \tag{4.27}$$

The model results in a bilinear $M - \theta$ mechanical behaviour of the nonlinear rotational spring. The difference between the real expected behaviour and the simplified model bilinear function is conceptually highlighted in Fig.4.12.

Failure criteria

Normally in a strain limited analysis the failure is assumed when the first steel fibre reaches a total strain of ϵ_{su}. This is normally done for the assessment of the resistance and the ductility of steel, reinforced concrete (RC) and composite sections under combined moment-axial force solicitation. In such cases the strain tensor $\underline{\underline{\epsilon}}$ at ultimate conditions is such that:

$$\underline{\underline{\epsilon}} = \begin{bmatrix} \epsilon_1 & \gamma_{12}/2 & \gamma_{13}/2 \\ \gamma_{12}/2 & \epsilon_2 & \gamma_{23}/2 \\ \gamma_{13}/2 & \gamma_{23}/2 & \epsilon_3 \end{bmatrix} \underset{\approx}{\text{ULS}} \begin{bmatrix} 0 & 0 & 0 \\ 0 & 0 & 0 \\ 0 & 0 & \epsilon_3 \end{bmatrix} \tag{4.28}$$

However, in the present case a plane strain field $\underline{\underline{\epsilon}}$ is assumed:

$$\underline{\underline{\epsilon}} = \begin{bmatrix} \epsilon_1 & \gamma_{12}/2 & \gamma_{13}/2 \\ \gamma_{12}/2 & \epsilon_2 & \gamma_{23}/2 \\ \gamma_{13}/2 & \gamma_{23}/2 & \epsilon_3 \end{bmatrix} \underset{\approx}{\text{ULS}} \begin{bmatrix} \epsilon_1 & \gamma/2 & 0 \\ \gamma/2 & 0 & 0 \\ 0 & 0 & 0 \end{bmatrix} \tag{4.29}$$

An equivalent plastic strain equation can be defined in a manner consistent with the definition of the Von Mises equation [79]. The equivalent Von Mieses plastic strain is computed according to the following relation:

$$\epsilon_{eq} = \frac{2}{3} \cdot \sqrt{\frac{3(e_1^2 + e_2^2 + e_3^2)}{2} + \frac{3(\gamma_{12}^2 + \gamma_{23}^2 + \gamma_{13}^2)}{4}} \tag{4.30}$$

$$e_1 = \frac{2}{3}\epsilon_1 - \frac{1}{3}\epsilon_2 - \frac{1}{3}\epsilon_3 \tag{4.31}$$

$$e_2 = -\frac{1}{3}\epsilon_1 + \frac{2}{3}\epsilon_2 - \frac{1}{3}\epsilon_3 \tag{4.32}$$

$$e_3 = -\frac{1}{3}\epsilon_1 - \frac{1}{3}\epsilon_2 + \frac{2}{3}\epsilon_3 \tag{4.33}$$

The equivalent Von Mieses (VM) strain is limited to the value ϵ_{su}. When the first fibre reaches an equivalent Von Mieses strain equal to the limit value of ϵ_{su}, failure is assumed to happen.

$$\epsilon_{eq} = \epsilon_{su} \qquad \rightarrow \text{Failure} \tag{4.34}$$

The total strains are considered to be approximately equal to the plastic strains, thus neglecting the elastic contributes:

$$\epsilon_{tot,ij} = \epsilon_{el,ij} + \epsilon_{pl,ij} \approx \epsilon_{pl,ij} \tag{4.35}$$

In a simplified approach, the strain component ϵ_2 is assumed to be zero. So the equivalent Von Mieses strain reduces to:

$$\epsilon_{eq} = \frac{2}{3} \cdot \sqrt{\frac{3\epsilon_1^2}{2} + \frac{3\gamma^2}{4}} \tag{4.36}$$

Note that if the out of plane strain component ϵ_3 is assumed to be zero, an out of plane stress σ_3 arises, where the value depends on the chosen material law. On the other hand if the out of plane stress component σ_3 is assumed to be zero, an out of plane strain ϵ_3 arises. The component $\epsilon_3 = 0$ has here been assumed.

The value of the angular slip γ, is computed by considering that the plastic failure surface due to. Having the value of the relative slip due to the nonlinear shear spring δ, it's possible to derive a mean value of the angular slip γ along the plastic plane height as:

$$\gamma = \delta / \Delta h_{pl,\delta} \tag{4.37}$$

The hypothesis behind this assumption in that the plasticity in the angular slip component is uniformly distributed in a height equal to $\Delta h_{pl,\delta}$. The following equation is considered to hold:

$$\delta = \int_{-\Delta h_{pl,\delta}/2}^{\Delta h_{pl,\delta}/2} \gamma(y)\, dy = \gamma_{max} \cdot \int_{-\Delta h_{pl,\delta}/2}^{\Delta h_{pl,\delta}/2} dy = \Delta h_{pl,\delta} \cdot \gamma \tag{4.38}$$

Here an equivalent concept of that used in the slab effective width computation was exploited. The first strain component $\epsilon_1 = \epsilon$ is considered to be consequence of the bending action on the dowel and is computed starting from:

$$\theta = \int_{-\Delta h_{pl,\theta}/2}^{\Delta h_{pl,\theta}/2} \chi(y)\, dy = \chi_{max} \cdot \int_{-\Delta h_{pl,\theta}/2}^{\Delta h_{pl,\theta}/2} dy = \Delta h_{pl,\theta} \cdot \chi \tag{4.39}$$

A linear strain distribution is assumed on the section. This leads to:

$$\epsilon = \chi\, b/2 \tag{4.40}$$

This leads to:

$$\epsilon_1 = \epsilon = \theta / \Delta h_{pl,\theta} \cdot b/2 \tag{4.41}$$

4.4.3 Sensitivity analysis

In order to gain confidence and sensitivity on the model results, a simple exemplar rectangular dowel of $b = 0.5 e_x$ and generic slenderness of h_P/b is considered. The height is assumed to be $h = 4/3 h_P$. Values of parameters summarized in figures are used. The resulting force-total slip diagram of the dowel is plotted for various slenderness values (Fig.4.14). The points where the failure criteria is reached are marked in the chart. As expected from the preliminary considerations, the resistance appears to be function of the dowel slenderness. For low values of the slenderness h_P/b, the resistance appear to be constant and conditioned by a shear failure. For higher values of slenderness a reduction of the resistance appears. As expected the resistance tends to zero with higher values of slenderness. Note that a transition in the behaviour appears between the values $h_P/b = 0.27$ and $h_P/b = 0.8$. As expected the transition from the shear to bending failure mode appears in the region surrounding the value $h_P/b = 0.433$. The ductility of the dowel is almost constant for a pure shear failure with low values of h_P/b and increases for high values of slenderness h_P/b.

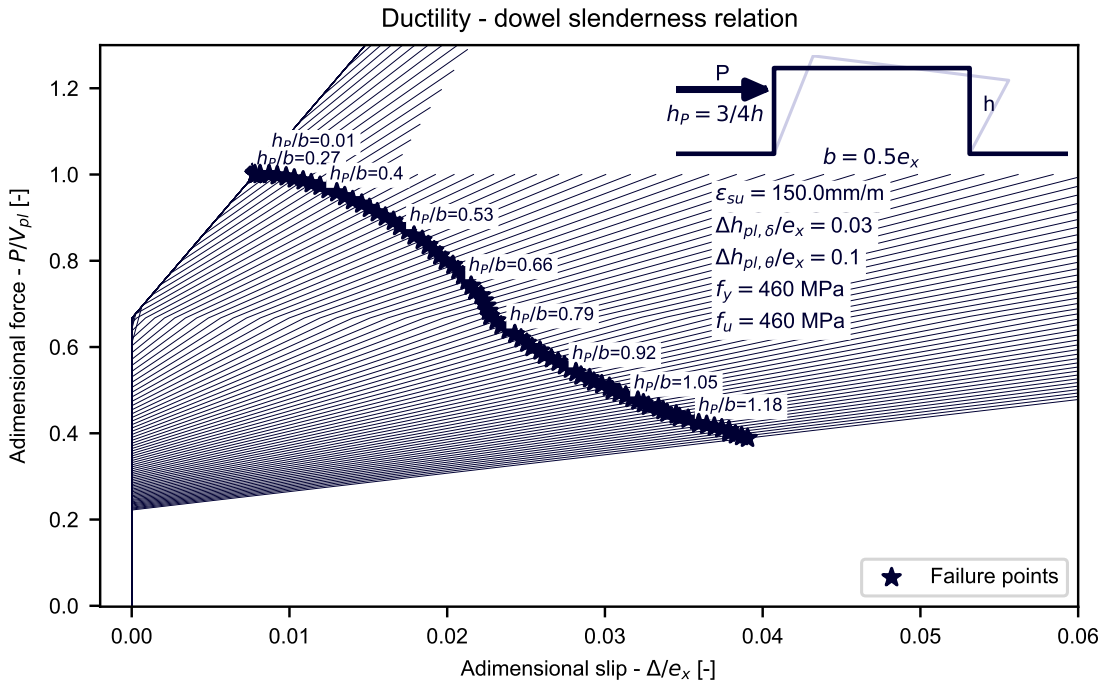

Figure 4.14: resulting load-total slip curves from the simplified analytical model for a test dowel of given listed data

The parameters $\Delta h_{pl,\delta}$, $\Delta h_{pl,\theta}$ and ϵ_{su} are supposed to play a significant role in the model, especially in the steel dowel ductility computation. Thus, a deeper study was made on the influence of these parameters. In order to have a better understanding of the influence of the parameters, the values where changed one-by-one. The reference case study is the same as the previous one and the quantities are summarized below:

$$f_y = 460\ MPa \qquad b = 0.5\, e_x\ mm \qquad h = 4/3\, e \tag{4.42}$$

The ductility of the failure point can be plotted as function of the slenderness for different values of the varied parameter.

In Fig.4.15 the results are summarized for varying $\Delta h_{pl,\delta}$ keeping the other parameters as constant. A visible difference can be observed in the three domains: for $h_P/b < 0.30$ a shear failure mode is observed with constant values of ductility. For $h_P/b > 0.75$ a bending failure mode is observed. The ductility value is affected by the plastic shear plane height $\Delta h_{pl,\delta}$ in the shear failure region. This value affects the ductility also in the mixed failure domain but does not have an influence in the bending failure mode domain.

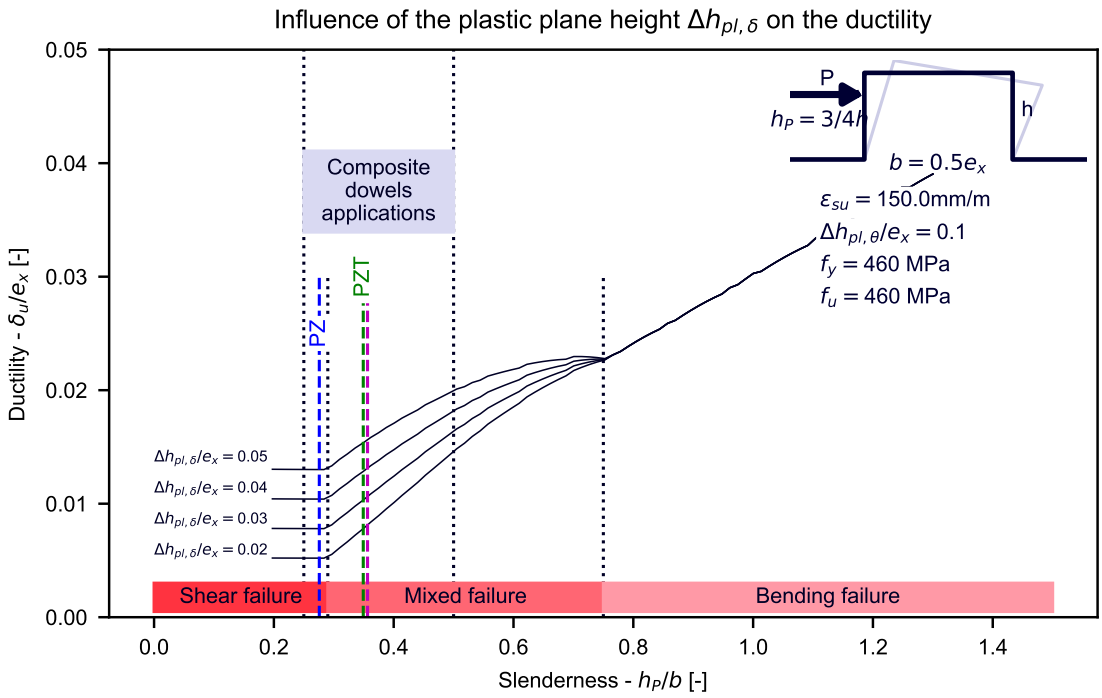

Figure 4.15: sensitivity analysis for the plastic plane height parameter as function of the slenderness of the dowel

In Fig.4.16 the results are summarized varying $\Delta h_{pl,\theta}$ and keeping the other parameters fixed. Again, a visible difference can be observed in the three domains: for $h_P/b < 0.23$ a shear failure mode is observed with constant values of ductility. For $h_P/b > 0.75$ a bending failure mode is observed. The ductility value is affected by the plastic shear plane height $\Delta h_{pl,\theta}$ in the bending failure region. This value affects the ductility also in the mixed failure domain but does not have an influence in the shear failure mode domain. In the bending failure domain the ductility appears to be a linear function of the slenderness.

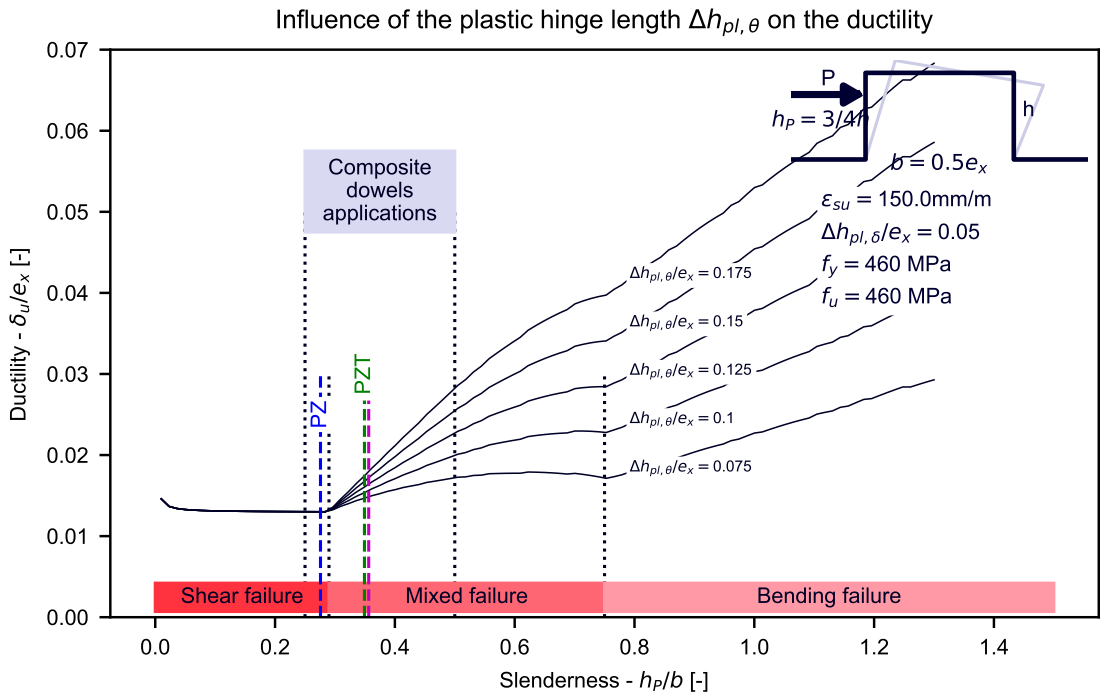

Figure 4.16: sensitivity analysis for the plastic hinge height parameter as function of the slenderness of the dowel

In Fig.4.17 the results are summarized varying ϵ_{su}. and keeping the other parameters fixed. Again, a visible difference can be observed in the three domains: for $h_P/b < 0.23$ a shear failure mode is observed with constant values of ductility. For $h_P/b > 0.75$ a bending failure mode is observed. All the three failure domains are affected by this parameter. In particular the most affected failure mode ductility is the one related with the bending failure. Here a much larger dependence is observed.

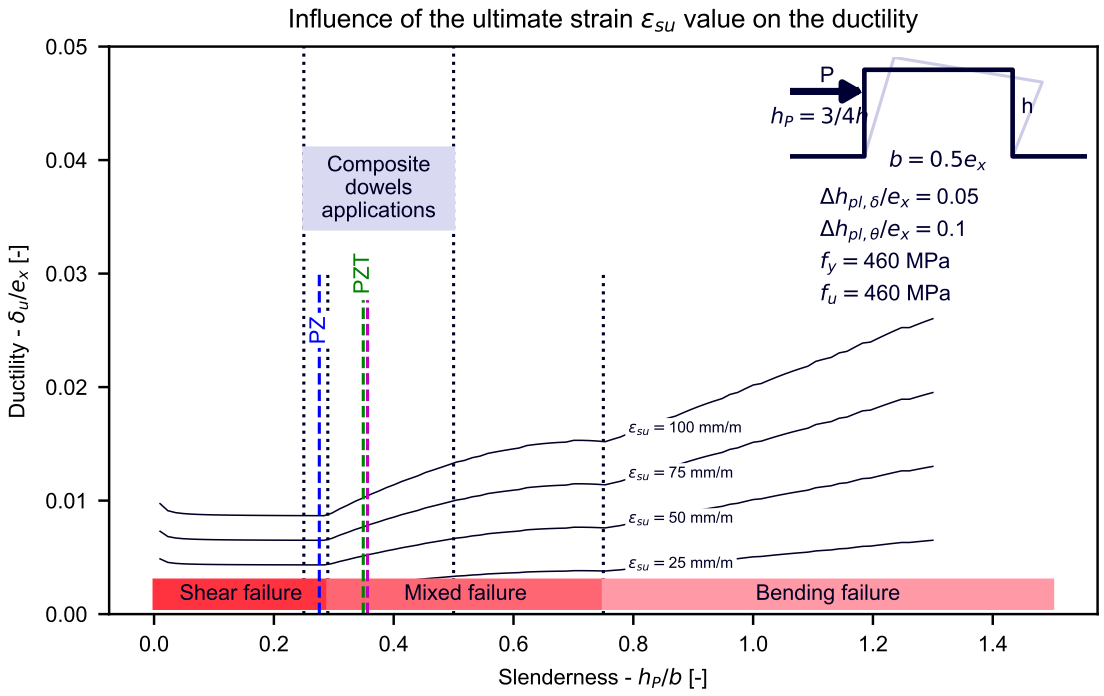

Figure 4.17: sensitivity analysis for the ultimate strain parameter as function of the slenderness of the dowel

This sensitivity study on the three parameters ϵ_{su}, $\Delta h_{pl,\delta}$ and $\Delta h_{pl,\theta}$ testifies that uncertainty of the complex situation is in the simplified model heavily dependent on these three parameters.

4.4.4 Model predictions for the standard steel dowel shapes

The standard steel dowel shapes MCL, PZ and PZT are used here, The considered generic size is e_x. The prediction of the simplified model is shown using the values:

$$f_y = 460\,MPa \qquad \epsilon_{su} = 50\,mm/m \qquad \Delta h_{pl,\theta} = 0.05\,e_x \qquad \Delta h_{pl,\delta} = 0.05\,e_x \tag{4.43}$$

The exploited values of h_P, b, h_{crit} and h for the different dowel shapes are summarized in the next table and the dowel geometry can be appreciated in Fig.4.18.

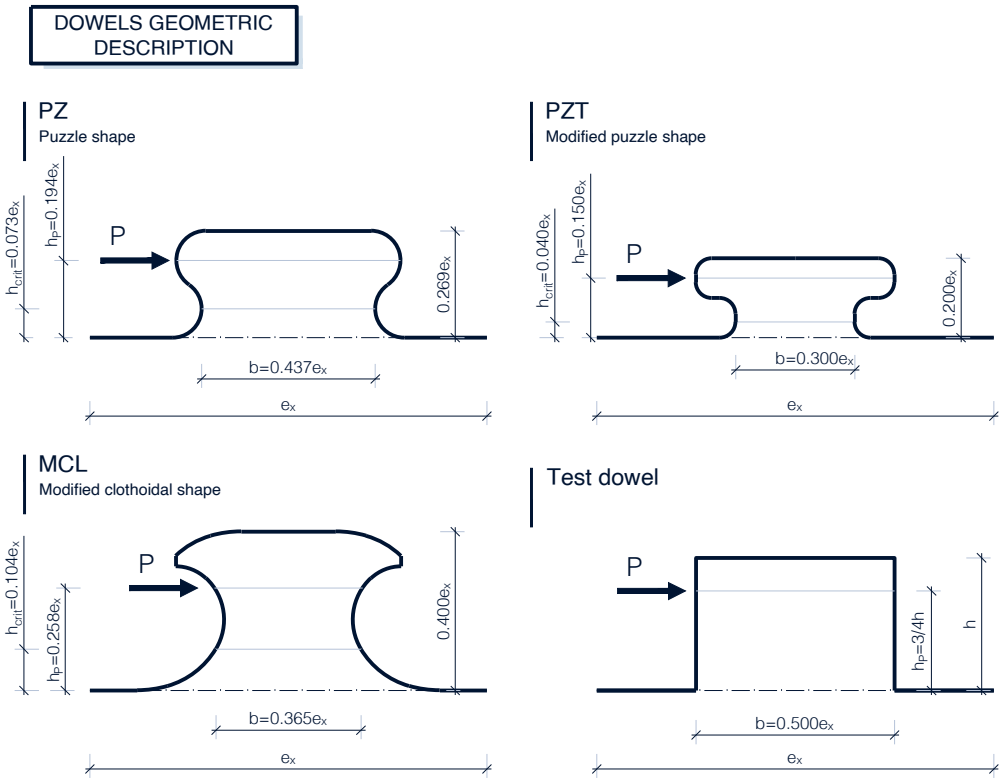

Figure 4.18: possible definition of the geometric quantities in accordance to the setup of the simplified analytical model for the three dowel shapes MCL, PZ and PZT

The material law is shown in Fig.4.19. The considered configurations lead to the nonlinear springs model of Fig.4.19. The MCL dowel appears to have a larger ductility value. The PZ and PZT dowels have lower but similar values of ultimate total slip Δ.

The derived values P/V_{pl} at failure can be used in order to check the correspondence between the literature coefficient λ_{geo} and the model results. This is done by writing:

$$\left(\frac{P_{\text{failure}}}{V_{pl}}\right) \cdot \frac{1}{\sqrt{3}}\, f_y\, b\, t_w = \lambda_{geo}\, f_y\, t_w\, e_x \tag{4.44}$$

The correspondent λ_{geo} values are derived by inverting the relation:

$$\lambda_{geo} = \left(\frac{P_{\text{failure}}}{V_{pl}}\right) \cdot \frac{1}{\sqrt{3}}\, \frac{b}{e_x} \tag{4.45}$$

These values can be compared directly with the values available in literature. This is done in Fig.4.20.

4.4.5 Comparison with literature available data

In Fig.4.21 a scatterplot of available literature test results is shown. Results are associated with a steel dowel yielding failure. Results are highly scattered and the presence of a negative R-squared parameter trying to summarize a linear model imposing zero slip capacity for size zero indicates the absence of additional information. Results have not been used for subsequent reasonings.

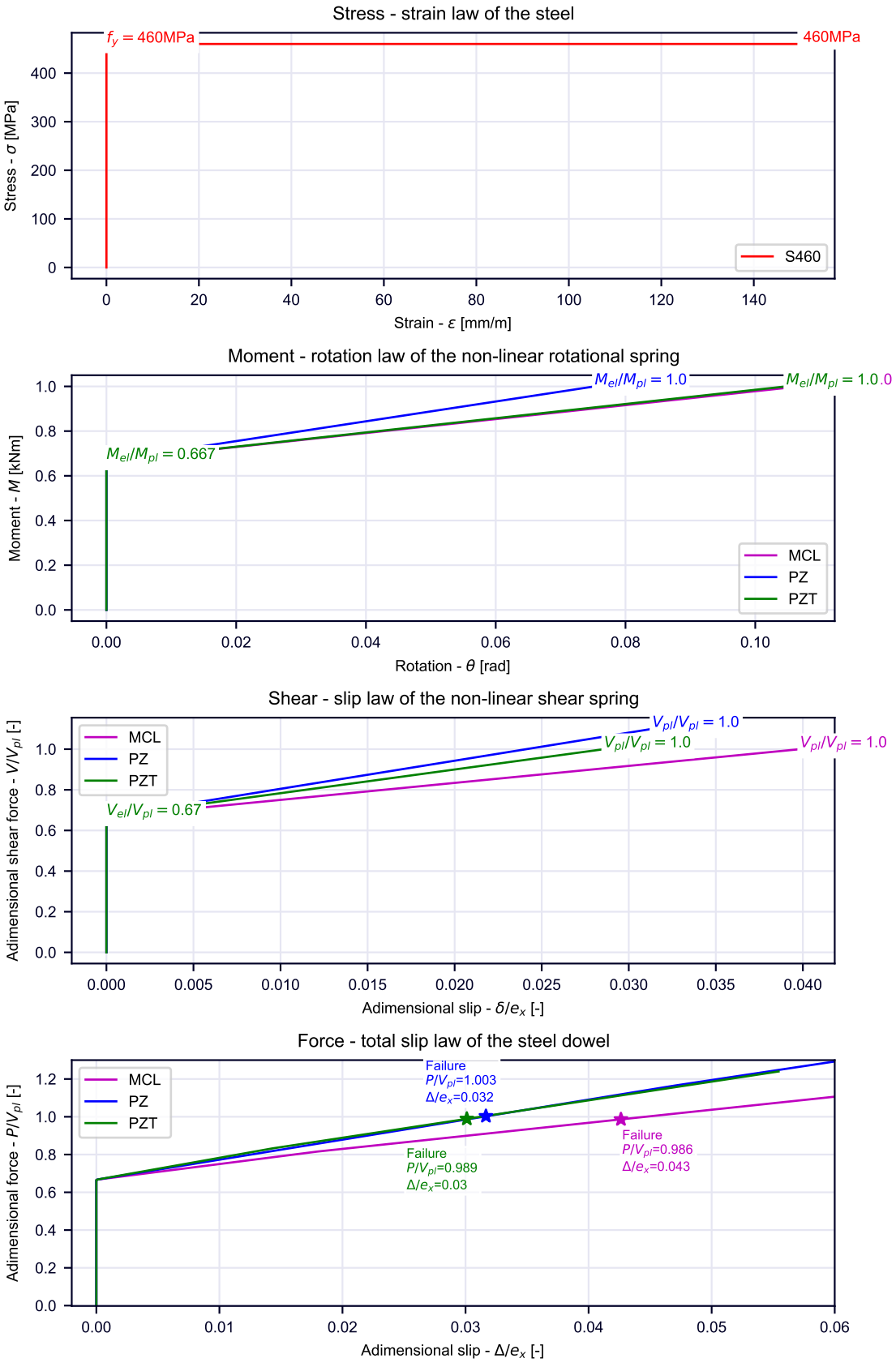

Figure 4.19: resulting curves for the three dowel shapes from the simplified analytical model for the steel dowel failure

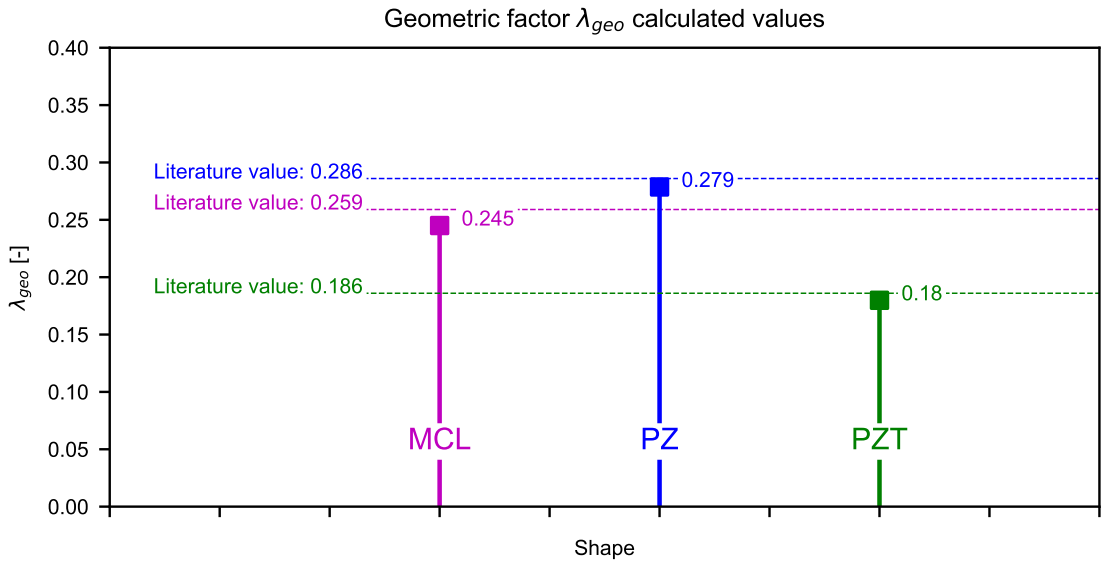

Figure 4.20: calibrated accordance of the resistance with the literature data

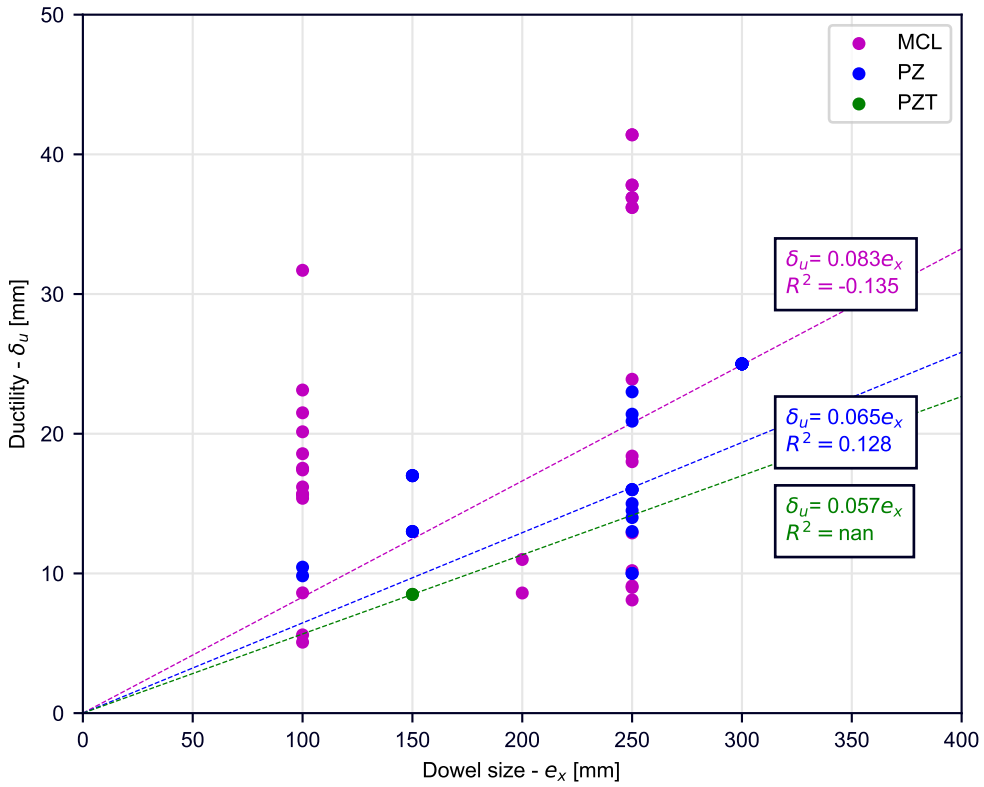

Figure 4.21: scatterplot of the available literature data for the steel dowel yielding failure ductility

4.5 Concrete crushing deformation contribute

The concrete crushing deformation contribute is added to the one of the steel dowel yielding. The assumption is that the concrete dowel of an approximate size of $0.5\, e_x$ is in compression with a linear variation of strains between the value of $\epsilon_{cu} = 3.5$ and $\epsilon = 0.0$. This results in a displacement contribute of:

$$\Delta_c = \epsilon_{cu}/4\, e_x \approx 0.01\, e_x \tag{4.46}$$

This is a contribute that is proportional to the size of the dowel. Note that the the computation in coarse and simplified.

4.6 Total plastic slip capacity estimation

The slip capacity is assumed to depend on the ratio between the concrete pryout failure resistance and the steel dowel yielding resistance ($P_{po,k}/P_{pl,k}$). The $P_{po,k}/P_{pl,k}$ ratio can be plotted in the input parameters plane $e_x - t_w - c - f_{ck}$. Here the steel grade is considered fixed and equal to the one associated with $f_y = 460\, MPa$. The concrete cover $c = c_{D,u} = c_{D,o}$ is used. Using the multi-linear relation of Fig.4.22 it is possible to map the minimum plastic slip capacity as function of the input parameters. A model has been derived. This will be in the subsequent sections compared with the model summarized from the results of the numerical analysis.
In Fig.4.25, Fig.4.23, Fig.4.24 the mapping of the resistances ratio is shown. In Fig.4.28, Fig.4.26, Fig.4.27 the mapping of the minimum plastic slip capacity is shown.

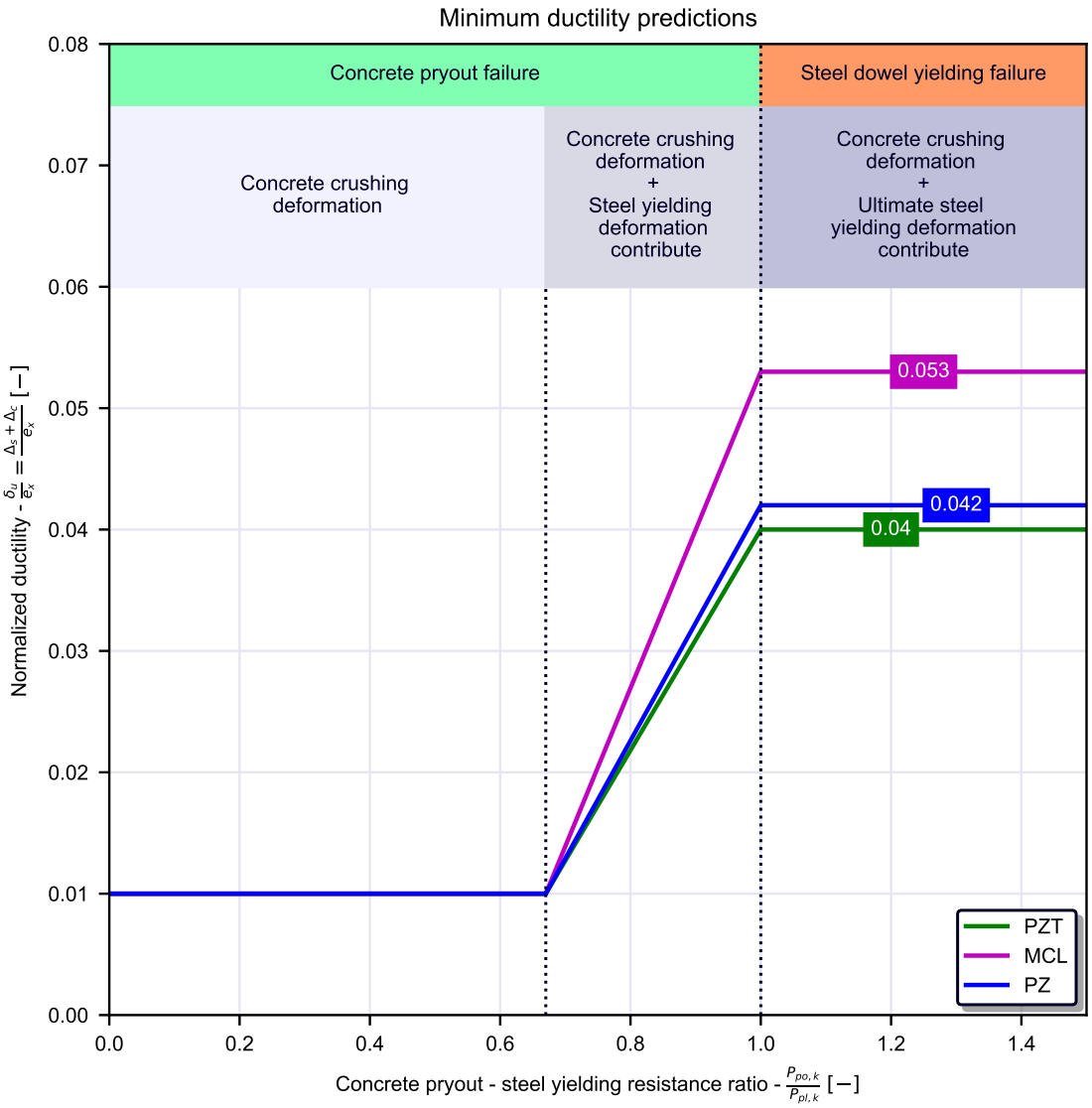

Figure 4.22: assumed normalized ductility as function of the concrete pryout-steel dowel yielding resistance ratio

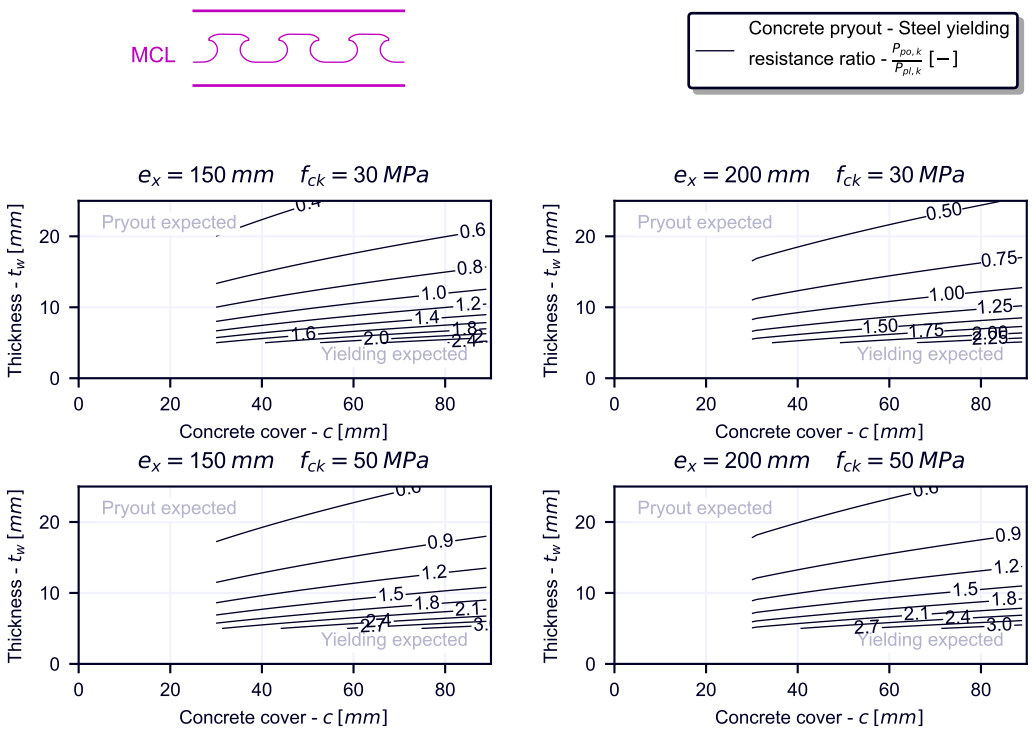

Figure 4.23: concrete pryout-steel dowel yielding resistance ratio mapping as function of the parameters e_x, f_{ck}, t_w and c for the MCL dowel shape

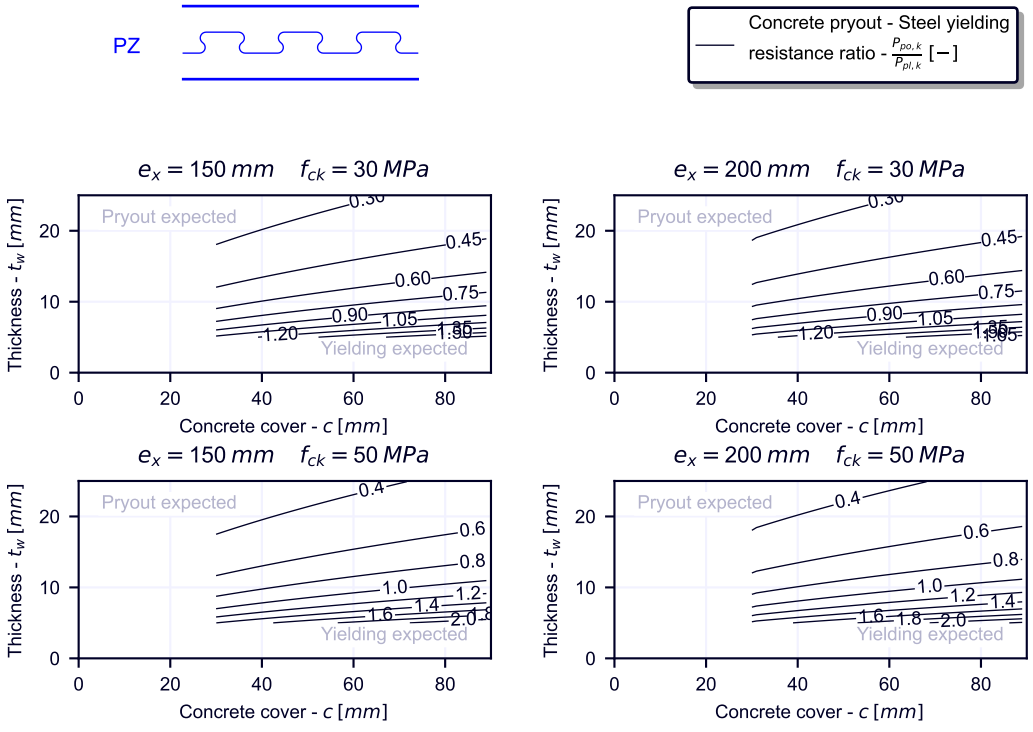

Figure 4.24: concrete pryout-steel dowel yielding resistance ratio mapping as function of the parameters e_x, f_{ck}, t_w and c for the PZ dowel shape

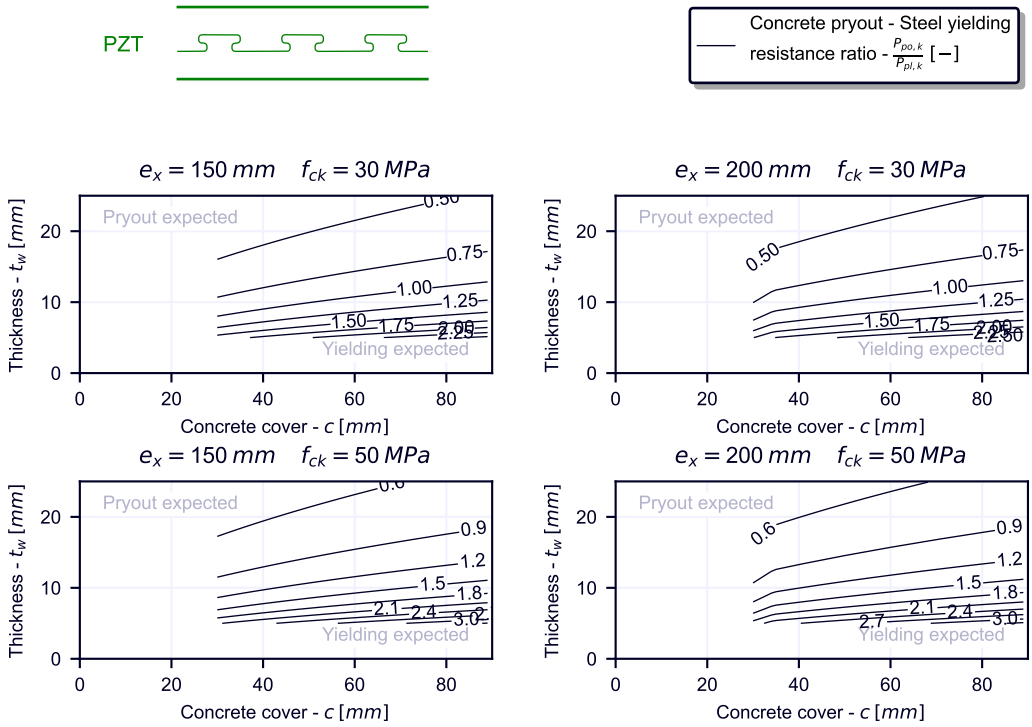

Figure 4.25: concrete pryout-steel dowel yielding resistance ratio mapping as function of the parameters e_x, f_{ck}, t_w and c for the PZT dowel shape

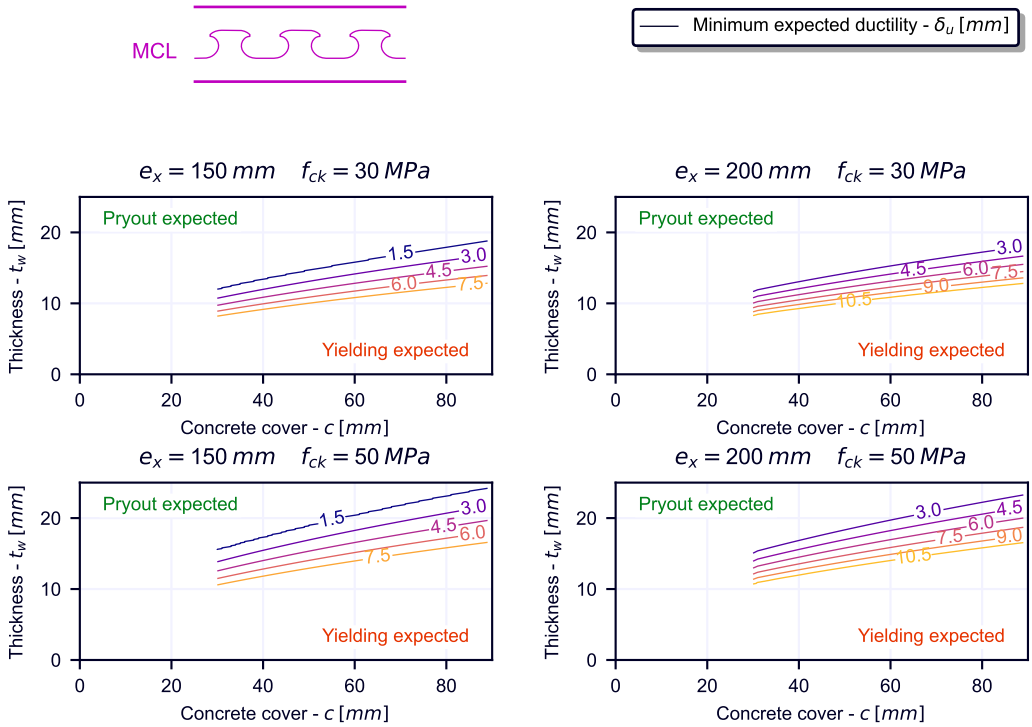

Figure 4.26: ductility model mapping derived from the analytical simplified model for the MCL dowel shape

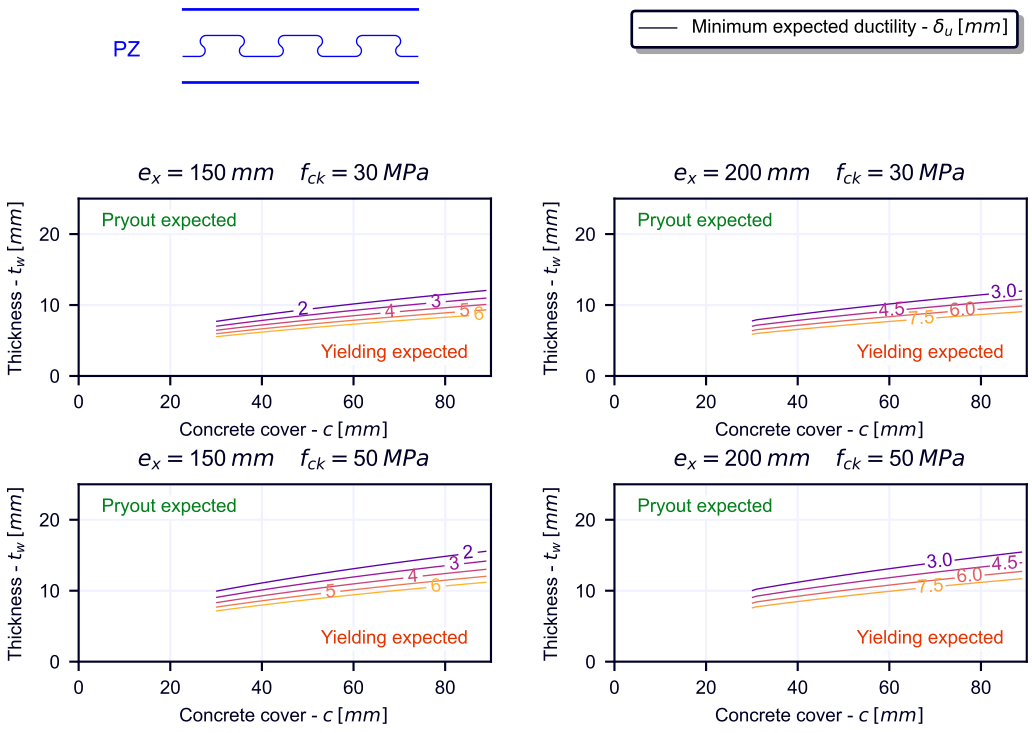

Figure 4.27: ductility model mapping derived from the analytical simplified model for the PZ dowel shape

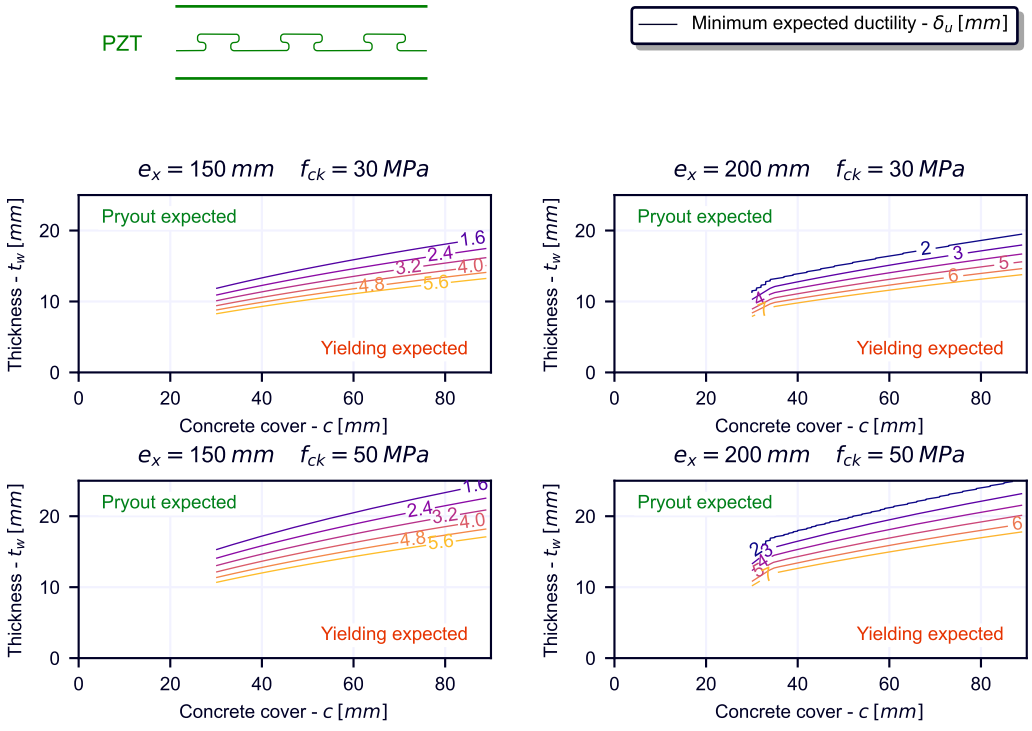

Figure 4.28: ductility model mapping derived from the analytical simplified model for the PZT dowel shape

Chapter 5

FEM analysis

5.1 Background information

5.1.1 Implicit versus explicit solver

The chosen solver can play a key role in determining the analysis consistency and simulation time. Between the two solvers different equations sets are used.

Explicit solver

In an explicit solver only a predictor step is used. The computational cost of the single increment is small. However to prevent numerical instabilities and drift errors in the solution the time increment can not be too large. The stable time increment Δt is the largest time increment that can be used by Abaqus. This is defined by:

$$\Delta t \approx L_{min}/c_d \tag{5.1}$$

$$c_d = \sqrt{\frac{\hat{\lambda} + 2\hat{\mu}}{\rho}} \tag{5.2}$$

Here L_{min} is the smaller element's size, ρ is the material's density, $\hat{\lambda}$ and $\hat{\mu}$ are the effective Lame's constants, c_d is the current dilation wave speed, E and ν the Young's modulus and Poisson's modulus of the material. For an elastic isotropic material these are:

$$\hat{\lambda} = \lambda_0 = \frac{E\nu}{(1+\nu)(1-2\nu)} \tag{5.3}$$

$$\hat{\mu} = \mu_0 = \frac{E}{2(1+\nu)} \tag{5.4}$$

In these circumstances:

$$c_d = \sqrt{\frac{\hat{\lambda} + 2\hat{\mu}}{\rho}} \propto \sqrt{\frac{E}{\rho}} \tag{5.5}$$

The stable time increment Δt reduces with smaller element size L_{min}, lower density, and higher stiffness. The smallest element is decisive for the analysis time. A badly shaped element can significantly influence

the analysis time. The loading rate does not influence the stable time increment. A large amount of simulated time will therefore also take a large amount of simulation time. In the explicit solver there are no convergency problems. The time increment is usually constant throughout the analysis. Time has a physical meaning. For contact problems the explicit solver is preferred. The Explicit solver can give more noisy results.

Implicit solver

In an implicit solver a predictor-corrector method is used. In this case after the predictor step, the solution is iterativelly corrected with a Newton-Raphson method. The computational cost of the single step is larger compared with the explicit solver case. On the other side the time increment is not limited by the stability and large time increments are allowed. Here convergency issues of the Newton-Raphson corrector step can arise. The time increment is not constant throughout the analysis. The more non-linear the problem is, the more computationally expensive it is to find a converged solution.
In Fig.5.1 a comparison between the two methods is made.

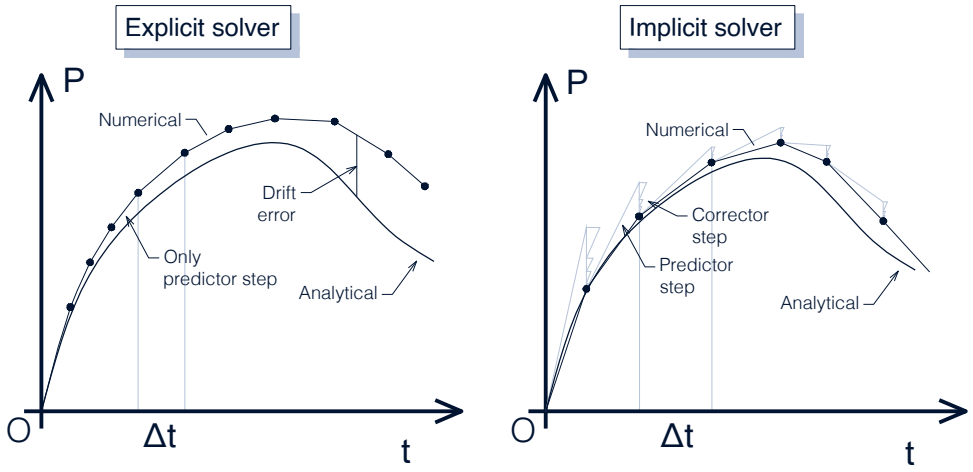

Figure 5.1: schematic representation of explicit and implicit analysis solver for one degree of freedom projection

5.1.2 Quasi-static solution in explicit analysis

The explicit solver calculates the dynamic equilibrium. Inertial contributes are accounted. More oscillatory results are expected in an explicit analysis. If a static phenomena is studied, dynamic effects are not of interest and the loading should be applied so slow that the force due to mass times acceleration does not play a role. A low load application rate is therefore required, thus implying high values of time step periods. Due to the fact that the stable time increment is not dependent on the step period, the computational cost will increase with higher values of step periods. In order to reduce the computational time a Mass Scaling Factor (MSF) can be applied to the masses of the model. A suggested value of MSF that keeps the problem

quasi-static is such that:

$$\sqrt{MSF} \cdot \delta_{max}/T \approx 10 \tag{5.6}$$

Applying a mass scaling allows for reducing the number of increments ($n_{increments} = T/\Delta t_{max}$).
Here δ_{max} and T are respectively the applied displacement and the step period. Their ratio is the load application ratio. In order to check the results consistency and the quasi-static assumption validity, the energy balance check should be carried out. In the whole model, the total energy E_{TOT} is constant. Due to numerical errors, an error can affect E_{TOT}, despite of that the error is generally contained in 1%.

$$\text{const.} = E_{TOT} = E_I + E_V + E_{FD} + E_{KE} + E_{IHE} - E_W - E_{PW} - E_{CW} - E_{MW} - E_{HF} \tag{5.7}$$

where E_I is the internal energy, E_V is the viscous energy dissipated, E_{FD} is the frictional energy dissipated, E_{KE} is the kinetic energy, E_{IHE} is the internal heat energy, E_W is the work done by the externally applied loads, and E_{PW}, E_{CW}, E_{MW} are the work done by contact penalties, by constraint penalties, and by propelling added mass, respectively. For the purposes of the present study:

$$\text{const.} = E_{TOT} = E_I + E_V + E_{FD} + E_{KE} + E_W \tag{5.8}$$

Under quasi-static conditions:

$$\text{const.} = E_{TOT} = E_I - E_W \qquad E_V \approx 0 \qquad E_{FD} \approx 0 \qquad E_{KE} \approx 0 \tag{5.9}$$

As a general rule the kinetic energy E_{KE} of the deforming material should not exceed a small fraction (typically 5% to 10%) of its internal energy E_I throughout most of the process (Fig.5.2).
In Fig.5.1 a comparison between the two methods is made.

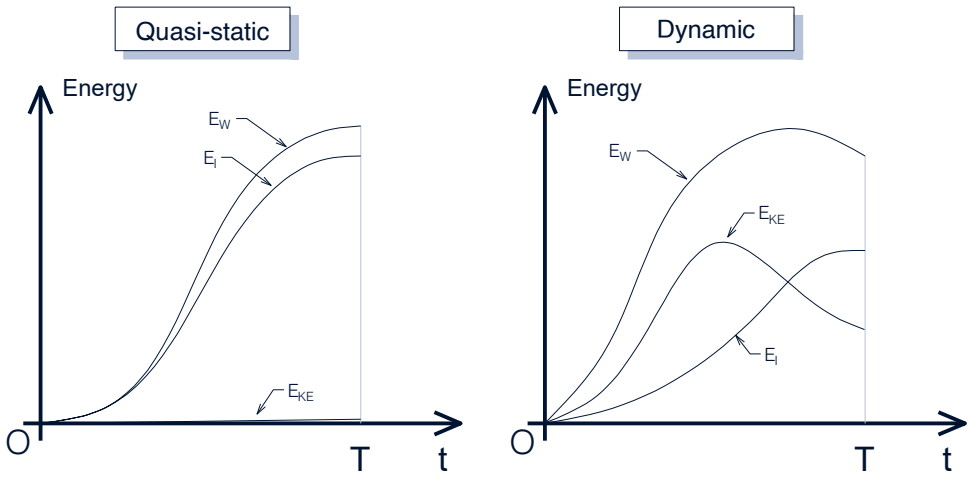

Figure 5.2: dynamic and quasi-static conditions energy balance comparison

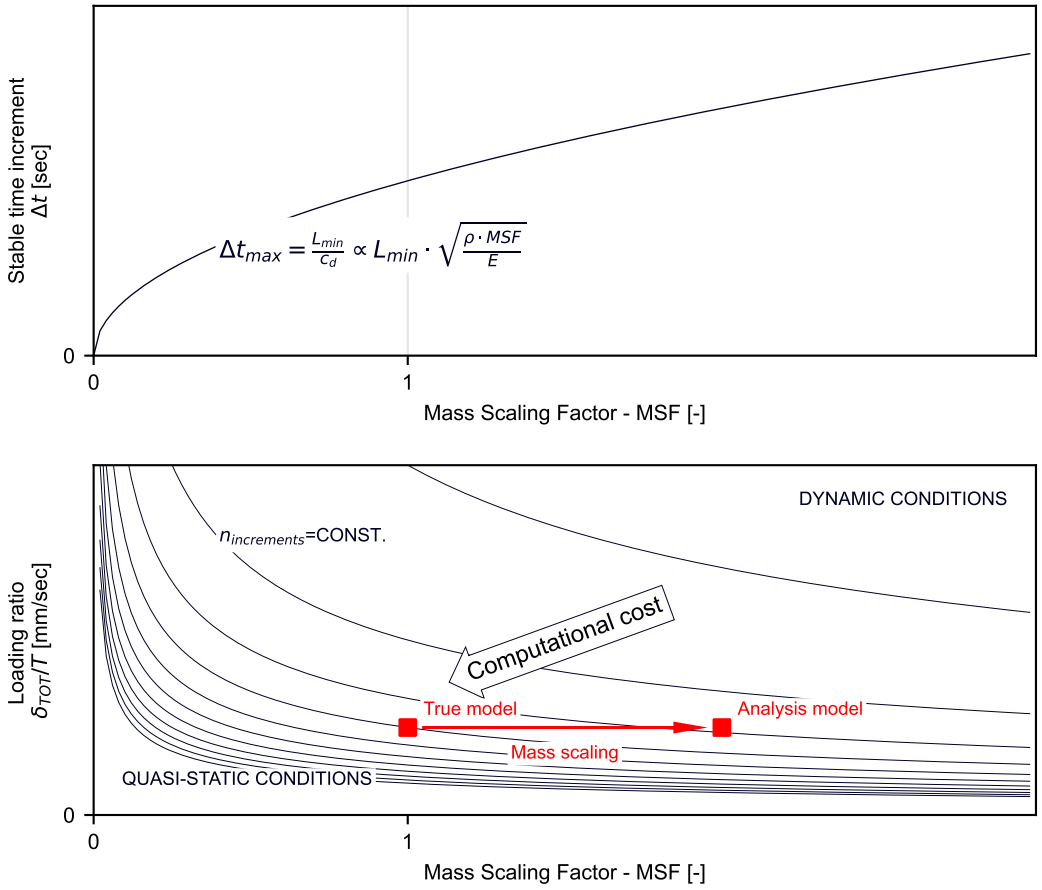

Figure 5.3: concept of mass scaling in the explicit numerical FEM analysis

5.1.3 Concrete CDP definition

An elastic property with elastic modulus E_{cm} has been defined. A mass property with density ρ has been used. A concrete damage plasticity model has been defined for the material non-linearity. Following parameters are used in the CDP model:

CDP parameters

Symbol	Parameter
Ψ	Concrete CDP dilation angle
f_{b0}/f_{c0}	Concrete CDP parameter (ratio of biaxial compressive yield stress to uniaxial compressive yield stress)
ϵ	Concrete CDP eccentricity parameter
K_c	Concrete CDP parameter (ratio of the second stress invariant on the tensile meridian to that on the compressive meridian for the yield function)
μ	Concrete CDP viscosity parameter

Compression law

The compression concrete CDP damage laws have been set according to the one used in [15]. The compression elastic-plastic behaviour is as follows:

$$\sigma_c(\epsilon_c) = f_{cm} \cdot \left(\frac{\frac{E_{cm}}{E_{c1}} \cdot \frac{\epsilon_c}{\epsilon_{c1}} - (\frac{\epsilon_c}{\epsilon_{c1}})^2}{1 + (\frac{E_{cm}}{E_{c1}} - 2) \cdot \frac{\epsilon_c}{\epsilon_{c1}}} \right) \tag{5.10}$$

Here:

$$\epsilon_c = \epsilon_{c,tot} = \epsilon_{c,el} + \epsilon_{c,in} \tag{5.11}$$

And:

$$\epsilon_{c,el} = \frac{\epsilon_c}{E_{cm}} \tag{5.12}$$

The Abaqus® input table for the uni-axial compression behaviour is given in σ_c and $\epsilon_{c,in}$ coordinates. Here the $i-th$ point is obtained as:

$$\{\sigma_{c,i}, \epsilon_{c,in,i}\} = \{\sigma_c(\epsilon_{c,i}), \epsilon_{c,in,i}\} = \{\sigma_c(\epsilon_{c,i}), \epsilon_{c,i} - \frac{\epsilon_{c,i}}{E_{cm}}\} \qquad \text{for } i = 1, ..., N \tag{5.13}$$

In order to prevent Abaqus® errors is important to define $\epsilon_{c,in,1} = 0$.
The damage d_c is computed according to:

$$d_c(\epsilon_c) = \begin{cases} 0 & \text{for } \epsilon_c <= \epsilon_{c,peak} \\ 1 - \frac{\sigma_c(\epsilon c)}{\sigma_{c,max}} & \text{for } \epsilon_c > \epsilon_{c,peak} \end{cases} \tag{5.14}$$

The Abaqus input table for the damage behaviour is given in d_c and $\epsilon_{c,in}$ coordinates. Here the $i-th$ point is obtained as:

$$\{d_{c,i}, \epsilon_{c,in,i}\} = \{d_c(\epsilon_{c,i}), \epsilon_{c,in,i}\} = \{1 - \frac{\sigma_c(\epsilon_{c,i})}{\sigma_{c,max}}, \epsilon_{c,i} - \frac{\epsilon_{c,i}}{E_{cm}}\} \qquad \text{for } i = 1, ..., N \tag{5.15}$$

Tensile law

A fracture energy criterion has been used in order to model the tension stiffening behaviour. The crack displacement w_c is introduced. The parameter G_F is the fracture energy and represents the amount of energy required to open a unit area of crack. This is a material property. The same exponential relation used in [36] is used:

$$\sigma_{ct}(w) = f_{ctm} \cdot e^{-w/w_u} \tag{5.16}$$

The integral should be equal to the fracture energy:

$$\int_{w=0}^{w=\infty} \sigma_{ct}(w) dw = G_F \qquad \rightarrow \qquad w_u = G_F / f_{ctm} \tag{5.17}$$

The parameter $G_F = 0.13\ N/mm$ is used. The Abaqus input points are:

$$\{\sigma_{ct,i}, w_{c,i}\} = \{\sigma_{ct}(w_{c,i}), w_{c,i}\} \tag{5.18}$$

The damage is defined as:

$$d_t(w_c) = 1 - \sigma_{ct}(w_c)/f_{ctm} \tag{5.19}$$

The Abaqus® input points are:

$$\{d_{t,i}, w_{c,i}\} = \{d_t(w_{c,i}), w_{c,i}\} \tag{5.20}$$

5.2 Parametric analysis setup

The model is shown in Fig.5.5. The FEM model is illustrated in Fig.5.4. Here the symmetry of the problem is considered.

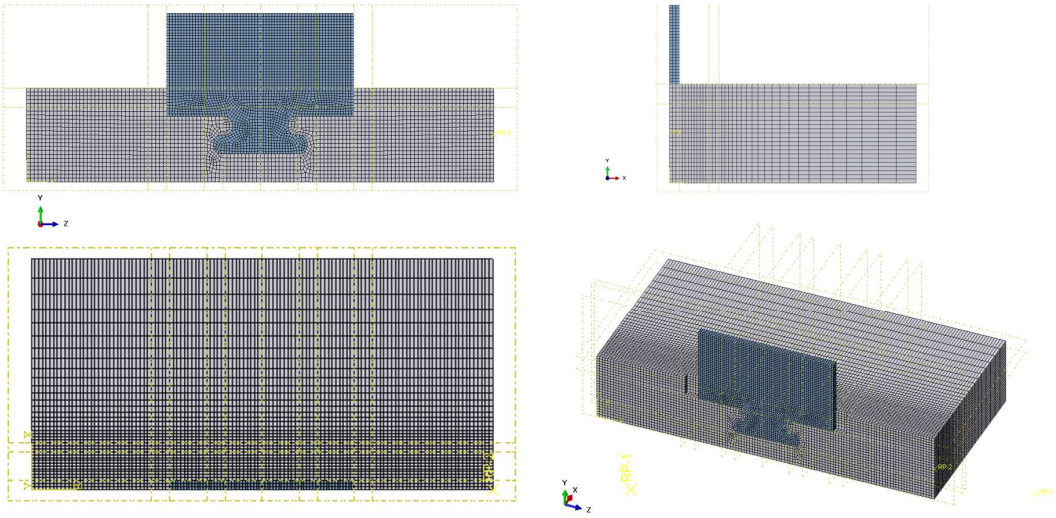

Figure 5.4: numerical model meshing

The listed parameters were varied in the parametric study:

- Shape={PZT, PZ, MCL}
- $t_w = \{5, 10, 20\}\ mm$
- $c = c_{Du} = c_{Do} = \{30, 45, 70\}\ mm$
- $e_x = \{150, 200\}\ mm$
- $f_{ck} = \{30, 50\}\ MPa$

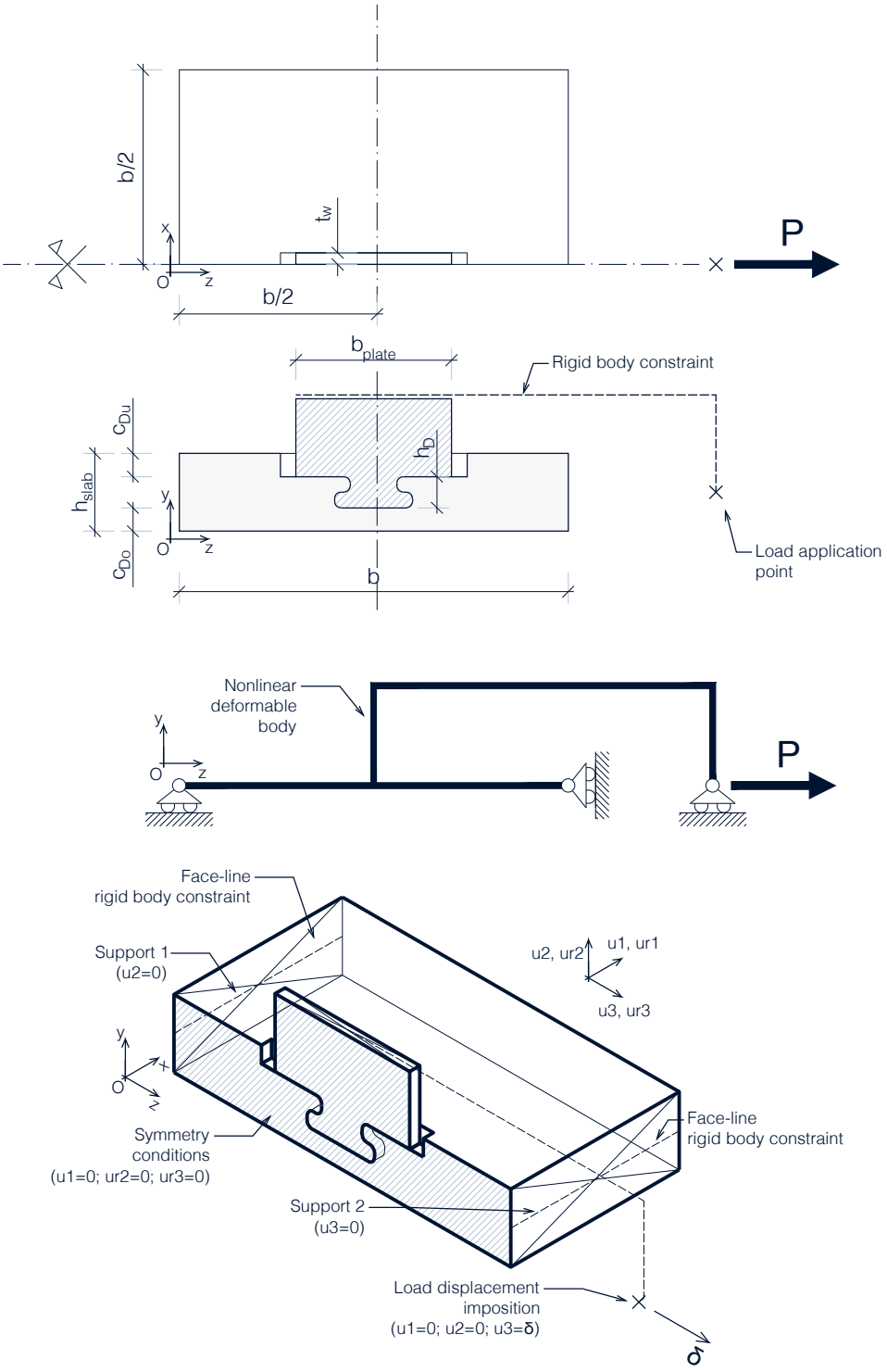

Figure 5.5: schematic representation of the numerical model: geometric parameters, boundary conditions

The plate dimensions in the $y-z$ plane are kept as constant for all the models. The considered steel grade is S460. Note that this was selected differently from the one used in the calibration study. This is in order to maintain a safe approach in the ductility assessment. The concrete cover of the reinforcement is fixed for $\Phi 10$ rebars and the relative position of the dowel with the reinforcement is fixed for $\Phi 12$ rebars.
A total number of 118 models are used in the parametric study, 36 per each dowel shape.
The models are named according to the following scheme:

$$Model - Shape - Size - Plate\,thickness - Concrete\,cover - Concrete\,class - Steel\,grade \quad (5.21)$$

$$Model - Shape - e_x - t_w - c - f_{ck} - f_y \quad (5.22)$$

The CDP model is implemented using the same formulation that has been described in section 5.1.3. The compression law is shown in Fig.5.6. The tension stiffening law is shown in Fig.5.7. The parameters used and the input tables are shown in Fig.5.9 and Fig.5.10 respectively for concrete C30/37 and C50/60. The steel material law is defined with an elastic-plastic hardening behaviour. This is a bi-linear model. The considered material's law is shown in Fig.5.8.

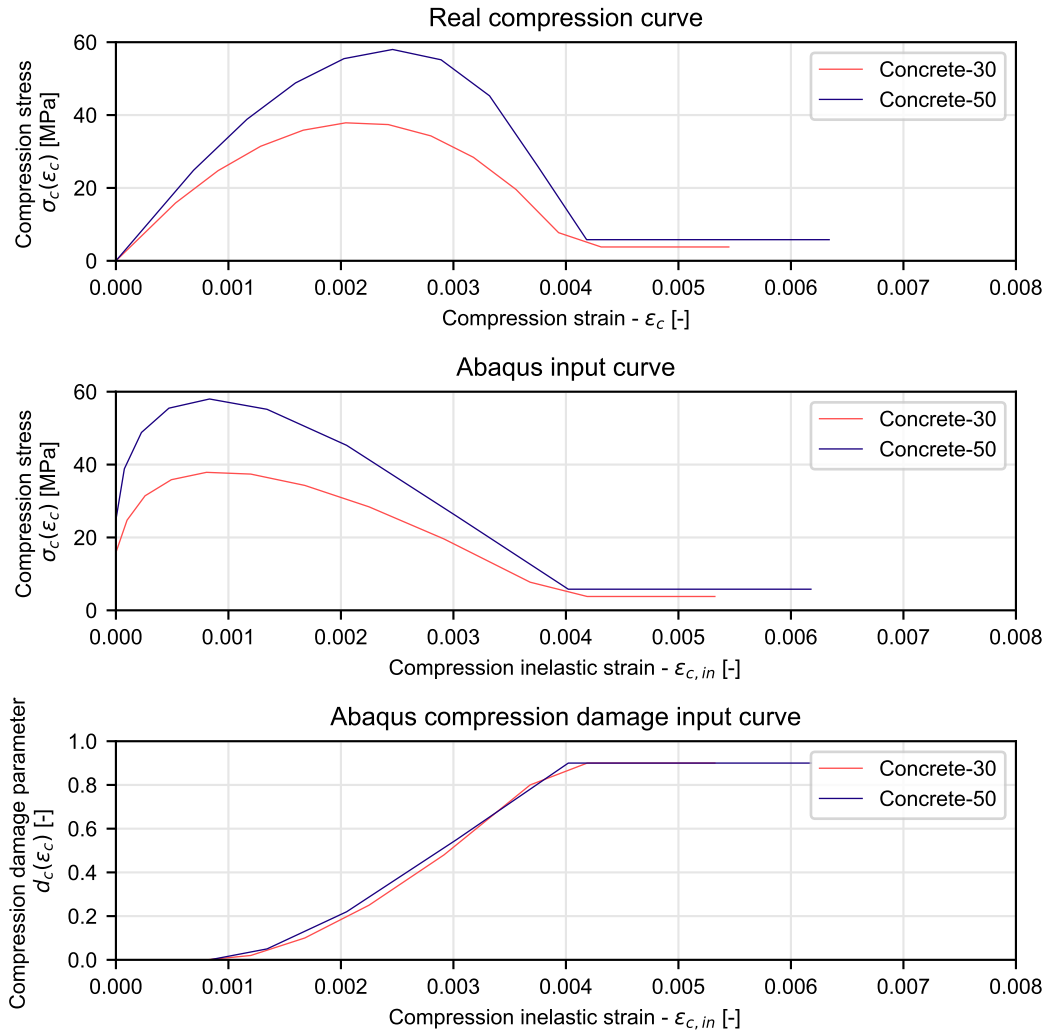

Figure 5.6: numerical parametric analysis input concrete curves: compression

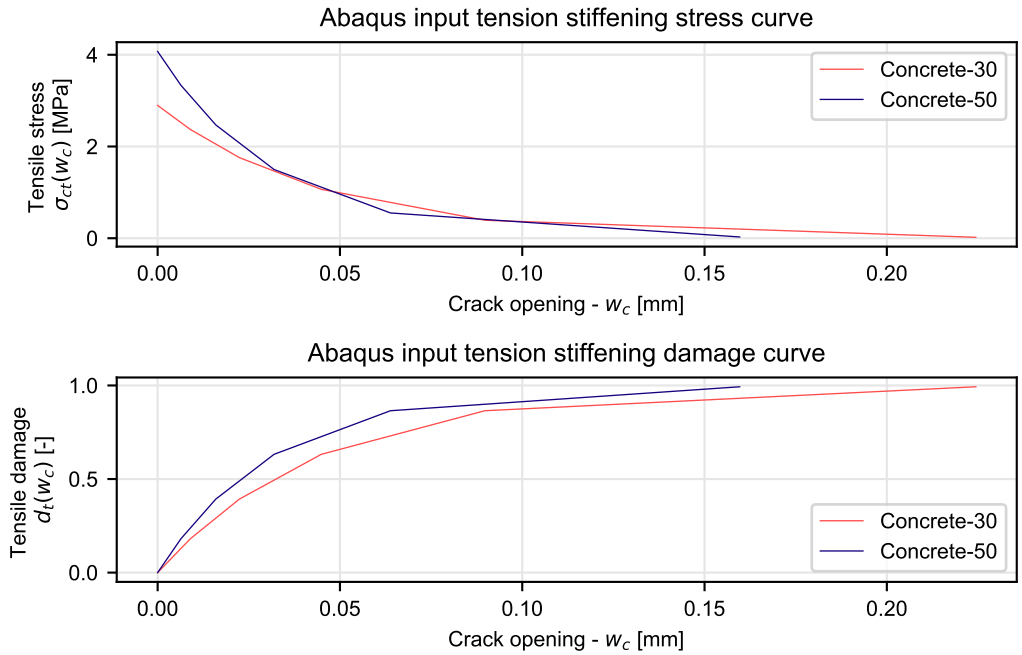

Figure 5.7: numerical parametric analysis input concrete curves: tension

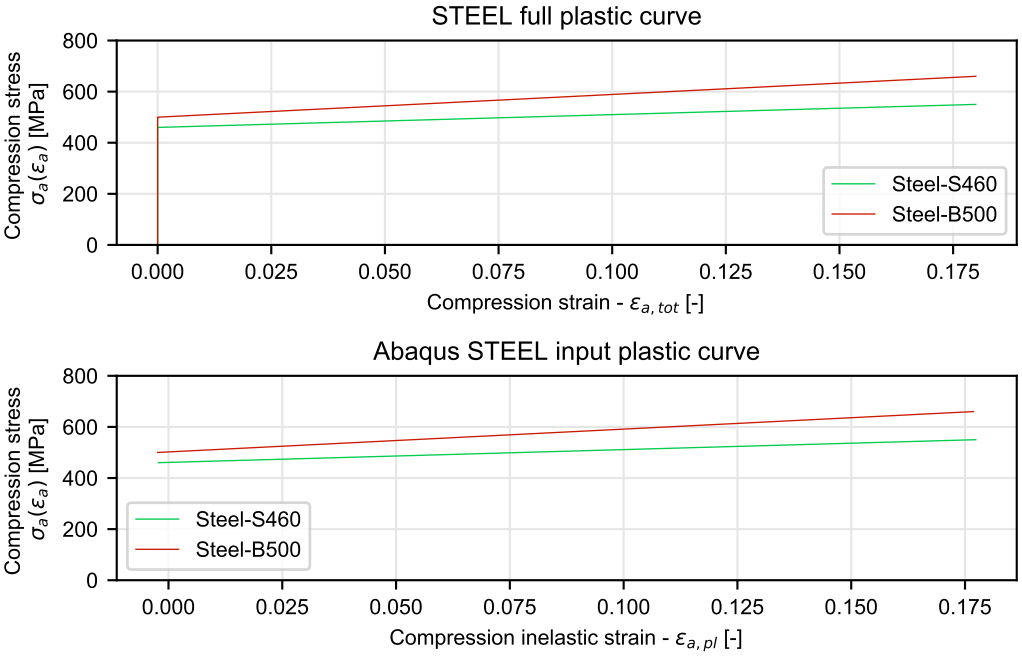

Figure 5.8: numerical parametric analysis input steel curves

Concrete <<Concrete-30>>: Parameters

$f_{ck}\,[MPa]$	$f_{cm}\,[MPa]$	$f_{ctm}\,[MPa]$	$E_{cm}\,[MPa]$	$\varepsilon_{c1}\,[-]$	$\rho\,[ton/mm^3]$
30.0	38.0	2.9	30588.56	0.0021619	2.5e-09

$\Psi\,[^o]$	$f_{b0}/f_{c0}\,[-]$	$\varepsilon\,[-]$	$K_c\,[-]$	$\mu\,[-]$	$G_F\,[N/mm]$
35.0	1.16	0.1	0.667	1e-05	0.13

Concrete <<Concrete-30>>: Compression law

i	$\sigma_{c,i}\,[MPa]$	$\varepsilon_{c,in,i}\,[-]$	$\varepsilon_{c,el,i}\,[-]$	$\varepsilon_{c,i}\,[-]$	$d_{c,i}\,[-]$
1.0	15.87	0.0	0.000519	0.00053	0.0
2.0	24.74	9.9e-05	0.000809	0.000908	0.0
3.0	31.43	0.000259	0.001028	0.001286	0.0
4.0	35.85	0.000493	0.001172	0.001665	0.0
5.0	37.87	0.000805	0.001238	0.002043	0.0
6.0	37.39	0.001199	0.001223	0.002421	0.02
7.0	34.28	0.001679	0.001121	0.0028	0.1
8.0	28.4	0.00225	0.000928	0.003178	0.25
9.0	19.59	0.002916	0.000641	0.003556	0.48
10.0	7.72	0.003682	0.000253	0.003935	0.8
11.0	3.8	0.004189	0.000124	0.004313	0.9
12.0	3.8	0.004567	0.000124	0.004691	0.9
13.0	3.8	0.004945	0.000124	0.00507	0.9
14.0	3.8	0.005324	0.000124	0.005448	0.9

Concrete <<Concrete-30>>: Tension stiffening law

i	$\sigma_{ct,i}\,[MPa]$	$w_{c,i}\,[mm]$	$d_{t,i}\,[-]$
1.0	2.896500992202708	0.0	0.0
2.0	2.371	0.00898	0.181
3.0	1.757	0.02244	0.393
4.0	1.066	0.04488	0.632
5.0	0.392	0.08976	0.865
6.0	0.02	0.22441	0.993

Figure 5.9: numerical parametric analysis input concrete curves table values

Concrete <<Concrete-50>>: Parameters

$f_{ck}\,[MPa]$	$f_{cm}\,[MPa]$	$f_{ctm}\,[MPa]$	$E_{cm}\,[MPa]$	$\varepsilon_{c1}\,[-]$	$\rho\,[ton/mm^3]$
50.0	58.0	4.07	35654.45	0.0024647	2.5e-09

$\Psi\,[^o]$	$f_{b0}/f_{c0}\,[-]$	$\varepsilon\,[-]$	$K_c\,[-]$	$\mu\,[-]$	$G_F\,[N/mm]$
35.0	1.16	0.1	0.667	1e-05	0.13

Concrete <<Concrete-50>>: Compression law

i	$\sigma_{c,i}\,[MPa]$	$\varepsilon_{c,in,i}\,[-]$	$\varepsilon_{c,el,i}\,[-]$	$\varepsilon_{c,i}\,[-]$	$d_{c,i}\,[-]$
1.0	24.84	0.0	0.000697	0.00069	0.0
2.0	38.84	7.5e-05	0.001089	0.001165	0.0
3.0	48.81	0.000227	0.001369	0.001596	0.0
4.0	55.48	0.000471	0.001556	0.002027	0.0
5.0	58.0	0.000832	0.001627	0.002459	0.0
6.0	55.17	0.001343	0.001547	0.00289	0.05
7.0	45.28	0.002051	0.00127	0.003321	0.22
8.0	25.85	0.003028	0.000725	0.003752	0.55
9.0	5.8	0.004021	0.000163	0.004184	0.9
10.0	5.8	0.004452	0.000163	0.004615	0.9
11.0	5.8	0.004884	0.000163	0.005046	0.9
12.0	5.8	0.005315	0.000163	0.005478	0.9
13.0	5.8	0.005746	0.000163	0.005909	0.9
14.0	5.8	0.006178	0.000163	0.00634	0.9

Concrete <<Concrete-50>>: Tension stiffening law

i	$\sigma_{ct,i}\,[MPa]$	$w_{c,i}\,[mm]$	$d_{t,i}\,[-]$
1.0	4.07167951955935	0.0	0.0
2.0	3.334	0.00639	0.181
3.0	2.47	0.01596	0.393
4.0	1.498	0.03193	0.632
5.0	0.551	0.06386	0.865
6.0	0.027	0.15964	0.993

Figure 5.10: numerical parametric analysis input concrete curves table values

5.2.1 Workflow automation

The generation of the model, the preliminary running of checks, the input files creation, the output file manipulation, the image saving, the energy and load-slip curves extraction and the data post-processing are automated in Python language. The workflow process is shown in Fig.5.11. Libraries such as Abaqus®, numpy, pandas, matplotlib and pillow were used.

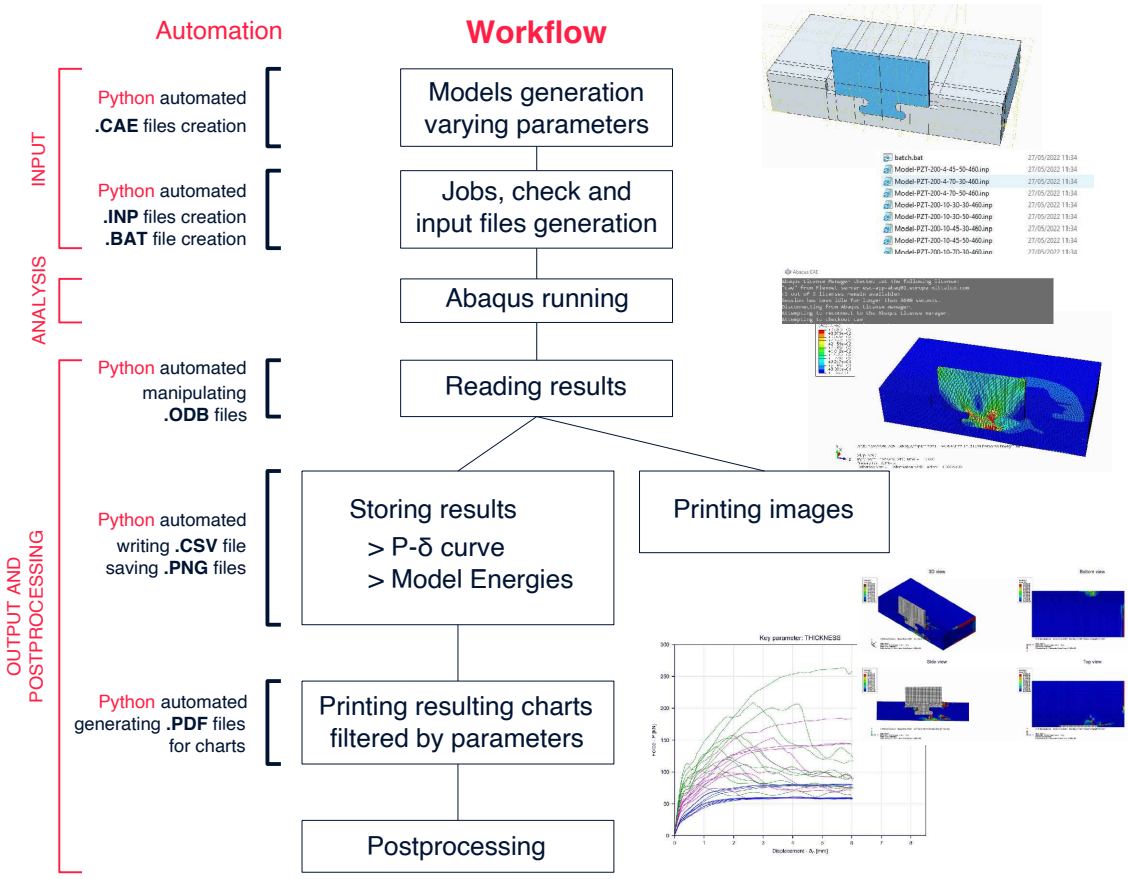

Figure 5.11: numerical analysis workflow automation scheme

5.3 Model calibration

5.3.1 Reference test

The reference test consists in a Push Out test. This was carried out at RWTH Aachen and can be found in [46]. A PZT dowel geometry was tested here under pure shear. The steel dowel is embedded in a 50x50x10 cm reinforced concrete block. The geometry and the load configuration are shown in Fig.5.13. Two equal specimens were tested. The reference cases are labelled in the reference as S-DV-PZKL-1 and S-DV-PZKL-2.

The material and geometry data are:

Materials

Value	Parameter
C40/50	Concrete class
$f_{cm,cube} = 53.8\ MPa$	Measured mean compression resistance
S355J0	Structural steel strength class
B500	Reinforcement steel

Geometry

Value	Parameter
$c_{Do} = 30\ mm$	Upper concrete cover
$c_{Du} = 30\ mm$	Lower concrete cover
$e_x = 200\ mm$	Dowel size
$t_w = 20\ mm$	Plate thickness
$h_{slab} = 100\ mm$	Concrete slab height
$b = 500\ mm$	Concrete block base

The test setup is shown in Fig.5.12.

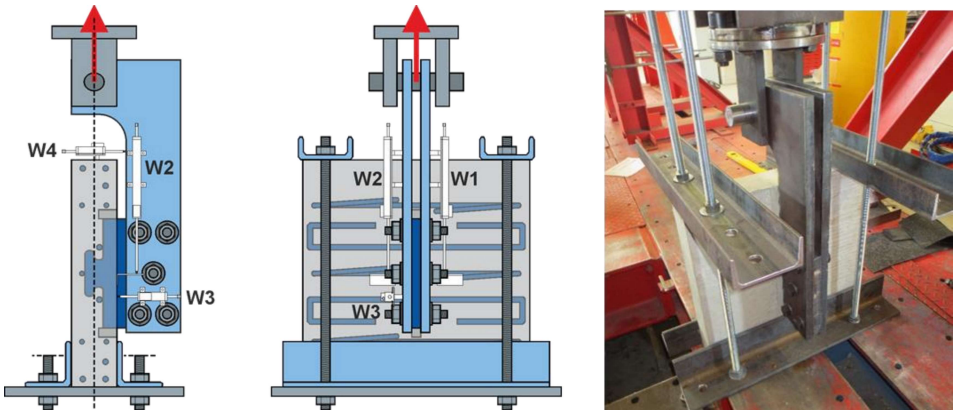

Figure 5.12: reference literature test setup from [46]

In Fig.5.13 a drawback of the test setup is shown. Due to the external restraints on the concrete block a small rotation is allowed and was observed. This must be taken into account for the subsequent calibration. The resulting loading curve is shown in Fig.5.14. The specimens failed under concrete pryout failure mode. The cone formations are clearly visible in Fig.5.15. The cracking pattern can be here appreciated. Note that the failure mode and the load-displacement curve is similar for the two specimens.

The reference test has been reproduced with Abaqus® with a Finite Element Analysis (FEA). Linear hexahedral finite elements () of type C3D8R are used for the solid sections. Linear truss elements of type T3D2 are used for the reinforcement. Solid homogeneous sections are used for the solid parts. Circular sections

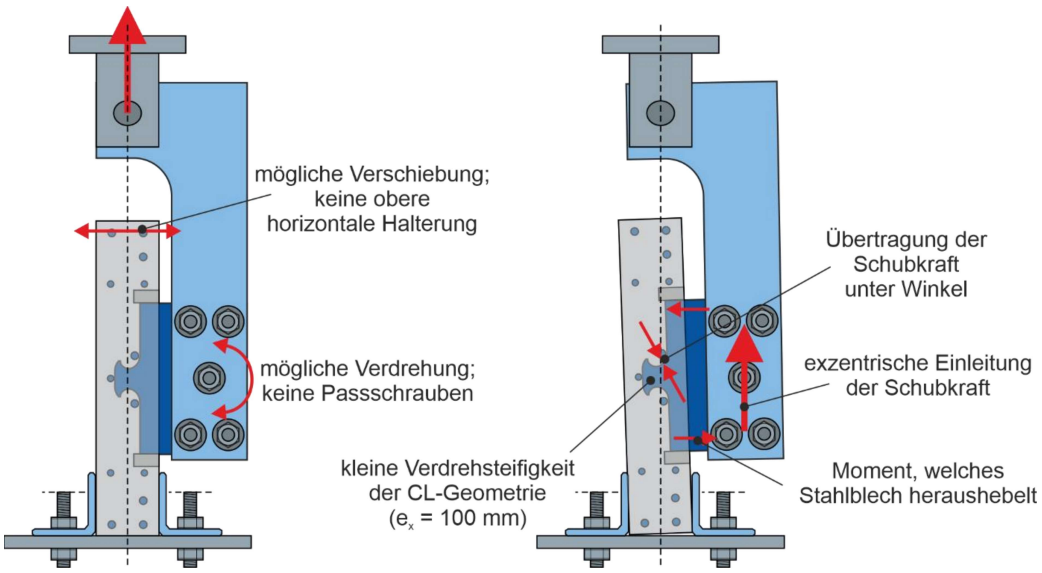

Abbildung 3-6: Problematik des Versuchsaufbaus der Schubversuche: mögliches Verdrehen und Aushebeln der Verbundmittel

Figure 5.13: reference literature test setup from [46]: rotation of specimen observed during test

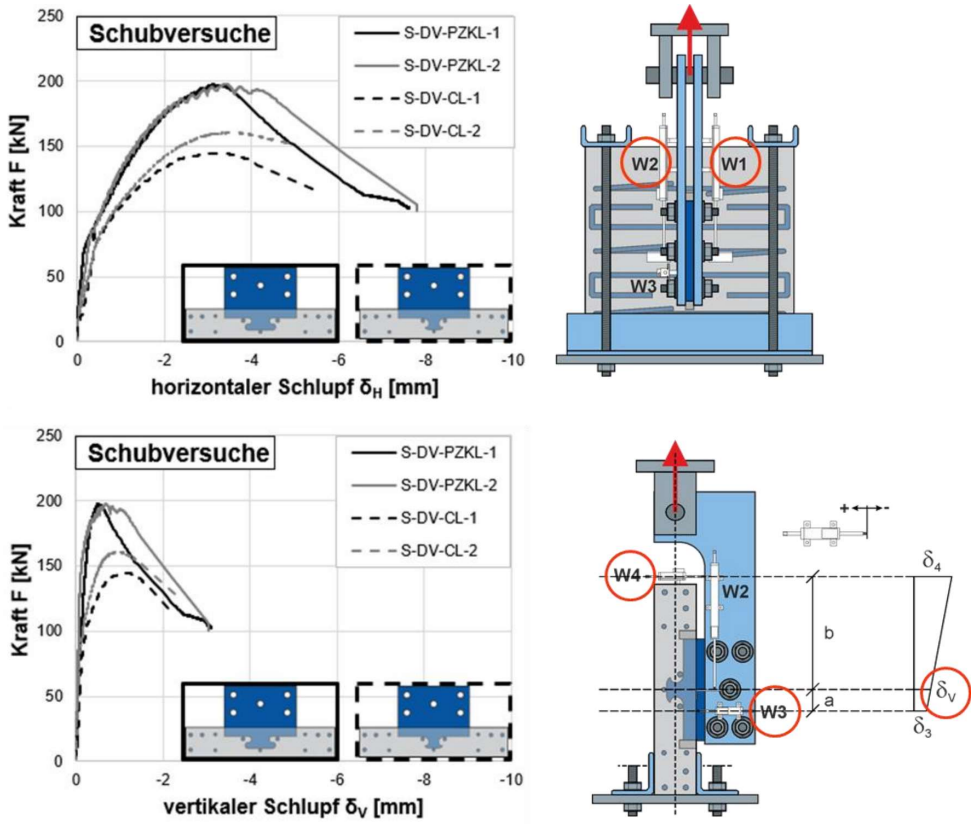

Figure 5.14: reference literature test from [46]: resulting curves

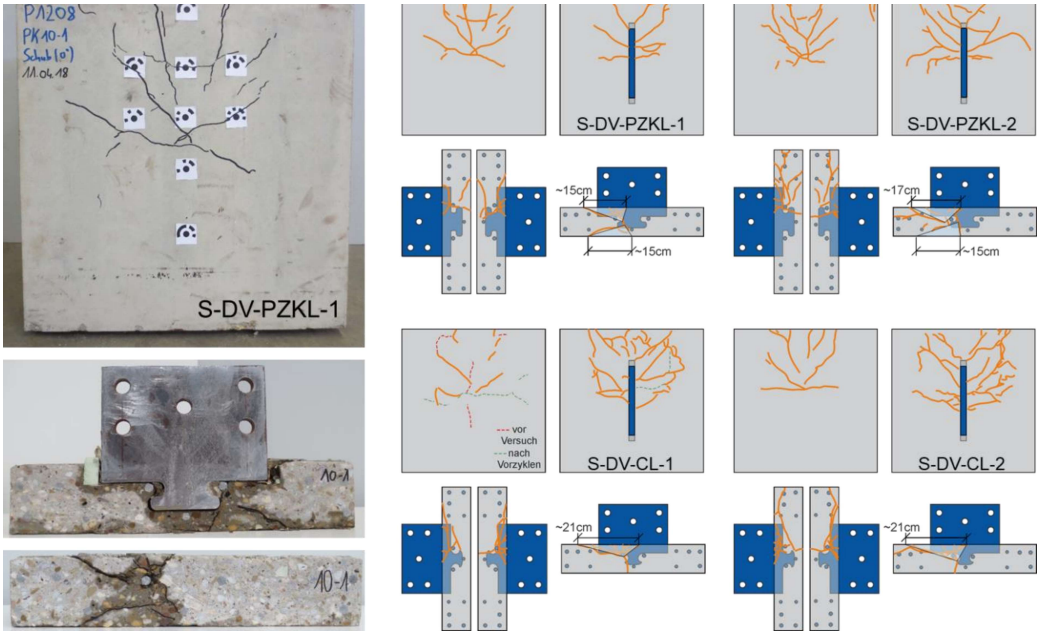

Abbildung 3-7: Rissbilder der Versuchsserie *S-DV*

Figure 5.15: reference literature test from [46]: failure mode and cracking pattern

with the same area as the reinforcement bars are used for the linear elements. An embedded region constraint relation has been defined between the concrete part and the reinforcement. No slip between the two parts is allowed. In order to optimize the analysis the mesh is refined in the steel dowel area and is coarser in the distant regions. A contact interaction property is used between the steel part and the concrete part. For the tangential behaviour a penalty method with friction coefficient $\mu_{Friction}$ is used. For the normal contact an hard contact is used.

An explicit analysis load step is defined. The load is applied in a period T. The Mass Scaling Factor MSF is defined. The geometric non-linearity is considered in the model

The load is applied as imposed displacement on the $RP1$ point. The maximum applied displacement is δ_{max} in the z direction. This is applied in a step time period T. In order to simplify the analysis progression in the first stages of contact a smooth amplitude has been used.

The boundary conditions are set as shown in Fig.5.5. These come directly from the simplified static scheme assumption of Fig.5.5. Displacement in the z direction is allowed for Face 1. Displacement in the direction y is allowed for the Face 2, simulating the imperfect test setup highlighted before which allows for a rotation of the specimen. No restrain has been set on Face 1 and Face 2 for the lateral contraction. The point $RP1$ is restrained in the y direction and the displacement δ_{max} is imposed in the z direction. A coupling constraint has been defined between the upper steel plate face (Face 4) and the point $RP1$.

5.3.2 Base model

The model under the name "Base model" has been used as reference.

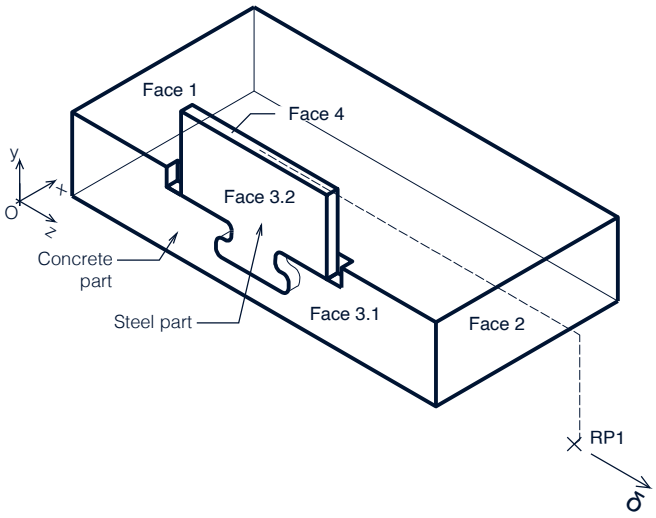

Figure 5.16: schematic representation of the numerical model. Symmetry is exploited

Base model settings

Setting	Description
$f_{ck} = f_{ck,0} = 45.8\,MPa$	characteristic value of concrete cylindric compression strength
$\mathrm{Concrete\text{-}40}$	CDP model according to Fig.5.19 and Fig.5.17
$\mu_{Friction} = 0.5$	steel-concrete tangential friction coefficient
$\mathrm{CDP\ parameters}$	see Fig.5.17
$T = 10\,sec$	load step time period
$\delta_{max} = 4.5\,mm$	applied displacement
$MSF = 1000$	Adopted mass scaling factor
$\mathrm{Smooth\ step}$	Amplitude type
$C3D8R$	Finite element formulation for the solid parts
$T3D2$	Finite element formulation for the reinforcement mesh

Concrete <<Concrete-40>>: Parameters

$f_{ck}\,[MPa]$	$f_{cm}\,[MPa]$	$f_{ctm}\,[MPa]$	$E_{cm}\,[MPa]$	$\varepsilon_{c1}\,[-]$	$\rho\,[ton/mm^3]$
45.8	53.8	3.84	36446.63	0.0024079	2.5e-09

$\Psi\,[^o]$	$f_{b0}/f_{c0}\,[-]$	$\varepsilon\,[-]$	$K_c\,[-]$	$\mu\,[-]$	$G_F\,[N/mm]$
35.0	1.16	0.1	0.667	1e-05	0.13

Concrete <<Concrete-40>>: Compression law

i	$\sigma_{c,i}\,[MPa]$	$\varepsilon_{c,in,i}\,[-]$	$\varepsilon_{c,el,i}\,[-]$	$\varepsilon_{c,i}\,[-]$	$d_{c,i}\,[-]$
1.0	22.87	0.0	0.000627	0.000632	0.0
2.0	35.09	9.1e-05	0.000963	0.001053	0.0
3.0	44.56	0.000252	0.001223	0.001475	0.0
4.0	50.9	0.0005	0.001397	0.001896	0.0
5.0	53.71	0.000844	0.001474	0.002318	0.0
6.0	52.47	0.001299	0.00144	0.002739	0.02
7.0	46.6	0.001882	0.001279	0.00316	0.13
8.0	35.38	0.002611	0.000971	0.003582	0.34
9.0	17.92	0.003511	0.000492	0.004003	0.67
10.0	5.38	0.004277	0.000148	0.004425	0.9
11.0	5.38	0.004698	0.000148	0.004846	0.9
12.0	5.38	0.00512	0.000148	0.005267	0.9
13.0	5.38	0.005541	0.000148	0.005689	0.9
14.0	5.38	0.005962	0.000148	0.00611	0.9

Concrete <<Concrete-40>>: Tension stiffening law

i	$\sigma_{ct,i}\,[MPa]$	$w_{c,i}\,[mm]$	$d_{t,i}\,[-]$
1.0	3.84	0.0	0.0
2.0	3.144	0.00677	0.181
3.0	2.329	0.01693	0.393
4.0	1.413	0.03385	0.632
5.0	0.52	0.0677	0.865
6.0	0.026	0.16926	0.993

Figure 5.17: numerical model meshing

5.3.3 Sensitivity analysis on the input parameters

In order to gain sensitivity with the model and choose the correct values of the parameters, a sensitivity study has been carried out on the input values.

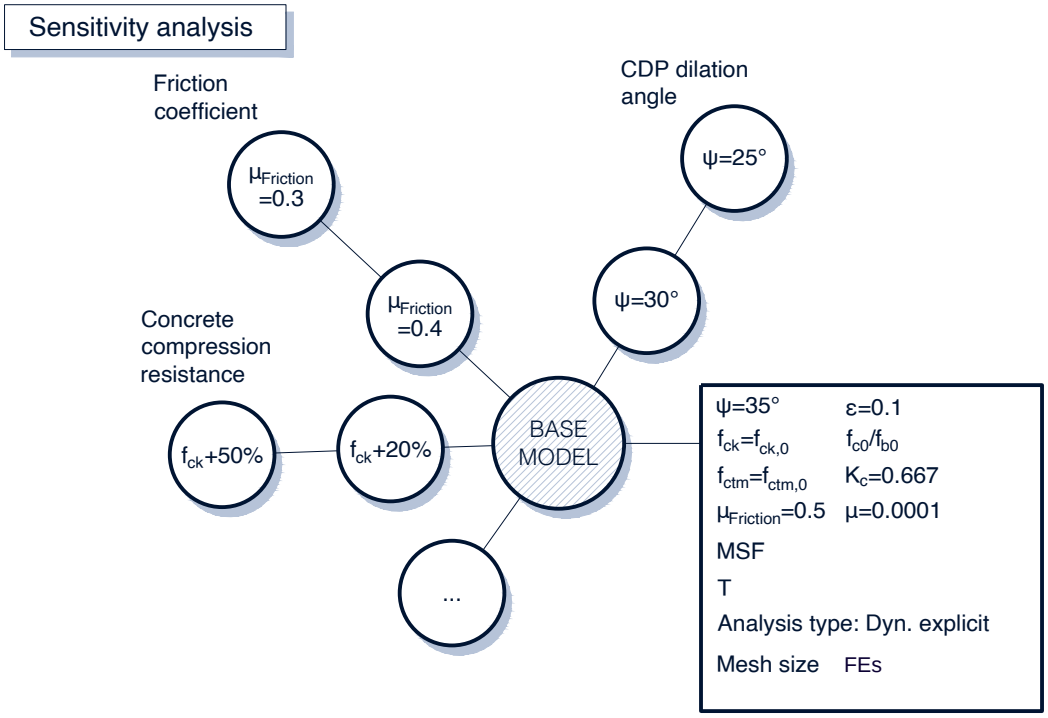

Figure 5.18: numerical model meshing

List of FEM models in the sensitivity analysis and related varied parameters

Model name	Varied parameter
Concrete-40-Psi30	CDP parameter $\psi = 30^o$
Concrete-40-Psi25	CDP parameter $\psi = 25^o$
Concrete-40-Friction03	steel-concrete tangential friction coefficient $\mu_{Friction} = 0.3$
Concrete-40-Friction04	steel-concrete tangential friction coefficient $\mu_{Friction} = 0.4$
Concrete-40-AsX200	area of reinforcement doubled $A_s = 2 \times A_{s,0}$
Concrete-40-fckX120	concrete class improved such that $f_{ck} = 1.2 \times f_{ck,0}$
Concrete-40-fckX150	concrete class improved such that $f_{ck} = 1.5 \times f_{ck,0}$
Concrete-40-fctmX150	tensile mean resistance of concrete multiplied to $f_{ctm} = 1.5 \times f_{ctm,0}$
Concrete-40-fctmX70	tensile mean resistance of concrete multiplied to $f_{ctm} = 0.7 \times f_{ctm,0}$
Concrete-40-NoDamage	no damage in the CDP compression and tension concrete model
Concrete-40-Confined	strains values according to [8] of confined concrete used

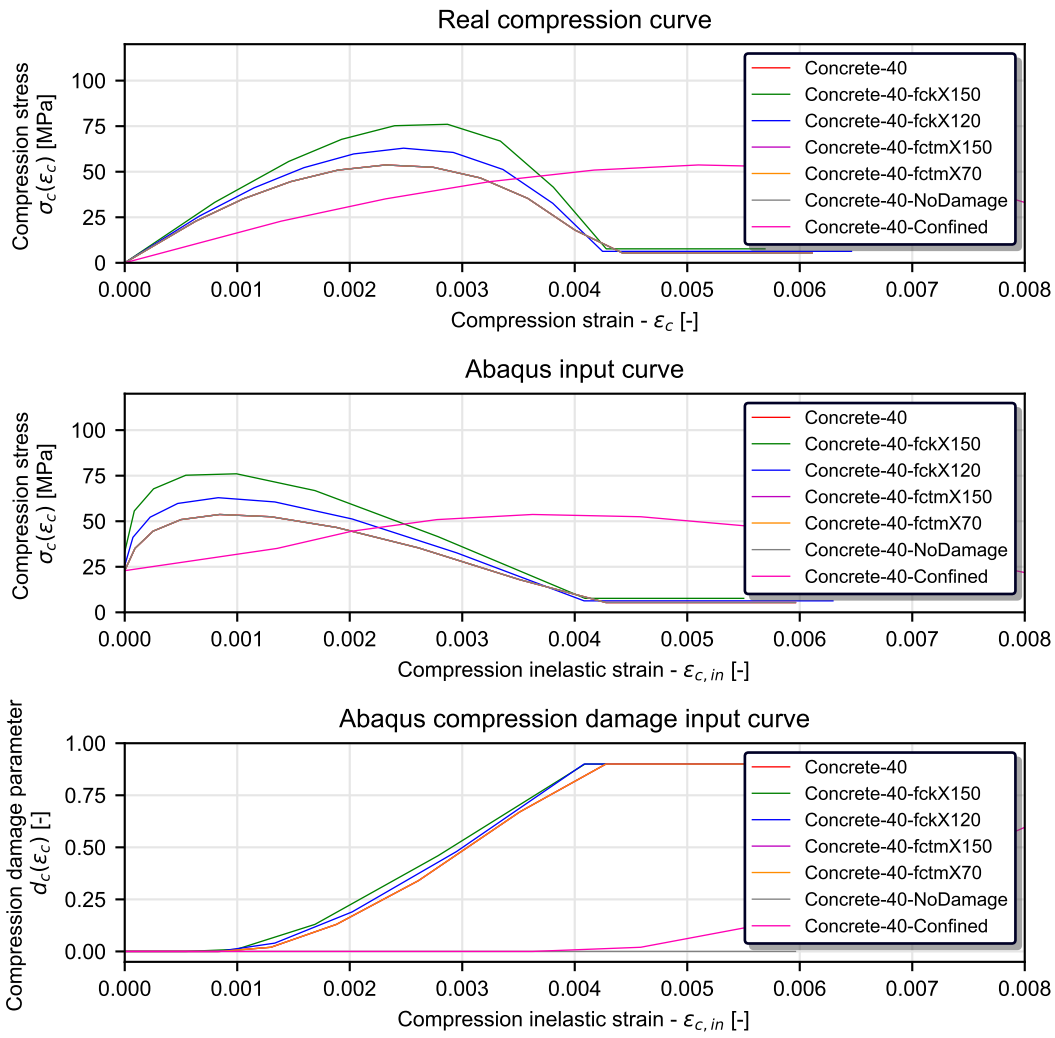

Figure 5.19: numerical model meshing

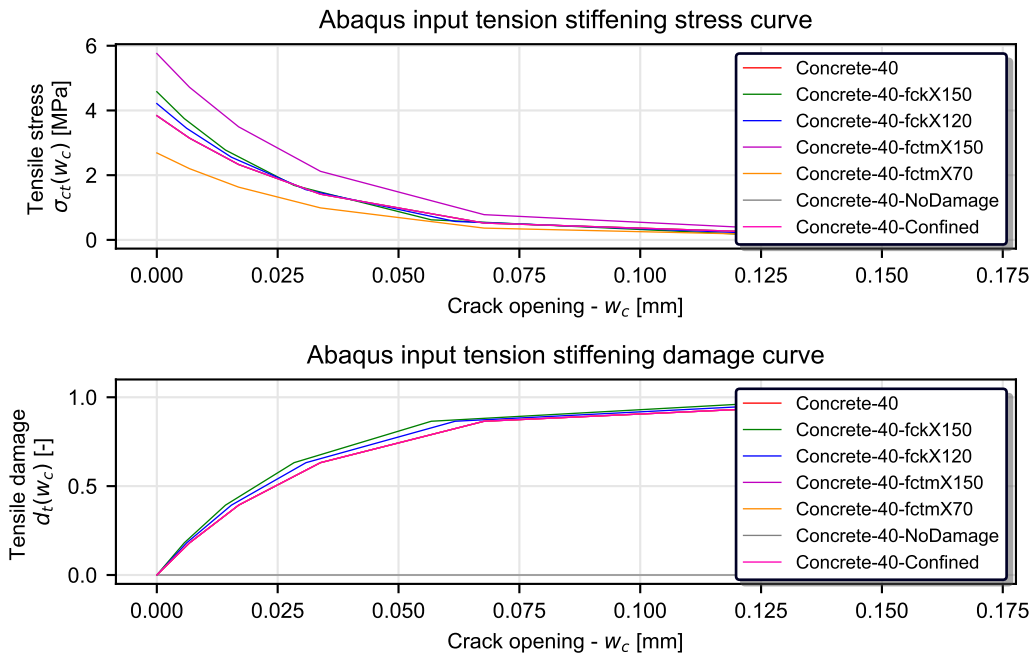

Figure 5.20: numerical model meshing

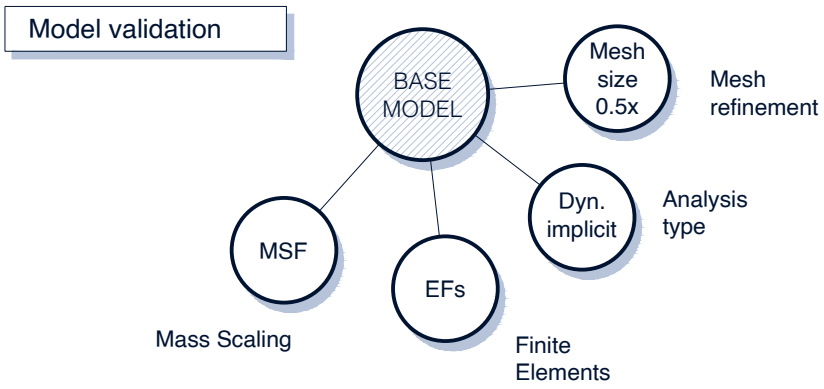

Figure 5.21: numerical model meshing

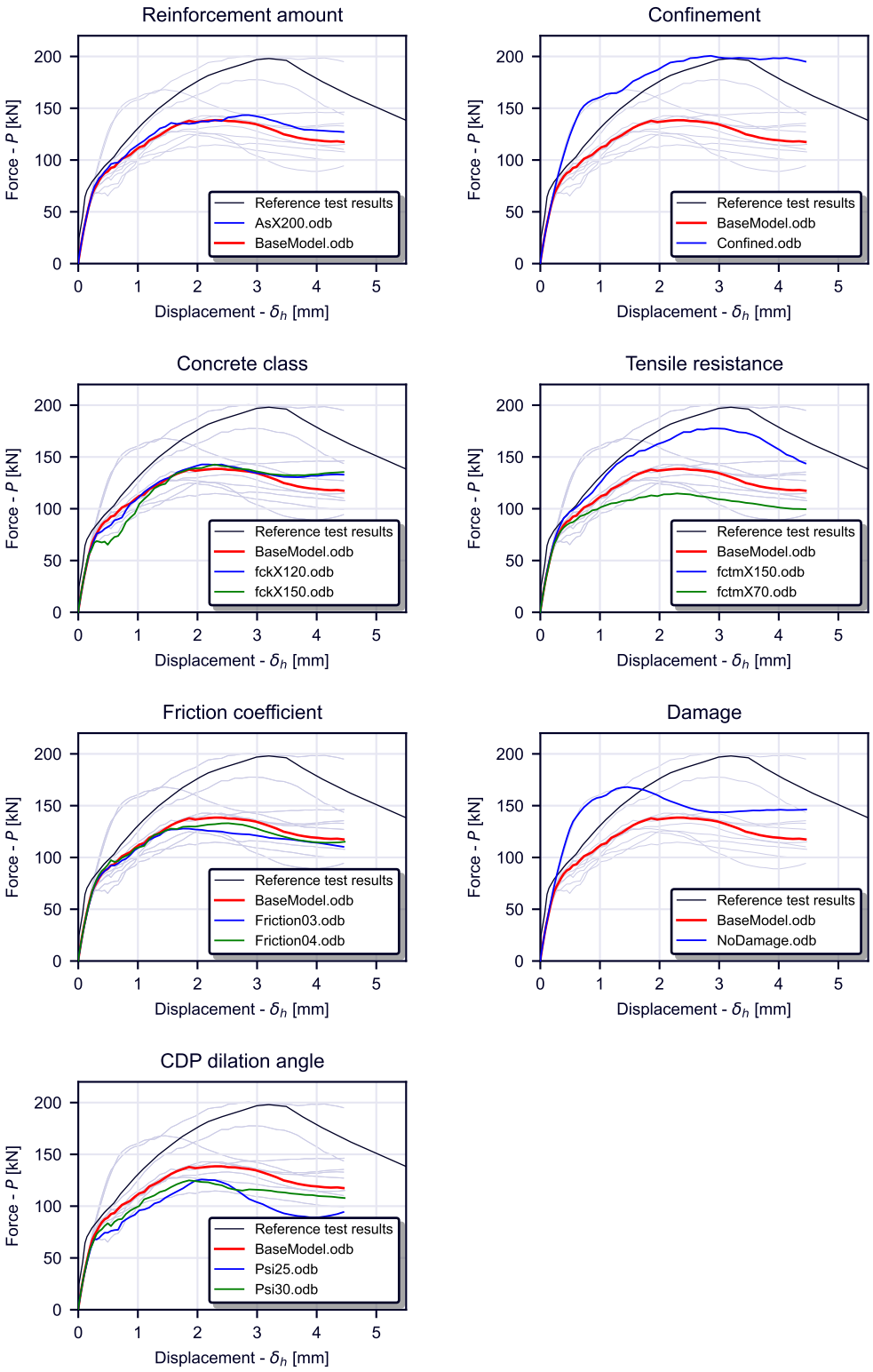

Figure 5.22: numerical model meshing

With reference to Fig.5.22 conclusions can be summarized as follows. From the analysis it can be concluded that the reinforcement area has influence only on the post-critical branch of the curve. This is probably a consequence of the tensile state activation of reinforcement for large displacements and activation of catenary action. Using confinement values of strains has a significant influence on the curve. If the confined values of strains are used, the curve misses the initial failure behaviour. A significant increase of the resistance is observed. Increasing the concrete class modifies the initial failure behaviour of the curve and the post-critical branch. It does not have however a significant influence on the resistance and in general on the curve. The tensile resistance of the concrete has a major influence on the curve. It is a crucial parameter for the initial failure branch, the resistance, the ductility, and the post-critical branch of the curve. The friction coefficient does not have a significant impact on the curves. It appears to have an influence on the resistance. The damage is of crucial importance for the results. The model with missing damage curve appears not having the expected behaviour. The dilation angle of the CDP has an influence on the curve.

5.3.4 Expected resistance

The expected resistance, if the actual failure mode of the test is considered, is:

$$P_{po,k} = k_1 \cdot \chi_x \cdot \chi_y \cdot h_{po}^{1.5} \cdot \sqrt{f_{ck}} \cdot (1 + \rho_{D,i}) \cdot \psi_{crack} = 121.5\, kN \tag{5.23}$$

Here $\psi_{crack} = 1$ as there is no transverse cracking, $k_1 = 71$, $\chi_x = 1.0$ because there is only one dowel, $\chi_y = 1.0$ because there is only one dowel. The value of f_{ck} has been taken as the equivalent value to a concrete having f_{cm} equal to the measured one, hence $f_{ck} = 53.8 - 8 = 45.8\, MPa$.

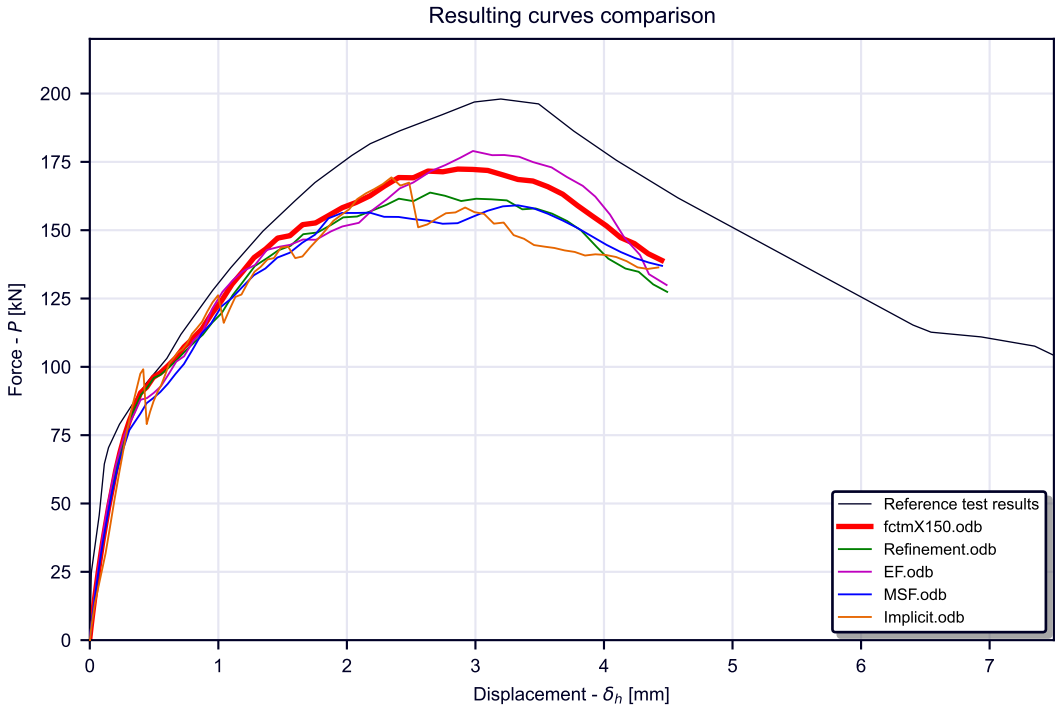

Figure 5.23: resulting curves of the validation analysis

5.3.5 Validation of the curves

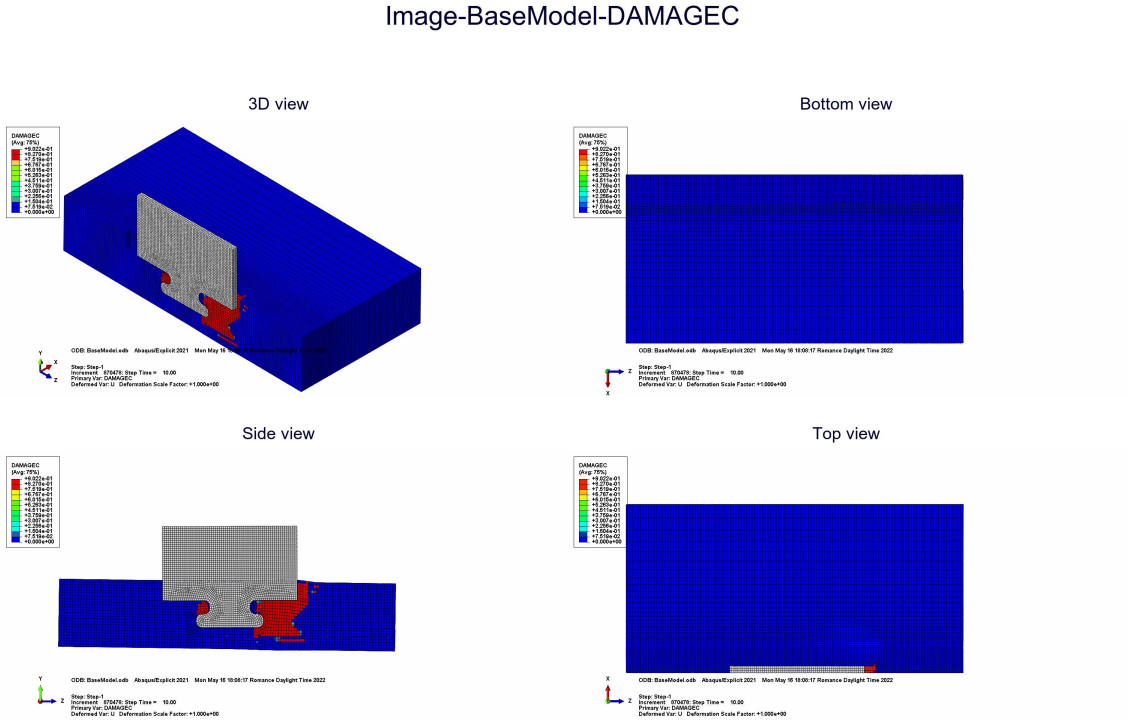

Figure 5.24: numerical model resulting concrete compression damage field

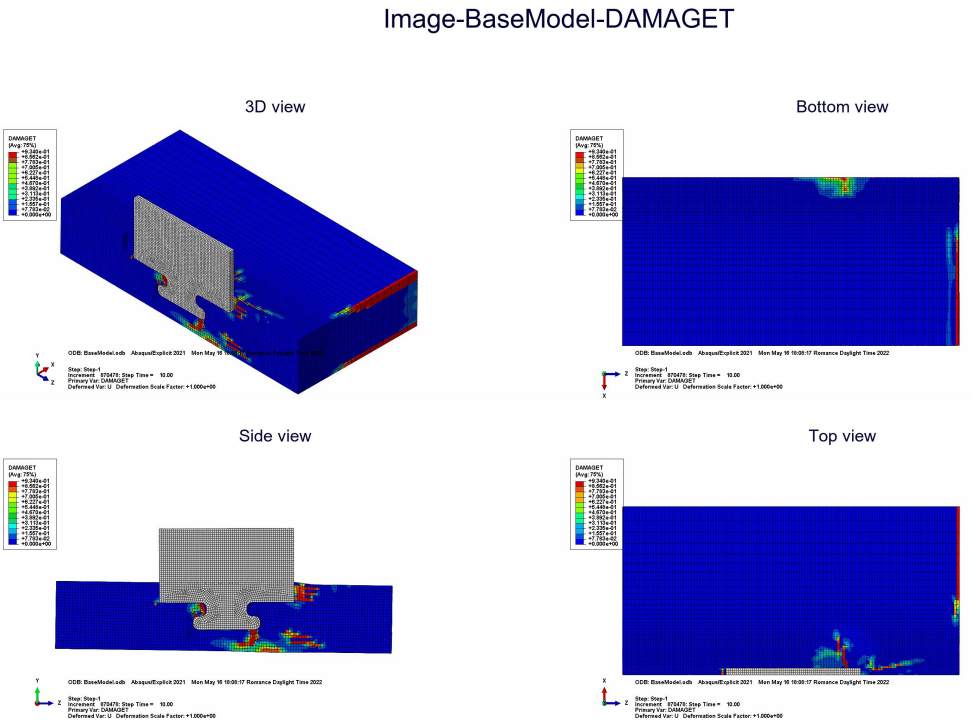

Figure 5.25: numerical model resulting concrete tensile damage field

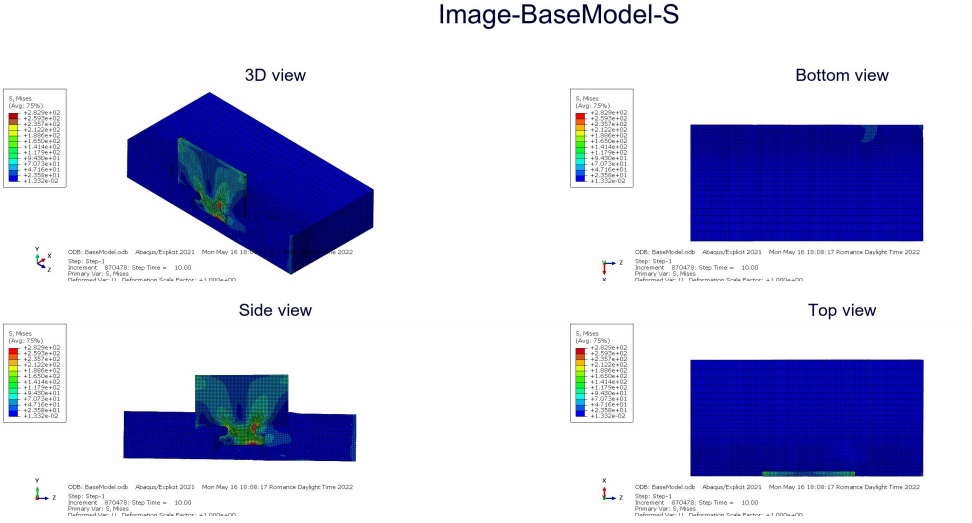

Figure 5.26: numerical model resulting Von Mieses stress field

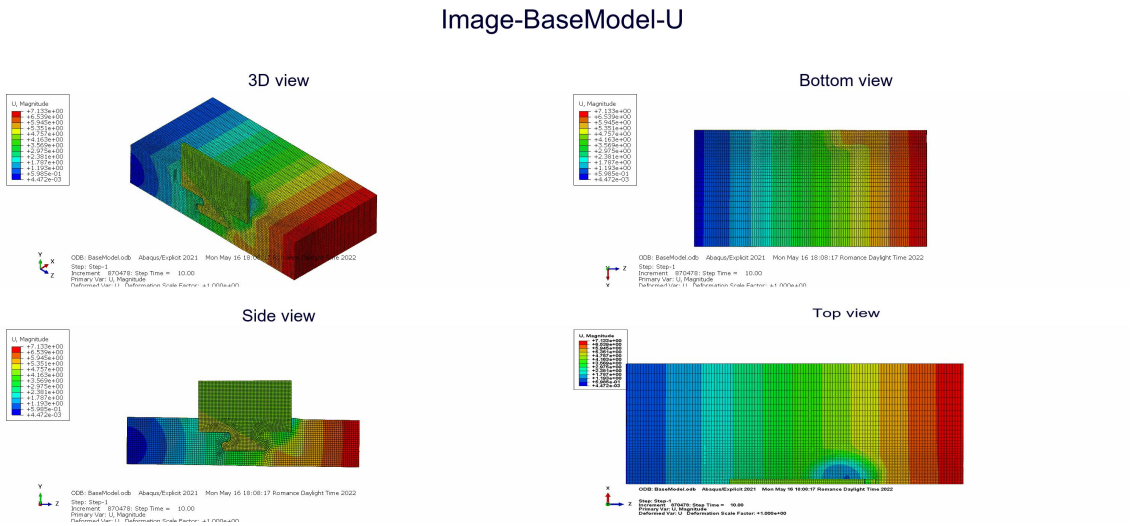

Figure 5.27: numerical model resulting displacement magnitude field

5.4 Parametric analysis results

The results are exported from the object database files (.odb) into comma separated values files (.csv). The load-displacement curves can be filtered and the influence of the different parameters can be observed. In Fig.5.28 the curves are filtered on the base of the dowel shape. The failure points are identified as that points having 90% of the peak resistance P_{max} on the post-critical branch. The ductility value δ_u is the slip δ in correspondence of the failure point. The force in correspondence of the failure point is $P(\delta_u)$.

5.4.1 PZT series results

In Fig.5.29 the influence of the plate thickness t_w is shown. This influences both the initial stiffness and the resistance. The failure mode is affected. In Fig.5.30 the influence of the size e_x is shown. In Fig.5.31 the influence of the concrete cover c is shown. Note that for high values of concrete cover the failure mode is yielding of the steel dowel. For Low values of t_w the failure is not affected by the concrete cover. For low values of concrete cover a pryout failure is likely to happen. In Fig.5.32 the influence of the concrete grade f_{ck} is shown. In case of pryout failure the load curve is not significantly affected by the concrete resistance. In Fig.5.33 the curves are filtered by the failure mode. The failure points are identified in Fig.5.34.

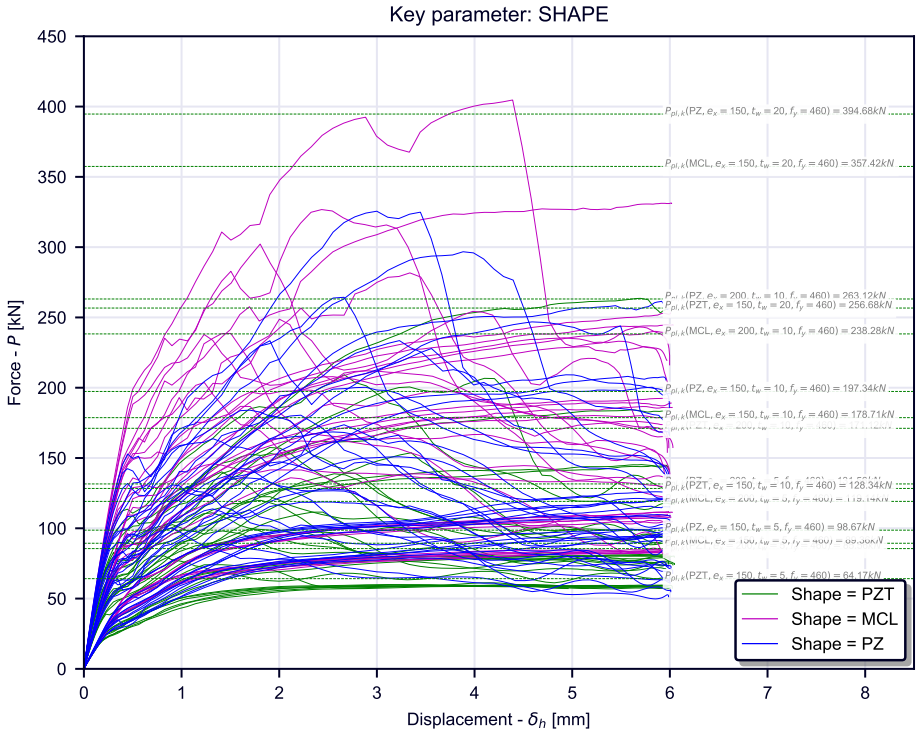

Figure 5.28: parametric numerical FEM simulation study: resulting curves sorted by dowel shape

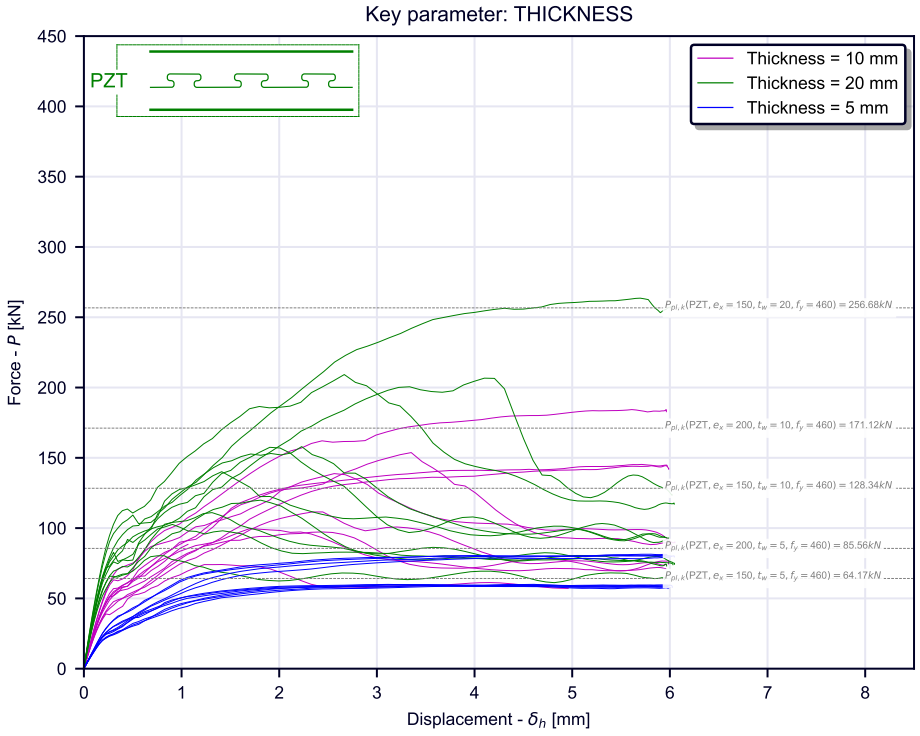

Figure 5.29: parametric numerical FEM simulation study: resulting curves sorted by thickness of plate for the filtered shape

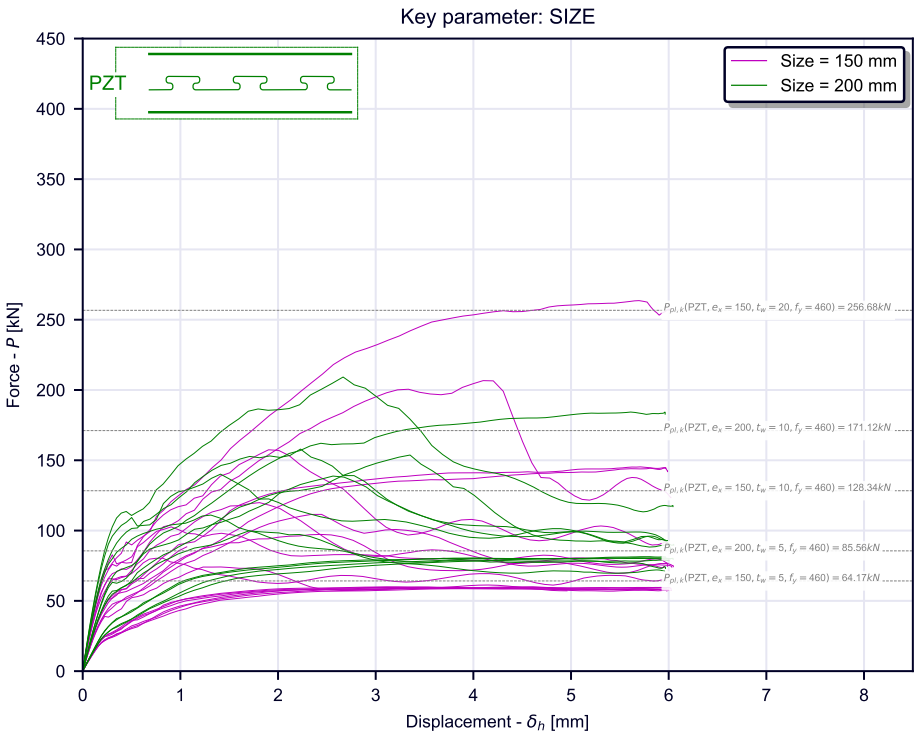

Figure 5.30: parametric numerical FEM simulation study: resulting curves sorted by size of dowel for the filtered shape

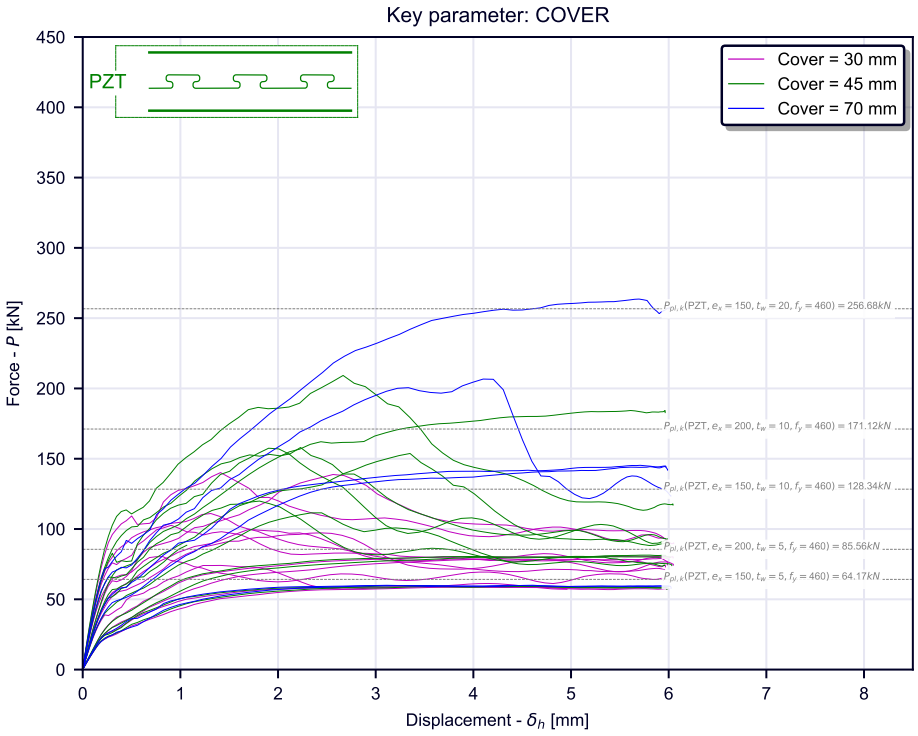

Figure 5.31: parametric numerical FEM simulation study: resulting curves sorted by concrete cover for the filtered shape

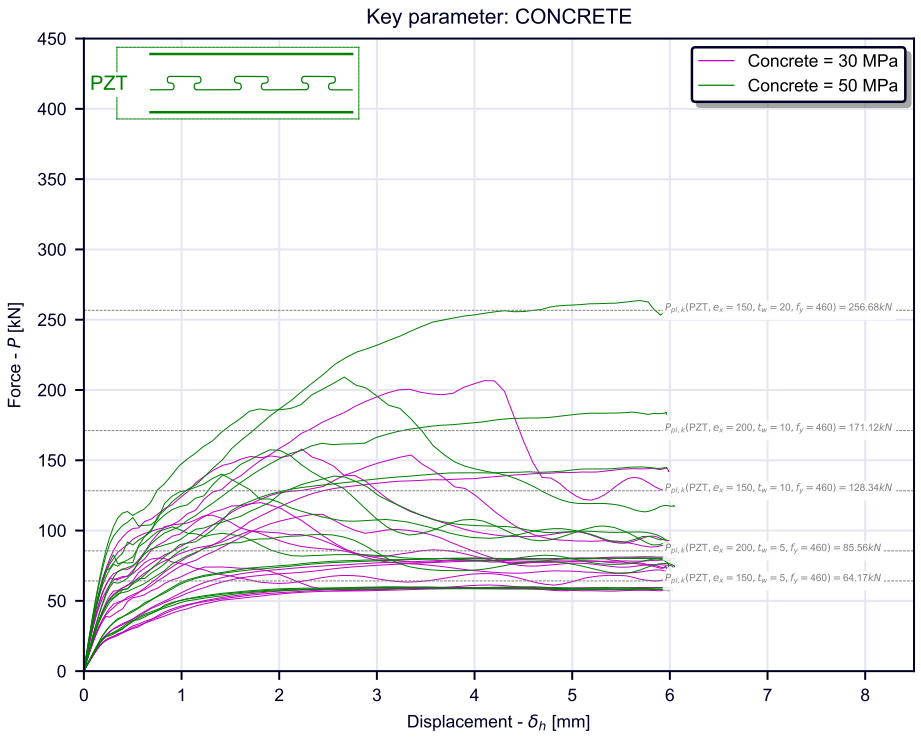

Figure 5.32: parametric numerical FEM simulation study: resulting curves sorted by concrete class for the filtered shape

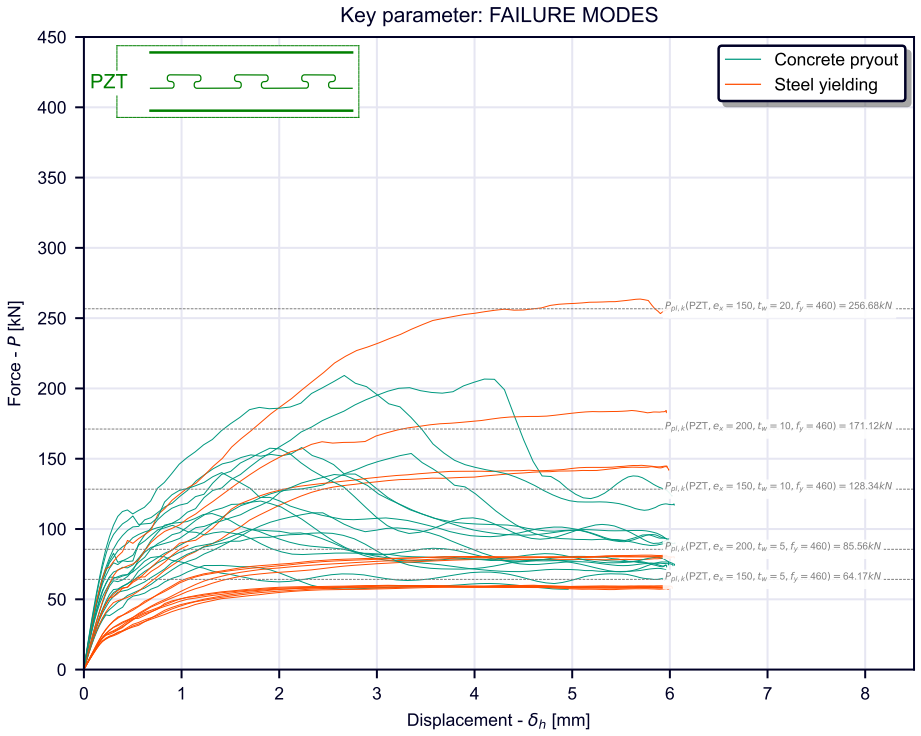

Figure 5.33: parametric numerical FEM simulation study: resulting curves sorted by observed failure mode for the filtered shape

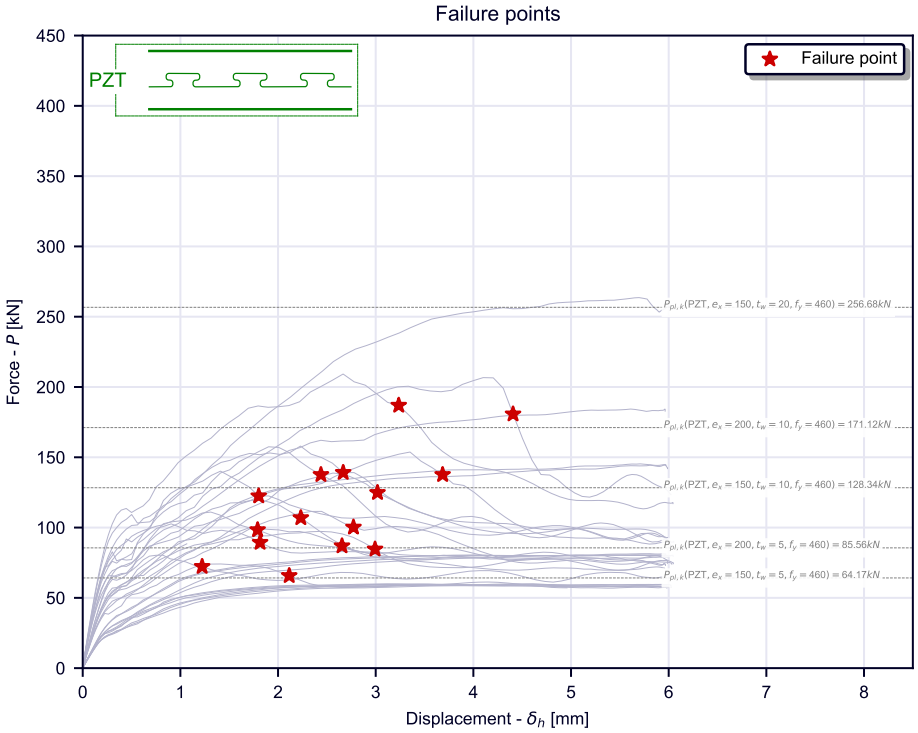

Figure 5.34: parametric numerical FEM simulation study: resulting curves failure points for the filtered shape

5.4.2 MCL series results

the considerations done for the PZT series hold also for the MCL series. In Fig.5.41 the influence of the plate thickness t_w is shown. This influences both the initial stiffness and the resistance. The failure mode is affected. In Fig.5.42 the influence of the size e_x is shown. In Fig.5.43 the influence of the concrete cover c is shown. Note that for high values of concrete cover the failure mode is yielding of the steel dowel. For Low values of t_w the failure is not affected by the concrete cover. For low values of concrete cover a pryout failure is likely to happen. In Fig.5.38 the influence of the concrete grade f_{ck} is shown. In case of pryout failure the load curve is not significantly affected by the concrete resistance. In Fig.5.39 the curves are filtered by the failure mode. The failure points are identified in Fig.5.40.

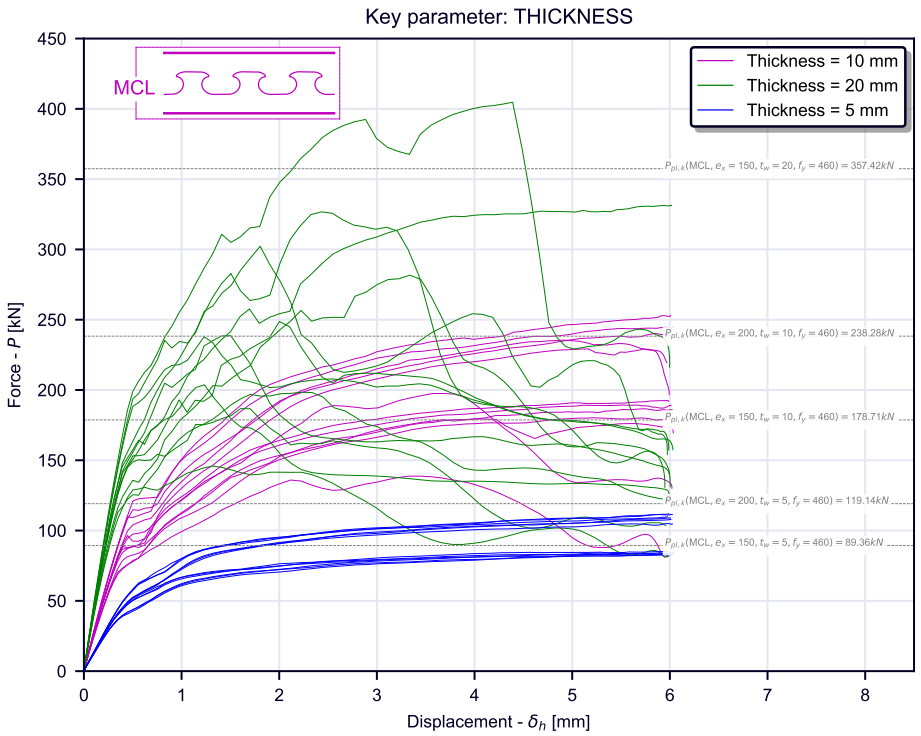

Figure 5.35: parametric numerical FEM simulation study: resulting curves sorted by thickness of plate for the filtered shape

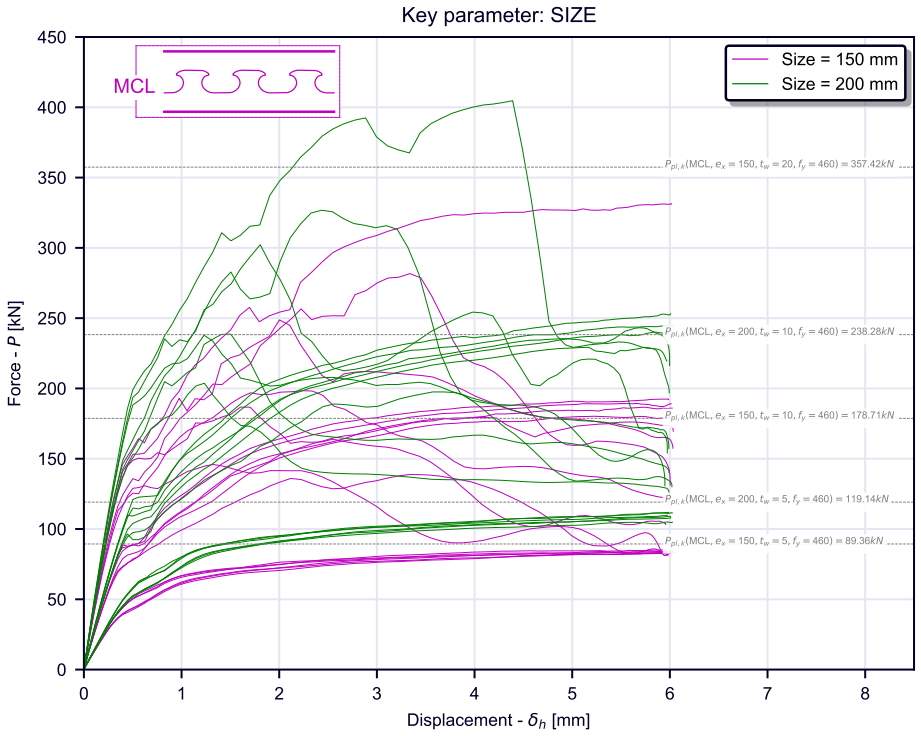

Figure 5.36: parametric numerical FEM simulation study: resulting curves sorted by size of dowel for the filtered shape

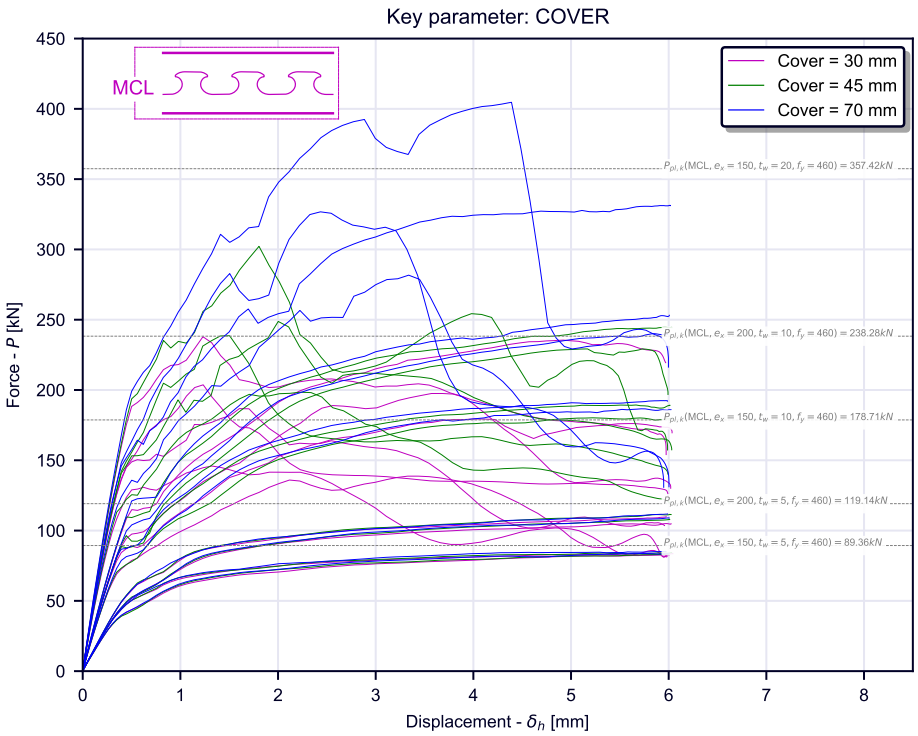

Figure 5.37: parametric numerical FEM simulation study: resulting curves sorted by concrete cover for the filtered shape

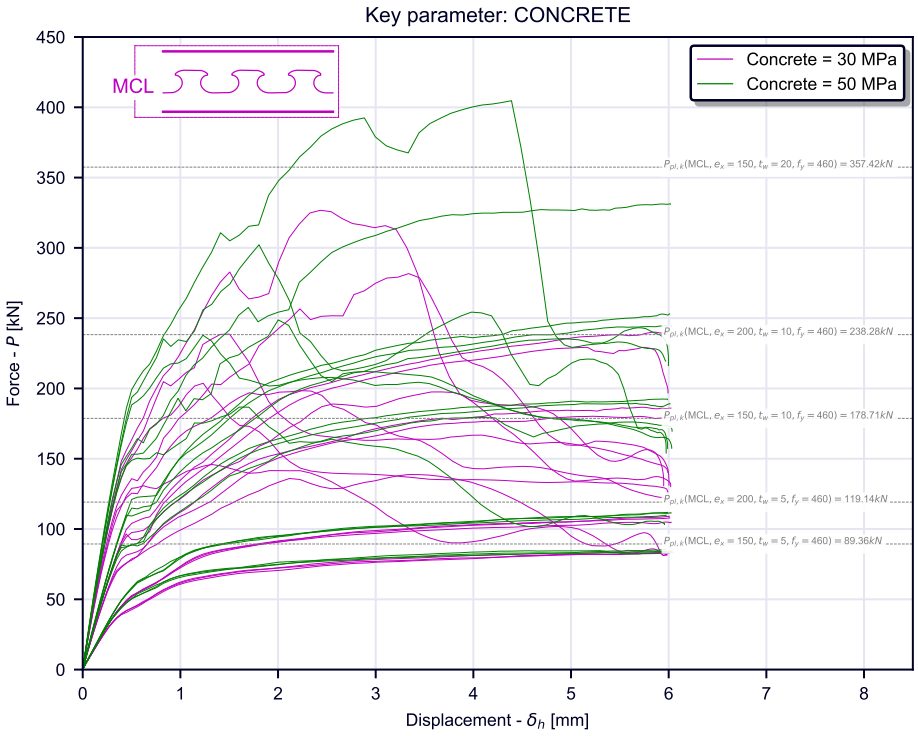

Figure 5.38: parametric numerical FEM simulation study: resulting curves sorted by concrete class for the filtered shape

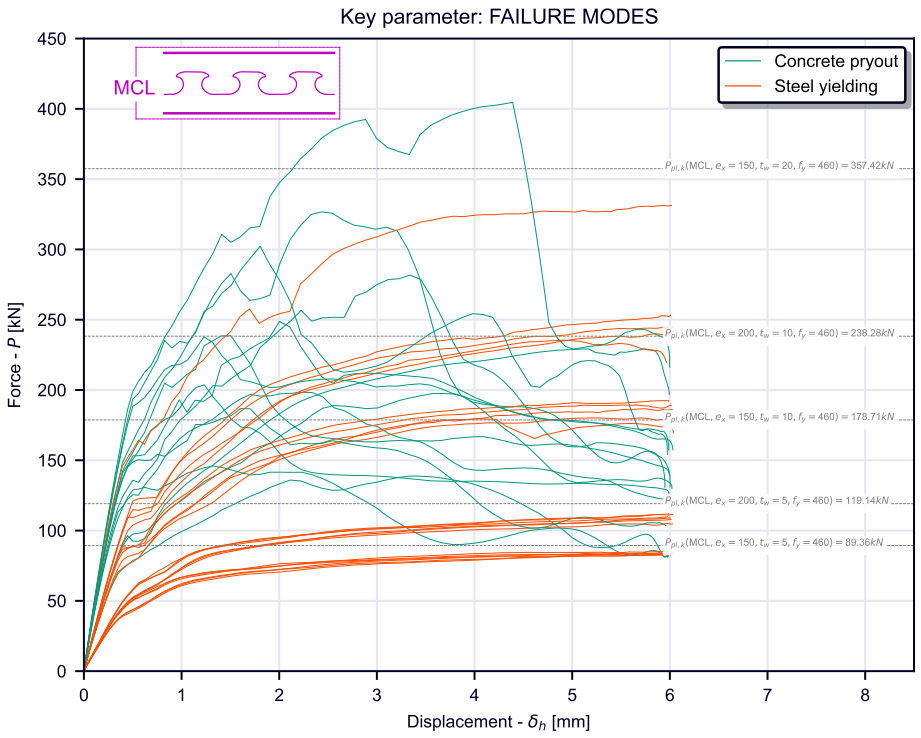

Figure 5.39: parametric numerical FEM simulation study: resulting curves sorted by observed failure mode for the filtered shape

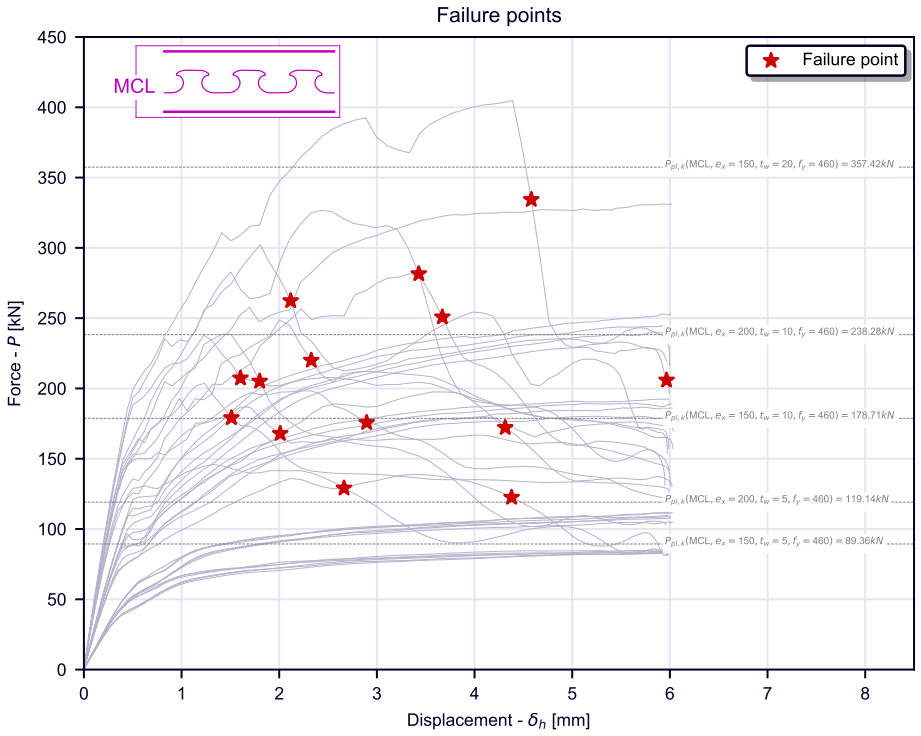

Figure 5.40: parametric numerical FEM simulation study: resulting curves failure points for the filtered shape

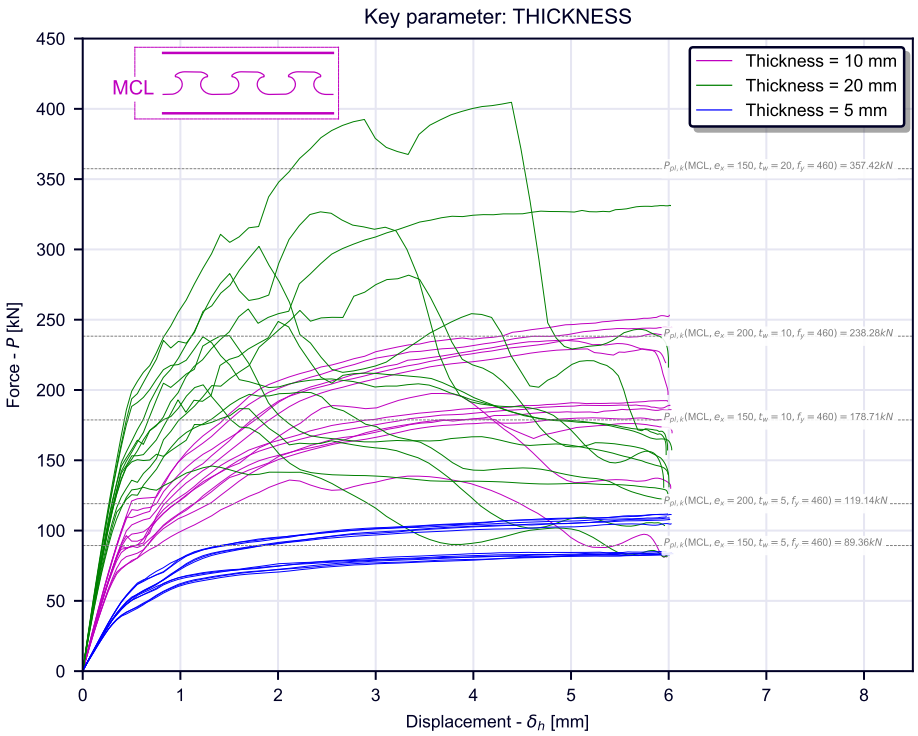

Figure 5.41: parametric numerical FEM simulation study: resulting curves sorted by thickness of plate for the filtered shape

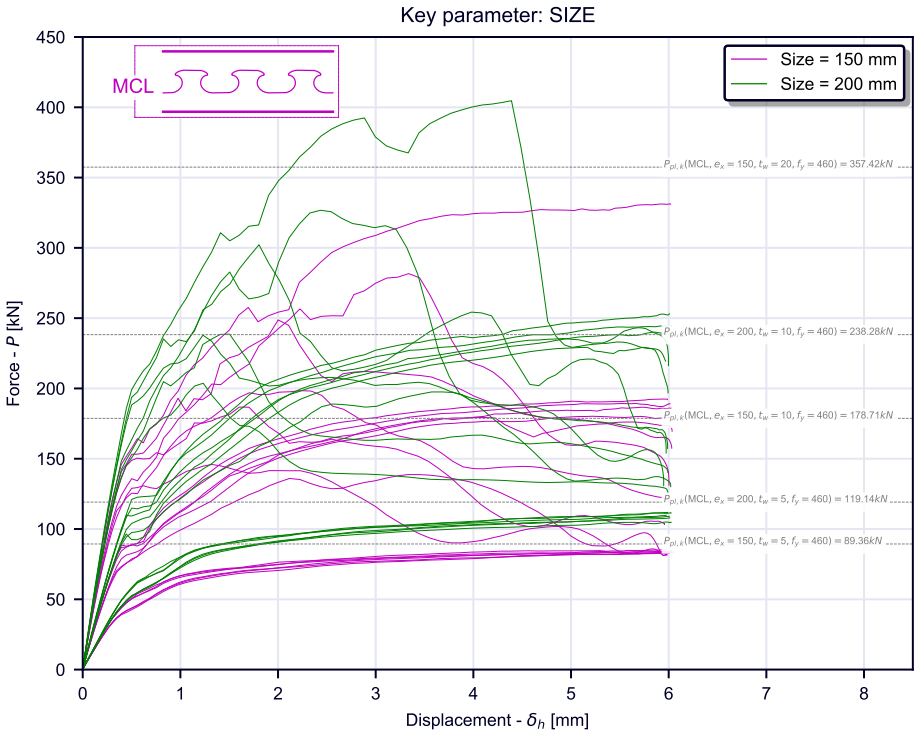

Figure 5.42: parametric numerical FEM simulation study: resulting curves sorted by size of dowel for the filtered shape

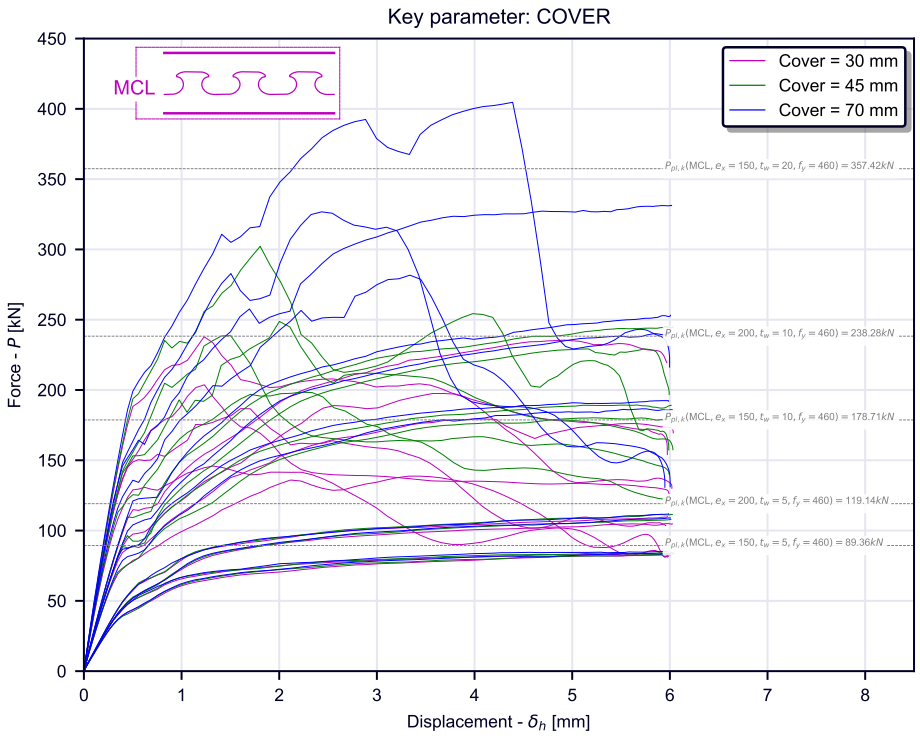

Figure 5.43: parametric numerical FEM simulation study: resulting curves sorted by concrete cover for the filtered shape

5.4.3 PZ series results

The considerations done for the PZT and MCL series hold also for the MCL series. In Fig.5.44 the influence of the plate thickness t_w is shown. This influences both the initial stiffness and the resistance. The failure mode is affected. In Fig.5.45 the influence of the size e_x is shown. In Fig.5.46 the influence of the concrete cover c is shown. Note that for high values of concrete cover the failure mode is yielding of the steel dowel. For Low values of t_w the failure is not affected by the concrete cover. For low values of concrete cover a pryout failure is likely to happen. In Fig.5.47 the influence of the concrete grade f_{ck} is shown. In case of pryout failure the load curve is not significantly affected by the concrete resistance. In Fig.5.48 the curves are filtered by the failure mode. The failure points are identified in Fig.5.49.

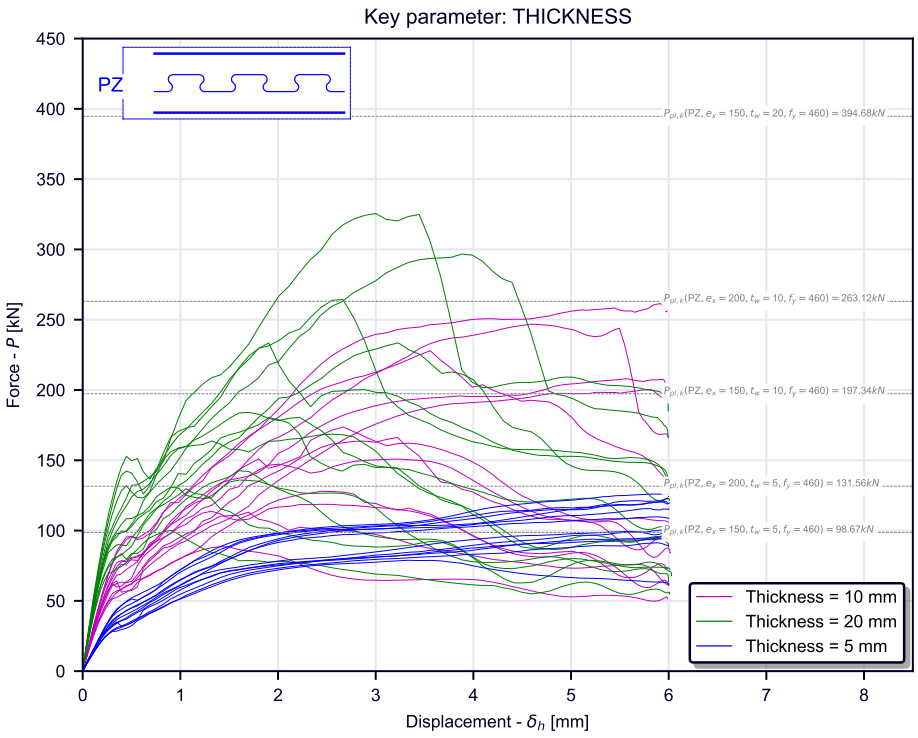

Figure 5.44: Example 1: diagrams

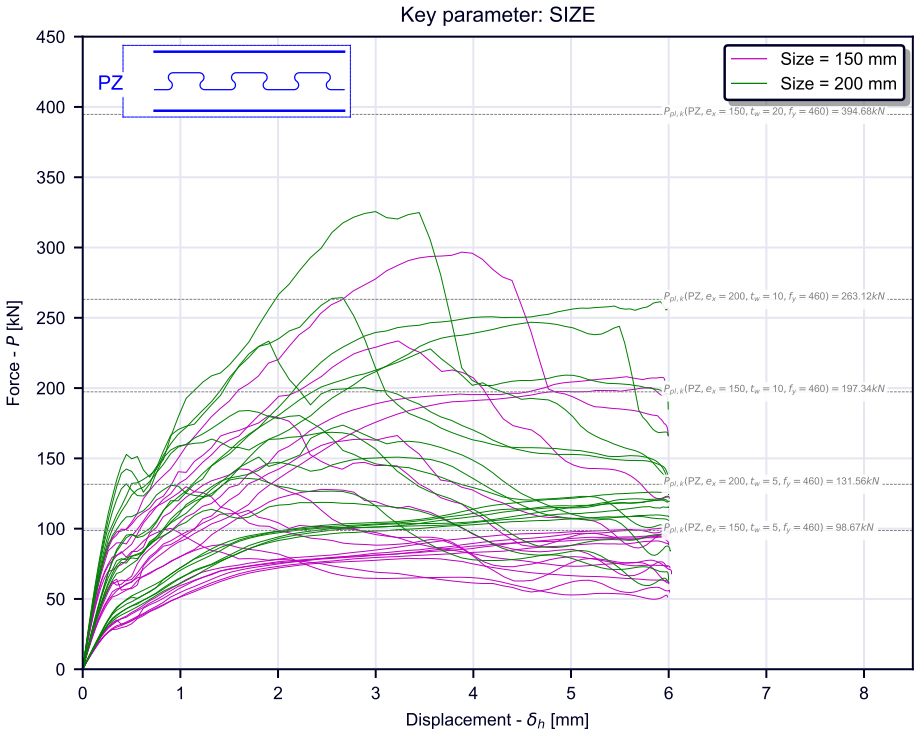

Figure 5.45: Example 1: diagrams

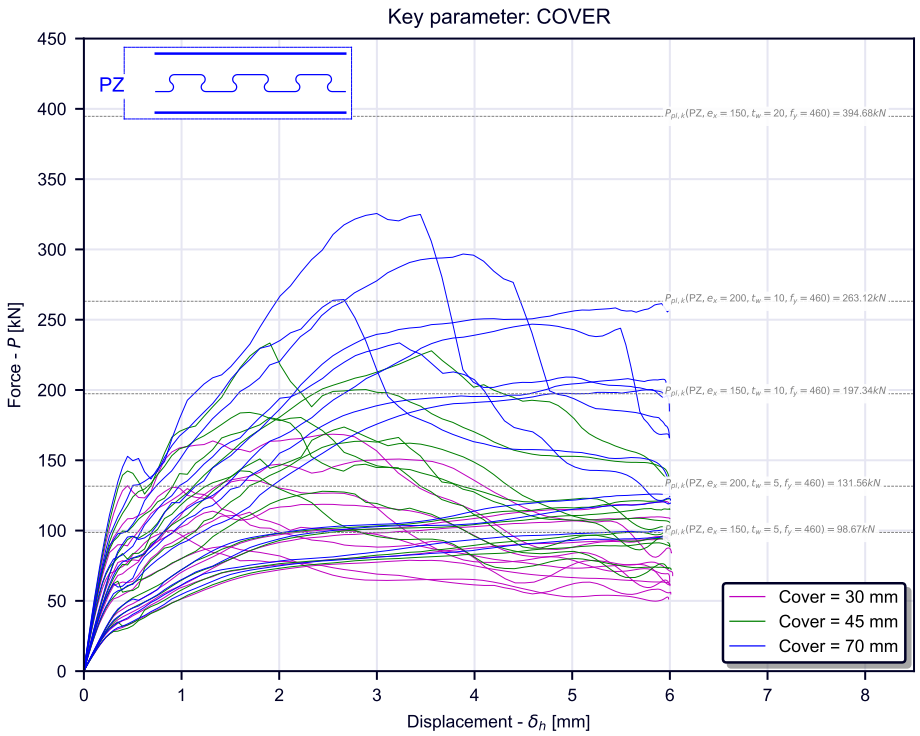

Figure 5.46: Example 1: diagrams

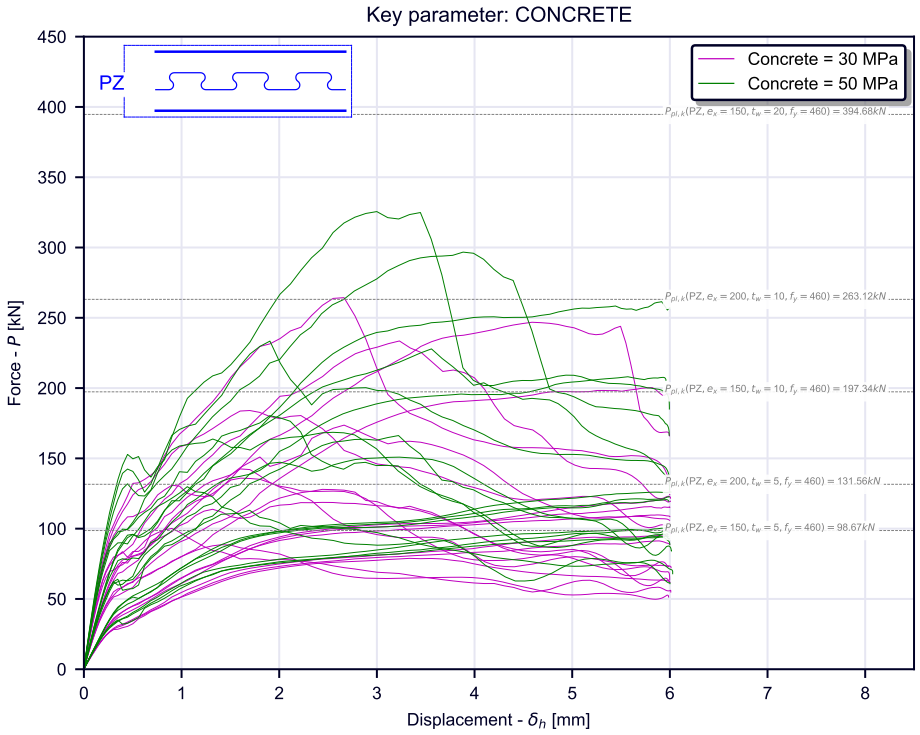

Figure 5.47: parametric numerical FEM simulation study: resulting curves sorted by concrete class for the filtered shape

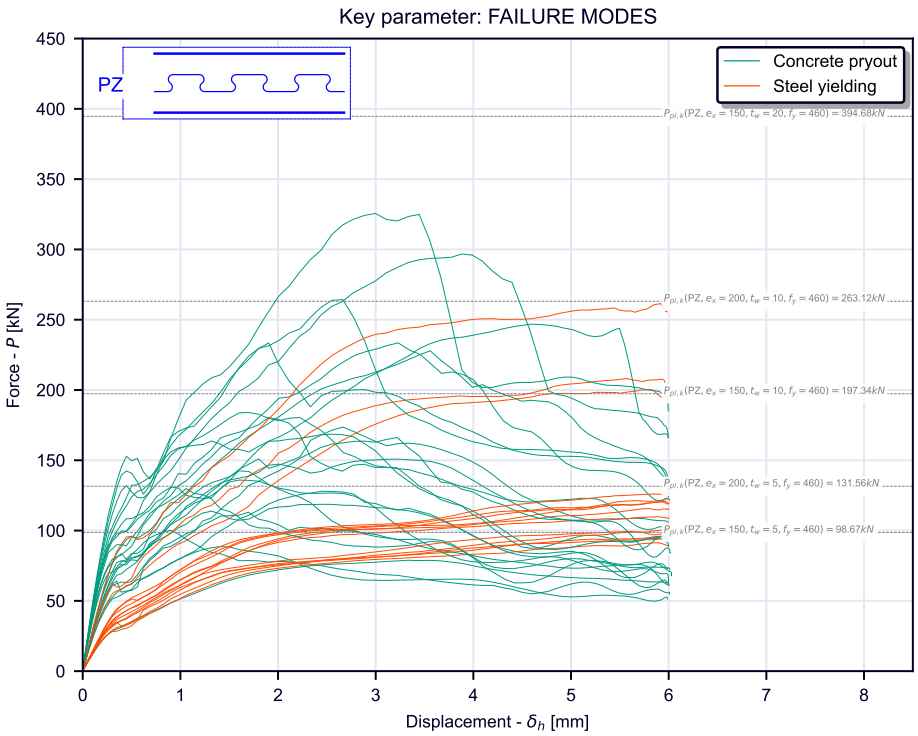

Figure 5.48: parametric numerical FEM simulation study: resulting curves sorted by observed failure mode for the filtered shape

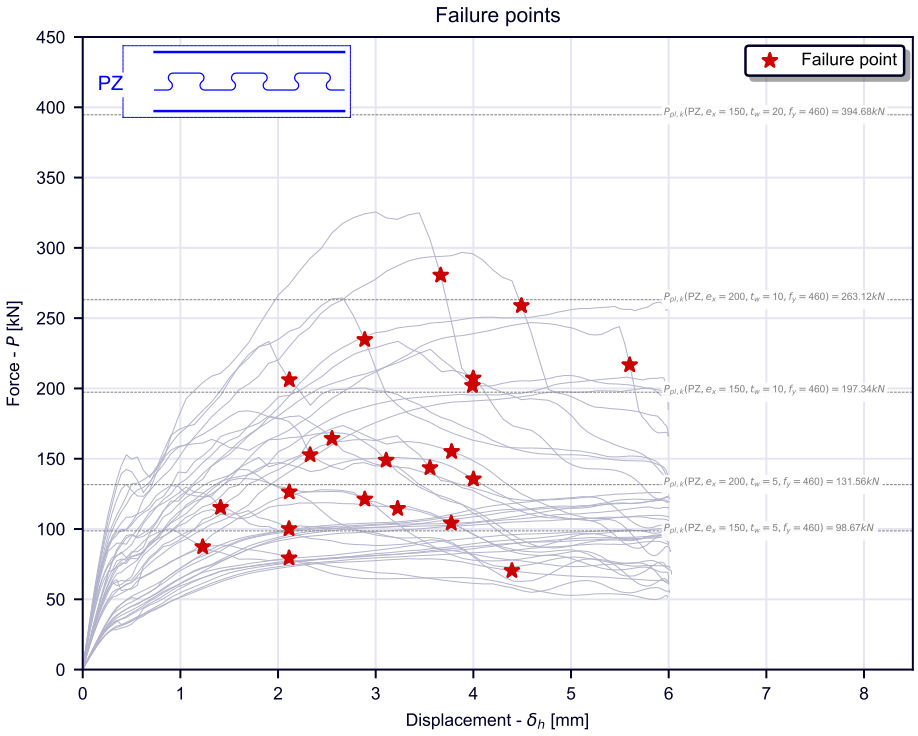

Figure 5.49: parametric numerical FEM simulation study: resulting curves failure points for the filtered shape

5.4.4 Results summary tables

In Fig.5.50, Fig.5.51, Fig.5.52 results regarding the peak force P_{max}, the failure mode, the value of the force in correspondence of the failure point $P(\delta_u)$ and of the ductility δ_u are summarised.

RESULTS SUMMARY: PZT shape

Model name	Shape	Size $e_x\,[mm]$	Thickness $t_w\,[mm]$	Cover $c\,[mm]$	Concrete $f_{ck}\,[MPa]$	Steel $f_y\,[MPa]$	$P_{max}\,[kN]$	$P(\delta_u)\,[kN]$	$\delta_u\,[mm]$	Failure mode
Model-PZT-150-10-30-30-460.odb	PZT	150	10	30	30	460	74.1	65.7	2.1	pryout
Model-PZT-150-10-30-50-460.odb	PZT	150	10	30	50	460	97.3	84.6	3.0	pryout
Model-PZT-150-10-45-30-460.odb	PZT	150	10	45	30	460	111.5	100.2	2.8	pryout
Model-PZT-150-10-45-50-460.odb	PZT	150	10	45	50	460	88.4	na	> 6.0	yielding
Model-PZT-150-10-70-30-460.odb	PZT	150	10	70	30	460	144.5	na	> 6.0	yielding
Model-PZT-150-10-70-50-460.odb	PZT	150	10	70	50	460	145.3	na	> 6.0	yielding
Model-PZT-150-20-30-30-460.odb	PZT	150	20	30	30	460	80.3	72.3	1.2	pryout
Model-PZT-150-20-30-50-460.odb	PZT	150	20	30	50	460	102.6	89.4	1.8	pryout
Model-PZT-150-20-45-30-460.odb	PZT	150	20	45	30	460	119.9	106.9	2.2	pryout
Model-PZT-150-20-45-50-460.odb	PZT	150	20	45	50	460	157.5	137.6	2.4	pryout
Model-PZT-150-20-70-30-460.odb	PZT	150	20	70	30	460	206.7	180.7	4.4	pryout
Model-PZT-150-20-70-50-460.odb	PZT	150	20	70	50	460	263.6	na	> 6.0	yielding
Model-PZT-150-4-30-30-460.odb	PZT	150	4	30	30	460	58.6	na	> 6.0	yielding
Model-PZT-150-4-30-50-460.odb	PZT	150	4	30	50	460	59.1	na	> 6.0	yielding
Model-PZT-150-4-45-30-460.odb	PZT	150	4	45	30	460	59.2	na	> 6.0	yielding
Model-PZT-150-4-45-50-460.odb	PZT	150	4	45	50	460	59.7	na	> 6.0	yielding
Model-PZT-150-4-70-30-460.odb	PZT	150	4	70	30	460	60.0	na	> 6.0	yielding
Model-PZT-150-4-70-50-460.odb	PZT	150	4	70	50	460	60.0	na	> 6.0	yielding
Model-PZT-200-10-30-30-460.odb	PZT	200	10	30	30	460	99.8	86.9	2.7	pryout
Model-PZT-200-10-30-50-460.odb	PZT	200	10	30	50	460	138.8	124.8	3.0	pryout
Model-PZT-200-10-45-30-460.odb	PZT	200	10	45	30	460	153.7	137.6	3.7	pryout
Model-PZT-200-10-45-50-460.odb	PZT	200	10	45	50	460	184.3	na	> 6.0	yielding
Model-PZT-200-20-30-30-460.odb	PZT	200	20	30	30	460	111.0	98.4	1.8	pryout
Model-PZT-200-20-30-50-460.odb	PZT	200	20	30	50	460	140.1	122.4	1.8	pryout
Model-PZT-200-20-45-30-460.odb	PZT	200	20	45	30	460	158.0	139.1	2.7	pryout
Model-PZT-200-20-45-50-460.odb	PZT	200	20	45	50	460	209.2	186.9	3.2	pryout
Model-PZT-200-4-30-30-460.odb	PZT	200	4	30	30	460	79.3	na	> 6.0	yielding
Model-PZT-200-4-30-50-460.odb	PZT	200	4	30	50	460	80.7	na	> 6.0	yielding
Model-PZT-200-4-45-30-460.odb	PZT	200	4	45	30	460	81.4	na	> 6.0	yielding
Model-PZT-200-4-45-50-460.odb	PZT	200	4	45	50	460	80.5	na	> 6.0	yielding

Figure 5.50: parametric numerical FEM simulation study: summary table for PZT dowel shape

RESULTS SUMMARY: MCL shape

Model name	Shape	Size $e_x\,[mm]$	Thickness $t_w\,[mm]$	Cover $c\,[mm]$	Concrete $f_{ck}\,[MPa]$	Steel $f_y\,[MPa]$	$P_{max}\,[kN]$	$P(\delta_u)\,[kN]$	$\delta_u\,[mm]$	Failure mode
Model-MCL-150-10-30-30-460.odb	MCL	150	10	30	30	460	138.7	122.5	4.4	pryout
Model-MCL-150-10-30-50-460.odb	MCL	150	10	30	50	460	179.4	na	> 6.0	yielding
Model-MCL-150-10-45-30-460.odb	MCL	150	10	45	30	460	180.2	na	> 6.0	yielding
Model-MCL-150-10-45-50-460.odb	MCL	150	10	45	50	460	189.3	na	> 6.0	yielding
Model-MCL-150-10-70-30-460.odb	MCL	150	10	70	30	460	186.6	na	> 6.0	yielding
Model-MCL-150-10-70-50-460.odb	MCL	150	10	70	50	460	192.4	na	> 6.0	yielding
Model-MCL-150-20-30-30-460.odb	MCL	150	20	30	30	460	145.9	129.0	2.7	pryout
Model-MCL-150-20-30-50-460.odb	MCL	150	20	30	50	460	186.7	167.9	2.0	pryout
Model-MCL-150-20-45-30-460.odb	MCL	150	20	45	30	460	198.4	175.7	2.9	pryout
Model-MCL-150-20-45-50-460.odb	MCL	150	20	45	50	460	248.8	220.0	2.3	pryout
Model-MCL-150-20-70-30-460.odb	MCL	150	20	70	30	460	281.7	250.8	3.7	pryout
Model-MCL-150-20-70-50-460.odb	MCL	150	20	70	50	460	331.3	na	> 6.0	yielding
Model-MCL-150-4-30-30-460.odb	MCL	150	4	30	30	460	82.8	na	> 6.0	yielding
Model-MCL-150-4-30-50-460.odb	MCL	150	4	30	50	460	83.6	na	> 6.0	yielding
Model-MCL-150-4-45-30-460.odb	MCL	150	4	45	30	460	83.2	na	> 6.0	yielding
Model-MCL-150-4-45-50-460.odb	MCL	150	4	45	50	460	84.3	na	> 6.0	yielding
Model-MCL-150-4-70-30-460.odb	MCL	150	4	70	30	460	83.7	na	> 6.0	yielding
Model-MCL-150-4-70-50-460.odb	MCL	150	4	70	50	460	85.2	na	> 6.0	yielding
Model-MCL-200-10-30-30-460.odb	MCL	200	10	30	30	460	197.5	172.1	4.3	pryout
Model-MCL-200-10-30-50-460.odb	MCL	200	10	30	50	460	235.5	na	> 6.0	yielding
Model-MCL-200-10-45-30-460.odb	MCL	200	10	45	30	460	229.3	205.9	6.0	pryout
Model-MCL-200-10-45-50-460.odb	MCL	200	10	45	50	460	244.7	na	> 6.0	yielding
Model-MCL-200-10-70-30-460.odb	MCL	200	10	70	30	460	240.1	na	> 6.0	yielding
Model-MCL-200-10-70-50-460.odb	MCL	200	10	70	50	460	253.1	na	> 6.0	yielding
Model-MCL-200-20-30-30-460.odb	MCL	200	20	30	30	460	203.7	179.1	1.5	pryout
Model-MCL-200-20-30-50-460.odb	MCL	200	20	30	50	460	237.9	207.4	1.6	pryout
Model-MCL-200-20-45-30-460.odb	MCL	200	20	45	30	460	238.6	205.1	1.8	pryout
Model-MCL-200-20-45-50-460.odb	MCL	200	20	45	50	460	302.2	262.3	2.1	pryout
Model-MCL-200-20-70-30-460.odb	MCL	200	20	70	30	460	326.7	281.5	3.4	pryout
Model-MCL-200-20-70-50-460.odb	MCL	200	20	70	50	460	404.7	334.3	4.6	pryout
Model-MCL-200-4-30-30-460.odb	MCL	200	4	30	30	460	105.0	na	> 6.0	yielding
Model-MCL-200-4-30-50-460.odb	MCL	200	4	30	50	460	109.8	na	> 6.0	yielding
Model-MCL-200-4-45-30-460.odb	MCL	200	4	45	30	460	108.0	na	> 6.0	yielding
Model-MCL-200-4-45-50-460.odb	MCL	200	4	45	50	460	111.5	na	> 6.0	yielding
Model-MCL-200-4-70-30-460.odb	MCL	200	4	70	30	460	109.0	na	> 6.0	yielding
Model-MCL-200-4-70-50-460.odb	MCL	200	4	70	50	460	112.0	na	> 6.0	yielding

Figure 5.51: parametric numerical FEM simulation study: summary table for MCL dowel shape

RESULTS SUMMARY: PZ shape

Model name	Shape	Size $e_x\,[mm]$	Thickness $t_w\,[mm]$	Cover $c\,[mm]$	Concrete $f_{ck}\,[MPa]$	Steel $f_y\,[MPa]$	$P_{max}\,[kN]$	$P(\delta_u)\,[kN]$	$\delta_u\,[mm]$	Failure mode
Model-PZ-150-10-30-30-460.odb	PZ	150	10	30	30	460	88.6	79.3	2.1	pryout
Model-PZ-150-10-30-50-460.odb	PZ	150	10	30	50	460	113.1	100.1	2.1	pryout
Model-PZ-150-10-45-30-460.odb	PZ	150	10	45	30	460	127.9	114.5	3.2	pryout
Model-PZ-150-10-45-50-460.odb	PZ	150	10	45	50	460	166.2	143.5	3.6	pryout
Model-PZ-150-10-70-30-460.odb	PZ	150	10	70	30	460	200.3	na	> 6.0	yielding
Model-PZ-150-10-70-50-460.odb	PZ	150	10	70	50	460	208.1	na	> 6.0	yielding
Model-PZ-150-20-30-30-460.odb	PZ	150	20	30	30	460	100.2	87.3	1.2	pryout
Model-PZ-150-20-30-50-460.odb	PZ	150	20	30	50	460	129.9	115.3	1.4	pryout
Model-PZ-150-20-45-30-460.odb	PZ	150	20	45	30	460	142.5	126.3	2.1	pryout
Model-PZ-150-20-45-50-460.odb	PZ	150	20	45	50	460	180.4	152.7	2.3	pryout
Model-PZ-150-20-70-30-460.odb	PZ	150	20	70	30	460	233.5	207.3	4.0	pryout
Model-PZ-150-20-70-50-460.odb	PZ	150	20	70	50	460	296.7	258.8	4.5	pryout
Model-PZ-150-4-30-30-460.odb	PZ	150	4	30	30	460	78.9	70.3	4.4	pryout
Model-PZ-150-4-30-50-460.odb	PZ	150	4	30	50	460	94.5	na	> 6.0	yielding
Model-PZ-150-4-45-30-460.odb	PZ	150	4	45	30	460	91.3	na	> 6.0	yielding
Model-PZ-150-4-45-50-460.odb	PZ	150	4	45	50	460	99.0	na	> 6.0	yielding
Model-PZ-150-4-70-30-460.odb	PZ	150	4	70	30	460	95.5	na	> 6.0	yielding
Model-PZ-150-4-70-50-460.odb	PZ	150	4	70	50	460	100.9	na	> 6.0	yielding
Model-PZ-200-10-30-30-460.odb	PZ	200	10	30	30	460	118.7	104.2	3.8	pryout
Model-PZ-200-10-30-50-460.odb	PZ	200	10	30	50	460	150.9	135.5	4.0	pryout
Model-PZ-200-10-45-30-460.odb	PZ	200	10	45	30	460	173.6	155.0	3.8	pryout
Model-PZ-200-10-45-50-460.odb	PZ	200	10	45	50	460	227.9	202.0	4.0	pryout
Model-PZ-200-10-70-30-460.odb	PZ	200	10	70	30	460	246.8	216.7	5.6	pryout
Model-PZ-200-10-70-50-460.odb	PZ	200	10	70	50	460	261.5	na	> 6.0	yielding
Model-PZ-200-20-30-30-460.odb	PZ	200	20	30	30	460	135.9	121.2	2.9	pryout
Model-PZ-200-20-30-50-460.odb	PZ	200	20	30	50	460	168.5	148.9	3.1	pryout
Model-PZ-200-20-45-30-460.odb	PZ	200	20	45	30	460	184.0	164.3	2.6	pryout
Model-PZ-200-20-45-50-460.odb	PZ	200	20	45	50	460	233.4	206.1	2.1	pryout
Model-PZ-200-20-70-30-460.odb	PZ	200	20	70	30	460	264.3	234.7	2.9	pryout
Model-PZ-200-20-70-50-460.odb	PZ	200	20	70	50	460	325.6	280.5	3.7	pryout
Model-PZ-200-4-30-30-460.odb	PZ	200	4	30	30	460	109.8	na	> 6.0	yielding
Model-PZ-200-4-30-50-460.odb	PZ	200	4	30	50	460	120.7	na	> 6.0	yielding
Model-PZ-200-4-45-30-460.odb	PZ	200	4	45	30	460	115.7	na	> 6.0	yielding
Model-PZ-200-4-45-50-460.odb	PZ	200	4	45	50	460	122.8	na	> 6.0	yielding
Model-PZ-200-4-70-30-460.odb	PZ	200	4	70	30	460	120.6	na	> 6.0	yielding
Model-PZ-200-4-70-50-460.odb	PZ	200	4	70	50	460	126.1	na	> 6.0	yielding

Figure 5.52: parametric numerical FEM simulation study: summary table for PZ dowel shape

5.4.5 Failure modes and resistances consistency

In Fig.5.53 the comparison between expected resistance of the observed failure mode and the actual resistance P_{max} is shown. Points above the bisector are safe ($P_{numerical} > P_{expected}$) and those under the bisector are unsafe ($P_{expected} > P_{numerical}$). The majority of the points is in the safe region and a good correspondence between the expected resistance of the observed failure mode and the actual resistance is observed. In Fig.5.54, Fig.5.56 and Fig.5.55 the analysis results are filtered for each input parameter of the study. The failure mode is represented. The line separating the expected failure domains is plotted. This is derived from the literature known relations. The numerical analysis results generally respects well the expected failure. Despite of the fact that the number of analyses done is moderate and the failure domains is coarsely represented by the colors of the points, the results are respecting the expected failure modes well. Some points in which a pryout failure is expected but in the numerical analysis a yielding failure appears can be identified, however this can probably be a consequence of a safe side approach in deriving the pryout resistance formulations from literature.

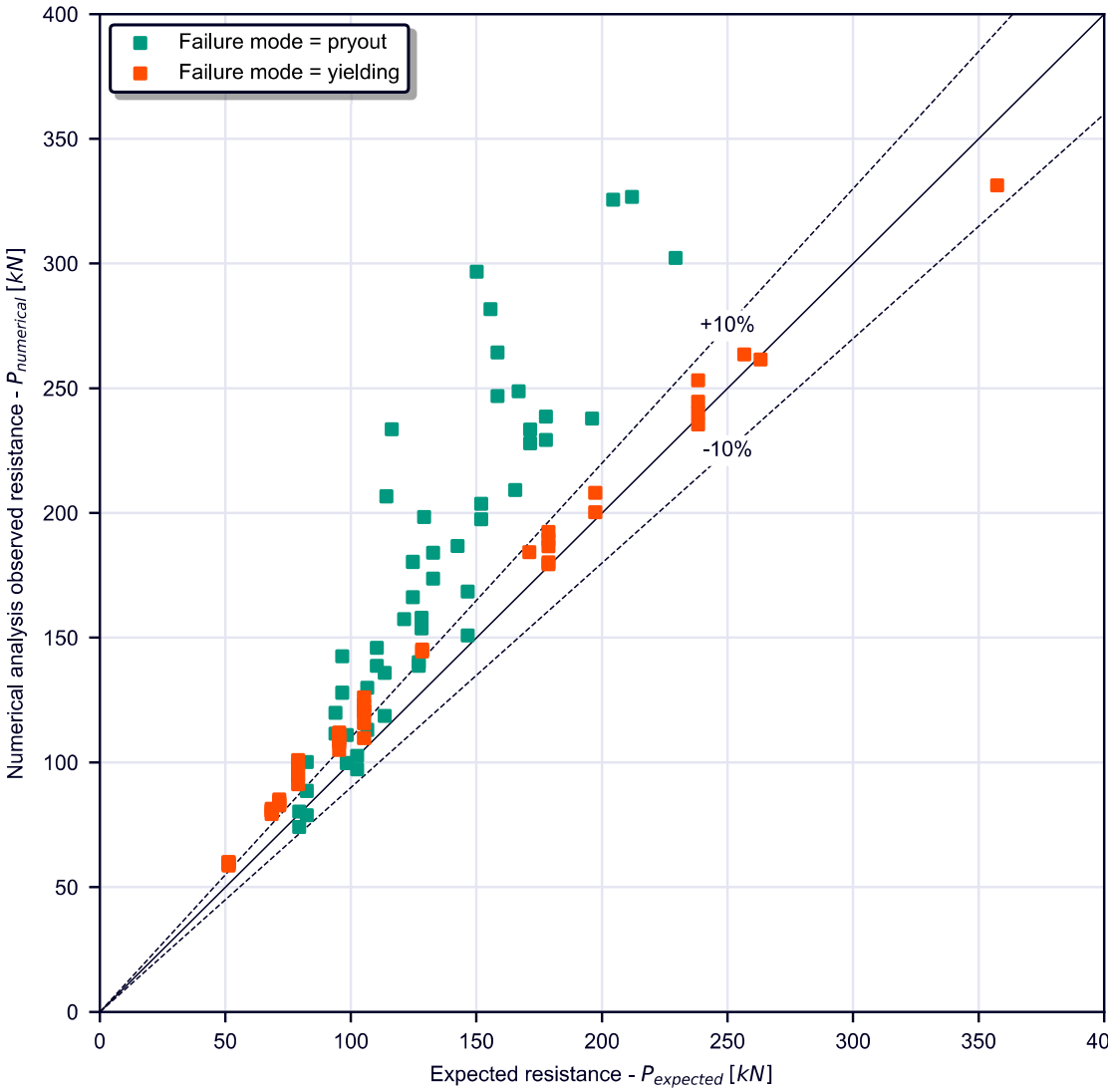

Figure 5.53: expected vs. numerically observed resistance

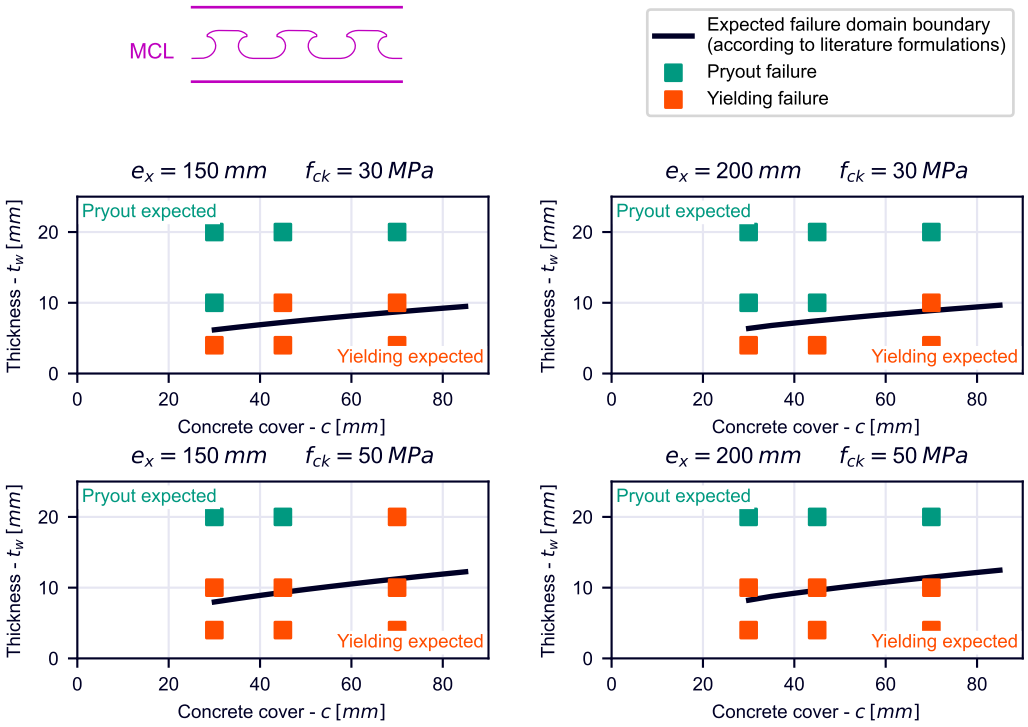

Figure 5.54: expected vs. numerically observed failure modes for the given shape

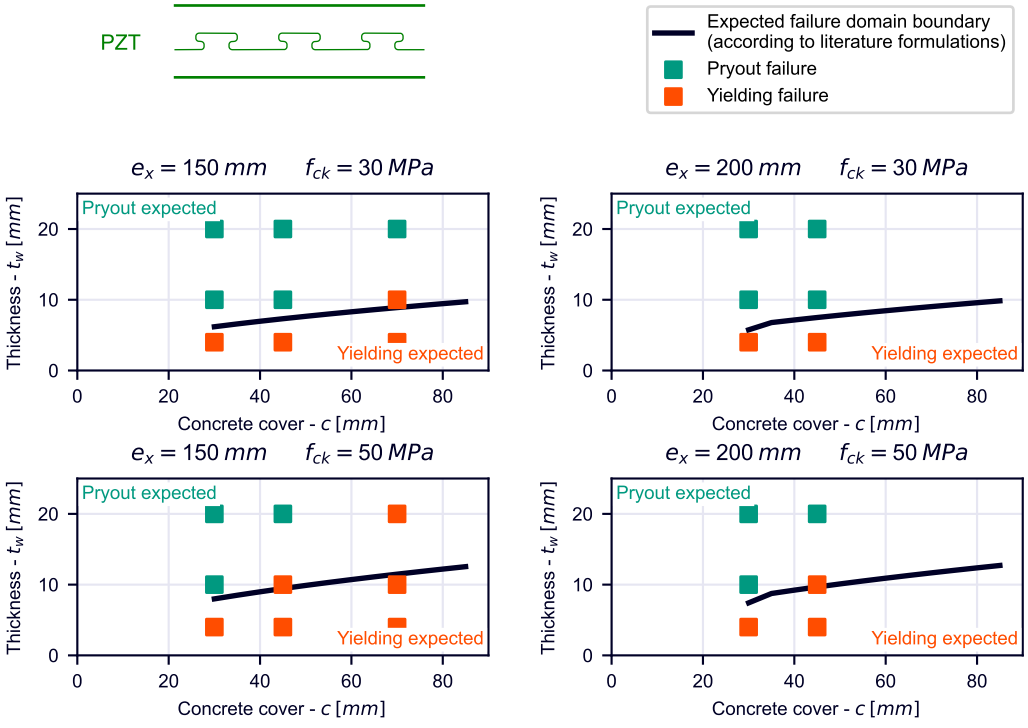

Figure 5.55: expected vs. numerically observed failure modes for the given shape

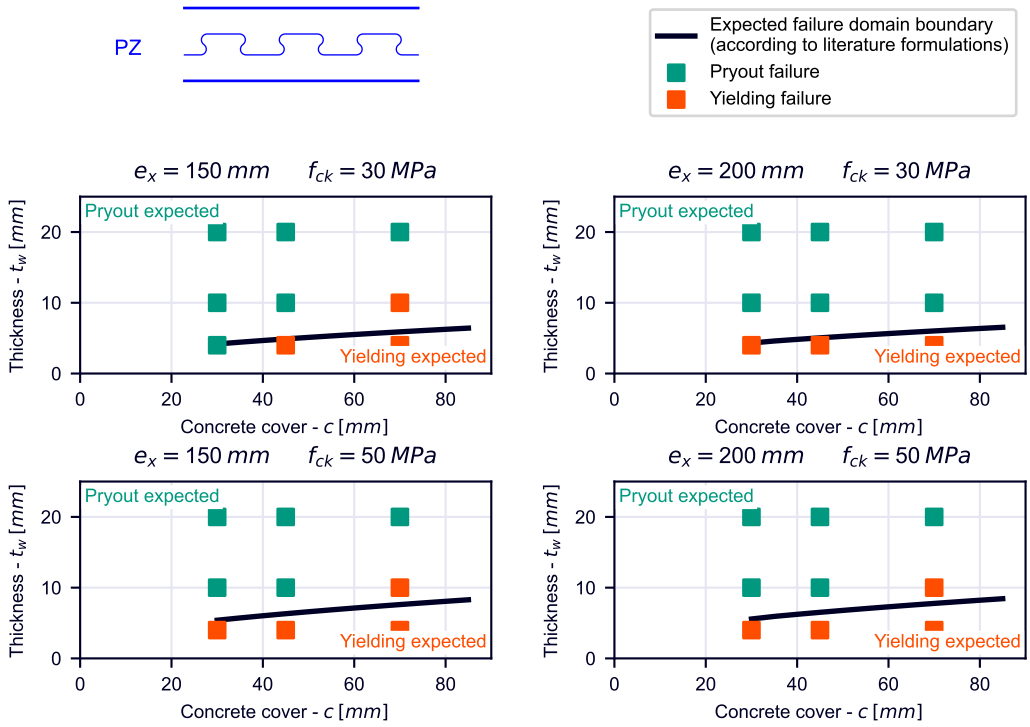

Figure 5.56: expected vs. numerically observed failure modes for the given shape

5.4.6 Ductility map and model for the ductility

In the same charts as the one used before the ductility results can be plotted. This is done in Fig.5.57, Fig.5.58 and Fig.5.59. A trend can be observed in the ductility result. Moving from top-left angle to bottom-right angle of the charts the ductility increases. This well respects the expectations. This is generally valid for all the three shapes. In case of steel yielding failure the ductility value has not been observed, it can only be concluded to be a value greater than 6mm.

A model for predicting the ductility as function of the input parameters has here been derived. The model is as follows:

$$\hat{\delta}_{u,Shape}(t_w, c, e_w, f_{ck}) = k_{1,Shape}\, 1/t_w + k_{2,Shape}\, c + k_{3,Shape}\, e_x + k_{4,Shape}\, f_{ck} \tag{5.24}$$

The model is intuitively introduced. It is assumed that the ductility increases linearly with the concrete cover c, the size of the dowel e_x and the concrete grade f_{ck}. It is assumed to reduce in an inverse proportional way with the steel plate thickness t_w. Note that the model is linear in the parameters $k_{1,Shape}$, $k_{2,Shape}$, $k_{3,Shape}$ and $k_{4,Shape}$. These parameters can be estimated according to a linear least square method. In this case the number of ductilities values $\delta_{u,i,Shape}$ observed for each shape is N. The number of parameters $k_{i,Shape}$ to be determined for each shape is $p = 4$.

$$\begin{pmatrix} \hat{\delta}_{u,1,Shape} \\ \hat{\delta}_{u,2,Shape} \\ ... \\ \hat{\delta}_{u,i,Shape} \\ ... \\ \hat{\delta}_{u,N,Shape} \end{pmatrix} = \begin{pmatrix} 1/t_{w,1} & c_1 & e_{x,1} & f_{ck,1} \\ 1/t_{w,2} & c_2 & e_{x,2} & f_{ck,2} \\ ... & & & \\ 1/t_{w,i} & c_i & e_{x,i} & f_{ck,i} \\ ... & & & \\ 1/t_{w,N} & c_N & e_{x,N} & f_{ck,N} \end{pmatrix} \begin{pmatrix} k_{1,Shape} \\ k_{2,Shape} \\ k_{3,Shape} \\ k_{4,Shape} \end{pmatrix} \tag{5.25}$$

The system can be written as:

$$\underline{\hat{\delta}}_{u,Shape} = \underline{\underline{A}}\, \underline{k}_{Shape} \tag{5.26}$$

Note that $\underline{\delta}_{u,Shape}$ is an N-vector, $\underline{k}_{Shape}$ is a 4-vector, the matrix $\underline{\underline{A}}$ is a $N \times 4$-matrix. The purpose is to find the parameter vector $\underline{k}_{Shape}$ that minimizes the sum of squared errors:

$$Err = \sum_{i=1}^{N} (\delta_{u,i,Shape} - \hat{\delta}_{u,i,Shape})^2 = \min \tag{5.27}$$

This condition can be solved by a minimum problem as function of the parameters $k_{i,Shape}$. Hence, imposing the gradient of the error Err equals to a zero vector:

$$\frac{\partial\, Err}{\partial \underline{k}_{Shape}} = \underline{0} \tag{5.28}$$

The previous condition leads to:

$$\underline{k}_{Shape} = (\underline{\underline{A}}^T\, \underline{\underline{A}})^{-1}\, A^T\, \underline{\delta}_{u,Shape} \tag{5.29}$$

This system is called normal system and the matrix $(\underline{\underline{A}}^T\, \underline{\underline{A}})$ is called normal matrix. The estimator of the variance of the model can be computed as:

$$\hat{\sigma}^2_{Shape} = \frac{1}{N-p} \sum_{i=1}^{N} (\delta_{u,i,Shape} - \hat{\delta}_{u,i,Shape})^2 = \frac{1}{N-p} ||(\underline{\delta}_{u,Shape} - \underline{\hat{\delta}}_{u,Shape})||^2 = \tag{5.30}$$

$$= \frac{1}{N-p} ||(\underline{\delta}_{u,Shape} - \underline{\underline{A}}\, \underline{k}_{Shape}||^2 \tag{5.31}$$

The model predictions can be shown in Fig.5.60, Fig.5.62 and Fig.5.61 for all the three shapes MCL, PZ and PZT respectively. Here the modelled ductility is shown as contour-plot as function of the input parameters.

A visual comparison of the model predictions and the observed ductilities is given in Fig.5.64, Fig.5.65 and Fig.5.63.

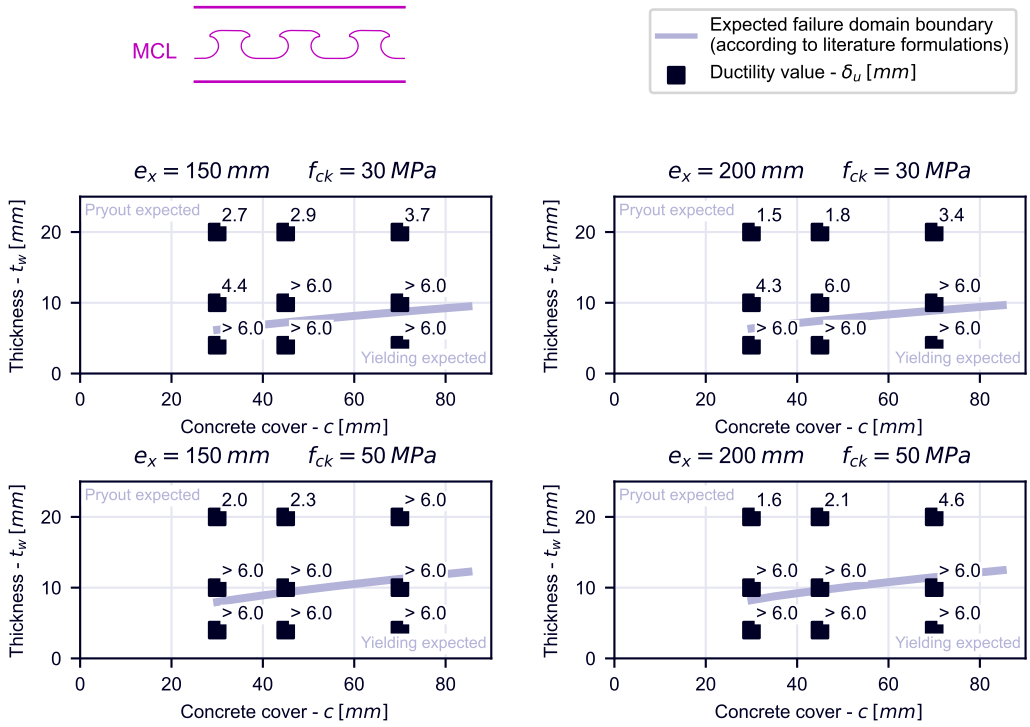

Figure 5.57: observed ductility values for the given shape

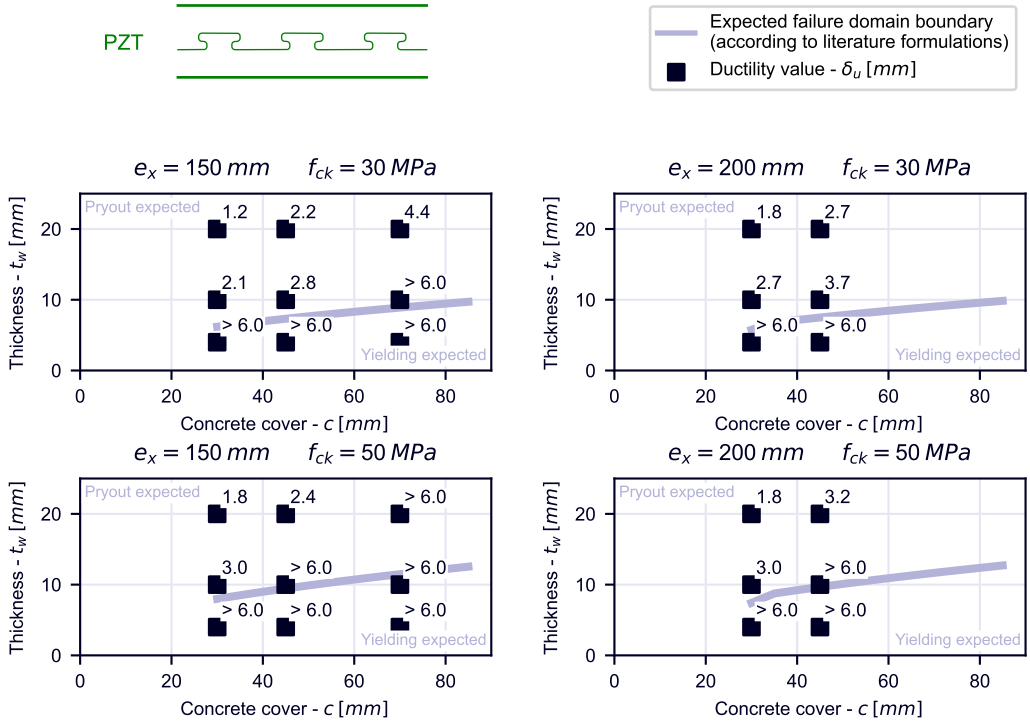

Figure 5.58: observed ductility values for the given shape

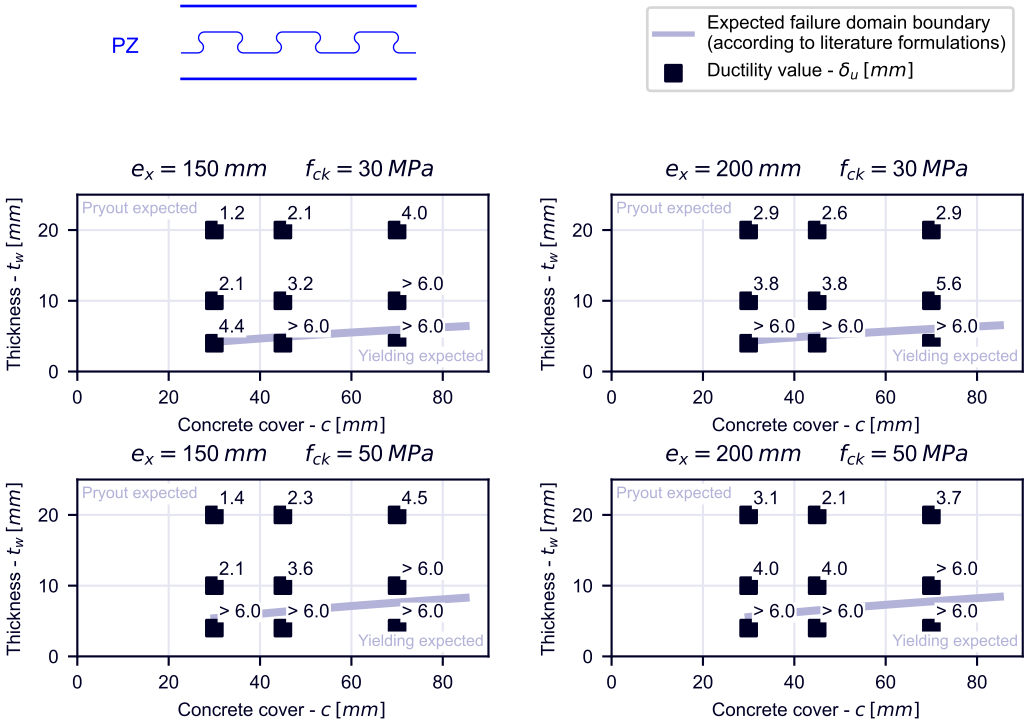

Figure 5.59: observed ductility values for the given shape

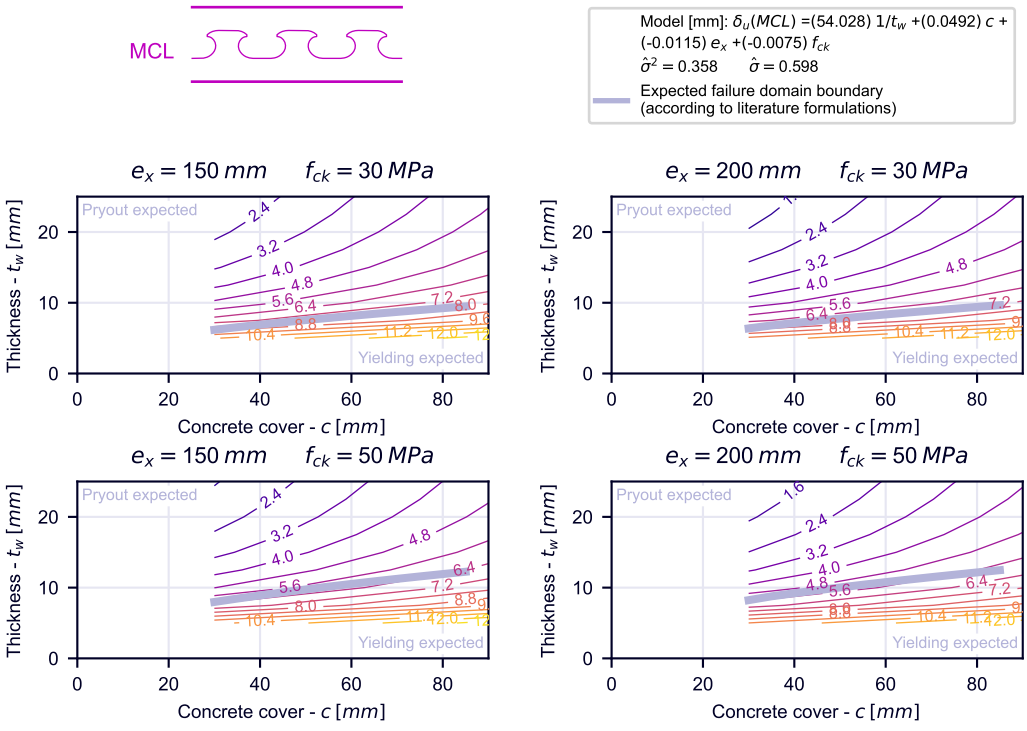

Figure 5.60: ductility model map for the given shape

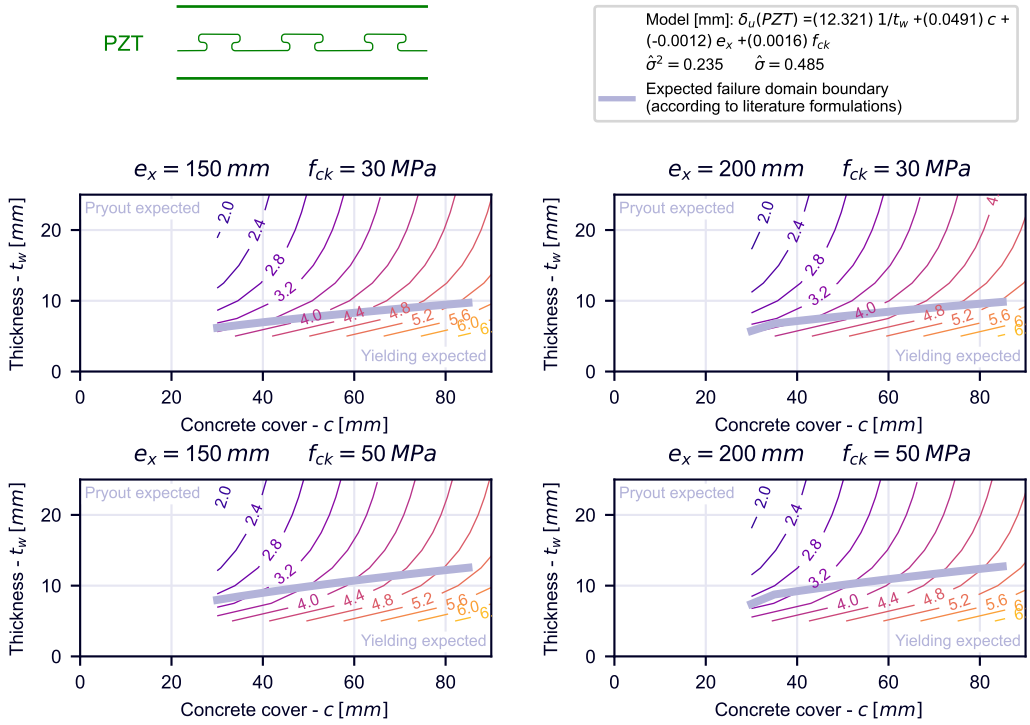

Figure 5.61: ductility model map for the given shape

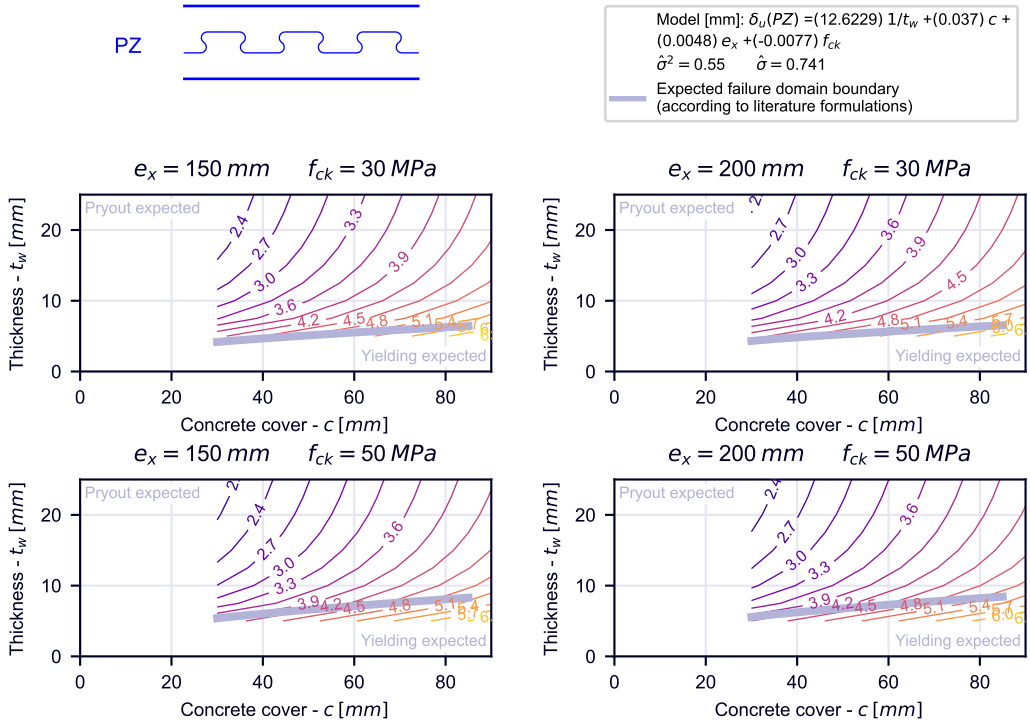

Figure 5.62: ductility model map for the given shape

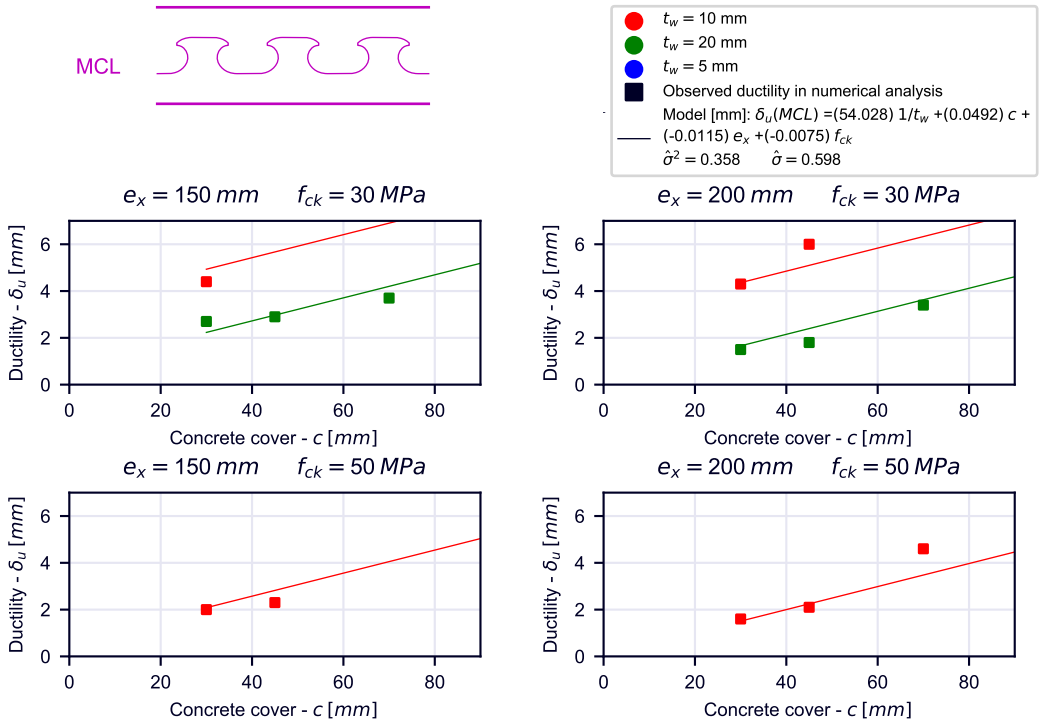

Figure 5.63: ductility model vs observed ductility comparison for the given shape

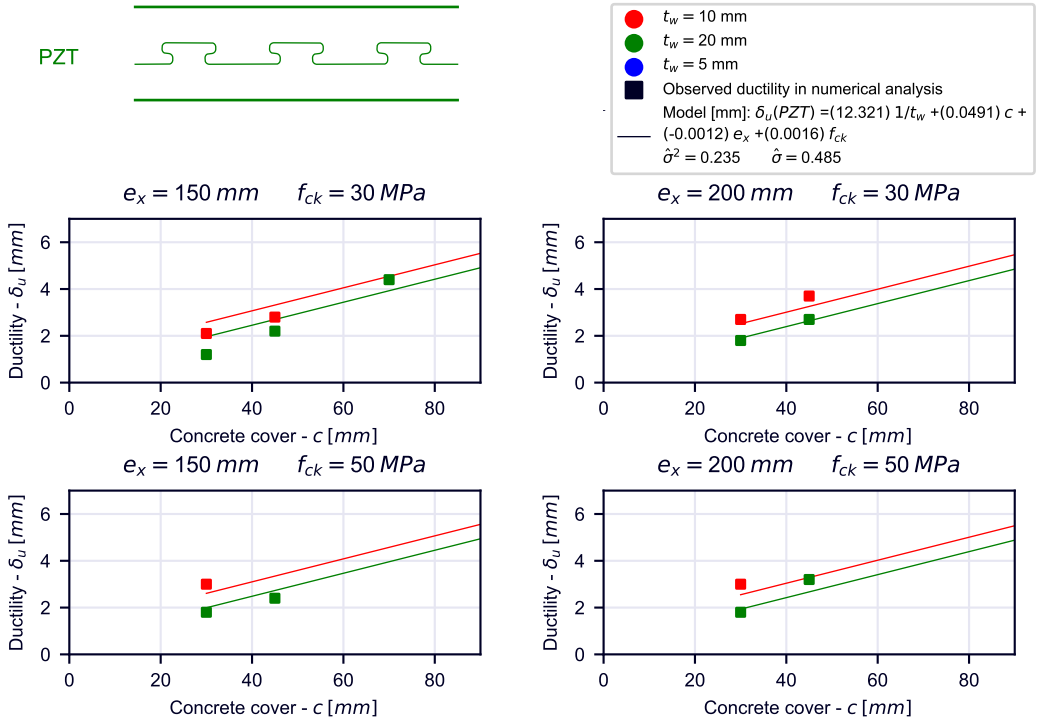

Figure 5.64: ductility model vs observed ductility comparison for the given shape

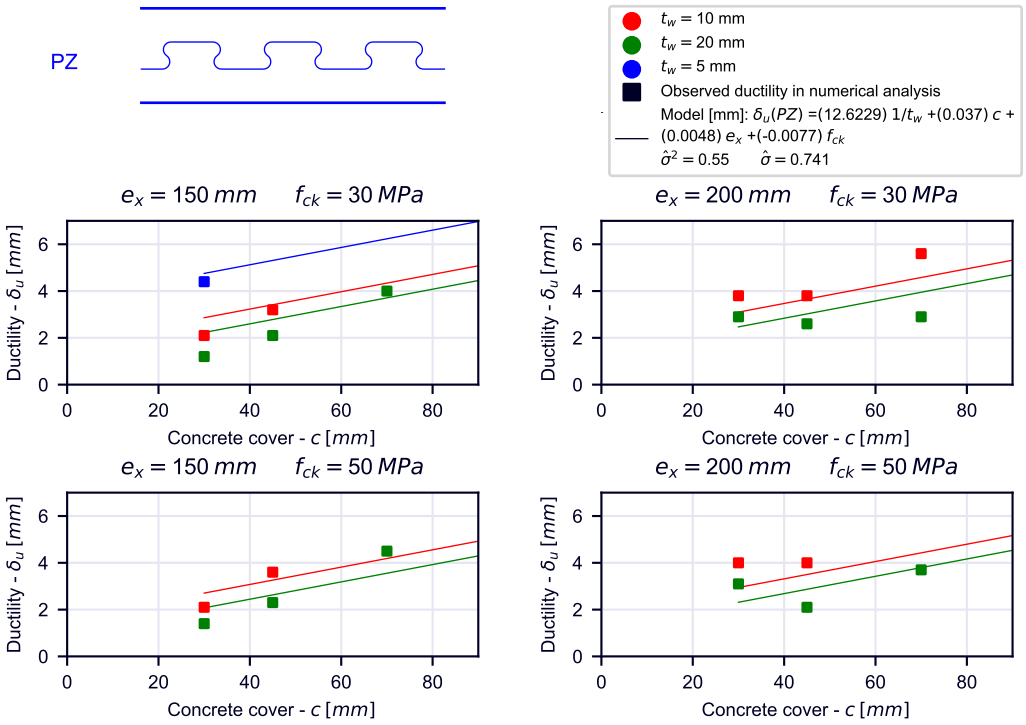

Figure 5.65: ductility model vs observed ductility comparison for the given shape

For both models it can be observed that hardly the composite dowels reach the threshold value of 6mm introduced by EC4 [11].

5.5 Comparison of the two models

The analytical model derived in section 4 and the one derived from numerical results in section 5 are in Fig.5.66, Fig.5.68 and Fig.5.67 for the three different shapes. The numerically derived model is valid for pry-out failure. The ductility expected range and the global trends are in good agreement. However the analytical derived model has an excessively sudden transition in the ductility compared with the numerically derived model.

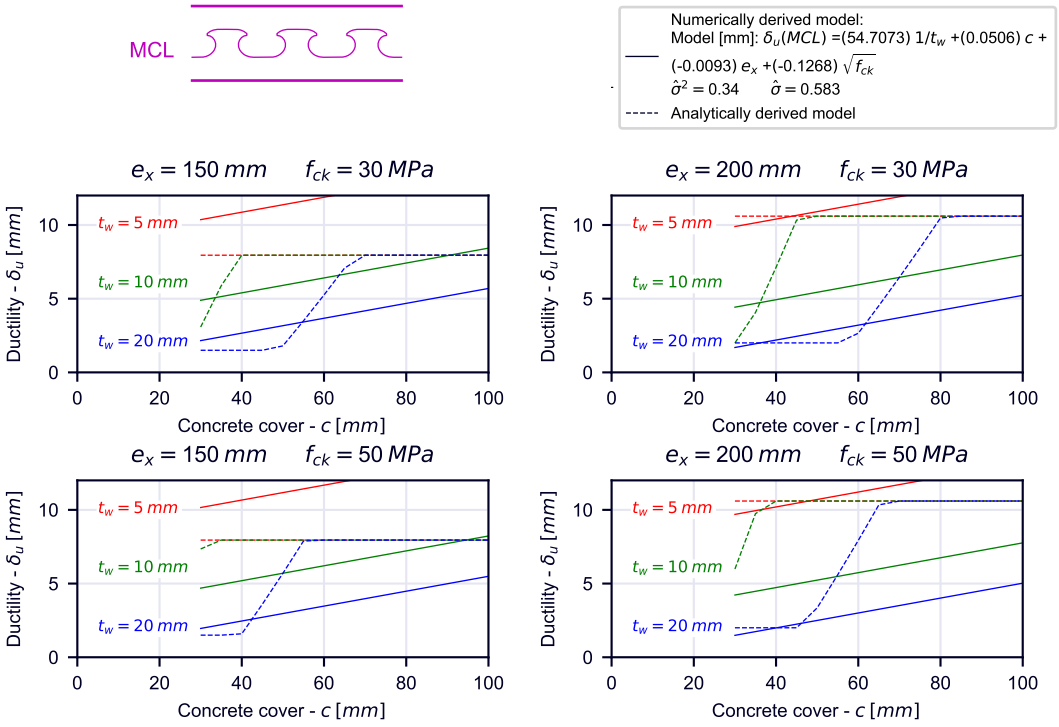

Figure 5.66: observed ductility values for the given shape

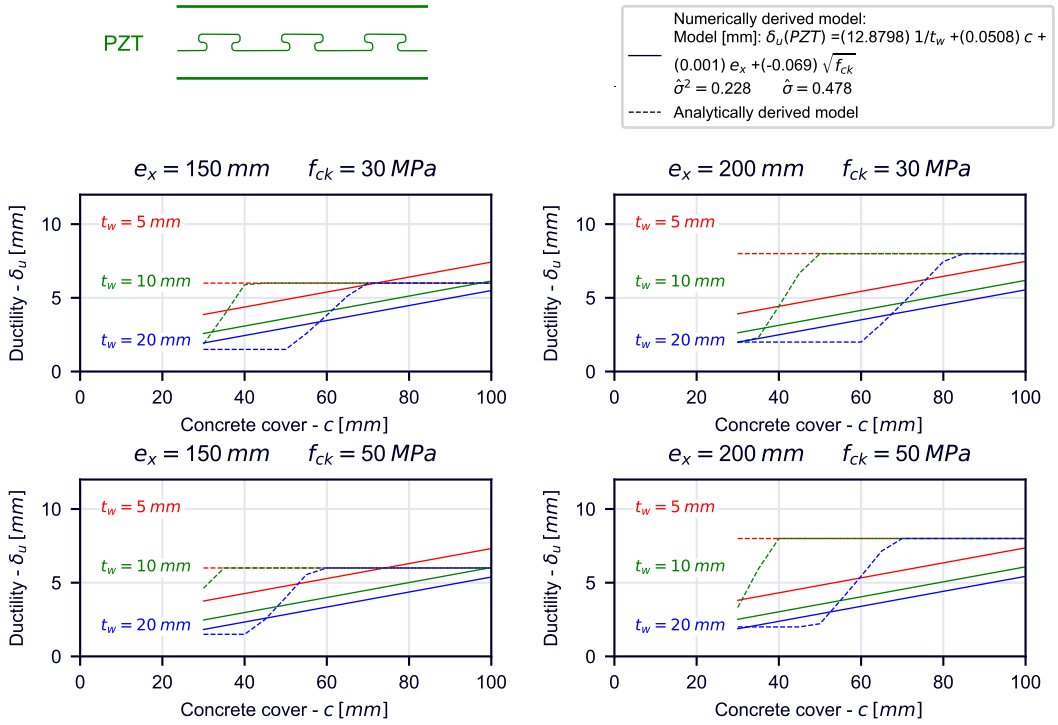

Figure 5.67: observed ductility values for the given shape

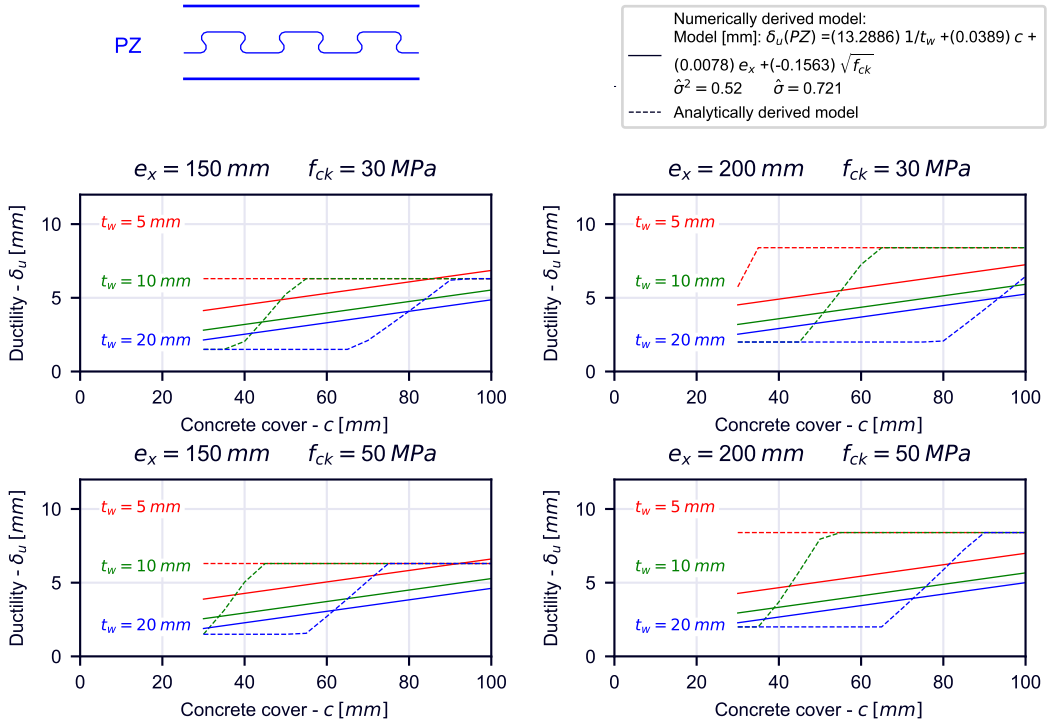

Figure 5.68: observed ductility values for the given shape

Chapter 6

Conclusions

In the research work different aspects of the composite shear connections have been studied. From one side, the problem of determining the slip demand on the shear connection has been studied. Despite of the fact that this part of the work was not innovative, it has been an important part of the work in order to gain confidence with the research topic. Moreover future comparisons can be done by using the results from the slip demand analysis method and the slip capacity thresholds used for the shear connector classifications introduced by the EC4 [11].

6.1 Plastic slip capacity assessment of composite dowels

From the plastic slip capacity assessment side of the composite dowels shear connection technology, two different methods have been used and compared in order to assess the value of slip capacity. First an analytical method has been developed starting from a simplified model of the shear connection. Secondly an analytical formulation has been proposed. This formulation is derived by mean of Least Squares Method from numerical analysis results. These have been derived from an intense FEM parametric study campaign. The influence of different input geometry and material parameters is studied. Reference to a real test developed at the University of Aachen is made.

The final comparison of the two different methods shows good agreement for the determination of the range of plastic slip capacity values. However the simplified analytical model presents a too sharp transition from low plastic slip capacity values with increasing concrete cover. A limitation of the model proposed starting from numerical analysis is that is valid only for the pryout failure. More intense analysis campaigns have to be done in order to refine the sampled region of the input parameters. Moreover also the influence of changing the steel grade has to be studied. The influence of considering different models of the steel mechanical behaviour have not been studied. This can be studied in future research work.

The two models, despite showing different transition from high slip capacity to low slip capacity region, can in future be used in order to classify the composite dowels shear connectors according to the forthcoming version of the EC4. Moreover the simplified analytical model presented is innovative and different from

those already present in literature. The novel model can be used as a starting point in order to enhance the method. The numerical analysis campaign is not innovative, but can be used in future again in order to extend the numerical analysis campaign.

A potential weakness of the numerical analysis campaign is that a reference test has been used in order to gain confidence and to learn the influence of the input parameters, trying to reproduce the load-slip curve resulting from the reference test with a calibration procedure. However a validation of the model has not been done. In fact a proper validation would come from taking the same model setup and trying to reproduce a second reference test, different from the first one used for the calibration procedure. The validity of the results of output from the numerical explicit analysis has been successfully tested by changing mesh refinement, finite elements, mass scaling factor and analysis type. The parametric numerical analysis campaign shows overall good agreement between the numerically observed values of resistances and the expected values of resistances. This is especially true for the steel yielding failure mode. Agreement has been demonstrated to exist also for the expected and numerically observed failure modes comparisons.

A further enhancement of the numerical analysis campaign can be to take as reference and as setup a Push Out Standard Test test according to EC4 [11], rather than considering a non standard push out test. By doing this, the results can for sure enhance the research value. In general it has been demonstrated that according to the present literature design formulas for the computation of the resistances of composite dowels, the common failure mode is concrete pryout. This is a result that is confirmed from literature observations of tests. In both the simplified analytical model and the model derived from numerical analysis, it has been demonstrated that composite dowels hardly reach the deformation capacity of 6mm under pryout failure used as threshold by EC4 [11] for the ductility classification of the shear connector.

6.2 Slip demand assessment on the shear connection

In the present research work a numerical one-dimensional forward finite differences method has been developed in order to compute the slip demand along the shear connection of a beam. This method can be enhanced in future with implicit methods instead of explicit. More extended analysis campaigns can be done in order to understand how the slip demand relates to the degree of shear connection of the beam and the span length. Moreover more research work has to be done in order to understand what is the impact of considering different material laws and shear connection mechanical behaviour in the numerical model.

The series of arguments developed in this research work, can be used in future in order to compare the slip demand on the shear connection with the plastic slip capacity of the shear connection. This can be used in order to identify minimum degree of shear connection requirements in accordance to the forthcoming version of EC4.

Bibliography

[1] Abaqus, Simulia - Dassault Systemes Simulia Corp

[2] Allgemeine bauaufsichtliche zulassung - z-26.4-3. Technical report, Z-26.4-39 - Deutsches Institut für Bautechnik: DIBt.

[3] Allgemeine bauaufsichtliche zulassung - z-26.4-38. Technical report, Z-26.4-38 - Deutsches Institut für Bautechnik: DIBt.

[4] Allgemeine bauaufsichtliche zulassung - z-26.4-56. Technical report, Deutsches Institut für Bautechnik: DIBt.

[5] The clt handbook clt structures-facts and planning.

[6] EN 1990 (2002): Eurocode - basis of structural design. Technical report.

[7] EN 1991-1-1 (2002): Eurocode 1: Actions on structures - part 1-1: General actions - densities, self-weight, imposed loads for buildings. Technical report.

[8] EN 1992-1-1 (2004) - eurocode 2: Design of concrete structures - part 1-1: General rules and rules for buildings design. Technical report.

[9] EN 1993-1-1 (2005): Eurocode 3: Design of steel structures — part 1-1: General rules and rules for buildings.

[10] EN 1993-1-9 - eurocode 3: Design of steel structures - part 1-9: Fatigue.

[11] EN 1994-1-1 (2004): Eurocode 4: Design of composite steel and concrete structures - part 1-1: General rules and rules for buildings. Technical report.

[12] EN 1994-2: Eurocode 4: Design of composite steel and concrete structures – part 2: General rules and rules for bridges. Technical report.

[13] EN 1995-1-1 (2004): Eurocode 5: Design of timber structures - part 1-1: General - common rules and rules for buildings. Technical report.

[14] Scopus. https://www.scopus.com/. Accessed: 2021-09-30.

[15] Shear transfer in heavy steel-concrete composite columns with multiple encased steel profiles - dissertation.

[16] SSF Ingenieure. https://www.ssf-ing.de/. Accessed: 2021-09-30.

[17] Partial interaction in composite steel and concrete beams with full shear connection a b e f f h i k l nomenclature area width young's modulus force material strength vertical distance second moment of area parametric material constant longitudinal distance 235 236, 1997.

[18] Trag- und verformungsverhalten von verbundträgern mit betondübeln zur Übertragung der längsschubkräfte (c. zapfe). *Stahlbau*, 70(11):913–913, 2001.

[19] Cen/tc 250 eurocode 5: Design of timber structures-structural design of timber-concrete composite structures-common rules and rules for buildings eurocode 5: Bemessung und berechnung von holzbeton-verbundbauteilen-allgemeine regeln und regeln für den hochbau, 2020.

[20] ArcelorMittal. Arcelormittal beams calculator.

[21] J. Berthellemy. Fatigue designed cl-cutting shape: A new economic steel-concrete connection system and some applications for bridges. In *Procedia Engineering*, volume 66, pages 138–149, 2013. Cited By :4.

[22] J. Berthellemy, W. Lorenc, M. Mensinger, S. Rauscher, and G. Seidl. Load bearing behaviour of composite dowels - static loads (part i). *Stahlbau*, 80(3):172–184, 2011. Cited By :33.

[23] J. Berthellemy, D. Schavits, and C. Erre. Crossing motorways under traffic without intermediate piers. *Steel Construction*, 9(3):200–206, 2016. Cited By :8.

[24] Y. Broschart, J. Gajda, and W. Kurz. Investigations on the load bearing behavior of composite dowels positioned close to the free concrete surface. *Stahlbau*, 87(5):438–445, 2018. Cited By :2.

[25] Y. Broschart and W. Kurz. Untersuchungen zu verbundträgern mit randnahen verbunddübelleisten. *Stahlbau*, 88(9):892–899, 2019. Cited By :2.

[26] Y. Broschart, W. Kurz, K. Wolters, G. Christou, and M. Claßen. Influencing parameters on the load-bearing behaviour of composite dowels positioned close to the free surface of concrete slabs. *Bauingenieur*, 94(6):199–205, 2019. Cited By :6.

[27] Yannick Micha Broschart. *Untersuchungen zum Trag- und Verformungsverhalten oberflächennaher Verbunddübelleisten*. PhD thesis, 2019.

[28] Roland Bärtschi. Load-bearing behaviour of composite beams in low degrees of partial shear connection.

[29] H. D. S. Cardoso, O. P. Aguiar, R. B. Caldas, and R. H. Fakury. Composite dowels as load introduction devices in concrete-filled steel tubular columns. *Engineering Structures*, 219, 2020.

[30] G. Christou, J. Ungermann, K. Wolters, J. Hegger, and M. Claßen. Fatigue of rib shear connectors - analysis and engineering model. *Beton- und Stahlbetonbau*, 115(5):355–363, 2020. Cited By :3.

[31] M. Classen and J. Hegger. Anchorage of composite dowels. *Steel Construction*, 9(2):138–150, 2016. Cited By :17.

[32] M. Classen and J. Hegger. Shear-slip behaviour and ductility of composite dowel connectors with pry-out failure. *Engineering Structures*, 150:428–437, 2017. Cited By :31.

[33] M. Classen and J. Hegger. Shear tests on composite dowel rib connectors in cracked concrete. *ACI Structural Journal*, 115(3):661–671, 2018. Cited By :14.

[34] M. Classen and M. Herbrand. Shear behaviour of composite dowels in transversely cracked concrete. *Structural Concrete*, 16(2):195–206, 2015. Cited By :25.

[35] M. Classen, M. Herbrand, V. Adam, D. Kueres, and M. Sarac. Puzzle-shaped rib shear connectors subjected to combined shear and tension. *Journal of Constructional Steel Research*, 145:232–243, 2018. Cited By :20.

[36] Martin Classen. Limitations on the use of partial shear connection in composite beams with steel t-sections and uniformly spaced rib shear connectors. *Journal of Constructional Steel Research*, 142:99–112, 3 2018.

[37] Martin Classen, Joerg Gallwoszus, and Alexander Stark. Anchorage of composite dowels in uhpc under fatigue loading. *Structural Concrete*, 17(2):183–193, 2016.

[38] Martin Classen, Martin Herbrand, and Alexander Stark. Dübelkennlinien von verbunddübelleisten mit stahlversagen/shear force-slip characteristic of composite dowels with steel failure. *Bauingenieur*, 92:237–244, 01 2017.

[39] M. Claßen and J. Hegger. Mechanical model with aggregate interlock for pry-out failure of composite dowels in cracked concrete. *Beton- und Stahlbetonbau*, 112(3):155–166, 2017. Cited By :10.

[40] Martin Claßen. Zum trag-und verformungsverhalten von verbundträgern mit verbunddübelleisten und großen stegöffnungen.

[41] Martin Claßen, Joerg Gallwoszus, and Josef Hegger. Einfluss von querrissen auf das schubtragverhalten von verbunddübelleisten in schlanken betongurten. *Beton- und Stahlbetonbau*, 109(12):882–894, 2014.

[42] Florian Eggert. und verbundbau einfluss der verdübelung auf das trag-und verformungsverhalten von verbundträgern mit und ohne profilblech mitteilungen, 2019.

[43] P. Enzinger, T. Petraschek, G. Seidl, C. Yu, R. Garn, and M. Daßler. Railway viaduct nearby schwarzach/st. veit - challenges by the realisation of a 46 m long vft composite frame. *Stahlbau*, 86(9):772–777, 2017. Cited By :3.

[44] M Feldmann, M Gündel, M Kopp, J Hegger, J Gallwoszus, S Heinemeyer, G Seidl, and O Hoyer. Neue systeme für stahlverbundbrücken–verbundfertigteilträger aus hochfesten werkstoffen und innovativen verbundmitteln (p804). forschungsbericht, endbericht nr. 2009-30-04, 2012.

[45] M. Feldmann, M. Gündel, M. Kopp, J. Hegger, J. Gallwoszus, S. Heinemeyer, G. Seidl, and O. Hoyer. Endbericht p804 - neue systeme für stahlverbundbrücken-verbundfertigteilträger aus hochfesten werkstoffen und innovativenverbundmitteln, 2012.

[46] M. Feldmann, Wolters K., W. Kurz, Y. Broschart, J. Hegger, M. Claßen, and G. Christou. Consistent design model for productionoptimized composite dowels – basis for dast guideline and transfer to eurocode 4.

[47] M. Feldmann, M. Kopp, and D. Pak. Composite dowels as shear connectors for composite beams – background to the german technical approval. *Steel Construction*, 9(2):80–88, 2016. Cited By :21.

[48] M. Feldmann, D. Pak, M. Kopp, N. Schillo, and J. Gallwoszus. *Design of composite dowels as shear connectors according to the German technical approval*, pages 57–71. Economical Bridge Solutions Based on Innovative Composite Dowels and Integrated Abutments: Ecobridge. 2015. Cited By :3.

[49] M. Feldmann, D. Pak, M. Kopp, N. Schillo, T. Wirth, G. Seidl, M. Mensinger, and E. Koch. Railway bridge simmerbach - monitoring of the composite dowels and the rail fasteners in the vft-rail system. *Stahlbau*, 81(10):737–747, 2012. Cited By :19.

[50] Markus Feldmann, Ch. Heinemeyer, and B. Völling. Sections and merchant bars design guide for floor vibrations.

[51] O. Fischer, T. Lechner, M. Mensinger, J. Ndogmo, G. Seidl, and M. Stambuk. Entwicklung dünnwandiger, flächenhafter konstruktionselemente aus uhpc und geeigneter verbindungstechniken zum einsatz im hoch- und industriebau. Technical report, Fraunhofer IRB, 2014.

[52] J. Gajda and W. Kurz. Load bearing behavior of concrete dowels in a location close to a free surface underlongitudinal shear stress. *Stahlbau*, 82(9):636–642, 2013. Cited By :6.

[53] J. Gallwoszus and M. Claßen. Fatigue of composite dowels in uhpc under cyclic pull out loading. *Bautechnik*, 92(7):509–521, 2015. Cited By :20.

[54] M. Gündel, M. Kopp, M. Feldmann, J. Gallwoszus, J. Hegger, and G. Seidl. Design of composite dowels according to the new national technical approval. *Stahlbau*, 83(2):112–121, 2014. Cited By :31.

[55] P. Harnatkiewicz, A. Kopczyński, M. Kozuch, W. Lorenc, and S. Rowiński. Research on fatigue cracks in composite dowel shear connection. *Engineering Failure Analysis*, 18(5):1279–1294, 2011. Cited By :19.

[56] O. Hechler, J. Berthellemy, W. Lorenc, G. Seidl, and E. Viefhues. Continuous shear connectors in bridge construction. In *Composite Construction in Steel and Concrete VI - Proceedings of the 2008 Composite Construction in Steel and Concrete Conference*, pages 78–91, 2011. Cited By :10.

[57] Oliver Hechler, Jacques Berthellemy, Wojciech Lorenc, Günter Seidl, and Eva Viefhues. *Continuous Shear Connectors in Bridge Construction*, pages 78–91.

[58] S. Heinemeyer. *Zum Trag- und Verformungsverhalten von Verbundträgern aus ultrahochfestem Beton mit Verbundleisten*. IMB, Lehrstuhl und Institut für Massivbau, RWTH Aachen. Eigenverl., 2011.

[59] S. Heinemeyer, J. Gallwoszus, and J. Hegger. Composite beams with puzzle strip shear connectors and high strength materials. *Stahlbau*, 81(8):595–603, 2012. Cited By :26.

[60] R P JOHNSON and N and MOLENSTRA. Partial shear connection in composite beams for buildings. *Proceedings of the Institution of Civil Engineers*, 91(4):679–704, 1991.

[61] R. Jung and T. Mansperger. The ortho-composite slab. *Stahlbau*, 89(2):129–137, 2020.

[62] F. Kong, P. Huang, B. Han, X. Wang, and C. Liu. Experimental study on behavior of corrugated steel-concrete composite bridge decks with mcl shape composite dowels. *Engineering Structures*, 227, 2021. Cited By :2.

[63] M. Kopp, K. Wolters, M. Claßen, J. Hegger, M. Gündel, J. Gallwoszus, S. Heinemeyer, and M. Feldmann. Composite dowels as shear connectors for composite beams – background to the design concept for static loading. *Journal of Constructional Steel Research*, 147:488–503, 2018. Cited By :33.

[64] M. Kożuch and W. Lorenc. The behaviour of clothoid-shaped composite dowels: Experimental and numerical investigations. *Journal of Constructional Steel Research*, 167, 2020. Cited By :3.

[65] M. Kożuch and S. Rowiński. Elastic behaviour of the steel part of a shear connection with mcl composite dowels design basis for serviceability and fatigue limit states. *Steel Construction*, 9(2):107–114, 2016. Cited By :7.

[66] Ulrike Kuhlmann and Jörg Schänzlin. A timber-concrete composite slab system for use in tall buildings. *Structural Engineering International: Journal of the International Association for Bridge and Structural Engineering (IABSE)*, 18:174–178, 5 2008.

[67] T. Lechner, S. Gehrlein, and O. Fischer. Structural behaviour of composite dowels in thin uhpc elements. *Steel Construction*, 9(2):132–137, 2016. Cited By :13.

[68] Thomas Lechner. *Zur Anwendung von Verbunddübelleisten in schlanken Verbundträgern aus ultrahochfestem Beton*. PhD thesis, 07 2018.

[69] W. Lorenc. The design concept for the steel part of composite dowel shear connection in steel-concrete composite structures. *Prace Naukowe Instytutu Budownictwa Politechniki Wroclawskiej*, (93):1–132, 2010.

[70] W. Lorenc. The design concept for the steel part of a composite dowel shear connection. *Steel Construction*, 9(2):89–97, 2016. Cited By :9.

[71] W. Lorenc. Non-linear behaviour of steel dowels in shear connections with composite dowels: Design models and approach using finite elements. *Steel Construction*, 9(2):98–106, 2016. Cited By :4.

[72] W. Lorenc. francesc cyclic loading during full-scale tests of beams for the “wierna rzeka” bridge. *Engineering Structures*, 209, 2020. Cited By :1.

[73] W. Lorenc, T. Kolakowski, A. Hukowicz, and G. Seidl. Composite bridge nearby elbląg - enhancements of the preco-beam construction method. *Stahlbau*, 86(2):167–174, 2017. Cited By :8.

[74] W. Lorenc, M. Kozuch, and S. Rowiński. The behaviour of puzzle-shaped composite dowels - part i: Experimental study. *Journal of Constructional Steel Research*, 101:482–499, 2014. Cited By :52.

[75] W. Lorenc, M. Kozuch, and S. Rowiński. The behaviour of puzzle-shaped composite dowels - part ii: Theoretical investigations. *Journal of Constructional Steel Research*, 101:500–518, 2014. Cited By :36.

[76] W. Lorenc, M. Kozuch, and G. Seidl. The ultimate load bearing capacity of composite dowels with clothoid form. *Stahlbau*, 82(3):196–207, 2013. Cited By :16.

[77] Khai Quang Mai, Aron Park, Khoa Tan Nguyen, and Kihak Lee. Full-scale static and dynamic experiments of hybrid clt–concrete composite floor. *Construction and Building Materials*, 170:55–65, 2018.

[78] C. Massonet and M. Save. *Calcolo plastico a rottura delle costruzioni*. Maggioli Editore, 2008.

[79] A. Mendelson. *Plasticity: Theory and Application*. Macmillan series in applied mechanics. Macmillan, 1968.

[80] K. Möhler. *Über das Tragverhalten von Biegeträgern und Druckstäben mit zusammengesetzten Querschnitten und nachgiebigen Verbindungsmitteln*. 1956.

[81] E. Petzek, V. Schmitt, E. Meteş, G. Ispăşoiu, and A. Ţurcan. Romanian projects and integral bridge solutions based on composite dowels. *Steel Construction*, 9(3):161–169, 2016. Cited By :6.

[82] Maurizio Piazza, Roberto Tomasi, and Roberto Modena. Strutture in legno. *Materiale, calcolo e progetto secondo le nuove normative europee (Wooden structures. Material, calculation and design according to the new European regulations). Biblioteca Tecnica Hoepli Milano, Milano*, pages 512–558, 2005.

[83] M. Sargin. *Stress-strain Relationship for Concrete and the Analysis of Structural Concrete Sections*. Studies series. Solid Mechanics Division University of Waterloo, 1971.

[84] V. Schmitt, G. Seidl, M. Hever, and C. Zapfe. The new road bridge over the railway line next to pöcking applied to a new construction method for composite bridges. *Stahlbau*, 73(6):387–393, 2004. Cited By :34.

[85] G. Seidl and W. Lorenc. Innovative solutions in bridge construction with composite dowel strips. *Stahlbau*, 87(6):547–554, 2018. Cited By :2.

[86] G. Seidl, W. Mariacher, J. Schmidt, and M. Daßler. Brücke über die salzach bei kaprun. *Stahlbau*, 88(5):488–498, 2019. Cited By :1.

[87] G. Seidl, M. Mensinger, E. Koch, and F. Hugle. Report on the railway overpass simmerbach, germany - pilot project in vft-rail construction method with external reinforcement. *Stahlbau*, 81(2):100–107, 2012. Cited By :13.

[88] G. Seidl, M. Stambuk, W. Lorenc, T. Kołakowski, and E. Petzek. Economic composite constructions for bridges - construction methods implementing composite dowel strips. *Stahlbau*, 82(7):510–521, 2013. Cited By :19.

[89] G. Seidl, E. Viefhues, J. Berthellemy, I. Mangerig, R. Wagner, W. Lorenc, M. Kozuch, J.-M. Franssen, D. Janssen, J. Ikäheimonen, R. Lundmark, O. Hechler, and N. Popa. Prefabricated enduring composite beams based on innovative shear transmission (preco-beam). final report, 2013. European Commission.

[90] Günter Seidl. *Behaviour and load bearing capacity of composite dowels in steel-concrete composite girders*. PhD thesis, 11 2009.

[91] Günter Seidl, Martin Hierl, Michael Breu, Martin Mensinger, and Mislav Stambuk. Segmentbrücke greißelbach als stahlverbundbrücke ohne abdichtung und asphalt. *Stahlbau*, 85(2):126–136, 2016.

[92] Ayesha Siddika, Md Abdullah Al Mamun, Farhad Aslani, Yan Zhuge, Rayed Alyousef, and Ailar Hajimohammadi. Cross-laminated timber–concrete composite structural floor system: A state-of-the-art review, 12 2021.

[93] Pavel Simon, Libor Hrdlicka, Aleš Dráb, and Vojtěch Zvěřina. A composite dowel bridge in the czech republic. *Steel Construction*, 9(3):191–199, 2016.

[94] J. Springer, H. Reuke, K. Wolters, and M. Kopp. Special features of the composite structure of the car park coulinstraße in wiesbaden, germany. *Stahlbau*, 87(7):695–703, 2018. Cited By :2.

[95] G. S. Veríssimo, J. L. R. Paes, I. Valente, P. J. S. Cruz, and R. H. Fakury. Design and experimental analysis of a new shear connector for steel and concrete composite structures. In *Proceedings of the 3rd International Conference on Bridge Maintenance, Safety and Management - Bridge Maintenance, Safety, Management, Life-Cycle Performance and Cost*, pages 807–809, 2006. Cited By :23.

[96] O. Wurzer. *Zur Tragfähigkeit von Betondübeln*. Baumechanik, Baustatik, Ingenieurinformatik, Holzbau, Massivbau, Stahlbau. Univ. der Bundeswehr, 1997.

[97] Qingjie Zhang. Moment and longitudinal resistance for composite beams based on strain limited design method-elastic-plastic design for composite beams considering deep, 2020.

Appendix A

Case study: integrated floor beam deck for office flooring system

The solution consists in a 10m spanlength simply supported beam with interaxis equal to 6m. It is designed for an office destination. A composite CLT panel-concrete decking solution is used in the transverse direction. The solution was originally used in [94].

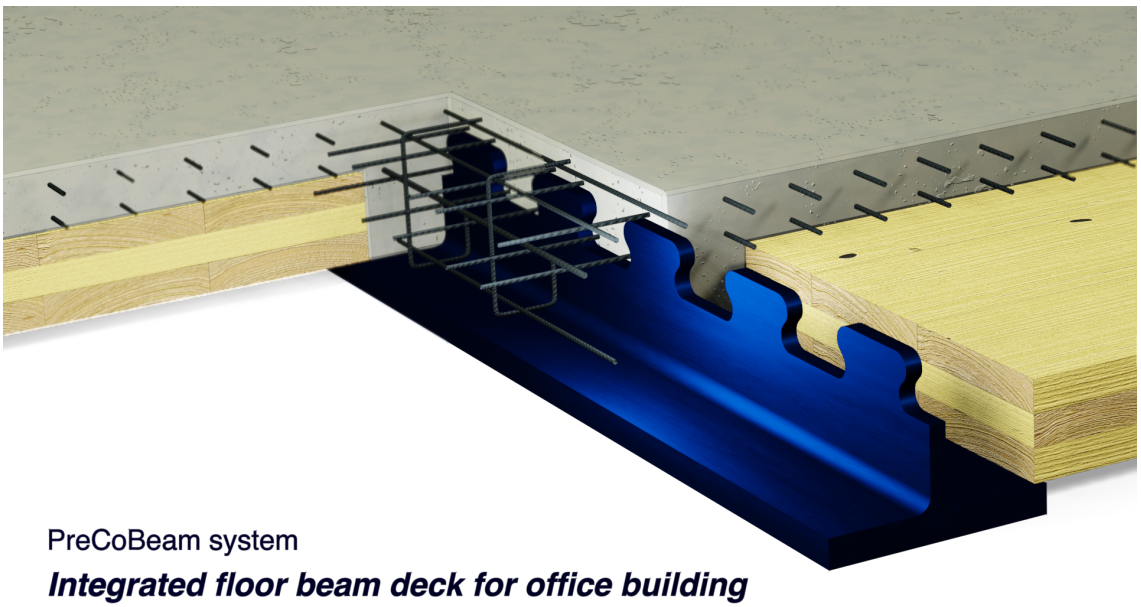

Figure A.1: rendering: integrated floor beam deck for office flooring system

A.1 Reference design rules and partial safety coefficients

In the following calculation reference at EN1990 [6], EN1991-1-1 [7], EN1992-1-1 [8], EN1993-1-1 [9], EN1994-1-1 [11] and the technical specification for the composite dowels is made.
The partial safety coefficients used are:

Partial safety coefficients	
$\gamma_c = 1.50$	Partial safety coefficient for concrete resistance
$\gamma_{M0} = 1.00$	Partial safety coefficient for structural steel resistance
$\gamma_s = 1.15$	Partial safety coefficient for reinforcement steel resistance
$\gamma_v = 1.00$	Partial safety coefficient for the shear connection resistance
$\gamma_{G1} = 1.35$	Partial safety coefficient for the permanent structural actions
$\gamma_{G2} = 1.35$	Partial safety coefficient for the permanent non structural actions
$\gamma_Q = 1.50$	Partial safety coefficient for the live load actions

A.2 Case study framework

A section composed by a single T steel profile and a top concrete slab is considered. The section has a concrete web. The single T steel profile is derived by mean of a cutting process from a standard double T steel hot-rolled section. The composite dowels shear connection is embedded in the concrete part.

A.3 Data

The geometry, materials and shear connection data are described in this section. The loading conditions and consequent design actions are computed.

A.3.1 Materials

Following materials are considered:

- Structural steel: S460
- Concrete: C35/45
- Reinforcement steel: B500
- CLT wood: C24

This leads to the following material properties:

Structural steel	
$f_y = 460\ MPa$	Structural steel yielding resistance
$E_a = 210000\ MPa$	Structural steel elastic modulus
Concrete	
$f_{ck} = 35.0\ MPa$	Concrete compression characteristic strength
$f_{cd} = f_{ck}/\gamma_c = 23.3\ MPa$	Concrete compression design strength
$f_{cm} = f_{ck} + 8 = 43.0\ MPa$	Concrete compression mean strength
$f_{ctm} = 3.21\ MPa$	Average concrete tensile strength
$E_{cm} = 22000 \cdot (f_{cm}/10)^{0.3} = 34077.1\ MPa$	Mean elastic modulus of concrete
Reinforcement steel	
$f_{sk} = 500.0\ MPa$	Characteristic yielding resistance
$f_{sd} = f_{sk}/\gamma_s = 434.8\ MPa$	Design yielding resistance
C24 CLT panel	
$f_{m,k} = 24.0\ MPa$	Characteristic value of bending resistance
$f_{t,0,k} = 14.5\ MPa$	Characteristic value of tensile resistance parallel to the fibres
$f_{t,90,k} = 0.4\ MPa$	Characteristic value of tensile resistance orthogonal to the fibres
$f_{c,0,k} = 21.0\ MPa$	characteristic value of compression resistance parallel to the grain fibres
$f_{c,90,k} = 2.5\ MPa$	characteristic value of compression resistance orthogonal to the fibres
$f_{v,k} = 4.0\ MPa$	Shear characteristic resistance
$E_{m,0,mean} = 11000.0\ MPa$	Mean value of the elastic modulus parallel to the fibres
$E_{m,0,0.05} = 74000.0\ MPa$	Characteristic value of elastic modulus parallel to the fibres
$G_{mean} = 690\ MPa$	Shear modulus mean value
$G_{rs} = 69\ MPa$	Rolling shear modulus
$\rho_k = 350.0\ kg/m^3$	Characteristic value of the density
$\rho_{mean} = 420\ kg/m^3$	Mean density

A.3.2 Geometry

A simply supported static scheme is considered with spanlength L. In the transversal direction the beams are spaced with an interaxis of L_{inter}. The used quantities are:

$L = 10000\,mm$	Span length
$L_{inter} = 6000\,mm$	Beams interaxis

An HE400M hot-rolled standard profile is used. The selected shear connection is a PZ type with size $e_x = 150\,mm$. The cross-section is shown in Fig.A.2. The static scheme (Fig.A.2) consists in a simply supported beam.

In this case the weight of the double T section is:

$$G = 256.0\,kg/m \tag{A.1}$$

This means that the oxycutted single T profile used for the composite beam solution has a weight of:

$$G/2 = 128\,kg/m \tag{A.2}$$

The following geometry related quantities are defined:

Shear connection dimensions	
$e_x = 150\,mm$	Dowel size
$h_D = 40\,mm$	Dowel height
Hot rolled profile dimensions	
$h = 432.0\,mm$	Profile height
$b = 307.0\,mm$	Flange width
$t_w = 21.0\,mm$	Web thickness
$t_f = 40.0\,mm$	Flange thickness
$r = 27.0\,mm$	Fillet radius
Concrete part dimensions	
$h_{slab} = 70.0\,mm$	Slab height
$b_{web} = 200.0\,mm$	Concrete web thickness
$h_{web} = 160.0\,mm$	Concrete web height
Concrete part dimensions	
$h_{CLT} = 160.0\,mm$	CLT panel height

The considered number of dowels in half-spanlength is:

$$n = \frac{L/2}{e_x} = 33 \tag{A.3}$$

In this case the concrete slab is placed relatively to the shear connection position in such a way that:

$$c_{D,o} = 34\,mm \tag{A.4}$$

An executive aspect is underlined. The standard hot-rolled section has to be selected considering the transverse composite -concrete configuration. The transverse bars have in fact to pass through the concrete dowels staying above the panel. A cutting of the upper part of the panel can be done in order to provide the proper anchorage of the reinforcement and bond.

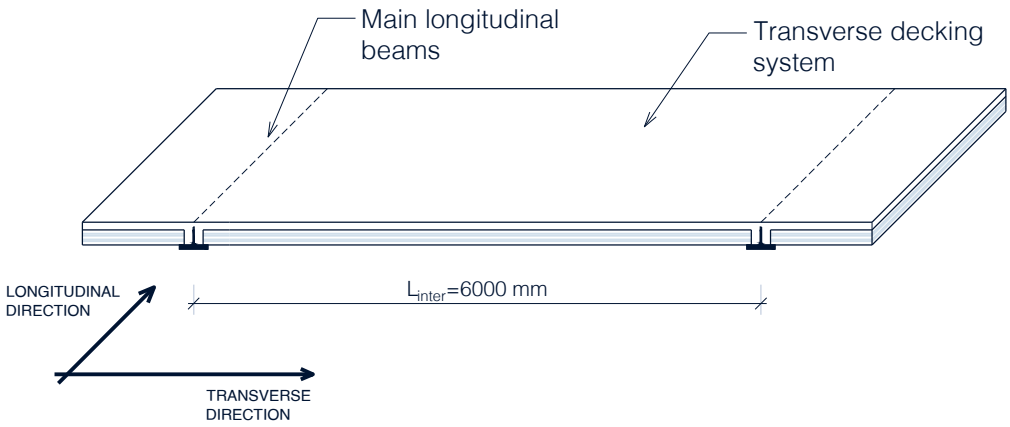

TRANSVERSE CROSS-SECTION

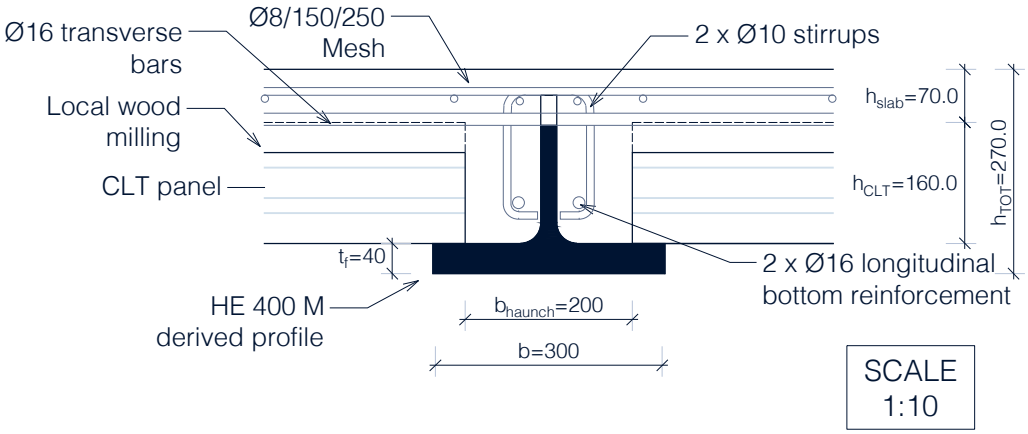

LONGITUDINAL SECTION

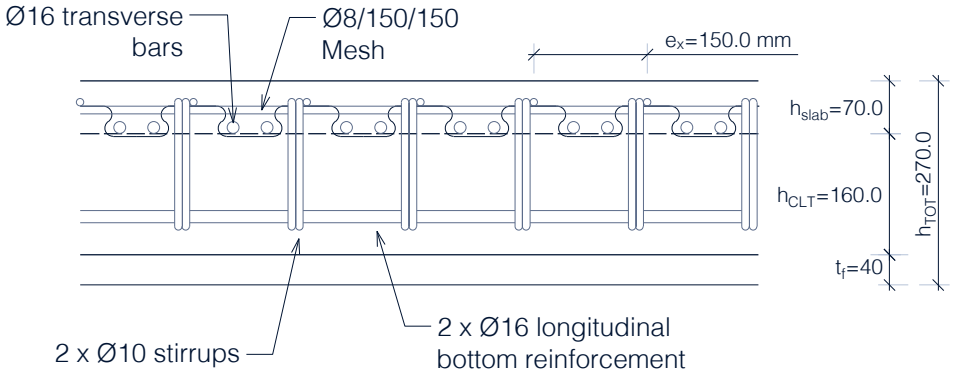

Figure A.2: geometry

The section results in a total height of:

$$h_{TOT} = h/2 + h_D/2 + c_{D,u} = 270\,mm \tag{A.5}$$

The structural element has a slenderness of:

$$L/h_{TOT} = 37 \tag{A.6}$$

A.3.3 Effective width

The effective width is computed according to EC4 [11] and the calculation is summarized below.

$$L_{e,support} = 0.25 \cdot L = 2500\,mm \tag{A.7}$$

$$L_{e,midspan} = L = 10000\,mm \tag{A.8}$$

$$\beta_1 = \min\left(0.55 + 0.025 \cdot L/b_{e,1}; 1\right) = 0.6 \tag{A.9}$$

$$\beta_2 = \min\left(0.55 + 0.025 \cdot L/b_{e,2}; 1\right) = 0.6 \tag{A.10}$$

$$b_{eff} = b_{eff,midspan} = b_0 + b_{e,1} + b_{e,2} = 2500\,mm \tag{A.11}$$

$$b_{eff,support} = b_0 + \beta_1 \cdot b_{e,1} + \beta_2 \cdot b_{e,2} = 1500\,mm \tag{A.12}$$

A.3.4 Reinforcement

The reinforcement amount and position can be appreciated in Fig.A.2. Two transverse horizontal $\phi 16$ bars are provided per each concrete dowel. This results in:

$$(A_{sf,passing\,bars}/e_x) = \frac{2 \cdot 201}{150} = 2680\,mm^2/m \tag{A.13}$$

Two transverse $\phi 10$ stirrups is provided per each dowel. A welded mesh of $\phi 8/150/150$ is placed on top of the shear connection. This provides an additional reinforcement density in the transverse direction and and a presence of longitudinal reinforcement:

$$(A_{sf,mesh}/e_x) = \frac{1 \cdot 50}{150} = 333\,mm^2/m \tag{A.14}$$

$$(A_{s,long}) = b_{eff}/150 \cdot 50 = 1333\,mm^2 \tag{A.15}$$

In the following sections the transverse reinforcement amount for each concrete dowel are referred as A_{b1} and the top transverse slab reinforcement per each dowel will be referred as A_{t1}. In this case:

$$A_{b1} = 2\phi 16 = 402\,mm^2 \tag{A.16}$$

$$A_{t1} = 1\phi 8 = 50\,mm^2 \tag{A.17}$$

A.3.5 Cross-section properties

In order to compute the following geometric quantities the y coordinate is introduced to identify the generic fibre of the section. The origin of the reference system is at the bottom part of the composite section, pointing upward. The reference coordinate of the shear connection position $y_{sh.connection}$ is:

$$y_{sh.connection} = h/2 = 216.0\, mm \tag{A.18}$$

The net height of the single T steel profile is:

$$h_{singleT} = h/2 - h_D/2 = 195.9\, mm \tag{A.19}$$

The structural steel area results in:

$$A_a = b \cdot t_f + t_w(h_{singleT} - h_f) = 155.5\, cm^2 \tag{A.20}$$

The centroid position of the steel part is:

$$y_{G,a} = (b \cdot t_f^2/2 + t_w(h_{singleT} - t_f) \cdot (t_f + h_{singleT}/2))/A_a = 40.6\, mm \tag{A.21}$$

The second moment of the steel part is:

$$\begin{aligned} I_a = {} & t_f \cdot b(t_f/2 - y_{G,a})^2 + t_w \cdot (h_{singleT} - h_f)((h_{singleT} + t_f)/2 - y_{G,a})^2 + \\ & + b \cdot t_f^3/12 + t_w(h_{singleT} - t_f)^3/12 = 3304.4\, cm^4 \end{aligned} \tag{A.22}$$

The lower surface of the concrete slab is placed at a distance from the bottom edge of the section of:

$$y_{c,bottom,slab} = h/2 - h_D/2 + c_{D,o} - h_{slab} = 200.0\, mm \tag{A.23}$$

The lower surface of the concrete slab is placed at a distance from the bottom edge of the section of:

$$y_{c,bottom,web} = t_f = 40.0\, mm \tag{A.24}$$

The upper surface of the concrete slab is placed at a distance from the bottom edge of the section of:

$$y_{c,top} = h/2 + h_D/2 + c_{D,o} = 270\, mm \tag{A.25}$$

The area of the concrete part of the section is:

$$A_c = h_{slab} \cdot b_{eff} + (h_{web} \cdot b_{web}) = 2070\, cm^2 \tag{A.26}$$

The centroid position of the concrete part is:

$$y_{G,c} = \frac{(h_{slab} \cdot b_{eff}) \cdot (y_{c,top} + y_{c,bottom,slab})/2 + (h_{web} \cdot b_{web}) \cdot (y_{c,bottom,web} + y_{c,bottom,slab})/2}{A_c} = \tag{A.27}$$

$$= 217\, mm \tag{A.28}$$

The second moment of the concrete part is:

$$I_c = h_{slab} \cdot b_{eff}^3/12 + h_{web} \cdot b_{web}^3/12 + (h_{slab} \cdot b_{eff}) \cdot ((y_{c,top} + y_{c,bottom,slab})/2 - y_{G,c})^2 + \quad \text{(A.29)}$$

$$+ (h_{web} \cdot b_{web}) \cdot ((y_{c,bottom,web} + y_{c,bottom,slab})/2 - y_{G,c})^2 = 49750.3\, cm^4 \quad \text{(A.30)}$$

The composite section geometric properties can be derived through an homogenization procedure of the section. The section is homogenized as an equivalent steel section. The homogenization coefficient n_0 is:

$$n_0 = \frac{E_s}{E_{cm}} = 6.16 \quad \text{(A.31)}$$

The coordinate of the centroid of the homogenized composite section is:

$$y_{G,homo} = (A_c \cdot y_{G,c}/n_0 + A_a \cdot y_{G,a})/(A_a + A_c/n_0) = 161.3\, mm \quad \text{(A.32)}$$

The second moment of the homogenized composite section is:

$$I_{homo} = I_a + I_c/n_0 + A_a \cdot (y_{G,a} - y_{G,homo})^2 + A_c/n_0 \cdot (y_{G,c} - y_{G,homo})^2 = 44537.6\, cm^4 \quad \text{(A.33)}$$

The bending stiffness of the steel section is defined as:

$$EI_a = E_a I_a \quad \text{(A.34)}$$

The bending stiffness of the composite section is defined as:

$$EI_{homo} = E_a I_{homo} \quad \text{(A.35)}$$

A.3.6 Loads

The structural permanent loads include the dead weights of the concrete and steel structural components. On the flooring system the characteristic values of loads per unit surface can be computed as follows:

Characteristic values of structural permanent loads per unit surface

$G_{1k,concrete} = \gamma_{concrete} \cdot h_{slab} = 1.75\, kN/m^2$

$G_{1k,CLT} = \gamma_{wood} \cdot h_{CLT} = 0.56\, kN/m^2$

Thus the structural permanent characteristic loads per unit length acting on the main beam can be derived by multiplying the per unit surface values by the interaxis length:

Characteristic values of structural permanent loads per unit length

$g_{1k,concrete} = G_{1k,concrete} \cdot L_{inter} + \gamma_{concrete} \cdot b_{web} \cdot$

$h_{web} = 10.50\, kN/m$

$g_{1k,CLT} = G_{1k,CLT} \cdot L_{inter} = 3.36\, kN/m$

$g_{1k,steel} = \gamma_{steel} \cdot A_a = 1.22\, kN/m$

The non structural permanent loads include the finishing permanent layers of the office building. The overall quantity that is:

Characteristic values of non structural permanent loads per unit surface	
$G_{2k,decking} = 1.50\ kN/m^2$	Non structural permanent loads

The non structural permanent characteristic loads per unit length acting on the main beam can be derived by multiplying the per unit surface values by the interaxis length:

Characteristic values of non structural permanent loads per unit length	
$g_{2k,decking} = G_{2k,decking} \cdot L_{inter} = 9.00\ kN/m$	Non structural permanent loads

The considered live load for an office destination is:

Characteristic values of live loads per unit surface	
$Q_{k,Cat} = 3.80\ kN/m^2$	Live loads

The live loads per unit length acting on the main beam can be derived by multiplying the per unit surface values by the interaxis length:

Characteristic values of live loads per unit length	
$q_{k,Cat} = Q_{k,Cat} \cdot L_{inter} = 22.80\ kN/m$	Live loads

The design values of the loads are:

$$Q_{d,ULS} = 1.35 \cdot G_{1k} + 1.35 \cdot G_{2k} + 1.50 \cdot Q_{k,Cat} = 10.80\ kN/m^2 \tag{A.36}$$

$$q_{d,ULS} = 1.35 \cdot g_{1k} + 1.35 \cdot g_{2k} + 1.50 \cdot q_{k,Cat} = 66.70\ kN/m \tag{A.37}$$

A.3.7 Design actions under fundamental load combination

Considering a simply supported beam under uniformly distributed loads leads to (Fig.A.3):

$V_{Ed} = q_{d,ULS} \cdot L/2 = 333.5\ kN$	Design shear at support
$M_{Ed} = q_{d,ULS} \cdot L^2/8 = 833.9\ kNm$	Design bending moment at midspan

A.4 Geometric detailing checks

According to the reference technical standard for the composite dowels, the accomplishment of the following geometric detailing checks should be verified:

Figure A.3: design actions - fundamental combination

$t_w < 40\,mm$	Verified
$4\,mm < t_w < 60\,mm$	Verified
$c_{D,o} \geq 30\,mm$	Verified
$t_f \geq t_w$	Verified
$(h_{singleT} - t_f) \geq 0.45 \cdot h_D$	Verified

A.5 Shear connection resistance

The shear connection resistance is computed according to the rules given in the technical specifications for the composite dowels.

The longitudinal shear resistance due to steel failure is computed as:

$$P_{pl,k} = \lambda_{geo} \cdot e_x \cdot t_w \cdot f_{yk} = 396.4\,kN \tag{A.38}$$

Where the value of λ_{geo} is $\lambda_{geo,PZ} = 0.286$.

The longitudinal shear resistance due to concrete shearing is:

$$P_{sh,k} = \eta_D \cdot e_x^2 \cdot \sqrt{f_{ck} \cdot (1 + \rho_D)} = 399.6\,kN \tag{A.39}$$

In this relation the values of $\eta_{D,PZ}$, ρ_D are:

$\eta_{D,PZ} = 2 - e_x/400 = 1.63$	Reduction factor for the surface of concrete dowel
$\rho_D = E_a \cdot A_b/(E_{cm} \cdot A_D) = 0.847$	Degree of reinforcement
$A_D = A_{D,PZ} = 0.13 \cdot e_x^2$	Area of concrete dowel for the chosen shape

The longitudinal resistance against concrete pryout is determined by:

$$P_{po,k} = k_1 \cdot \chi_x \cdot \chi_y \cdot h_{po}^{1.5} \cdot \sqrt{f_{ck}} \cdot (1 + \rho_{D,i}) \cdot \psi_{crack} = 133.6\,kN \tag{A.40}$$

The concrete pryout cone height is:

$$h_{po} = \min\left(c_{D,o} + 0.07\,e_x;\ c_{D,u} + 0.08\,e_x\right) = 44.5\,mm \tag{A.41}$$

The used values are:

$k_1 = 71$	Factor for calculation of pry-out failure for a PZ shape
$\chi_x = 1 \quad for \quad e_x \geq 4.5 \cdot h_{po}$ $\chi_x = e_x/(4.5 \cdot h_{po}) \leq 1.0 \quad for \quad e_x < 4.5 \cdot h_{po}$ $\rightarrow \chi_x = 1.0$	Reduction factor for overlapping of pry-out cones in longitudinal direction
$\chi_y = 1.0$	Reduction factor for overlapping of concrete cones in the transverse direction for one dowel strip
$\rho_{D,i} = E_a \cdot A_{sf}/(E_{cm} \cdot A_{D,i}) = 0.072$ $A_{D,i} = h_c \cdot e_x$	Reinforcement ratio for pry-out failure
$\psi_{crack} = \psi_{crack,PZ} = 1.0$	Reduction factor for transverse cracking of concrete due to longitudinal tensile stresses

The characteristic value of the shear connection longitudinal shear resistance $P_{S,Rk}$ is computed as follows:

$$P_{S,Rk} = \min\left(P_{pl,k}; P_{sh,k}; P_{po,k}\right) 133.6\ kN \tag{A.42}$$

The design value of the longitudinal shear resistance $P_{S,Rd}$ is:

$$P_{S,Rd} = P_{S,Rk}/\gamma_v = 106.9\ kN \tag{A.43}$$

A.6 ULS vertical shear resistance check

The ULS vertical shear check is done in accordance with the forthcoming version of EC4. For the present case study no web openings have to be taken into account.

A.6.1 Plastic resistance to vertical shear

The plastic resistance to vertical shear $V_{pl,a,Rd}$ is computed in accordance with [9]. There is no torsional effect. The considered shear area A_v is:

$$A_v = A_a - b \cdot t_f + (t_w + 2r) = 2945.6\ mm^2 \tag{A.44}$$

$$V_{pl,Rd} = \frac{A_v \cdot f_y}{\sqrt{3} \cdot \gamma_{M0}} = 748.3\ kN \tag{A.45}$$

A.6.2 Shear buckling resistance

It must be determined whether shear buckling is prevented. This is done by verifying the following inequality:

$$h_w/t_w = 7.1 \leq 72/\eta \cdot \epsilon = 43.8 \qquad Verified \tag{A.46}$$

In this relation $\eta = 1.2$ is considered.

A.6.3 Shear design resistance

The shear design resistance is the lower between the shear buckling resistance and the plastic shear resistance. Thus:

$$V_{Rd} = \min\left(V_{pl,Rd}; V_{b,Rd}\right) = 748.3\, kN \tag{A.47}$$

The V_{Ed}/V_{Rd} radio is:

$$V_{Ed}/V_{Rd} = 0.446 < 0.5 \tag{A.48}$$

The shear utilization ratio is less then 0.5. This implies that no account should be taken for moment-shear interaction according to EC4 [11].

A.7 ULS bottom flange bending resistance check

The bottom flange of the T profile is offering support reaction for the transverse decking system. Thus, a force is acting on the bottom flange generating a bending moment with the flange acting as a cantilever beam under an end point load. According to the forthcoming version of EC4, account should be taken for this local effect. The considered scheme is shown in Fig.A.4. The reaction force per unit length can be computed as:

$$rf = Q_{d,ULS} \cdot L_{inter}/2 = 32.5\, kN/m \tag{A.49}$$

According to this configuration, the acting bending moment per unit length is:

$$m_{ybt,Ed} = rf \cdot (b/2 - r/2 - d_{support}/3) = 3.6\, kNm/m \tag{A.50}$$

This has to be compared with the resistant design bending moment per unit length, which is the elastic resistant bending moment of the bottom flange, times an increasing factor of 1.2:

$$m_{ybt,Rd} = 1.2 \cdot 1/6 \cdot f_y \cdot t_w^2 = 140.8\, kNm/m \tag{A.51}$$

The check consists in:

$$m_{ybt,Ed}/m_{ybt,Rd} =\leq 1.0 \qquad Verified \tag{A.52}$$

In the RP and SL analysis a reduced yielding resistance of the steel bottom flange is used ($f_{y,red}$).

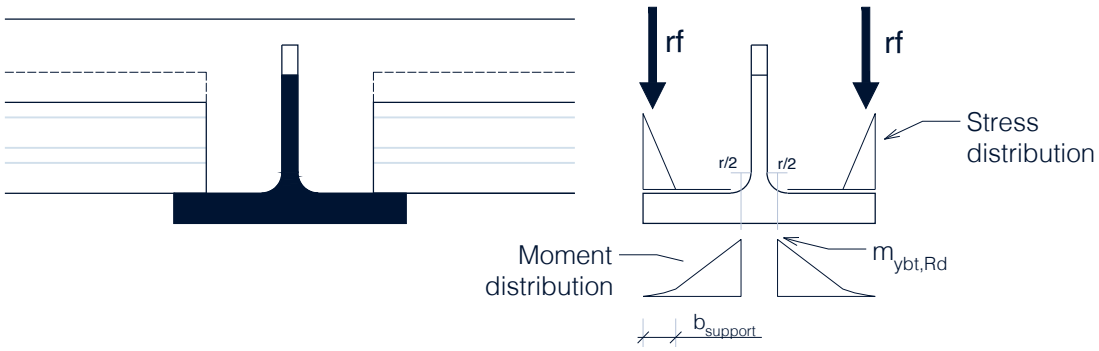

Figure A.4: bending action on bottom flange

A.8 ULS bending resistance check

The bending resistant moment is here computed according to two different methods. The first is a rigid plastic (RP) analysis. The second is a strain limitation (SL) method.

The strain limited analysis is conduced with a section discretization of 1 mm height fibres. The nonlinear material laws used are the parabola-rectangle according to EC2 [8] and an elastic-plastic hardening law for structural steel and reinforcement steel. A pure bending condition is assumed, thus $N = 0.00\,kN$ is imposed as equilibrium target. For the RP analysis the moment-curvature curve cannot be derived. In the SL analysis the moment-curvature diagram for a full interaction case is computed and is shown in Fig.A.6. The partial shear connection diagram is illustrated in Fig.A.5. The stress-strain relations on the section at failure are shown in Fig.A.7. In both results cases the shear connection position is above the PNA. So the shear connection is in the compression zone of the section.

At the ULS condition with full shear interaction assumption the following quantities are derived in the analysis:

$(1/r)_u = 2.02 \times 10^{-5}\,1/mm$	Ultimate curvature of the composite section
$x_u = 171.2\,mm$	Neutral axis position at failure
$M_{pl,f,Rd} = 847.7\,kNm$	Plastic resistant design bending moment under full shear interaction assumption
$N_{cf} = 3745.4\,kN$	Concrete compression force at ULS condition with full shear interaction assumption
Concrete crushing	Failure type (ULS condition)

The degree of shear connection can be derived as follows:

$$\eta = n \cdot P_{S,Rd}/N_{cf} = 0.94 \tag{A.53}$$

By a simplified approach this means that plastic redistribution occurs, as $\eta < 2$ and furthermore the Partial

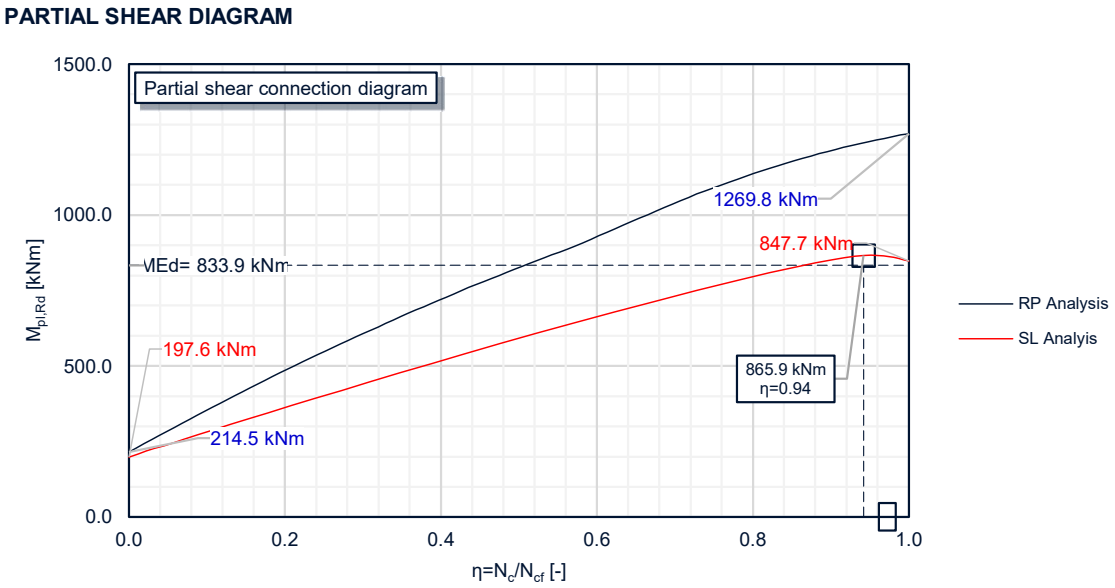

Figure A.5: Partial Shear Diagram (PSD)

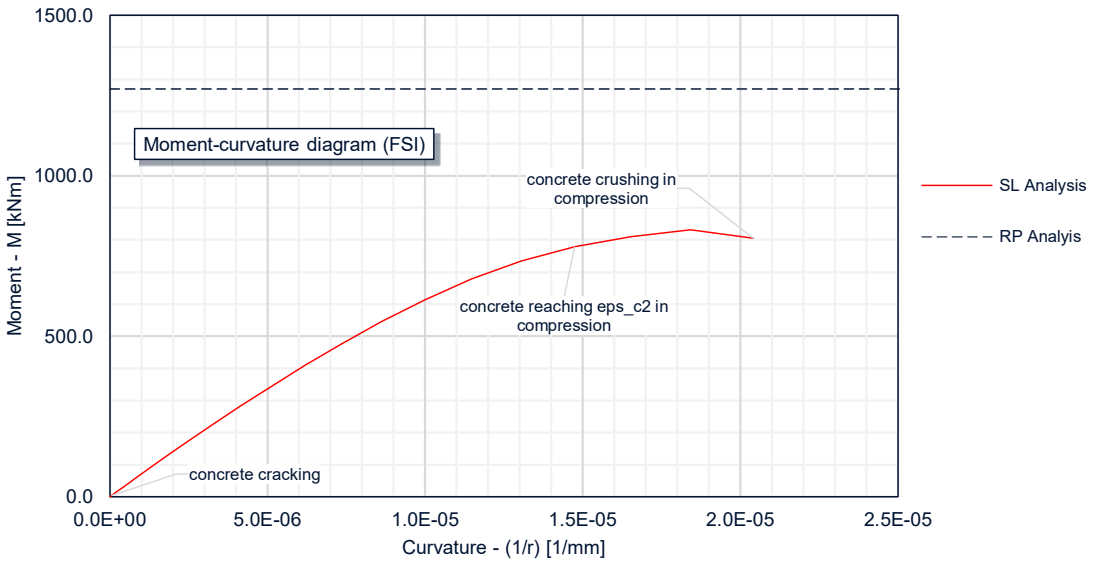

Figure A.6: Moment-curvature diagram in Full Shear Interaction (FSI) condition

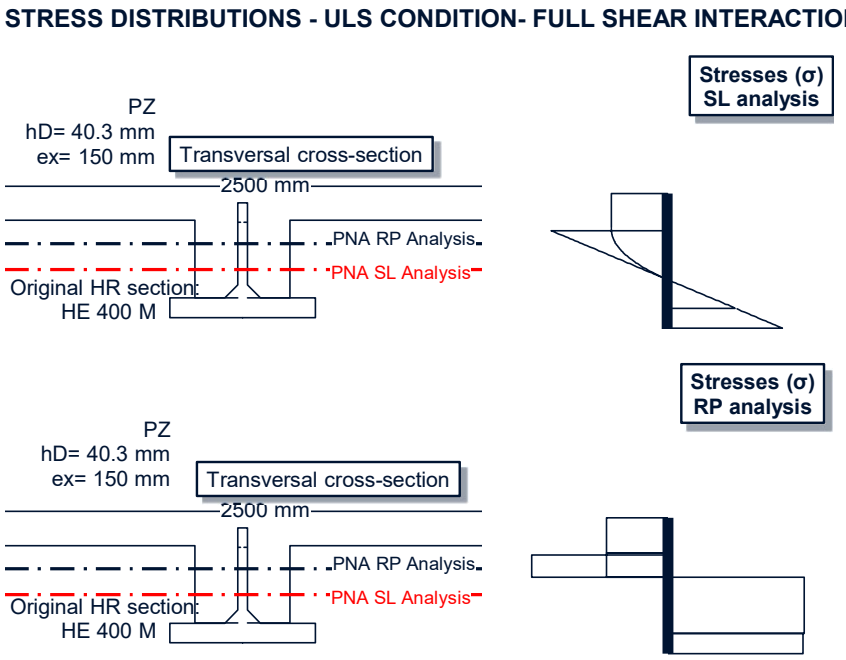

Figure A.7: Stress distributions derived from RP and SL analysis

Shear Connection (PSC) case is reached as $\eta < 1$. Thus the maximum shear flow along the beam is exactly the one associated with the dowel yielding:

$$v_{L,max} = P_{S,Rd}/e_x = 712.8\, kN/m \tag{A.54}$$

By exploiting the partial shear connection diagram derived in the SL analysis, the plastic bending resistant design moment for the calculated degree of shear connection η is:

$$M_{pl,Rd} = M_{pl,Rd}(\eta = 0.94) = 865.9\, kNm \tag{A.55}$$

The bending ULS resistant check consists in:

$$M_{Ed}/M_{pl,Rd} = \frac{833.9}{865.9} = 0.908 \leq 1.0 \tag{A.56}$$

Summarizing the results, the composite element is in a partial shear connection condition with redistribution along the shear connection. The ULS bending checks are satisfied and the solution presents a high utilization ratio in bending. The solution satisfies the requirement on the minimum degree of shear connection:

$$\eta = 0.94 > \eta_{min} = 1 - (355/f_y) * (0.3 - 0.015 * L/1000) = 0.88 \qquad \text{Verified} \tag{A.57}$$

A.9 ULS longitudinal shear in concrete slab check

According to EC4 [11] the forthcoming version of EC4 longitudinal shear failure of the concrete slab shall be prevented. Here two potential shear failure surfaces are checked. Failure surface a-a, failure surface b-b and failure surface c-c according to Fig.A.8 are considered.

A.9.1 Model overview

According to the reference design codes a strut-and-tie model contained in the slab is used in order to do the checks. The truss model is symmetric to the longitudinal beam axis. The local bearing force transmitted by a steel dowel to the concrete slab diffuses through the slab according to inclined struts. The diffusion angle can be chosen in the range $[26.5^o, 45^o]$. Here the chosen angle is:

$$\theta = 45^o \qquad \rightarrow \qquad \cot\theta = 1.00 \tag{A.58}$$

The transverse force component is balanced by the passing bars that have to resist the tensile force. Both the shear resistance of the concrete slab and the resistance of the passing bars have to be checked. The shear resistance of the concrete slab is computed according to [8]. Here the value v_{Rd} has to be computed:

$$v_{Rd} = \nu \cdot f_{cd} \cdot \sin\theta\cos\theta = 6.02\, MPa \tag{A.59}$$

Here $\nu = 0.6(1 - f_{ck}/250) = 0.516$ according to [8] is used.

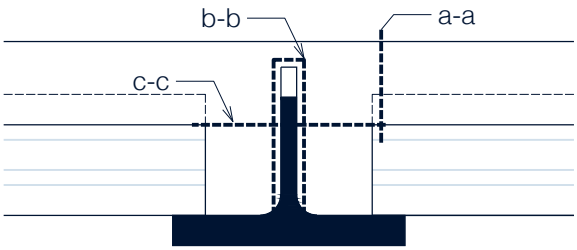

Figure A.8: Failure surfaces considered in the longitudinal shear checks

A.9.2 Failure surface a-a

In failure surface a-a the considered shear flow is half the maximum force transmitted by the dowel to the concrete slab divided by the dowels spacing, namely:

$$v_{L,a-a} = 1/2 \cdot P_{S,Rd}/e_x = 356.4\, kN/m \tag{A.60}$$

This shear flow transits through a surface of unit longitudinal length and a height equal to the concrete slab height h_{slab}:

$$h_{f,a-a} = h_{slab} = 70\, mm \tag{A.61}$$

So, the shear stress can be computed by considering the shear flow v_L and dividing it by the slab height h_{slab}:

$$v_{Ed,a-a} = v_L/h_{slab} = 5.09\, MPa \tag{A.62}$$

The shear stress is compared with the shear concrete resistance of the concrete slab and the first check is carried out:

$$v_{Ed,a-a} = 5.09\, MPa \leq v_{Rd} = 6.02\, MPa \qquad \text{Verified} \tag{A.63}$$

The transverse component of the transmitted bearing force which is $P_{S,Rd}/\cot\theta$ should be balanced by the transverse reinforcement tensile force. At limit this force should be equal to the one at yielding point of the reinforcement:

$$1/2 \cdot P_{S,Rd}/\cot\theta \leq A_{sf,a-a} \cdot f_{sd} \tag{A.64}$$

The reinforcement amount $A_{sf,a-a}$ accounted here is the quantity $A_{b1} + A_{t1}$ that is the transverse steel bars area per each dowel. The reinforcement density here is $A_{sf,a-a}/s_f$ where s_f is the spacing of the transverse bars that coincides with the dowel spacing e_x. In term of shear flow the same expression can be written as follows, by dividing both sides by $e_x = s_f$:

$$v_{L,a-a}/\cot\theta \leq A_{sf}/s_f \cdot f_{sd} \tag{A.65}$$

or equivalently:

$$v_{Ed,a-a}\, h_{f,a-a}/\cot\theta = 356.4\, kN/m \leq A_{sf,a-a}/s_f \cdot f_{sd} = 1393.2\, kN/m \tag{A.66}$$

A minimum amount of transverse reinforcement can be computed as:

$$(A_{sf,a-a}/s_f)_{min} = \frac{v_{Ed,a-a}\, h_{f,a-a}}{\cot\theta f_{sd}} = 8.2\, cm^2/m \tag{A.67}$$

A.9.3 Failure surface b-b

In the failure surface b-b the total force flowing through the surface is all the force transmitted by the steel dowel to the concrete slab. So:

$$v_{L,b-b} = P_{S,Rd}/e_x = 712.8\, kN/m \tag{A.68}$$

This shear flow transits through a surface of unit longitudinal length and a perimeter equal to $h_{f,b-b}$:

$$h_{f,b-b} = 2(h_{singleT} - t_f + h_D) + t_w = 413.0\, mm \tag{A.69}$$

The considered reinforcement area here is just the bottom amount $2A_{b1}$ according to the forthcoming version of EC4: The two checks, are done similarly as before, and consist in:

$$v_{Ed,b-b} = 1.73\, MPa \leq v_{Rd} = 6.02\, MPa \qquad \text{Verified} \tag{A.70}$$

$$v_{Ed,b-b}\, h_{f,b-b}/\cot\theta = 712.8\, kN/m \leq A_{sf,b-b}/s_f \cdot f_{sd} = 2331.2\, kN/m \tag{A.71}$$

A minimum amount of transverse reinforcement can be computed as:

$$(A_{sf,b-b}/s_f)_{min} = \frac{v_{Ed,b-b}\, h_{f,b-b}}{\cot\theta f_{sd}} = 16.4\, cm^2/m \tag{A.72}$$

$$(A_{b1}/s_f)_{min} = 1/2 \cdot (A_{sf,b-b}/s_f)_{min} = 8.2\, cm^2/m \leq (A_{b1}/e_x) = 26.8\, cm^2/m \tag{A.73}$$

A.9.4 Failure surface c-c

In the failure surface c-c the total force flowing through the surface is all the force transmitted by the steel dowel to the concrete slab. So:

$$v_{L,c-c} = P_{S,Rd}/e_x = 712.8\,kN/m \tag{A.74}$$

This shear flow transits through a surface of unit longitudinal length and a perimeter equal to $h_{f,c-c}$:

$$h_{f,b-b} = 2(b_{web} - t_w) = 179.0\,mm \tag{A.75}$$

The considered reinforcement area here is the transverse stirrups $A_{sw,stirrups}$ according to the forthcoming version of EC4. Here 4 legs have been considered for the computation of $A_{sw,stirrups}$. The two checks, are done similarly as before, and consist in:

$$v_{Ed,c-c} = 3.98\,MPa \leq v_{Rd} = 6.02\,MPa \qquad \text{Verified} \tag{A.76}$$

$$v_{Ed,c-c}\,h_{f,c-c}/\cot\theta = 712.8\,kN/m \leq A_{sf,c-c}/s_f \cdot f_{sd} = 910.6\,kN/m \tag{A.77}$$

A minimum amount of transverse reinforcement can be computed as:

$$(A_{sf,c-c}/s_f)_{min} = \frac{v_{Ed,c-c}\,h_{f,c-c}}{\cot\theta f_{sd}} = 16.4\,cm^2/m \tag{A.78}$$

$$(A_{b1}/s_f)_{min} = (A_{sf,c-c}/s_f)_{min} = 16.4\,cm^2/m \leq (A_{sw,stirrups}/e_x) = 21.3\,cm^2/m \tag{A.79}$$

A.9.5 Minimum reinforcement ratio check

The minimum reinforcement ratio check is done in accordance with EN1994-1-1, 6.6.6.3 [11] and EN1992-1-1, 9.2.2(5) [8]. The transverse reinforcement density is:

$$\left(\frac{A_{sw}}{s_w}\right) = (A_{b1} + A_{t1})/e_x = 3204\,mm^2/m \tag{A.80}$$

This leads to the transverse reinforcement density:

$$\rho_w = \frac{(A_{sw}/s_w)}{h_{slab}} = 4.578\,\% \tag{A.81}$$

The following inequality should be checked:

$$\rho_{w,min} = 0.08\frac{\sqrt{f_{ck}}}{f_{sk}} = 0.095\,\% \leq \rho_w \qquad \text{Verified} \tag{A.82}$$

A.10 SLS stress computations

The stresses are computed according to an effects summation due to all load contributes taking into account the concrete creep, the shrinkage, the load history and the construction stages. Here a propped construction is considered. The concrete properties and geometric values are:

N	Cement type according to [8]
RH=50%	Considered relative humidity (RH)
$u = 2L_{inter} = 5000\,mm$	Perimeter of the concrete part exposed to drying
$A_c = 2070\,cm^2$	Concrete sectional area subjected to drying
$h_0 = 2A_c/u = 82.8\,mm$	Equivalent hydraulic radius

Following construction stages are considered:

Considered loading stages

t=0 days	Concrete pouring
t=28 days	Propping removal
t=100 days	First loading
t=infinity	Long term effect

At the different times, the concrete elastic modulus is computed as:

$$E_{c,eff}(t) = \frac{E_{cm}}{1 + \psi_L \cdot \phi(t, t_0)} \tag{A.83}$$

Consequently, the homogenization factor n is:

$$n_L(t) = \frac{E_s}{E_{c,eff}(t)} = \frac{E_s}{E_{cm}} \cdot (1 + \psi_L \cdot \phi(t, t_0)) = n_0 \cdot (1 + \psi_L \cdot \phi(t, t_0)) \tag{A.84}$$

Note that this coefficient is both dependent on the loading type (L subscript) and its application instant t_0 and also to the considered time.

Permanent structural loads are considered to be applied at the same time of the propping removal. The accounted loading contributes together with the application instant t_0 and the related load types are:

Considered loading contributes

Load	t_0 [days]	Load type and ψ_L
G1 - steel profile	28	Permanent loading
G1 - concrete	28	Permanent loading
G2 - decking system	100	Permanent loading
Q - category load	100	Short term loading
Shrinkage	2	Shrinkage effect

The various moment contributes $M_{d,i}$ are computed according to:

$$M_{d,i} = q_{d,i} \cdot L^2/8 \tag{A.85}$$

A shrinkage strain value of $\epsilon_{cs} = 325 \times 10^-6$ is used according to the forthcoming version of EC4 Annex C. As the shrinkage exhibits, the shortening of the concrete slab is impeded by the steel part of the element

which is not subject to shrinkage. The internal constraint conditions generate an internal stress state which is self balanced and creates on the section an additional positive bending moment. In the steel part a compression with a bending component generates, while on the concrete part a tensile state with a bending component generates. The total positive additional moment acting on the section due to shrinkage of concrete is M_{cs}. The value of this moment is generally computed in a simplified way (neglecting the strain due to compression on the steel) as $\epsilon_{cs} \cdot E_{c,eff}(t) A_c$. Note that this force is time dependent, because of the fictitious dependency of the elastic modulus of concrete which is introduced to simulate the time dependent effect of creep. The tensile resultant force acts in correspondence of the centroid of the concrete part y_c. So with respect of the composite section, the lever arm of the force will be the difference between this point and the centroid of the composite section. Note that this last value is also dependent on time.
The moment due to shrinkage is:

$$M_{cs} = \epsilon_{cs} \cdot E_{c,eff}(t) A_c \cdot (y_c - y_{G,homo,cs}(t)) \tag{A.86}$$

Note that every load contribute has a different homogenization factor $n_{L,i}$. This is because of the different load coefficients ψ_L and of the different load application times t_0. Thus, for every load contribute a different effective second moment of section and a different centroid position of the homogenized section exists. For every load contribute i the related effective second moment of section can be computed:

$$I_{eff,i}(t) = I_a + \frac{I_c}{n_{L,i}(t)} + A_a \cdot (y_{G,a} - y_{G,homo,i})^2 + \frac{A_c}{n_{L,i}(t)} \cdot (y_{G,c} - y_{G,homo,i})^2 \tag{A.87}$$

Here the neutral axis position of the homogenized steel section is $y_{G,homo}$:

$$y_{G,homo,i}(t) = \frac{A_a \cdot y_{G,a} + A_c \cdot y_{G,c}/n_{L,i}(t)}{A_a + A_c/n_{L,i}(t)} \tag{A.88}$$

For the given time t the total stress acting at a particular point of the composite section can be computed by adding linearly the contributes. Note that in case of concrete cracking the phenomena would became nonlinear and an effects linear summation would not be suitable. However it has to be recognized that all the applied method is a simplified approach. First of all because of the linear effects summation of the creep effect which a nonlinear phenomena, and because of the simplified method for the homogenization factor of the concrete. Moreover, no reliable literature has been found on how to consider the effect of concrete cracking in the stress distribution computation. If a rigorous computation of the effects of concrete cracking is requested, a more sophisticated analysis should be carried out. So, for the present computation, in order to preserve the simplicity of the calculation method, it was decided not to take into account potential effects of concrete cracking at this computational stage. If tensile stresses greater than the concrete tensile resistance f_{ctm} are detected, a following reduction of the stiffness of the composite element will be carried out.
The significant points of the section where the stresses have to be computed are the top and the bottom fibers of both the concrete part and the steel part of the section, namely:

$$\sigma_{c,inf}(t) \qquad \text{normal stress on the bottom concrete fibre} \tag{A.89}$$

$\sigma_{c,sup}(t)$ normal stress on the top concrete fibre (A.90)

$\sigma_{a,inf}(t)$ normal stress on the bottom steel fibre (A.91)

$\sigma_{a,sup}(t)$ normal stress on the top steel fibre (A.92)

Stresses are therefore derived by an effect summation. Here the load contributes i accounted for are the ones applied before the considered time, i.e. $t > t_{0,i}$:

$$\sigma_{c,inf}(t) = \frac{1}{n_{L,i}(t)} \cdot \sum_{i=1}^{\text{load contrib.}} \frac{M_{d,i}}{I_{eff,i}(t)} \cdot y_{c,inf} + \frac{1}{n_{L,i}(t)} \cdot \frac{M_{cs}}{I_{eff,cs}(t)} y_{c,inf} + E_{c,eff,cs}(t)\epsilon_{cs} \quad \text{(A.93)}$$

$$\sigma_{c,sup}(t) = \frac{1}{n_{L,i}(t)} \cdot \sum_{i=1}^{\text{load contrib.}} \frac{M_{d,i}}{I_{eff,i}(t)} \cdot y_{c,sup} + \frac{1}{n_{L,i}(t)} \cdot \frac{M_{cs}}{I_{eff,cs}(t)} y_{c,sup} + E_{c,eff,cs}(t)\epsilon_{cs} \quad \text{(A.94)}$$

$$\sigma_{a,inf}(t) = \sum_{i=1}^{\text{load contrib.}} \frac{M_{d,i}}{I_{eff,i}(t)} \cdot y_{a,inf} + \frac{M_{cs}}{I_{eff,cs}(t)} y_{a,inf} - A_c E_{c,eff,cs}(t)\epsilon_{cs}/A_a \quad \text{(A.95)}$$

$$\sigma_{a,sup}(t) = \sum_{i=1}^{\text{load contrib.}} \frac{M_{d,i}}{I_{eff,i}(t)} \cdot y_{a,sup} + \frac{M_{cs}}{I_{eff,cs}(t)} y_{a,sup} - A_c E_{c,eff,cs}(t)\epsilon_{cs}/A_a \quad \text{(A.96)}$$

The shear stresses are considered to be balanced just by the steel profile. This is because of the smaller elastic modulus, the smaller partial static moment, and the large width of the concrete slab that in the Jourawski formula would return small shear stresses on the concrete part. So the concrete slab contribute is neglected. This simplification is reasonable and furthermore implies that no homogenization should be carried out. Moreover it stays on the safe side. The generic shear stress on the steel part is computed as:

$$\tau(y) = \frac{V_d \cdot S^*(y)}{b(y) \cdot I_a} \quad \text{(A.97)}$$

The maximum shear stress on the steel web is computed according to the Jourawski formula at steel neutral axis height which is the steel centroid position τ_{max}:

$$\tau_{max} = \tau(y_{G,a}) = \frac{V_d \cdot S^*(y_{G,a})}{b(y_{G,a}) \cdot I_a} \quad \text{(A.98)}$$

Here the considered shear action is derived with a linear summation of the shear contributes due to the various loads:

$$V_d = \sum_{i=1}^{\text{load contrib.}} V_{d,i} \qquad V_{d,i} = q_{d,i} \cdot L/2 \quad \text{(A.99)}$$

A.11 SLS deflection check

The total deflection $\delta_{TOT}(t)$ at a specific time t is computed as the sum of the permanent plus the shrinkage $\delta_{cs+g}(t)$, the live load $\delta_q(t)$ and the precamber δ_c contributes:

$$\delta_{TOT}(t) = \delta_{cs+g}(t) + \delta_q(t) - \delta_c \quad \text{(A.100)}$$

A precambering δ_c of the beam is considered. This amount is a design value. The precambering contribute is prescribed in order to balance the deflection under permanent loads and shrinkage at time infinite. Thus,

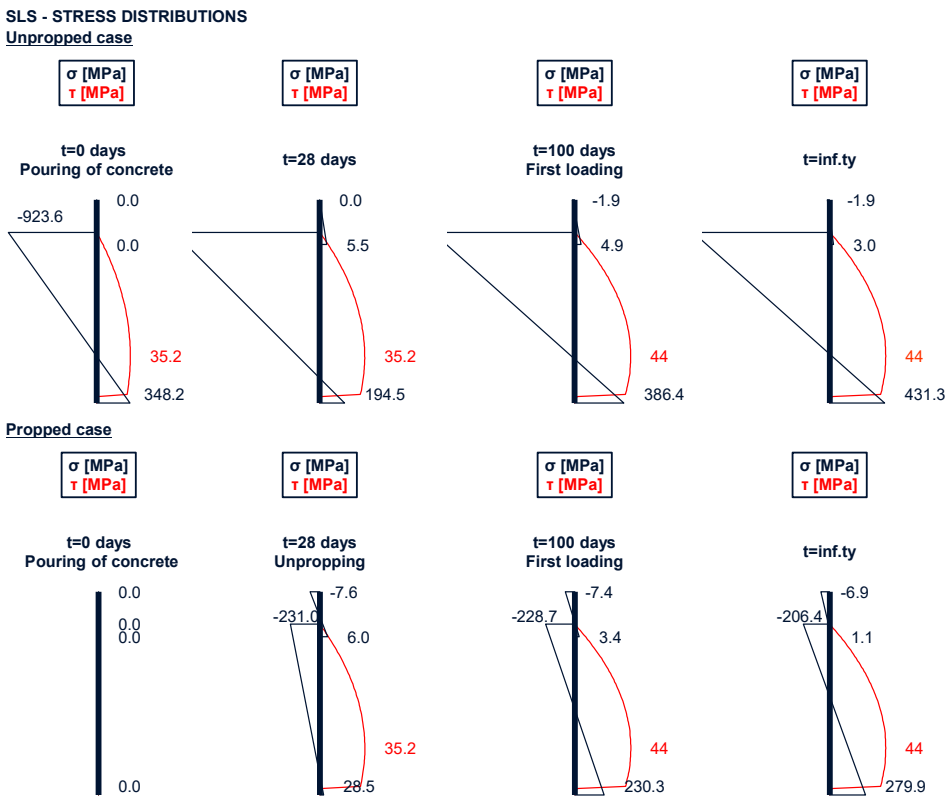

Figure A.9: SLS normal and shear stress distributions

the total deflection under long term load is computed by adding the different contributes of the permanent loads and the shrinkage contribute:

$$\delta_{g+cs}(t) = \sum_{i=1}^{G_1+G_2 \text{ contrib.}} \frac{5}{384}\frac{q_{d,i}L^4}{E_s I_{homo,i}(t)} + \frac{1}{8}\frac{M_{cs}L^2}{E_s I_{homo,cs}(t)} \tag{A.101}$$

Effects of partial shear interaction due to the shear connection deformation are taken into account with:

$$EI_p = EI_a + N/N_{cf}(EI_{homo} - EI_a) \tag{A.102}$$

Here effects of cracking have been taken into account by taking:

$$EI_{homo,red} = 0.5(EI_{I,homo} + EI_{II,homo}) \tag{A.103}$$

In this last equation EI_I, EI_{II} are respectively the bending stiffness in case of non cracked section (state I), and cracked section (state II).

So the chosen value δ_c is:

$$\delta_c = \delta_{g+cs}(t \to \infty) = 86.7\, mm \tag{A.104}$$

In this circumstances the total deflection under long term action is:

$$\delta_{TOT}(t \to \infty) = \delta_q(t \to \infty) = \frac{5}{384}\frac{q_{Cat}L^4}{E_s I_{homo,q}(t=\infty)} = 32.4\, mm \tag{A.105}$$

The deflection check consists in limiting the deflection-span $\delta_{TOT}(t)/L$ length ratio at a specific value. Here this value is chosen to $1/300$, so:

$$\delta_{TOT}(t)/L = 2/617 \leq \delta_{lim}/L = \frac{1}{300} \qquad \text{Verified} \tag{A.106}$$

The SLS deflection check is therefore verified, and the prescribed amount of precambering is $\delta_c = 87\,mm$.

A.12 SLS vibrations check

The vibration frequency is limited to a value of $f_{lim} = 3.00\,Hz$. The proper frequency of the structure can be assessed according to various methods. Due to the simplicity in the static scheme no sophisticated analysis is used here, instead the assessment is carried out just by using literature formulations. These formulations are derived according to dynamic theory of structures. The actual structural proper first mode vibration frequency is here computed according to the methods provided by the technical document [50].

$$f = \frac{\pi}{2} \cdot \sqrt{\frac{\alpha_{b,dyn} E_s I_{homo,dyn}}{\mu L^4}} \tag{A.107}$$

Here the $\alpha_{b,dyn}$ coefficient takes into account that at serviceability condition the static scheme is not a perfect pinned-pinned situation and restraints are an intermediate situation between pinned-pinned $\alpha_{b,dyn} = 1$ and clamped-clamped $\alpha_{b,dyn} = 5$. Supports can in fact in a serviceability condition provide a non zero reaction moment, partially impeding the support rotation. Considering a pinned-pinned static scheme would surely be on the safe side. Moreover the value of μ consists in the distributed modal mass per unit length of beam:

$$\mu = g_d/9.81 \approx (g_1 + g_2)/10 = 2408.1\,kg/m \tag{A.108}$$

The second moment of inertia of the section is corrected taking into account the dynamic elastic modulus of concrete $E_{c,dyn}$ instead of the common mean value E_{cm} and the short term condition is considered. The value of $E_{c,dyn}$ is derived by increasing the value of E_{cm} by 10%.

$$I_{homo,dyn} = I_a + \frac{E_{c,dyn}}{E_s} I_c + A_a (y_{G,a} - y_{G,homo})^2 + \frac{E_{c,dyn}}{E_s} A_c (y_{G,c} - y_{G,homo})^2 = 46394\,cm^4 \tag{A.109}$$

The frequency and the related check results in:

$$f = 4.47 \geq f_{lim} = 2.30\,Hz \qquad \text{Verified} \tag{A.110}$$

The composite frequency is computed. This is done on the basis of Dunkerley approach for natural frequency computation of the reference document [50]:

$$\frac{1}{f^2} = \frac{1}{f_1^2} + \frac{1}{f_2^2} \tag{A.111}$$

Here f_1 and f_2 are the vibration frequencies of the longitudinal and the transverse direction vibration mode respectively.

A.13 Solution summary

A summary of the solution results is given in the table below.

Solution summary

Parameter	Numerical result	Specification
$G/2$	$128.0\ kg/m$	Structural steel amount
L/h	37	Slenderness of the structural system
$M_{Ed,max}$	$833.9\ kNm$	Design bending moment at midspan (fundamental combination)
$V_{Ed,max}$	$333.5\ kN$	Design shear action st support (fundamental combination)
$V_{Ed,max}/V_{Rd}$	0.446	Utilization ratio for shear action
P_{Rd}	$106.9\ kN$	Design resistance of the connectors
$M_{pl,Rd}$	$865.9\ kNm$	Plastic resistant design bending moment
$M_{Ed}/M_{pl,Rd}$	0.963	Moment degree of utilization
η	$0.94 < 1.00$	Degree of shear connection
	PSC	Full (FSC) vs. Partial (PSC) Shear Connection
	0.772	Longitudinal shear utilization ratio
$(A_{sw}/s_w)_{min}$	$8.2\ cm^2/m$	Minimum transverse reinforcement for longitudinal shear
δ_c	$87\ mm$	Precambering
δ_Q	$32.4\ mm$	Deflection under live loads
f	$4.47\ Hz$	Vibration frequency for a $\alpha_b = 2.0$ static scheme and with only the permanent load as modal mass

A.14 Computational report

PreCoBeam Floor beams system - Design sheet v.1.02

Created by UNITN / AMR&D: CIA061-22
Author: **Francesco PROFICO**
Check: Riccardo ZANON

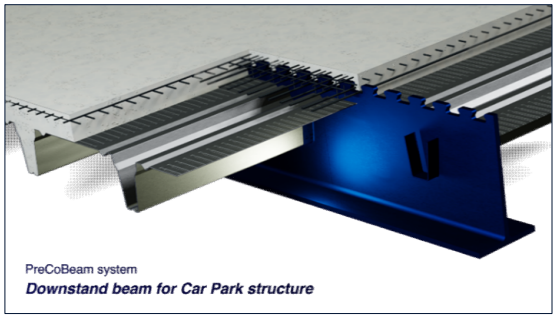

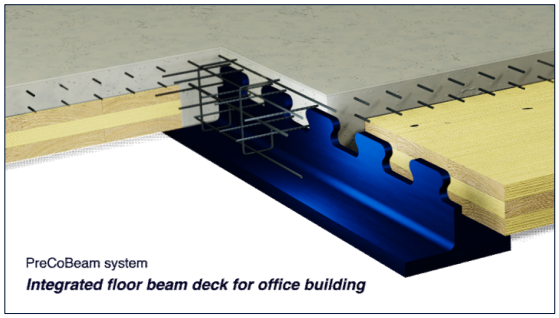

1) Reference

Project reference:	**Test car park project**	User:	**Gustave EIFFEL**
Beam Reference:	**Internal beam**	Company:	**Eiffel Cie**

2) Scope of the calculation sheet

Design is based on structural Eurocodes (EN1990; EN1992-1-1; EN1993-1-1; EN1994-1-1) as well as CEN-TS - Composite dowels (Draft version 2022).
Materials according EN1994-1-1 - Section 3. Structural steel: EN10025-2, -3, -4, -5:2019; ETA-10/0156; Reinforcement: EN10080:2005; Concrete: EN206
Section: composite section with concrete slab (eventually with concrete web) and single T structural steel profile obtained with cutting process from an hot-rolled H section.
Shear connection: continuous shear connection in accordance with "CEN-TS-Composite dowels" document.
Element: Simply supported composite element with section and shear connection in accordance with previous assumptions. Application field: Buildings
Loads: only uniformly distributed loads. Concentrated loads are NOT covered.
Structural analysis: strain-based design of the cross-section resistance, redistribution of shear flow based on a ductile shear connection.
Verification procedure: semi-probabilistic at limit states approach with safety factors.

3) Input fields

Input field	Main input values	Ref.	References
Input field	General input field with default values (not necessary to modify)	Text	Specifications
Output field	Calculated value	Key:	Comments

4) General geometric parametes

ORIGINAL HOT ROLLED SECTION

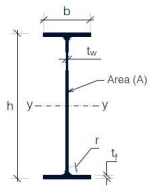

DOWEL SHAPES

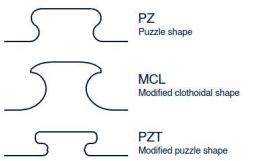

CONCRETE

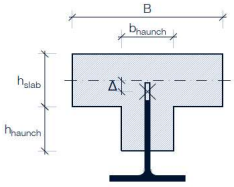

GEOMETRIC PARAMETERS

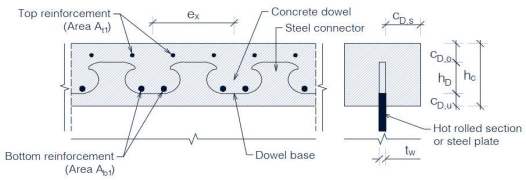

ELEMENT DIMENTIONS

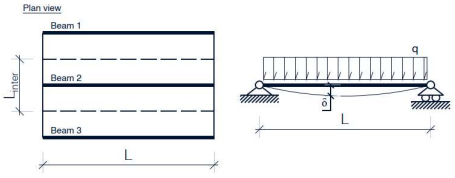

5) Parameters presentting

Partial safety factors

Materials
Ref. EN1994-1-1, 2.4.1

γ_c [-]	1.50	
γ_M [-]	1.00	
γ_v [-]	1.25	
γ_{M0} [-]	1.00	
γ_s [-]	1.15	
γ_{M1} [-]	1.00	
$\gamma_{M,fi,a}$ [-]	1.00	Ref. prEN1994-1-2, 4.5(1)
$\gamma_{M,fi,c}$ [-]	1.00	Ref. prEN1994-1-2, 4.5(1)
$\gamma_{M,fi,s}$ [-]	1.00	Ref. prEN1994-1-2, 4.5(1)

Actions

Load type	γ_{UNFAV} [-]	
γ_{G1} [-]	1.35	Permanent loads: structural
γ_{G2} [-]	1.35	Permanent loads: non structural
γQ [-]	1.50	Live loads

6) Comments about the project

7) Element definition

7.1) Materials

Ref. EN1994-1-1 - Sec.3, CEN document Annex B.2

Steel grade:	S460M	Acc to EN10025-2, -3, -4, -5:2019; ETA-10/0156
Concrete class:	C35/45	Acc to EN1992-1-1
Reinforc. steel:	B500	Acc to EN10080:2005

Material properties

Steel:

Standard:	EN10025-4 (Thermon	Reference standard
Nom. thick. [mm]	16mm <t<=40mm	Nominal thickness of steel section
γ_s [kN/m^3]	78.5	Steel specific weight
f_y [MPa]	440.0	Yealding resistance of structural steel
f_u [MPa]	-	
E_a [MPa]	210000.0	Young's modulus of structural steel
Message:	-	

270 200 40

Concrete:

γ_c [kN/m^3]	25.0	Concrete specific weight
f_{ck} [MPa]	35.0	Characteristic concrete compressive strength
f_{cd} [MPa]	23.3	Design concrete compressive strength
f_{cm} [MPa]	43	Average concrete compressive strength
f_{ctm} [MPa]	3.21	Average concrete tensile strength
E_{cm} [MPa]	34077.1	Young's modulus of concrete
Message:	-	

Reinforcement steel:

f_{sk} [MPa]	500.0	Characteristic yeald resistance of rebar
f_{sd} [MPa]	434.8	Design yealding resistance of rebar

Other derived quantities

ε [-]	0.731	

7.2) Geometry

Ref. EN1994-1-1 - 2.4.1.3

Element

L [mm]	10000	Span length
L_{inter} [mm]	6000	Beams interaxis

Shear connection

Dowel shape:	PZ	Dowel shape
e_x [mm]	150.0	Longitudinal distance between connectors
h_D [mm]	40.3	Height of dowel
n_{Dowels} [-]	33.0	Nb. connectors btw. critical sections
Dowel area coeff.	0.13	
A_D [mm^2]	2925	Concrete dowel area
$A_{D,i}$ [mm^2]	34500	Effective concrete area
b_{CD} [mm]	300.0	Maximum length steel connector parallel to the lon
strips/steel section	1.0	Nb. strips of longitudinal shear connection
e_y [mm]	-	Spacing between strips

Section

Original hot-rolled H section

Hot-r. double-T sec	HE 400 M	
G [kg/m]	256.0	Weight per unit length
G/2 [kg/m]	128	Weight per unit length of
h [mm]	432.0	Height of H section
b [mm]	307.0	Base of H section
t_w [mm]	21.0	Web thickness of H secti
t_f [mm]	40.0	Flange thickness of H se
r [mm]	27.0	Fillet radius of H section
A [cm^2]	325.8	Area of H section
$I_{a,HR}$ [cm^4]	104110.0	Second order central mo
$W_{pl,y}$ [cm^3]	5570.0	Plastic resistant moment

Classification of double-T section under bending

Ref. EN 1993-1-1, 5.6

> Web		
c [mm]	-648	
c/t_w [-]	-30.9	c/t ratio
72 ε [-]	52.6	Class 1 limit for part in bending
83 ε [-]	60.7	Class 2 limit for part in be
124 ε [-]	90.6	Class 3 limit for part in be
Bending:	Class 1	Resulting class
> Flange		
c [mm]	116	
c/t_f [-]	2.9	c/t ratio
9 ε [-]	6.6	Class 1 limit for part in compression
10 ε [-]	7.3	Class 2 limit for part in co
14 ε [-]	10.2	Class 3 limit for part in co
Compression:	Class 1	Resulting class
Profile class:	Class 1	

Single-T section

$y_{Sh.connection}$ [mm]	216.0	Reference coordinate of s
$h_{singleT}$ [mm]	195.9	Single T profile height
A_a [cm^2]	155.5	Net area of steel part
$y_{G,a}$ [mm]	40.61	Centroid position of steel
I_a [cm^4]	3304.4	Second order central mo

Concrete part

h_{slab} [mm]	70.0	Slab height
Δ [mm]	19.0	Offset between slab centr =h_slab/2+clt_height+t_f-
B [mm]	6000.0	Slab width
h_{haunch} [mm]	160.0	Type "=snap_to_flange" if contact with the steel flan
b_{haunch} [mm]	200.0	Haunch width
B_{eff} [mm]	2500.0	Effective width
h_c [mm]	230	Height of concrete part
A_c [cm^2]	2070	Concrete part area
$y_{G,c}$ [mm]	217	Centroid concrete part acc. to reference (*)
I_c [cm^4]	49750.3	Second moment of concrete section

Dowel position relative to the concrete part:

$c_{D,o}$ [mm]	34.0	Concrete cover over the connectors
$c_{D,u}$ [mm]	156.0	Concrete cover beyond the connectors
$c_{D,s}$ [mm]	89.5	Dowel concrete cover transverse to beam axis
c_o [mm]	50	For tensile load on dowel used as anchorage

Derived quantities

h_{po} [mm]	44.5	Pryout cone height
b_c [mm]	200	Concrete web thickness
h/L [-]	1/37	

Composite section

n_0 [-]	6.16	Homogenization factor
$y_{G,homo}$ [mm]	161.3	Centroid position of homo
I_{homo} [cm^4]	44537.6	Second moment of homo

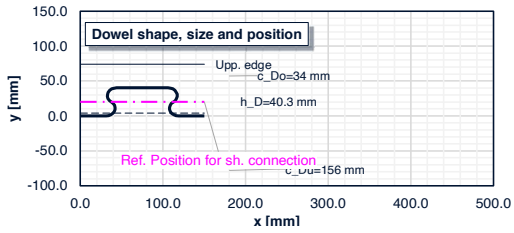

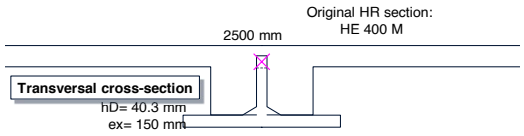

6.3) Effective width of concrete flange (Shear Lag effect)

Ref. EN 1994-1-1, 5.4.1.2

b_0 [mm]	0.0
b_1 [mm]	3000
b_2 [mm]	3000
$L_{e,support}$ [mm]	2500
$L_{e,midspan}$ [mm]	10000
b_{e1} [mm]	1250
b_{e2} [mm]	1250
β_1 [-]	0.600
β_2 [-]	0.600
$b_{eff,support}$ [mm]	1500
$b_{eff,midspan}$ [mm]	2500

Geometry limitations checks

Ref. CEN document - Annex A

Concrete pry-out on lower slab edge:

Prevented [Y/N]	Y	Y if CLT or concrete precast panel are used.
Possib. p.o.e. [Y/N]	N	Recommended N; Y if dowel close to vertical edge
Dowel in slab [Y/N]	Y	Y if dowel is in a concrete slab; N if in concrete Wel

Limitations

e_y >= 120mm	Undefined	
t_w<40 mm	VERO	
4mm < t_w<60 mm	VERO	
$c_{D,o}$>=30 mm	VERO	
cD,u>=20 mm	VERO	
$c_{D,s}$>=45 mm	na	
t_f>=t_w	VERO	Ref. CEN document - Fig.A.5
($h_{singleT}$-t_f)>=0.45 h_D	VERO	Ref. CEN document - Fig.A.6

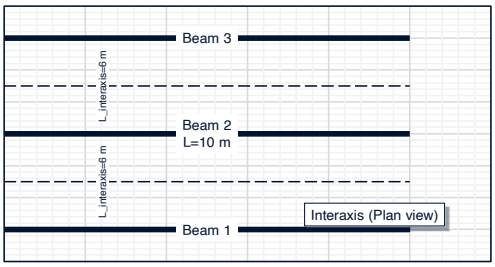

8) Reinforcement definition

Longitudinal slab reinforcement

Top

Presence [Y/N]:	Y
Φ [mm]	8
Spacing [mm]	150
Conc. cover [mm]	30

Bottom

Presence [Y/N]:	N
Φ [mm]	16
Spacing [mm]	100
Conc. cover [mm]	25

Transverse reinforcement: "passing" stirrups

Reinforcement position and amount

Presence [Y/N]:	N	
Φ [mm]	10.0	Stirrups diameter
n. stirrups/dowel [-]	2	Number of stirrups per dowel
Offset [mm]	30.0	Offset from centre of concrete dowel
$A_{s,pass.stirrups}$ [mm^2]	0.0	

Transverse reinforcement: conc. slab bars - Bottom

Reinforcement position and amount

Presence [Y/N]:	Y	
Φ [mm]	16.0	Bar diameter
n. bars/dowel [-]	2	Number of bars
Offset [mm]	37.5	Offset from centre of concrete dowel
Conc. cover [mm]	3.9	Concrete cover
$A_{s,pass.bottom\ bars}$ [mm	402.1	

Transverse reinforcement: conc. slab bars - Top

Reinforcement position and amount

Presence [Y/N]:	Y	
Φ [mm]	8.0	Bar diameter
n. bars/dowel [-]	1.000	Number of bars
Spacing [mm]	150.0	Offset from centre of concrete dowel
Conc. cover [mm]	20	Concrete cover
$A_{s,pass.top\ bars}$ [mm^2]	50.3	

Transverse reinforcement: confinement stirrups

Reinforcement position and amount

Φ [mm]	10.0	Stirrups diameter
n. stirrups/dowel [-]	2.0	Number of stirrups per dowel
n. legs [-]	2.0	Number of legs (4 if internal leg is anchored)
s [mm]	75.0	Spacing
Enbedded in:	Conc. web	
A_{sw} [mm^2]	314.2	

Minimum ratio check

Ref. EN1994-1-1, 6.6.6.3; EN1992-1-1, 9.2.2(5)

A_{sw}/s [mm^2/m]	2094.4	Area of transverse reinforcement / m
α [°]	90.0	Angle between stirrups and long. Axis
ρ_w [-]	1.047%	Angle between stirrups and long. Axis
$\rho_{w,min}$ [-]	0.095%	Density of transverse reinforcement
ρ_w > $\rho_{w,min}$	VERO	Minimum transverse rein

Details check

If embedded in concrete slab:

Ref. CEN document - Annex A.6.2

φ >=8 mm	VERO	
s_{max} [mm]	210.0	s_{max}=min(4.5 h_{po}; 300 mm) Max spacing
s<=s_{max}	VERO	

If embedded in concrete web:

> Geometry:

Ref. CEN document - Annex A.6.3(1)

b_c>=$b_{c,min}$=250 mm	na	
$e_{V,min}$ [mm]	114.5	
$c_{D,s}$=e_V>=$e_{V,min}$	na	
h_{po}<=e_V+0.13 e_x	na	

> Splitting:

Ref. CEN document - Annex A.6.3(2); … Annex A.6.3(9)

$A_{s,conf}$ [mm^2]	314.2	
$A_{s,conf}$ >= 0.3 $P_{S,Rd}$/f	na	
φ >=10 mm	na	
Further checks [T/F	VERO	…
b_s [mm]	300	
b_s > min(h_c, 360mm	na	

Derived quantities

A_t [mm^2]	
A_b [mm^2]	402.1
ρ_D [-]	0.847
$\rho_{D,i}$ [-]	0.072 Reinforcement ratio for pry-out failure
$A_{s,conc.slab,1}$ [mm^2]	452.4 Transversal reinforcement in slab

Minimum quantity of transverse reinforcement

Ref. CEN document - Annex A.6.1

$A_{b,min}$ [mm^2]	123.0	
A_b>$A_{b,min}$	VERO	
n=2	VERO	Number of bars in each concrete dowel
A_b(1ϕ)>=0.5A_b	VERO	

Dowels close to a concrete edge

Ref. CEN document - Annex A.6.4

h_c + t_s *10 >=100 mr	VERO	
$c_{D,s}$>=45 mm	VERO	
φ [mm]	10	
φ >=8 mm	VERO	

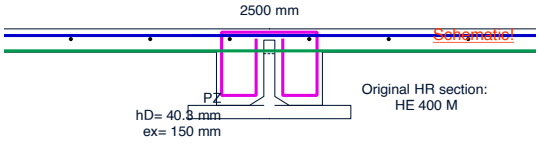

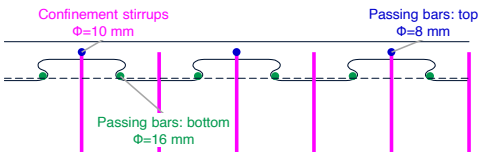

9) Complementary elements

Transversal ribbed slab

Type:	None	Ribs shape
Sheet th. t_s [mm]	1.25	Profiled sheet thickness
Dowel-ribs compatibility:		
mod(spac.;e_x)=0	No ribs	
Sh. perimeter/m [m	0.0	Profiled sheet length per unit length
Additional area [m^2/	0.000	Rib additional long. cross sectional area
Ribs spacing [m]	None	Ribs spacing
Ribs depth [m]	0.000	Ribs depth from slab bottom
Additional weight [k	0.00	Additional concrete weight due to ribs (including p
Wings add. weight	0.000	

Wood CLT panel

Thickness [mm]	160.0	
γ_{wood} [kN/m^3]	3.5	
Weight [kN/m^2]	0.56	
Support width [mm]	53.5	CLT panel support width on bottom flange (assumed to be half of the difference between b and the concrete web thickness)

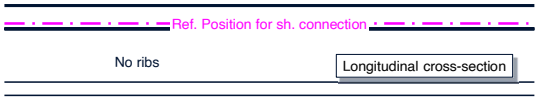

Consistency check

Consistency: VERO

10) Loads definition

Loads list

Permanent loads: structural

Item [i]	Load name	G_k [kN/m^2]	g_k [kN/m]	ULS Coefficient
1.1	G1 - Steel section		1.22	1.35
1.2	G1 - Concrete	1.75	10.50	1.35
1.3	G1 - Wood	0.56	3.36	1.35

Permanent loads: non structural

Item [i]	Load name	G_k [kN/m^2]	g_k [kN/m]	ULS Coefficient
2.1	G2 - Decking	1.50	9.00	1.35
2.2				1.35

Live loads

Note: First listed imposed load is assumed to be the principal load

Item [i]	Load name	Q_k [kN/m^2]	q_k [kN/m]	ψ_{0i} [-]	ULS Coefficient
3.1	Q - Cat.	3.80	22.80	1	1.50
3.2				1	1.50
3.3				1	1.50

Load on the main beam

q_{ULS} [kN/m] 66.7

Load on the decking system

$q_{ULS,transv}$ [kN/m^2] 10.8 Considering a 1m strip

11) Further inputs

Construction stage setting

Type of construction: Propped Specify if the construc

Frequency limitation settings

1≤ $\alpha_{b,dyn}$ [-] ≤ 5	2.0	1 for perfect isostatic b
f_{lim} [Hz]	2.3	Limit frequency

Deflection limitation settings

δ_{lim}/L [-] 1/300

Slab-main beam composite checks

Composed checks	N	Activate if composed
1≤ $\alpha_{b,dyn}$ [-] ≤ 5	2.0	
Slab w/L deflection	1/500	Insert deflection of sla
$f_{transv.}$ [Hz]	2.50	Transversal mode fre

Bottom flange as support

Is support [Y/N] Y 'Y' if the bottom flange is a support for the slal

11) Run sheet calculations

Press to launch:

- ULS Rigid Plastic (RP) analysis;
- ULS Strain Limitation (SL) analysis;
- SLS stress computations in the different construction stages and for both propped and unpropped conditions

Note: specific analysis settings (gray highlighted) are available in the specific modules

Note: buttons for the specific modules are also available in the related sections

12) Structural analysis

Actions

M_{Ed} [kNm]	833.9	Design moment
V_{Ed} [kN]	333.5	Design shear

Actions on dowel (For separated checks)

$P_{S,Ed}$ [kN]	106.9	Shear design action on single dowel
$P_{T,Ed}$ [kN]	0.0	Tension design action on single dowel

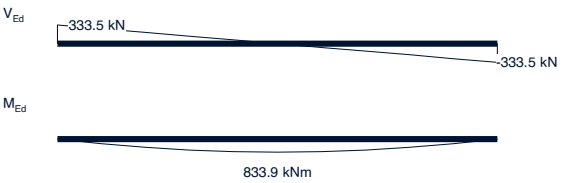

13) Shear connection ductility

Deformation capacity

Ref. prEN1994-1-1 - Tab. 5.1

Identify ductility class

> D0

δ_{ek} [mm]	
δ_{ek}<2 mm	VERO

> D1.a

δ_{ek} [mm]	
δ_{ek}>2 mm	FALSO

> D1.b

δ_{ek1} [mm]	
δ_{ek2} [mm]	
δ_{ek}>2 mm	FALSO

> D2

δ_{ek} [mm]	
δ_{uk} [mm]	
$(\delta_{uk}-\delta_{ek})/\delta_{uk}$<0.70	na
δ_{uk} >6 mm	FALSO

> D3

δ_{ek} [mm]	
δ_{uk} [mm]	
$(\delta_{uk}-\delta_{ek})/\delta_{uk}$<0.80	na
δ_{uk} >10 mm	FALSO

Identified ductility class

Ductility class: D2

13) ULS dowel resistance

Ref. EN1994-1-1 - 6.6: Shear connection; CEN document; CEN Document Annex A.3

Dowel: shear

> Splitting

Ref. CEN document - XXX

Excluded via sufficient transverse reinforcement

Force [kN]	53.5	Tensile force of 50% the
$A_{s,min}$ [mm^2]	123.0	
A_b>$A_{b,min}$	VERO	

> Local compression

Ref. CEN document - XXX

Allowed

> Shearing

Ref. CEN document - XXX; CEN Document Annex A.X

η_D [-]	1.63	
$P_{sh,k}$ [kN]	399.6	Shearing resistance of concrete dowel

> Pry-out

Ref. CEN document - 6.3.5; CEN Document Annex A.3

k_1 [-]	71	Factor dependent on dowel geometry
χ_x [-]	1.00	Red. overlapping pry-out cones - Long
e_x<4.5 h_{po}	FALSO	
χ_y [-]	1.00	Red. overlapping pry-out cones - Transv
e_y<9 h_{po}	Undefined	
$y_{G,omo}$<$y_{sh,connection}$	VERO	
Dowel in compressi	VERO	
ψ_{crack} [-]	1.000	Red. for transverse concrete cracking
$P_{po,k}$ [kN]	133.6	Pry-out char. Resistance of concrete cone

> Edge pry-out

Ref. CEN document Annex A.3

ζ_{geo} [-]	0.194	
$h_{d,eff}$ [mm]	29.1	Effective height of steel connector
k [-]	2.495	Size effect coefficient
$P_{poe,k}$ [kN]	128.7	Pry-out char. Resistance
$P_{pl,k}$>=1.5 $P_{poe,k}$	VERO	
Message:	-	

> Steel dowel plastifying

λ_{GEO} [-]	0.286	Factor dependent on geometry
$P_{pl,k}$ [kN]	396.4	Plastifying of steel char. resistance

> Dowel connector resistance

$P_{S,Rk}$ [kN]	133.6	Shear char. resistance of single dowel
$P_{S,Rd}$ [kN]	106.9	Shear design resistance of single dowel

14) ULS shear resistance

Buckling resistance of web

Ref. EN1994-1-1, 6.2.2.3; EN1993-1-1, 5

η [-]	1.2	
h_w [mm]	149.0	Steel web height
h_w/t_w [-]	7.1	
72/η ε	43.8	
h_w/t_w < 72/η ε	VERO	
Message:	-	

Plastic shear resistance of web

Ref. EN1994-1-1, 6.2.2.2

A_v [mm^2]	2945.6
$V_{pl,Rd}$ [kN]	748.3

Note: shear conservatively ensured by single-T section web (height=h/2-t_f-h_D)

Interaction

Ref. EN1994-1-1, 6.2.2.4

V_{Rd} [kN]	748.3	Design shear resistance
V_{Ed}/V_{Rd} [-]	0.446	Shear design / resistance check
V_{Ed}/V_{Rd}>0.5	FALSO	Check for need of reduction
ρ [-]	No reduction	Reduction factor
(1-ρ) f_{yd} [MPa]	No reduction	Reduced steel yielding stress in the shear area

15) Bending on bottom flange check

Ref. prEN1994-1-1, Annex I.3.1

Support on fl. [Y/N]	Y	"Y" if the bottom flange consists in a support of the transversal flooring system
$m_{ybt,Rd}$ [kNm/m]	140.8	Resistant elastic bending moment of the bottom flange
V [kN/m]	32.5	Reaction force of the bottom flange on the transversal system
$m_{ybt,Ed}$ [kNm/m]	3.6	Acting design bending moment on the bottom flange
$m_{ybt,Ed}$ < $m_{ybt,Rd}$	VERO	
η_m [-]	0.026	Utilization ratio in trasverse bending (parameter defined according to prEN1994-1-1, Annex I.3.1.2)
$f_{y,red}$ [MPa]	437.1	Reduced yealding resistance of bottom flange due to transverse bending interaction

16) ULS bending resistance

Ref. EN1994-1-1 - Sec.6

ULS analysis - FSC case (η=1)

Ref. EN1994-1-1 - 6.2.1.2

Analysis:	RP - Rigid-plastic (--)	SL - Strain limitation (--)	
x_{pl} [mm]	117.9	171.2	Position of the plastic neutral axis in case of FSC
y_{PNA} [mm]	152.1	98.78	Position of the plastic neutral axis in case of FSC
N [kN]	0.00	0.00	Residual tensile force along the section for numerical evaluation procedure
$M_{pl,Rd,FSC}$ [kNm]	1269.8	847.7	Plastic resistance design bending moment in case of FSC
N_{cf} [kN]	-6035.0	-3745.4	Compressive normal force in concrete flange in case of FSC (<0 if compressive)
$(1/r)_u$ [1/mm]	na	2.02E-05	Ultimate curvature
Failure type:	na	concrete crushing	Failure type

Reduction

x_{pl}/h [-]	0.634	
$x_{pl}/h>0.15$	VERO	
S420/S460	VERO	
β [-]	>0.4!	
Reduction:	Yes	
$M_{pl,Rd,FSC,red}$ [kNm]	847.7	Not reduced according to prEN1994-1-1 new appro

Shear flow

$P_{max,el}$ [kN]	227.0	
$N_{cf,el}$ [kN]	1764.1	Limit value of N_{cf} that does'nt imply redistribution
$N_{cf}<=N_{cf,el}$	FALSO	
$N_{cf}<=2*N_{cf,el}$	FALSO	
Redistribution:	YES	
Sh. connection:	PARTIAL (PSC)	
$v_{L,max}$ [kN/m]	712.8	Maximum shear flow

Degree of shear connection

N_c [kN]	3528.3	Transmissible shear force
$N_c<N_{c,f}$	VERO	
Sh. connection:	PARTIAL (PSC)	Type of connection
η [-]	0.94	
L<18m with PSC	VERO	Ref. CEN Document - 8
η > 0.5	VERO	Ref. CEN Document - A.
$\eta_{min}(L, f_y)$	0.88	
$\eta > \eta_{min}(L, f_y)$	VERO	Minimum degree of shear
$M_{pl,Rd}$ [kNm]	865.9	

Degree of utilization

$M_{Ed}/M_{pl,Rd}$ [-]	0.963	

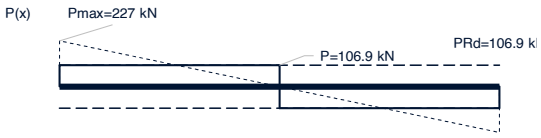

Settings for SL design

Discretization

Δy [mm]	2.0	Discretization step (fibre height)

Material laws

Structural steel:	Elastic-plastic hardeni	Structural steel material law
Reinforcement stee	Elastic-plastic hardeni	Reinforcement steel material law (Reinf. Bars
Concrete:	Parabola-rectangle	Concrete material law

Concrete law parameters:

n [-]	2.000	Parabola-rectangle law exponent
ε_{c1} [-]	0.225%	
ε_{cu1} [-]	0.350%	
ε_{c2} [-]	0.200%	
ε_{cu2} [-]	0.350%	

Structural steel law parameters:

ε_{ay} [-]	0.210%	Yealding strain for stru
ε_{au} [-]	15.0%	Ultimate strain for stru
E' [MPa]	210.0	Hardening slope

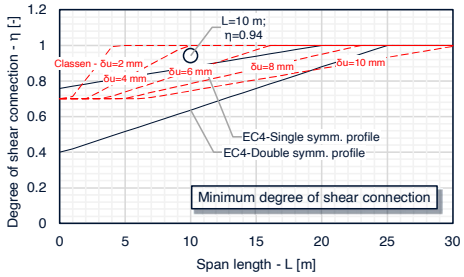

Material laws

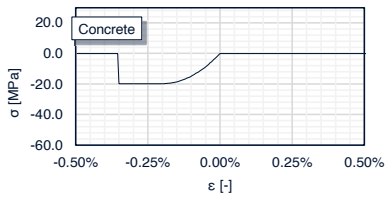

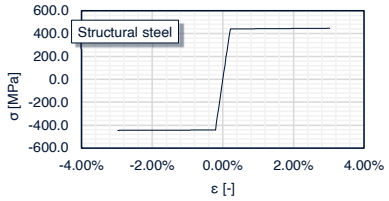

Stresses and strains along section: FSC-ULS

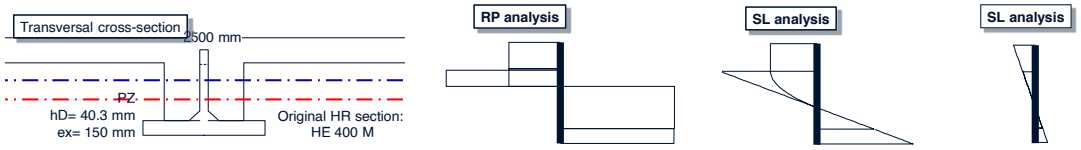

Partial shear connection diagram

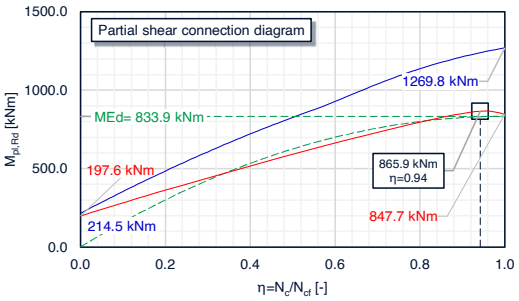

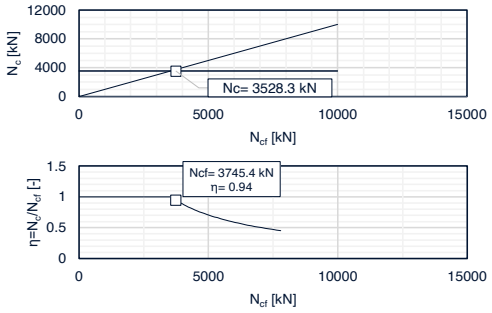

Moment-curvature diagram

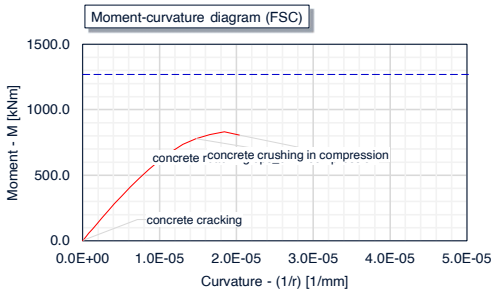

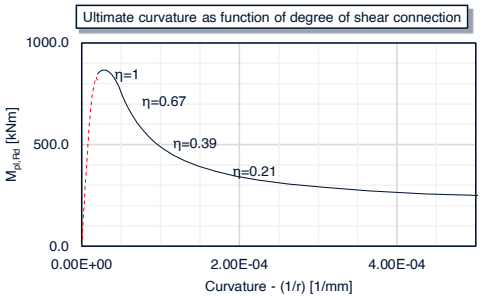

17) ULS longit. shear resistance of concrete flange

Transverse reinforcement

Reinforcement:

Ref. EN1994-1-1, 6.6.6; EN1992-1-1, 6.2.4

$A_{b1}+A_{t1}$ [mm²]	452.4
$A_{b1,passing\ bars}$ [mm²]	402.1
s_f [mm]	150.0

Crushing of concrete parameters:

Ref. EN1992-1-1, expr.6.22

ν [-]	0.516
v_{Rd} [MPa]	6.02

Additional force

Ref. CEN TS. A.7.1(1)

0.5 $P_{S,Rd}/f_{sd}$ [kN]	123.0
$A_{sf} \geq 0.5\ P_{S,Rd}/f_{sd}$	VERO

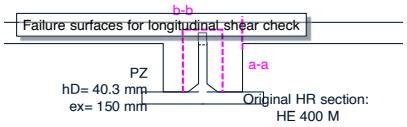

Failure surface d-d

> Resistance of reinforcement

v_L [kN/m]	712.8	
h_f [mm]	179.0	
v_{Ed} [MPa]	3.98	
A_{sf}/s_f [mm²/m]	2094.4	
θ [°]	45.0	
26.5°<=θ<=45°	VERO	Angle limits check
cot(θ) [-]	1.00	
$A_{sf}/s_f\ f_{sd}$ [kN/m]	910.6	
$v_{Ed}\ h_f/\cot(\theta)$ [kN/m]	712.8	
$A_{sf}/s_f\ f_{sd} \geq v_{Ed}\ h_f/\cot$	VERO	

Failure surface a-a

> Resistance of reinforcement

v_L [kN/m]	356.4	Considered shear flow
h_f [mm]	70	Height of potential failure surface
v_{Ed} [MPa]	5.09	Design shear stress
A_{sf}/s_f [mm²/m]	3015.9	transversal reinforcement density
θ [°]	45.0	Strut angle
26.5°<=θ<=45°	VERO	Angle limits check
cot(θ) [-]	1.00	Cotangent of strut angle
$A_{sf}/s_f\ f_{sd}$ [kN/m]	1311.3	Reinforcement resistance per unit length
$v_{Ed}\ h_f/\cot(\theta)$ [kN/m]	356.4	Force applied on reinforcement / m
$A_{sf}/s_f\ f_{sd} \geq v_{Ed}\ h_f/\cot$	VERO	Check

> Crushing of concrete flange

v_{Ed}/v_{Rd} [-]	0.846
$v_{Ed} < v_{Rd}$	VERO

Failure surface b-b

> Resistance of reinforcement EN1994-1-1, 6.6.6.2(2)

v_L [kN/m]	712.8	Considered shear flow
h_f [mm]	413.0	Height of potential failure surface
v_{Ed} [MPa]	1.73	Design shear stress
A_{sf}/s_f [mm²/m]	5361.7	transversal reinforcement density
θ [°]	45.0	Strut angle
26.5°<=θ<=45°	VERO	Angle limits check
cot(θ) [-]	1.00	Cotangent of strut angle
$A_{sf}/s_f\ f_{sd}$ [kN/m]	2331.2	Reinforcement resistance per unit length
$v_{Ed}\ h_f/\cot(\theta)$ [kN/m]	712.8	Force applied on reinforcement per unit length
$A_{sf}/s_f\ f_{sd} \geq v_{Ed}\ h_f/\cot$	VERO	Check

> Crushing of concrete flange

v_{Ed}/v_{Rd} [-]	0.287
$v_{Ed} < v_{Rd}$	VERO

Minimum ratio of transverse reinforcement

ρ_w [-]	4.308%
$\rho_{w,min}$ [-]	0.095%
$\rho_w > \rho_{w,min}$	VERO

18) SLS

Creep coefficient computation parameters

Ref. EN1992-1-1

u [mm]	5000	Perimeter exposed to drying
A_c [mm^2]	207000	Concrete cross-sectional area
h_0 [mm]	82.8	Notional size (Equivalent hydraulic radius)
CEM [S/R/N]	N	Tipe of cement
RH [%]	50	Relative humidity

Type of construction: **Propped**

Settings

t [days]	1E+11	Unpropping [days]	28	Time of unpropping (f
Propping [Y/N]	Y	First loading [days]	100	Time of first loading
Concrete collaborat	2	Begin of shrinkage [da	2	Beginning of applicatic

Loads list

Permanent loads: structural

Item [i]	Load name	g_k [kN/m]	M_d [kNm]	V_d [kN]	$t_{0,unpropped}$ [days]	$t_{0,propped}$ [days]	Load category
1.1	G1 - Steel section	1.22	15.3	6.1	0	28	Permanent loading
1.2	G1 - Concrete	10.50	131.3	52.5	0	28	Permanent loading
1.3	G1 - Wood	3.36	42.0	16.8	0	28	Permanent loading

Permanent loads: non structural

Item [i]	Load name	g_k [kN/m]	M_d [kNm]	V_d [kN]	$t_{0,unpropped}$ [days]	$t_{0,propped}$ [days]	Load category
2.1	G2 - Decking	9.00	112.5	45.0	100	100	Permanent loading
2.2					100	100	Permanent loading

Live loads — Note: First listed imposed load is assumed to be the principal load

Item [i]	Load name	q_k [kN/m]	M_d [kNm]	V_d [kN]	$t_{0,unpropped}$ [days]	$t_{0,propped}$ [days]	Load category
3.1	Q - Cat.	22.80	285.0	114.0	100	100	Short-term
3.2					100	100	Short-term
3.3					100	100	Short-term

Shrinkage

Item [i]	Load name	ε_{cs} [-]	M_{cs} [kNm]	$t_{0,unpropped}$ [days]	$t_{0,propped}$ [days]	Load category
4.1	Shrinkage	0.000325	76.1	2	2	Shrinkage effect

Computation of stresses and deflection

Loads list		Time of application	$t > t_0$	Creep multiplier	Creep coefficient	Effective concrete stiff	Modular ratio
Load name		t_0 [days]	Flag	ψ_L [-]	φ_t [-]	$E_{c,eff}$ [MPa]	n_L [-]
G1 - Steel section	…	28	VERO	1.1	2.4	9379.7	22.4
G1 - Concrete	…	28	VERO	1.1	2.4	9379.7	22.4
G1 - Wood	…	28	VERO	1.1	2.4	9379.7	22.4
G2 - Decking	…	100	VERO	1.1	1.9	11122.1	18.9
	…						
Q - Cat.	…	100	VERO	0.0	1.9	34077.1	6.2
	…						
	…						
Shrinkage	…	2.00	VERO	0.6	3.9	10789.0	19.5

Loads list		Centroid position	Homogenized second	Lower edge steel stre	Upper edge steel stre	Lower edge concrete	per edge concrete stre
Load name		$y_G(t,t_0)$ [mm]	I_{homo} [cm^4]	$\sigma_{a,inf}$ [MPa]	$\sigma_{a,sup}$ [MPa]	$\sigma_{c,inf}$ [MPa]	$\sigma_{c,sup}$ [MPa]
G1 - Steel section	…	106.5	23614.0	6.9	-5.8	0.2	-0.5
G1 - Concrete	…	106.5	23614.0	59.2	-49.7	1.6	-4.1
G1 - Wood	…	106.5	23614.0	18.9	-15.9	0.5	-1.3
G2 - Decking	…	113.6	25997.6	49.2	0.0	1.7	0.0
	…			0.0	0.0	0.0	0.0
Q - Cat.	…	161.3	44537.6	103.2	-8.7	12.6	-4.5
	…			0.0	0.0	0.0	0.0
	…			0.0	0.0	0.0	0.0
Shrinkage	…	112.33	25561.8	-13.2	-65.5	4.6	0.0
Sum	**…**			**224.2**	**-145.6**	**21.3**	**-10.3**

Loads list		δ [mm]	V_d [kN]
Load name			
G1 - Steel section	…	3.5	6.1
G1 - Concrete	…	30.3	52.5
G1 - Wood	…	9.7	16.8
G2 - Decking	…	23.6	0.0
	…		
Q - Cat.	…	31.7	45.0
	…		
	…		
Shrinkage	…	17.73	
Sum of permanent contributes:		84.9	
Sum of live loads contributes:		31.7	

Unpropped case

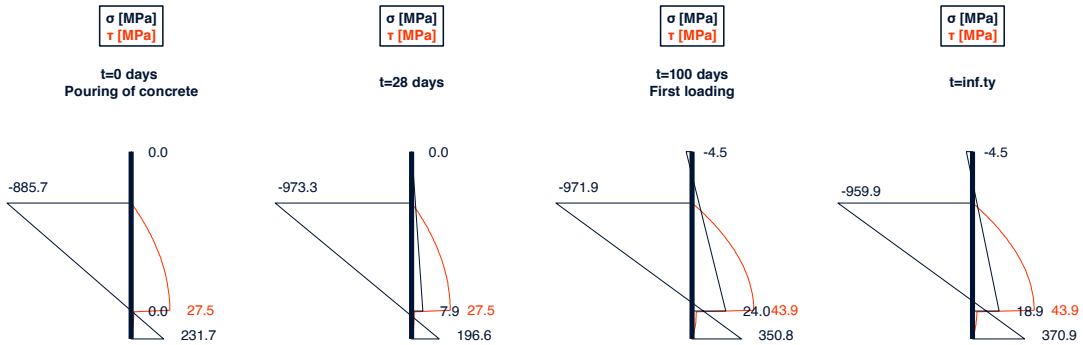

Propped case

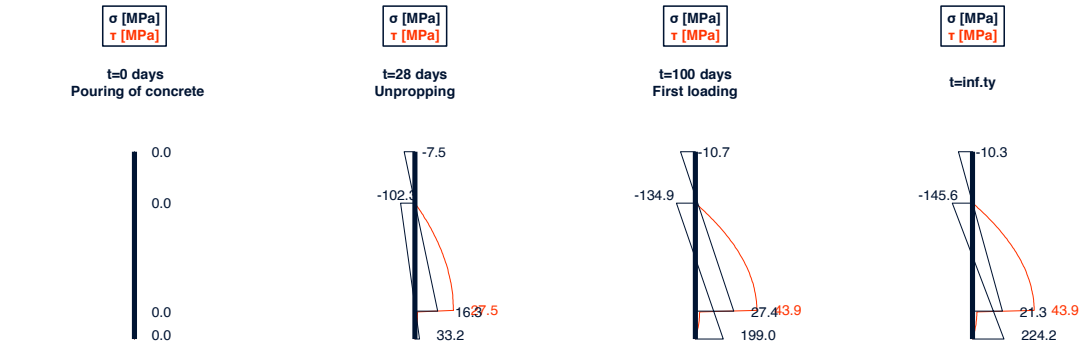

Summary

Unpropped case

Time - t [days]	$\sigma_{a,inf}$ [MPa]	$\sigma a_{,sup}$ [MPa]	$\sigma_{c,inf}$ [MPa]	$\sigma_{c,sup}$ [MPa]	$\tau_{a,max}$ [MPa]	δ_g [mm]	δ_q [mm]
0.0	231.7	-885.7	0.0	0.0	27.5	311.3	0.0
28	196.6	-973.3	7.9	0.0	27.5	329.1	0.0
100	350.8	-971.9	24.0	-4.5	43.9	342.9	31.7
inf.ty	370.9	-959.9	18.9	-4.5	43.9	352.6	31.7

Propped case

Time - t [days]	$\sigma_{a,inf}$ [MPa]	$\sigma_{a,sup}$ [MPa]	$\sigma_{c,inf}$ [MPa]	$\sigma_{c,sup}$ [MPa]	$\tau_{a,max}$ [MPa]	δ_g [mm]	δ_q [mm]
0.0	0.0	0.0	0.0	0.0	0.0	0.0	0.0
28	33.2	-102.3	16.3	-7.5	27.5	40.9	0.0
100	199.0	-134.9	27.4	-10.7	43.9	67.4	31.7
inf.ty	224.2	-145.6	21.3	-10.3	43.9	84.9	31.7

Results for the chosen case: Propped

Max. normal stresses:

$\sigma_{a,max,comp}$ [MPa]	-145.6	Max compression stre
$\sigma_{a,max,tens}$ [MPa]	224.2	Max tensile stress on
$\sigma_{c,max,comp}$ [MPa]	-10.7	Max compression stre
$\sigma_{c,max,tens}$ [MPa]	27.4	Max tensile stress on
Cracking [Y/N]	Y	Check if concrete is cr

Composed checks: N

Deflection

$I_{homo,2}$ [cm^4]	42685.8	Second moment in partialized state
$I_{red}=0.5(I_1+I_2)$ [cm^4]	43611.7	Composite section in cracked situation
I_1/I_{red} [-]	1.02	Amplification due to cracking of concrete
δ_{lim}/L [-]	**1/300**	**Limitation on deflection**
δ_c [mm]	**86.7**	**Precambering**
δ_{TOT} [mm]	**32.4**	**Deflection under live loads**
δ_{TOT}/L [-]	**2/617**	**Deflection/span length ratio**

Instantaneous deflection check:

Slab w/L deflection	1/500
Slab deflection	12
$\delta_{TOT,lim}$ [mm]	**17.2**
$\delta_{TOT}<\delta_{TOT,lim}$ [mm]	FALSO

Vibration frequency

Ref. EN1994-1-1, 7.3.2

$1\leq \alpha_{b,dyn}$ [-] ≤ 5	2	
f_{lim} [Hz]	2.3	
$E_{c,dyn}/E_{cm}$ [-]	1.1	
$I_{homo,dyn}$ [cm^4]	46394.4	
μ [kg/m]	2408.1	Distributed mass per unit length
f [Hz]	**4.47**	**Vibration frequency**

Composed frequency check

$1\leq \alpha_{b,dyn}$ [-] ≤ 5	2.0	
$E_{c,dyn}/E_{cm}$ [-]	1.1	
$I_{homo,dyn}$ [cm^4]	46394.4	
μ [kg/m]	2408.1	
f_{long} [Hz]	4.468	Longitudinal frequency
$f_{transv.}$ [Hz]	2.5	
$f_{composed}$ [Hz]	**2.18**	Resulting frequency

19) Checks

General

> Materials	
Steel grade	S460M
Concrete class	C35/45
> Element	
L [m]	10.00
h_{tot} [m]	0.27
h_{tot}/L [-]	1/37
> Shear connection:	
Dowel:	PZ
Dowel size (h_D) [mm	40.3
Ductility class:	D2
Redistribution:	YES
Type:	PARTIAL (PSC)
η [-]	0.9

Top concrete cover

c [mm]	26

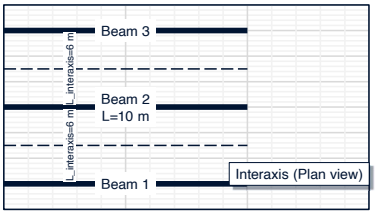

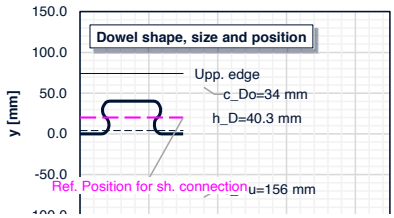

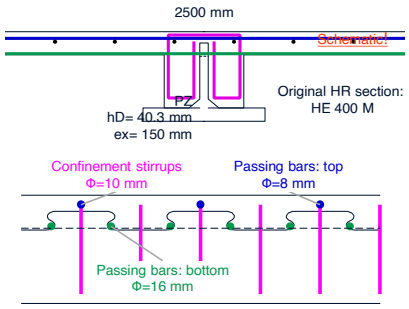

ULS

> Bending resistance		
$M_{Ed}/M_{pl,Rd} \le 1$	VERO	0.963
> Shear resistance		
$h_w/t_w < 72/\eta\ \varepsilon$	VERO	0.162
$V_{Ed}/V_{pl,Rd} \le 1$	VERO	0.446
> Dowel resistance		
$P_{S,Ed}/P_{S,Rd} \le 1$	VERO	1.000
> Long. shear in concrete slab		
Surface a-a:		
$A_{sf}/s_f\ f_{sd} \ge v_{L,Ed}\ h_f/\cot(\theta)$	VERO	0.272
$v_{L,Ed} < v_{Rd}$	VERO	0.846
Surface b-b:		
$A_{sf}/s_f\ f_{sd} \ge v_{Ed}\ h_f/\cot(\theta)$	VERO	0.306
$v_{Ed} < v_{Rd}$	VERO	0.287
Bottom flange moment check		
$m_{el,Rd,flange} < m_{el,Rd,flange}$	VERO	

SLS

$\delta_{TOT}/L < \delta_{lim}/L$	VERO	0.972
$\delta_{TOT,composed} < \delta_{TOT,composed,lim}$ [mm]	na	
f≥2.3 Hz	VERO	0.515
$f_{composed} \ge f_{lim}$	na	

Degree of connection

L<18m with PSC	VERO	
η > 0.5	VERO	0.531
$\eta > \eta_{min}(L, f_y)$	VERO	

Details and geometric limitations

> Geometry limitations		
$e_y \ge 120$mm	na	
t_w<40 mm	VERO	
4mm < t_w<60 mm	VERO	
$c_{D,o} \ge 30$ mm	VERO	
$c_{D,u} \ge 30$ mm	VERO	
$c_{D,s} \ge 45$ mm	na	
$t_f \ge t_w$	VERO	
$(h_{singleT}-t_f) \ge 0.45\ h_D$	VERO	
> Transverse reinforcement		
$A_b > A_{b,min}$	VERO	
n=2	VERO	
$A_b(1\phi) \ge 0.5 A_b$	VERO	
> Confinement stirrups		
$\rho_w > \rho_{w,min}$	VERO	
> Reinforcement in slabs		
φ ≥8 mm	VERO	
$s <= s_{max}$	VERO	
> Reinforcement in web		
$d_c \ge b_{c,min}$=250 mm	na	
$c_{D,s} = e_V > e_{V,min}$	na	
$h_{po} \le e_V + 0.13\ e_x$	na	
$A_{s,conf} \ge 0.3\ P_{S,Rd}/f_{sd}$	na	
φ ≥10 mm	na	
$b_s > \min(h_c, 360mm)$	na	
Further checks:	na	
> Dowels close to concrete edge		
$h_c \ge 100$ mm	na	
$c_{D,s} \ge 45$ mm	na	
φ >=8 mm	na	
> Concrete slab		
$A_{s,prov} > A_{s,min}$	VERO	
26.5°≤θ≤45°	VERO	

Declaration consistencies:

Lower pryout prevention:	VERO

ULS checks	VERO
SLS checks	VERO
Geometric limitations checks	VERO
Reinforcement details checks	VERO
Consistency in declarations checks	VERO
Degree of shear connection	VERO

Global check status

Summary check:	VERO

Appendix B

Case study: downstand beam for car park flooring system

The solution consists in a 16m spanlength simply supported beam with interaxis equal to 5m. It is designed for a carpark destination. A Cofraplus®220 technology is used in the transverse direction. The solution was originally used in [94].

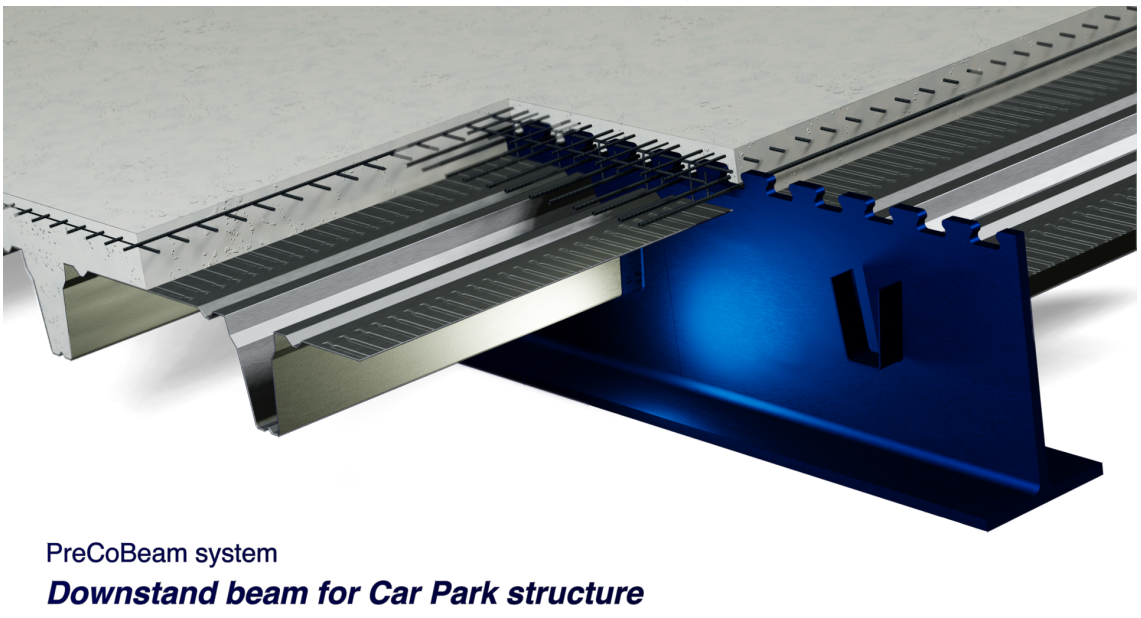

Figure B.1: rendering: downstand beam for car park flooring system

B.1 Reference design rules and partial safety coefficients

In the following calculation reference at EN1990 [6], EN1991-1-1 [7], EN1992-1-1 [8], EN1993-1-1 [9], EN1994-1-1 [11], and the technical specification for the composite dowels is made.
The partial safety coefficients used are:

Partial safety coefficients	
$\gamma_c = 1.50$	Partial safety coefficient for concrete resistance
$\gamma_{M0} = 1.00$	Partial safety coefficient for structural steel resistance
$\gamma_s = 1.15$	Partial safety coefficient for reinforcement steel resistance
$\gamma_v = 1.00$	Partial safety coefficient for the shear connection resistance
$\gamma_{G1} = 1.35$	Partial safety coefficient for the permanent structural actions
$\gamma_{G2} = 1.35$	Partial safety coefficient for the permanent non structural actions
$\gamma_Q = 1.50$	Partial safety coefficient for the live load actions

B.2 Case study framework

A section composed by a single T steel profile and a top concrete slab is considered. The single T steel profile is derived by mean of a cutting process from a standard double T steel hot-rolled section. The composite dowels shear connection is embedded in the concrete slab. According to the reference technical specification for the composite dowels, the considered section is classified as conventional member. This is because the section does not include a concrete web. In this case the only concrete member is the concrete slab. Differently, hybrid members include a concrete web or a concrete member that due to its size its contribute can be taken into account for the vertical shear resistance check.

B.3 Data

The geometry, materials and shear connection data are described in this section. The loading conditions and consequent design actions are computed.

B.3.1 Materials

Following materials are considered:

- Structural steel: S460
- Concrete: C35/45
- Reinforcement steel: B500

This leads to the following material properties:

Structural steel	
$f_y = 460\ MPa$	Structural steel yielding resistance
$E_a = 210000\ MPa$	Structural steel elastic modulus
Concrete	
$f_{ck} = 35.0\ MPa$	Concrete compression characteristic strength
$f_{cd} = f_{ck}/\gamma_c = 23.3\ MPa$	Concrete compression design strength
$f_{cm} = f_{ck} + 8 = 43.0\ MPa$	Concrete compression mean strength
$f_{ctm} = 3.21\ MPa$	Average concrete tensile strength
$E_{cm} = 22000 \cdot (f_{cm}/10)^{0.3} = 34077.1\ MPa$	Mean elastic modulus of concrete
Reinforcement steel	
$f_{sk} = 500.0\ MPa$	Characteristic yielding resistance
$f_{sd} = f_{sk}/\gamma_s = 434.8\ MPa$	Design yielding resistance

B.3.2 Geometry

A simply supported static scheme is considered with spanlength L. In the transversal direction the beams are spaced with an interaxis of L_{inter}. The used quantities are:

$L = 16000\ mm$	Span length
$L_{inter} = 5000\ mm$	Beams interaxis

For a carpark destination, an exposure class XC4 is considered according to EC2. This leads to a minimum concrete cover of 40 mm.

An HE900AA hot-rolled standard profile is used. The selected shear connection is a PZT type with size $e_x = 150\ mm$. The cross-section is shown in Fig.B.2. The static scheme (Fig.B.3) consists in a simply supported beam.

The amount of steel used is an important parameter in order to identify the potential appeal of the solution for the construction industry. In this case the weight of the double T section is:

$$G = 198.0\ kg/m \tag{B.1}$$

This means that the oxycutted single T profile used for the composite beam solution has a weight of:

$$G/2 = 99.0\ kg/m \tag{B.2}$$

The following geometry related quantities are defined:

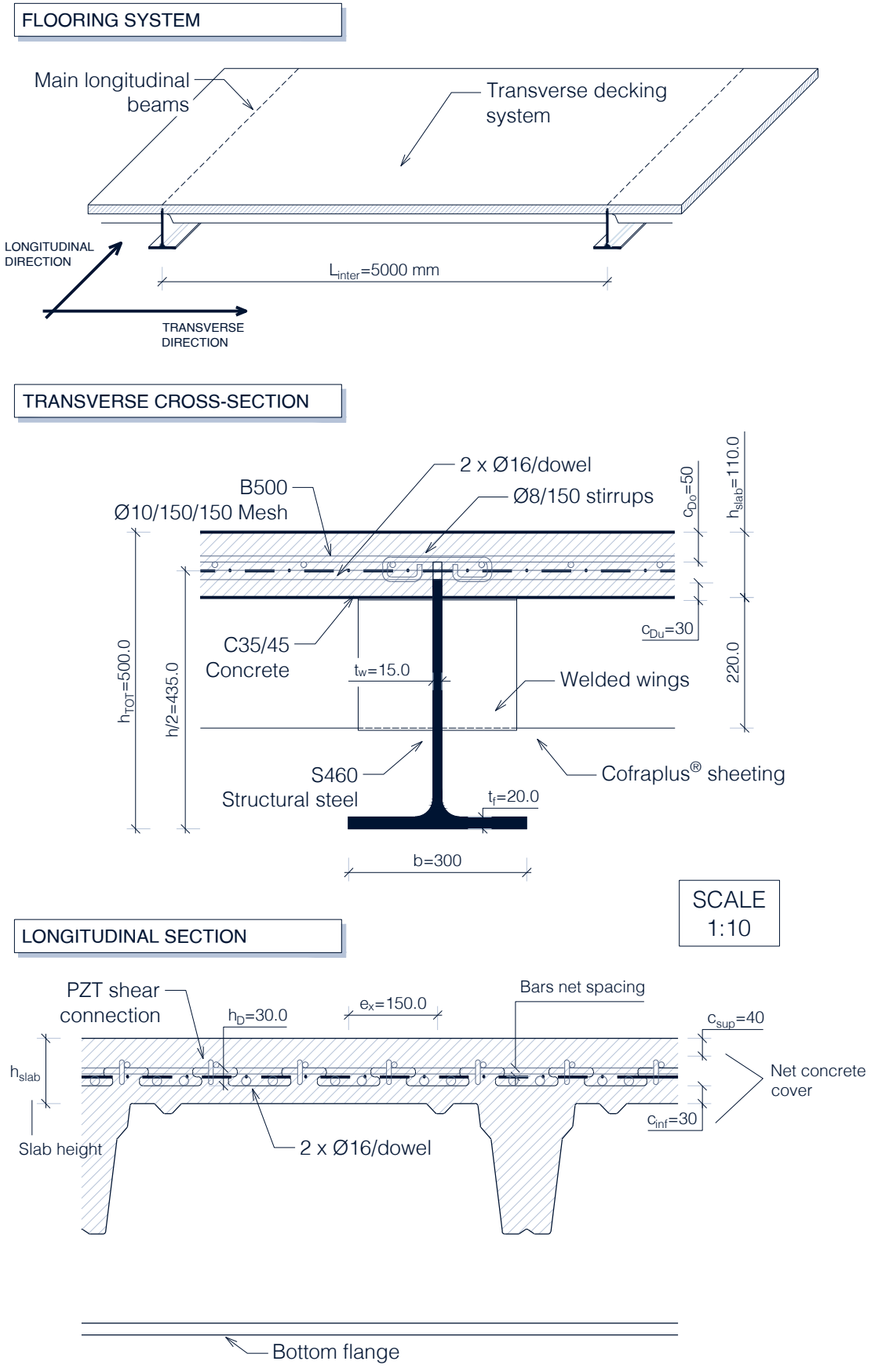

Figure B.2: case study configuration, geometry and materials

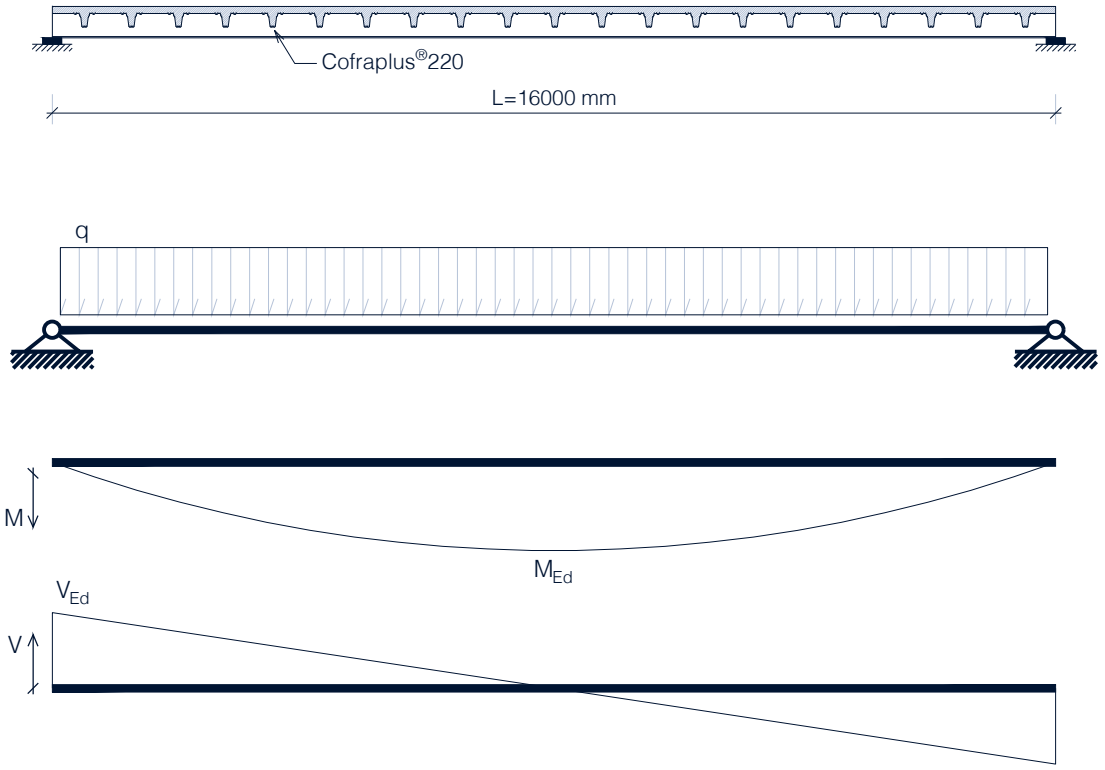

Figure B.3: static scheme, loading configuration and internal actions diagrams

Shear connection dimensions	
$e_x = 150\,mm$	Dowel size
$h_D = 30\,mm$	Dowel height
Hot rolled profile dimensions	
$h = 870.0\,mm$	Profile height
$b = 300.0\,mm$	Flange width
$t_w = 15.0\,mm$	Web thickness
$t_f = 20.0\,mm$	Flange thickness
$r = 30.0\,mm$	Fillet radius
Concrete part dimensions	
$h_{slab} = 110.0\,mm$	Slab height

The considered number of dowels in half-spanlength is:

$$n = \frac{L/2}{e_x} = 53 \tag{B.3}$$

In this case the concrete slab is placed relatively to the shear connection position in such a way that:

$$c_{D,u} = 30\,mm$$
$$c_{D,o} = 50\,mm$$

The dimensions $c_{Du} = 30\,mm$ and $c_{Do} = 30\,mm$ have to be provided according to the technical specification for the composite dowels. If the lower side pryout is prevented for the presence of a Cofraplus® sheeting, like in the present casestudy, the requirement on the c_{Du} value drops to a minimum of $c_{Du} = 20\,mm$. Despite of that, according to the actual technical specification, the pryout cone height h_{po} would drop by reducing c_{Du}. This is affecting also the dowel resistance, in particular for the pryout failure mode. Thus, the beam can be in a low degree of shear connection. Because of this reason a dimension of $c_{Du} = 30\,mm$ is used. Note that due to the XC4 exposure class of the reinforced concrete, according to EC2 a minimum of 40 mm of concrete cover has to be considered. This of course creates significant limitations if the designer wants to minimize the concrete slab height. A PZT dowel is considered leading to $h_D = 30\,mm$. A welded reinforcement mesh is put on the top of the dowel, leading to additional 6 to 10 mm depending on the reinforcement mesh diameter. With respect of this reinforcement external boundary an additional $40\,mm$ concrete cover has to be provided. By summing all of this contributes, the concrete slab height of $h_{slab} = 110\,mm$ is reached. According to the Cofraplus® design solution design manual, the profiled sheeting can be used without propping only if the concrete slab does not reach $120\,mm$.
An executive aspect is underlined. The Cofraplus® sheeting has an interaxis of $0.75\,m$. For simplicity in the design and executive process and compatibility of the reinforcement, this sheeting dimension has to be a multiple of the dowel size e_x and the transverse spacing of the welded mesh reinforcement positioned in the slab should also be spaced with the same amount e_x.

The section results in a total height of:

$$h_{TOT} = h/2 + h_D/2 + c_{D,u} = 500\,mm \tag{B.4}$$

The structural element has a slenderness of:

$$L/h_{TOT} = 32 \tag{B.5}$$

B.3.3 Effective width

The effective width is computed according to EC4 [11] and the calculation is summarized below.

$$L_{e,support} = 0.25 \cdot L = 4000\,mm \tag{B.6}$$

$$L_{e,midspan} = L = 16000\,mm \tag{B.7}$$

$$\beta_1 = \min\left(0.55 + 0.025 \cdot L/b_{e,1}; 1\right) = 0.6 \tag{B.8}$$

$$\beta_2 = \min\left(0.55 + 0.025 \cdot L/b_{e,2}; 1\right) = 0.6 \tag{B.9}$$

$$b_{eff} = b_{eff,midspan} = b_0 + b_{e,1} + b_{e,2} = 4000\,mm \tag{B.10}$$

$$b_{eff,support} = b_0 + \beta_1 \cdot b_{e,1} + \beta_2 \cdot b_{e,2} = 2500\,mm \tag{B.11}$$

B.3.4 Reinforcement

The reinforcement amount and position can be appreciated in Fig.B.2. Two transverse horizontal $\phi 16$ bars are provided per each concrete dowel. This results in:

$$(A_{sf,passing\,bars}/e_x) = \frac{2 \cdot 201}{150} = 2680\,mm^2/m \tag{B.12}$$

One transverse $\phi 8$ stirrup is provided per each dowel. A welded mesh of $\phi 8/150/150$ is placed on top of the shear connection. This provides an additional reinforcement density in the transverse direction and and a presence of longitudinal reinforcement:

$$(A_{sf,mesh}/e_x) = \frac{1 \cdot 50}{150} = 333\,mm^2/m \tag{B.13}$$

$$(A_{s,long}) = b_{eff}/150 \cdot 50 = 1333\,mm^2 \tag{B.14}$$

In the following sections the transverse reinforcement amount for each concrete dowel are referred as A_{b1} and the top transverse slab reinforcement per each dowel will be referred as A_{t1}. In this case:

$$A_{b1} = 2\phi 16 = 402\,mm^2 \tag{B.15}$$

$$A_{t1} = 1\phi 8 = 50\,mm^2 \tag{B.16}$$

B.3.5 Cross-section properties

In order to compute the following geometric quantities the y coordinate is introduced to identify the generic fibre of the section. The origin of the reference system is at the bottom part of the composite section, pointing upward. The reference coordinate of the shear connection position $y_{sh.connection}$ is:

$$y_{sh.connection} = h/2 = 435\,mm \tag{B.17}$$

The net height of the single T steel profile is:

$$h_{singleT} = h/2 - h_D/2 = 420\,mm \tag{B.18}$$

The structural steel area results in:

$$A_a = b \cdot t_f + t_w(h_{singleT} - h_f) = 120.0\,cm^2 \tag{B.19}$$

The centroid position of the steel part is:

$$y_{G,a} = (b \cdot t_f^2/2 + t_w(h_{singleT} - t_f) \cdot (t_f + h_{singleT}/2))/A_a = 115.0\,mm \tag{B.20}$$

The second moment of the steel part is:

$$\begin{aligned} I_a = {} & t_f \cdot b(t_f/2 - y_{G,a})^2 + t_w \cdot (h_{singleT} - h_f)((h_{singleT} + t_f)/2 - y_{G,a})^2 + \\ & + b \cdot t_f^3/12 + t_w(h_{singleT} - t_f)^3/12 = 21250.0\,cm^4 \end{aligned} \tag{B.21}$$

The lower surface of the concrete slab is placed at a distance from the bottom edge of the section of:

$$y_{c,bottom} = h/2 - h_D/2 - c_{D,u} = 390\,mm \tag{B.22}$$

The upper surface of the concrete slab is placed at a distance from the bottom edge of the section of:

$$y_{c,top} = h/2 + h_D/2 + c_{D,o} = 500\,mm \tag{B.23}$$

The area of the concrete part of the section is:

$$A_c = h_{slab} \cdot b_{eff} = 4400\,cm^2 \tag{B.24}$$

The centroid position of the concrete part is:

$$y_{G,c} = (y_{c,top} + y_{c,bottom})/2 = 445\,mm \tag{B.25}$$

The second moment of the concrete part is:

$$I_c = b_{eff} \cdot h_slab^3/12 = 44366.7\,cm^4 \tag{B.26}$$

The composite section geometric properties can be derived through an homogenization procedure of the section. The section is homogenized as an equivalent steel section. The homogenization coefficient n_0 is:

$$n_0 = \frac{E_s}{E_{cm}} = 6.16 \tag{B.27}$$

The coordinate of the centroid of the homogenized composite section is:

$$y_{G,homo} = (A_c \cdot y_{G,c}/n_0 + A_a \cdot y_{G,a})/(A_a + A_c/n_0) = 397.5\,mm \tag{B.28}$$

The second moment of the homogenized composite section is:

$$I_{homo} = I_a + I_c/n_0 + A_a \cdot (y_{G,a} - y_{G,homo})^2 + A_c/n_0 \cdot (y_{G,c} - y_{G,homo})^2 = 140326.5\,cm^4 \tag{B.29}$$

The bending stiffness of the steel section is defined as:

$$EI_a = E_a I_a \tag{B.30}$$

The bending stiffness of the composite section is defined as:

$$EI_{homo} = E_a I_{homo} \tag{B.31}$$

B.3.6 Loads

The structural permanent loads include the dead weights of the concrete and steel structural components. On the flooring system the characteristic values of loads per unit surface can be computed as follows:

Characteristic values of structural permanent loads per unit surface

$G_{1k,concrete} = \gamma_{concrete} \cdot h_{slab} + G_{1k,conc.ribs} = 3.77\,kN/m^2$

Here an additional contribute $G_{1k,conc.ribs}$ is added in order to take into account the Cofraplus® technology concrete ribs. These are equally spaced with a distance of $0.75\,m$. Thus the structural permanent characteristic loads per unit length acting on the main beam can be derived by multiplying the per unit surface values by the interaxis length:

Characteristic values of structural permanent loads per unit length

$g_{1k,concrete} = g_{1,concrete} \cdot L_{inter} = 18.85\,kN/m$

$g_{1k,steel} = \gamma_{steel} \cdot A_a = 1.26\,kN/m$

In the structural steel weight quantity the profiled steel sheeting weight is also included. This consists in a cold formed sheeting of $1.25\,mm$ thickness.
The non structural permanent loads include the finishing permanent layers of the carpark structure, thus comprehensive of the asphalt layer. The overall quantity that is used is:

Characteristic values of non structural permanent loads per unit surface

$G_{2k,decking} = 1.00\,kN/m^2$	Non structural permanent loads

The non structural permanent characteristic loads per unit length acting on the main beam can be derived by multiplying the per unit surface values by the interaxis length:

Characteristic values of non structural permanent loads per unit length

$g_{2k,decking} = G_{2k,decking} \cdot L_{inter} = 5.00\ kN/m$	Non structural permanent loads

The considered live load comes from the Eurocode 1 [7] and for a carpark destination is:

Characteristic values of live loads per unit surface

$Q_{k,Cat} = 2.50\ kN/m^2$	Live loads

The live loads per unit length acting on the main beam can be derived by multiplying the per unit surface values by the interaxis length:

Characteristic values of live loads per unit length

$q_{k,Cat} = Q_{k,Cat} \cdot L_{inter} = 12.50\ kN/m$	Live loads

The design values of the loads are:

$$Q_{d,ULS} = 1.35 \cdot G_{1k} + 1.35 \cdot G_{2k} + 1.50 \cdot Q_{k,Cat} = 10.20\ kN/m^2 \tag{B.32}$$

$$q_{d,ULS} = 1.35 \cdot g_{1k} + 1.35 \cdot g_{2k} + 1.50 \cdot q_{k,Cat} = 52.6\ kN/m \tag{B.33}$$

B.3.7 Design actions under fundamental load combination

Considering a simply supported beam under uniformly distributed loads leads to:

$V_{Ed} = q_{d,ULS} \cdot L/2 = 421.2\ kN$	Design shear at support
$M_{Ed} = q_{d,ULS} \cdot L^2/8 = 1684.7\ kNm$	Design bending moment at midspan

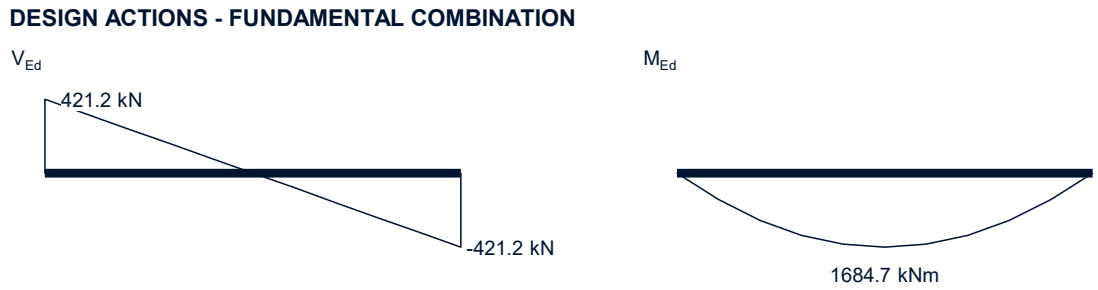

Figure B.4: design actions - fundamental combination

B.4 Geometric detailing checks

According to the reference technical standard for the composite dowels, the accomplishment of the following geometric detailing checks should be verified:

$t_w < 40\,mm$	Verified
$4\,mm < t_w < 60\,mm$	Verified
$c_{D,u} \geq 20\,mm$	Verified
$c_{D,o} \geq 30\,mm$	Verified
$t_f \geq t_w$	Verified
$(h_{singleT} - t_f) \geq 0.45 \cdot h_D$	Verified

B.5 Shear connection resistance

The shear connection resistance is computed according to the rules given in for the composite dowels.

The longitudinal shear resistance due to steel failure is computed as:

$$P_{pl,k} = \lambda_{geo} \cdot e_x \cdot t_w \cdot f_{yk} = 184.1\,kN \tag{B.34}$$

Where the value of λ_{geo} is $\lambda_{geo,PZT} = 0.186$.

The longitudinal shear resistance due to concrete shearing is:

$$P_{sh,k} = \eta_D \cdot e_x^2 \cdot \sqrt{f_{ck} \cdot (1 + \rho_D)} = 339.2\,kN \tag{B.35}$$

In this relation the values of $\eta_{D,PZT}$, ρ_D are:

$\eta_{D,PZT} = 1.4 - e_x/590 = 1.15$	Reduction factor for the surface of concrete dowel
$\rho_D = E_a \cdot A_b/(E_{cm} \cdot A_D) = 1.224$	Degree of reinforcement
$A_D = A_{D,PZT} = 0.09 \cdot e_x^2$	Area of concrete dowel for the chosen shape

The longitudinal resistance against pry-out of the concrete cone is determined by:

$$P_{po,k} = k_1 \cdot \chi_x \cdot \chi_y \cdot h_{po}^{1.5} \cdot \sqrt{f_{ck}} \cdot (1 + \rho_{D,i}) \cdot \psi_{crack} = 117.7\,kN \tag{B.36}$$

The concrete pryout cone height is:

$$h_{po} = \min\left(c_{D,o} + 0.05\,e_x;\; c_{D,u} + 0.06\,e_x\right) = 39.0\,mm \tag{B.37}$$

The used values are:

$k_1 = 71$	Factor for calculation of pry-out failure for a PZT shape
$\chi_x = 1 \quad for \quad e_x \geq 4.5 \cdot h_{po}$ $\chi_x = e_x/(4.5 \cdot h_{po}) \leq 1.0 \quad for \quad e_x < 4.5 \cdot h_{po}$ $\rightarrow \chi_x 1.00 =$	Reduction factor for overlapping of pry-out cones in longitudinal direction
$\chi_y = 1.0$	Reduction factor for overlapping of concrete cones in the transverse direction for one dowel strip
$\rho_{D,i} = E_a \cdot A_{sf}/(E_{cm} \cdot A_{D,i}) = 0.150$ $A_{D,i} = h_c \cdot e_x$	Reinforcement ratio for pry-out failure
$\psi_{crack} = \psi_{crack,PZT} = 1.0$	Reduction factor for transverse cracking of concrete due to longitudinal tensile stresses

The characteristic value of the shear connection longitudinal shear resistance $P_{S,Rk}$ is computed as follows:

$$P_{S,Rk} = \min\left(P_{pl,k}; P_{sh,k}; P_{po,k}\right) = 117.7\, kN \tag{B.38}$$

The design value of the longitudinal shear resistance $P_{S,Rd}$ is:

$$P_{S,Rd} = P_{S,Rk}/\gamma_v = 94.1\, kN \tag{B.39}$$

B.6 ULS vertical shear resistance check

The ULS vertical shear check is done in accordance with the forthcoming version of EC4. For the present case study no web openings have to be taken into account.

B.6.1 Plastic resistance to vertical shear

The plastic resistance to vertical shear $V_{pl,a,Rd}$ is computed in accordance with [9]. There is no torsional effect. The considered shear area A_v is:

$$A_v = A_a - b \cdot t_f + (t_w + 2r) = 6750.0\, mm^2 \tag{B.40}$$

$$V_{pl,Rd} = \frac{A_v \cdot f_y}{\sqrt{3} \cdot \gamma_{M0}} = 1714.7\, kN \tag{B.41}$$

No shear stress computation in accordance to for the composite dowels.

B.6.2 Shear buckling resistance

It must be determined whether shear buckling is prevented. This is done by verifying the following inequality:

$$h_w/t_w = 25.7 \leq 72/\eta \cdot \epsilon = 43.8 \qquad Verified \tag{B.42}$$

In this relation $\eta = 1.2$ is considered.

If the above written inequality had not been verified, the shear buckling resistance $V_{b,Rd}$ should have been determined in accordance with the forthcoming version of EC4. No account has been taken from the concrete slab contribution.

B.6.3 Shear design resistance

The shear design resistance is the lower between the shear buckling resistance and the plastic shear resistance. Thus:

$$V_{Rd} = \min\left(V_{pl,Rd}; V_{b,Rd}\right) = 1714.7\ kN \tag{B.43}$$

The V_{Ed}/V_{Rd} radio is:

$$V_{Ed}/V_{Rd} = 0.246 < 0.5 \tag{B.44}$$

The shear utilization ratio is less then 0.5. This implies that no account should be taken for moment-shear interaction according to EC4 [11].

B.7 ULS bending resistance check

The bending resistant moment is here computed according to two different methods. The first is a rigid plastic (RP) analysis. The second is a strain limitation (SL) method.

The strain limited analysis is conduced with a section discretization of 1 mm height fibres. The nonlinear material laws used are the parabola-rectangle according to EC2 [8] and an elastic-plastic hardening law for structural steel and reinforcement steel. A pure bending condition is assumed, thus $N = 0.00\ kN$ is imposed as equilibrium target. For the RP analysis the moment-curvature curve cannot be derived. In the SL analysis the moment-curvature diagram for a full interaction case is computed and is shown in Fig.B.6. The partial shear connection diagram is illustrated in Fig.B.5. The stress-strain relations on the section at failure are shown in Fig.B.7. In both results cases the shear connection position is above the PNA. So the shear connection is in the compression zone of the section.

At the ULS condition with full shear interaction assumption the following quantities are derived in the analysis:

$(1/r)_u = 4.30 \times 10^{-5}\ 1/mm$	Ultimate curvature of the composite section
$x_u = 79.3\ mm$	Neutral axis position at failure
$M_{pl,f,Rd} = 1857.1\ kNm$	Plastic resistant design bending moment under full shear interaction assumption
$N_{cf} = 5145.0\ kN$	Concrete compression force at ULS condition with full shear interaction assumption
Concrete crushing	Failure type (ULS condition)

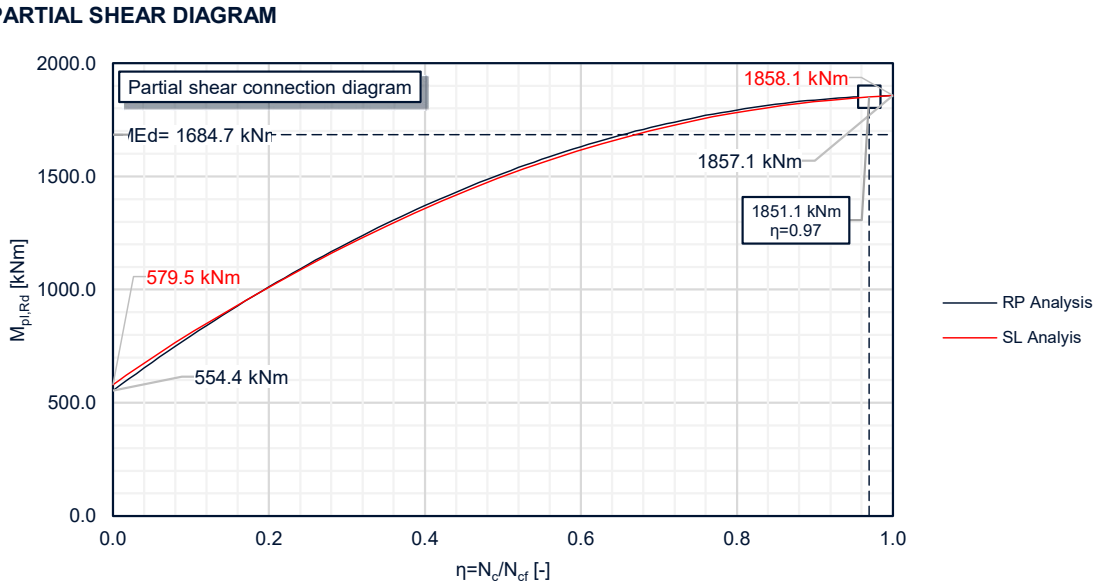

Figure B.5: Partial Shear Diagram (PSD)

The degree of shear connection can be derived as follows:

$$\eta = n \cdot P_{S,Rd}/N_{cf} = 0.97 \tag{B.45}$$

By a simplified approach this means that plastic redistribution occurs, as $\eta < 2$ and furthermore the partial shear connection case is reached as $\eta < 1$. Thus the maximum shear flow along the beam is exactly the one associated with the dowel plastification:

$$v_{L,max} = P_{S,Rd}/e_x = 627.6\ kN \tag{B.46}$$

By exploiting the partial shear connection diagram derived in the SL analysis, the plastic bending resistant design moment for the calculated degree of shear connection η is:

$$M_{pl,Rd} = M_{pl,Rd}(\eta = 0.97) = 1851.1\ kNm \tag{B.47}$$

The bending ULS resistant check consists in:

$$M_{Ed}/M_{pl,Rd} = \frac{1681.6}{1851.1} = 0.908 \leq 1.0 \tag{B.48}$$

Summarizing the results, the composite element is in a partial shear connection condition with redistribution along the shear connection. The ULS bending checks are satisfied and the solution presents a high utilization ratio in bending. From the moment curvature diagram a ductile behaviour is observed.

B.8 ULS longitudinal shear in concrete slab check

According to EC4 [11] the forthcoming version of EC4 part 8.6.11 longitudinal shear failure of the concrete slab shall be prevented. Here two potential shear failure surfaces are checked. Failure surface a-a and failure surface b-b according to Fig.B.8 are considered.

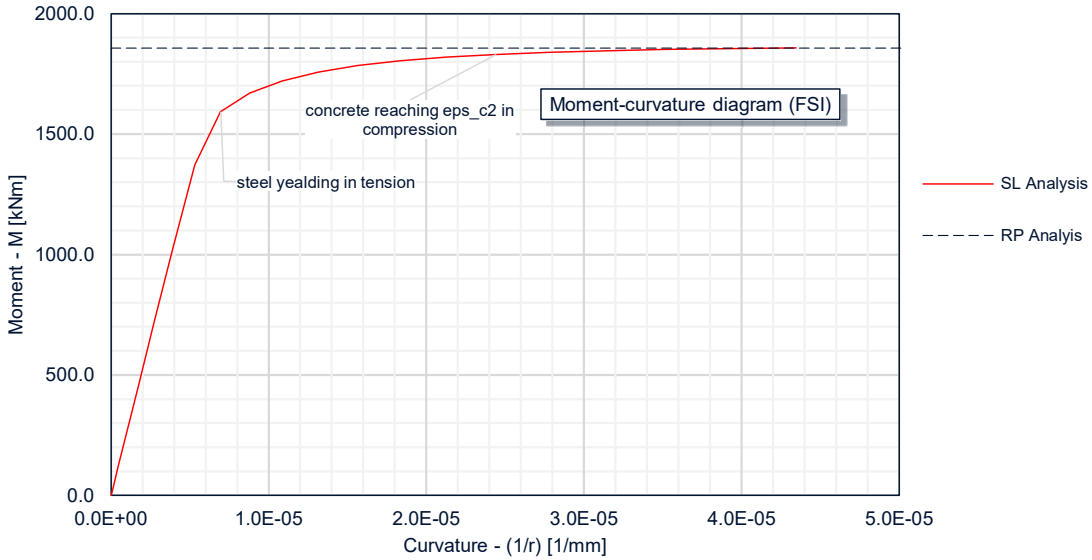

Figure B.6: moment-curvature diagram in Full Shear Interaction (FSI) condition

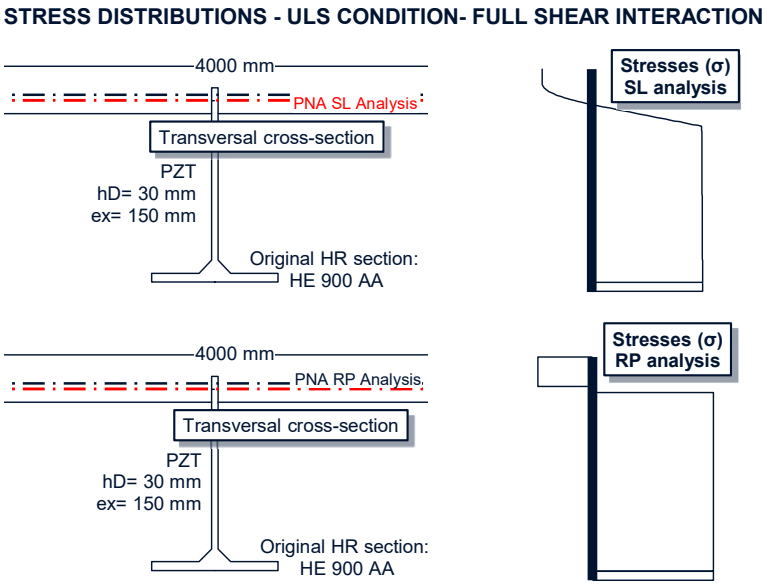

Figure B.7: stress distributions derived from RP and SL analysis

B.8.1 Model overview

According to the reference design codes a strut-and-tie model contained in the slab is used in order to do the checks. The truss model is symmetric to the longitudinal beam axis. The local bearing force transmitted by a steel dowel to the concrete slab diffuses through the slab according to inclined struts. The diffusion angle can be chosen in the range $[26.5, 45]$. Here the chosen angle is:

$$\theta = 45 \qquad \rightarrow \qquad \cot\theta = 1.00 \tag{B.49}$$

The transverse force component is balanced by the passing bars that have to resist the tensile force. Both the shear resistance of the concrete slab and the resistance of the passing bars have to be checked. The shear resistance of the concrete slab is computed according to []. Here the value v_{Rd} has to be computed:

$$v_{Rd} = \nu \cdot f_{cd} \cdot \sin\theta\cos\theta = 6.02\, MPa \tag{B.50}$$

Here $\nu = 0.6(1 - f_{ck}/250) = 0.516$ according to [8] is used.

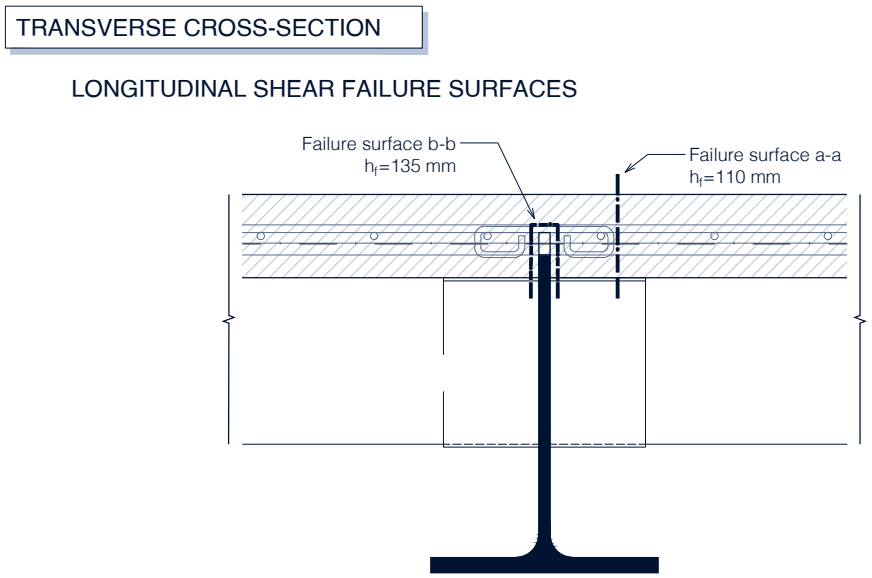

Figure B.8: failure surfaces considered in the longitudinal shear checks

B.8.2 Failure surface a-a

In failure surface a-a the considered shear flow is half the maximum force transmitted by the dowel to the concrete slab divided by the dowels spacing, namely:

$$v_{L,a-a} = 1/2 \cdot P_{S,Rd}/e_x = 313.8\, kN/m \tag{B.51}$$

This shear flow transits through a surface of unit longitudinal length and a height equal to the concrete slab height h_{slab}:

$$h_{f,a-a} = h_{slab} = 110\, mm \tag{B.52}$$

So, the shear stress can be computed by considering the shear flow v_L and dividing it by the slab height h_{slab}:

$$v_{Ed,a-a} = v_L/h_{slab} = 2.85\,MPa \tag{B.53}$$

The shear stress is compared with the shear concrete resistance of the concrete slab and the first check is carried out:

$$v_{Ed,a-a} = 2.85\,MPa \leq v_{Rd} = 6.02\,MPa \qquad \text{Verified} \tag{B.54}$$

The transverse component of the transmitted bearing force which is $P_{S,Rd}/\cot\theta$ should be balanced by the transverse reinforcement tensile force. At limit this force should be equal to the one at yielding point of the reinforcement:

$$1/2 \cdot P_{S,Rd}/\cot\theta \leq A_{sf,a-a} \cdot f_{sd} \tag{B.55}$$

The reinforcement amount $A_{sf,a-a}$ accounted here is the quantity $A_{b1} + A_{t1}$ that is the transverse steel bars area per each dowel. The reinforcement density here is $A_{sf,a-a}/s_f$ where s_f is the spacing of the transverse bars that coincides with the dowel spacing e_x. In term of shear flow the same expression can be expressed as follows, by dividing both sides by $e_x = s_f$:

$$v_{L,a-a}/\cot\theta \leq A_{sf}/s_f \cdot f_{sd} \tag{B.56}$$

or equivalently:

$$v_{Ed,a-a}\, h_{f,a-a}/\cot\theta = 313.8\,kN/m \leq A_{sf,a-a}/s_f \cdot f_{sd} = 1311.3\,kN/m \tag{B.57}$$

A minimum amount of transverse reinforcement can be computed as:

$$(A_{sf,a-a}/s_f)_{min} = \frac{v_{Ed,a-a}\, h_{f,a-a}}{\cot\theta f_{sd}} = 7.21\,cm^2/m \tag{B.58}$$

$$((A_{b1} + A_{t1})/s_f)_{min} = (A_{sf,a-a}/s_f)_{min} = 7.21\,cm^2/m \leq ((A_{b1} + A_{t1})/e_x) = 30.1\,cm^2/m \tag{B.59}$$

B.8.3 Failure surface b-b

In the failure surface b-b the total force flowing through the surface is all the force transmitted by the steel dowel to the concrete slab. So:

$$v_{L,b-b} = P_{S,Rd}/e_x = 627.6\,kN/m \tag{B.60}$$

This shear flow transits through a surface of unit longitudinal length and a perimeter equal to $h_{f,b-b}$:

$$h_{f,b-b} = 2(c_{Du} + h_D) + t_w = 135.0\,mm \tag{B.61}$$

The considered reinforcement area here is just the bottom amount $2A_{b1}$ according to the forthcoming version of EC4: The two checks, are done similarly as before, and consist in:

$$v_{Ed,b-b} = 4.65\,MPa \leq v_{Rd} = 6.02\,MPa \qquad \text{Verified} \tag{B.62}$$

$$v_{Ed,b-b}\, h_{f,b-b}/\cot\theta = 627.6\, kN/m \leq A_{sf,b-b}/s_f \cdot f_{sd} = 2331.2\, kN/m \tag{B.63}$$

A minimum amount of transverse reinforcement can be computed as:

$$(A_{sf,b-b}/s_f)_{min} = \frac{v_{Ed,b-b}\, h_{f,b-b}}{\cot\theta f_{sd}} = 14.46\, cm^2/m \tag{B.64}$$

$$(A_{b1}/s_f)_{min} = 1/2 \cdot (A_{sf,b-b}/s_f)_{min} = 7.23\, cm^2/m \leq (A_{b1}/e_x) = 26.8\, cm^2/m \tag{B.65}$$

B.8.4 Minimum reinforcement ratio check

The minimum reinforcement ratio check is done in accordance with EN1994-1-1, 6.6.6.3 [11] and EN1992-1-1, 9.2.2(5) [8]. The transverse reinforcement density is:

$$\left(\frac{A_{sw}}{s_w}\right) = (A_{b1} + A_{t1})/e_x = 3204\, mm^2/m \tag{B.66}$$

This leads to the transverse reinforcement density:

$$\rho_w = \frac{(A_{sw}/s_w)}{h_{slab}} = 2.742\,\% \tag{B.67}$$

The following inequality should be checked:

$$\rho_{w,min} = 0.08\frac{\sqrt{f_{ck}}}{f_{sk}} = 0.095\,\% \leq \rho_w \qquad \text{Verified} \tag{B.68}$$

B.9 SLS stress computations

The stresses are computed according to an effects summation due to all load contributes taking into account the concrete creep, the shrinkage, the load history and the construction stages. Here a propped construction is considered. The concrete properties and geometric values are:

N	Cement type according to [8]
RH=50%	Considered relative humidity (RH)
$u = 2L_{inter} = 10000\, mm$	Perimeter of the concrete part exposed to drying
$A_c = 4400\, cm^2$	Concrete sectional area subjected to drying
$h_0 = 2A_c/u = 110\, mm$	Equivalent hydraulic radius

Following construction stages are considered:

Considered loading stages	
t=0 days	Concrete pouring
t=28 days	Propping removal
t=100 days	First loading
t=infinity	Long term effect

At the different times, the concrete elastic modulus is computed as:

$$E_{c,eff}(t) = \frac{E_{cm}}{1 + \psi_L \cdot \phi(t, t_0)} \tag{B.69}$$

Consequently, the homogenization factor n is:

$$n_L(t) = \frac{E_s}{E_{c,eff}(t)} = \frac{E_s}{E_{cm}} \cdot (1 + \psi_L \cdot \phi(t, t_0)) = n_0 \cdot (1 + \psi_L \cdot \phi(t, t_0)) \tag{B.70}$$

Note that this coefficient is both dependent on the loading type (L subscript) and its application instant t_0 and also to the considered time.

Permanent structural loads are considered to be applied at the same time of the propping removal. The accounted loading contributes together with the application instant t_0 and the related load types are:

Considered loading contributes

Load	t_0 [days]	Load type and ψ_L
G1 - steel profile	28	Permanent loading
G1 - concrete	28	Permanent loading
G2 - decking system	100	Permanent loading
Q - category load	100	Short term loading
Shrinkage	2	Shrinkage effect

The various moment contributes $M_{d,i}$ are computed according to:

$$M_{d,i} = q_{d,i} \cdot L^2/8 \tag{B.71}$$

A shrinkage strain value of $\epsilon_{cs} = 325 \times 10^-6$ is used according to the forthcoming version of EC4. As the shrinkage exhibits, the shortening of the concrete slab is impeded by the steel part of the element which is not subject to shrinkage. The internal constraint conditions generate an internal stress state which is self balanced and creates on the section an additional positive bending moment. In the steel part a compression with a bending component generates, while on the concrete part a tensile state with a bending component generates. The total positive additional moment acting on the section due to shrinkage of concrete is M_{cs}. The value of this moment is generally computed in a simplified way (neglecting the strain due to compression on the steel) as $\epsilon_{cs} \cdot E_{c,eff}(t) A_c$. Note that this force is time dependent, because of the fictitious dependency of the elastic modulus of concrete which is introduced to simulate the time dependent effect of creep. The tensile resultant force acts in correspondence of the centroid of the concrete part y_c. So with respect of the composite section, the lever arm of the force will be the difference between this point and the centroid of the composite section. Note that this last value is also dependent on time.

The moment due to shrinkage is:

$$M_{cs} = \epsilon_{cs} \cdot E_{c,eff}(t) A_c \cdot (y_c - y_{G,homo,cs}(t)) \tag{B.72}$$

Note that every load contribute has a different homogenization factor $n_{L,i}$. This is because of the different load coefficients ψ_L and of the different load application times t_0. Thus, for every load contribute a different

effective second moment of section and a different centroid position of the homogenized section exists. For every load contribute i the related effective second moment of section can be computed:

$$I_{eff,i}(t) = I_a + \frac{I_c}{n_{L,i}(t)} + A_a \cdot (y_{G,a} - y_{G,homo,i})^2 + \frac{A_c}{n_{L,i}(t)} \cdot (y_{G,c} - y_{G,homo,i})^2 \tag{B.73}$$

Here the neutral axis position of the homogenized steel section is $y_{G,homo}$:

$$y_{G,homo,i}(t) = \frac{A_a \cdot y_{G,a} + A_c \cdot y_{G,c}/n_{L,i}(t)}{A_a + A_c/n_{L,i}(t)} \tag{B.74}$$

For the given time t the total stress acting at a particular point of the composite section can be computed by adding linearly the contributes. Note that in case of concrete cracking the phenomena would became nonlinear and an effects linear summation would not be suitable. However it has to be recognized that all the applied method is a simplified approach. First of all because of the linear effects summation of the creep effect which a nonlinear phenomena, and because of the simplified method for the homogenization factor of the concrete. Moreover, no reliable literature has been found on how to consider the effect of concrete cracking in the stress distribution computation. If a rigorous computation of the effects of concrete cracking is requested, a more sophisticated analysis should be carried out. So, for the present computation, in order to preserve the simplicity of the calculation method, it was decided not to take into account potential effects of concrete cracking at this computational stage. If tensile stresses greater than the concrete tensile resistance f_{ctm} are detected, a following reduction of the stiffness of the composite element will be carried out.

The significant points of the section where the stresses have to be computed are the top and the bottom fibers of both the concrete part and the steel part of the section, namely:

$$\sigma_{c,inf}(t) \qquad \text{normal stress on the bottom concrete fibre} \tag{B.75}$$

$$\sigma_{c,sup}(t) \qquad \text{normal stress on the top concrete fibre} \tag{B.76}$$

$$\sigma_{a,inf}(t) \qquad \text{normal stress on the bottom steel fibre} \tag{B.77}$$

$$\sigma_{a,sup}(t) \qquad \text{normal stress on the top steel fibre} \tag{B.78}$$

Stresses are therefore derived by an effect summation. Here the load contributes i accounted for are the ones applied before the considered time, i.e. $t > t_{0,i}$:

$$\sigma_{c,inf}(t) = \frac{1}{n_{L,i}(t)} \cdot \sum_{i=1}^{\text{load contrib.}} \frac{M_{d,i}}{I_{eff,i}(t)} \cdot y_{c,inf} + \frac{1}{n_{L,i}(t)} \cdot \frac{M_{cs}}{I_{eff,cs}(t)} y_{c,inf} + E_{c,eff,cs}(t)\epsilon_{cs} \tag{B.79}$$

$$\sigma_{c,sup}(t) = \frac{1}{n_{L,i}(t)} \cdot \sum_{i=1}^{\text{load contrib.}} \frac{M_{d,i}}{I_{eff,i}(t)} \cdot y_{c,sup} + \frac{1}{n_{L,i}(t)} \cdot \frac{M_{cs}}{I_{eff,cs}(t)} y_{c,sup} + E_{c,eff,cs}(t)\epsilon_{cs} \tag{B.80}$$

$$\sigma_{a,inf}(t) = \sum_{i=1}^{\text{load contrib.}} \frac{M_{d,i}}{I_{eff,i}(t)} \cdot y_{a,inf} + \frac{M_{cs}}{I_{eff,cs}(t)} y_{a,inf} - A_c E_{c,eff,cs}(t)\epsilon_{cs}/A_a \tag{B.81}$$

$$\sigma_{a,sup}(t) = \sum_{i=1}^{\text{load contrib.}} \frac{M_{d,i}}{I_{eff,i}(t)} \cdot y_{a,sup} + \frac{M_{cs}}{I_{eff,cs}(t)} y_{a,sup} - A_c E_{c,eff,cs}(t)\epsilon_{cs}/A_a \tag{B.82}$$

The shear stresses are considered to be balanced just by the steel profile. This is because of the smaller elastic modulus, the smaller partial static moment, and the large width of the concrete slab that in the Jourawski formula would return small shear stresses on the concrete part. So the concrete slab contribute is neglected. This simplification is reasonable and furthermore implies that no homogenization should be carried out. Moreover it stays on the safe side. The generic shear stress on the steel part is computed as:

$$\tau(y) = \frac{V_d \cdot S^*(y)}{b(y) \cdot I_a} \tag{B.83}$$

The maximum shear stress on the steel web is computed according to the Jourawski formula at steel neutral axis height which is the steel centroid position τ_{max}:

$$\tau_{max} = \tau(y_{G,a}) = \frac{V_d \cdot S^*(y_{G,a})}{b(y_{G,a}) \cdot I_a} \tag{B.84}$$

Here the considered shear action is derived with a linear summation of the shear contributes due to the various loads:

$$V_d = \sum_{i=1}^{\text{load contrib.}} V_{d,i} \qquad V_{d,i} = q_{d,i} \cdot L/2 \tag{B.85}$$

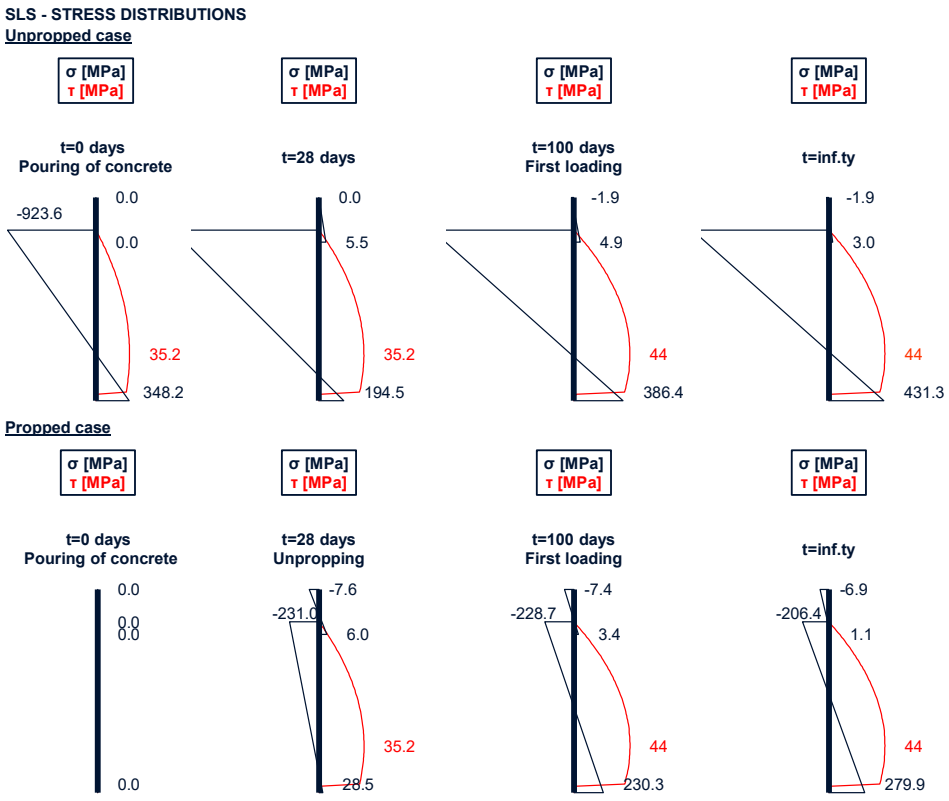

Figure B.9: SLS normal and shear stress distributions

B.10 SLS deflection check

The total deflection $\delta_{TOT}(t)$ at a specific time t is computed as the sum of the permanent plus the shrinkage $\delta_{cs+g}(t)$, the live load $\delta_q(t)$ and the precamber δ_c contributes:

$$\delta_{TOT}(t) = \delta_{cs+g}(t) + \delta_q(t) - \delta_c \tag{B.86}$$

A precambering δ_c of the beam is considered. This amount is a design value. The precambering contribute is prescribed in order to balance the deflection under permanent loads and shrinkage at time infinite. Thus, the total deflection under long term load is computed by adding the different contributes of the permanent loads and the shrinkage contribute:

$$\delta_{g+cs}(t) = \sum_{i=1}^{G_1+G_2 \text{ contrib.}} \frac{5}{384}\frac{q_{d,i}L^4}{E_s I_{homo,i}(t)} + \frac{1}{8}\frac{M_{cs}L^2}{E_s I_{homo,cs}(t)} \tag{B.87}$$

Effects of partial shear interaction due to the shear connection deformation are taken into account with:

$$EI_p = EI_a + N/N_{cf}(EI_{homo} - EI_a) \tag{B.88}$$

Here effects of cracking have been taken into account by taking:

$$EI_{homo,red} = 0.5(EI_{I,homo} + EI_{II,homo}) \tag{B.89}$$

In this last equation EI_I, EI_{II} are respectively the bending stiffness in case of non cracked section (state I), and cracked section (state II).
So the chosen value δ_c is:

$$\delta_c = \delta_{g+cs}(t \to \infty) = 130.7\, mm \tag{B.90}$$

Note that the value L/δ_c is at around 120. In general the precambering is clearly visible in high performance composite steel concrete building solutions. In this circumstances the total deflection under long term action is:

$$\delta_{TOT}(t \to \infty) = \delta_q(t \to \infty) = \frac{5}{384}\frac{q_{Cat}L^4}{E_s I_{homo,q}(t=\infty)} = 36.4\, mm \tag{B.91}$$

Due to the fact that concrete cracks, a reduction in stiffness occurs and a consequent larger deflection shows. The deflection check consists in limiting the deflection-span $\delta_{TOT}(t)/L$ length ratio at a specific value. Here this value is chosen to $1/250$, so:

$$\delta_{TOT}(t)/L = 1/439 \leq \delta_{lim}/L = \frac{1}{250} \qquad \text{Verified} \tag{B.92}$$

The SLS deflection check is therefore verified, and the prescribed amount of precambering is $\delta_c = 130mm$.

B.11 SLS vibrations check

The vibration frequency is limited to a value of $f_{lim} = 2.30\, Hz$. The proper frequency of the structure can be assessed according to various methods. Due to the simplicity in the static scheme no sophisticated

analysis is used here, instead the assessment is carried out just by using literature formulations. These formulations are derived according to dynamic theory of structures. The actual structural proper first mode vibration frequency is here computed according to the methods provided by the technical document [50].

$$f = \frac{\pi}{2} \cdot \sqrt{\frac{\alpha_{b,dyn} E_s I_{homo,dyn}}{\mu L^4}} \tag{B.93}$$

Here the $\alpha_{b,dyn}$ coefficient takes into account that at serviceability condition the static scheme is not a perfect pinned-pinned situation and restraints are an intermediate situation between pinned-pinned $\alpha_{b,dyn} = 1$ and clamped-clamped $\alpha_{b,dyn} = 5$. Supports can in fact in a serviceability condition provide a non zero reaction moment, partially impeding the support rotation. Considering a pinned-pinned static scheme would surely be on the safe side. Moreover the value of μ consists in the distributed modal mass per unit length of beam:

$$\mu = g_d/9.81 \approx (g_1 + g_2)/10 = 2503.6\ kg/m \tag{B.94}$$

The second moment of inertia of the section is corrected taking into account the dynamic elastic modulus of concrete $E_{c,dyn}$ instead of the common mean value E_{cm} and the short term condition is considered. The value of $E_{c,dyn}$ is derived by increasing the value of E_{cm} by 10%.

$$I_{homo,dyn} = I_a + \frac{E_{c,dyn}}{E_s} I_c + A_a (y_{G,a} - y_{G,homo})^2 + \frac{E_{c,dyn}}{E_s} A_c (y_{G,c} - y_{G,homo})^2 = 142656\, cm^4 \tag{B.95}$$

The frequency and the related check results in:

$$f = 3.00 \geq f_{lim} = 2.30\ Hz \qquad \text{Verified} \tag{B.96}$$

The frequency and the related check results in:

$$f(\alpha_{b,dyn} = 2.0) = 3.00\ Hz \tag{B.97}$$

$$f(\alpha_{b,dyn} = 1.0) = 2.12\ Hz \tag{B.98}$$

B.12 Comparison with classical solution

A common solution in composite structures is the adoption of a double T hot rolled profile with a top concrete slab. Head stud connectors are used as shear connection devices. A particular configuration with a high performance degree is that exploiting an IPE550A profile, in conjunction with a Cofraplus decking technology. The final solutions has a high degree of utilization and minimizes the amount of steel used in the construction. One example of external park structure exploiting this technology is the one in Belval (Luxembourg), shown in Fig.B.10. In this case a solution with bars sustaining the Cofraplus sheeting is adopted. A welded wings solution can also be chosen.
A rendering of the traditional IPE550A solution is given in Fig.B.11. This has been taken from the technical document where additional technical information can be found.

Figure B.10: an example of carpark application of the IPE550A solution. Sheeting is not fixed with welded wings in this configuration: bars welded on the top flange are used for supports.

A calculation of this solution can be made quickly with the ABC Software [20] which provides a practical tool for simply supported composite beams calculations. A comparison is done in the subsequent paragraphs with the HE900AA with composite dowels solution that has been presented so far. The direct comparison of the two sections is made in Fig.B.12. In both solutions the used materials are an S460 structural steel, a C35/45 concrete, a B500 reinforcement steel. The considered spanlengths and interaxis lengths are the same and equal to $L = 16000\ mm$ and $L_{inter} = 5000\ mm$ respectively. While in the single T HE900AA solution the composite connection is made by the composite dowels, in the double T IPE550A option the shear connection is realized with diameter 22 mm, height 75 mm welded studs. The studs are aligned in a single row with uniform spacing of $e_x = 150\ mm$. In the double T solution an upward translation of the Cofraplus sheeting of 20mm is provided. This allows for minimizing the concrete slab height at a height of 80 mm, thus reducing the dead weight of the concrete. This solution presents a total height of 647 mm, thus leading to a slenderness of $(L/h_{TOT})_{IPE550A} = 16000/647 \approx 25$. The double T HE900AA solution has already been proven to satisfy the checks, in this case the slenderness is $(L/h_{TOT})_{HE900AA} = 16000/647 \approx 32$. Under this perspective the novel composite dowels solution is demonstrating competitiveness and advantages. The traditional double T solution presents a structural steel weight of $92.1\ kg/m$. If the head studs amount is included this increases to $(G)_{IPE550A} = 94\ kg/m$. Differently, the novel single T HE900AA solution presents an amount of steel of $(G)_{HE900AA} = 99\ kg/m$. Here no additional weight for the shear connection has to be added. The Cofraplus sheeting steel amount is the same in the two solutions, thus not being a discriminant factor.

By exploiting the ABC software [20] results can be derived. A direct comparison of the main results between the two solutions is given in the subsequent table.

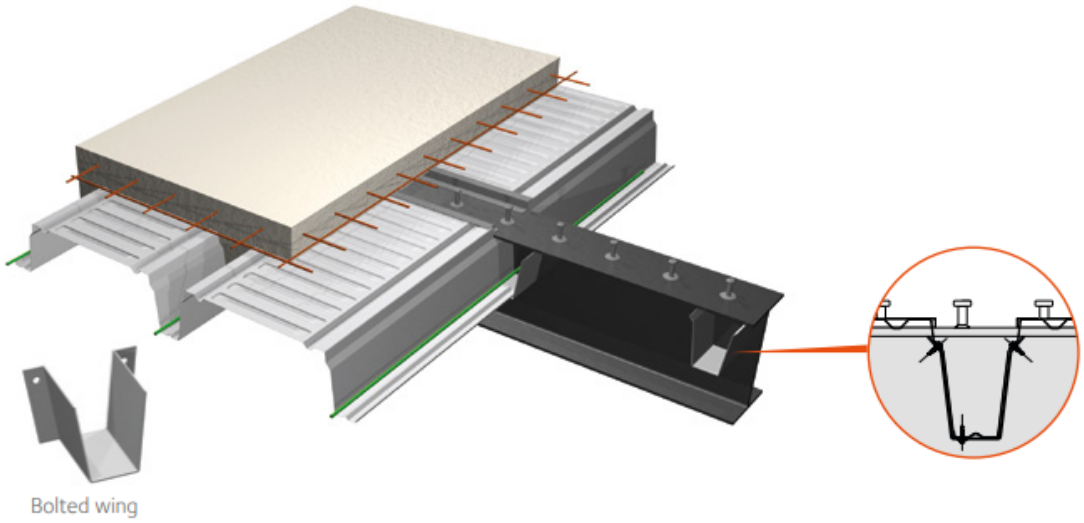

Figure B.11: IPE550A solution rendering

ABC software results

Parameter	IPE550A double T solution	HE900AA single T solution	
G	$94.0\ kg/m$	$99.0\ kg/m$	Structural steel amount
$M_{Ed,max}$	$1524.54\ kNm$	$1684.7\ kNm$	Design bending moment at midspan (fundamental combination)
$V_{Ed,max}$	$381.11\ kN$	$421.2\ kN$	Design shear action st support (fundamental combination)
$V_{Ed,max}/V_{Rd,pl}$	0.202	0.246	Utilization ratio for shear action
P_{Rd}	$108.14\ kN$	$94.1\ kN$	Design resistance of the connectors
$M_{pl,Rd}$	$1712.56\ kNm$	$1851.1\ kNm$	Plastic resistant design bending moment
$M_{Ed}/M_{pl,Rd}$	0.89	0.908	Plastic resistant design bending moment
η	$1.204 > 1.00$	$0.908 > 1.00$	Degree of shear connection
	FSC	PSC	Full (FSC) vs. Partial (PSC) Shear Connection
	0.996	0.772	Longitudinal shear utilization ratio
$(A_{sw}/s_w)_{min}$	$5.99\ cm^2/m$	$7.23\ cm^2/m$	Minimum transverse reinforcement for longitudinal shear
δ_c	$143\ mm$	$130\ mm$	Precambering
δ_Q	$33\ mm$	$36.4\ mm$	Deflection under live loads
f	$2.38\ Hz$	na*	Vibration frequency for a perfect pinned-pinned static scheme and with only the permanent load as modal mass

*The value can not be compared due to the different static scheme assumed

The solution, analogously to the novel single T option, presents a high degree of utilization both in bending

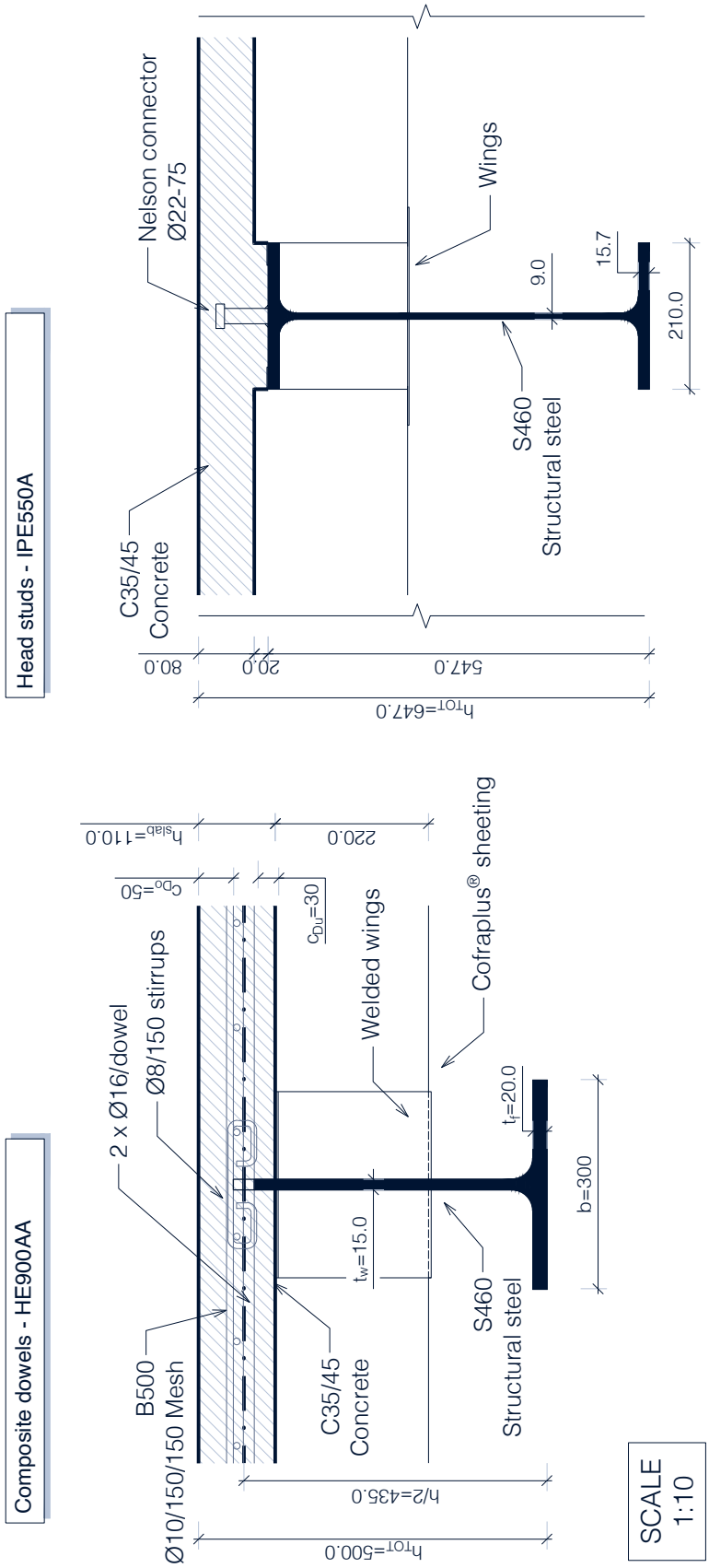

Figure B.12: comparison of the two solutions

and under vertical shear. The precambering and the deflection under live loads are in both cases similar. The vibration frequency comparison is not immediate as the ABC software considers a perfectly pinned-pinned situation (parameter $\alpha_b = 1.0$), while the single T section was computed with imperfect pins at the beam ends (parameter $\alpha_b = 2.0$. While the double T solution stands in a full shear connection condition (FSC), the single T solution slightly stands in a partial shear connection condition (PSC).

In conclusion the IPE550A solution with a traditional head studs shear connection can minimize the structural steel weight. The difference in the two solutions under this point of view is of the order of 5%. On the other hand if the main objective of the project is to reduce the structural height of the decking system the single T HE900AA option consists in a valid solution. Here the slenderness is significantly higher. The slenderness gets in fact increased by a +25% order.

B.13 Computational report

PreCoBeam Floor beams system - Design sheet v.1.02

Created by UNITN / AMR&D: CIA061-22
Author: **Francesco PROFICO**
Check: Riccardo ZANON

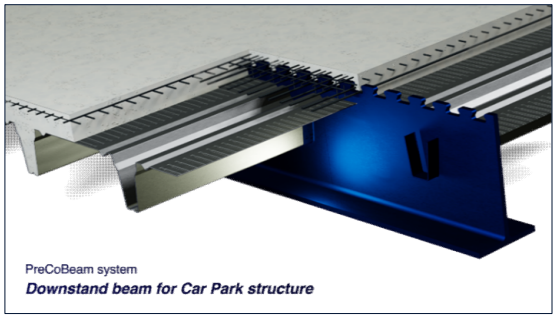

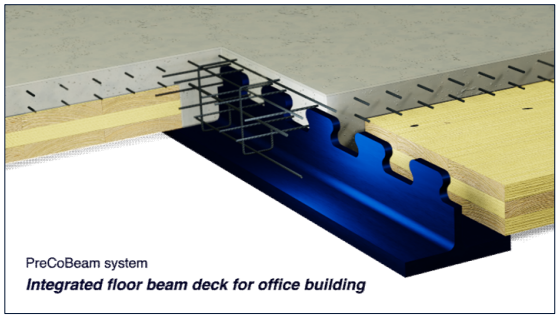

1) Reference

Project reference:	**Test car park project**	User:	**Gustave EIFFEL**
Beam Reference:	**Internal beam**	Company:	**Eiffel Cie**

2) Scope of the calculation sheet

Design is based on structural Eurocodes (EN1990; EN1992-1-1; EN1993-1-1; EN1994-1-1) as well as CEN-TS - Composite dowels (Draft version 2022).
Materials according EN1994-1-1 - Section 3. Structural steel: EN10025-2, -3, -4, -5:2019; ETA-10/0156; Reinforcement: EN10080:2005; Concrete: EN206
Section: composite section with concrete slab (eventually with concrete web) and single T structural steel profile obtained with cutting process from an hot-rolled H section.
Shear connection: continuous shear connection in accordance with "CEN-TS-Composite dowels" document.
Element: Simply supported composite element with section and shear connection in accordance with previous assumptions. Application field: Buildings
Loads: only uniformly distributed loads. Concentrated loads are NOT covered.
Structural analysis: strain-based design of the cross-section resistance, redistribution of shear flow based on a ductile shear connection.
Verification procedure: semi-probabilistic at limit states approach with safety factors.

3) Input fields

Input field	Main input values	Ref.	References
Input field	General input field with default values (not necessary to modify)	Text	Specifications
Output field	Calculated value	Key:	Comments

4) General geometric parametes

ORIGINAL HOT ROLLED SECTION

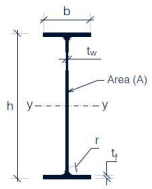

DOWEL SHAPES

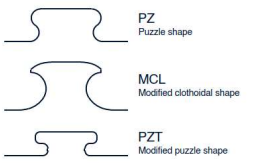

CONCRETE

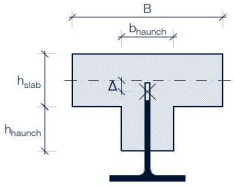

GEOMETRIC PARAMETERS

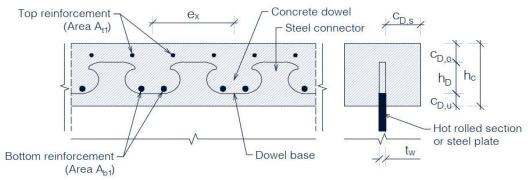

ELEMENT DIMENTIONS

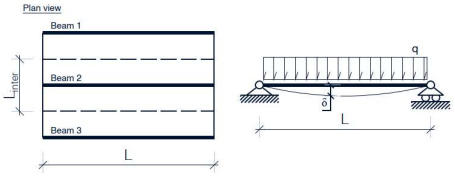

5) Parameters presentting

Partial safety factors

Materials
Ref. EN1994-1-1, 2.4.1

γ_c [-]	1.50	
γ_M [-]	1.00	
γ_v [-]	1.25	
γ_{M0} [-]	1.00	
γ_s [-]	1.15	
γ_{M1} [-]	1.00	
$\gamma_{M,fi,a}$ [-]	1.00	Ref. prEN1994-1-2, 4.5(1)
$\gamma_{M,fi,c}$ [-]	1.00	Ref. prEN1994-1-2, 4.5(1)
$\gamma_{M,fi,s}$ [-]	1.00	Ref. prEN1994-1-2, 4.5(1)

Actions

Load type	γ_{UNFAV} [-]	
γ_{G1} [-]	1.35	Permanent loads: structural
γ_{G2} [-]	1.35	Permanent loads: non structural
γQ [-]	1.50	Live loads

6) Comments about the project

7) Element definition

7.1) Materials

Ref. EN1994-1-1 - Sec.3, CEN document Annex B.2

Steel grade:	S460M	Acc to EN10025-2, -3, -4, -5:2019; ETA-10/0156
Concrete class:	C35/45	Acc to EN1992-1-1
Reinforc. steel:	B500	Acc to EN10080:2005

Material properties

Steel:

Standard:	EN10025-4 (Thermon	Reference standard
Nom. thick. [mm]	16mm <t<=40mm	Nominal thickness of steel section
γ_s [kN/m^3]	78.5	Steel specific weight
f_y [MPa]	440.0	Yealding resistance of structural steel
f_u [MPa]	-	
E_a [MPa]	210000.0	Young's modulus of structural steel
Message:	-	

500	390	390

Concrete:

γ_c [kN/m^3]	25.0	Concrete specific weight
f_{ck} [MPa]	35.0	Characteristic concrete compressive strength
f_{cd} [MPa]	23.3	Design concrete compressive strength
f_{cm} [MPa]	43	Average concrete compressive strength
f_{ctm} [MPa]	3.21	Average concrete tensile strength
E_{cm} [MPa]	34077.1	Young's modulus of concrete
Message:	-	

Reinforcement steel:

f_{sk} [MPa]	500.0	Characteristic yeald resistance of rebar
f_{sd} [MPa]	434.8	Design yealding resistance of rebar

Other derived quantities

ε [-]	0.731	

7.2) Geometry

Ref. EN1994-1-1 - 2.4.1.3

Element

L [mm]	16000	Span length
L_{inter} [mm]	5000	Beams interaxis

Shear connection

Dowel shape:	PZT	Dowel shape
e_x [mm]	150.0	Longitudinal distance between connectors
h_D [mm]	30.0	Height of dowel
n_{Dowels} [-]	53.0	Nb. connectors btw. critical sections
Dowel area coeff.	0.09	
A_D [mm^2]	2025	Concrete dowel area
$A_{D,i}$ [mm^2]	16500	Effective concrete area
b_{CD} [mm]	300.0	Maximum length steel connector parallel to the lon
strips/steel section	1.0	Nb. strips of longitudinal shear connection
e_y [mm]	-	Spacing between strips

Section

Original hot-rolled H section

Hot-r. double-T sec	HE 900 AA	
G [kg/m]	198.0	Weight per unit length
G/2 [kg/m]	99	Weight per unit length of
h [mm]	870.0	Height of H section
b [mm]	300.0	Base of H section
t_w [mm]	15.0	Web thickness of H secti
t_f [mm]	20.0	Flange thickness of H se
r [mm]	30.0	Fillet radius of H section
A [cm^2]	252.2	Area of H section
$I_{a,HR}$ [cm^4]	301140.0	Second order central mo
$W_{pl,y}$ [cm^3]	7998.0	Plastic resistant moment

Classification of double-T section under bending

Ref. EN 1993-1-1, 5.6

> Web		
c [mm]	270	
c/t_w [-]	18.0	c/t ratio
72 ε [-]	52.6	Class 1 limit for part in bending
83 ε [-]	60.7	Class 2 limit for part in be
124 ε [-]	90.6	Class 3 limit for part in be
Bending:	Class 1	Resulting class
> Flange		
c [mm]	112.5	
c/t_f [-]	5.6	c/t ratio
9 ε [-]	6.6	Class 1 limit for part in compression
10 ε [-]	7.3	Class 2 limit for part in co
14 ε [-]	10.2	Class 3 limit for part in co
Compression:	Class 1	Resulting class

Profile class: Class 1

Single-T section

$y_{Sh.connection}$ [mm]	435.0	Reference coordinate of s
$h_{singleT}$ [mm]	420.0	Single T profile height
A_a [cm^2]	120.0	Net area of steel part
$y_{G,a}$ [mm]	115.00	Centroid position of steel
I_a [cm^4]	21250.0	Second order central mo

Concrete part

h_{slab} [mm]	110.0	Slab height
Δ [mm]	10.0	Offset between slab centr =h_slab/2+clt_height+t_f-
B [mm]	5000.0	Slab width
h_{haunch} [mm]	0.0	Type "=snap_to_flange" if contact with the steel flan
b_{haunch} [mm]	200.0	Haunch width
B_{eff} [mm]	4000.0	Effective width
h_c [mm]	110	Height of concrete part
A_c [cm^2]	4400	Concrete part area
$y_{G,c}$ [mm]	445	Centroid concrete part acc. to reference (*)
I_c [cm^4]	44366.7	Second moment of concrete section

Dowel position relative to the concrete part:

$c_{D,o}$ [mm]	50.0	Concrete cover over the connectors
$c_{D,u}$ [mm]	30.0	Concrete cover beyond the connectors
$c_{D,s}$ [mm]	2492.5	Dowel concrete cover transverse to beam axis
c_o [mm]	50	For tensile load on dowel used as anchorage

Derived quantities

h_{po} [mm]	39.0	Pryout cone height
b_c [mm]	200	Concrete web thickness
h/L [-]	1/32	

Composite section

n_0 [-]	6.16	Homogenization factor
$y_{G,homo}$ [mm]	397.5	Centroid position of homo
I_{homo} [cm^4]	140326.5	Second moment of homo

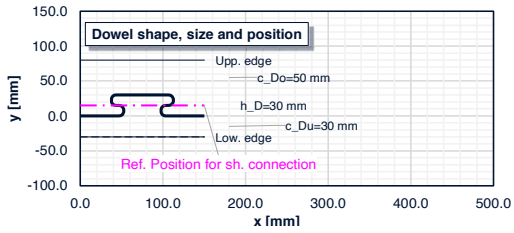

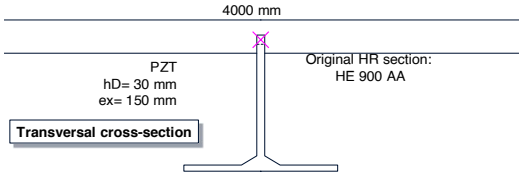

6.3) Effective width of concrete flange (Shear Lag effect)

Ref. EN 1994-1-1, 5.4.1.2

b_0 [mm]	0.0
b_1 [mm]	2500
b_2 [mm]	2500
$L_{e,support}$ [mm]	4000
$L_{e,midspan}$ [mm]	16000
b_{e1} [mm]	2000
b_{e2} [mm]	2000
β_1 [-]	0.600
β_2 [-]	0.600
$b_{eff,support}$ [mm]	2400
$b_{eff,midspan}$ [mm]	4000

Geometry limitations checks

Ref. CEN document - Annex A

Concrete pry-out on lower slab edge:

Prevented [Y/N]	Y	Y if CLT or concrete precast panel are used.
Possib. p.o.e. [Y/N]	N	Recommended N; Y if dowel close to vertical edge
Dowel in slab [Y/N]	Y	Y if dowel is in a concrete slab; N if in concrete Wel

Limitations

e_y >= 120mm	Undefined	
t_w<40 mm	VERO	
4mm < t_w<60 mm	VERO	
$c_{D,o}$>=30 mm	VERO	
cD,u>=20 mm	VERO	
$c_{D,s}$>=45 mm	na	
t_f>=t_w	VERO	Ref. CEN document - Fig.A.5
($h_{singleT}$-t_f)>=0.45 h_D	VERO	Ref. CEN document - Fig.A.6

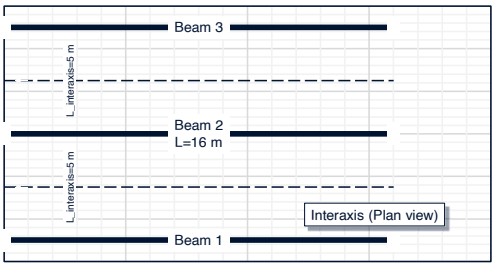

8) Reinforcement definition

Longitudinal slab reinforcement

Top

Presence [Y/N]:	Y
Φ [mm]	10
Spacing [mm]	150
Conc. cover [mm]	30

Bottom

Presence [Y/N]:	N
Φ [mm]	16
Spacing [mm]	100
Conc. cover [mm]	25

Transverse reinforcement: "passing" stirrups

Reinforcement position and amount

Presence [Y/N]:	N	
Φ [mm]	10.0	Stirrups diameter
n. stirrups/dowel [-]	2	Number of stirrups per dowel
Offset [mm]	30.0	Offset from centre of concrete dowel
$A_{s,pass.stirrups}$ [mm^2]	0.0	

Transverse reinforcement: conc. slab bars - Bottom

Reinforcement position and amount

Presence [Y/N]:	Y	
Φ [mm]	16.0	Bar diameter
n. bars/dowel [-]	2	Number of bars
Offset [mm]	37.5	Offset from centre of concrete dowel
Conc. cover [mm]	38.0	Concrete cover
$A_{s,pass.bottom\ bars}$ [mm	402.1	

Transverse reinforcement: conc. slab bars - Top

Reinforcement position and amount

Presence [Y/N]:	Y	
Φ [mm]	10.0	Bar diameter
n. bars/dowel [-]	1.000	Number of bars
Spacing [mm]	150.0	Offset from centre of concrete dowel
Conc. cover [mm]	20	Concrete cover
$A_{s,pass.top\ bars}$ [mm^2]	78.5	

Transverse reinforcement: confinement stirrups

Reinforcement position and amount

Φ [mm]	8.0	Stirrups diameter
n. stirrups/dowel [-]	1.0	Number of stirrups per dowel
n. legs [-]	2.0	Number of legs (4 if internal leg is anchored)
s [mm]	150.0	Spacing
Enbedded in:	Conc. slab	
A_{sw} [mm^2]	100.5	

Minimum ratio check

Ref. EN1994-1-1, 6.6.6.3; EN1992-1-1, 9.2.2(5)

A_{sw}/s [mm^2/m]	670.2	Area of transverse reinforcement / m
α [°]	90.0	Angle between stirrups and long. Axis
ρ_w [-]	0.335%	Angle between stirrups and long. Axis
$\rho_{w,min}$ [-]	0.095%	Density of transverse reinforcement
ρ_w > $\rho_{w,min}$	VERO	Minimum transverse reinf

Details check

If embedded in concrete slab:

Ref. CEN document - Annex A.6.2

φ >=8 mm	VERO	
s_{max} [mm]	180.0	s_{max}=min(4.5 h_{po}; 300 mm) Max spacing
s<=s_{max}	VERO	

If embedded in concrete web:

> Geometry:

Ref. CEN document - Annex A.6.3(1)

b_c>=$b_{c,min}$=250 mm	na	
$e_{V,min}$ [mm]	117.5	
$c_{D,s}$=e_V>=$e_{V,min}$	na	
h_{po}<=e_V+0.13 e_x	na	

> Splitting:

Ref. CEN document - Annex A.6.3(2); … Annex A.6.3(9)

$A_{s,conf}$ [mm^2]	100.5	
$A_{s,conf}$ >= 0.3 $P_{S,Rd}$/f	na	
φ >=10 mm	na	
Further checks [T/F	VERO	…
b_s [mm]	300	
b_s > min(h_c, 360mm	na	

Derived quantities

A_t [mm^2]	
A_b [mm^2]	402.1
ρ_D [-]	1.224
$\rho_{D,i}$ [-]	0.150 Reinforcement ratio for pry-out failure
$A_{s,conc.slab,1}$ [mm^2]	480.7 Transversal reinforcement in slab

Minimum quantity of transverse reinforcement

Ref. CEN document - Annex A.6.1

$A_{b,min}$ [mm^2]	108.3	
A_b>$A_{b,min}$	VERO	
n=2	VERO	Number of bars in each concrete dowel
A_b(1ϕ)>=0.5A_b	VERO	

Dowels close to a concrete edge

Ref. CEN document - Annex A.6.4

h_c + t_s *10 >=100 mr	VERO	
$c_{D,s}$>=45 mm	VERO	
φ [mm]	8	
φ >=8 mm	VERO	

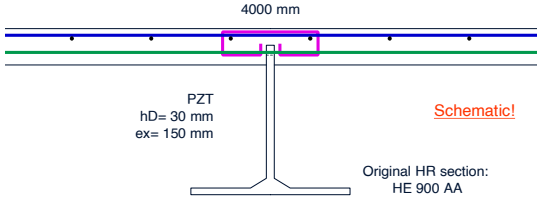

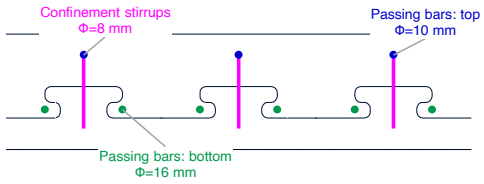

9) Complementary elements

Transversal ribbed slab

Type:	Cofraplus® 220	Ribs shape
Sheet th. t_s [mm]	1.25	Profiled sheet thickness
Dowel-ribs compatibility:		
mod(spac.;e_x)=0	VERO	
Sh. perimeter/m [m	1533.3	Profiled sheet length per unit length
Additional area [m^2/	0.026	Rib additional long. cross sectional area
Ribs spacing [m]	0.750	Ribs spacing
Ribs depth [m]	0.220	Ribs depth from slab bottom
Additional weight [k	1.02	Additional concrete weight due to ribs (including p
Wings add. weight	0.321	

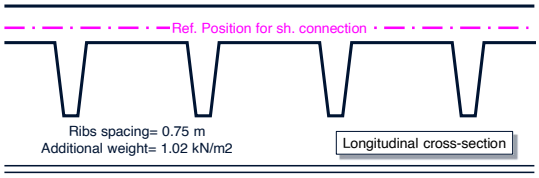

Wood CLT panel

Thickness [mm]	0.0	
γ_{wood} [kN/m^3]	3.5	
Weight [kN/m^2]	0.00	
Support width [mm]	50	CLT panel support width on bottom flange (assumed to be half of the difference between b and the concrete web thickness)

Consistency check

Consistency: VERO

10) Loads definition

Loads list

Permanent loads: structural

Item [i]	Load name	G_k [kN/m^2]	g_k [kN/m]	ULS Coefficient
1.1	G1 - Steel section		1.26	1.35
1.2	G1 - Concrete	3.77	18.85	1.35
1.3				1.35

Permanent loads: non structural

Item [i]	Load name	G_k [kN/m^2]	g_k [kN/m]	ULS Coefficient
2.1	G2 - Decking	1.00	5.00	1.35
2.2				1.35

Live loads — Note: First listed imposed load is assumed to be the principal load

Item [i]	Load name	Q_k [kN/m^2]	q_k [kN/m]	ψ_{0i} [-]	ULS Coefficient
3.1	Q - Cat.	2.50	12.50	1	1.50
3.2				1	1.50
3.3				1	1.50

Load on the main beam

q_{ULS} [kN/m] 52.6

Load on the decking system

$q_{ULS,transv}$ [kN/m^2] 10.2 Considering a 1m strip

11) Further inputs

Construction stage setting

Type of construction: Propped — Specify if the construc

Frequency limitation settings

1≤ $\alpha_{b,dyn}$ [-] ≤ 5	2.0	1 for perfect isostatic b
f_{lim} [Hz]	2.3	Limit frequency

Deflection limitation settings

δ_{lim}/L [-] 1/250

Slab-main beam composite checks

Composed checks	N	Activate if composed
1≤ $\alpha_{b,dyn}$ [-] ≤ 5	2.0	
Slab w/L deflection	1/500	Insert deflection of sla
$f_{transv.}$ [Hz]	2.50	Transversal mode fre

Bottom flange as support

Is support [Y/N] N — 'Y' if the bottom flange is a support for the slal

11) Run sheet calculations

Press to launch:

- ULS Rigid Plastic (RP) analysis;
- ULS Strain Limitation (SL) analysis;
- SLS stress computations in the different construction stages and for both propped and unpropped conditions

Note: specific analysis settings (gray highlighted) are available in the specific modules

Note: buttons for the specific modules are also available in the related sections

12) Structural analysis

Actions

M_{Ed} [kNm]	1684.7	Design moment
V_{Ed} [kN]	421.2	Design shear

Actions on dowel (For separated checks)

$P_{S,Ed}$ [kN]	94.1	Shear design action on single dowel
$P_{T,Ed}$ [kN]	0.0	Tension design action on single dowel

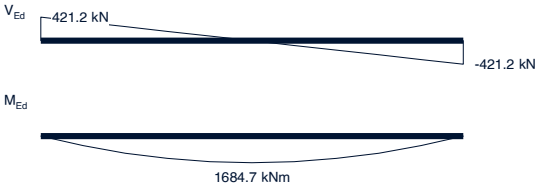

13) Shear connection ductility

Deformation capacity

Ref. prEN1994-1-1 - Tab. 5.1

Identify ductility class

> D0

δ_{ek} [mm]	
δ_{ek}<2 mm	VERO

> D1.a

δ_{ek} [mm]	
δ_{ek}>2 mm	FALSO

> D1.b

δ_{ek1} [mm]	
δ_{ek2} [mm]	
δ_{ek}>2 mm	FALSO

> D2

δ_{ek} [mm]	
δ_{uk} [mm]	
$(\delta_{uk}-\delta_{ek})/\delta_{uk}$<0.70	na
δ_{uk} >6 mm	FALSO

> D3

δ_{ek} [mm]	
δ_{uk} [mm]	
$(\delta_{uk}-\delta_{ek})/\delta_{uk}$<0.80	na
δ_{uk} >10 mm	FALSO

Identified ductility class

Ductility class: D2

13) ULS dowel resistance

Ref. EN1994-1-1 - 6.6: Shear connection; CEN document; CEN Document Annex A.3

Dowel: shear

> Splitting

Ref. CEN document - XXX

Excluded via sufficient transverse reinforcement

Force [kN]	47.1	Tensile force of 50% the
$A_{s,min}$ [mm^2]	108.3	
A_b>$A_{b,min}$	VERO	

> Local compression

Ref. CEN document - XXX

Allowed

> Shearing

Ref. CEN document - XXX; CEN Document Annex A.X

η_D [-]	1.15	
$P_{sh,k}$ [kN]	339.2	Shearing resistance of concrete dowel

> Pry-out

Ref. CEN document - 6.3.5; CEN Document Annex A.3

k_1 [-]	71	Factor dependent on dowel geometry
χ_x [-]	1.00	Red. overlapping pry-out cones - Long
e_x<4.5 h_{po}	FALSO	
χ_y [-]	1.00	Red. overlapping pry-out cones - Transv
e_y<9 h_{po}	Undefined	
$y_{G,omo}$<$y_{sh,connection}$	VERO	
Dowel in compressi	VERO	
ψ_{crack} [-]	1.000	Red. for transverse concrete cracking
$P_{po,k}$ [kN]	117.7	Pry-out char. Resistance of concrete cone

> Edge pry-out

Ref. CEN document Annex A.3

ζ_{geo} [-]	0.1	
$h_{d,eff}$ [mm]	15.0	Effective height of steel connector
k [-]	1.283	Size effect coefficient
$P_{poe,k}$ [kN]	1320.9	Pry-out char. Resistance
$P_{pl,k}$>=1.5 $P_{poe,k}$	FALSO	
Message:	-	

> Steel dowel plastifying

λ_{GEO} [-]	0.186	Factor dependent on geometry
$P_{pl,k}$ [kN]	184.1	Plastifying of steel char. resistance

> Dowel connector resistance

$P_{S,Rk}$ [kN]	117.7	Shear char. resistance of single dowel
$P_{S,Rd}$ [kN]	94.1	Shear design resistance of single dowel

14) ULS shear resistance

Buckling resistance of web

Ref. EN1994-1-1, 6.2.2.3; EN1993-1-1, 5

η [-]	1.2	
h_w [mm]	385.0	Steel web height
h_w/t_w [-]	25.7	
72/η ε	43.8	
h_w/t_w < 72/η ε	VERO	
Message:	-	

Plastic shear resistance of web

Ref. EN1994-1-1, 6.2.2.2

A_v [mm^2]	5400.0
$V_{pl,Rd}$ [kN]	1371.8

Note: shear conservatively ensured by single-T section web (height=h/2-t_f-h_D)

Interaction

Ref. EN1994-1-1, 6.2.2.4

V_{Rd} [kN]	1371.8	Design shear resistance
V_{Ed}/V_{Rd} [-]	0.307	Shear design / resistance check
V_{Ed}/V_{Rd}>0.5	FALSO	Check for need of reduction
ρ [-]	No reduction	Reduction factor
(1-ρ) f_{yd} [MPa]	No reduction	Reduced steel yielding stress in the shear area

15) Bending on bottom flange check

Ref. prEN1994-1-1, Annex I.3.1

Support on fl. [Y/N]	N	"Y" if the bottom flange consists in a support of the transversal flooring system
$m_{ybt,Rd}$ [kNm/m]	35.2	Resistant elastic bending moment of the bottom flange
V [kN/m]	25.5	Reaction force of the bottom flange on the transversal system
$m_{ybt,Ed}$ [kNm/m]	0.0	Acting design bending moment on the bottom flange
$m_{ybt,Ed}$ < $m_{ybt,Rd}$	No reduction	
η_m [-]	0.000	Utilization ratio in trasverse bending (parameter defined according to prEN1994-1-1, Annex I.3.1.2)
$f_{y,red}$ [MPa]	440.0	Reduced yealding resistance of bottom flange due to transverse bending interaction

16) ULS bending resistance

Ref. EN1994-1-1 - Sec.6

ULS analysis - FSC case (η=1)

Ref. EN1994-1-1 - 6.2.1.2

Analysis:	RP - Rigid-plastic (--)	SL - Strain limitation (--)	
x_{pl} [mm]	66.6	79.3	Position of the plastic neutral axis in case of FSC
y_{PNA} [mm]	433.4	420.66	Position of the plastic neutral axis in case of FSC
N [kN]	0.00	0.00	Residual tensile force along the section for numerical evaluation procedure
$M_{pl,Rd,FSC}$ [kNm]	1857.1	1858.1	Plastic resistance design bending moment in case of FSC
N_{cf} [kN]	-5280.0	-5145.0	Compressive normal force in concrete flange in case of FSC (<0 if compressive)
$(1/r)_u$ [1/mm]	na	4.30E-05	Ultimate curvature
Failure type:	na	concrete crushing	Failure type

Reduction

x_{pl}/h [-]	0.159	
x_{pl}/h>0.15	VERO	
S420/S460	VERO	
β [-]	0.995	
Reduction:	Yes	
$M_{pl,Rd,FSC,red}$ [kNm]	1858.1	Not reduced according to prEN1994-1-1 new appro

Shear flow

$P_{max,el}$ [kN]	194.2	
$N_{cf,el}$ [kN]	2494.6	Limit value of N_{cf} that does'nt imply redistribution
N_{cf}<=$N_{cf,el}$	FALSO	
N_{cf}<=2*$N_{cf,el}$	FALSO	
Redistribution:	YES	
Sh. connection:	PARTIAL (PSC)	
$v_{L,max}$ [kN/m]	627.6	Maximum shear flow

Degree of shear connection

N_c [kN]	4989.1	Transmissible shear force
N_c<$N_{c,f}$	VERO	
Sh. connection:	PARTIAL (PSC)	Type of connection
η [-]	0.97	
L<18m with PSC	VERO	Ref. CEN Document - 8
η > 0.5	VERO	Ref. CEN Document - A.
$\eta_{min}(L, f_y)$	0.95	
η > $\eta_{min}(L, f_y)$	VERO	Minimum degree of shear
$M_{pl,Rd}$ [kNm]	1851.1	

Degree of utilization

$M_{Ed}/M_{pl,Rd}$ [-]	0.910

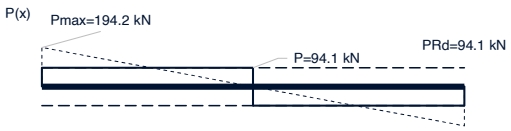

Settings for SL design

Discretization

Δy [mm]	2.0	Discretization step (fibre height)

Material laws

Structural steel:	Elastic-plastic harden	Structural steel material law
Reinforcement stee	Elastic-plastic harden	Reinforcement steel material law (Reinf. Bars
Concrete:	Parabola-rectangle	Concrete material law

Concrete law parameters:

n [-]	2.000	Parabola-rectangle law exponent
ε_{c1} [-]	0.225%	
ε_{cu1} [-]	0.350%	
ε_{c2} [-]	0.200%	
ε_{cu2} [-]	0.350%	

Structural steel law parameters:

ε_{ay} [-]	0.210%	Yealding strain for stru
ε_{au} [-]	15.0%	Ultimate strain for stru
E' [MPa]	210.0	Hardening slope

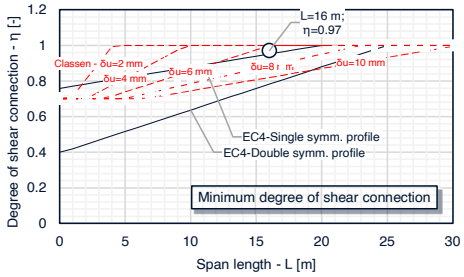

Material laws

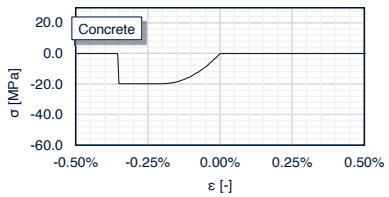

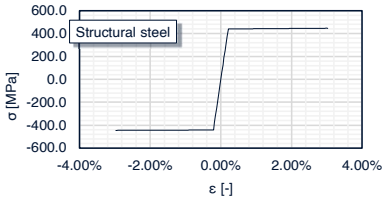

Stresses and strains along section: FSC-ULS

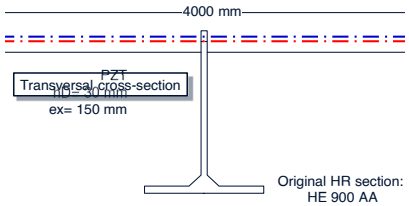

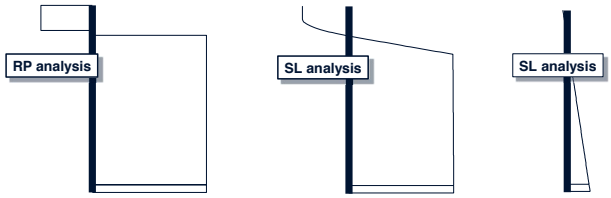

Partial shear connection diagram

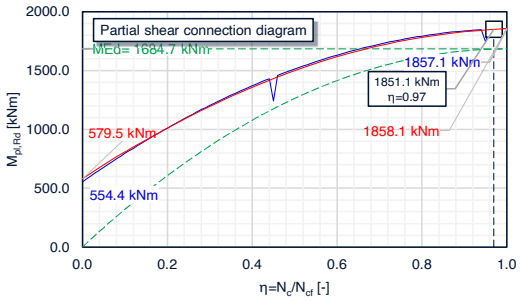

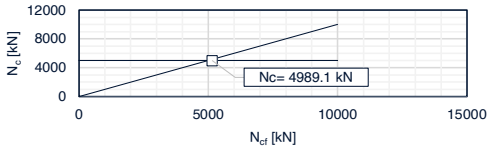

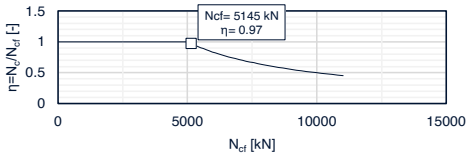

Moment-curvature diagram

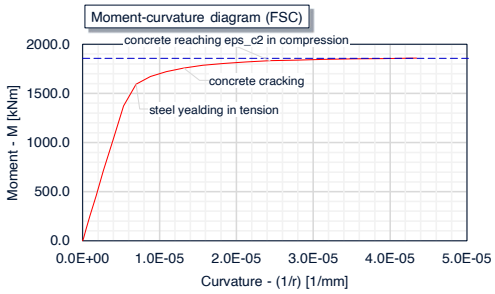

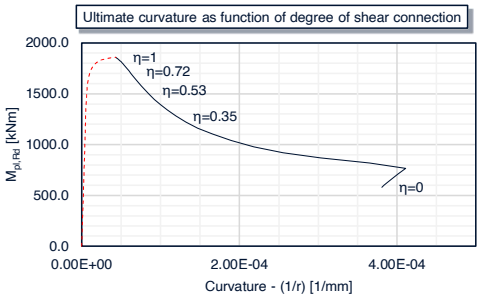

17) ULS longit. shear resistance of concrete flange

Transverse reinforcement

Reinforcement:

Ref. EN1994-1-1, 6.6.6; EN1992-1-1, 6.2.4

$A_{b1}+A_{t1}$ [mm²]	480.7
$A_{b1,passing\ bars}$ [mm²]	402.1
s_f [mm]	150.0

Crushing of concrete parameters:

Ref. EN1992-1-1, expr.6.22

ν [-]	0.516
v_{Rd} [MPa]	6.02

Additional force

Ref. CEN TS. A.7.1(1)

0.5 $P_{S,Rd}/f_{sd}$ [kN]	108.3
$A_{sf} \geq 0.5\ P_{S,Rd}/f_{sd}$	VERO

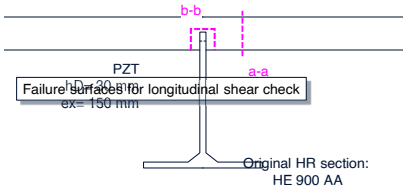

Failure surface d-d

> Resistance of reinforcement

v_L [kN/m]	627.6	
h_f [mm]	185.0	
v_{Ed} [MPa]	3.39	
A_{sf}/s_f [mm²/m]	670.2	
θ [°]	45.0	
26.5°<=θ<=45°	VERO	
cot(θ) [-]	1.00	
$A_{sf}/s_f\ f_{sd}$ [kN/m]	291.4	
$v_{Ed}\ h_f/\cot(\theta)$ [kN/m]	627.6	
$A_{sf}/s_f\ f_{sd} \geq v_{Ed}\ h_f/\cot$	FALSO	

Failure surface a-a

> Resistance of reinforcement

v_L [kN/m]	313.8	Considered shear flow
h_f [mm]	110	Height of potential failure surface
v_{Ed} [MPa]	2.85	Design shear stress
A_{sf}/s_f [mm²/m]	3204.4	transversal reinforcement density
θ [°]	45.0	Strut angle
26.5°<=θ<=45°	VERO	Angle limits check
cot(θ) [-]	1.00	Cotangent of strut angle
$A_{sf}/s_f\ f_{sd}$ [kN/m]	1393.2	Reinforcement resistance per unit length
$v_{Ed}\ h_f/\cot(\theta)$ [kN/m]	313.8	Force applied on reinforcement / m
$A_{sf}/s_f\ f_{sd} \geq v_{Ed}\ h_f/\cot$	VERO	Check

> Crushing of concrete flange

v_{Ed}/v_{Rd} [-]	0.474
$v_{Ed} < v_{Rd}$	VERO

Failure surface b-b

> Resistance of reinforcement EN1994-1-1, 6.6.6.2(2)

v_L [kN/m]	627.6	Considered shear flow
h_f [mm]	135.0	Height of potential failure surface
v_{Ed} [MPa]	4.65	Design shear stress
A_{sf}/s_f [mm²/m]	5361.7	transversal reinforcement density
θ [°]	45.0	Strut angle
26.5°<=θ<=45°	VERO	Angle limits check
cot(θ) [-]	1.00	Cotangent of strut angle
$A_{sf}/s_f\ f_{sd}$ [kN/m]	2331.2	Reinforcement resistance per unit length
$v_{Ed}\ h_f/\cot(\theta)$ [kN/m]	627.6	Force applied on reinforcement per unit length
$A_{sf}/s_f\ f_{sd} \geq v_{Ed}\ h_f/\cot$	VERO	Check

> Crushing of concrete flange

v_{Ed}/v_{Rd} [-]	0.772
$v_{Ed} < v_{Rd}$	VERO

Minimum ratio of transverse reinforcement

ρ_w [-]	2.913%
$\rho_{w,min}$ [-]	0.095%
$\rho_w > \rho_{w,min}$	VERO

18) SLS

Creep coefficient computation parameters

Ref. EN1992-1-1

u [mm]	8000	Perimeter exposed to drying
A_c [mm^2]	440000	Concrete cross-sectional area
h_0 [mm]	110.0	Notional size (Equivalent hydraulic radius)
CEM [S/R/N]	N	Tipe of cement
RH [%]	50	Relative humidity

Type of construction: **Propped**

Settings

t [days]	1E+11	Unpropping [days]	28	Time of unpropping (f
Propping [Y/N]	Y	First loading [days]	100	Time of first loading
Concrete collaboral	2	Begin of shrinkage [da	2	Beginning of applicati

Loads list

Permanent loads: structural

Item [i]	Load name	g_k [kN/m]	M_d [kNm]	V_d [kN]	$t_{0,unpropped}$ [days]	$t_{0,propped}$ [days]	Load category
1.1	G1 - Steel section	1.26	40.4	10.1	0	28	Permanent loading
1.2	G1 - Concrete	18.85	603.1	150.8	0	28	Permanent loading
1.3					0	28	Permanent loading

Permanent loads: non structural

Item [i]	Load name	g_k [kN/m]	M_d [kNm]	V_d [kN]	$t_{0,unpropped}$ [days]	$t_{0,propped}$ [days]	Load category
2.1	G2 - Decking	5.00	160.0	40.0	100	100	Permanent loading
2.2					100	100	Permanent loading

Live loads — Note: First listed imposed load is assumed to be the principal load

Item [i]	Load name	q_k [kN/m]	M_d [kNm]	V_d [kN]	$t_{0,unpropped}$ [days]	$t_{0,propped}$ [days]	Load category
3.1	Q - Cat.	12.50	400.0	100.0	100	100	Short-term
3.2					100	100	Short-term
3.3					100	100	Short-term

Shrinkage

Item [i]	Load name	ε_{cs} [-]	M_{cs} [kNm]	$t_{0,unpropped}$ [days]	$t_{0,propped}$ [days]	Load category
4.1	Shrinkage	0.000325	178.5	2	2	Shrinkage effect

Computation of stresses and deflection

Loads list		Time of application	$t > t_0$	Creep multiplier	Creep coefficient	Effective concrete stiff	Modular ratio
Load name		t_0 [days]	Flag	ψ_L [-]	φ_t [-]	$E_{c,eff}$ [MPa]	n_L [-]
G1 - Steel section	…	28	VERO	1.1	2.3	9696.0	21.7
G1 - Concrete	…	28	VERO	1.1	2.3	9696.0	21.7
	…						
G2 - Decking	…	100	VERO	1.1	1.8	11470.0	18.3
	…						
Q - Cat.	…	100	VERO	0.0	1.8	34077.1	6.2
	…						
	…						
Shrinkage	…	2.00	VERO	0.6	3.7	11131.4	18.9

Loads list		Centroid position	Homogenized second	Lower edge steel stre	Upper edge steel stre	Lower edge concrete	per edge concrete stre
Load name		$y_G(t,t_0)$ [mm]	I_{homo} [cm^4]	$\sigma_{s,inf}$ [MPa]	$\sigma_{s,sup}$ [MPa]	$\sigma_{c,inf}$ [MPa]	$\sigma_{c,sup}$ [MPa]
G1 - Steel section	…	322.5	105451.9	12.4	-3.7	-0.1	-0.3
G1 - Concrete	…	322.5	105451.9	184.4	-55.8	-1.8	-4.7
	…			0.0	0.0	0.0	0.0
G2 - Decking	…	335.1	110832.3	48.4	0.0	-0.4	0.0
	…			0.0	0.0	0.0	0.0
Q - Cat.	…	397.5	140326.5	113.3	-2.6	0.3	-1.9
	…			0.0	0.0	0.0	0.0
	…			0.0	0.0	0.0	0.0
Shrinkage	…	332.89	109886.8	-78.6	-144.4	3.1	0.0
Sum	…			**279.9**	**-206.4**	**1.1**	**-6.9**

Loads list		δ [mm]	V_d [kN]
Load name			
G1 - Steel section	…	5.4	10.1
G1 - Concrete	…	79.9	150.8
	…		
G2 - Decking	…	20.2	0.0
	…		
Q - Cat.	…	36.2	40.0
	…		
	…		
Shrinkage	…	24.75	
Sum of permanent contributes:		130.1	
Sum of live loads contributes:		36.2	

Unpropped case

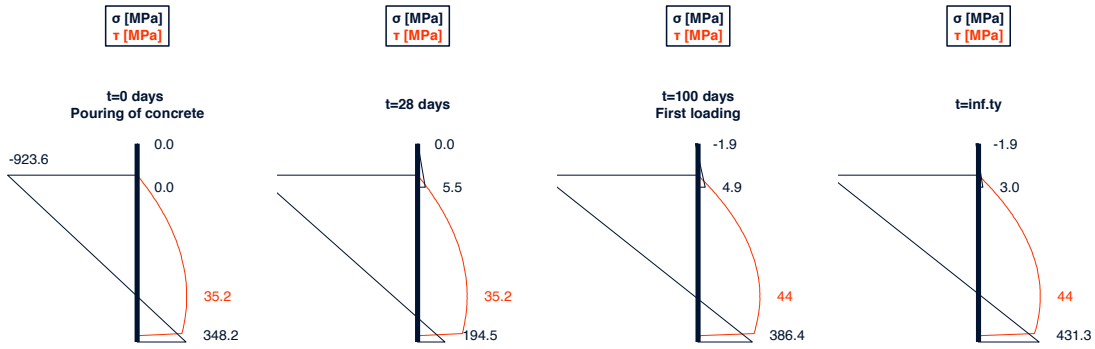

Propped case

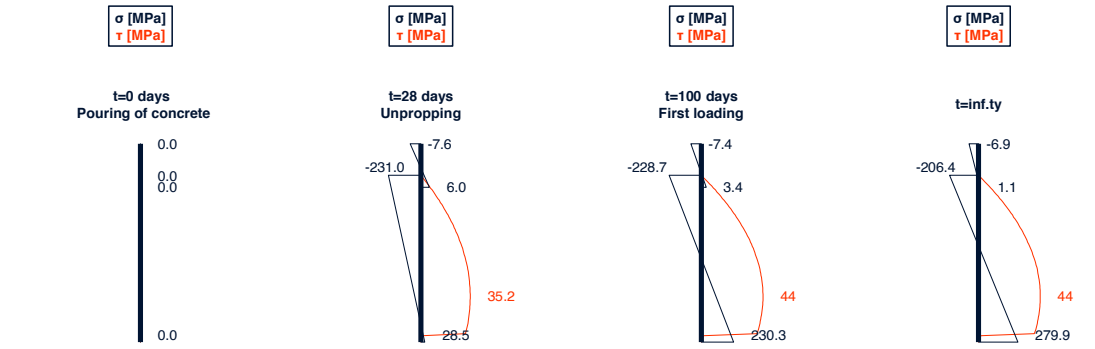

Summary

Unpropped case

Time - t [days]	$\sigma_{a,inf}$ [MPa]	$\sigma a_{,sup}$ [MPa]	$\sigma_{c,inf}$ [MPa]	$\sigma_{c,sup}$ [MPa]	$\tau_{a,max}$ [MPa]	δ_g [mm]	δ_q [mm]
0.0	348.2	-923.6	0.0	0.0	35.2	423.0	0.0
28	194.5	-1144.2	5.5	0.0	35.2	448.1	0.0
100	386.4	-1113.2	4.9	-1.9	44.0	464.0	36.2
inf.ty	431.3	-1070.5	3.0	-1.9	44.0	467.9	36.2

Propped case

Time - t [days]	$\sigma_{a,inf}$ [MPa]	$\sigma_{a,sup}$ [MPa]	$\sigma_{c,inf}$ [MPa]	$\sigma_{c,sup}$ [MPa]	$\tau_{a,max}$ [MPa]	δ_g [mm]	δ_q [mm]
0.0	0.0	0.0	0.0	0.0	0.0	0.0	0.0
28	28.5	-231.0	6.0	-7.6	35.2	89.2	0.0
100	230.3	-228.7	3.4	-7.4	44.0	117.9	36.2
inf.ty	279.9	-206.4	1.1	-6.9	44.0	130.1	36.2

Results for the chosen case: Propped

Max. normal stresses:

$\sigma_{a,max,comp}$ [MPa]	-231.0	Max compression stre
$\sigma_{a,max,tens}$ [MPa]	279.9	Max tensile stress on
$\sigma_{c,max,comp}$ [MPa]	-7.6	Max compression stre
$\sigma_{c,max,tens}$ [MPa]	6.0	Max tensile stress on
Cracking [Y/N]	Y	Check if concrete is cr

Composed checks: N

Deflection

$I_{homo,2}$ [cm^4]	138484.2	Second moment in partialized state
$I_{red}=0.5(I_1+I_2)$ [cm^4]	139405.4	Composite section in cracked situation
I_1/I_{red} [-]	1.01	Amplification due to cracking of concrete
δ_{lim}/L [-]	**1/250**	**Limitation on deflection**
δ_c [mm]	**131.0**	**Precambering**
δ_{TOT} [mm]	**36.4**	**Deflection under live loads**
δ_{TOT}/L [-]	**1/439**	**Deflection/span length ratio**

Instantaneous deflection check:

Slab w/L deflection	1/500
Slab deflection	10
$\delta_{TOT,lim}$ [mm]	**31.9**
$\delta_{TOT}<\delta_{TOT,lim}$ [mm]	FALSO

Vibration frequency

Ref. EN1994-1-1, 7.3.2

$1\leq \alpha_{b,dyn}$ [-] ≤ 5	2	
f_{lim} [Hz]	2.3	
$E_{c,dyn}/E_{cm}$ [-]	1.1	
$I_{homo,dyn}$ [cm^4]	142656.2	
μ [kg/m]	2510.9	Distributed mass per unit length
f [Hz]	**3.00**	**Vibration frequency**

Composed frequency check

$1\leq \alpha_{b,dyn}$ [-] ≤ 5	2.0	
$E_{c,dyn}/E_{cm}$ [-]	1.1	
$I_{homo,dyn}$ [cm^4]	142656.2	
μ [kg/m]	2510.9	
f_{long} [Hz]	2.997	Longitudinal frequency
$f_{transv.}$ [Hz]	2.5	
$f_{composed}$ [Hz]	**1.92**	Resulting frequency

19) Checks

General

> Materials	
Steel grade	S460M
Concrete class	C35/45
> Element	
L [m]	16.00
h_{tot} [m]	0.50
h_{tot}/L [-]	1/32
> Shear connection:	
Dowel:	PZT
Dowel size (h_D) [mm	30.0
Ductility class:	D2
Redistribution:	YES
Type:	PARTIAL (PSC)
η [-]	1.0

Top concrete cover

c [mm]	40

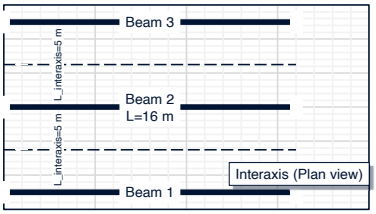

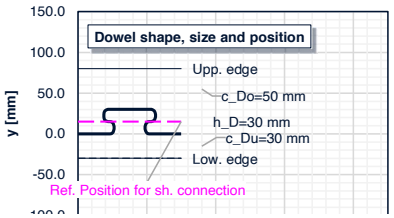

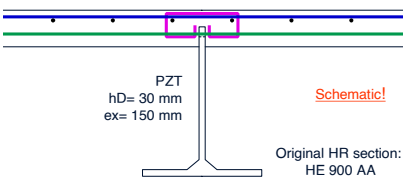

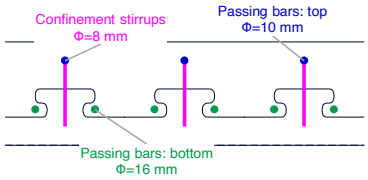

ULS

> Bending resistance		
$M_{Ed}/M_{pl,Rd} \leq 1$	VERO	0.910
> Shear resistance		
$h_w/t_w < 72/\eta\ \varepsilon$	VERO	0.585
$V_{Ed}/V_{pl,Rd} \leq 1$	VERO	0.307
> Dowel resistance		
$P_{S,Ed}/P_{S,Rd} \leq 1$	VERO	1.000
> Long. shear in concrete slab		
Surface a-a:		
$A_{sf}/s_f\ f_{sd} \geq v_{L,Ed}\ h_f/\cot(\theta)$	VERO	0.225
$v_{L,Ed} < v_{Rd}$	VERO	0.474
Surface b-b:		
$A_{sf}/s_f\ f_{sd} \geq v_{Ed}\ h_f/\cot(\theta)$	VERO	0.269
$v_{Ed} < v_{Rd}$	VERO	0.772
Bottom flange moment check		
$m_{el,Rd,flange} < m_{el,Rd,flange}$	No reduction	

SLS

$\delta_{TOT}/L < \delta_{lim}/L$	VERO	0.569
$\delta_{TOT,composed} < \delta_{TOT,composed,lim}$ [mm]	na	
f≥2.3 Hz	VERO	0.767
$f_{composed} \geq f_{lim}$	na	

Degree of connection

L<18m with PSC	VERO	
η > 0.5	VERO	0.516
$\eta > \eta_{min}(L, f_y)$	VERO	

Details and geometric limitations

> Geometry limitations		
$e_y \geq 120$mm	na	
t_w<40 mm	VERO	
4mm < t_w<60 mm	VERO	
$c_{D,o} \geq 30$ mm	VERO	
$c_{D,u} \geq 30$ mm	VERO	
$c_{D,s} \geq 45$ mm	na	
$t_f >= t_w$	VERO	
$(h_{singleT}-t_f) \geq 0.45\ h_D$	VERO	
> Transverse reinforcement		
$A_b > A_{b,min}$	VERO	
n=2	VERO	
$A_b(1\phi) \geq 0.5 A_b$	VERO	
> Confinement stirrups		
$\rho_w > \rho_{w,min}$	VERO	
> Reinforcement in slabs		
φ ≥8 mm	VERO	
$s <= s_{max}$	VERO	
> Reinforcement in web		
$d_c \geq b_{c,min}$=250 mm	na	
$c_{D,s} = e_V > e_{V,min}$	na	
$h_{po} \leq e_V + 0.13\ e_x$	na	
$A_{s,conf} \geq 0.3\ P_{S,Rd}/f_{sd}$	na	
φ ≥10 mm	na	
b_s > min(h_c, 360mm)	na	
Further checks:	na	
> Dowels close to concrete edge		
$h_c \geq 100$ mm	na	
$c_{D,s} \geq 45$ mm	na	
φ >=8 mm	na	
> Concrete slab		
$A_{s,prov} > A_{s,min}$	VERO	
26.5°≤θ≤45°	VERO	

Declaration consistencies:

Lower pryout prevention:	VERO

ULS checks	VERO
SLS checks	VERO
Geometric limitations checks	VERO
Reinforcement details checks	VERO
Consistency in declarations checks	VERO
Degree of shear connection	VERO

Global check status

Summary check:	VERO

Appendix C

Parametric study

For both the two composite dowel based studied decking technologies a parametric analysis has been carried out. The main objective of this part of the work is to analyse the potential for multi-storey buildings, identifying the most optimised configurations according with the latest research available results. The performance capability of these solutions is investigated by means of parametric analysis campaigns for the two innovative structural solutions. In both cases, the possibility of plastic redistribution of the shear flow at the level of the composite connection is considered. The two cases are analysed on the basis of the recent design rules proposals for the dimensioning of this type of steel-concrete connectors. Within the parametric analysis, the length of the span, the beam spacing, the thickness of the load-bearing concrete slab, the hot-rolled profile used for the construction of the steel-concrete T-section and the shape and type of the shear connector are varied. The parametric study is carried out using a code routine in Python language. The program systematically varies through different loops the input parameters in the Excel spreadsheet developed in this research work framework and by running the checks, collects the output results into a CSV database. Resulting charts are then post-processed and printed using Python.

C.1 Integrated beam for office building

The first solution analysed considers steel T-profiles integrated in a composite wood-concrete slab. In the longitudinal direction the structural function is ensured by the steel-concrete composite beam with continuous shear connection. In the transverse direction, Cross-laminated timber (CLT) panels with composite wood-concrete solutions are used. The structure is dimensioned for office or residential use. The applied non structural and live loads are here considered fixed and equal to:

$$G_2 = 1.50\,kN/m^2 \qquad \text{Permanent non structural load} \tag{C.1}$$

$$Q = 3.80\,kN/m^2 \qquad \text{Live load} \tag{C.2}$$

The general geometric scheme is shown in Fig.C.1.

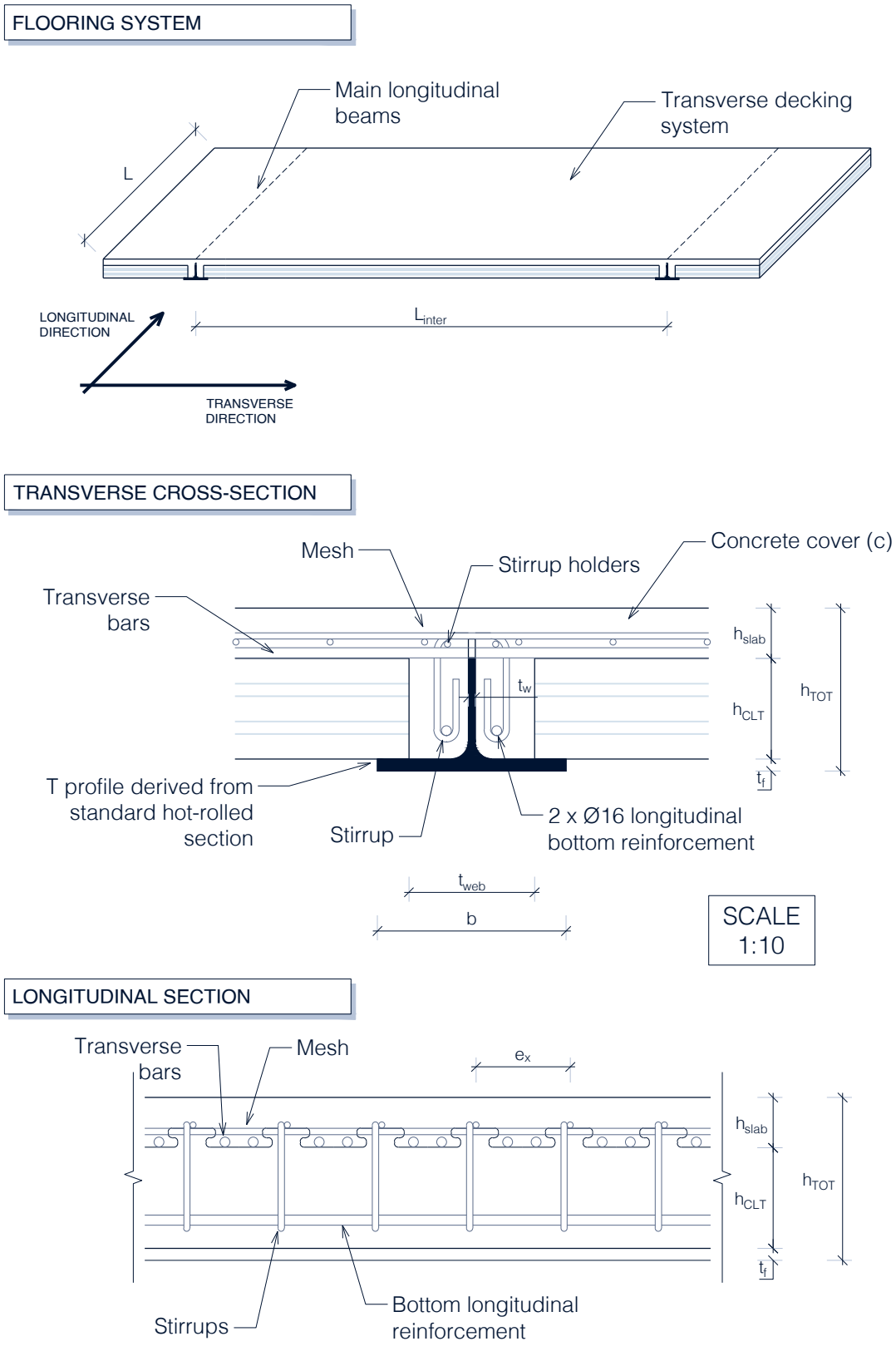

Figure C.1: Case study: element, static scheme and acting moment diagram

C.1.1 Parametric study setup

The considered materials are:

- S460 structural steel
- C35/45 concrete
- B500 reinforcement steel

For the integrated beam section for office building case the examined parameters and the relative ranges of values are:

- the spanlength L in the range [6000, 7000, ..., 14000 mm];
- the beams interaxis L_{inter} in the range [5000, 5500, ..., 7500 mm]. For each interaxis length L_{inter} an hot-rolled standard section family is considered, for example HE320. A more detailed explanation of the association between the steel profile family and the interaxis length can be found below;
- the hot rolled standard section from which the steel T profile is derived. In the selected family of profiles strictly associated to the beams interaxis L_{inter} the profile is varied within the possible solutions according to the European framework. As an example if the family HE320 is considered, the exploited sections in the family will vary within [HE320AA, HE320A, HE320B, HE320M, HE320C];
- the dowel shape. This is varied between the PS shape and the PZT one.
- the slab height h_{slab} varied within [70,80,...,100 mm] for the PZ dowel shape and within [60,70,...,100 mm] for the PZT shape.

The different geometric configurations and the parametric study setup can be seen in Fig.C.2.
As said in the introduction section, the reason for carrying out the present parametric analysis is to identify a set of optimized solutions for chosen values of L and L_{inter}. In order to do that a more extended parametric analysis should be carried out involving also the transverse decking system parameters such as the CLT panel used and the related CLT panel height h_{CLT}. The slab height parameter is instead the same as the one of the longitudinal beam section, thus not constituting an additional parameter to be varied. Related with the additional study, additional SLS and ULS checks would have to be done for the transverse system, by checking the vibration frequency, the deflection limitation and the ULS stresses of the section. The exploited approach here is to run a secondary, minor parametric analysis involving the transverse concrete-wood composite system. This is done because of the importance of reaching an optimized solution in both directions. Note that the secondary transverse concrete-wood system cannot be separated from the analysis of the composite section study as the system consists of a unique technology and the geometric dimensions are strictly related. The sectional total height h_{TOT} is in fact the same for the transverse system an the longitudinal beam (at less than the steel profile flange), the slab height h_{slab} is also the same and for executive reasons the transverse reinforcement bars need to pass through the concrete dowels and of

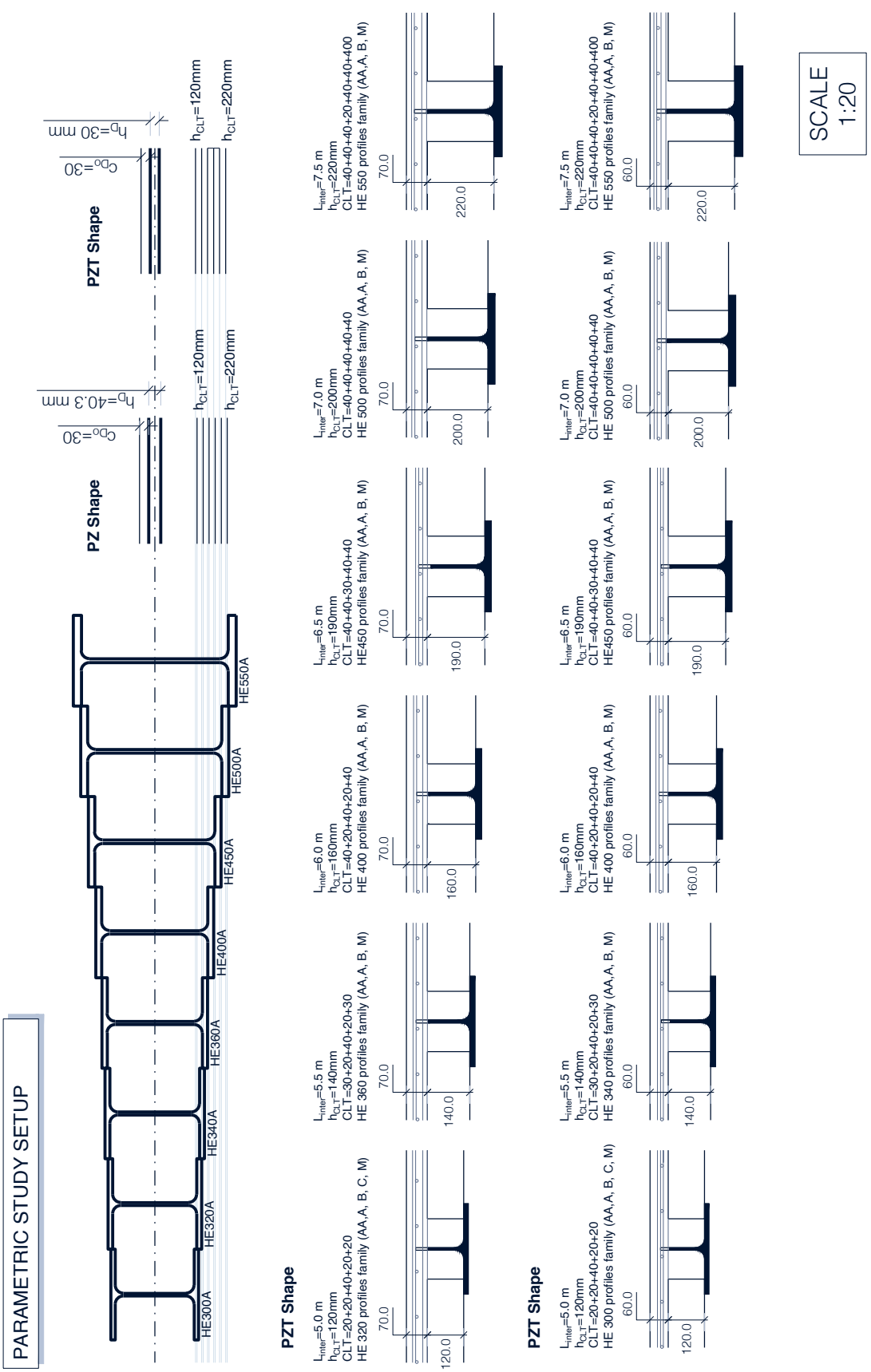

Figure C.2: Case study: element, static scheme and acting moment diagram

course lay over the CLT panels. Geometric dimensions are therefore strictly constrained. This fact has been outlined also in the Annex A. Here the secondary parametric analysis implementation, and results can be appreciated. This results have been used as a starting point in order to choose the minimum CLT panel plus slab heights that satisfy the checks for the transverse wood-concrete system for a given L_{inter}. Summarizing the general scheme chosing an interaxis length L_{inter}, the CLT panel is selected in accordance with the secondary parametric study presented in annex D, and the steel section family choice is than constrained due to the geometric and executive relations of the overall structural steel-concrete-wood typology. The concrete cover is of course a significant aspect of the design in reinforced concrete and composite structures. The approach here is to take trace of the concrete cover between the slab reinforcement and the concrete surface as result parameter. The slab height is varied regardless of the required concrete cover value. A significant observation that needs to be done, which is related with the executive aspects, is that within the different options belonging to one family the distance d between the flanges and the fillet radius r are constant. Varying the section in the family only the web thickness t_w and the flange thickness t_f vary. This implicates that if a particular section in the selected family well fits with the chosen CLT panel, the reinforcement details both passing through the dowels and over the CLT panel and the concrete slab height, then also another section of the same family will be suitable to the rest of the section.

C.1.2 Parametric study results

The parametric analysis results have been post-processed. This is done by exploiting the Python Pandas library. The dataframe has been appropriately filtered in order to identify the optimal solutions. For each couple of span length and beams interaxis length (L, L_{inter}) the best solution has been identified. Results are first filtered keeping those cases which satisfy the ULS and SLS checks. Then within the cases belonging to particular values (L, L_{inter}) the optimal solution has been identified by the particular solution that minimizes the total sectional height. This is obtained as the sum of the slab height, the CLT panel thickness and the bottom flange thickness of the steel profile. The solution minimizing the total sectional height and satisfying the checks is plotted for each (L, L_{inter}) couple in the presented charts, both for the case of PZ shaped dowel (Fig.C.3) and for PZT shaped dowel (Fig.C.4). These figures represent a condensed summary of the results, while extended results can be found in F.

The different solutions present a high level of performance under a height-span length ratio h_{TOT}/L. The line $h_{TOT}/L = 1/35$ can be interpreted as a limit to the element performance as under about this value of height-span length ratios, the examined cases do not satisfy the ULS bending checks for the steel-concrete section. Cases with a h_{TOT}/L value greater than 1/30 are those in which the sectional height is governed by the transverse decking system checks. The optimal design solutions can be interpreted to be those with $h_{TOT}/L < 1/30$. For these solutions both the transverse functioning and the longitudinal one are optimized.

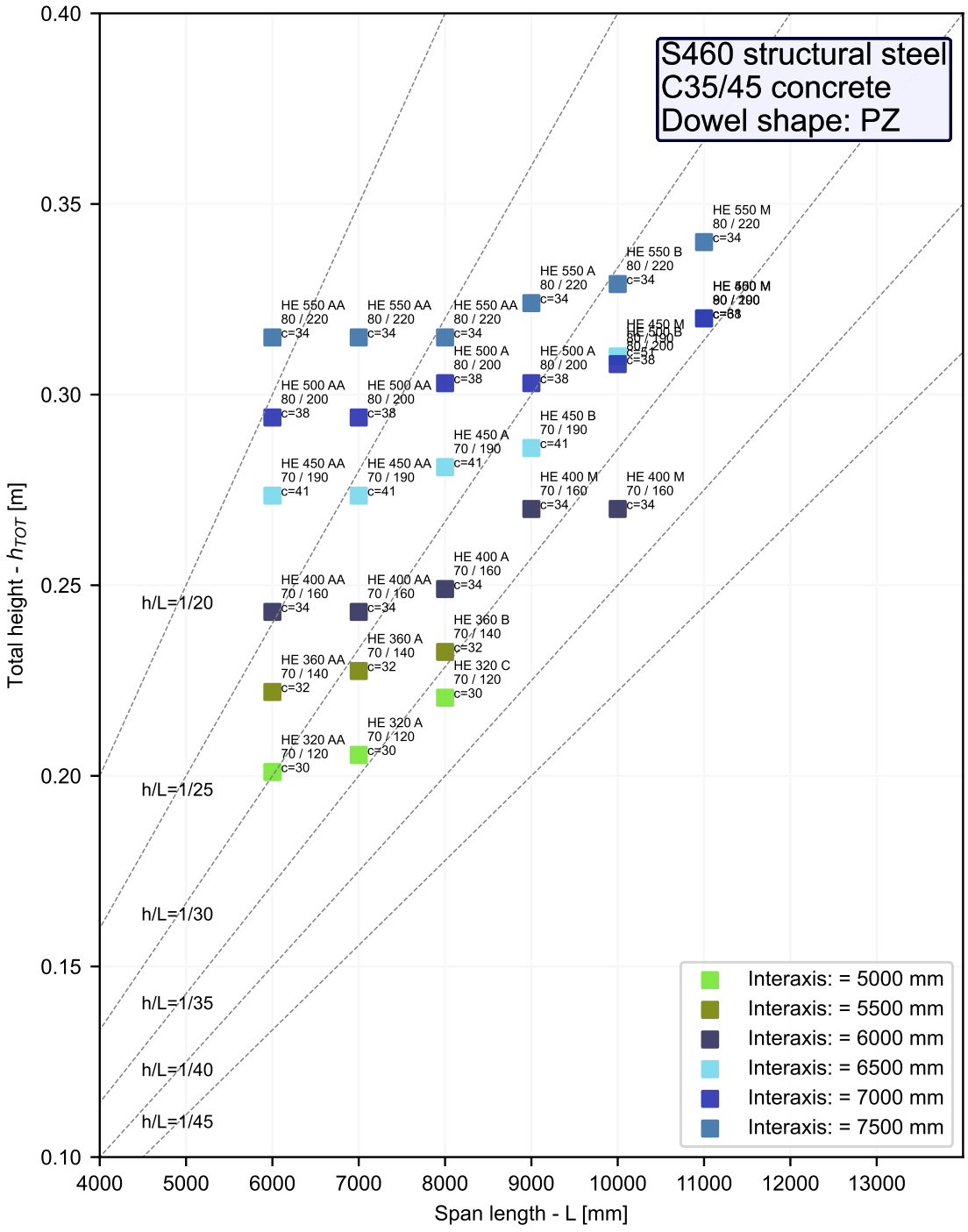

Figure C.3: Case study: element, static scheme and acting moment diagram

C.2 Car park section

The second solution examined is a floor beam for multi-storey car-park structures. Transversely, the floor is built using Cofraplus® technology, which has already been successfully used for traditional composite beams with a double-T profile, and fixed directly to the web of the steel T-profile. There are already two projects in Germany with this type of section, so the study will focus on verifying the optimisation of the sections in the light of the new regulations for the dimensioning of the connection. The technology was

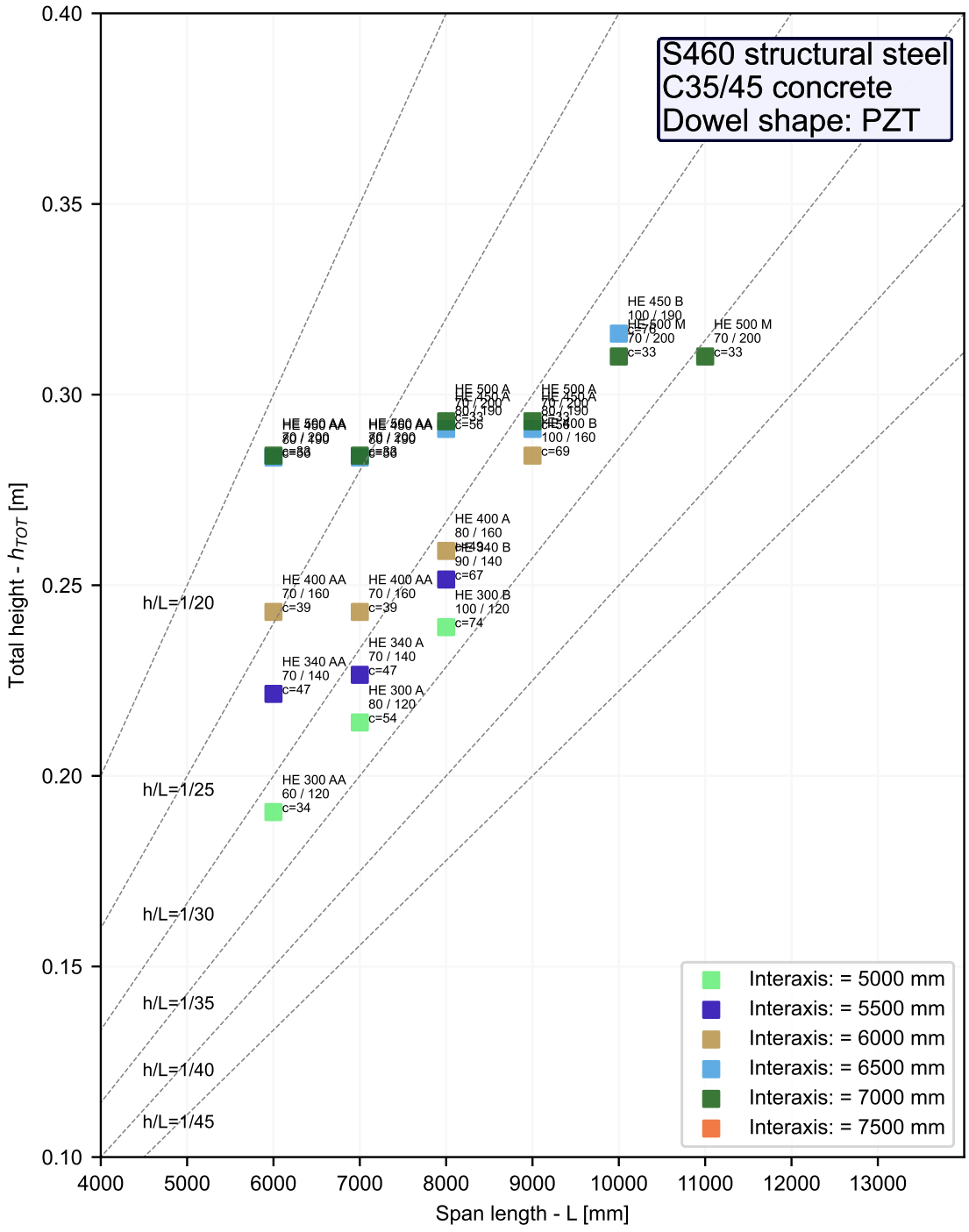

Figure C.4: Case study: element, static scheme and acting moment diagram succsessfully exploited in [94].

The applied non structural and live loads are here considered fixed and equal to:

$$G_2 = 1.00\ kN/m^2 \qquad \text{Permanent non structural load} \tag{C.3}$$

$$Q = 2.50\ kN/m^2 \qquad \text{Live load} \tag{C.4}$$

C.2.1 Parametric study setup

For parking constructions standard spanlengths and interaxis between the main beams are used. So the dimensions of the spanlegth L and the interaxis length L_{inter} are fixed to:

$$L = 16000\,mm \qquad L_{inter} = 5000\,mm \tag{C.5}$$

The considered materials are:

- S460 structural steel
- C35/45 concrete
- B500 reinforcement steel

For the integrated beam section for office building case the examined parameters and the relative ranges of values are:

- the hot rolled standard section from which the steel T profile is derived;
- the dowel shape. This is varied between the PZ shape and the PZT one.
- the slab height h_{slab} varied within [100,105,...,120 mm] for the PZ dowel shape and within [90,95,...,120 mm] for the PZT shape.
- the hot rolled standard section from which the steel T profile is derived. Families [HE800, HE900, HE1000] are considered. In each family the members [_AA, _A, _B, _M] are used.

C.2.2 Parametric study results

Results are extensively presented in Annex F. Various results are shown such as the vibration frequency, the deflection-span length ratio δ/L, the plastic resistant bending moment, the bending utilization coefficient M_{Ed}/M_{Rd}, the shear connection degree η. The influence of the various parameters can be visualized. Solutions having the same hot-rolled profile appear as "clusters" in the charts. The hot rolled profile selection appears being the major affecting parameter in the solution choice. Varying the hot rolled section within a family does not affect significantly the h_{tot}/L ratio. It has a significant influence on the analyzed parameters (y axis in the charts). By changing the profile family a significant influence can be observed also in the h_{tot}/L ratio due to the fact that the parameter h of the hot rolled profile varies significantly by changing family. The variation in the slab height h_{slab} and the shear connector shape can be visualized as well. The slab height appears not having a significant effect on the vibration frequency. Differently it has a weak influence on the deflection-span ratio and on the plastic resistant design bending moment. The dowel shape does not have an influence on the vibration frequency and on the deflection. Despite of that it has an influence on the shear connection degree η, with the PZT shape solutions exhibiting a reduction in the value of η with the other parameters kept as fixed. This generates as a direct consequence a reduction

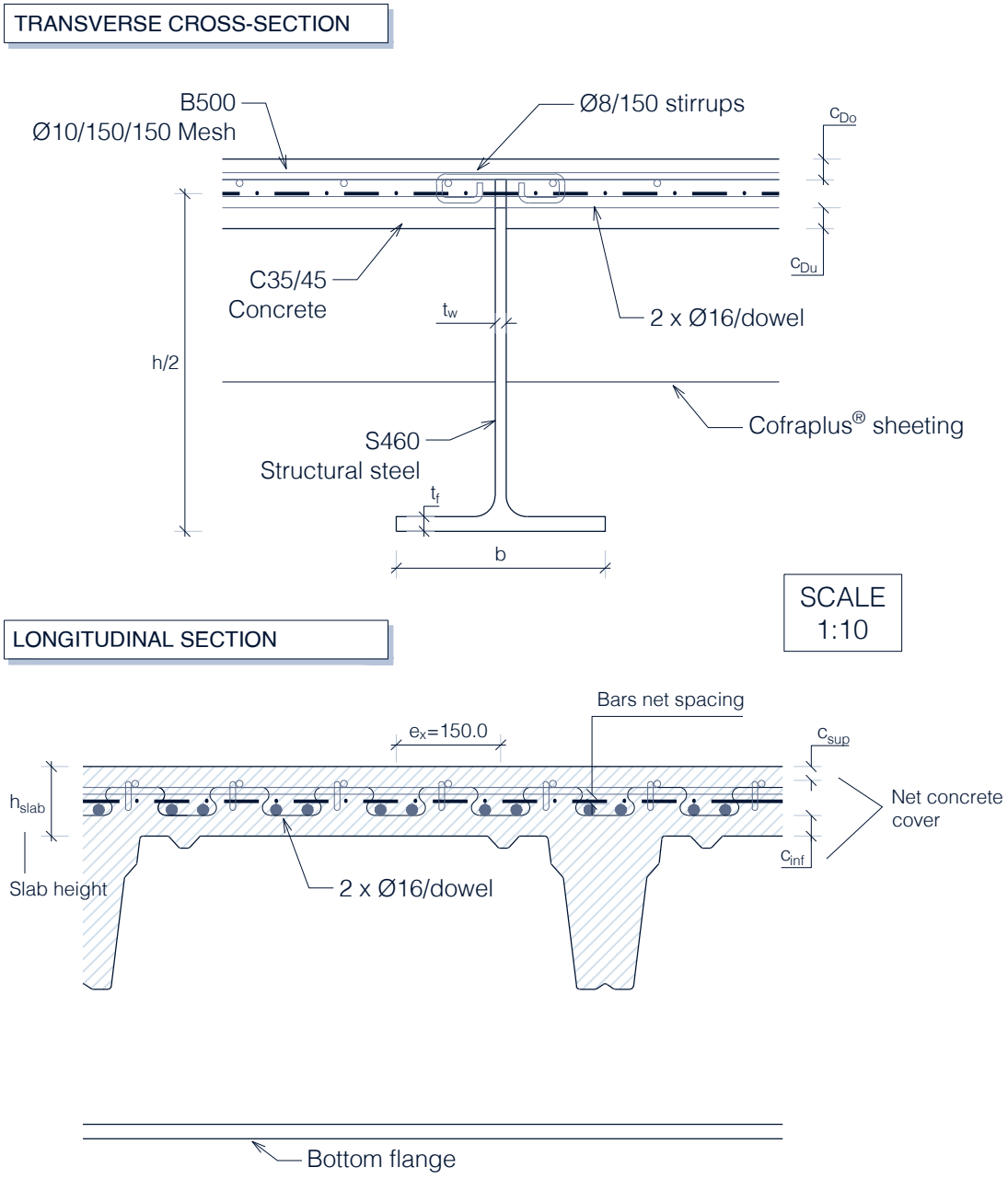

Figure C.5: Case study: element, static scheme and acting moment diagram

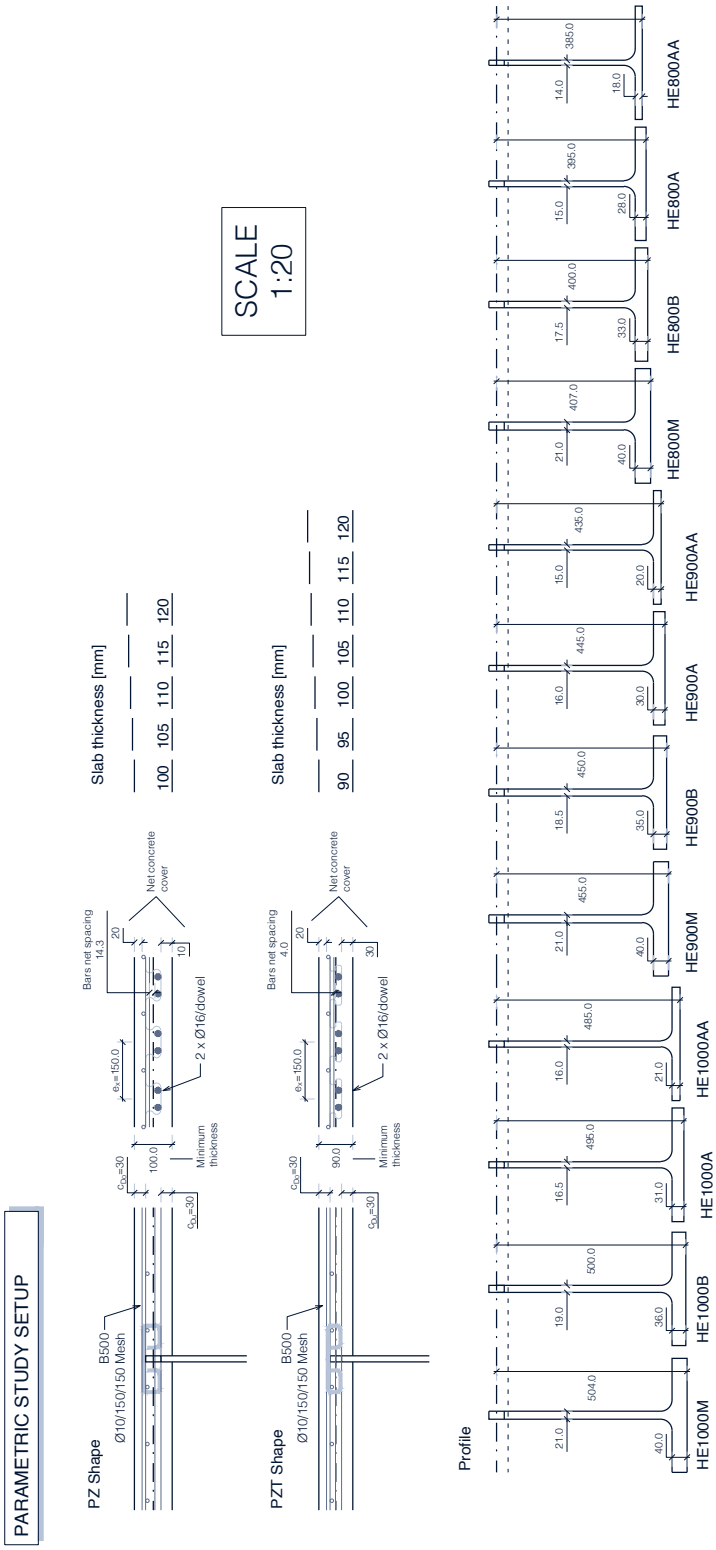

Figure C.6: Case study: element, static scheme and acting moment diagram

in the resistant plastic bending moment $M_{pl,Rd}(\eta)$ as it depends on the parameter η. The solutions which pass all the checks are considered to be valid solutions. Valid solutions range in total sectional height-span length rations between about 1/35 and 1/28. The most severe check appears being the one on the vibration frequency at serviceability limit states (SLS). In the vibration frequency charts, a net division of the passing cases and the non-passing cases can be observed exactly in correspondence at the limit that was set of $f_{lim} = 2.3\ Hz$. Optimal solutions are identified in terms of h_{tot}/L ratios. The cases minimizing this value can be interpreted as optimal ones. In order to minimize this value, the choice should fall on the HE800M hot rolled section. Minimizing the slab height helps in the h_{tot}/L ratio reduction but has a minor influence. The drawback in selecting low h_{tot}/L ratios appears in the degree of shear connection η: while choosing an HE1000AA hot rolled section the solution has nearly $\eta \approx 1$ values, in adopting hot rolled solutions with an HE800M profile the shear connection parameter significantly reduces to the value $\eta \approx 0.6$. Selecting a PZT shaped connector rather than a PZ one can additionally reduce the degree of shear connection.

Appendix D

CLT wood panel-concrete composite decking

Despite of the fact that composite wood concrete structures are not the subject of this study, one of the examined solution involves this type of structural typology in the transverse direction. I order to realise the flooring system in the "integrated floor beam for office building" case study, the decking in the transverse direction is realized by a coupled CLT panel-concrete slab system. A correct design of this component leads to a higher performance also in the longitudinal steel-concrete composite beam project (Fig.D.1). The sectional height of the flooring system is in fact both dependent on the transversal functioning and longitudinal beam functioning. An optimum project is the one that best exploits the structural material in both directions. An over-dimensioning of the CLT-concrete system in the transversal direction would cause also an incorrect, or non-optimized design for the longitudinal steel concrete beam. The correctness in the study of the transverse system has for this reason been considered as crucial part of the work. However it has to be underlined that in the following procedure only SLS and ULS stresses checks are taken into account. A complete approach must take into account also the structural fire behaviour for example. Useful considerations on composite wood-concrete system with slim floor steel beams can be found in [66].
A general review of composite concrete-wood elements can be found in [92]. The concrete-wood interface shear connection may rely on different technologies. A first option consists in a notched shear connection. Mechanical devices such as screws can be exploited as well. A last type of connection is provided by glued surfaces. In order to conduce the SLS deflection and vibration and ULS stresses checks, the widely exploited γ-method is exploited. This method is also contained in the wood structures design codes such as EC [13]. The method can be exploited also on concrete-wood structures. According to [77] that compares full scale testing and analytical results of the γ-method on composite CLT-concrete systems, the method understimates the capacity with a margin of around 20%, thus remaining on the safe side. In order to conduce the checks reference to the recent developed design rules for concrete-wood elements [19] and Eurocode 5 [13] was made.

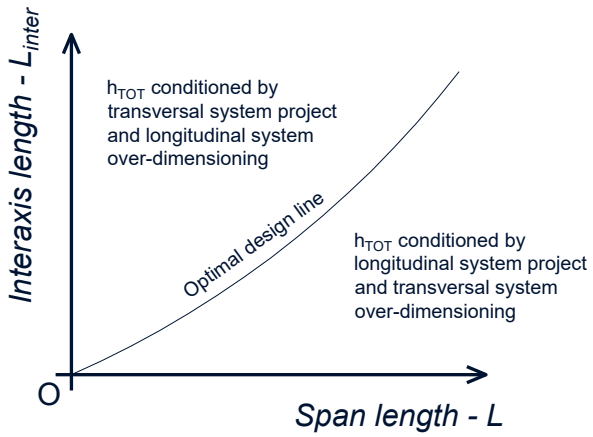

Figure D.1: Numerical shooting method visualisation

D.1 Gamma method for wood-concrete sections

Documents such as [5], provide the formulas for the γ-method for 3 to 5 CLT layer panels. In the present work the formulas are needed for a 3 to 5 layered CLT panel in conjuction with an upper concrete slab. So a formula providing the value of J_{eff} for 3+1 longitudinal layers is needed, where these are divided by 3 shear deformable interfaces. So a derivation of the formulas for such a case is needed. In [82] the derivation of the γ-method is explained and the reference is used to extend the approach.

D.1.1 Derivation for the 2-layer case

The formulas are derived from a simplified approach by considering a simply supported beam of span length l. A sinusoidal load q is considered on the beam:

$$q = q_0 \sin(\pi x/l) \tag{D.1}$$

The section is considered to be composed of two resistant layers distanced with a. These have axial stiffness of EA_1 and EA_2 and flexural stiffness of EJ_1 and EJ_2. The two layers deform axially by $u_1(x)$ and $u_2(x)$, so the strains will be u_1' and u_2'.
Between these two layers a shear deformable layer exists. The shear deformation stiffness of this is k. The overall system deforms with a deflection $w(x)$. Equations imposing the equilibrium condition and the kinematic congruence of the layers are needed. For a three layered CLT panel the system consists in:

$$\begin{cases} EA_1 u_1'' + k(u_2 - u_1 + w'a) = 0 \\ EA_2 u_2'' - k(u_2 - u_1 + w'a) = 0 \\ \sum_i EJ_i w^{IV} - ka(u_2' - u_1' + w''a) = q \end{cases} \tag{D.2}$$

Having a three equations system with three unknown functions $u_1(x)$, $u_2(x)$, $w(x)$, the solution can be derived. The sinusoidal load assumption implies that the solution of the previous written equations system

is in the form of:

$$u_1 = u_{10}\cos(\pi x/l) \qquad u_2 = u_{20}\cos(\pi x/l) \qquad w = w_0 \sin(\pi x/l) \tag{D.3}$$

The constants u_{10}, u_{20} and w_0 can be proven to be proportional to q_0 and functions of the parameters k, a, EA_1, EA_2, EJ_1, EJ_2 and l. The explicit solution is here not reported. The solution can be easily obtained by exploiting programs such as Wolfram Mathematica or the Simpy library in the Python programming language. Both have tools that allow to run symbolic analytical calculations in few steps. After having done this the deflection $w(x)$ of the actual system is imposed to be equal to the one of a homogeneus beam of flexural stiffness EJ_{eff} under a sinusoidal loading:

$$w(x) = w_0 \sin(\pi x/l) = \frac{q_0 L^4}{\pi^4 EJ_{eff}} \sin(\pi x/l) \tag{D.4}$$

Here the effective bending stiffness EJ_{eff} can be derived by considering:

$$EJ_{eff} = \frac{q_0 L^4}{\pi^4 w_0} \tag{D.5}$$

As already said, w_0 is proportional to q_0 so that the solution is not dependent on the load coefficient q_0. This provides the γ-method formulas also contained in EC5 [13], which are here written:

$$(EJ)_{ef} = \sum_i EJ_i + \gamma_2 EA_2 a_2^2 + \gamma_1 EA_1 a_1^2 \tag{D.6}$$

$$\gamma_2 = 1 \qquad \gamma_1 = \frac{1}{1 + \pi^2 EA_1/(k \cdot l^2)} \tag{D.7}$$

D.1.2 Extension to the 4-layer case

The previously presented approach can be extended to a system composed by N longitudinal layers divided by $N-1$ shear deformable layers. Here the case of $N = 4$ is of interest because the effective bending stiffness EJ_{eff} of a 5 layered CLT panel with an upper concrete slab is needed.

The mechanical system is here composed of 4 longitudinal layers of axial stiffness EA_i and bending stiffness EJ_i with $i = 1, ..., 4$. These deform axially with displacement $u_i(x)$ and vertically by a deflection $w(x)$ common to all layers. Layers are distanced by quantities b_i as shown in Fig.D.2 and the intermediate layers have shear stiffness k_i with $i = 1, 2, 3$. In order to do that the equations system D.2 is extended. The equations system is here reported:

$$\begin{cases} EA_1 u_1' + k_1(u_2 - u_1 + w' b_1) = 0 \\ EA_2 u_2'' - k_1(u_2 - u_1 + w' b_1) + k_2(u_3 - u_2 + w' b_2) = 0 \\ EA_3 u_3'' - k_2(u_3 - u_2 + w' b_2) + k_3(u_4 - u_3 + w' b_3) = 0 \\ EA_4 u_4'' - k_3(u_4 - u_3 + w' b_3) = 0 \\ \sum_i EJ_i w^{IV} - k_1 b_1(u_2' - u_1' + w'' b_1) - k_2 b_2(u_3' - u_2' + w'' b_2) - k_3 b_3(u_3' - u_2' + w'' b_3) = q \end{cases} \tag{D.8}$$

Here w, u_1, u_2, u_3, q are all functions of x. Moreover, similarly to the 2-layer case, as consequence of the sinusoidal load distribution assumption, the following can be proven:

$$u_1 = u_{10}\cos(\pi x/l) \qquad u_2 = u_{20}\cos(\pi x/l) \tag{D.9}$$

$$u_3 = u_{30}\cos(\pi x/l) \qquad u_4 = u_{40}\cos(\pi x/l) \qquad w = w_0\sin(\pi x/l) \tag{D.10}$$

Here u_{i0} and w_0 are all functions of the different coefficients EA_i, EJ_i, l, b_j, k_j for $i = 1, ..., 4$ and $j = 1, 2, 3$ and proportional to q_0. By equationg the deflection of a homogeneus beam of bending stiffness EJ_{eff} with the deflection of the actual system the expression of the EJ_{eff} can be derived. The solution is again not function of the parameter q_0. The explicit function is here not reported. Expressions can be derived by exploiting tools such as Wolfram Mathematica or the Simpy library in the Python language. Adding layers, N gets bigger and terms tends to proliferate. The used expression in the subsequent analysis is in the form:

$$EJ_{eff} = EJ_{eff}(EA_1, ..., EA_4, EJ_1, ..., EJ_4, b_1, ..., b_3, k_1, ...k_3, l) \tag{D.11}$$

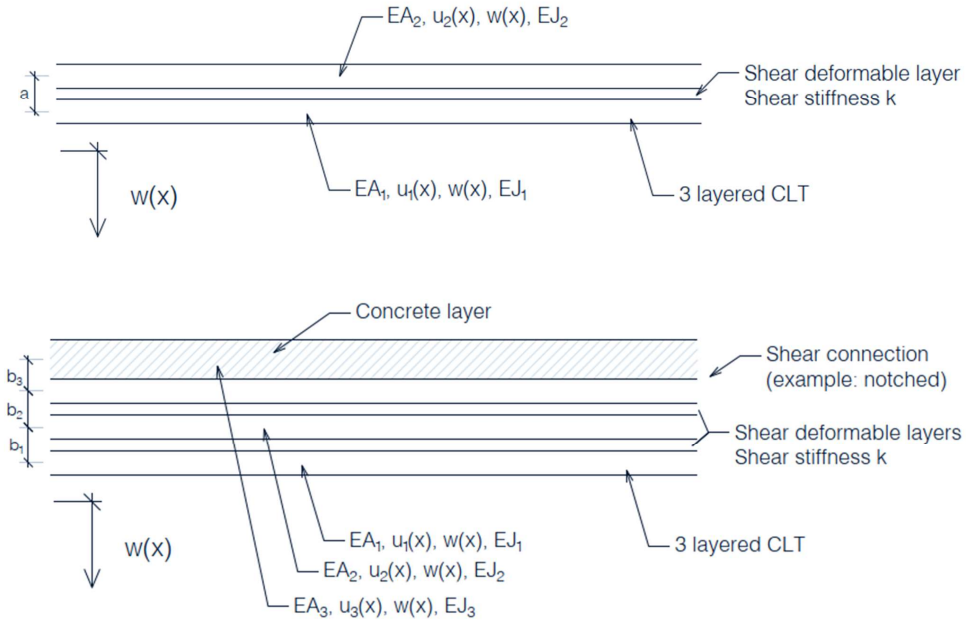

Figure D.2: layers of the wood-concrete composite system

D.2 Checks

The CLT-concrete composite system is studied. Every possible solution has a specific slab height h_{slab} that coincides with the longitudinal steel-concrete composite slab height. Furthermore a specific CLT panel has to be chosen. The CLT panel in detail has an own composition made of different layers thicknesses $t_1 - t_2 - t_3$ if a 3-layered CLT is considered and $t_1 - t_2 - t_3 - t_4 - t_5$ if a 5-layered CLT is taken. The static scheme is the one of a simply supported beam of span length L_{inter}.

The chosen materials are C35/45 concrete and C24 CLT panel. Related relevant properties are:

C35/45 concrete	
$f_{ck} = 35.0\ MPa$	cylindric characteristic value of compression resistance
$f_{cd} = 25.9\ MPa$	design value of compression resistance
$f_{cm} = 43.0\ MPa$	mean value of compression resistance
$f_{ctm} = 3.2\ MPa$	mean value of tensile resistance
$E_{cm} = 34077.1\ MPa$	mean value of elastic modulus
C24 CLT panel	
$f_{m,k} = 24.0\ MPa$	characteristic value of bending resistance
$f_{t,0,k} = 14.5\ MPa$	characteristic value of tensile resistance parallel to fibres
$f_{t,90,k} = 0.4\ MPa$	characteristic value of tensile resistance orthogonal to fibres
$f_{c,0,k} = 21.0\ MPa$	characteristic value of compression resistance parallel to fibres
$f_{c,90,k} = 2.5\ MPa$	characteristic value of compression resistance orthogonal to fibres
$f_{v,k} = 4.0\ MPa$	characteristic value of shear resistance
$E_{m,0,mean} = 11000.0\ MPa$	mean elastic modulus parallel to fibres
$E_{m,0,0.05} = 74000.0\ MPa$	characteristic value of elastic modulus parallel to fibres
$G_{mean} = 690\ MPa$	mean shear modulus
$G_{rs} = 69\ MPa$	rolling shear modulus
$\rho_k = 350.0\ kg/m^3$	characteristic value of density
$\rho_{mean} = 420\ kg/m^3$	mean density

After having specified the materials and the sectional composition, the following relevant quantities can be obtained:

$$h_{CLT} = \sum t_i = \begin{cases} t_1 + t_2 + t_3 \quad \text{3-layered CLT} \\ t_1 + t_2 + t_3 + t_4 + t_5 \quad \text{5-layered CLT} \end{cases} \tag{D.12}$$

$$h_x = \begin{cases} t_1 + t_3 \quad \text{3-layered CLT} \\ t_1 + t_3 + t_5 \quad \text{5-layered CLT} \end{cases} \tag{D.13}$$

$$h_y = \begin{cases} t_2 \quad \text{3-layered CLT} \\ t_2 + t_4 \quad \text{5-layered CLT} \end{cases} \tag{D.14}$$

$$A_{x,net} = h_x \cdot b_{ref} \qquad A_{y,net} = h_y \cdot b_{ref} \tag{D.15}$$

$$h_{TOT} = h_{CLT} + h_{slab} \tag{D.16}$$

The shear connection type affects the shear stiffness at the CLT-concrete interface. Here a notched connection is taken into account. The notch depth is $h_n = 30\ mm$ and the notch spacing is $s_{ef} = 200\ mm$. The standard [19] provides the values to be taken into account for the shear stiffness. For the selected

notch height:

$$K_u = K_{ser} = \begin{cases} 1000 \frac{N/mm}{mm} & \text{for } h_n = 20mm \\ 1500 \frac{N/mm}{mm} & \text{for } h_n \geq 30mm \end{cases} \tag{D.17}$$

Precambering is allowed by [19]. However in the present work the precambering possibility is not considered. This is because it's not commonly done in practice. In order to run the SLS checks the time effects have to be taken into account both on the concrete and the wood side. Moreover the different construction stages have to be taken into account. The structure is considered to be propped. As a propped solution is definitely needed in order for the steel-concrete solution to work. So, a propped solution will be also considered for the wood-concrete solution in transverse direction. The deflection checks are performed both at short term and long term. In order to do that the effective bending stiffness has been computed both at short term and infinite time taking into account the wood and concrete time dependent effects. At section 4.3.2 the standard rule [19] specifies how the elastic properties must take into account for time effects. This is done as follows:

$$E_{c,fin} = \frac{E_{cm}}{1 + \psi_{conc}\phi(\infty, t_0)} \tag{D.18}$$

$$E_{tim,fin} = \frac{E_{0,mean}}{1 + \psi_{tim}k_{def}} \tag{D.19}$$

$$K_{ser,fin} = \frac{K_{ser}}{1 + \psi_{conn}k'_{def}} \tag{D.20}$$

$$K_{u,fin} = \frac{K_u}{1 + \psi_{conn}k'_{def}} \tag{D.21}$$

For the wood shear deformable layers the stiffness k is computed as:

$$k_i = G_{rs}/t_i \cdot b_{ref} \qquad \text{for i=2,4 if 5-layered CLT or i=2 if 3-layered CLT} \tag{D.22}$$

For the wood-concrete interface the used stiffness is K_{ser}. The effective bending stiffness is then computed as proposed by formula D.11. The following values are computed:

$EJ_{eff,ST}$	Instantaneous value of bending stiffness
$EJ_{eff,LT}$	Long term value of bending stiffness

A partially clamped static scheme is here considered. So the coefficient $\beta = 3/384$ is used. The deflection is computed under short term load in the characteristic load combination:

$$w_{ST} = w_{ST,G} + w_{ST,Q} = \beta\frac{(g_1 + g_2)L^4}{EJ_{eff,ST}} + \beta\frac{(q)L^4}{EJ_{eff,ST}} \tag{D.23}$$

The deflection is computed under long term load in the quasi permanent load combination and added to a short term component given by the live load term in a difference between the characteristic and quasi-permanent load contribution:

$$w_{LT} = w_{LT,G,qp} + w_{LT,Q,qp} + w_{LT,Q,char-qp} = \beta\frac{(g_1 + g_2)L^4}{EJ_{eff,LT}} + \beta\frac{(q)L^4}{EJ_{eff,LT}} + (1-\psi_{2Q})\beta\frac{(q)L^4}{EJ_{eff,ST}} \tag{D.24}$$

Furthermore, the long term load under self weight G is computed as:

$$w_{LT,G,qp} = \beta \frac{(g_1 + g_2)L^4}{EJ_{eff,LT}} \tag{D.25}$$

The instantaneous deflection under Q is:

$$w_{ST,Q,char} = \beta \frac{(q)L^4}{EJ_{eff,ST}} \tag{D.26}$$

Following limits are imposed:

$w_{ST,lim} = 1/500$	Short term limit under G+Q
$w_{LT,lim} = 1/300$	Long term limit under G+Q
$w_{LT,G,lim} = 1/500$	Long term limit under G
$w_{ST,Q,lim} = 1/500$	Short term limit under Q

The SLS vibration check is performed by considering:

$$f = \frac{2}{\pi}\sqrt{\frac{\alpha_{b,dyn} EJ_{eff,ST,dyn}}{\mu}} \tag{D.27}$$

Here μ is the distributed mass per unit length. The value of $EJ_{eff,ST,dyn}$ is computed by using the value of the dynamic elastic modulus of concrete $E_{c,dyn} = 1.1 \cdot E_{cm}$. According to the assumed partially clamped static scheme the value $\alpha_{b,dyn} = 3$ is used. The minimum frequency allowed is set to $f_{lim} = 4\,Hz$.

D.3 Parametric analysis

In order to collect data for the steel-concrete longitudinal system design, to better understand the transverse decking system performance and improve the design of the overall structural flooring system, a restricted parametric study was done on the behaviour of the wood-concrete composite system. Here the slab height was varied between in the range $h_{slab} = [50, 55, ..., 135mm]$. The used CLT panels have been varied within all the common commercial possibilities of 3- and 5-layered CLT solutions. The list has been extracted from [5]. The CLT heights consequently range between $h_{CLT} = [60, 70, ..., 200mm]$ and the total heights range in $h_{TOT} = [110, 115, ..., 335]$. The interaxis length l has been also varied. Here the chosen range is $l = [4.5, 5.0, ..., 7.5m]$.

The computation of the long term deflection, short term deflection and vibration frequency have been performed for every case studied. Results are shown in charts of Fig.D.4. Most critical check is the one on the long term deflection. In Fig.D.3 the minimum height of the section in order to satisfy the SLS long term deflection checks for variable deflection-spanlength limits is shown. The static scheme has also been varied between $\alpha = 0$ for a perfect pinned-pinned situation, to $\alpha = 1$ for a perfect clamped-clamped situation. The reference case for this study is $\alpha = 0.5$ for a partially clamped scheme.

As reminder the present parametric study is specific for the present decking technology and for the particular load values.

Considering a $1/300$ deflection-span limit on a partially clamped situation results in $h_{TOT}/L \approx 1/25$.

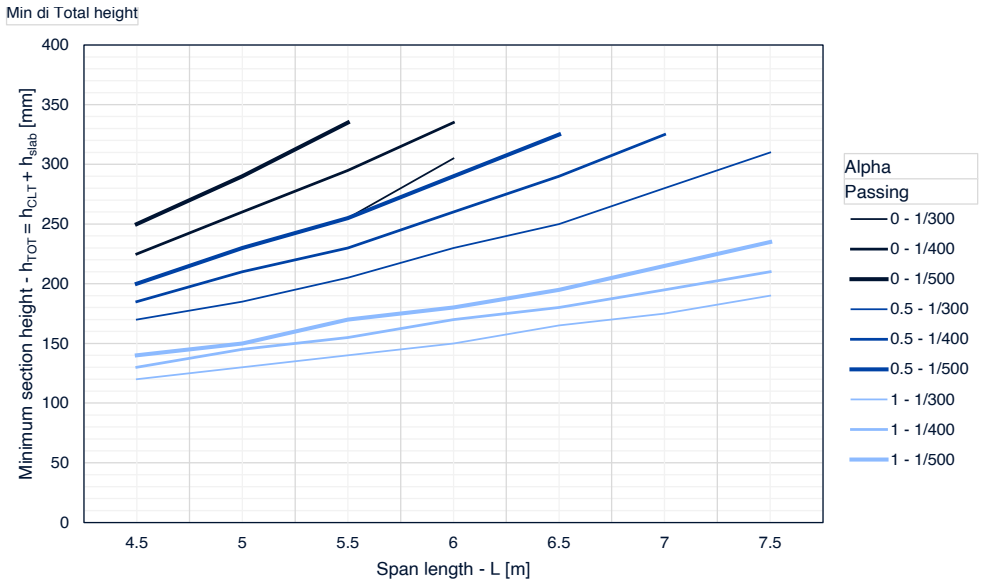

Figure D.3: Numerical shooting method visualisation

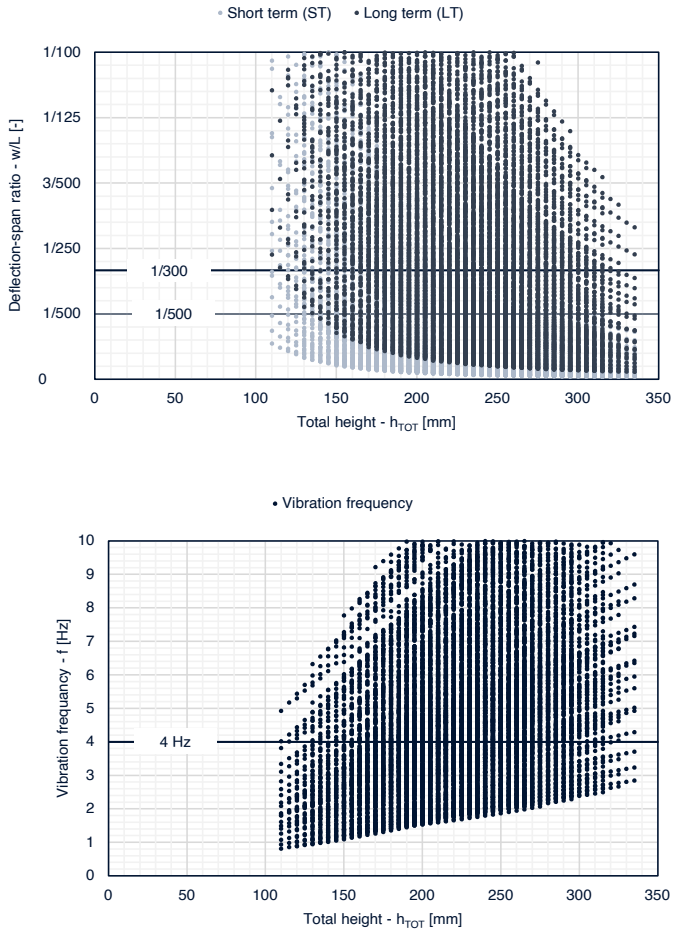

Figure D.4: Numerical shooting method visualisation

Appendix E

Numerical analysis energy curves

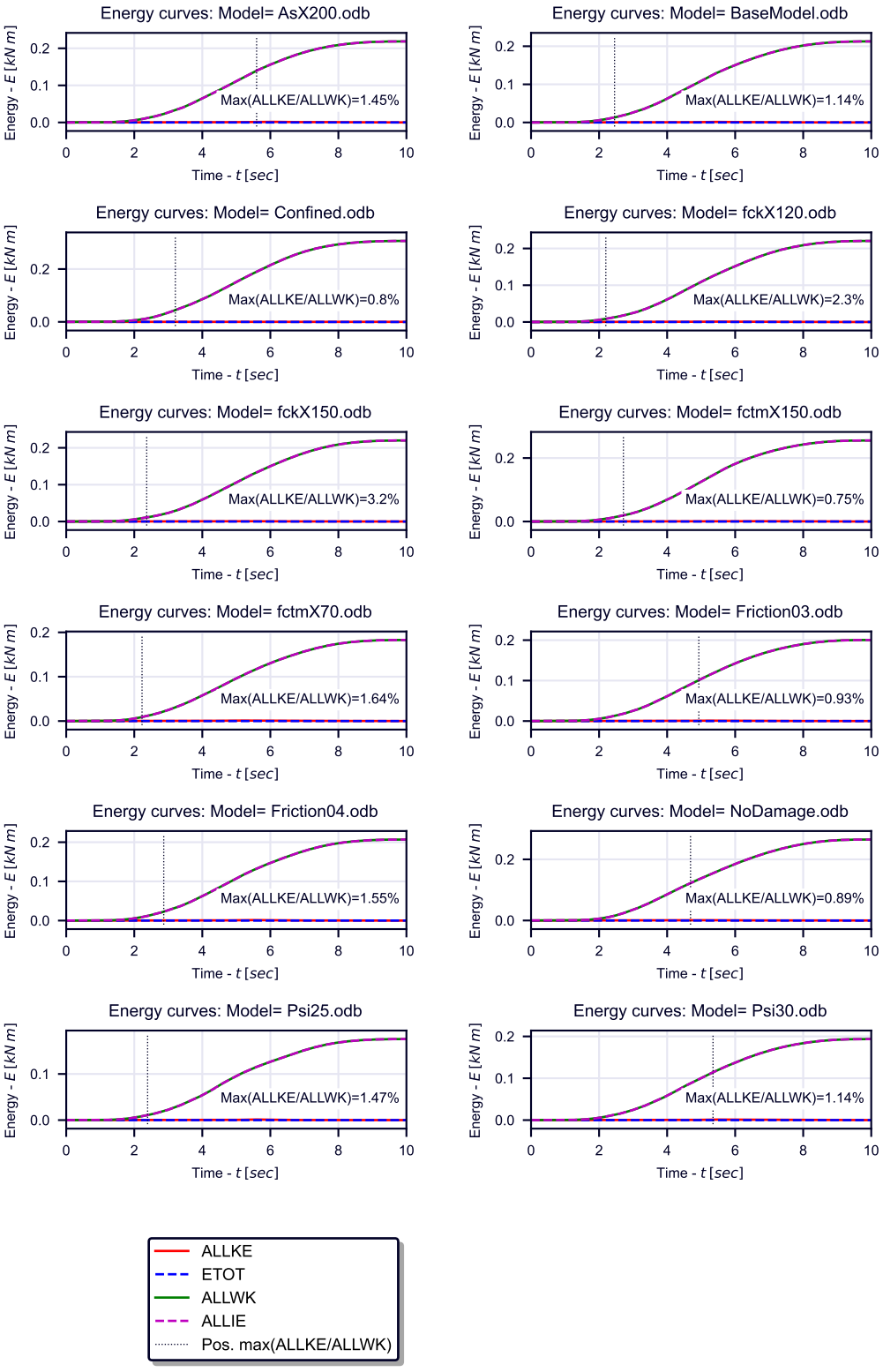
Energy curves: Model= AsX200.odb
Max(ALLKE/ALLWK)=1.45%
Energy curves: Model= BaseModel.odb
Max(ALLKE/ALLWK)=1.14%
Energy curves: Model= Confined.odb
Max(ALLKE/ALLWK)=0.8%
Energy curves: Model= fckX120.odb
Max(ALLKE/ALLWK)=2.3%
Energy curves: Model= fckX150.odb
Max(ALLKE/ALLWK)=3.2%
Energy curves: Model= fctmX150.odb
Max(ALLKE/ALLWK)=0.75%
Energy curves: Model= fctmX70.odb
Max(ALLKE/ALLWK)=1.64%
Energy curves: Model= Friction03.odb
Max(ALLKE/ALLWK)=0.93%
Energy curves: Model= Friction04.odb
Max(ALLKE/ALLWK)=1.55%
Energy curves: Model= NoDamage.odb
Max(ALLKE/ALLWK)=0.89%
Energy curves: Model= Psi25.odb
Max(ALLKE/ALLWK)=1.47%
Energy curves: Model= Psi30.odb
Max(ALLKE/ALLWK)=1.14%
Energy - E [kN m]
Time - t [sec]
ALLKE
ETOT
ALLWK
ALLIE
Pos. max(ALLKE/ALLWK)

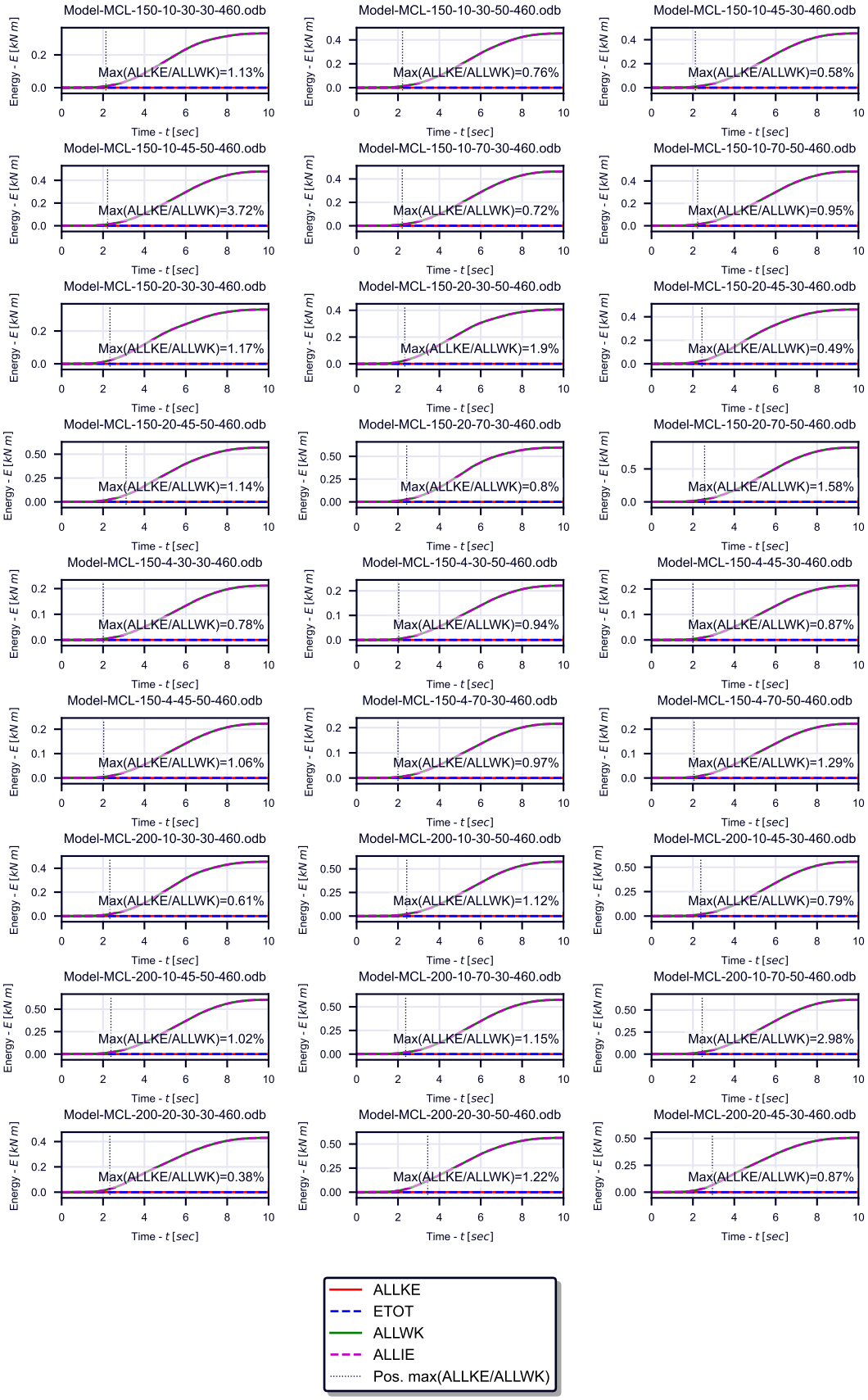
Model-MCL-150-10-30-30-460.odb
Max(ALLKE/ALLWK)=1.13%
Model-MCL-150-10-30-50-460.odb
Max(ALLKE/ALLWK)=0.76%
Model-MCL-150-10-45-30-460.odb
Max(ALLKE/ALLWK)=0.58%
Model-MCL-150-10-45-50-460.odb
Max(ALLKE/ALLWK)=3.72%
Model-MCL-150-10-70-30-460.odb
Max(ALLKE/ALLWK)=0.72%
Model-MCL-150-10-70-50-460.odb
Max(ALLKE/ALLWK)=0.95%
Model-MCL-150-20-30-30-460.odb
Max(ALLKE/ALLWK)=1.17%
Model-MCL-150-20-30-50-460.odb
Max(ALLKE/ALLWK)=1.9%
Model-MCL-150-20-45-30-460.odb
Max(ALLKE/ALLWK)=0.49%
Model-MCL-150-20-45-50-460.odb
Max(ALLKE/ALLWK)=1.14%
Model-MCL-150-20-70-30-460.odb
Max(ALLKE/ALLWK)=0.8%
Model-MCL-150-20-70-50-460.odb
Max(ALLKE/ALLWK)=1.58%
Model-MCL-150-4-30-30-460.odb
Max(ALLKE/ALLWK)=0.78%
Model-MCL-150-4-30-50-460.odb
Max(ALLKE/ALLWK)=0.94%
Model-MCL-150-4-45-30-460.odb
Max(ALLKE/ALLWK)=0.87%
Model-MCL-150-4-45-50-460.odb
Max(ALLKE/ALLWK)=1.06%
Model-MCL-150-4-70-30-460.odb
Max(ALLKE/ALLWK)=0.97%
Model-MCL-150-4-70-50-460.odb
Max(ALLKE/ALLWK)=1.29%
Model-MCL-200-10-30-30-460.odb
Max(ALLKE/ALLWK)=0.61%
Model-MCL-200-10-30-50-460.odb
Max(ALLKE/ALLWK)=1.12%
Model-MCL-200-10-45-30-460.odb
Max(ALLKE/ALLWK)=0.79%
Model-MCL-200-10-45-50-460.odb
Max(ALLKE/ALLWK)=1.02%
Model-MCL-200-10-70-30-460.odb
Max(ALLKE/ALLWK)=1.15%
Model-MCL-200-10-70-50-460.odb
Max(ALLKE/ALLWK)=2.98%
Model-MCL-200-20-30-30-460.odb
Max(ALLKE/ALLWK)=0.38%
Model-MCL-200-20-30-50-460.odb
Max(ALLKE/ALLWK)=1.22%
Model-MCL-200-20-45-30-460.odb
Max(ALLKE/ALLWK)=0.87%
Energy - E [kN m]
Time - t [sec]
ALLKE
ETOT
ALLWK
ALLIE
Pos. max(ALLKE/ALLWK)

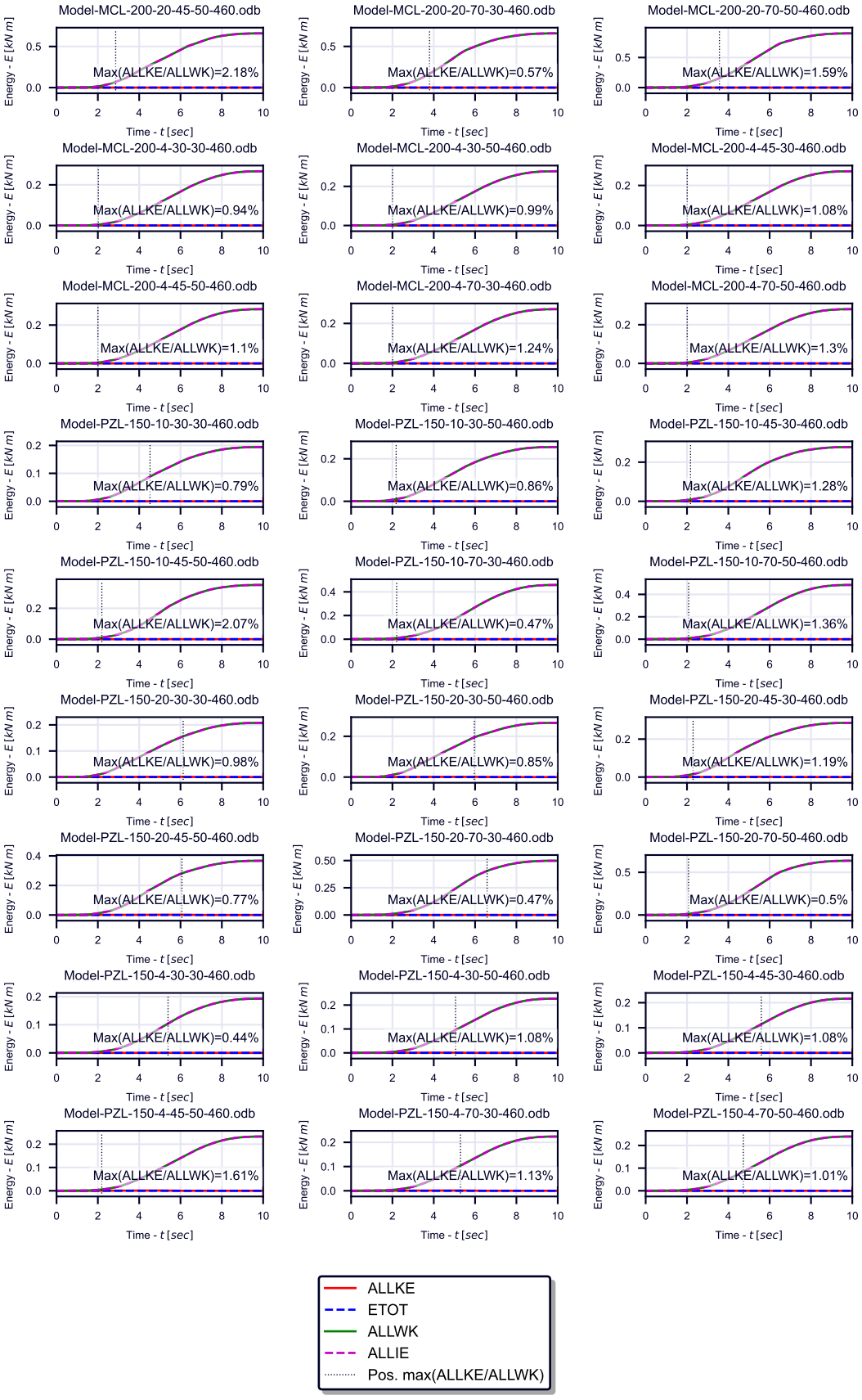
Model-MCL-200-20-45-50-460.odb
Max(ALLKE/ALLWK)=2.18%
Model-MCL-200-20-70-30-460.odb
Max(ALLKE/ALLWK)=0.57%
Model-MCL-200-20-70-50-460.odb
Max(ALLKE/ALLWK)=1.59%
Model-MCL-200-4-30-30-460.odb
Max(ALLKE/ALLWK)=0.94%
Model-MCL-200-4-30-50-460.odb
Max(ALLKE/ALLWK)=0.99%
Model-MCL-200-4-45-30-460.odb
Max(ALLKE/ALLWK)=1.08%
Model-MCL-200-4-45-50-460.odb
Max(ALLKE/ALLWK)=1.1%
Model-MCL-200-4-70-30-460.odb
Max(ALLKE/ALLWK)=1.24%
Model-MCL-200-4-70-50-460.odb
Max(ALLKE/ALLWK)=1.3%
Model-PZL-150-10-30-30-460.odb
Max(ALLKE/ALLWK)=0.79%
Model-PZL-150-10-30-50-460.odb
Max(ALLKE/ALLWK)=0.86%
Model-PZL-150-10-45-30-460.odb
Max(ALLKE/ALLWK)=1.28%
Model-PZL-150-10-45-50-460.odb
Max(ALLKE/ALLWK)=2.07%
Model-PZL-150-10-70-30-460.odb
Max(ALLKE/ALLWK)=0.47%
Model-PZL-150-10-70-50-460.odb
Max(ALLKE/ALLWK)=1.36%
Model-PZL-150-20-30-30-460.odb
Max(ALLKE/ALLWK)=0.98%
Model-PZL-150-20-30-50-460.odb
Max(ALLKE/ALLWK)=0.85%
Model-PZL-150-20-45-30-460.odb
Max(ALLKE/ALLWK)=1.19%
Model-PZL-150-20-45-50-460.odb
Max(ALLKE/ALLWK)=0.77%
Model-PZL-150-20-70-30-460.odb
Max(ALLKE/ALLWK)=0.47%
Model-PZL-150-20-70-50-460.odb
Max(ALLKE/ALLWK)=0.5%
Model-PZL-150-4-30-30-460.odb
Max(ALLKE/ALLWK)=0.44%
Model-PZL-150-4-30-50-460.odb
Max(ALLKE/ALLWK)=1.08%
Model-PZL-150-4-45-30-460.odb
Max(ALLKE/ALLWK)=1.08%
Model-PZL-150-4-45-50-460.odb
Max(ALLKE/ALLWK)=1.61%
Model-PZL-150-4-70-30-460.odb
Max(ALLKE/ALLWK)=1.13%
Model-PZL-150-4-70-50-460.odb
Max(ALLKE/ALLWK)=1.01%
Energy - E [kN m]
Time - t [sec]
ALLKE
ETOT
ALLWK
ALLIE
Pos. max(ALLKE/ALLWK)

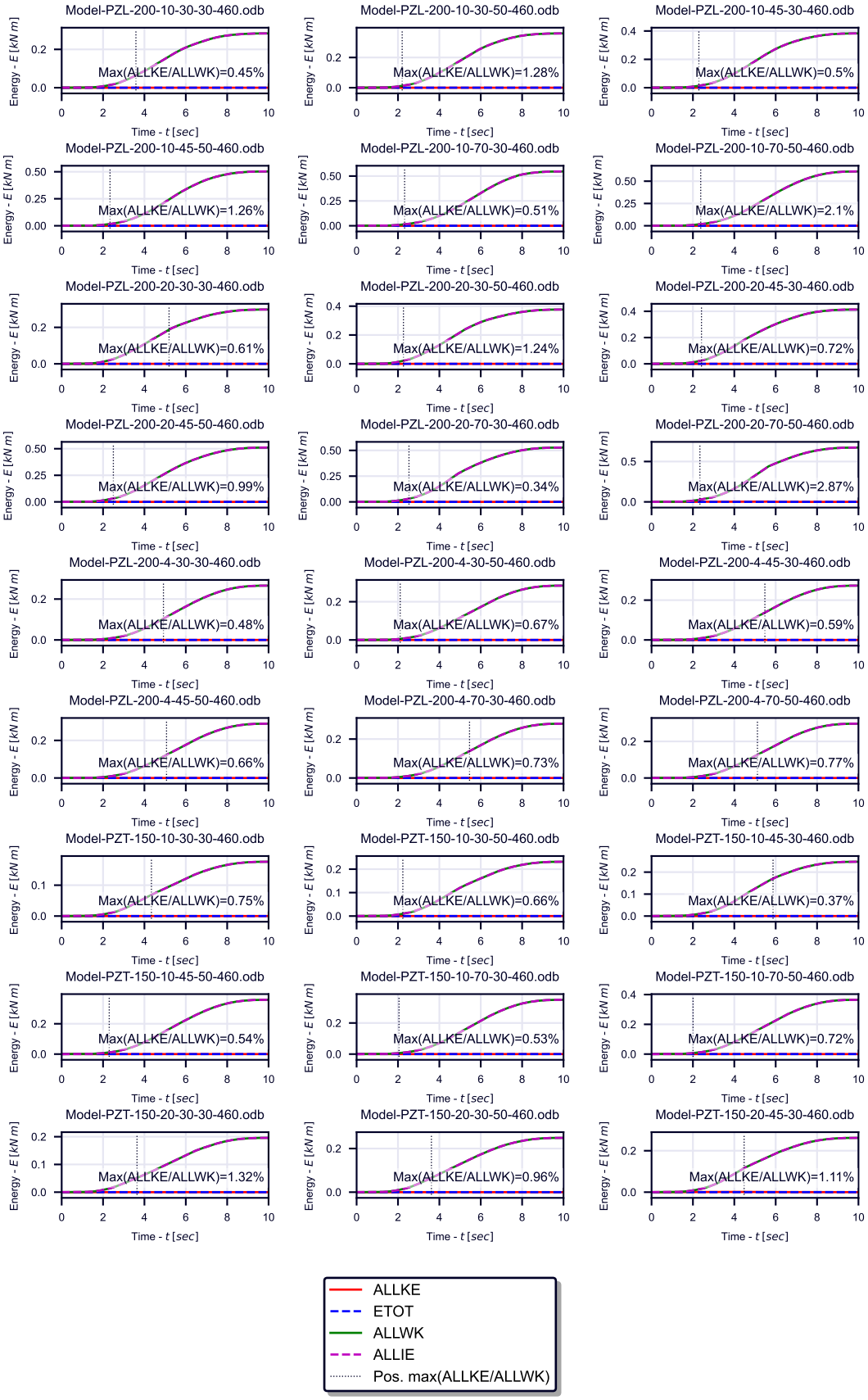
Model-PZL-200-10-30-30-460.odb
Max(ALLKE/ALLWK)=0.45%
Model-PZL-200-10-30-50-460.odb
Max(ALLKE/ALLWK)=1.28%
Model-PZL-200-10-45-30-460.odb
Max(ALLKE/ALLWK)=0.5%
Model-PZL-200-10-45-50-460.odb
Max(ALLKE/ALLWK)=1.26%
Model-PZL-200-10-70-30-460.odb
Max(ALLKE/ALLWK)=0.51%
Model-PZL-200-10-70-50-460.odb
Max(ALLKE/ALLWK)=2.1%
Model-PZL-200-20-30-30-460.odb
Max(ALLKE/ALLWK)=0.61%
Model-PZL-200-20-30-50-460.odb
Max(ALLKE/ALLWK)=1.24%
Model-PZL-200-20-45-30-460.odb
Max(ALLKE/ALLWK)=0.72%
Model-PZL-200-20-45-50-460.odb
Max(ALLKE/ALLWK)=0.99%
Model-PZL-200-20-70-30-460.odb
Max(ALLKE/ALLWK)=0.34%
Model-PZL-200-20-70-50-460.odb
Max(ALLKE/ALLWK)=2.87%
Model-PZL-200-4-30-30-460.odb
Max(ALLKE/ALLWK)=0.48%
Model-PZL-200-4-30-50-460.odb
Max(ALLKE/ALLWK)=0.67%
Model-PZL-200-4-45-30-460.odb
Max(ALLKE/ALLWK)=0.59%
Model-PZL-200-4-45-50-460.odb
Max(ALLKE/ALLWK)=0.66%
Model-PZL-200-4-70-30-460.odb
Max(ALLKE/ALLWK)=0.73%
Model-PZL-200-4-70-50-460.odb
Max(ALLKE/ALLWK)=0.77%
Model-PZT-150-10-30-30-460.odb
Max(ALLKE/ALLWK)=0.75%
Model-PZT-150-10-30-50-460.odb
Max(ALLKE/ALLWK)=0.66%
Model-PZT-150-10-45-30-460.odb
Max(ALLKE/ALLWK)=0.37%
Model-PZT-150-10-45-50-460.odb
Max(ALLKE/ALLWK)=0.54%
Model-PZT-150-10-70-30-460.odb
Max(ALLKE/ALLWK)=0.53%
Model-PZT-150-10-70-50-460.odb
Max(ALLKE/ALLWK)=0.72%
Model-PZT-150-20-30-30-460.odb
Max(ALLKE/ALLWK)=1.32%
Model-PZT-150-20-30-50-460.odb
Max(ALLKE/ALLWK)=0.96%
Model-PZT-150-20-45-30-460.odb
Max(ALLKE/ALLWK)=1.11%
Energy - E [kN m]
Time - t [sec]
ALLKE
ETOT
ALLWK
ALLIE
Pos. max(ALLKE/ALLWK)

Appendix F

Parametric study full results

F.1 Integrated floor beam for office building

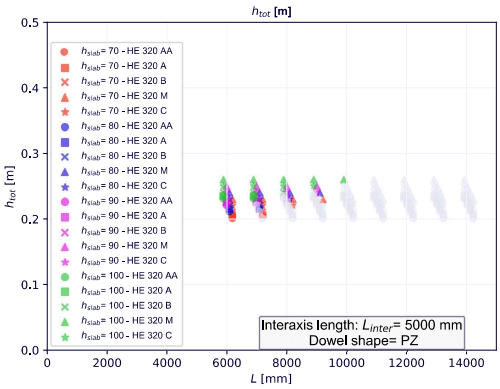
h_{tot} [m]
h_{tot} [m]
L [mm]
h_{slab}= 70 - HE 320 AA
h_{slab}= 70 - HE 320 A
h_{slab}= 70 - HE 320 B
h_{slab}= 70 - HE 320 M
h_{slab}= 70 - HE 320 C
h_{slab}= 80 - HE 320 AA
h_{slab}= 80 - HE 320 A
h_{slab}= 80 - HE 320 B
h_{slab}= 80 - HE 320 M
h_{slab}= 80 - HE 320 C
h_{slab}= 90 - HE 320 AA
h_{slab}= 90 - HE 320 A
h_{slab}= 90 - HE 320 B
h_{slab}= 90 - HE 320 M
h_{slab}= 90 - HE 320 C
h_{slab}= 100 - HE 320 AA
h_{slab}= 100 - HE 320 A
h_{slab}= 100 - HE 320 B
h_{slab}= 100 - HE 320 M
h_{slab}= 100 - HE 320 C
Interaxis length: L_{inter}= 5000 mm
Dowel shape= PZ

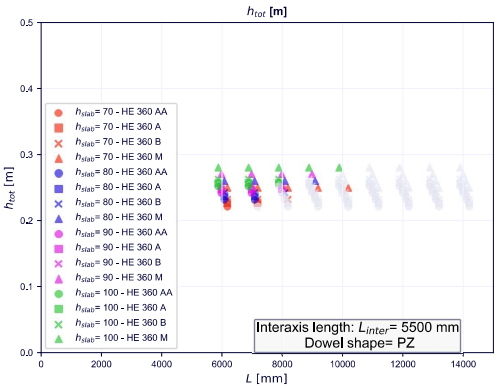
h_{tot} [m]
h_{tot} [m]
L [mm]
h_{slab}= 70 - HE 360 AA
h_{slab}= 70 - HE 360 A
h_{slab}= 70 - HE 360 B
h_{slab}= 70 - HE 360 M
h_{slab}= 80 - HE 360 AA
h_{slab}= 80 - HE 360 A
h_{slab}= 80 - HE 360 B
h_{slab}= 80 - HE 360 M
h_{slab}= 90 - HE 360 AA
h_{slab}= 90 - HE 360 A
h_{slab}= 90 - HE 360 B
h_{slab}= 90 - HE 360 M
h_{slab}= 100 - HE 360 AA
h_{slab}= 100 - HE 360 A
h_{slab}= 100 - HE 360 B
h_{slab}= 100 - HE 360 M
Interaxis length: L_{inter}= 5500 mm
Dowel shape= PZ

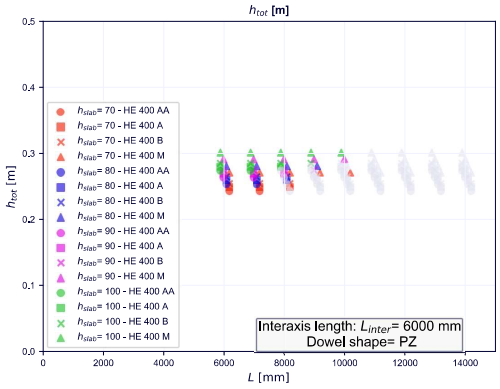
h_{tot} [m]
h_{tot} [m]
L [mm]
h_{slab}= 70 - HE 400 AA
h_{slab}= 70 - HE 400 A
h_{slab}= 70 - HE 400 B
h_{slab}= 70 - HE 400 M
h_{slab}= 80 - HE 400 AA
h_{slab}= 80 - HE 400 A
h_{slab}= 80 - HE 400 B
h_{slab}= 80 - HE 400 M
h_{slab}= 90 - HE 400 AA
h_{slab}= 90 - HE 400 A
h_{slab}= 90 - HE 400 B
h_{slab}= 90 - HE 400 M
h_{slab}= 100 - HE 400 AA
h_{slab}= 100 - HE 400 A
h_{slab}= 100 - HE 400 B
h_{slab}= 100 - HE 400 M
Interaxis length: L_{inter}= 6000 mm
Dowel shape= PZ

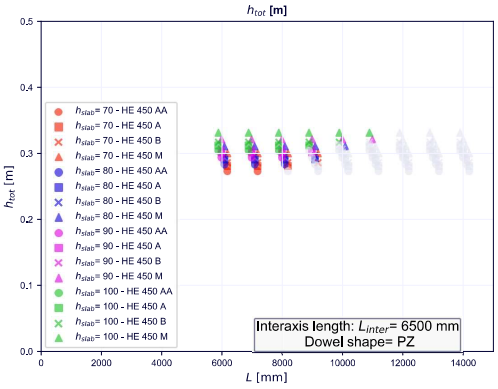
h_{tot} [m]
h_{tot} [m]
L [mm]
h_{slab}= 70 - HE 450 AA
h_{slab}= 70 - HE 450 A
h_{slab}= 70 - HE 450 B
h_{slab}= 70 - HE 450 M
h_{slab}= 80 - HE 450 AA
h_{slab}= 80 - HE 450 A
h_{slab}= 80 - HE 450 B
h_{slab}= 80 - HE 450 M
h_{slab}= 90 - HE 450 AA
h_{slab}= 90 - HE 450 A
h_{slab}= 90 - HE 450 B
h_{slab}= 90 - HE 450 M
h_{slab}= 100 - HE 450 AA
h_{slab}= 100 - HE 450 A
h_{slab}= 100 - HE 450 B
h_{slab}= 100 - HE 450 M
Interaxis length: L_{inter}= 6500 mm
Dowel shape= PZ

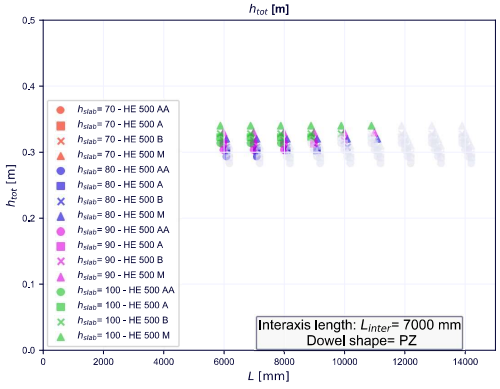
h_{tot} [m]
h_{tot} [m]
L [mm]
h_{slab}= 70 - HE 500 AA
h_{slab}= 70 - HE 500 A
h_{slab}= 70 - HE 500 B
h_{slab}= 70 - HE 500 M
h_{slab}= 80 - HE 500 AA
h_{slab}= 80 - HE 500 A
h_{slab}= 80 - HE 500 B
h_{slab}= 80 - HE 500 M
h_{slab}= 90 - HE 500 AA
h_{slab}= 90 - HE 500 A
h_{slab}= 90 - HE 500 B
h_{slab}= 90 - HE 500 M
h_{slab}= 100 - HE 500 AA
h_{slab}= 100 - HE 500 A
h_{slab}= 100 - HE 500 B
h_{slab}= 100 - HE 500 M
Interaxis length: L_{inter}= 7000 mm
Dowel shape= PZ

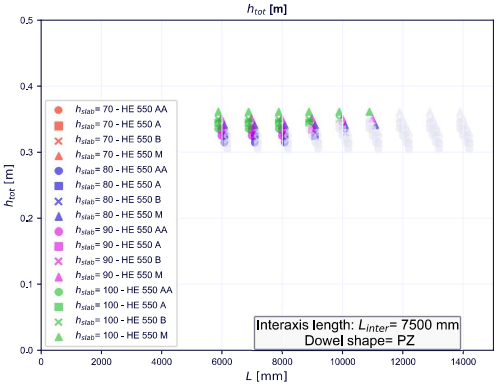
h_{tot} [m]
h_{tot} [m]
L [mm]
h_{slab}= 70 - HE 550 AA
h_{slab}= 70 - HE 550 A
h_{slab}= 70 - HE 550 B
h_{slab}= 70 - HE 550 M
h_{slab}= 80 - HE 550 AA
h_{slab}= 80 - HE 550 A
h_{slab}= 80 - HE 550 B
h_{slab}= 80 - HE 550 M
h_{slab}= 90 - HE 550 AA
h_{slab}= 90 - HE 550 A
h_{slab}= 90 - HE 550 B
h_{slab}= 90 - HE 550 M
h_{slab}= 100 - HE 550 AA
h_{slab}= 100 - HE 550 A
h_{slab}= 100 - HE 550 B
h_{slab}= 100 - HE 550 M
Interaxis length: L_{inter}= 7500 mm
Dowel shape= PZ

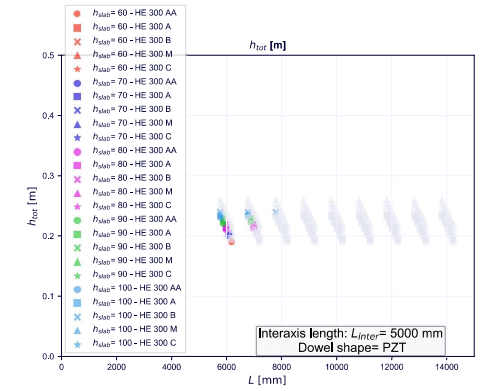
h_{tot} [m]
h_{tot} [m]
L [mm]
h_{slab}= 60 - HE 300 AA
h_{slab}= 60 - HE 300 A
h_{slab}= 60 - HE 300 B
h_{slab}= 60 - HE 300 M
h_{slab}= 60 - HE 300 C
h_{slab}= 70 - HE 300 AA
h_{slab}= 70 - HE 300 A
h_{slab}= 70 - HE 300 B
h_{slab}= 70 - HE 300 M
h_{slab}= 70 - HE 300 C
h_{slab}= 80 - HE 300 AA
h_{slab}= 80 - HE 300 A
h_{slab}= 80 - HE 300 B
h_{slab}= 80 - HE 300 M
h_{slab}= 80 - HE 300 C
h_{slab}= 90 - HE 300 AA
h_{slab}= 90 - HE 300 A
h_{slab}= 90 - HE 300 B
h_{slab}= 90 - HE 300 M
h_{slab}= 90 - HE 300 C
h_{slab}= 100 - HE 300 AA
h_{slab}= 100 - HE 300 A
h_{slab}= 100 - HE 300 B
h_{slab}= 100 - HE 300 M
h_{slab}= 100 - HE 300 C
Interaxis length: L_{inter}= 5000 mm
Dowel shape= PZT

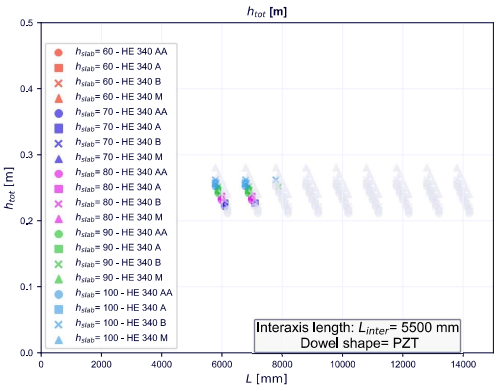
h_{tot} [m]
h_{tot} [m]
L [mm]
h_{slab}= 60 - HE 340 AA
h_{slab}= 60 - HE 340 A
h_{slab}= 60 - HE 340 B
h_{slab}= 60 - HE 340 M
h_{slab}= 70 - HE 340 AA
h_{slab}= 70 - HE 340 A
h_{slab}= 70 - HE 340 B
h_{slab}= 70 - HE 340 M
h_{slab}= 80 - HE 340 AA
h_{slab}= 80 - HE 340 A
h_{slab}= 80 - HE 340 B
h_{slab}= 80 - HE 340 M
h_{slab}= 90 - HE 340 AA
h_{slab}= 90 - HE 340 A
h_{slab}= 90 - HE 340 B
h_{slab}= 90 - HE 340 M
h_{slab}= 100 - HE 340 AA
h_{slab}= 100 - HE 340 A
h_{slab}= 100 - HE 340 B
h_{slab}= 100 - HE 340 M
Interaxis length: L_{inter}= 5500 mm
Dowel shape= PZT

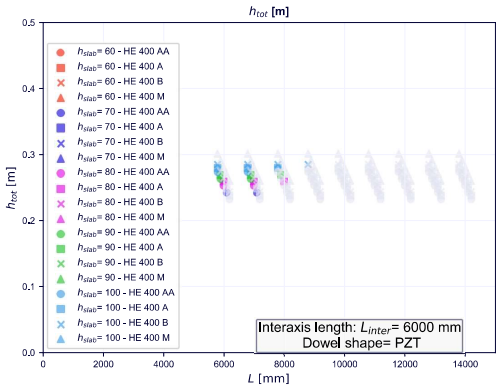
h_{tot} [m]
h_{tot} [m]
L [mm]
h_{slab}= 60 - HE 400 AA
h_{slab}= 60 - HE 400 A
h_{slab}= 60 - HE 400 B
h_{slab}= 60 - HE 400 M
h_{slab}= 70 - HE 400 AA
h_{slab}= 70 - HE 400 A
h_{slab}= 70 - HE 400 B
h_{slab}= 70 - HE 400 M
h_{slab}= 80 - HE 400 AA
h_{slab}= 80 - HE 400 A
h_{slab}= 80 - HE 400 B
h_{slab}= 80 - HE 400 M
h_{slab}= 90 - HE 400 AA
h_{slab}= 90 - HE 400 A
h_{slab}= 90 - HE 400 B
h_{slab}= 90 - HE 400 M
h_{slab}= 100 - HE 400 AA
h_{slab}= 100 - HE 400 A
h_{slab}= 100 - HE 400 B
h_{slab}= 100 - HE 400 M
Interaxis length: L_{inter}= 6000 mm
Dowel shape= PZT

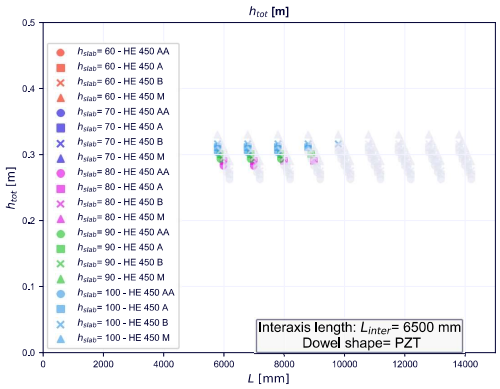
h_{tot} [m]
h_{tot} [m]
L [mm]
h_{slab}= 60 - HE 450 AA
h_{slab}= 60 - HE 450 A
h_{slab}= 60 - HE 450 B
h_{slab}= 60 - HE 450 M
h_{slab}= 70 - HE 450 AA
h_{slab}= 70 - HE 450 A
h_{slab}= 70 - HE 450 B
h_{slab}= 70 - HE 450 M
h_{slab}= 80 - HE 450 AA
h_{slab}= 80 - HE 450 A
h_{slab}= 80 - HE 450 B
h_{slab}= 80 - HE 450 M
h_{slab}= 90 - HE 450 AA
h_{slab}= 90 - HE 450 A
h_{slab}= 90 - HE 450 B
h_{slab}= 90 - HE 450 M
h_{slab}= 100 - HE 450 AA
h_{slab}= 100 - HE 450 A
h_{slab}= 100 - HE 450 B
h_{slab}= 100 - HE 450 M
Interaxis length: L_{inter}= 6500 mm
Dowel shape= PZT

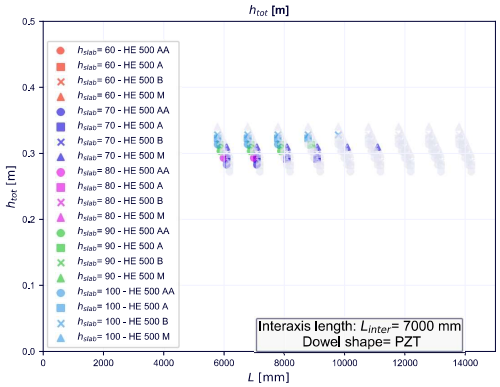
h_{tot} [m]
h_{tot} [m]
L [mm]
h_{slab}= 60 - HE 500 AA
h_{slab}= 60 - HE 500 A
h_{slab}= 60 - HE 500 B
h_{slab}= 60 - HE 500 M
h_{slab}= 70 - HE 500 AA
h_{slab}= 70 - HE 500 A
h_{slab}= 70 - HE 500 B
h_{slab}= 70 - HE 500 M
h_{slab}= 80 - HE 500 AA
h_{slab}= 80 - HE 500 A
h_{slab}= 80 - HE 500 B
h_{slab}= 80 - HE 500 M
h_{slab}= 90 - HE 500 AA
h_{slab}= 90 - HE 500 A
h_{slab}= 90 - HE 500 B
h_{slab}= 90 - HE 500 M
h_{slab}= 100 - HE 500 AA
h_{slab}= 100 - HE 500 A
h_{slab}= 100 - HE 500 B
h_{slab}= 100 - HE 500 M
Interaxis length: L_{inter}= 7000 mm
Dowel shape= PZT

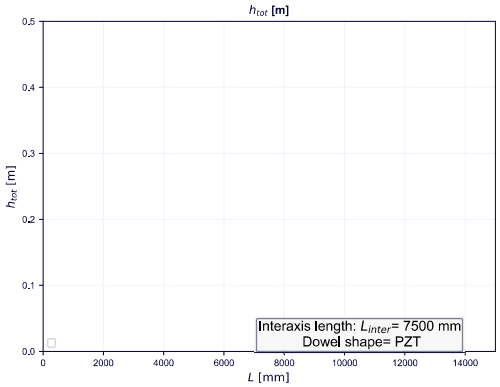
h_{tot} [m]
h_{tot} [m]
L [mm]
Interaxis length: L_{inter}= 7500 mm
Dowel shape= PZT

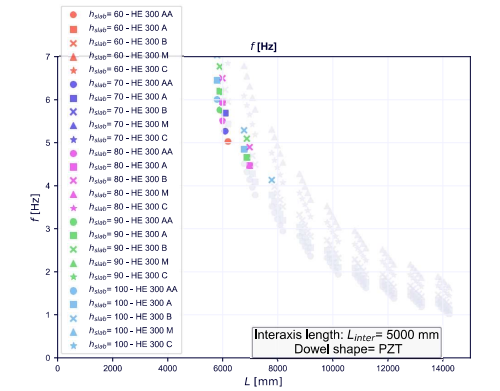
f [Hz]
f [Hz]
L [mm]
h_{slab}= 60 - HE 300 AA
h_{slab}= 60 - HE 300 A
h_{slab}= 60 - HE 300 B
h_{slab}= 60 - HE 300 M
h_{slab}= 60 - HE 300 C
h_{slab}= 70 - HE 300 AA
h_{slab}= 70 - HE 300 A
h_{slab}= 70 - HE 300 B
h_{slab}= 70 - HE 300 M
h_{slab}= 70 - HE 300 C
h_{slab}= 80 - HE 300 AA
h_{slab}= 80 - HE 300 A
h_{slab}= 80 - HE 300 B
h_{slab}= 80 - HE 300 M
h_{slab}= 80 - HE 300 C
h_{slab}= 90 - HE 300 AA
h_{slab}= 90 - HE 300 A
h_{slab}= 90 - HE 300 B
h_{slab}= 90 - HE 300 M
h_{slab}= 90 - HE 300 C
h_{slab}= 100 - HE 300 AA
h_{slab}= 100 - HE 300 A
h_{slab}= 100 - HE 300 B
h_{slab}= 100 - HE 300 M
h_{slab}= 100 - HE 300 C
Interaxis length: L_{inter}= 5000 mm
Dowel shape= PZT

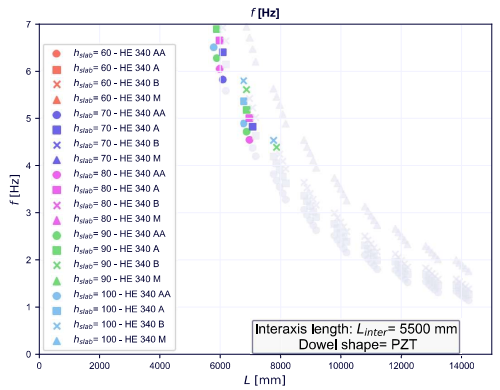
f [Hz]
f [Hz]
L [mm]
h_{slab}= 60 - HE 340 AA
h_{slab}= 60 - HE 340 A
h_{slab}= 60 - HE 340 B
h_{slab}= 60 - HE 340 M
h_{slab}= 70 - HE 340 AA
h_{slab}= 70 - HE 340 A
h_{slab}= 70 - HE 340 B
h_{slab}= 70 - HE 340 M
h_{slab}= 80 - HE 340 AA
h_{slab}= 80 - HE 340 A
h_{slab}= 80 - HE 340 B
h_{slab}= 80 - HE 340 M
h_{slab}= 90 - HE 340 AA
h_{slab}= 90 - HE 340 A
h_{slab}= 90 - HE 340 B
h_{slab}= 90 - HE 340 M
h_{slab}= 100 - HE 340 AA
h_{slab}= 100 - HE 340 A
h_{slab}= 100 - HE 340 B
h_{slab}= 100 - HE 340 M
Interaxis length: L_{inter}= 5500 mm
Dowel shape= PZT

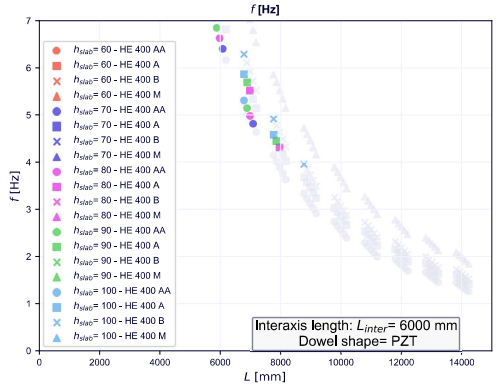
f [Hz]
f [Hz]
L [mm]
h_{slab}= 60 - HE 400 AA
h_{slab}= 60 - HE 400 A
h_{slab}= 60 - HE 400 B
h_{slab}= 60 - HE 400 M
h_{slab}= 70 - HE 400 AA
h_{slab}= 70 - HE 400 A
h_{slab}= 70 - HE 400 B
h_{slab}= 70 - HE 400 M
h_{slab}= 80 - HE 400 AA
h_{slab}= 80 - HE 400 A
h_{slab}= 80 - HE 400 B
h_{slab}= 80 - HE 400 M
h_{slab}= 90 - HE 400 AA
h_{slab}= 90 - HE 400 A
h_{slab}= 90 - HE 400 B
h_{slab}= 90 - HE 400 M
h_{slab}= 100 - HE 400 AA
h_{slab}= 100 - HE 400 A
h_{slab}= 100 - HE 400 B
h_{slab}= 100 - HE 400 M
Interaxis length: L_{inter}= 6000 mm
Dowel shape= PZT

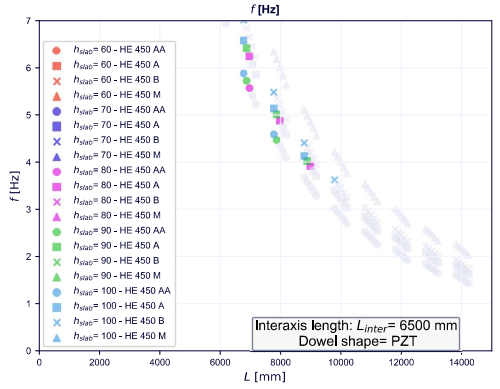
f [Hz]
f [Hz]
L [mm]
h_{slab}= 60 - HE 450 AA
h_{slab}= 60 - HE 450 A
h_{slab}= 60 - HE 450 B
h_{slab}= 60 - HE 450 M
h_{slab}= 70 - HE 450 AA
h_{slab}= 70 - HE 450 A
h_{slab}= 70 - HE 450 B
h_{slab}= 70 - HE 450 M
h_{slab}= 80 - HE 450 AA
h_{slab}= 80 - HE 450 A
h_{slab}= 80 - HE 450 B
h_{slab}= 80 - HE 450 M
h_{slab}= 90 - HE 450 AA
h_{slab}= 90 - HE 450 A
h_{slab}= 90 - HE 450 B
h_{slab}= 90 - HE 450 M
h_{slab}= 100 - HE 450 AA
h_{slab}= 100 - HE 450 A
h_{slab}= 100 - HE 450 B
h_{slab}= 100 - HE 450 M
Interaxis length: L_{inter}= 6500 mm
Dowel shape= PZT

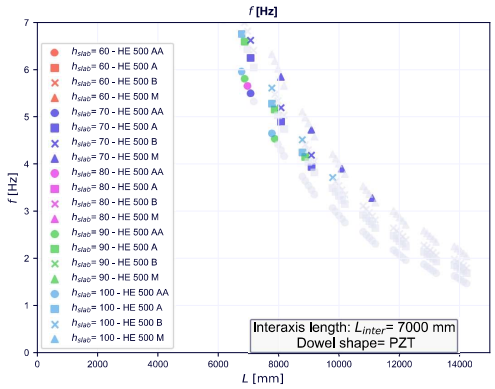
f [Hz]
f [Hz]
L [mm]
Interaxis length: L_{inter}= 7000 mm
Dowel shape= PZT

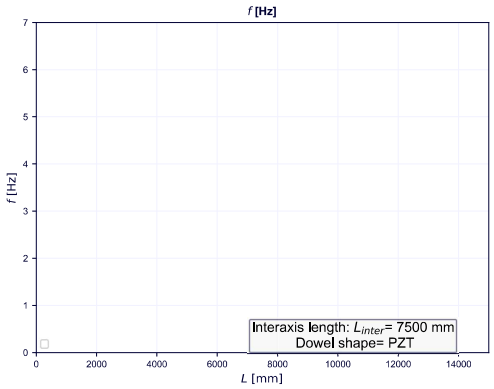
f [Hz]
f [Hz]
L [mm]
Interaxis length: L_{inter}= 7500 mm
Dowel shape= PZT

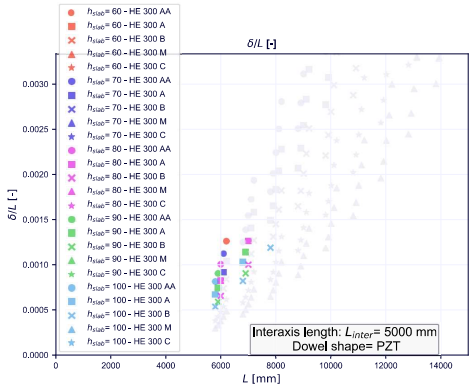
δ/L [-]
δ/L [-]
L [mm]
Interaxis length: L_{inter}= 5000 mm
Dowel shape= PZT

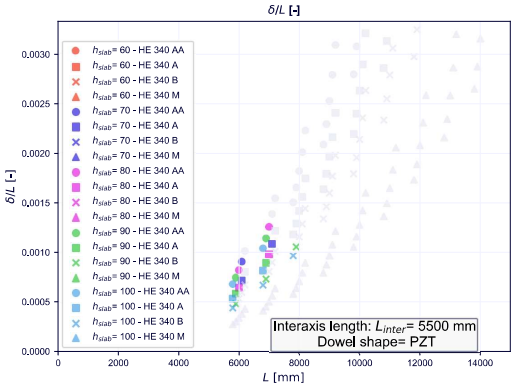
δ/L [-]
δ/L [-]
L [mm]
Interaxis length: L_{inter}= 5500 mm
Dowel shape= PZT

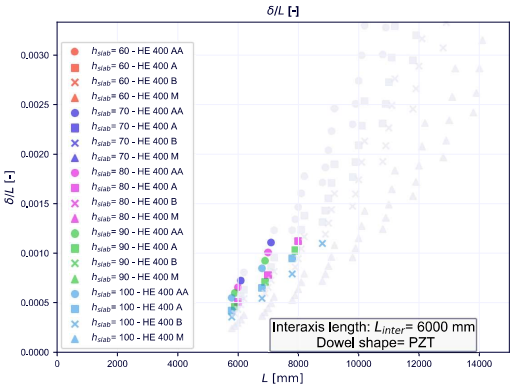
δ/L [-]
δ/L [-]
L [mm]
Interaxis length: L_{inter}= 6000 mm
Dowel shape= PZT

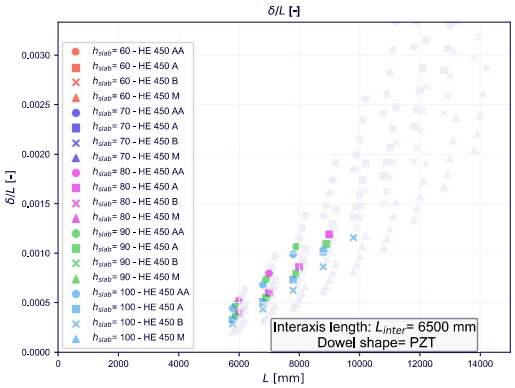
δ/L [-]
δ/L [-]
L [mm]
Interaxis length: L_{inter}= 6500 mm
Dowel shape= PZT

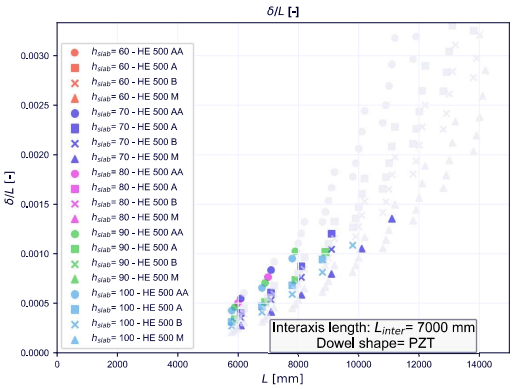
δ/L [-]
δ/L [-]
L [mm]
Interaxis length: L_{inter}= 7000 mm
Dowel shape= PZT

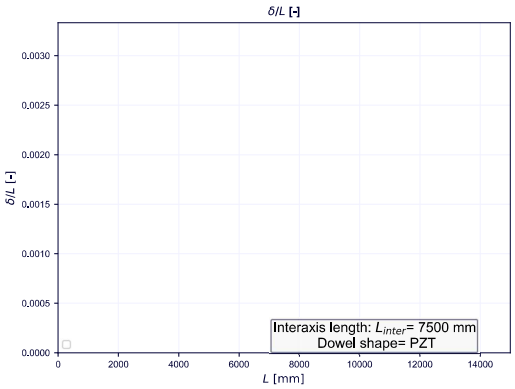
δ/L [-]
δ/L [-]
L [mm]
Interaxis length: L_{inter}= 7500 mm
Dowel shape= PZT

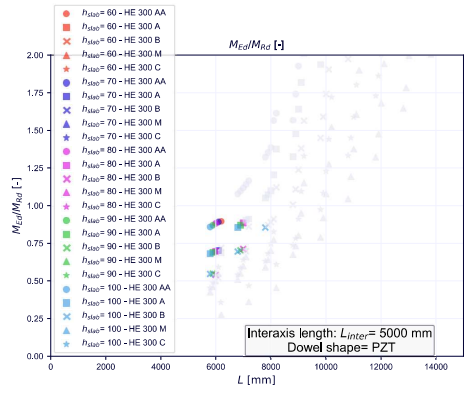
M_{Ed}/M_{Rd} [-]
h_{Slab}= 60 - HE 300 AA
h_{Slab}= 60 - HE 300 A
h_{Slab}= 60 - HE 300 B
h_{Slab}= 60 - HE 300 M
h_{Slab}= 60 - HE 300 C
h_{Slab}= 70 - HE 300 AA
h_{Slab}= 70 - HE 300 A
h_{Slab}= 70 - HE 300 B
h_{Slab}= 70 - HE 300 M
h_{Slab}= 70 - HE 300 C
h_{Slab}= 80 - HE 300 AA
h_{Slab}= 80 - HE 300 A
h_{Slab}= 80 - HE 300 B
h_{Slab}= 80 - HE 300 M
h_{Slab}= 80 - HE 300 C
h_{Slab}= 90 - HE 300 AA
h_{Slab}= 90 - HE 300 A
h_{Slab}= 90 - HE 300 B
h_{Slab}= 90 - HE 300 M
h_{Slab}= 90 - HE 300 C
h_{Slab}= 100 - HE 300 AA
h_{Slab}= 100 - HE 300 A
h_{Slab}= 100 - HE 300 B
h_{Slab}= 100 - HE 300 M
h_{Slab}= 100 - HE 300 C
Interaxis length: L_{inter}= 5000 mm
Dowel shape= PZT
M_{Ed}/M_{Rd} [-]
L [mm]

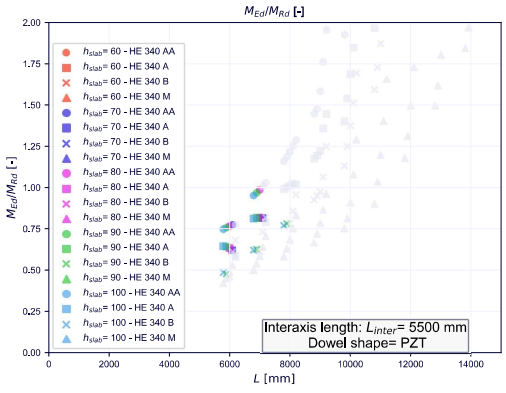
M_{Ed}/M_{Rd} [-]
h_{Slab}= 60 - HE 340 AA
h_{Slab}= 60 - HE 340 A
h_{Slab}= 60 - HE 340 B
h_{Slab}= 60 - HE 340 M
h_{Slab}= 70 - HE 340 AA
h_{Slab}= 70 - HE 340 A
h_{Slab}= 70 - HE 340 B
h_{Slab}= 70 - HE 340 M
h_{Slab}= 80 - HE 340 AA
h_{Slab}= 80 - HE 340 A
h_{Slab}= 80 - HE 340 B
h_{Slab}= 80 - HE 340 M
h_{Slab}= 90 - HE 340 AA
h_{Slab}= 90 - HE 340 A
h_{Slab}= 90 - HE 340 B
h_{Slab}= 90 - HE 340 M
h_{Slab}= 100 - HE 340 AA
h_{Slab}= 100 - HE 340 A
h_{Slab}= 100 - HE 340 B
h_{Slab}= 100 - HE 340 M
Interaxis length: L_{inter}= 5500 mm
Dowel shape= PZT
M_{Ed}/M_{Rd} [-]
L [mm]

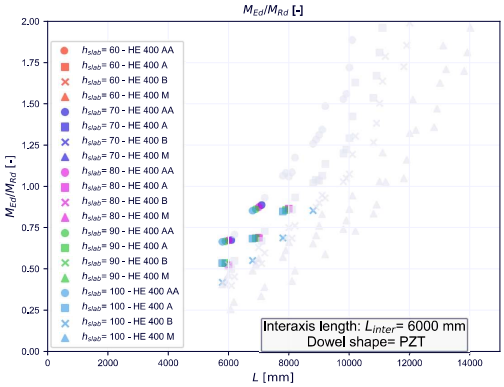
M_{Ed}/M_{Rd} [-]
h_{Slab}= 60 - HE 400 AA
h_{Slab}= 60 - HE 400 A
h_{Slab}= 60 - HE 400 B
h_{Slab}= 60 - HE 400 M
h_{Slab}= 70 - HE 400 AA
h_{Slab}= 70 - HE 400 A
h_{Slab}= 70 - HE 400 B
h_{Slab}= 70 - HE 400 M
h_{Slab}= 80 - HE 400 AA
h_{Slab}= 80 - HE 400 A
h_{Slab}= 80 - HE 400 B
h_{Slab}= 80 - HE 400 M
h_{Slab}= 90 - HE 400 AA
h_{Slab}= 90 - HE 400 A
h_{Slab}= 90 - HE 400 B
h_{Slab}= 90 - HE 400 M
h_{Slab}= 100 - HE 400 AA
h_{Slab}= 100 - HE 400 A
h_{Slab}= 100 - HE 400 B
h_{Slab}= 100 - HE 400 M
Interaxis length: L_{inter}= 6000 mm
Dowel shape= PZT
M_{Ed}/M_{Rd} [-]
L [mm]

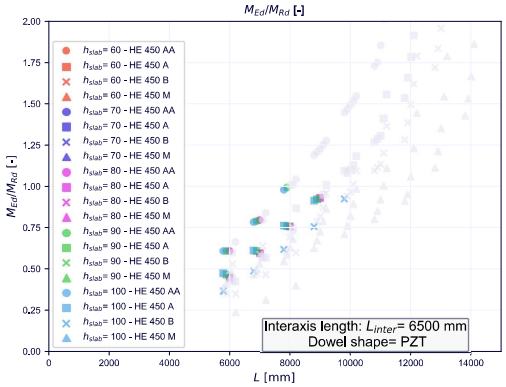
M_{Ed}/M_{Rd} [-]
h_{Slab}= 60 - HE 450 AA
h_{Slab}= 60 - HE 450 A
h_{Slab}= 60 - HE 450 B
h_{Slab}= 60 - HE 450 M
h_{Slab}= 70 - HE 450 AA
h_{Slab}= 70 - HE 450 A
h_{Slab}= 70 - HE 450 B
h_{Slab}= 70 - HE 450 M
h_{Slab}= 80 - HE 450 AA
h_{Slab}= 80 - HE 450 A
h_{Slab}= 80 - HE 450 B
h_{Slab}= 80 - HE 450 M
h_{Slab}= 90 - HE 450 AA
h_{Slab}= 90 - HE 450 A
h_{Slab}= 90 - HE 450 B
h_{Slab}= 90 - HE 450 M
h_{Slab}= 100 - HE 450 AA
h_{Slab}= 100 - HE 450 A
h_{Slab}= 100 - HE 450 B
h_{Slab}= 100 - HE 450 M
Interaxis length: L_{inter}= 6500 mm
Dowel shape= PZT
M_{Ed}/M_{Rd} [-]
L [mm]

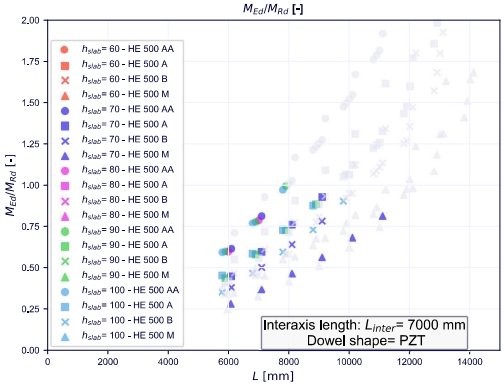
M_{Ed}/M_{Rd} [-]
h_{Slab}= 60 - HE 500 AA
h_{Slab}= 60 - HE 500 A
h_{Slab}= 60 - HE 500 B
h_{Slab}= 60 - HE 500 M
h_{Slab}= 70 - HE 500 AA
h_{Slab}= 70 - HE 500 A
h_{Slab}= 70 - HE 500 B
h_{Slab}= 70 - HE 500 M
h_{Slab}= 80 - HE 500 AA
h_{Slab}= 80 - HE 500 A
h_{Slab}= 80 - HE 500 B
h_{Slab}= 80 - HE 500 M
h_{Slab}= 90 - HE 500 AA
h_{Slab}= 90 - HE 500 A
h_{Slab}= 90 - HE 500 B
h_{Slab}= 90 - HE 500 M
h_{Slab}= 100 - HE 500 AA
h_{Slab}= 100 - HE 500 A
h_{Slab}= 100 - HE 500 B
h_{Slab}= 100 - HE 500 M
Interaxis length: L_{inter}= 7000 mm
Dowel shape= PZT
M_{Ed}/M_{Rd} [-]
L [mm]

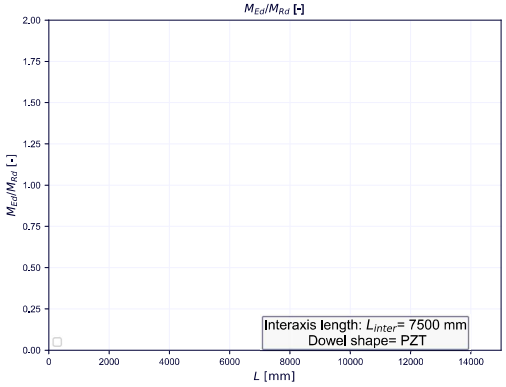
M_{Ed}/M_{Rd} [-]
Interaxis length: L_{inter}= 7500 mm
Dowel shape= PZT
M_{Ed}/M_{Rd} [-]
L [mm]

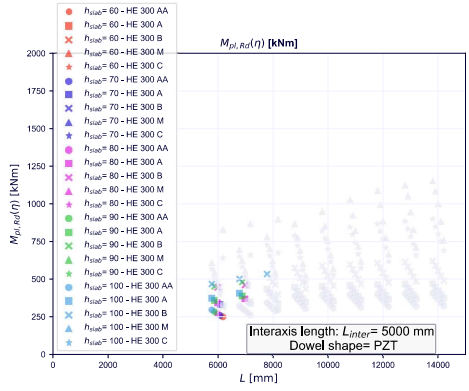
$M_{pl,Rd}(\eta)$ [kNm]
h_{Slab}= 60 - HE 300 AA
h_{Slab}= 60 - HE 300 A
h_{Slab}= 60 - HE 300 B
h_{Slab}= 60 - HE 300 M
h_{Slab}= 60 - HE 300 C
h_{Slab}= 70 - HE 300 AA
h_{Slab}= 70 - HE 300 A
h_{Slab}= 70 - HE 300 B
h_{Slab}= 70 - HE 300 M
h_{Slab}= 70 - HE 300 C
h_{Slab}= 80 - HE 300 AA
h_{Slab}= 80 - HE 300 A
h_{Slab}= 80 - HE 300 B
h_{Slab}= 80 - HE 300 M
h_{Slab}= 80 - HE 300 C
h_{Slab}= 90 - HE 300 AA
h_{Slab}= 90 - HE 300 A
h_{Slab}= 90 - HE 300 B
h_{Slab}= 90 - HE 300 M
h_{Slab}= 90 - HE 300 C
h_{Slab}= 100 - HE 300 AA
h_{Slab}= 100 - HE 300 A
h_{Slab}= 100 - HE 300 B
h_{Slab}= 100 - HE 300 M
h_{Slab}= 100 - HE 300 C
Interaxis length: L_{inter}= 5000 mm
Dowel shape= PZT
$M_{pl,Rd}(\eta)$ [kNm]
L [mm]

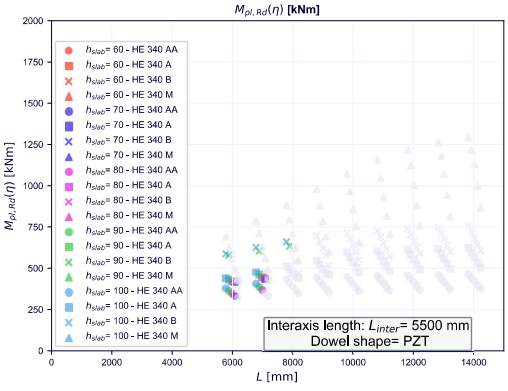
$M_{pl,Rd}(\eta)$ [kNm]
h_{Slab}= 60 - HE 340 AA
h_{Slab}= 60 - HE 340 A
h_{Slab}= 60 - HE 340 B
h_{Slab}= 60 - HE 340 M
h_{Slab}= 70 - HE 340 AA
h_{Slab}= 70 - HE 340 A
h_{Slab}= 70 - HE 340 B
h_{Slab}= 70 - HE 340 M
h_{Slab}= 80 - HE 340 AA
h_{Slab}= 80 - HE 340 A
h_{Slab}= 80 - HE 340 B
h_{Slab}= 80 - HE 340 M
h_{Slab}= 90 - HE 340 AA
h_{Slab}= 90 - HE 340 A
h_{Slab}= 90 - HE 340 B
h_{Slab}= 90 - HE 340 M
h_{Slab}= 100 - HE 340 AA
h_{Slab}= 100 - HE 340 A
h_{Slab}= 100 - HE 340 B
h_{Slab}= 100 - HE 340 M
Interaxis length: L_{inter}= 5500 mm
Dowel shape= PZT
$M_{pl,Rd}(\eta)$ [kNm]
L [mm]

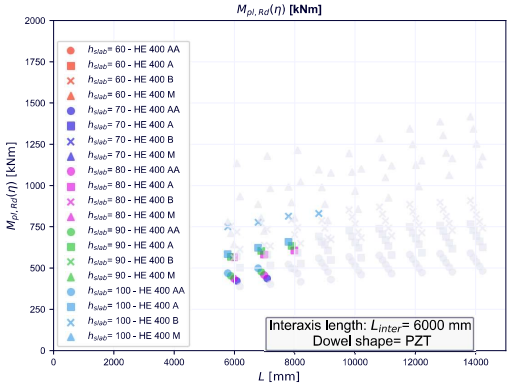
$M_{pl,Rd}(\eta)$ [kNm]
h_{slab}= 60 - HE 400 AA
h_{slab}= 60 - HE 400 A
h_{slab}= 60 - HE 400 B
h_{slab}= 60 - HE 400 M
h_{slab}= 70 - HE 400 AA
h_{slab}= 70 - HE 400 A
h_{slab}= 70 - HE 400 B
h_{slab}= 70 - HE 400 M
h_{slab}= 80 - HE 400 AA
h_{slab}= 80 - HE 400 A
h_{slab}= 80 - HE 400 B
h_{slab}= 80 - HE 400 M
h_{slab}= 90 - HE 400 AA
h_{slab}= 90 - HE 400 A
h_{slab}= 90 - HE 400 B
h_{slab}= 90 - HE 400 M
h_{slab}= 100 - HE 400 AA
h_{slab}= 100 - HE 400 A
h_{slab}= 100 - HE 400 B
h_{slab}= 100 - HE 400 M
Interaxis length: L_{inter}= 6000 mm
Dowel shape= PZT
L [mm]

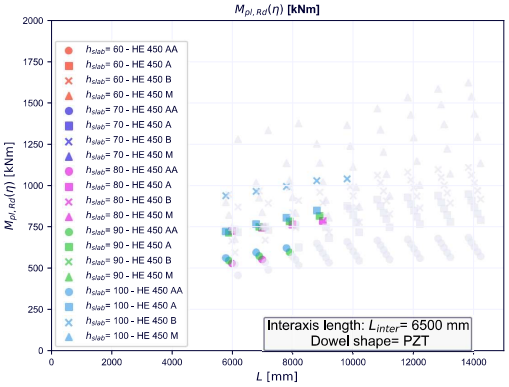
$M_{pl,Rd}(\eta)$ [kNm]
h_{slab}= 60 - HE 450 AA
h_{slab}= 60 - HE 450 A
h_{slab}= 60 - HE 450 B
h_{slab}= 60 - HE 450 M
h_{slab}= 70 - HE 450 AA
h_{slab}= 70 - HE 450 A
h_{slab}= 70 - HE 450 B
h_{slab}= 70 - HE 450 M
h_{slab}= 80 - HE 450 AA
h_{slab}= 80 - HE 450 A
h_{slab}= 80 - HE 450 B
h_{slab}= 80 - HE 450 M
h_{slab}= 90 - HE 450 AA
h_{slab}= 90 - HE 450 A
h_{slab}= 90 - HE 450 B
h_{slab}= 90 - HE 450 M
h_{slab}= 100 - HE 450 AA
h_{slab}= 100 - HE 450 A
h_{slab}= 100 - HE 450 B
h_{slab}= 100 - HE 450 M
Interaxis length: L_{inter}= 6500 mm
Dowel shape= PZT
L [mm]

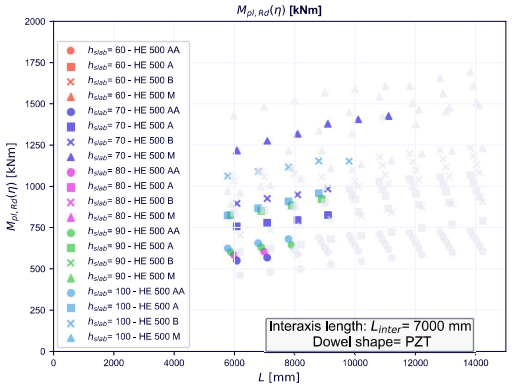
$M_{pl,Rd}(\eta)$ [kNm]
h_{slab}= 60 - HE 500 AA
h_{slab}= 60 - HE 500 A
h_{slab}= 60 - HE 500 B
h_{slab}= 60 - HE 500 M
h_{slab}= 70 - HE 500 AA
h_{slab}= 70 - HE 500 A
h_{slab}= 70 - HE 500 B
h_{slab}= 70 - HE 500 M
h_{slab}= 80 - HE 500 AA
h_{slab}= 80 - HE 500 A
h_{slab}= 80 - HE 500 B
h_{slab}= 80 - HE 500 M
h_{slab}= 90 - HE 500 AA
h_{slab}= 90 - HE 500 A
h_{slab}= 90 - HE 500 B
h_{slab}= 90 - HE 500 M
h_{slab}= 100 - HE 500 AA
h_{slab}= 100 - HE 500 A
h_{slab}= 100 - HE 500 B
h_{slab}= 100 - HE 500 M
Interaxis length: L_{inter}= 7000 mm
Dowel shape= PZT
L [mm]

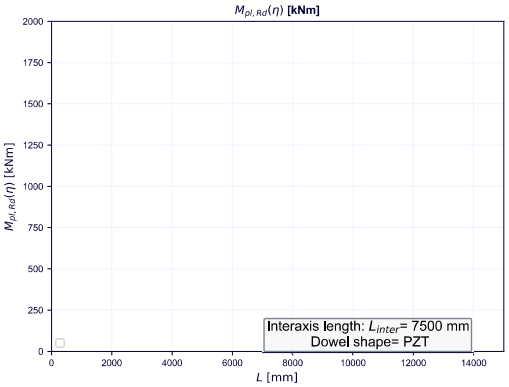
$M_{pl,Rd}(\eta)$ [kNm]
Interaxis length: L_{inter}= 7500 mm
Dowel shape= PZT
L [mm]

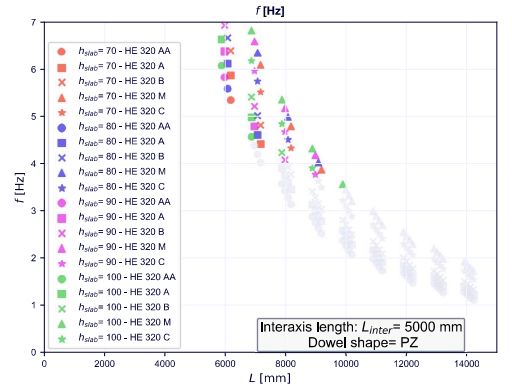
f [Hz]
h_{slab}= 70 - HE 320 AA
h_{slab}= 70 - HE 320 A
h_{slab}= 70 - HE 320 B
h_{slab}= 70 - HE 320 M
h_{slab}= 70 - HE 320 C
h_{slab}= 80 - HE 320 AA
h_{slab}= 80 - HE 320 A
h_{slab}= 80 - HE 320 B
h_{slab}= 80 - HE 320 M
h_{slab}= 80 - HE 320 C
h_{slab}= 90 - HE 320 AA
h_{slab}= 90 - HE 320 A
h_{slab}= 90 - HE 320 B
h_{slab}= 90 - HE 320 M
h_{slab}= 90 - HE 320 C
h_{slab}= 100 - HE 320 AA
h_{slab}= 100 - HE 320 A
h_{slab}= 100 - HE 320 B
h_{slab}= 100 - HE 320 M
h_{slab}= 100 - HE 320 C
Interaxis length: L_{inter}= 5000 mm
Dowel shape= PZ
L [mm]

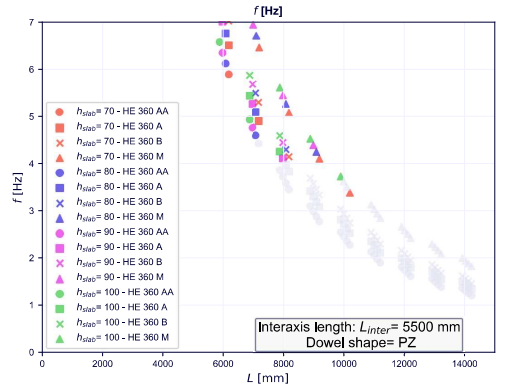
f [Hz]
h_{slab}= 70 - HE 360 AA
h_{slab}= 70 - HE 360 A
h_{slab}= 70 - HE 360 B
h_{slab}= 70 - HE 360 M
h_{slab}= 80 - HE 360 AA
h_{slab}= 80 - HE 360 A
h_{slab}= 80 - HE 360 B
h_{slab}= 80 - HE 360 M
h_{slab}= 90 - HE 360 AA
h_{slab}= 90 - HE 360 A
h_{slab}= 90 - HE 360 B
h_{slab}= 90 - HE 360 M
h_{slab}= 100 - HE 360 AA
h_{slab}= 100 - HE 360 A
h_{slab}= 100 - HE 360 B
h_{slab}= 100 - HE 360 M
Interaxis length: L_{inter}= 5500 mm
Dowel shape= PZ
L [mm]

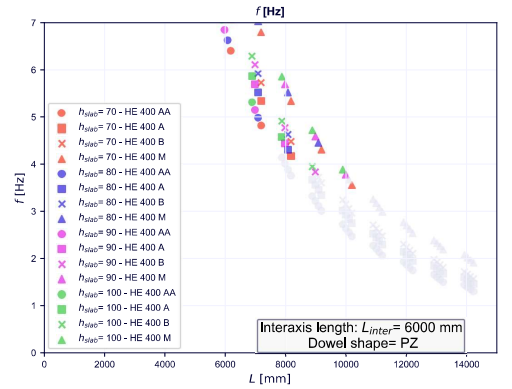
f [Hz]
h_{slab}= 70 - HE 400 AA
h_{slab}= 70 - HE 400 A
h_{slab}= 70 - HE 400 B
h_{slab}= 70 - HE 400 M
h_{slab}= 80 - HE 400 AA
h_{slab}= 80 - HE 400 A
h_{slab}= 80 - HE 400 B
h_{slab}= 80 - HE 400 M
h_{slab}= 90 - HE 400 AA
h_{slab}= 90 - HE 400 A
h_{slab}= 90 - HE 400 B
h_{slab}= 90 - HE 400 M
h_{slab}= 100 - HE 400 AA
h_{slab}= 100 - HE 400 A
h_{slab}= 100 - HE 400 B
h_{slab}= 100 - HE 400 M
Interaxis length: L_{inter}= 6000 mm
Dowel shape= PZ
L [mm]

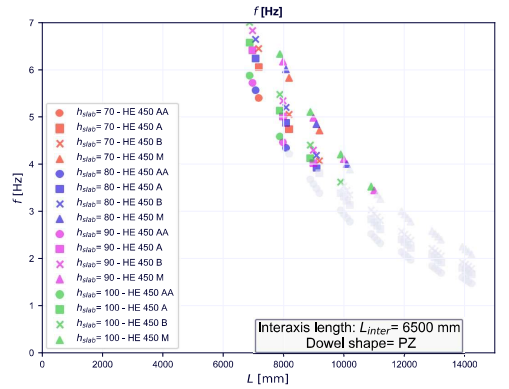
f [Hz]
h_{slab}= 70 - HE 450 AA
h_{slab}= 70 - HE 450 A
h_{slab}= 70 - HE 450 B
h_{slab}= 70 - HE 450 M
h_{slab}= 80 - HE 450 AA
h_{slab}= 80 - HE 450 A
h_{slab}= 80 - HE 450 B
h_{slab}= 80 - HE 450 M
h_{slab}= 90 - HE 450 AA
h_{slab}= 90 - HE 450 A
h_{slab}= 90 - HE 450 B
h_{slab}= 90 - HE 450 M
h_{slab}= 100 - HE 450 AA
h_{slab}= 100 - HE 450 A
h_{slab}= 100 - HE 450 B
h_{slab}= 100 - HE 450 M
Interaxis length: L_{inter}= 6500 mm
Dowel shape= PZ
L [mm]

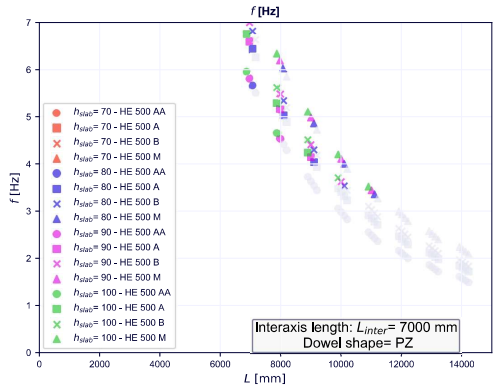
f [Hz]
f [Hz]
L [mm]
Interaxis length: L_{inter}= 7000 mm
Dowel shape= PZ
h_{slab}= 70 - HE 500 AA
h_{slab}= 70 - HE 500 A
h_{slab}= 70 - HE 500 B
h_{slab}= 70 - HE 500 M
h_{slab}= 80 - HE 500 AA
h_{slab}= 80 - HE 500 A
h_{slab}= 80 - HE 500 B
h_{slab}= 80 - HE 500 M
h_{slab}= 90 - HE 500 AA
h_{slab}= 90 - HE 500 A
h_{slab}= 90 - HE 500 B
h_{slab}= 90 - HE 500 M
h_{slab}= 100 - HE 500 AA
h_{slab}= 100 - HE 500 A
h_{slab}= 100 - HE 500 B
h_{slab}= 100 - HE 500 M

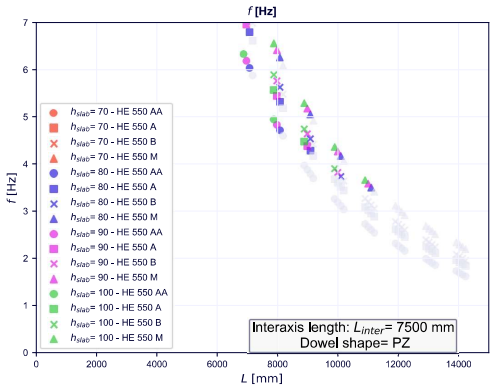
f [Hz]
f [Hz]
L [mm]
Interaxis length: L_{inter}= 7500 mm
Dowel shape= PZ
h_{slab}= 70 - HE 550 AA
h_{slab}= 70 - HE 550 A
h_{slab}= 70 - HE 550 B
h_{slab}= 70 - HE 550 M
h_{slab}= 80 - HE 550 AA
h_{slab}= 80 - HE 550 A
h_{slab}= 80 - HE 550 B
h_{slab}= 80 - HE 550 M
h_{slab}= 90 - HE 550 AA
h_{slab}= 90 - HE 550 A
h_{slab}= 90 - HE 550 B
h_{slab}= 90 - HE 550 M
h_{slab}= 100 - HE 550 AA
h_{slab}= 100 - HE 550 A
h_{slab}= 100 - HE 550 B
h_{slab}= 100 - HE 550 M

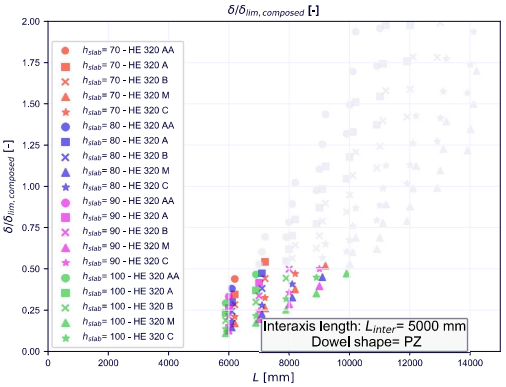
$\delta/\delta_{lim,composed}$ [-]
$\delta/\delta_{lim,composed}$ [-]
L [mm]
Interaxis length: L_{inter}= 5000 mm
Dowel shape= PZ
h_{slab}= 70 - HE 320 AA
h_{slab}= 70 - HE 320 A
h_{slab}= 70 - HE 320 B
h_{slab}= 70 - HE 320 M
h_{slab}= 70 - HE 320 C
h_{slab}= 80 - HE 320 AA
h_{slab}= 80 - HE 320 A
h_{slab}= 80 - HE 320 B
h_{slab}= 80 - HE 320 M
h_{slab}= 80 - HE 320 C
h_{slab}= 90 - HE 320 AA
h_{slab}= 90 - HE 320 A
h_{slab}= 90 - HE 320 B
h_{slab}= 90 - HE 320 M
h_{slab}= 90 - HE 320 C
h_{slab}= 100 - HE 320 AA
h_{slab}= 100 - HE 320 A
h_{slab}= 100 - HE 320 B
h_{slab}= 100 - HE 320 M
h_{slab}= 100 - HE 320 C

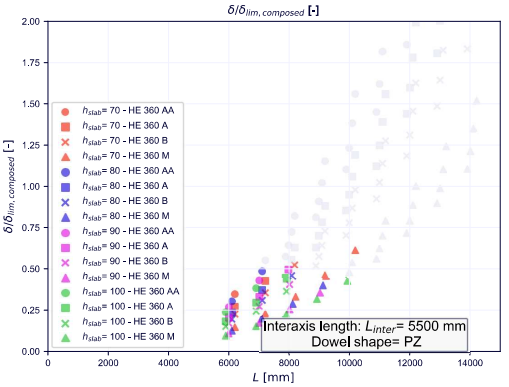
$\delta/\delta_{lim,composed}$ [-]
$\delta/\delta_{lim,composed}$ [-]
L [mm]
Interaxis length: L_{inter}= 5500 mm
Dowel shape= PZ
h_{slab}= 70 - HE 360 AA
h_{slab}= 70 - HE 360 A
h_{slab}= 70 - HE 360 B
h_{slab}= 70 - HE 360 M
h_{slab}= 80 - HE 360 AA
h_{slab}= 80 - HE 360 A
h_{slab}= 80 - HE 360 B
h_{slab}= 80 - HE 360 M
h_{slab}= 90 - HE 360 AA
h_{slab}= 90 - HE 360 A
h_{slab}= 90 - HE 360 B
h_{slab}= 90 - HE 360 M
h_{slab}= 100 - HE 360 AA
h_{slab}= 100 - HE 360 A
h_{slab}= 100 - HE 360 B
h_{slab}= 100 - HE 360 M

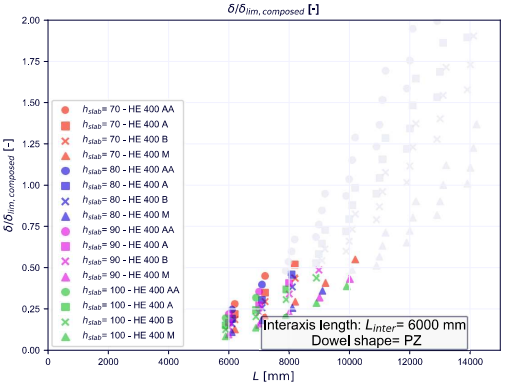
$\delta/\delta_{lim,composed}$ [-]
$\delta/\delta_{lim,composed}$ [-]
L [mm]
Interaxis length: L_{inter}= 6000 mm
Dowel shape= PZ
h_{slab}= 70 - HE 400 AA
h_{slab}= 70 - HE 400 A
h_{slab}= 70 - HE 400 B
h_{slab}= 70 - HE 400 M
h_{slab}= 80 - HE 400 AA
h_{slab}= 80 - HE 400 A
h_{slab}= 80 - HE 400 B
h_{slab}= 80 - HE 400 M
h_{slab}= 90 - HE 400 AA
h_{slab}= 90 - HE 400 A
h_{slab}= 90 - HE 400 B
h_{slab}= 90 - HE 400 M
h_{slab}= 100 - HE 400 AA
h_{slab}= 100 - HE 400 A
h_{slab}= 100 - HE 400 B
h_{slab}= 100 - HE 400 M

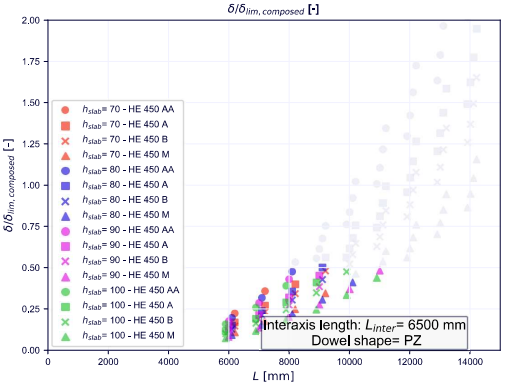
$\delta/\delta_{lim,composed}$ [-]
$\delta/\delta_{lim,composed}$ [-]
L [mm]
Interaxis length: L_{inter}= 6500 mm
Dowel shape= PZ
h_{slab}= 70 - HE 450 AA
h_{slab}= 70 - HE 450 A
h_{slab}= 70 - HE 450 B
h_{slab}= 70 - HE 450 M
h_{slab}= 80 - HE 450 AA
h_{slab}= 80 - HE 450 A
h_{slab}= 80 - HE 450 B
h_{slab}= 80 - HE 450 M
h_{slab}= 90 - HE 450 AA
h_{slab}= 90 - HE 450 A
h_{slab}= 90 - HE 450 B
h_{slab}= 90 - HE 450 M
h_{slab}= 100 - HE 450 AA
h_{slab}= 100 - HE 450 A
h_{slab}= 100 - HE 450 B
h_{slab}= 100 - HE 450 M

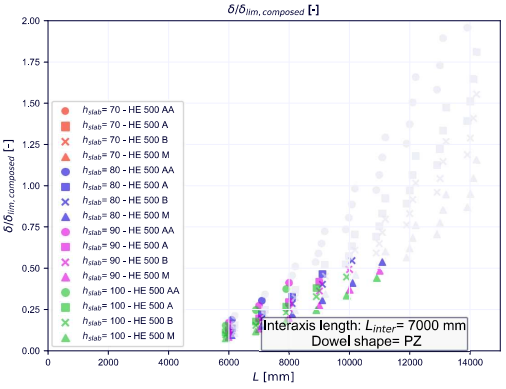
$\delta/\delta_{lim,composed}$ [-]
$\delta/\delta_{lim,composed}$ [-]
L [mm]
Interaxis length: L_{inter}= 7000 mm
Dowel shape= PZ
h_{slab}= 70 - HE 500 AA
h_{slab}= 70 - HE 500 A
h_{slab}= 70 - HE 500 B
h_{slab}= 70 - HE 500 M
h_{slab}= 80 - HE 500 AA
h_{slab}= 80 - HE 500 A
h_{slab}= 80 - HE 500 B
h_{slab}= 80 - HE 500 M
h_{slab}= 90 - HE 500 AA
h_{slab}= 90 - HE 500 A
h_{slab}= 90 - HE 500 B
h_{slab}= 90 - HE 500 M
h_{slab}= 100 - HE 500 AA
h_{slab}= 100 - HE 500 A
h_{slab}= 100 - HE 500 B
h_{slab}= 100 - HE 500 M

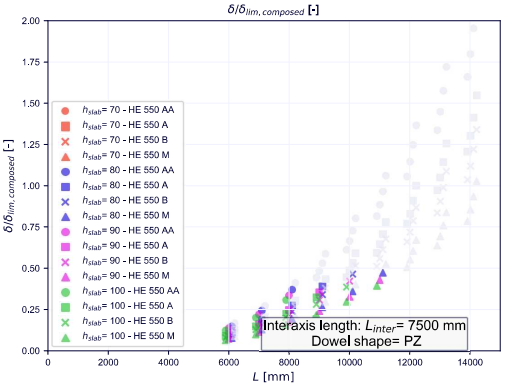
$\delta/\delta_{lim,composed}$ [-]
$\delta/\delta_{lim,composed}$ [-]
L [mm]
Interaxis length: L_{inter}= 7500 mm
Dowel shape= PZ
h_{slab}= 70 - HE 550 AA
h_{slab}= 70 - HE 550 A
h_{slab}= 70 - HE 550 B
h_{slab}= 70 - HE 550 M
h_{slab}= 80 - HE 550 AA
h_{slab}= 80 - HE 550 A
h_{slab}= 80 - HE 550 B
h_{slab}= 80 - HE 550 M
h_{slab}= 90 - HE 550 AA
h_{slab}= 90 - HE 550 A
h_{slab}= 90 - HE 550 B
h_{slab}= 90 - HE 550 M
h_{slab}= 100 - HE 550 AA
h_{slab}= 100 - HE 550 A
h_{slab}= 100 - HE 550 B
h_{slab}= 100 - HE 550 M

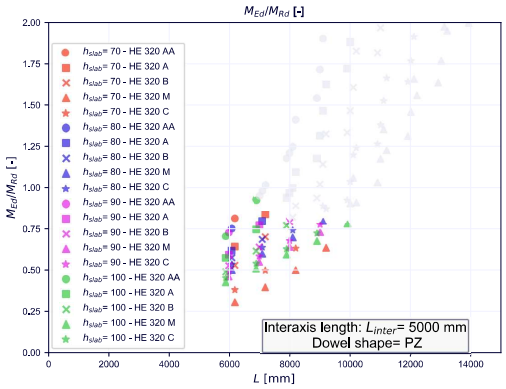
M_{Ed}/M_{Rd} [-]
h_{slab}= 70 - HE 320 AA
h_{slab}= 70 - HE 320 A
h_{slab}= 70 - HE 320 B
h_{slab}= 70 - HE 320 M
h_{slab}= 70 - HE 320 C
h_{slab}= 80 - HE 320 AA
h_{slab}= 80 - HE 320 A
h_{slab}= 80 - HE 320 B
h_{slab}= 80 - HE 320 M
h_{slab}= 80 - HE 320 C
h_{slab}= 90 - HE 320 AA
h_{slab}= 90 - HE 320 A
h_{slab}= 90 - HE 320 B
h_{slab}= 90 - HE 320 M
h_{slab}= 90 - HE 320 C
h_{slab}= 100 - HE 320 AA
h_{slab}= 100 - HE 320 A
h_{slab}= 100 - HE 320 B
h_{slab}= 100 - HE 320 M
h_{slab}= 100 - HE 320 C
Interaxis length: L_{inter}= 5000 mm
Dowel shape= PZ
M_{Ed}/M_{Rd} [-]
L [mm]

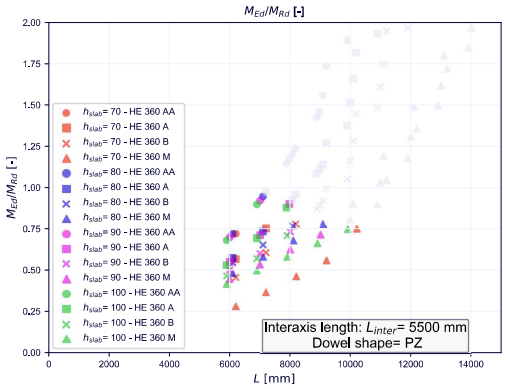
M_{Ed}/M_{Rd} [-]
h_{slab}= 70 - HE 360 AA
h_{slab}= 70 - HE 360 A
h_{slab}= 70 - HE 360 B
h_{slab}= 70 - HE 360 M
h_{slab}= 80 - HE 360 AA
h_{slab}= 80 - HE 360 A
h_{slab}= 80 - HE 360 B
h_{slab}= 80 - HE 360 M
h_{slab}= 90 - HE 360 AA
h_{slab}= 90 - HE 360 A
h_{slab}= 90 - HE 360 B
h_{slab}= 90 - HE 360 M
h_{slab}= 100 - HE 360 AA
h_{slab}= 100 - HE 360 A
h_{slab}= 100 - HE 360 B
h_{slab}= 100 - HE 360 M
Interaxis length: L_{inter}= 5500 mm
Dowel shape= PZ
M_{Ed}/M_{Rd} [-]
L [mm]

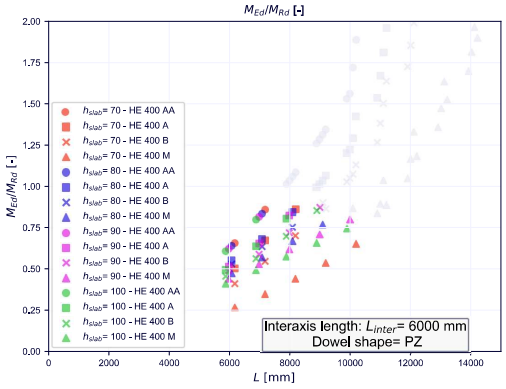
M_{Ed}/M_{Rd} [-]
h_{slab}= 70 - HE 400 AA
h_{slab}= 70 - HE 400 A
h_{slab}= 70 - HE 400 B
h_{slab}= 70 - HE 400 M
h_{slab}= 80 - HE 400 AA
h_{slab}= 80 - HE 400 A
h_{slab}= 80 - HE 400 B
h_{slab}= 80 - HE 400 M
h_{slab}= 90 - HE 400 AA
h_{slab}= 90 - HE 400 A
h_{slab}= 90 - HE 400 B
h_{slab}= 90 - HE 400 M
h_{slab}= 100 - HE 400 AA
h_{slab}= 100 - HE 400 A
h_{slab}= 100 - HE 400 B
h_{slab}= 100 - HE 400 M
Interaxis length: L_{inter}= 6000 mm
Dowel shape= PZ
M_{Ed}/M_{Rd} [-]
L [mm]

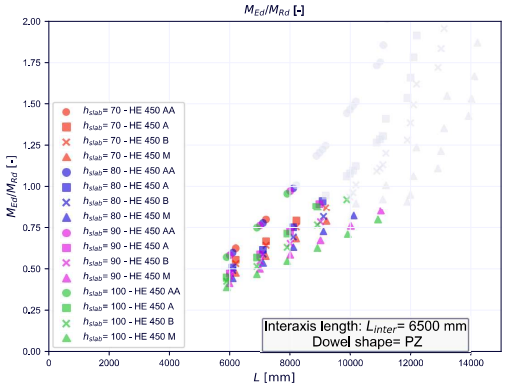
M_{Ed}/M_{Rd} [-]
h_{slab}= 70 - HE 450 AA
h_{slab}= 70 - HE 450 A
h_{slab}= 70 - HE 450 B
h_{slab}= 70 - HE 450 M
h_{slab}= 80 - HE 450 AA
h_{slab}= 80 - HE 450 A
h_{slab}= 80 - HE 450 B
h_{slab}= 80 - HE 450 M
h_{slab}= 90 - HE 450 AA
h_{slab}= 90 - HE 450 A
h_{slab}= 90 - HE 450 B
h_{slab}= 90 - HE 450 M
h_{slab}= 100 - HE 450 AA
h_{slab}= 100 - HE 450 A
h_{slab}= 100 - HE 450 B
h_{slab}= 100 - HE 450 M
Interaxis length: L_{inter}= 6500 mm
Dowel shape= PZ
M_{Ed}/M_{Rd} [-]
L [mm]

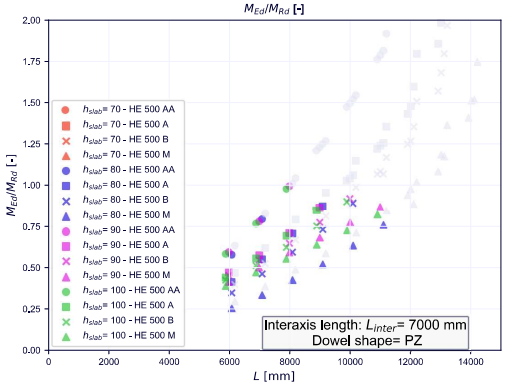
M_{Ed}/M_{Rd} [-]
h_{slab}= 70 - HE 500 AA
h_{slab}= 70 - HE 500 A
h_{slab}= 70 - HE 500 B
h_{slab}= 70 - HE 500 M
h_{slab}= 80 - HE 500 AA
h_{slab}= 80 - HE 500 A
h_{slab}= 80 - HE 500 B
h_{slab}= 80 - HE 500 M
h_{slab}= 90 - HE 500 AA
h_{slab}= 90 - HE 500 A
h_{slab}= 90 - HE 500 B
h_{slab}= 90 - HE 500 M
h_{slab}= 100 - HE 500 AA
h_{slab}= 100 - HE 500 A
h_{slab}= 100 - HE 500 B
h_{slab}= 100 - HE 500 M
Interaxis length: L_{inter}= 7000 mm
Dowel shape= PZ
M_{Ed}/M_{Rd} [-]
L [mm]

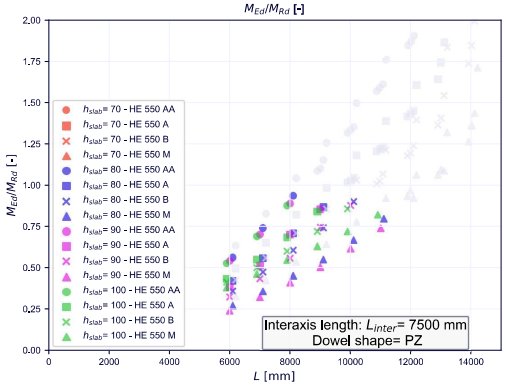
M_{Ed}/M_{Rd} [-]
h_{slab}= 70 - HE 550 AA
h_{slab}= 70 - HE 550 A
h_{slab}= 70 - HE 550 B
h_{slab}= 70 - HE 550 M
h_{slab}= 80 - HE 550 AA
h_{slab}= 80 - HE 550 A
h_{slab}= 80 - HE 550 B
h_{slab}= 80 - HE 550 M
h_{slab}= 90 - HE 550 AA
h_{slab}= 90 - HE 550 A
h_{slab}= 90 - HE 550 B
h_{slab}= 90 - HE 550 M
h_{slab}= 100 - HE 550 AA
h_{slab}= 100 - HE 550 A
h_{slab}= 100 - HE 550 B
h_{slab}= 100 - HE 550 M
Interaxis length: L_{inter}= 7500 mm
Dowel shape= PZ
M_{Ed}/M_{Rd} [-]
L [mm]

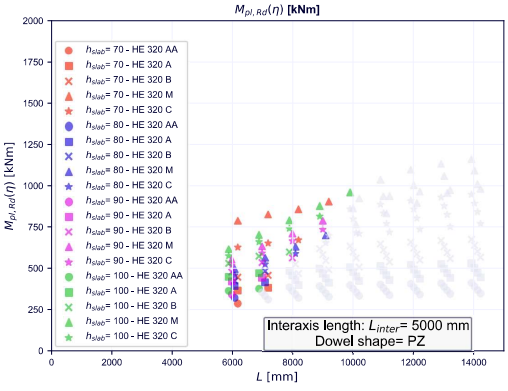
$M_{pl,Rd}(\eta)$ [kNm]
h_{slab}= 70 - HE 320 AA
h_{slab}= 70 - HE 320 A
h_{slab}= 70 - HE 320 B
h_{slab}= 70 - HE 320 M
h_{slab}= 70 - HE 320 C
h_{slab}= 80 - HE 320 AA
h_{slab}= 80 - HE 320 A
h_{slab}= 80 - HE 320 B
h_{slab}= 80 - HE 320 M
h_{slab}= 80 - HE 320 C
h_{slab}= 90 - HE 320 AA
h_{slab}= 90 - HE 320 A
h_{slab}= 90 - HE 320 B
h_{slab}= 90 - HE 320 M
h_{slab}= 90 - HE 320 C
h_{slab}= 100 - HE 320 AA
h_{slab}= 100 - HE 320 A
h_{slab}= 100 - HE 320 B
h_{slab}= 100 - HE 320 M
h_{slab}= 100 - HE 320 C
Interaxis length: L_{inter}= 5000 mm
Dowel shape= PZ
$M_{pl,Rd}(\eta)$ [kNm]
L [mm]

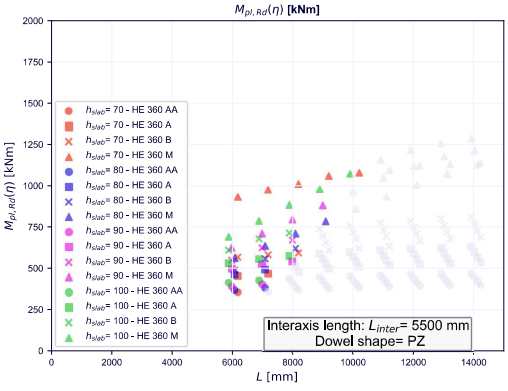
$M_{pl,Rd}(\eta)$ [kNm]
h_{slab}= 70 - HE 360 AA
h_{slab}= 70 - HE 360 A
h_{slab}= 70 - HE 360 B
h_{slab}= 70 - HE 360 M
h_{slab}= 80 - HE 360 AA
h_{slab}= 80 - HE 360 A
h_{slab}= 80 - HE 360 B
h_{slab}= 80 - HE 360 M
h_{slab}= 90 - HE 360 AA
h_{slab}= 90 - HE 360 A
h_{slab}= 90 - HE 360 B
h_{slab}= 90 - HE 360 M
h_{slab}= 100 - HE 360 AA
h_{slab}= 100 - HE 360 A
h_{slab}= 100 - HE 360 B
h_{slab}= 100 - HE 360 M
Interaxis length: L_{inter}= 5500 mm
Dowel shape= PZ
$M_{pl,Rd}(\eta)$ [kNm]
L [mm]

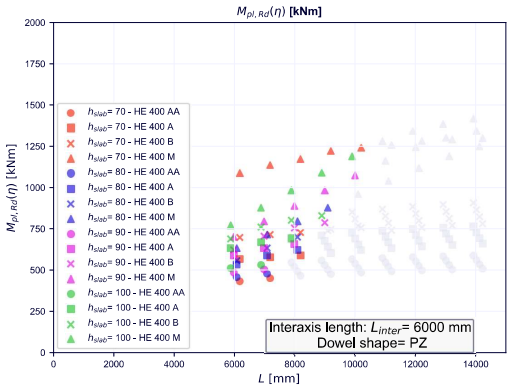
$M_{pl,Rd}(\eta)$ [kNm]
L [mm]
$h_{sl/ab}$= 70 - HE 400 AA
$h_{sl/ab}$= 70 - HE 400 A
$h_{sl/ab}$= 70 - HE 400 B
$h_{sl/ab}$= 70 - HE 400 M
$h_{sl/ab}$= 80 - HE 400 AA
$h_{sl/ab}$= 80 - HE 400 A
$h_{sl/ab}$= 80 - HE 400 B
$h_{sl/ab}$= 80 - HE 400 M
$h_{sl/ab}$= 90 - HE 400 AA
$h_{sl/ab}$= 90 - HE 400 A
$h_{sl/ab}$= 90 - HE 400 B
$h_{sl/ab}$= 90 - HE 400 M
$h_{sl/ab}$= 100 - HE 400 AA
$h_{sl/ab}$= 100 - HE 400 A
$h_{sl/ab}$= 100 - HE 400 B
$h_{sl/ab}$= 100 - HE 400 M
Interaxis length: L_{inter}= 6000 mm
Dowel shape= PZ

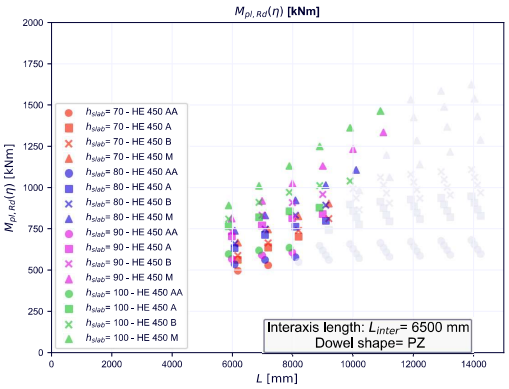
$M_{pl,Rd}(\eta)$ [kNm]
L [mm]
$h_{sl/ab}$= 70 - HE 450 AA
$h_{sl/ab}$= 70 - HE 450 A
$h_{sl/ab}$= 70 - HE 450 B
$h_{sl/ab}$= 70 - HE 450 M
$h_{sl/ab}$= 80 - HE 450 AA
$h_{sl/ab}$= 80 - HE 450 A
$h_{sl/ab}$= 80 - HE 450 B
$h_{sl/ab}$= 80 - HE 450 M
$h_{sl/ab}$= 90 - HE 450 AA
$h_{sl/ab}$= 90 - HE 450 A
$h_{sl/ab}$= 90 - HE 450 B
$h_{sl/ab}$= 90 - HE 450 M
$h_{sl/ab}$= 100 - HE 450 AA
$h_{sl/ab}$= 100 - HE 450 A
$h_{sl/ab}$= 100 - HE 450 B
$h_{sl/ab}$= 100 - HE 450 M
Interaxis length: L_{inter}= 6500 mm
Dowel shape= PZ

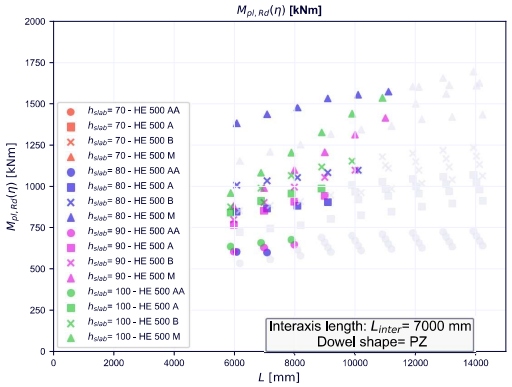
$M_{pl,Rd}(\eta)$ [kNm]
L [mm]
$h_{sl/ab}$= 70 - HE 500 AA
$h_{sl/ab}$= 70 - HE 500 A
$h_{sl/ab}$= 70 - HE 500 B
$h_{sl/ab}$= 70 - HE 500 M
$h_{sl/ab}$= 80 - HE 500 AA
$h_{sl/ab}$= 80 - HE 500 A
$h_{sl/ab}$= 80 - HE 500 B
$h_{sl/ab}$= 80 - HE 500 M
$h_{sl/ab}$= 90 - HE 500 AA
$h_{sl/ab}$= 90 - HE 500 A
$h_{sl/ab}$= 90 - HE 500 B
$h_{sl/ab}$= 90 - HE 500 M
$h_{sl/ab}$= 100 - HE 500 AA
$h_{sl/ab}$= 100 - HE 500 A
$h_{sl/ab}$= 100 - HE 500 B
$h_{sl/ab}$= 100 - HE 500 M
Interaxis length: L_{inter}= 7000 mm
Dowel shape= PZ

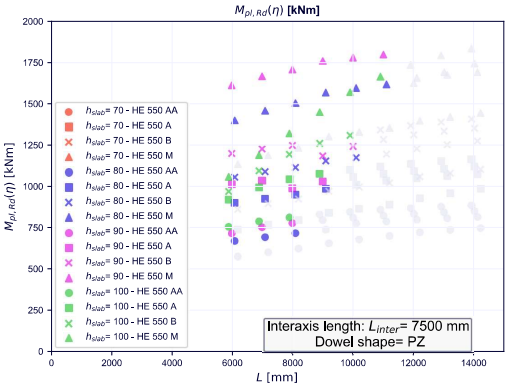
$M_{pl,Rd}(\eta)$ [kNm]
L [mm]
$h_{sl/ab}$= 70 - HE 550 AA
$h_{sl/ab}$= 70 - HE 550 A
$h_{sl/ab}$= 70 - HE 550 B
$h_{sl/ab}$= 70 - HE 550 M
$h_{sl/ab}$= 80 - HE 550 AA
$h_{sl/ab}$= 80 - HE 550 A
$h_{sl/ab}$= 80 - HE 550 B
$h_{sl/ab}$= 80 - HE 550 M
$h_{sl/ab}$= 90 - HE 550 AA
$h_{sl/ab}$= 90 - HE 550 A
$h_{sl/ab}$= 90 - HE 550 B
$h_{sl/ab}$= 90 - HE 550 M
$h_{sl/ab}$= 100 - HE 550 AA
$h_{sl/ab}$= 100 - HE 550 A
$h_{sl/ab}$= 100 - HE 550 B
$h_{sl/ab}$= 100 - HE 550 M
Interaxis length: L_{inter}= 7500 mm
Dowel shape= PZ

F.2 Downstand beam for carpark decking

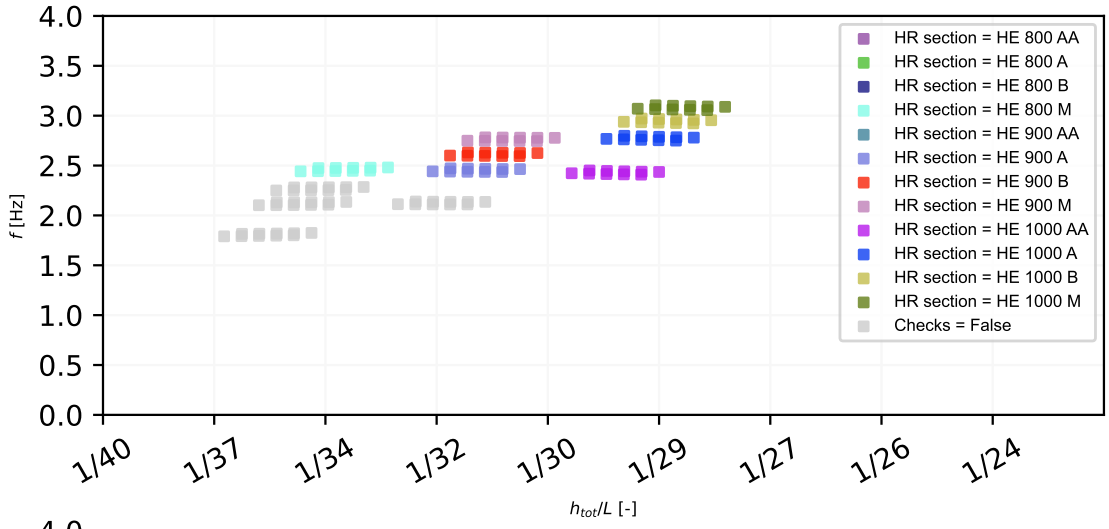
4.0
3.5
3.0
2.5
2.0
1.5
1.0
0.5
0.0
f [Hz]
1/40
1/37
1/34
1/32
1/30
1/29
1/27
1/26
1/24
h_{tot}/L [-]
HR section = HE 800 AA
HR section = HE 800 A
HR section = HE 800 B
HR section = HE 800 M
HR section = HE 900 AA
HR section = HE 900 A
HR section = HE 900 B
HR section = HE 900 M
HR section = HE 1000 AA
HR section = HE 1000 A
HR section = HE 1000 B
HR section = HE 1000 M
Checks = False

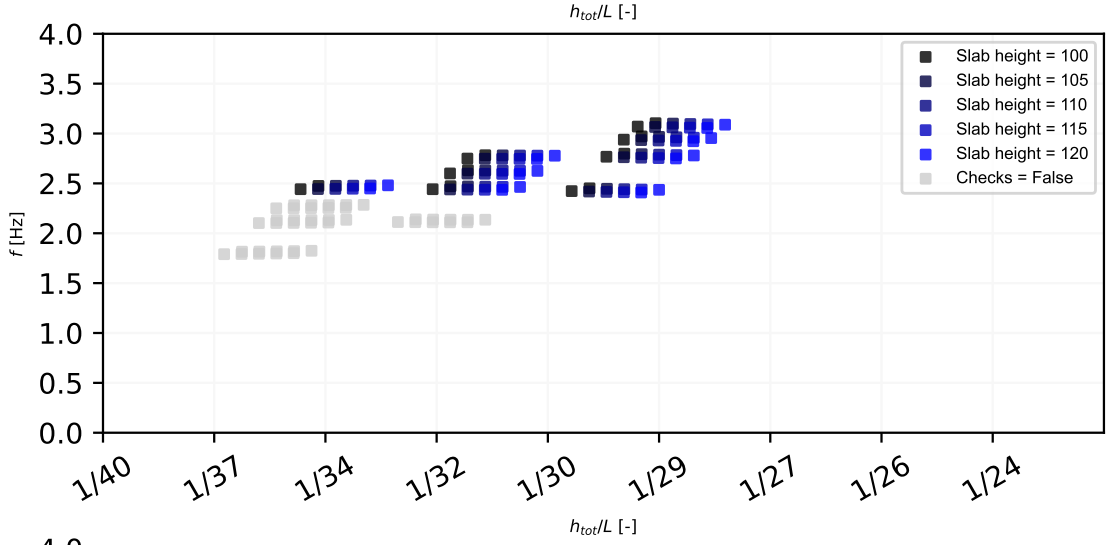
4.0
3.5
3.0
2.5
2.0
1.5
1.0
0.5
0.0
f [Hz]
1/40
1/37
1/34
1/32
1/30
1/29
1/27
1/26
1/24
h_{tot}/L [-]
Slab height = 100
Slab height = 105
Slab height = 110
Slab height = 115
Slab height = 120
Checks = False

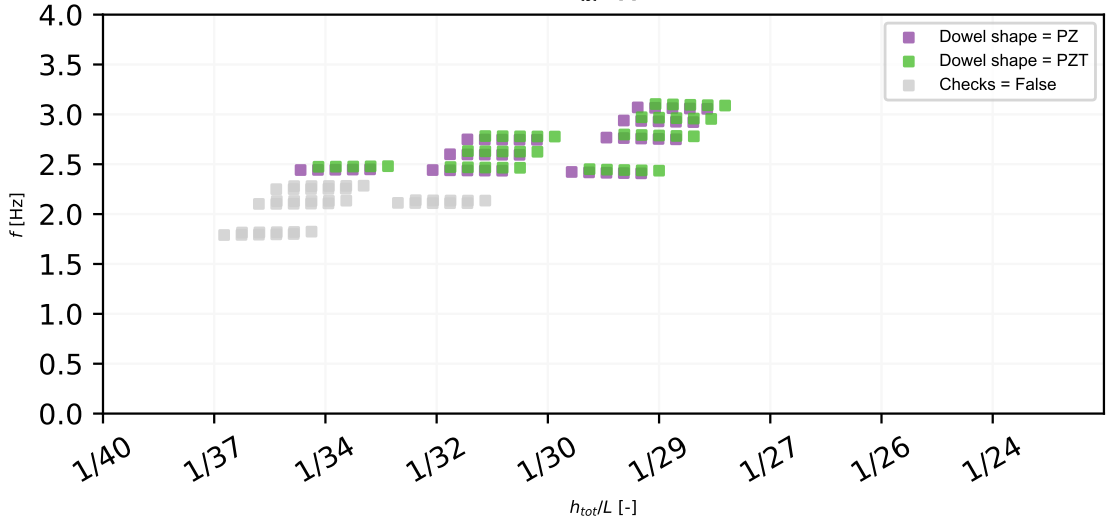
4.0
3.5
3.0
2.5
2.0
1.5
1.0
0.5
0.0
f [Hz]
1/40
1/37
1/34
1/32
1/30
1/29
1/27
1/26
1/24
h_{tot}/L [-]
Dowel shape = PZ
Dowel shape = PZT
Checks = False

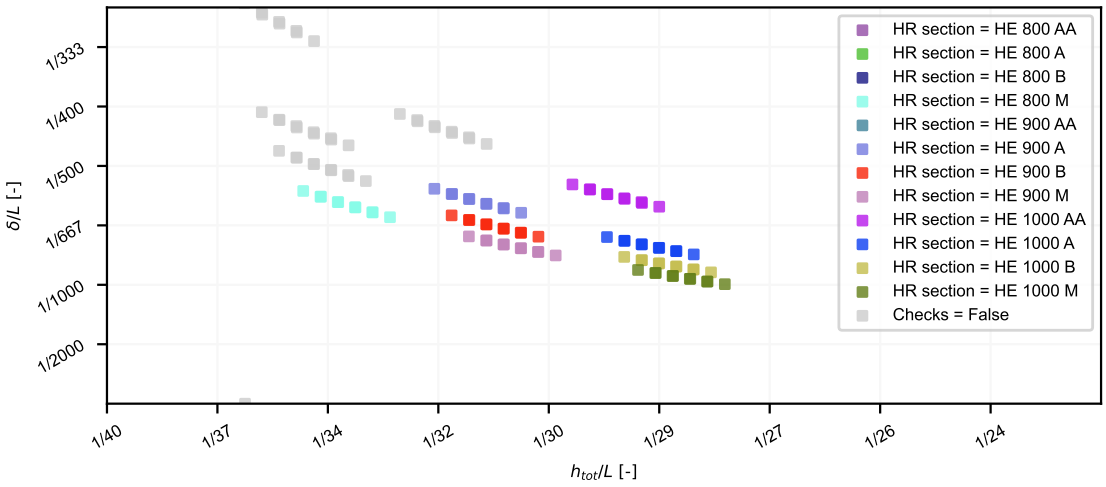
δ/L [-]
1/333
1/400
1/500
1/667
1/1000
1/2000
1/40
1/37
1/34
1/32
1/30
1/29
1/27
1/26
1/24
h_tot/L [-]
HR section = HE 800 AA
HR section = HE 800 A
HR section = HE 800 B
HR section = HE 800 M
HR section = HE 900 AA
HR section = HE 900 A
HR section = HE 900 B
HR section = HE 900 M
HR section = HE 1000 AA
HR section = HE 1000 A
HR section = HE 1000 B
HR section = HE 1000 M
Checks = False

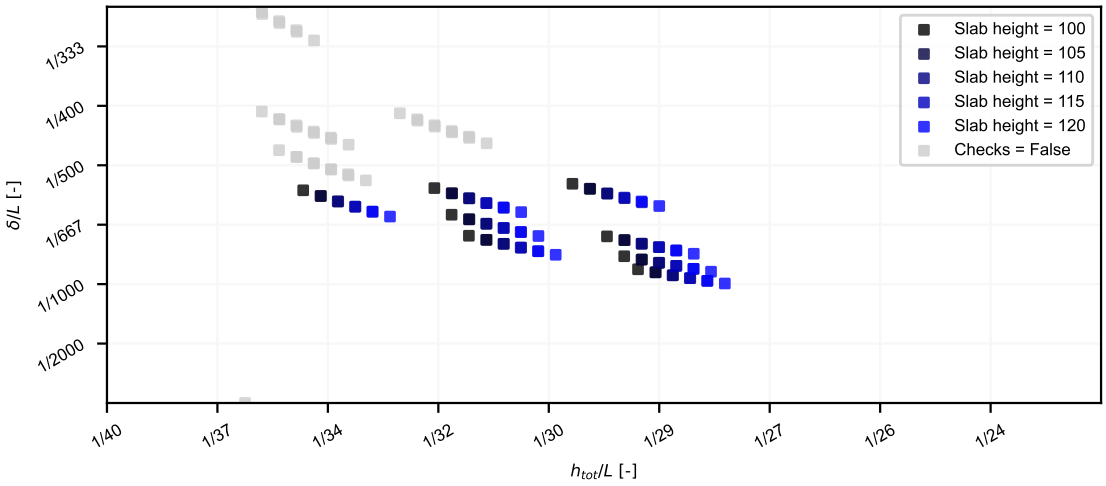
δ/L [-]
1/333
1/400
1/500
1/667
1/1000
1/2000
1/40
1/37
1/34
1/32
1/30
1/29
1/27
1/26
1/24
h_tot/L [-]
Slab height = 100
Slab height = 105
Slab height = 110
Slab height = 115
Slab height = 120
Checks = False

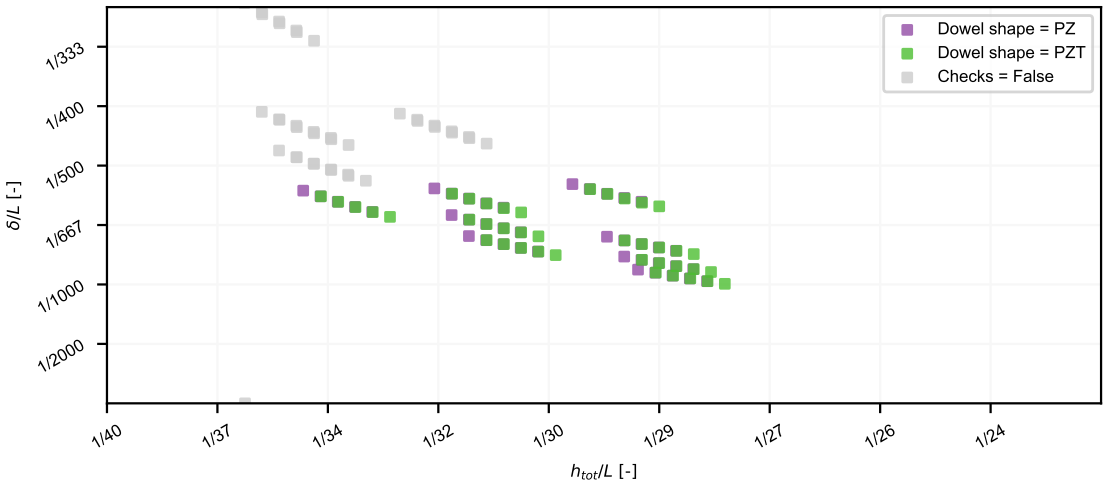
δ/L [-]
1/333
1/400
1/500
1/667
1/1000
1/2000
1/40
1/37
1/34
1/32
1/30
1/29
1/27
1/26
1/24
h_tot/L [-]
Dowel shape = PZ
Dowel shape = PZT
Checks = False

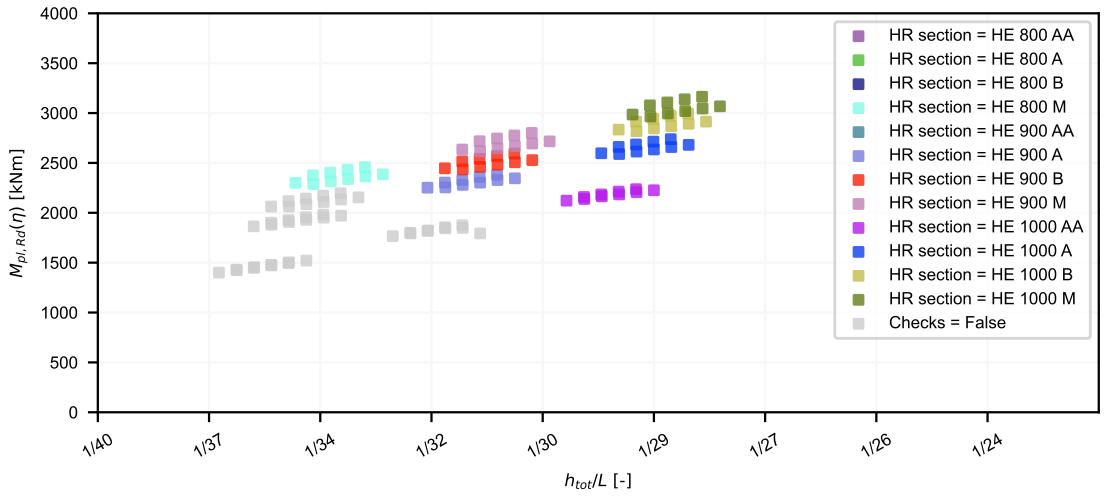
4000
3500
3000
2500
2000
1500
1000
500
0
$M_{pl,Rd}(\eta)$ [kNm]
1/40
1/37
1/34
1/32
1/30
1/29
1/27
1/26
1/24
h_{tot}/L [-]
HR section = HE 800 AA
HR section = HE 800 A
HR section = HE 800 B
HR section = HE 800 M
HR section = HE 900 AA
HR section = HE 900 A
HR section = HE 900 B
HR section = HE 900 M
HR section = HE 1000 AA
HR section = HE 1000 A
HR section = HE 1000 B
HR section = HE 1000 M
Checks = False

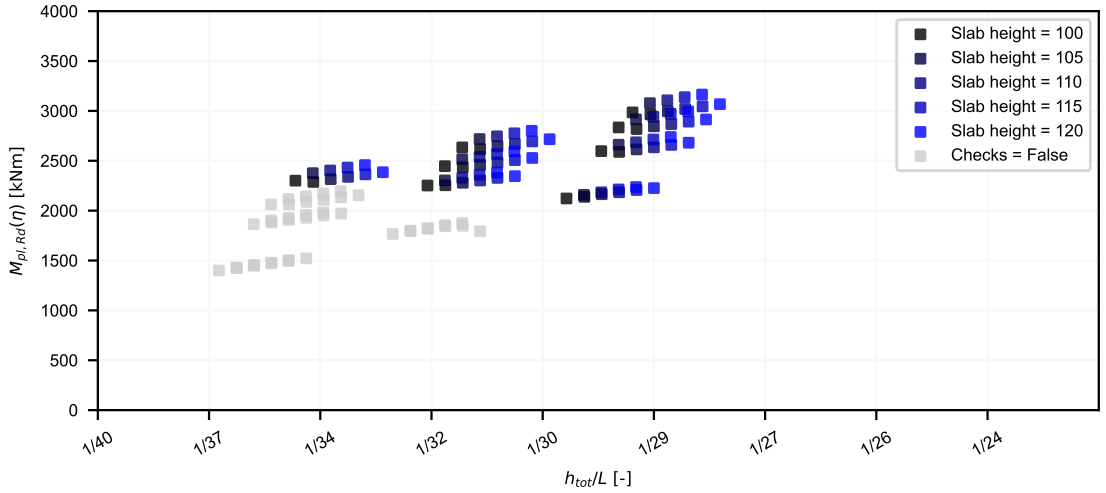
4000
3500
3000
2500
2000
1500
1000
500
0
$M_{pl,Rd}(\eta)$ [kNm]
1/40
1/37
1/34
1/32
1/30
1/29
1/27
1/26
1/24
h_{tot}/L [-]
Slab height = 100
Slab height = 105
Slab height = 110
Slab height = 115
Slab height = 120
Checks = False

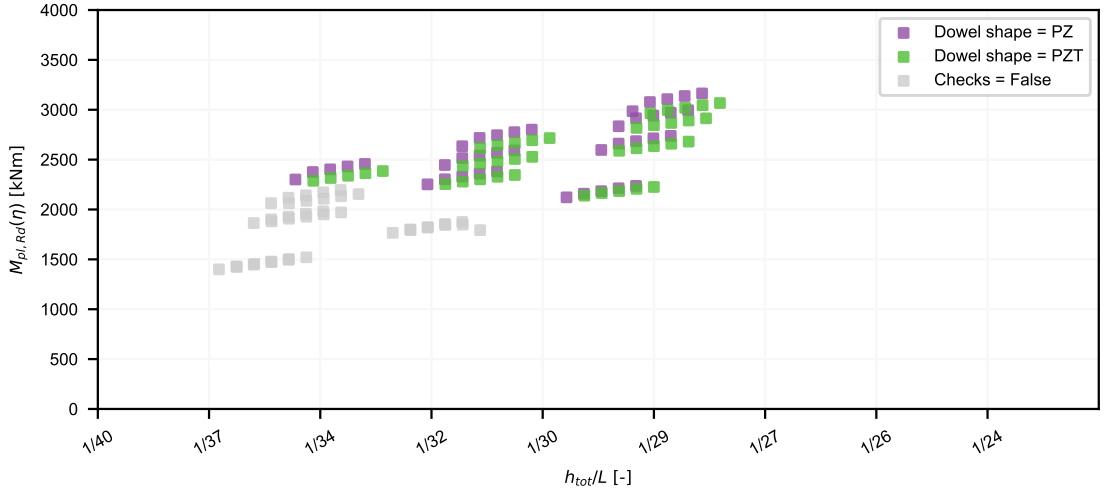
4000
3500
3000
2500
2000
1500
1000
500
0
$M_{pl,Rd}(\eta)$ [kNm]
1/40
1/37
1/34
1/32
1/30
1/29
1/27
1/26
1/24
h_{tot}/L [-]
Dowel shape = PZ
Dowel shape = PZT
Checks = False

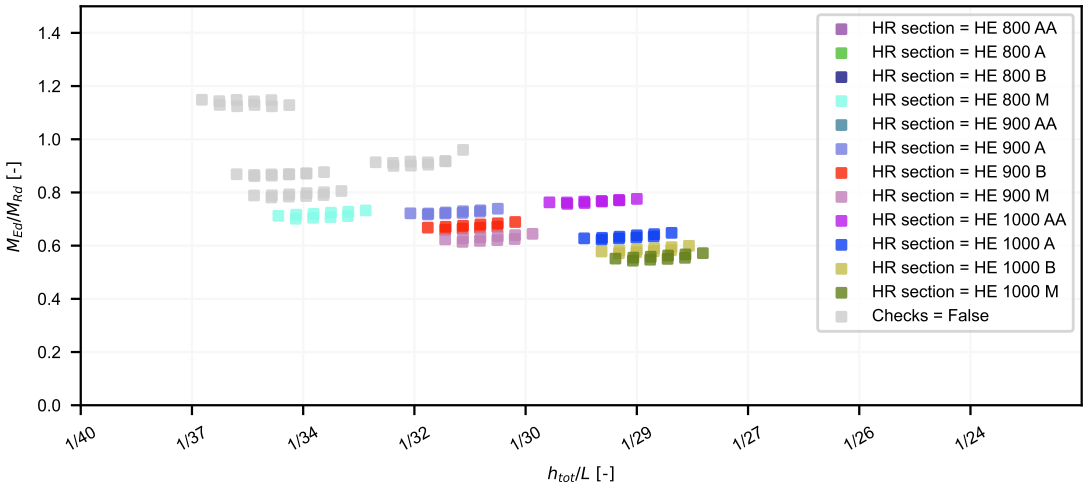
HR section = HE 800 AA
HR section = HE 800 A
HR section = HE 800 B
HR section = HE 800 M
HR section = HE 900 AA
HR section = HE 900 A
HR section = HE 900 B
HR section = HE 900 M
HR section = HE 1000 AA
HR section = HE 1000 A
HR section = HE 1000 B
HR section = HE 1000 M
Checks = False
M_{Ed}/M_{Rd} [-]
h_{tot}/L [-]

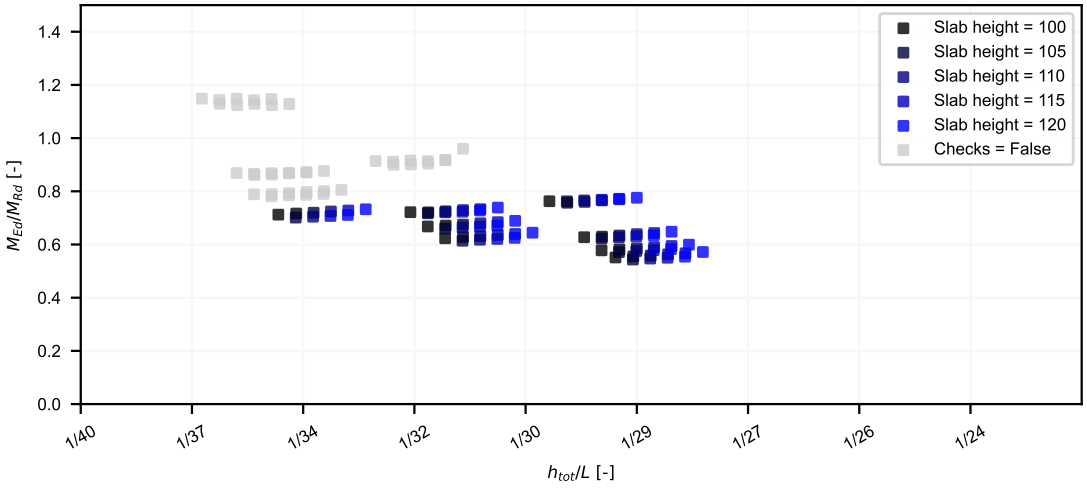
Slab height = 100
Slab height = 105
Slab height = 110
Slab height = 115
Slab height = 120
Checks = False
M_{Ed}/M_{Rd} [-]
h_{tot}/L [-]

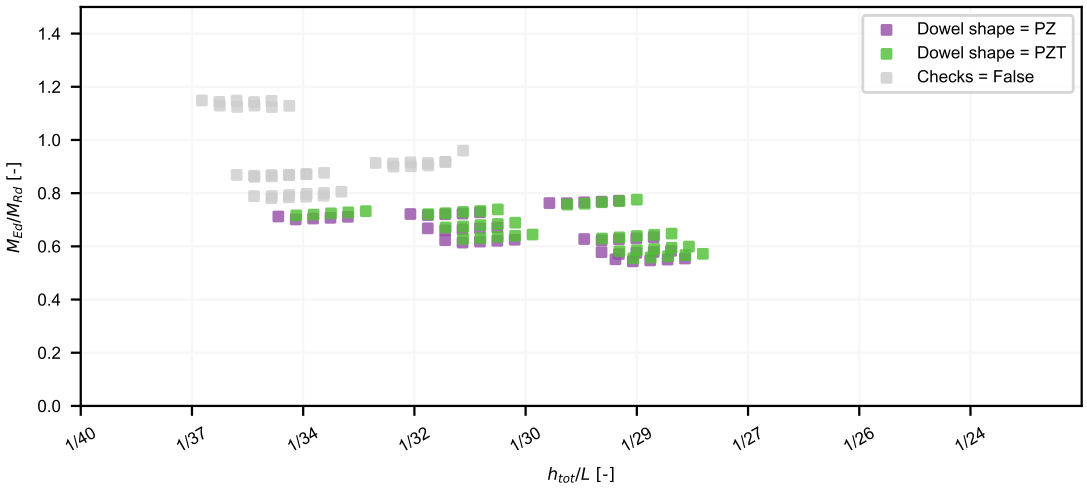
Dowel shape = PZ
Dowel shape = PZT
Checks = False
M_{Ed}/M_{Rd} [-]
h_{tot}/L [-]

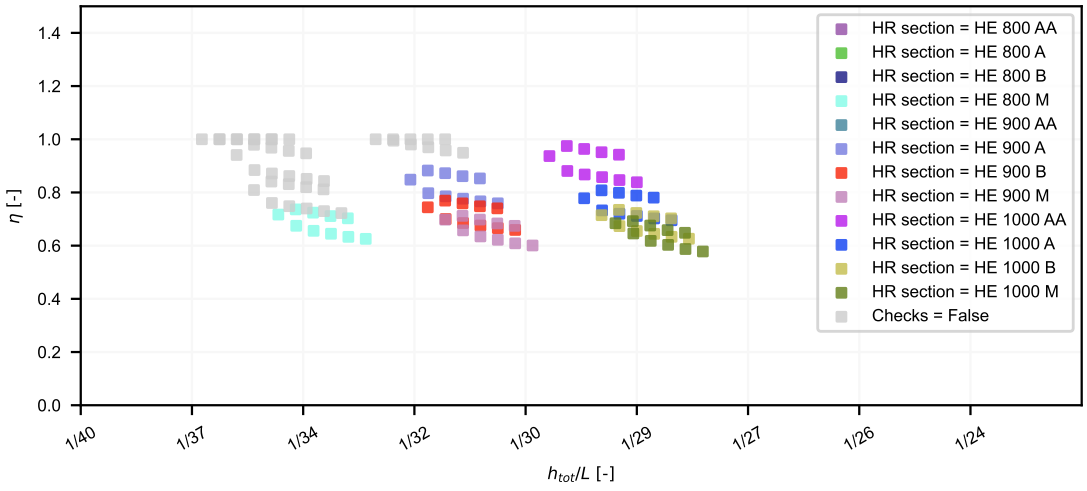
HR section = HE 800 AA
HR section = HE 800 A
HR section = HE 800 B
HR section = HE 800 M
HR section = HE 900 AA
HR section = HE 900 A
HR section = HE 900 B
HR section = HE 900 M
HR section = HE 1000 AA
HR section = HE 1000 A
HR section = HE 1000 B
HR section = HE 1000 M
Checks = False
η [-]
0.0
0.2
0.4
0.6
0.8
1.0
1.2
1.4
1/40
1/37
1/34
1/32
1/30
1/29
1/27
1/26
1/24
h_{tot}/L [-]

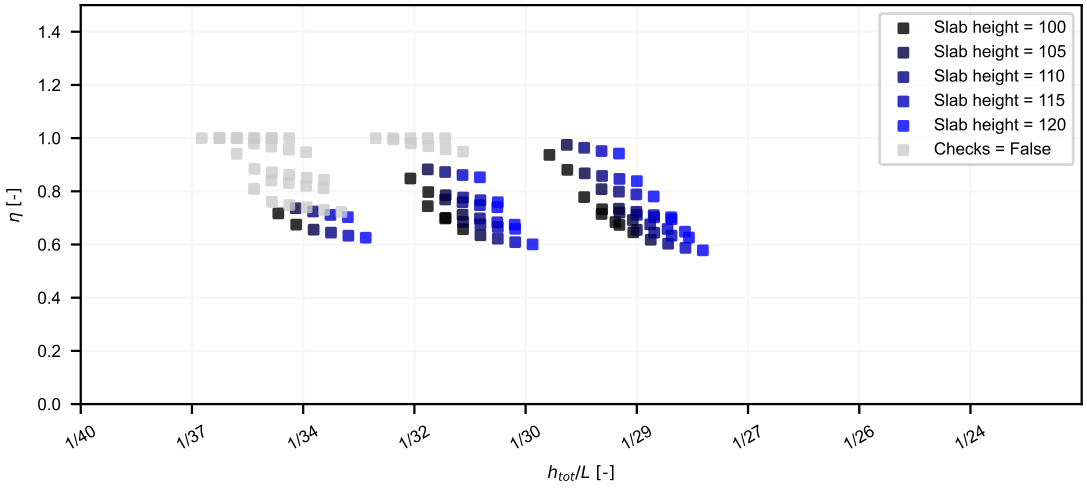
Slab height = 100
Slab height = 105
Slab height = 110
Slab height = 115
Slab height = 120
Checks = False
η [-]
0.0
0.2
0.4
0.6
0.8
1.0
1.2
1.4
1/40
1/37
1/34
1/32
1/30
1/29
1/27
1/26
1/24
h_{tot}/L [-]

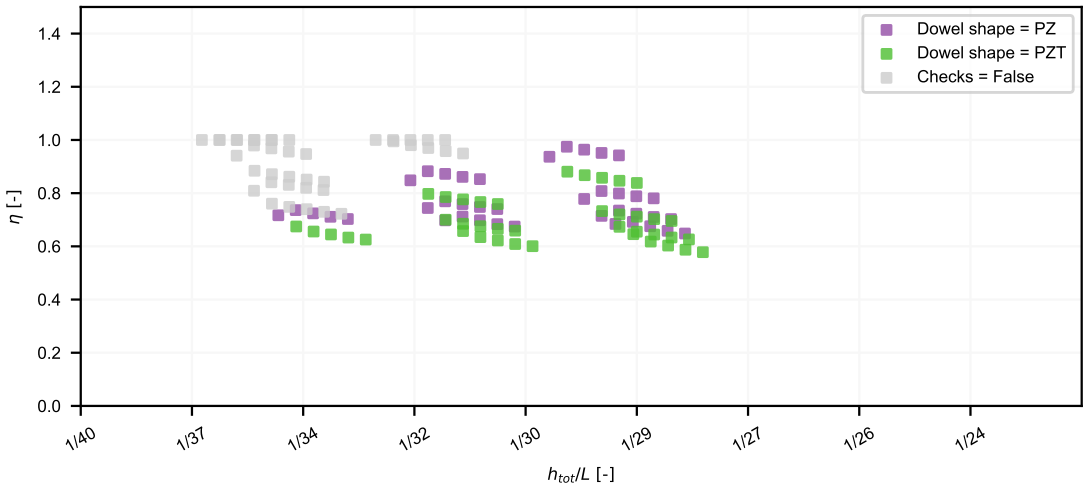
Dowel shape = PZ
Dowel shape = PZT
Checks = False
η [-]
0.0
0.2
0.4
0.6
0.8
1.0
1.2
1.4
1/40
1/37
1/34
1/32
1/30
1/29
1/27
1/26
1/24
h_{tot}/L [-]